

*sensors*

Special Issue Reprint

---

# Sensors and Robotics for Digital Agriculture

---

Edited by  
Dionysis Bochtis and Aristotelis C. Tagarakis

[mdpi.com/journal/sensors](https://mdpi.com/journal/sensors)



# **Sensors and Robotics for Digital Agriculture**



# Sensors and Robotics for Digital Agriculture

Editors

**Dionysis Bochtis**

**Aristotelis C. Tagarakis**



Basel • Beijing • Wuhan • Barcelona • Belgrade • Novi Sad • Cluj • Manchester



*Editors*

Dionysis Bochtis  
Institute for Bio-economy and  
Agri-technology (iBO)  
Centre for Research &  
Technology Hellas (CERTH)  
Volos, Greece

Aristotelis C. Tagarakis  
Institute for Bio-economy and  
Agri-technology (iBO)  
Centre for Research &  
Technology Hellas (CERTH)  
Volos, Greece

*Editorial Office*

MDPI  
St. Alban-Anlage 66  
4052 Basel, Switzerland

This is a reprint of articles from the Topical Collection published online in the open access journal *Sensors* (ISSN 1424-8220) (available at: [https://www.mdpi.com/journal/sensors/topical\\_collections/SRDA](https://www.mdpi.com/journal/sensors/topical_collections/SRDA)).

For citation purposes, cite each article independently as indicated on the article page online and as indicated below:

Lastname, A.A.; Lastname, B.B. Article Title. <i>Journal Name</i> <b>Year</b> , <i>Volume Number</i> , Page Range.
--

**ISBN 978-3-0365-8808-7 (Hbk)**

**ISBN 978-3-0365-8809-4 (PDF)**

**[doi.org/10.3390/books978-3-0365-8809-4](https://doi.org/10.3390/books978-3-0365-8809-4)**

© 2023 by the authors. Articles in this book are Open Access and distributed under the Creative Commons Attribution (CC BY) license. The book as a whole is distributed by MDPI under the terms and conditions of the Creative Commons Attribution-NonCommercial-NoDerivs (CC BY-NC-ND) license.

# Contents

<b>About the Editors</b> . . . . .	vii
<b>Aristotelis C. Tagarakis and Dionysis Bochtis</b> Sensors and Robotics for Digital Agriculture Reprinted from: <i>Sensors</i> <b>2023</b> , <i>23</i> , 7255, doi:10.3390/s23167255 . . . . .	1
<b>Lefteris Benos, Aristotelis C. Tagarakis, Georgios Dolias, Remigio Berruto, Dimitrios Kateris and Dionysis Bochtis</b> Machine Learning in Agriculture: A Comprehensive Updated Review Reprinted from: <i>Sensors</i> <b>2021</b> , <i>21</i> , 3758, doi:10.3390/s21113758 . . . . .	7
<b>Sadaf Farkhani, Søren Kelstrup Skovsen, Mads Dyrmann, Rasmus Nyholm Jørgensen and Henrik Karstoft</b> Weed Classification Using Explainable Multi-Resolution Slot Attention Reprinted from: <i>Sensors</i> <b>2021</b> , <i>21</i> , 6705, doi:10.3390/s21206705 . . . . .	63
<b>Athanasios Anagnostis, Aristotelis C. Tagarakis, Dimitrios Kateris, Vasileios Moysiadis, Claus Grøn Sørensen, Simon Pearson and Dionysis Bochtis</b> Orchard Mapping with Deep Learning Semantic Segmentation Reprinted from: <i>Sensors</i> <b>2021</b> , <i>21</i> , 3813, doi:10.3390/s21113813 . . . . .	81
<b>Martin Wutke, Felix Heinrich, Pronaya Prosun Das, Anita Lange, Maria Gentz, Imke Traulsen, et al.</b> Detecting Animal Contacts—A Deep Learning-Based Pig Detection and Tracking Approach for the Quantification of Social Contacts Reprinted from: <i>Sensors</i> <b>2021</b> , <i>21</i> , 7512, doi:10.3390/s21227512 . . . . .	101
<b>Dejan Pavlovic, Mikolaj Czerkawski, Christopher Davison, Oskar Marko, Craig Michie, Robert Atkinson, et al.</b> Behavioural Classification of Cattle Using Neck-Mounted Accelerometer-Equipped Collars Reprinted from: <i>Sensors</i> <b>2022</b> , <i>22</i> , 2323, doi:10.3390/s22062323 . . . . .	117
<b>Eduardo Navas, Roemi Fernández, Delia Sepúlveda, Manuel Armada and Pablo Gonzalez-de-Santos</b> Soft Grippers for Automatic Crop Harvesting: A Review Reprinted from: <i>Sensors</i> <b>2021</b> , <i>21</i> , 2689, doi:10.3390/s21082689 . . . . .	135
<b>Goran Kitić, Damir Krklješ, Marko Panić, Csaba Petes, Slobodan Birgermajer and Vladimir Crnojević</b> Agrobot Lala—An Autonomous Robotic System for Real-Time, In-Field Soil Sampling, and Analysis of Nitrates Reprinted from: <i>Sensors</i> <b>2022</b> , <i>22</i> , 4207, doi:10.3390/s22114207 . . . . .	163
<b>Aristotelis C. Tagarakis, Evangelia Filippou, Damianos Kalaitzidis, Lefteris Benos, Patrizia Busato and Dionysis Bochtis</b> Proposing UGV and UAV Systems for 3D Mapping of Orchard Environments Reprinted from: <i>Sensors</i> <b>2022</b> , <i>22</i> , 1571, doi:10.3390/s22041571 . . . . .	183
<b>Lefteris Benos, Vasileios Moysiadis, Dimitrios Kateris, Aristotelis C. Tagarakis, Patrizia Busato, Simon Pearson and Dionysis Bochtis</b> Human–Robot Interaction in Agriculture: A Systematic Review Reprinted from: <i>Sensors</i> <b>2023</b> , <i>23</i> , 6776, doi:10.3390/s23156776 . . . . .	197

**Abozar Nasirahmadi and Oliver Hensel**

Toward the Next Generation of Digitalization in Agriculture Based on Digital Twin Paradigm

Reprinted from: *Sensors* **2022**, *22*, 498, doi:10.3390/s22020498 . . . . . **221**

# About the Editors

## **Dionysis Bochtis**

Prof. Dionysis D. Bochtis (M) works in Systems Engineering, focused on bio-production and related provision systems including conventional systems with enhanced ICT and automation technologies up to fully robotized systems, holding various positions during his scientific career, including Director of the Institute for Bio-economy and Agri-Technology, CERTH; Professor (Agri-Robotics) at the Lincoln Institute for Agritechnology (LIAT), University of Lincoln; and Senior Scientist (Operations Management) at the Dept. of Engineering, Aarhus University, Denmark. In parallel, he is involved in agri-technology product development in the private sector and is the founder of the company “farmB digital agriculture S.A.”.

## **Aristotelis C. Tagarakis**

Dr. Aristotelis C. Tagarakis is Senior Researcher (Grade B') at the Institute for Bio-economy and Agri-technology (iBO/CERTH) with expertise in precision agriculture. Dr. Tagarakis received an MSc degree in Automation in Irrigation, Farm Structures and Farm Mechanization and PhD degree in Precision Agriculture from the University of Thessaly, Greece. In the framework of his PhD, he worked as a research scholar at Auburn University, Biosystems Engineering Department, AL, U.S.A., in the area of Precision Agriculture, studying variable rate fertilization and automated irrigation in maize. He was also a Postdoctoral Associate at Cornell University, N.Y., U.S.A., leading the Precision Agriculture program. Before joining the iBO, he was a Senior Researcher at the BioSense Institute in Serbia. He has significant research experience working on numerous national, European, and other international projects. His main research interests include precision agriculture, digital farming, agricultural automation, agri-robotics, remote and proximal sensing and sensor networks in agriculture.



# Sensors and Robotics for Digital Agriculture

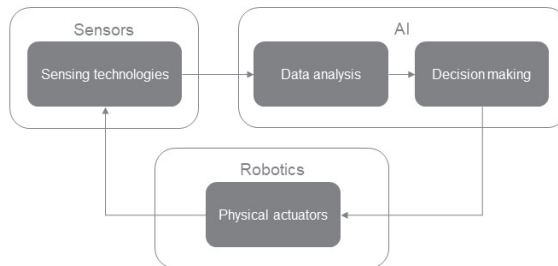
Aristotelis C. Tagarakis \* and Dionysis Bochtis

Institute for Bio-Economy and Agri-Technology (iBO), Centre for Research and Technology-Hellas (CERTH), 6th km Charilaou-Thermi Rd., 57001 Thessaloniki, Greece; d.bochtis@certh.gr

\* Correspondence: a.tagarakis@certh.gr

The latest advances in innovative sensing and data technologies have led to an increasing implementation of autonomous systems in agricultural production processes. Physical autonomous systems can accomplish even more complex tasks, while cyber ones can support timely, accurate and informed decision making, leading to more efficient farm management and improved profitability in the context of precision agriculture and Agriculture 4.0. This combination has transformed agricultural robots to machines with embedded awareness [1,2] also capable of interacting with other machines [3–5], as well as with human labor [6–8]. On the other hand, sensing technologies in agriculture continuously provide a vast amount of data necessary for the development and implementation of AI technologies [9–11].

All the above constitutes a closed-loop interaction between the disciplines of sensing, AI, and robotics technologies (Figure 1). This interaction is the basis of the present Topical Collection under the purpose of highlighting the corresponding advancements in the domain of precision agriculture. In this collection, a total of 10 articles are included covering different aspects of this interaction approach, including topics such as agri-robotics awareness, human–robot interaction, AI in crop and livestock production, and digital twins in the context of modern agriculture.



**Figure 1.** The closed-loop approach for the interaction of the sensors, AI, and robotics entities.

With the recent advances in sensing methods and data acquisition technologies in agriculture, a vast amount of data became available, paving the way to exploring the utilization of artificial intelligence in agriculture. This is the main topic that is analyzed in the comprehensive review provided by Benos et al. [12], as an update of the previous review presented in [9]. Machine learning refers to a subset of artificial intelligence and has considerable potential for handling numerous challenges in the establishment of knowledge-based farming systems. In this study, a thorough review of recent literature on machine learning in crop, water, soil, and livestock management is analyzed. Maize, wheat, cattle, and sheep were the most investigated crops and animals, respectively. This study is anticipated to constitute a guide of the potential advantages of machine learning in agriculture.

Regarding machine learning applications in crop management, two works are presented in the collection. Farkhani et al. [13] propose the use of a multi-layer attention

**Citation:** Tagarakis, A.C.; Bochtis, D. Sensors and Robotics for Digital Agriculture. *Sensors* **2023**, *23*, 7255. <https://doi.org/10.3390/s23167255>

Received: 15 August 2023

Accepted: 17 August 2023

Published: 18 August 2023



**Copyright:** © 2023 by the authors. Licensee MDPI, Basel, Switzerland. This article is an open access article distributed under the terms and conditions of the Creative Commons Attribution (CC BY) license (<https://creativecommons.org/licenses/by/4.0/>).

procedure to present an interpretation of the Deep Neural Network's (DNN) decisions through a high-resolution attention map for the classification of weeds. The proposed architecture can improve the resolution and location of weed areas for efficient weed management. The second work deals with the mapping of agricultural environments. The study presented by Anagnostis et al. [14] proposes an approach for the segmentation of trees in commercial orchards using aerial images obtained by unmanned aerial vehicles (UAVs). The methodology is based on a deep learning convolutional neural network and was proven to be efficient for the automated detection and localization of tree canopies. The trained model was tested on never-before-seen orthomosaic images, achieving performance levels up to 99%, demonstrating the robustness of the proposed approach.

Deep learning was also utilized in livestock management for the detection and tracking of pigs for the quantification of social contacts as described in Wutke et al. [15]. A convolutional neural network (CNN) was applied on video footage to detect the location and orientation of pigs tracking the animals' movement trajectories over a given period using a Kalman filter (KF) algorithm. This enabled the automatic identification of social contacts in the form of head-head and head-tail contacts. The specific study demonstrated the effectiveness of the methodology to enhance animal monitoring systems. The second study in this collection concerning technological and digital advances in livestock regards the use of neck-mounted collars equipped with accelerometers for monitoring and classifying dairy cattle behaviors (Pavlovic et al.) [16]. Such sensor systems automatically provide information about key cattle behaviors, such as level of restlessness and ruminating and eating time, assessing the overall welfare, at animal level. Within this work, the development of algorithms for the classification of cattle states is described. The results showed that the classification model that was based on linear discriminant analysis using features selected through Backward Feature Elimination provided the most balanced tradeoff between performance and computational complexity.

The second group of works regard applications of robotics in agriculture. Crop harvesting is one of the most demanding, time-consuming, and labor-intensive operations in high-value crops such as fruit and nut trees, grapes, and various vegetable crops. Due to its seasonal character, securing the work force to address this task is a great challenge [17]. Therefore, a lot of effort has been invested in the development of autonomous or semi-autonomous crop-harvesting systems. In most cases, due to the complexity of the operation, intelligent systems are needed [18]. A review conducted by Navas et al. [19] has been included in the current collection that addresses the task of automatic crop harvesting, focusing on the specifications of soft grippers. Soft robotics and soft grippers are promising approaches in this field due to the specifications required to meet hygiene and manipulation requirements in unstructured environments when working with delicate products. This review provides an insight into soft end-effectors for agricultural applications, emphasizing robotic harvesting, aiming to serve as a guide in the design of soft grippers for fruit harvesting robots in soft robotics for Agriculture 4.0.

Apart from harvesting, there is a plethora of other field management activities that are laborious and time-consuming and are subjected to automation. In the study presented by Kitic et al. [20] an Autonomous Robotic System was developed for real-time, in-field soil sampling and analysis of nitrates in the soil. The system combines a set of modules including a commercial robotic platform, an anchoring module, a sampling module, a sample preparation module, a sample analysis module, and a communication module. The procedure starts with the definition of the sampling locations using a dedicated cloud-based platform which processes satellite images using artificial intelligence. Then, automated soil sampling takes place; each sample is analyzed on the spot and georeferenced, providing a map which can be used for precision-based fertilizing.

The situational awareness and navigation of autonomous robotic platforms in agricultural fields is a particularly challenging and demanding task due to the irregular nature and the complexity of such environments. Therefore, mapping the environment for targeted robotic applications in agricultural fields is challenging due to the high spatial and temporal

variability which make these environments highly unpredictable [21]. The aim of the study presented by Tagarakis et al. [22] was to investigate the use of consumer-grade RGB-D (red, green, blue and depth) and unmanned aerial (UAV) and ground vehicles (UGV) for autonomous mapping of the environment in commercial orchards and for providing structural information of the trees such as height and canopy volume. Two systems were used; the ground-based system consisting of a UGV with an RGB-D camera and the aerial-based system which consisted of a UAV equipped with high accuracy RTK-GPS and a precise imaging system. The results from the ground-based mapping system were compared with the three-dimensional (3D) orthomosaics acquired by the UAV. Both systems performed adequately well. The fusion of the two datasets (from the ground and above) provided the most precise representation of the trees. In the pursuit of optimizing the efficiency, flexibility, and adaptability of agricultural operations, digitalization and automatization of agricultural practices are considered as the means to achieving the goals of agricultural production and addressing its modern challenges. However, unmanned systems, aerial or ground, show autonomy at some level and interact with other dynamic elements in the fields such as agricultural machinery and humans. Consequently, a new sector has emerged focused on human–robot interaction (HRI) in agriculture. A systematic review of the advances in the interaction between humans and agricultural robots was conducted by Benos et al. [23], reviewing the scholarly literature to capture the current progress and trends in this promising field while identifying future research directions. Based on the findings of the review, there is a growing interest in the specific research field which combines perspectives from several disciplines. In terms of crops, melons, grapes, and strawberries were the ones with the highest interest for HRI applications, mainly due to their high value perspective and the low availability of traditional machinery automations due to the nature of these cropping systems. Collaboration and cooperation were the most preferred interaction modes, with various levels of automation being examined in the cited studies. Due to the complexity of the agricultural environments and the tasks taking place in agricultural operations, there is still a long way to go towards the establishment of viable, functional, and safe human–robot systems [24,25].

As already mentioned, the digitalization of agriculture is the way forward to the future of farming in the framework of Agriculture 4.0, improving production systems and addressing food security, climate protection, and resource management. Due to the complexity and dynamic nature of agricultural production, sophisticated management systems are required supporting farmers and farm managers in making informed and improved decisions. In the review presented by Nasirahmadi et al. [26], the concept of utilizing digital twins and digital technologies and techniques is presented. A digital twin is the virtual representation of a physical system. In agriculture, this can be regarded as the virtual representation of a farm, providing the potential for enhancing productivity and efficiency while minimizing energy usage and losses. A general framework of digital twins in soil, irrigation, robotics, farm machinery, and food post-harvest processing in agriculture is provided.

To conclude, the current Topical Collection provides insights into advanced ICT systems applied in precision agriculture and digital farming steering towards Agriculture 4.0. The collection includes works that cover multi-disciplinary applications in both crop and livestock production systems. The outcomes from the reported articles highlight the importance of digital systems, sensing technologies, and advanced data analysis methodologies for making informed decisions supporting the sustainability of future farming.

**Author Contributions:** Writing—original draft preparation, A.C.T.; writing—review and editing, D.B. and A.C.T.; supervision, D.B. All authors have read and agreed to the published version of the manuscript.

**Acknowledgments:** The Guest Editors would like to thank all the authors for their contribution to this Topical Collection, as well as the peer reviewers for their valuable edits and comments that



improved the quality of the published documents. The Guest Editors would also like to express their gratitude to all the staff and people involved in this collection for all their efforts.

**Conflicts of Interest:** The authors declare no conflict of interest.

## References

- Lasota, P.A.; Shah, J.A. Analyzing the Effects of Human-Aware Motion Planning on Close-Proximity Human–Robot Collaboration. *Hum. Factors* **2015**, *57*, 21–33. [[CrossRef](#)] [[PubMed](#)]
- Benos, L.; Sørensen, C.G.; Bochtis, D. Field Deployment of Robotic Systems for Agriculture in Light of Key Safety, Labor, Ethics and Legislation Issues. *Curr. Robot. Rep.* **2022**, *3*, 49–56. [[CrossRef](#)]
- Katkaridis, D.; Moysiadis, V.; Tsolakis, N.; Busato, P.; Kateris, D.; Pearson, S.; Sørensen, C.G.; Bochtis, D. UAV-Supported Route Planning for UGVs in Semi-Deterministic Agricultural Environments. *Agronomy* **2022**, *12*, 1937. [[CrossRef](#)]
- Vu, Q.; Raković, M.; Delic, V.; Ronzhin, A. Trends in development of UAV-UGV cooperation approaches in precision agriculture. In Proceedings of the Interactive Collaborative Robotics: Third International Conference, ICR 2018, Leipzig, Germany, 18–22 September 2018; Springer: New York, NY, USA; pp. 213–221. [[CrossRef](#)]
- Mammarella, M.; Comba, L.; Biglia, A.; Dabbene, F.; Gay, P. Cooperation of unmanned systems for agricultural applications: A theoretical framework. *Biosyst. Eng.* **2022**, *223*, 61–80. [[CrossRef](#)]
- Benos, L.; Bechar, A.; Bochtis, D. Safety and ergonomics in human-robot interactive agricultural operations. *Biosyst. Eng.* **2020**, *200*, 55–72. [[CrossRef](#)]
- Adamides, G.; Edan, Y. Human–robot collaboration systems in agricultural tasks: A review and roadmap. *Comput. Electron. Agric.* **2023**, *204*, 107541. [[CrossRef](#)]
- Moysiadis, V.; Katkaridis, D.; Benos, L.; Busato, P.; Anagnostis, A.; Kateris, D.; Pearson, S.; Bochtis, D. An Integrated Real-Time Hand Gesture Recognition Framework for Human–Robot Interaction in Agriculture. *Appl. Sci.* **2022**, *12*, 8160. [[CrossRef](#)]
- Liakos, K.G.; Busato, P.; Moshou, D.; Pearson, S.; Bochtis, D. Machine learning in agriculture: A review. *Sensors* **2018**, *18*, 2674. [[CrossRef](#)]
- Van Klompenburg, T.; Kassahun, A.; Catal, C. Crop yield prediction using machine learning: A systematic literature review. *Comput. Electron. Agric.* **2020**, *177*, 105709. [[CrossRef](#)]
- Martínez, M.; Moore, N.J.; Cavalcante de Oliveira, R.; Diogne de Souza Silva, R. Artificial Intelligence in Agriculture: Benefits, Challenges, and Trends. *Appl. Sci.* **2023**, *13*, 7405. [[CrossRef](#)]
- Benos, L.; Tagarakis, A.C.; Doliias, G.; Berruto, R.; Kateris, D.; Bochtis, D. Machine learning in agriculture: A comprehensive updated review. *Sensors* **2021**, *21*, 3758. [[CrossRef](#)]
- Farkhani, S.; Skovsen, S.K.; Dyrmann, M.; Jørgensen, R.N.; Karstoft, H. Weed classification using explainable multi-resolution slot attention. *Sensors* **2021**, *21*, 6705. [[CrossRef](#)] [[PubMed](#)]
- Anagnostis, A.; Tagarakis, A.C.; Kateris, D.; Moysiadis, V.; Sørensen, C.G.; Pearson, S.; Bochtis, D. Orchard mapping with deep learning semantic segmentation. *Sensors* **2021**, *21*, 3813. [[CrossRef](#)]
- Wutke, M.; Heinrich, F.; Das, P.P.; Lange, A.; Gentz, M.; Traulsen, I.; Warns, F.K.; Schmitt, A.O.; Gültas, M. Detecting animal contacts—A deep learning-based pig detection and tracking approach for the quantification of social contacts. *Sensors* **2021**, *21*, 7512. [[CrossRef](#)] [[PubMed](#)]
- Pavlovic, D.; Czerkawski, M.; Davison, C.; Marko, O.; Michie, C.; Atkinson, R.; Crnojevic, V.; Andonovic, I.; Rajovic, V.; Kvascev, G.; et al. Behavioural Classification of Cattle Using Neck-Mounted Accelerometer-Equipped Collars. *Sensors* **2022**, *22*, 2323. [[CrossRef](#)] [[PubMed](#)]
- Marinoudi, V.; Lampridi, M.; Kateris, D.; Pearson, S.; Sørensen, C.G.; Bochtis, D. The Future of Agricultural Jobs in View of Robotization. *Sustainability* **2021**, *13*, 12109. [[CrossRef](#)]
- Bechar, A.; Vigneault, C. Agricultural robots for field operations: Concepts and components. *Biosyst. Eng.* **2016**, *149*, 94–111. [[CrossRef](#)]
- Navas, E.; Fernández, R.; Sepúlveda, D.; Armada, M.; Gonzalez-De-santos, P. Soft grippers for automatic crop harvesting: A review. *Sensors* **2021**, *21*, 2689. [[CrossRef](#)]
- Kitić, G.; Krklješ, D.; Panić, M.; Petes, C.; Birgermajer, S.; Crnojević, V. Agrobot Lala—An Autonomous Robotic System for Real-Time, In-Field Soil Sampling, and Analysis of Nitrates. *Sensors* **2022**, *22*, 4207. [[CrossRef](#)]
- Moysiadis, V.; Tsolakis, N.; Katkaridis, D.; Sørensen, C.G.; Pearson, S.; Bochtis, D. Mobile Robotics in Agricultural Operations: A Narrative Review on Planning Aspects. *Appl. Sci.* **2020**, *10*, 3453. [[CrossRef](#)]
- Tagarakis, A.C.; Filippou, E.; Kalaitzidis, D.; Benos, L.; Busato, P.; Bochtis, D. Proposing UGV and UAV Systems for 3D Mapping of Orchard Environments. *Sensors* **2022**, *22*, 1571. [[CrossRef](#)] [[PubMed](#)]
- Benos, L.; Moysiadis, V.; Kateris, D.; Tagarakis, A.C.; Busato, P.; Pearson, S.; Bochtis, D. Human–Robot Interaction in Agriculture: A Systematic Review. *Sensors* **2023**, *23*, 6776. [[CrossRef](#)]
- Benos, L.; Tsaopoulos, D.; Bochtis, D. A review on ergonomics in agriculture. Part II: Mechanized operations. *Appl. Sci.* **2020**, *10*, 3484. [[CrossRef](#)]
- Bechar, A.; Edan, Y. Human-robot collaboration for improved target recognition of agricultural robots. *Ind. Robot Int. J.* **2003**, *30*, 432–436. [[CrossRef](#)]

26. Nasirahmadi, A.; Hensel, O. Toward the Next Generation of Digitalization in Agriculture Based on Digital Twin Paradigm. *Sensors* **2022**, *22*, 498. [[CrossRef](#)] [[PubMed](#)]

**Disclaimer/Publisher's Note:** The statements, opinions and data contained in all publications are solely those of the individual author(s) and contributor(s) and not of MDPI and/or the editor(s). MDPI and/or the editor(s) disclaim responsibility for any injury to people or property resulting from any ideas, methods, instructions or products referred to in the content.



Review

# Machine Learning in Agriculture: A Comprehensive Updated Review

Lefteris Benos <sup>1</sup>, Aristotelis C. Tagarakis <sup>1</sup>, Georgios Dolias <sup>1</sup>, Remigio Berruto <sup>2</sup>, Dimitrios Kateris <sup>1</sup> and Dionysis Bochtis <sup>1,3,\*</sup>

<sup>1</sup> Centre of Research and Technology-Hellas (CERTH), Institute for Bio-Economy and Agri-Technology (IBO), 6th km Charilaou-Thermi Rd, GR 57001 Thessaloniki, Greece; e.benos@certh.gr (L.B.); a.tagarakis@certh.gr (A.C.T.); g.dolias@certh.gr (G.D.); d.kateris@certh.gr (D.K.)

<sup>2</sup> Department of Agriculture, Forestry and Food Science (DISAFA), University of Turin, Largo Braccini 2, 10095 Grugliasco, Italy; remigio.berruto@unito.it

<sup>3</sup> FarmB Digital Agriculture P.C., Doiranis 17, GR 54639 Thessaloniki, Greece

\* Correspondence: d.bochtis@certh.gr

**Abstract:** The digital transformation of agriculture has evolved various aspects of management into artificial intelligent systems for the sake of making value from the ever-increasing data originated from numerous sources. A subset of artificial intelligence, namely machine learning, has a considerable potential to handle numerous challenges in the establishment of knowledge-based farming systems. The present study aims at shedding light on machine learning in agriculture by thoroughly reviewing the recent scholarly literature based on keywords' combinations of "machine learning" along with "crop management", "water management", "soil management", and "livestock management", and in accordance with PRISMA guidelines. Only journal papers were considered eligible that were published within 2018–2020. The results indicated that this topic pertains to different disciplines that favour convergence research at the international level. Furthermore, crop management was observed to be at the centre of attention. A plethora of machine learning algorithms were used, with those belonging to Artificial Neural Networks being more efficient. In addition, maize and wheat as well as cattle and sheep were the most investigated crops and animals, respectively. Finally, a variety of sensors, attached on satellites and unmanned ground and aerial vehicles, have been utilized as a means of getting reliable input data for the data analyses. It is anticipated that this study will constitute a beneficial guide to all stakeholders towards enhancing awareness of the potential advantages of using machine learning in agriculture and contributing to a more systematic research on this topic.

**Keywords:** machine learning; crop management; water management; soil management; livestock management; artificial intelligence; precision agriculture; precision livestock farming

**Citation:** Benos, L.; Tagarakis, A.C.; Dolias, G.; Berruto, R.; Kateris, D.; Bochtis, D. Machine Learning in Agriculture: A Comprehensive Updated Review. *Sensors* **2021**, *21*, 3758. <https://doi.org/10.3390/s21113758>

Academic Editors: Giovanni Agati and Asim Biswas

Received: 6 April 2021  
Accepted: 24 May 2021  
Published: 28 May 2021

**Publisher's Note:** MDPI stays neutral with regard to jurisdictional claims in published maps and institutional affiliations.



**Copyright:** © 2021 by the authors. Licensee MDPI, Basel, Switzerland. This article is an open access article distributed under the terms and conditions of the Creative Commons Attribution (CC BY) license (<https://creativecommons.org/licenses/by/4.0/>).

## 1. Introduction

### 1.1. General Context of Machine Learning in Agriculture

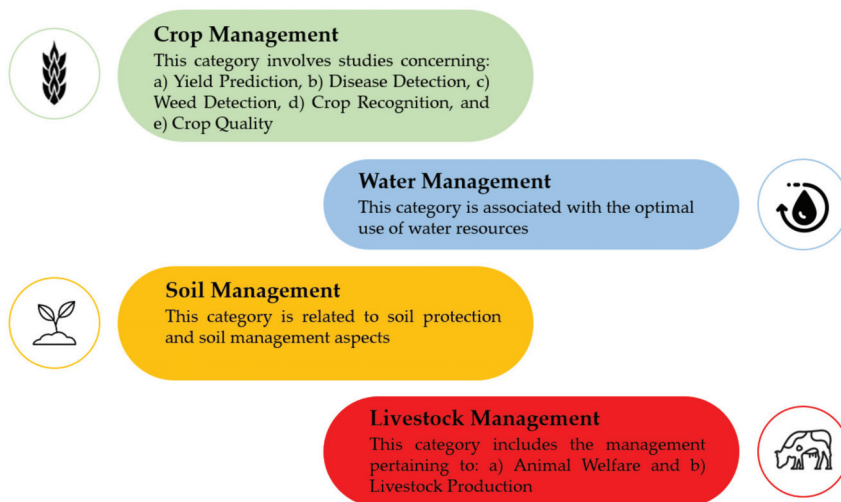
Modern agriculture has to cope with several challenges, including the increasing call for food, as a consequence of the global explosion of earth's population, climate changes [1], natural resources depletion [2], alteration of dietary choices [3], as well as safety and health concerns [4]. As a means of addressing the above issues, placing pressure on the agricultural sector, there exists an urgent necessity for optimizing the effectiveness of agricultural practices by, simultaneously, lessening the environmental burden. In particular, these two essentials have driven the transformation of agriculture into precision agriculture. This modernization of farming has a great potential to assure sustainability, maximal productivity, and a safe environment [5]. In general, smart farming is based on four key pillars in order to deal with the increasing needs; (a) optimal natural resources' management, (b) conservation of the ecosystem, (c) development of adequate services, and (d) utilization

of modern technologies [6]. An essential prerequisite of modern agriculture is, definitely, the adoption of Information and Communication Technology (ICT), which is promoted by policy-makers around the world. ICT can indicatively include farm management information systems, humidity and soil sensors, accelerometers, wireless sensor networks, cameras, drones, low-cost satellites, online services, and automated guided vehicles [7].

The large volume of data, which is produced by digital technologies and usually referred to as “big data”, needs large storage capabilities in addition to editing, analyzing, and interpreting. The latter has a considerable potential to add value for society, environment, and decision-makers [8]. Nevertheless, big data encompass challenges on account of their so-called “5-V” requirements; (a) Volume, (b) Variety, (c) Velocity, (d) Veracity, and (e) Value [9]. The conventional data processing techniques are incapable of meeting the constantly growing demands in the new era of smart farming, which is an important obstacle for extracting valuable information from field data [10]. To that end, Machine Learning (ML) has emerged, which is a subset of artificial intelligence [11], by taking advantage of the exponential computational power capacity growth.

There is a plethora of applications of ML in agriculture. According to the recent literature survey by Liakos et al. [12], regarding the time period of 2004 to 2018, four generic categories were identified (Figure 1). These categories refer to crop, water, soil, and livestock management. In particular, as far as crop management is concerned, it represented the majority of the articles amongst all categories (61% of the total articles) and was further sub-divided into:

- Yield prediction;
- Disease detection;
- Weed detection;
- Crop recognition;
- Crop quality.



**Figure 1.** The four generic categories in agriculture exploiting machine learning techniques, as presented in [12].

The generic categories dealing with the management of water and soil were found to be less investigated, corresponding cumulatively to 20% of the total number of papers (10% for each category).

Finally, two main sub-categories were identified for the livestock-related applications corresponding to a total 19% of journal papers:

- Livestock production;

- Animal welfare.

### 1.2. Open Problems Associated with Machine Learning in Agriculture

Due to the broad range of applications of ML in agriculture, several reviews have been published in this research field. The majority of these review studies have been dedicated to crop disease detection [13–16], weed detection [17,18], yield prediction [19,20], crop recognition [21,22], water management [23,24], animal welfare [25,26], and livestock production [27,28]. Furthermore, other studies were concerned with the implementation of ML methods regarding the main grain crops by investigating different aspects including quality and disease detection [29]. Finally, focus has been paid on big data analysis using ML, aiming at finding out real-life problems that originated from smart farming [30], or dealing with methods to analyze hyperspectral and multispectral data [31].

Although ML in agriculture has made considerable progress, several open problems remain, which have some common points of reference, despite the fact that the topic covers a variety of sub-fields. According to [23,24,28,32], the main problems are associated with the implementation of sensors on farms for numerous reasons, including high costs of ICT, traditional practices, and lack of information. In addition, the majority of the available datasets do not reflect realistic cases, since they are normally generated by a few people getting images or specimens in a short time period and from a limited area [15,21–23]. Consequently, more practical datasets coming from fields are required [18,20]. Moreover, the need for more efficient ML algorithms and scalable computational architectures has been pointed out, which can lead to rapid information processing [18,22,23,31]. The challenging background, when it comes to obtaining images, video, or audio recordings, has also been mentioned owing to changes in lighting [16,29], blind spots of cameras, environmental noise, and simultaneous vocalizations [25]. Another important open problem is that the vast majority of farmers are non-experts in ML and, thus, they cannot fully comprehend the underlying patterns obtained by ML algorithms. For this reason, more user-friendly systems should be developed. In particular, simple systems, being easy to understand and operate, would be valuable, as for example a visualization tool with a user-friendly interface for the correct presentation and manipulation of data [25,30,31]. Taking into account that farmers are getting more and more familiar with smartphones, specific smartphone applications have been proposed as a possible solution to address the above challenge [15,16,21]. Last but not least, the development of efficient ML techniques by incorporating expert knowledge from different stakeholders should be fostered, particularly regarding computing science, agriculture, and the private sector, as a means of designing realistic solutions [19,22,24,33]. As stated in [12], currently, all of the efforts pertain to individual solutions, which are not always connected with the process of decision-making, as seen for example in other domains.

### 1.3. Aim of the Present Study

As pointed out above, because of the multiple applications of ML in agriculture, several review studies have been published recently. However, these studies usually concentrate purely on one sub-field of agricultural production. Motivated by the current tremendous progress in ML, the increasing interest worldwide, and its impact in various domains of agriculture, a systematic bibliographic survey is presented on the range of the categories proposed in [12], which were summarized in Figure 1. In particular, we focus on reviewing the relevant literature of the last three years (2018–2020) for the intention of providing an updated view of ML applications in agricultural systems. In fact, this work is an updated continuation of the work presented at [12]; following, consequently, exactly the same framework and inclusion criteria. As a consequence, the scholarly literature was screened in order to cover a broad spectrum of important features for capturing the current progress and trends, including the identification of: (a) the research areas which are interested mostly in ML in agriculture along with the geographical distribution of the

contributing organizations, (b) the most efficient ML models, (c) the most investigated crops and animals, and (d) the most implemented features and technologies.

As will be discussed next, overall, a 745% increase in the number of journal papers took place in the last three years as compared to [12], thus justifying the need for a new updated review on the specific topic. Moreover, crop management remained as the most investigated topic, with a number of ML algorithms having been exploited as a means of tackling the heterogeneous data that originated from agricultural fields. As compared to [12], more crop and animal species have been investigated by using an extensive range of input parameters coming mainly from remote sensing, such as satellites and drones. In addition, people from different research fields have dealt with ML in agriculture, hence, contributing to the remarkable advancement in this field.

#### 1.4. Outline of the Paper

The remainder of this paper is structured as follows. The second section briefly describes the fundamentals of ML along with the subject of the four generic categories for the sake of better comprehension of the scope of the present study. The implemented methodology, along with the inclusive criteria and the search engines, is analyzed in the third section. The main performance metrics, which were used in the selected articles, are also presented in this section. The main results are shown in the fourth section in the form of bar and pie charts, while in the fifth section, the main conclusions are drawn by also discussing the results from a broader perspective. Finally, all the selected journal papers are summarized in Tables A1–A9, in accordance with their field of application, and presented in the Appendix A, together with Tables A10 and A11 that contain commonly used abbreviations, with the intention of not disrupting the flow of the main text.

## 2. Background

### 2.1. Fundamentals of Machine Learning: A Brief Overview

In general, the objective of ML algorithms is to optimize the performance of a task, via exploiting examples or past experience. In particular, ML can generate efficient relationships regarding data inputs and reconstruct a knowledge scheme. In this data-driven methodology, the more data are used, the better ML works. This is similar to how well a human being performs a particular task by gaining more experience [34]. The central outcome of ML is a measure of generalizability; the degree to which the ML algorithm has the ability to provide correct predictions, when new data are presented, on the basis of learned rules originated from preceding exposure to similar data [35]. More specifically, data involve a set of examples, which are described by a group of characteristics, usually called features. Broadly speaking, ML systems operate at two processes, namely the learning (used for training) and testing. In order to facilitate the former process, these features commonly form a feature vector that can be binary, numeric, ordinal, or nominal [36]. This vector is utilized as an input within the learning phase. In brief, by relying on training data, within the learning phase, the machine learns to perform the task from experience. Once the learning performance reaches a satisfactory point (expressed through mathematical and statistical relationships), it ends. Subsequently, the model that was developed through the training process can be used to classify, cluster, or predict.

An overview of a typical ML system is illustrated in Figure 2. With the intention of forming the derived complex raw data into a suitable state, a pre-processing effort is required. This usually includes: (a) data cleaning for removing inconsistent or missing items and noise, (b) data integration, when many data sources exist and (c) data transformation, such as normalization and discretization [37]. The extraction/selection feature aims at creating or/and identifying the most informative subset of features in which, subsequently, the learning model is going to be implemented throughout the training phase [38]. Regarding the feedback loop, which is depicted in Figure 2, it serves for adjustments pertaining to the feature extraction/selection unit as well as the pre-processing one that further improves the overall learning model's performance. During the phase of testing, previously unseen

samples are imported to the trained model, which are usually represented as feature vectors. Finally, an appropriate decision is made by the model (for example, classification or regression) in reliance of the features existing in each sample. Deep learning, a subfield of ML, utilizes an alternative architecture via shifting the process of converting raw data to features (feature engineering) to the corresponding learning system. Consequently, the feature extraction/selection unit is absent, resulting in a fully trainable system; it starts from a raw input and ends with the desired output [39,40].

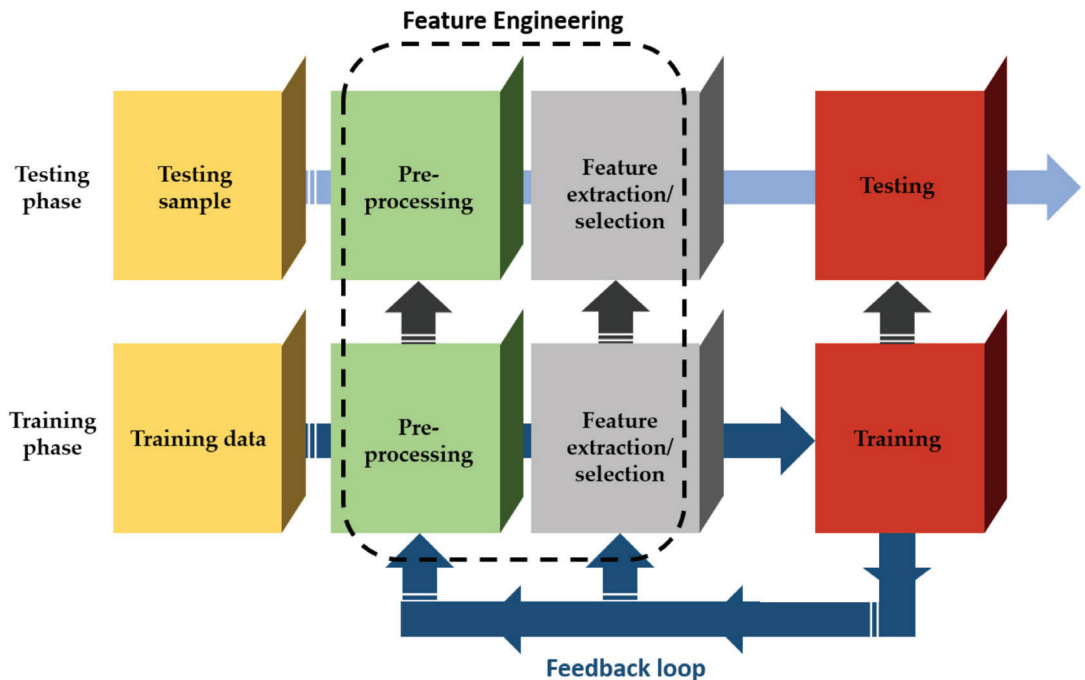


Figure 2. A graphical illustration of a typical machine learning system.

Based on the learning type, ML can be classified according to the relative literature [41,42] as:

- Supervised learning: The input and output are known and the machine tries to find the optimal way to reach an output given an input;
- Unsupervised learning: No labels are provided, leaving the learning algorithm itself to generate structure within its input;
- Semi-supervised learning: Input data constitute a mixture of labeled and non-labeled data;
- Reinforcement learning: Decisions are made towards finding out actions that can lead to the more positive outcome, while it is solely determined by trial and error method and delayed outcome.

Nowadays, ML is used in facilitating several management aspects in agriculture [12] and in a plethora of other applications, such as image recognition [43], speech recognition [44], autonomous driving [45], credit card fraud detection [46], stock market forecasting [47], fluid mechanics [48], email, spam and malware filtering [49], medical diagnosis [40], contamination detection in urban water networks [50], and activity recognition [51], to mention but a few.



## 2.2. Brief Description of the Four Generic Categories

### 2.2.1. Crop Management

The crop management category involves versatile aspects that originated from the combination of farming techniques in the direction of managing the biological, chemical and physical crop environment with the aim of reaching both quantitative and qualitative targets [52]. Using advanced approaches to manage crops, such as yield prediction, disease detection, weed detection, crop recognition, and crop quality, contributes to the increase of productivity and, consequently, the financial income. The above aspects constitute key goals of precision agriculture.

#### Yield Prediction

In general, yield prediction is one of the most important and challenging topics in modern agriculture. An accurate model can help, for instance, the farm owners to take informed management decisions on what to grow towards matching the crop to the existing market's demands [20]. However, this is not a trivial task; it consists of various steps. Yield prediction can be determined by several factors such as environment, management practices, crop genotypic and phenotypic characteristics, and their interactions. Hence, it necessitates a fundamental comprehension of the relationship between these interactive factors and yield. In turn, identifying such kinds of relationships mandates comprehensive datasets along with powerful algorithms such as ML techniques [53].

#### Disease Detection

Crop diseases constitute a major threat in agricultural production systems that deteriorate yield quality and quantity at production, storage, and transportation level. At farm level, reports on yield losses, due to plant diseases, are very common [54]. Furthermore, crop diseases pose significant risks to food security at a global scale. Timely identification of plant diseases is a key aspect for efficient management. Plant diseases may be provoked by various kinds of bacteria, fungi, pests, viruses, and other agents. Disease symptoms, namely the physical evidence of the presence of pathogens and the changes in the plants' phenotype, may consist of leaf and fruit spots, wilting and color change [55], curling of leaves, etc. Historically, disease detection was conducted by expert agronomists, by performing field scouting. However, this process is time-consuming and solely based on visual inspection. Recent technological advances have made commercially available sensing systems able to identify diseased plants before the symptoms become visible. Furthermore, in the past few years, computer vision, especially by employing deep learning, has made remarkable progress. As highlighted by Zhang et al. [56], who focused on identifying cucumber leaf diseases by utilizing deep learning, due to the complex environmental background, it is beneficial to eliminate background before model training. Moreover, accurate image classifiers for disease diagnosis need a large dataset of both healthy and diseased plant images. In reference to large-scale cultivations, such kinds of automated processes can be combined with autonomous vehicles, to timely identify phytopathological problems by implementing regular inspections. Furthermore, maps of the spatial distribution of the plant disease can be created, depicting the zones in the farm where the infection has been spread [57].

#### Weed Detection

As a result of their prolific seed production and longevity, weeds usually grow and spread invasively over large parts of the field very fast, competing with crops for the resources, including space, sunlight, nutrients, and water availability. Besides, weeds frequently arise sooner than crops without having to face natural enemies, a fact that adversely affects crop growth [18]. In order to prevent crop yield reduction, weed control is an important management task by either mechanical treatment or application of herbicides. Mechanical treatment is, in most cases, difficult to be performed and ineffective if not properly performed, making herbicide application the most widely used operation. Using

large quantities of herbicides, however, turns out to be both costly and detrimental for the environment, especially in the case of uniform application without taking into account the spatial distribution of the weeds. Remarkably, long-term herbicide use is very likely to make weeds more resistant, thus, resulting in more demanding and expensive weed control. In recent years, considerable achievements have been made pertaining to the differentiation of weeds from crops on the basis of smart agriculture. This discrimination can be accomplished by using remote or proximal sensing with sensors attached on satellites, aerial, and ground vehicles, as well as unmanned vehicles (both ground (UGV) and aerial (UAV)). The transformation of data gathered by UAVs into meaningful information is, however, still a challenging task, since both data collection and classification need painstaking effort [58]. ML algorithms coupled with imaging technologies or non-imaging spectroscopy can allow for real-time differentiation and localization of target weeds, enabling precise application of herbicides to specific zones, instead of spraying the entire fields [59] and planning of the shortest weeding path [60].

### Crop Recognition

Automatic recognition of crops has gained considerable attention in several scientific fields, such as plant taxonomy, botanical gardens, and new species discovery. Plant species can be recognized and classified via analysis of various organs, including leaves, stems, fruits, flowers, roots, and seeds [61,62]. Using leaf-based plant recognition seems to be the most common approach by examining specific leaf's characteristics like color, shape, and texture [63]. With the broader use of satellites and aerial vehicles as means of sensing crop properties, crop classification through remote sensing has become particularly popular. As in the above sub-categories, the advancement on computer software and image processing devices combined with ML has led to the automatic recognition and classification of crops.

### Crop Quality

Crop quality is very consequential for the market and, in general, is related to soil and climate conditions, cultivation practices and crop characteristics, to name a few. High quality agricultural products are typically sold at better prices, hence, offering larger earnings to farmers. For instance, as regards fruit quality, flesh firmness, soluble solids content, and skin color are among the most ordinary maturity indices utilized for harvesting [64]. The timing of harvesting greatly affects the quality characteristics of the harvested products in both high value crops (tree crops, grapes, vegetables, herbs, etc.) and arable crops. Therefore, developing decision support systems can aid farmers in taking appropriate management decisions for increased quality of production. For example, selective harvesting is a management practice that may considerably increase quality. Furthermore, crop quality is closely linked with food waste, an additional challenge that modern agriculture has to cope with, since if the crop deviates from the desired shape, color, or size, it may be thrown away. Similarly to the above sub-section, ML algorithms combined with imaging technologies can provide encouraging results.

#### 2.2.2. Water Management

The agricultural sector constitutes the main consumer of available fresh water on a global scale, as plant growth largely relies on water availability. Taking into account the rapid depletion rate of a lot of aquifers with negligible recharge, more effective water management is needed for the purpose of better conserving water in terms of accomplishing a sustainable crop production [65]. Effective water management can also lead to the improvement of water quality as well as reduction of pollution and health risks [66]. Recent research on precision agriculture offers the potential of variable rate irrigation so as to attain water savings. This can be realized by implementing irrigation at rates, which vary according to field variability on the basis of specific water requirements of separate management zones, instead of using a uniform rate in the entire field. The effectiveness and feasibility of the variable rate irrigation approach depend on agronomic

factors, including topography, soil properties, and their effect on soil water in order to accomplish both water savings and yield optimization [67]. Carefully monitoring the status of soil water, crop growth conditions, and temporal and spatial patterns in combination with weather conditions monitoring and forecasting, can help in irrigation programming and efficient management of water. Among the utilized ICTs, remote sensing can provide images with spatial and temporal variability associated with the soil moisture status and crop growth parameters for precision water management. Interestingly, water management is challenging enough in arid areas, where groundwater sources are used for irrigation, with the precipitation providing only part of the total crop evapotranspiration (ET) demands [68].

### 2.2.3. Soil Management

Soil, a heterogeneous natural resource, involves mechanisms and processes that are very complex. Precise information regarding soil on a regional scale is vital, as it contributes towards better soil management consistent with land potential and, in general, sustainable agriculture [5]. Better management of soil is also of great interest owing to issues like land degradation (loss of the biological productivity), soil-nutrient imbalance (due to fertilizers overuse), and soil erosion (as a result of vegetation overcutting, improper crop rotations rather than balanced ones, livestock overgrazing, and unsustainable fallow periods) [69]. Useful soil properties can entail texture, organic matter, and nutrients content, to mention but a few. Traditional soil assessment methods include soil sampling and laboratory analysis, which are normally expensive and take considerable time and effort. However, remote sensing and soil mapping sensors can provide low-cost and effortless solution for the study of soil spatial variability. Data fusion and handling of such heterogeneous “big data” may be important drawbacks, when traditional data analysis methods are used. ML techniques can serve as a trustworthy, low-cost solution for such a task.

### 2.2.4. Livestock Management

It is widely accepted that livestock production systems have been intensified in the context of productivity per animal. This intensification involves social concerns that can influence consumer perception of food safety, security, and sustainability, based on animal welfare and human health. In particular, monitoring both the welfare of animals and overall production is a key aspect so as to improve production systems [70]. The above fields take place in the framework of precision livestock farming, aiming at applying engineering techniques to monitor animal health in real time and recognizing warning messages, as well as improving the production at the initial stages. The role of precision livestock farming is getting more and more significant by supporting the decision-making processes of livestock owners and changing their role. It can also facilitate the products’ traceability, in addition to monitoring their quality and the living conditions of animals, as required by policy-makers [71]. Precision livestock farming relies on non-invasive sensors, such as cameras, accelerometers, gyroscopes, radio-frequency identification systems, pedometers, and optical and temperature sensors [25]. IoT sensors leverage variable physical quantities (VPQs) as a means of sensing temperature, sound, humidity, etc. For instance, IoT sensors can warn if a VPQ falls out of regular limits in real-time, giving valuable information regarding individual animals. As a result, the cost of repetitively and arduously checking each animal can be reduced [72]. In order to take advantage of the large amounts of data, ML methodologies have become an integral part of modern livestock farming. Models can be developed that have the capability of defining the manner a biological system operates, relying on causal relationships and exploiting this biological awareness towards generating predictions and suggestions.

### Animal Welfare

There is an ongoing concern for animal welfare, since the health of animals is strongly associated with product quality and, as a consequence, predominantly with the health

of consumers and, secondarily, with the improvement of economic efficiency [73]. There exist several indexes for animal welfare evaluation, including physiological stress and behavioral indicators. The most commonly used indicator is animal behavior, which can be affected by diseases, emotions, and living conditions, which have the potential to demonstrate physiological conditions [25]. Sensors, commonly used to detect behavioral changes (for example, changes in water or food consumption, reduced animal activity), include microphone systems, cameras, accelerometers, etc.

### Livestock Production

The use of sensor technology, along with advanced ML techniques, can increase livestock production efficiency. Given the impact of practices of animal management on productive elements, livestock owners are getting cautious of their asset. However, as the livestock holdings get larger, the proper consideration of every single animal is very difficult. From this perspective, the support to farmers via precision livestock farming, mentioned above, is an auspicious step for aspects associated with economic efficiency and establishment of sustainable workplaces with reduced environmental footprint [74]. Generally, several models have been used in animal production, with their intentions normally revolving around growing and feeding animals in the best way. However, the large volumes of data being involved, again, call for ML approaches.

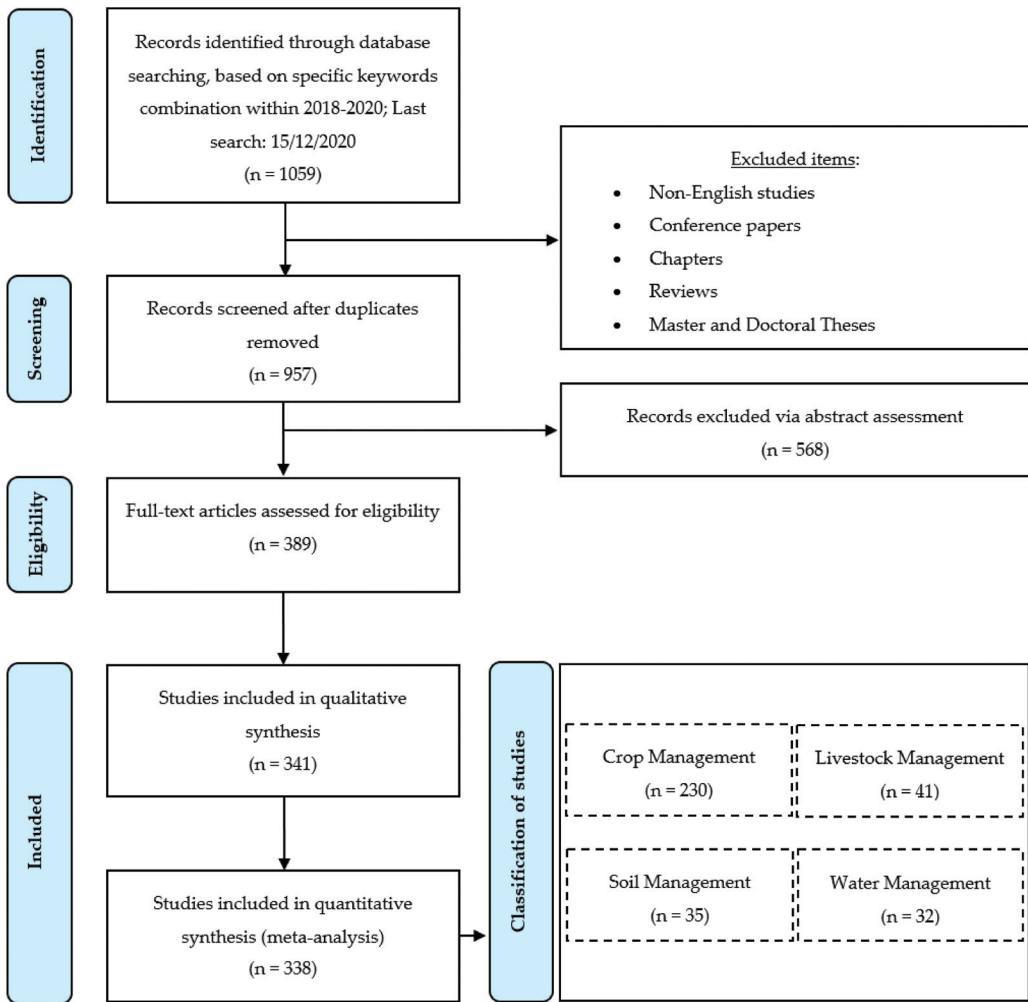
## 3. Methods

### 3.1. Screening of the Relative Literature

In order to identify the relevant studies concerning ML in respect to different aspects of management in agriculture, the search engines of Scopus, Google Scholar, ScienceDirect, PubMed, Web of Science, and MDPI were utilized. In addition, keywords' combinations of "machine learning" in conjunction with each of the following: "crop management", "water management", "soil management", and "livestock management" were used. Our intention was to filter the literature on the same framework as [12]; however, focusing solely within the period 2018–2020. Once a relevant study was being identified, the references of the paper at hand were being scanned to find studies that had not been found throughout the initial searching procedure. This process was being iterated until no relevant studies occurred. In this stage, only journal papers were considered eligible. Thus, non-English studies, conferences papers, chapters, reviews, as well as Master and Doctoral Theses were excluded. The latest search was conducted on 15 December 2020. Subsequently, the abstract of each paper was being reviewed, while, at a next stage, the full text was being read to decide its appropriateness. After a discussion between all co-authors with reference to the appropriateness of the selected papers, some of them were excluded, in the case they did not meet the two main inclusion criteria, namely: (a) the paper was published within 2018–2020 and (b) the paper referred to one of the categories and sub-categories, which were summarized in Figure 1. Finally, the papers were classified in these sub-categories. Overall, 338 journal papers were identified. The flowchart of the present review methodology is depicted in Figure 3, based on the PRISMA guidelines [75], along with information about at which stage each exclusive criterion was imposed similarly to recent systematic review studies such as [72,76–78].

### 3.2. Definition of the Performance Metrics Commonly Used in the Reviewed Studies

In this subsection, the most commonly used performance metrics of the reviewed papers are briefly described. In general, these metrics are utilized in an effort to provide a common measure to evaluate the ML algorithms. The selection of the appropriate metrics is very important, since: (a) how the algorithm's performance is measured relies on these metrics and (b) the metric itself can influence the way the significance of several characteristics is weighted.



**Figure 3.** The flowchart of the methodology of the present systematic review along with the flow of information regarding the exclusive criteria, based on PRISMA guidelines [75].

Confusion matrix constitutes one of the most intuitive metrics towards finding the correctness of a model. It is used for classification problems, where the result can be of at least two types of classes. Let us consider a simple example, by giving a label to a target variable: for example, “1” when a plant has been infected with a disease and “0” otherwise. In this simplified case, the confusion matrix (Figure 4) is a  $2 \times 2$  table having two dimensions, namely “Actual” and “Predicted”, while its dimensions have the outcome of the comparison between the predictions with the actual class label. Concerning the above simplified example, this outcome can acquire the following values:

- True Positive (TP): The plant has a disease (1) and the model classifies this case as diseased (1);
- True Negative (TN): The plant does not have a disease (0) and the model classifies this case as a healthy plant (0);
- False Positive (FP): The plant does not have a disease (0), but the model classifies this case as diseased (1);

- False Negative (FN): The plant has a disease (1), but the model classifies this case as a healthy plant (0).

		Actual	
		1	0
Predicted	1	TP	FP
	0	FN	TN

**Figure 4.** Representative illustration of a simplified confusion matrix.

As can be shown in Table 1, the aforementioned values can be implemented in order to estimate the performance metrics, typically observed in classification problems [79].

**Table 1.** Summary of the most commonly used evaluation metrics of the reviewed studies.

Name	Formula
Accuracy	$(TP + TN)/(TP + FP + FN + TN)$
Recall	$TP/(TP + FN)$
Precision	$TP/(TP + FP)$
Specificity	$TN/(TN + FP)$
F1 score	$(2 \times \text{Recall} \times \text{Precision})/(\text{Recall} + \text{Precision})$

Other common evaluation metrics were the coefficient of correlation ( $R$ ), coefficient of determination ( $R^2$ ; basically, the square of the correlation coefficient), Mean Absolute Error (MAE), Mean Absolute Percentage Error (MAPE), and Mean Squared Error (MSE), which can be given via the following relationships [80,81]:

$$R = \frac{T \cdot \sum_{t=1}^T Z(t) \cdot X(t) - \left(\sum_{t=1}^T Z(t)\right) \cdot \left(\sum_{t=1}^T X(t)\right)}{\sqrt{T \cdot \sum_{t=1}^T (Z(t))^2 - \left(\sum_{t=1}^T Z(t)\right)^2} \cdot \sqrt{T \cdot \sum_{t=1}^T (X(t))^2 - \left(\sum_{t=1}^T X(t)\right)^2}}, \quad (1)$$

$$MAE = \frac{1}{T} \cdot \sum_{t=1}^T |Z(t) - X(t)|, \quad (2)$$

$$MAPE = \frac{1}{T} \cdot \sum_{t=1}^T \left| \frac{Z(t) - X(t)}{Z(t)} \right|, \quad (3)$$

$$MSE = \frac{1}{T} \cdot \sum_{t=1}^T (Z(t) - X(t))^2, \quad (4)$$

where  $X(t)$  and  $Z(t)$  correspond to the predicted and real value, respectively,  $t$  stands for the iteration at each point, while  $T$  for the testing records number. Accordingly, low values of MAE, MAPE, and MSE values denote a small error and, hence, better performance. In contrast,  $R^2$  near 1 is desired, which demonstrates better model performance and also that the regression curve efficiently fits the data.

## 4. Results

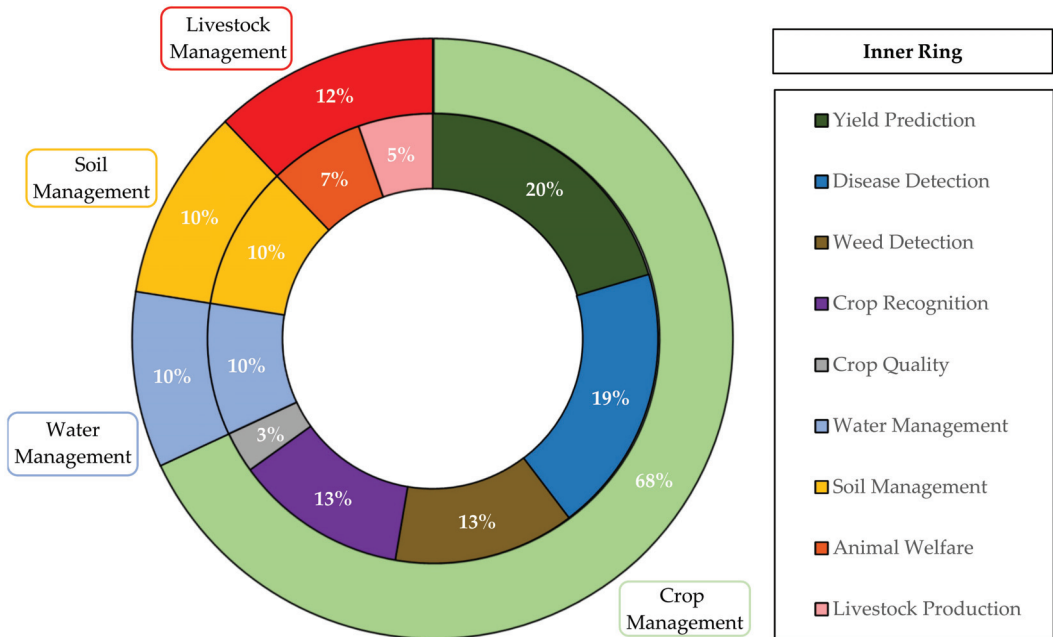
### 4.1. Preliminary Data Visualization Analysis

Graphical representation of data related to the reviewed studies, by using maps, bar or pie charts, for example, can provide an efficient approach to demonstrate and interpret the patterns of data. The data visualization analysis, as it usually refers to, can be vital in the context of analyzing large amounts of data and has gained remarkable attention in the past few years, including review studies. Indicatively, significant results can be deduced

in an effort to identify: (a) the most contributing authors and organizations, (b) the most contributing international journals (or equivalently which research fields are interested in this topic), and (c) the current trends in this field [82].

#### 4.1.1. Classification of the Studies in Terms of Application Domain

As can be seen in the flowchart of the present methodology (Figure 3), the literature survey on ML in agriculture resulted in 338 journal papers. Subsequently, these studies were classified into the four generic categories as well as into their sub-categories, as already mentioned above. Figure 5 depicts the aforementioned papers' distribution. In particular, the majority of the studies were intended for crop management (68%), while soil management (10%), water management (10%), and livestock management (12% in total; animal welfare: 7% and livestock production: 5%) had almost equal contribution in the present bibliographic survey. Focusing on crop management, the most contributing sub-categories were yield prediction (20%) and disease detection (19%). The former research field arises as a consequence of the increasing interest of farmers in taking decisions based on efficient management that can lead to the desired yield. Disease detection, on the other hand, is also very important, as diseases constitute a primary menace for food security and quality assurance. Equal percentages (13%) were observed for weed detection and crop recognition, both of which are essential in crop management at farm and agricultural policy making level. Finally, examination of crop quality was relatively scarce corresponding to 3% of all studies. This can be attributed to the complexity of monitoring and modeling the quality-related parameters.



**Figure 5.** The classification of the reviewed studies according to the field of application.

In this fashion, it should be mentioned again that all the selected journal papers are summarized in Tables A1–A9, depending on their field of application, and presented in the Appendix A. The columns of the tables correspond (from left to right) to the “Reference number” (Ref), “Input Data”, “Functionality”, “Models/Algorithms”, and “Best Output”. One additional column exists for the sub-categories belonging in crop management, namely “Crop”, whereas the corresponding column in the sub-categories pertaining to livestock



management refers to “Animal”. The present systematic review deals with a plethora of different ML models and algorithms. For the sake of brevity, the commonly used abbreviations are used instead of the entire names, which are summarized in Tables A10 and A11 (presented also in the Appendix A). The list of the aforementioned Tables, along with their content, is listed in Table 2.

**Table 2.** List of the tables appearing in the Appendix A related to: (a) the categories and sub-categories of the machine learning applications in agriculture (Tables A1–A9) and (b) the abbreviations of machine learning models and algorithms (Tables A10 and A11, respectively).

Table	Content
A1	Crop Management: Yield Prediction
A2	Crop Management: Disease Detection
A3	Crop Management: Weed Detection
A4	Crop Management: Crop Recognition
A5	Crop Management: Crop Quality
A6	Water Management
A7	Soil Management
A8	Livestock Management: Animal Welfare
A9	Livestock Management: Livestock Production
A10	Abbreviations of machine learning models
A11	Abbreviations of machine learning algorithms

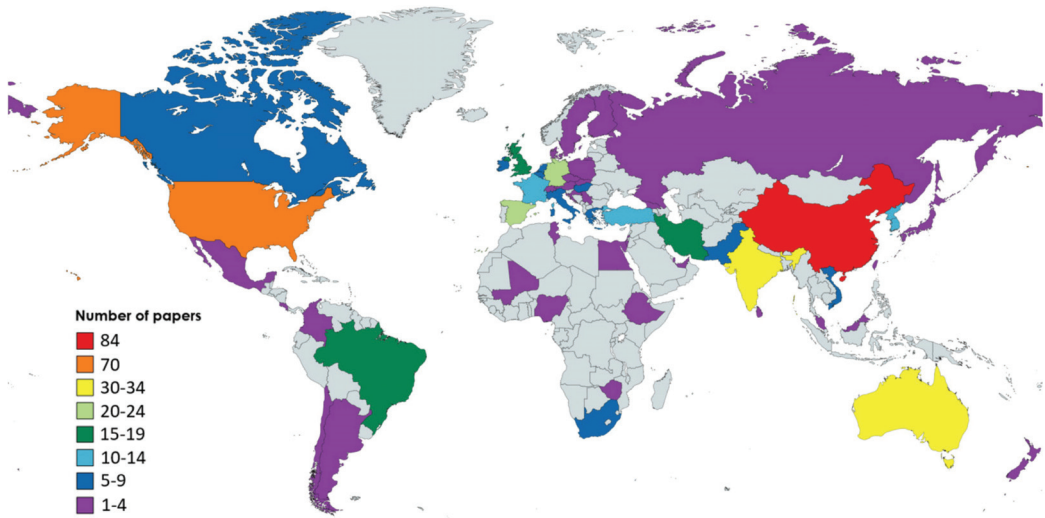
#### 4.1.2. Geographical Distribution of the Contributing Organizations

The subject of this sub-section is to find out the geographical distribution of all the contributing organizations in ML applications in agriculture. To that end, the author’s affiliation was taken into account. In case a paper included more than one author, which was the most frequent scenario, each country could contribute only once in the final map chart (Figure 6), similarly to [83,84]. As can be gleaned from Figure 6, investigating ML in agriculture is distributed worldwide, including both developed and developing economies. Remarkably, out of the 55 contributing countries, the least contribution originated from African countries (3%), whereas the major contribution came from Asian countries (55%). The latter result is attributed mainly to the considerable contribution of Chinese (24.9%) as well as Indian organizations (10.1%). USA appeared to be the second most contributing country with 20.7% percentage, while Australia (9.5%), Spain (6.8%), Germany (5.9%), Brazil, UK, and Iran (5.62%) seem to be particularly interested in ML in agriculture. It should be stressed that livestock management, which is a relatively different sub-field comparing to crop, water, and soil management, was primary examined from studies coming from Australia, USA, China, and UK, while all the papers regarding Ireland were focused on animals. Finally, another noteworthy observation is that a large number of articles were a result of international collaboration, with the synergy of China and USA standing out.

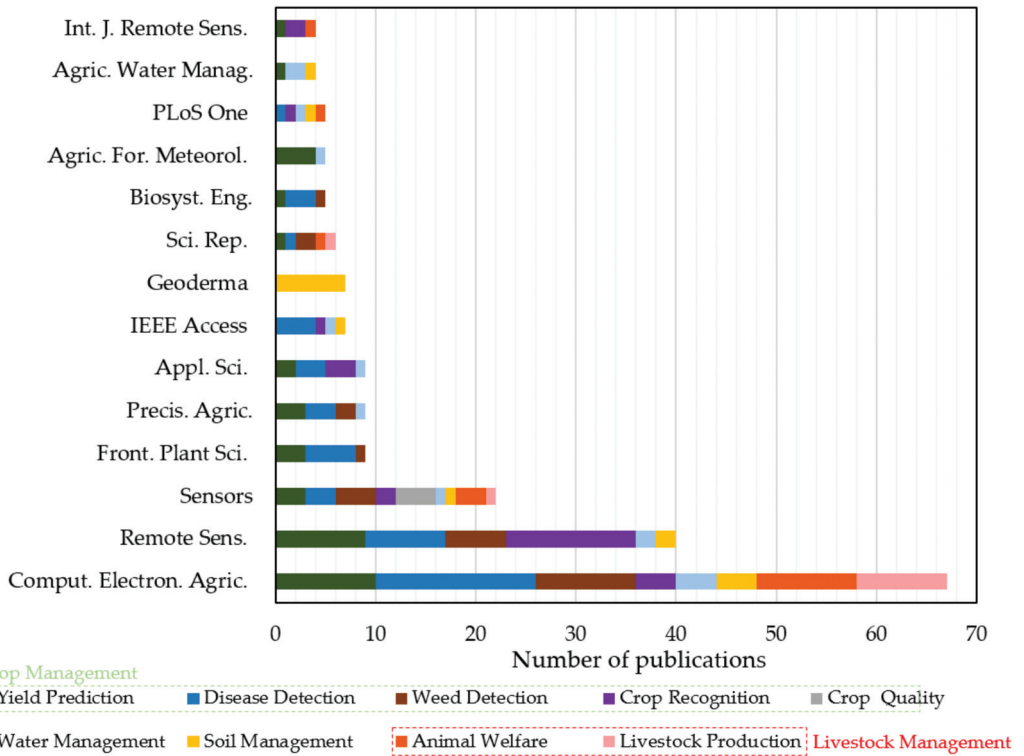
#### 4.1.3. Distribution of the Most Contributing Journal Papers

For the purpose of identifying the research areas that are mostly interested in ML in agriculture, the most frequently appeared international journal papers are depicted in Figure 7. In total, there were 129 relevant journals. However, in this bar chart, only the journals contributing with at least 4 papers are presented for brevity. As a general remark, remote sensing was of particular importance, since reliable data from satellites and UAV, for instance, constitute valuable input data for the ML algorithms. In addition, smart farming, environment, and agricultural sustainability were of central interest. Journals associated with computational techniques were also presented with considerable frequency. A typical example of such type of journals, which was presented in the majority of the studies with a percentage of 19.8%, was “*Computers and Electronics in Agriculture*”. This journal aims at providing the advances in relation to the application of computers and electronic systems for solving problems in plant and animal production.





**Figure 6.** Geographical distribution of the contribution of each country to the research field focusing on machine learning in agriculture.



**Figure 7.** Distribution of the most contributing international journals (published at least four articles) concerning applications of machine learning in agriculture.

The “*Remote Sensing*” and “*Sensors*” journals followed with approximately 11.8% and 6.5% of the total number of publications, respectively. These are cross-sectoral journals that are concentrated on applications of science and sensing technologies in various fields, including agriculture. Other journals, covering this research field, were also “*IEEE Access*” and “*International Journal of Remote Sensing*” with approximately 2.1% and 1.2% contribution, respectively. Moreover, agriculture-oriented journals were also presented in Figure 7, including “*Precision Agriculture*”, “*Frontiers in Plant Science*”, “*Agricultural and Forest Meteorology*”, and “*Agricultural Water Management*” with 1–3% percentage. These journals deal with several aspects of agriculture ranging from management strategies (so as to incorporate spatial and temporal data as a means of optimizing productivity, resource use efficiency, sustainability and profitability of agricultural production) up to crop molecular genetics and plant pathogens. An interdisciplinary journal concentrating on soil functions and processes also appeared with 2.1%, namely “*Geoderma*”, plausibly covering the soil management generic category. Finally, several journals focusing on physics and applied natural sciences, such as “*Applied Sciences*” (2.7%), “*Scientific Reports*” (1.8%), “*Biosystems Engineering*” (1.5%), and “*PLOS ONE*” (1.5%), had a notable contribution to ML studies. As a consequence, ML in agriculture concerns several disciplines and constitutes a fundamental area for developing various techniques, which can be beneficial to other fields as well.

#### 4.2. Synopsis of the Main Features Associated with the Relative Literature

##### 4.2.1. Machine Learning Models Providing the Best Results

A wide range of ML algorithms was implemented in the selected studies; their abbreviations are given in Table A11. The ML algorithms that were used by each study as well as those that provided the best output have been listed in the last two columns of Tables A1–A9. These algorithms can be classified into the eight broad families of ML models, which are summarized in Table A10. Figure 8 focuses on the best performed ML models as a means of capturing a broad picture of the current situation and demonstrating advancement similarly to [12].

As can be demonstrated in Figure 8, the most frequent ML model providing the best output was, by far, Artificial Neural Networks (ANNs), which appeared in almost half of the reviewed studies (namely, 51.8%). More specifically, ANN models provided the best results in the majority of the studies concerning all sub-categories. ANNs have been inspired by the biological neural networks that comprise human brains [85], while they allow for learning via examples from representative data describing a physical phenomenon. A distinct characteristic of ANNs is that they can develop relationships between dependent and independent variables, and thus extract useful information from representative datasets. ANN models can offer several benefits, such as their ability to handle noisy data [86], a situation that is very common in agricultural measurements. Among the most popular ANNs are the Deep Neural Networks (DNNs), which utilize multiple hidden layers between input and output layers. DNNs can be unsupervised, semi-supervised, or supervised. A usual kind of DNNs are the Convolutional Neural Networks (CNNs), whose layers, unlike common neural networks, can set up neurons in three dimensions [87]. In fact, CNNs were presented as the algorithms that provide the best output in all sub-categories, with an almost 50% of the individual percentage of ANNs. As stressed in recent studies, such as that of Yang et al. [88], CNNs are receiving more and more attention because of their efficient results when it comes to detection through images’ processing.

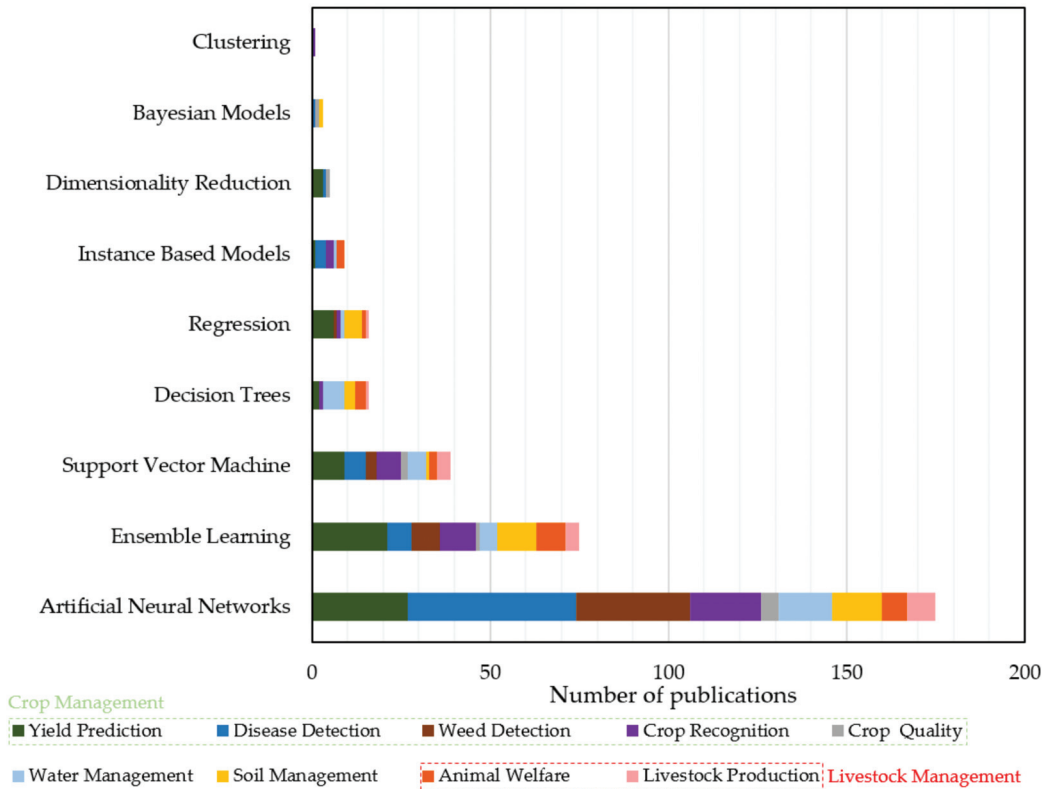


Figure 8. Machine Learning models giving the best output.

Recurrent Neural Networks (RNNs) followed, representing approximately 10% of ANNs, with Long Short-Term Memory (LSTM) standing out. They are called “recurrent” as they carry out the same process for every element, with the previous computations determining the current output, while they have a “memory” that stores information pertaining to what has been calculated so far. RNNs can face problems concerning vanishing gradients and inability to “memorize” many sequential data. Towards addressing these issues, the cell structures of LSTM can control which part of information will be either stored in long memory or discarded, resulting in optimization of the memorizing process [51]. Moreover, Multi-Layer Perceptron (MLP), Fully Convolutional Networks (FCNs), and Radial Basis Function Networks (RBFNs) appeared to have the best performance in almost 3–5% of ANNs. Finally, ML algorithms, belonging to ANNs with low frequency, were Back-Propagation Neural Networks (BPNNs), Modular Artificial Neural Networks (MANNs), Deep Belief Networks (DBNs), Adaptive-Neuro Fuzzy Inference System (ANFIS), Subtractive Clustering Fuzzy Inference System (SCFIS), Takagi-Sugeno Fuzzy Neural Networks (TS-FNN), and Feed Forward Neural Networks (FFNNs).

The second most accurate ML model was Ensemble Learning (EL), contributing to the ML models used in agricultural systems with approximately 22.2%. EL is a concise term for methods that integrate multiple inducers for the purpose of making a decision, normally in supervised ML tasks. An inducer is an algorithm, which gets as an input a number of labeled examples and creates a model that can generalize these examples. Thus, predictions can be made for a set of new unlabeled examples. The key feature of EL is that via combining various models, the errors coming from a single inducer is likely to be compensated from other inducers. Accordingly, the prediction of the overall

performance would be superior comparing to a single inducer [89]. This type of ML model was presented in all sub-categories, apart from crop quality, perhaps owing to the small number of papers belonging in this subcategory. Support Vector Machine (SVM) followed, contributing in approximately 11.5% of the studies. The strength of the SVM stems from its capability to accurately learn data patterns while showing reproducibility. Despite the fact that it can also be applied for regression applications, SVM is a commonly used methodology for classification extending across numerous data science settings [90], including agricultural research.

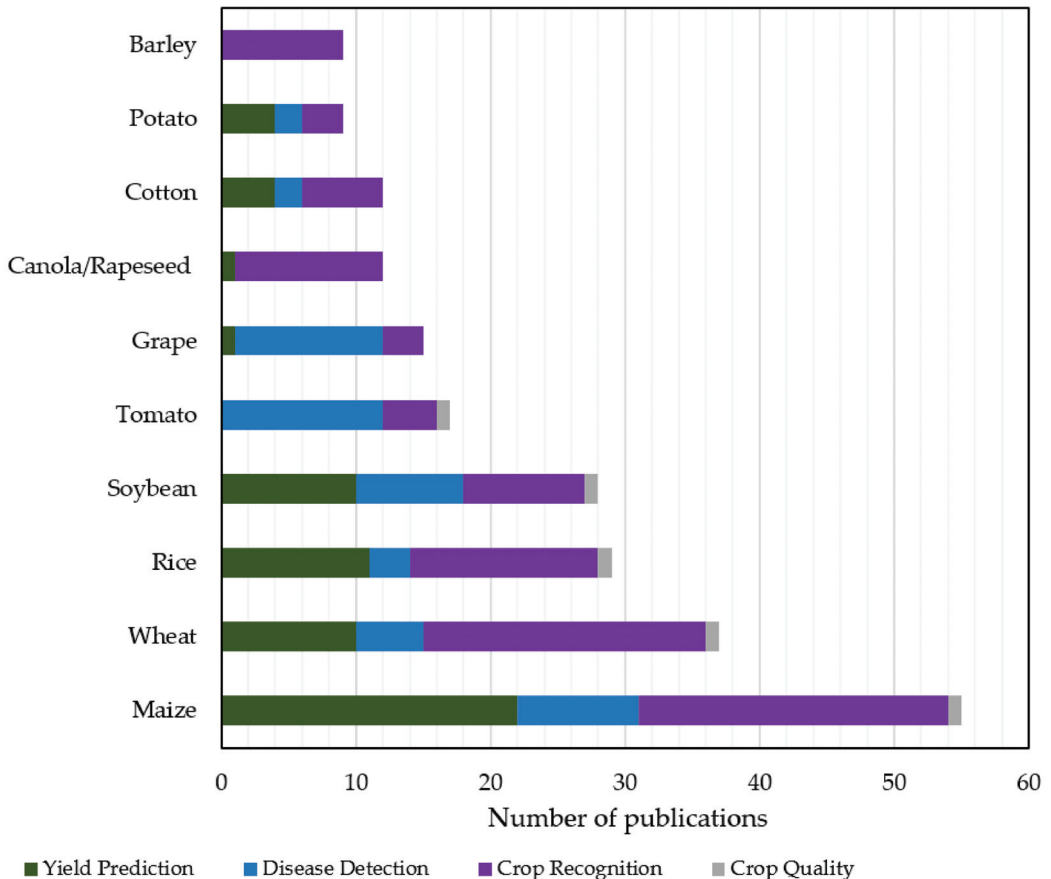
Decision Trees (DT) and Regression models came next with equal percentage, namely 4.7%. Both these ML models were presented in all generic categories. As far as DT are concerned, they are either regression or classification models structured in a tree-like architecture. Interestingly, handling missing data in DT is a well-established problem. By implementing DT, the dataset can be gradually organized into smaller subsets, whereas, in parallel, a tree graph is created. In particular, each tree's node denotes a dissimilar pairwise comparison regarding a certain feature, while each branch corresponds to the result of this comparison. As regards leaf nodes, they stand for the final decision/prediction provided after following a certain rule [91,92]. As for Regression, it is used for supervised learning models intending to model a target value on the basis of independent predictors. In particular, the output can be any number based on what it predicts. Regression is typically applied for time series modeling, prediction, and defining the relationships between the variables.

Finally, the ML models, leading to optimal performance (although with lower contribution to literature), were those of Instance Based Models (IBM) (2.7%), Dimensionality Reduction (DR) (1.5%), Bayesian Models (BM) (0.9%), and Clustering (0.3%). IBM appeared only in crop, water, and livestock management, whereas BM only in crop and soil management. On the other hand, DR and Clustering appeared as the best solution only in crop management. In brief, IBM are memory-based ML models that can learn through comparison of the new instances with examples within the training database. DR can be executed both in unsupervised and supervised learning types, while it is typically carried out in advance of classification/regression so as to prevent dimensionality effects. Concerning the case of BM, they are a family of probabilistic models whose analysis is performed within the Bayesian inference framework. BM can be implemented in both classification and regression problems and belong to the broad category of supervised learning. Finally, Clustering belongs to unsupervised ML models. It contains automatically discovering of natural grouping of data [12].

#### 4.2.2. Most Studied Crops and Animals

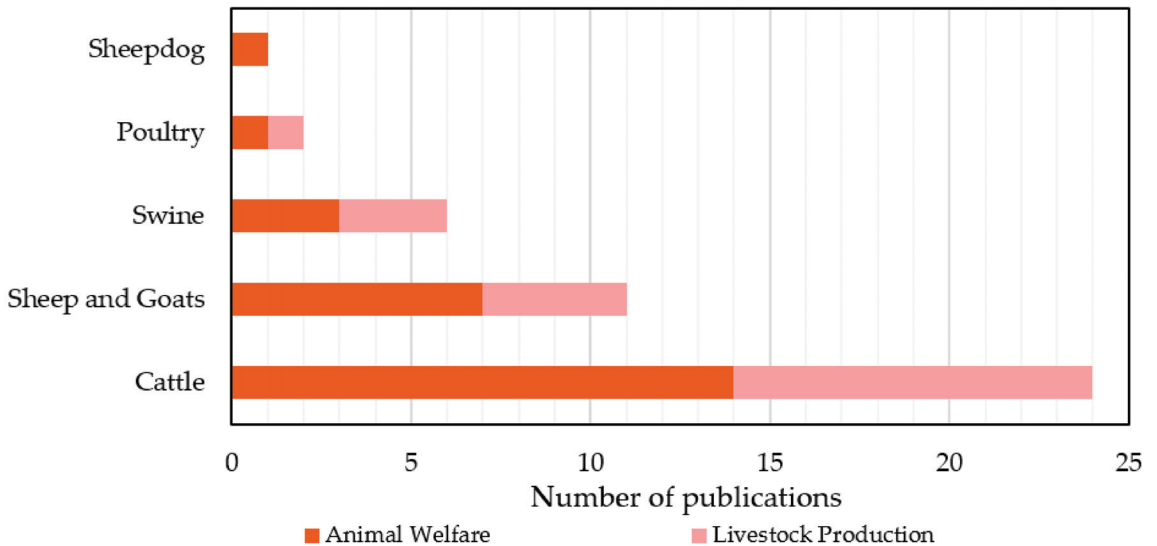
In this sub-section, the most examined crops and animals that were used in the ML models are discussed as a result of our searching within the four sub-categories of crop management similarly to [12]. These sub-categories refer to yield prediction, disease detection, crop recognition, and crop quality. Overall, approximately 80 different crop species were investigated. The 10 most utilized crops are summarized in Figure 9. Specifically, the remarkable interest on maize (also known as corn) can be attributed to the fact that it is cultivated in many parts across the globe as well as its versatile usage (for example, direct consumption by humans, animal feed, producing ethanol, and other biofuels). Wheat and rice follow, which are two of the most widely consumed cereal grains. According to the Food and Agriculture Organization (FAO) [93], the trade in wheat worldwide is more than the summation of all other crops. Concerning rice, it is the cereal grain with the third-highest production and constitutes the most consumed staple food in Asia [94]. The large contribution of Asian countries presented in Figure 6, like China and India, justifies the interest in this crop. In the same vein, soybeans, which are broadly distributed in East Asia, USA, Africa, and Australia [95], were presented in many studies. Finally, tomato, grape, canola/rapeseed (cultivated primarily for its oil-rich seed), potato, cotton, and barley complete the top 10 examined crops. All these species are widely

cultivated all over the world. Some other indicative species, which were investigated at least five times in the present reviewed studies, were also alfalfa, citrus, sunflower, pepper, pea, apple, squash, sugarcane, and rye.



**Figure 9.** The 10 most investigated crops using machine learning models; the results refer to crop management.

As far as livestock management is concerned, the examined animal species can be classified, in descending order of frequency, into the categories of cattle (58.5%), sheep and goats (26.8%), swine (14.6%), poultry (4.9%), and sheepdog (2.4%). As can be depicted in Figure 10, the last animal, which is historically utilized with regard to the raising of sheep, was investigated only in one study belonging to animal welfare, whereas all the other animals were examined in both categories of livestock management. In particular, the most investigated animal in both animal welfare and livestock production was cattle. Sheep and goats came next, which included nine studies for sheep and two studies for goats. Cattles are usually raised as livestock aimed at meat, milk, and hide used for leather. Similarly, sheep are raised for meat and milk as well as fleece. Finally, swine (often called domestic pigs) and poultry (for example, chicken, turkey, and duck), which are used mainly for their meat or eggs (poultry), had equal contribution from the two livestock sub-categories.

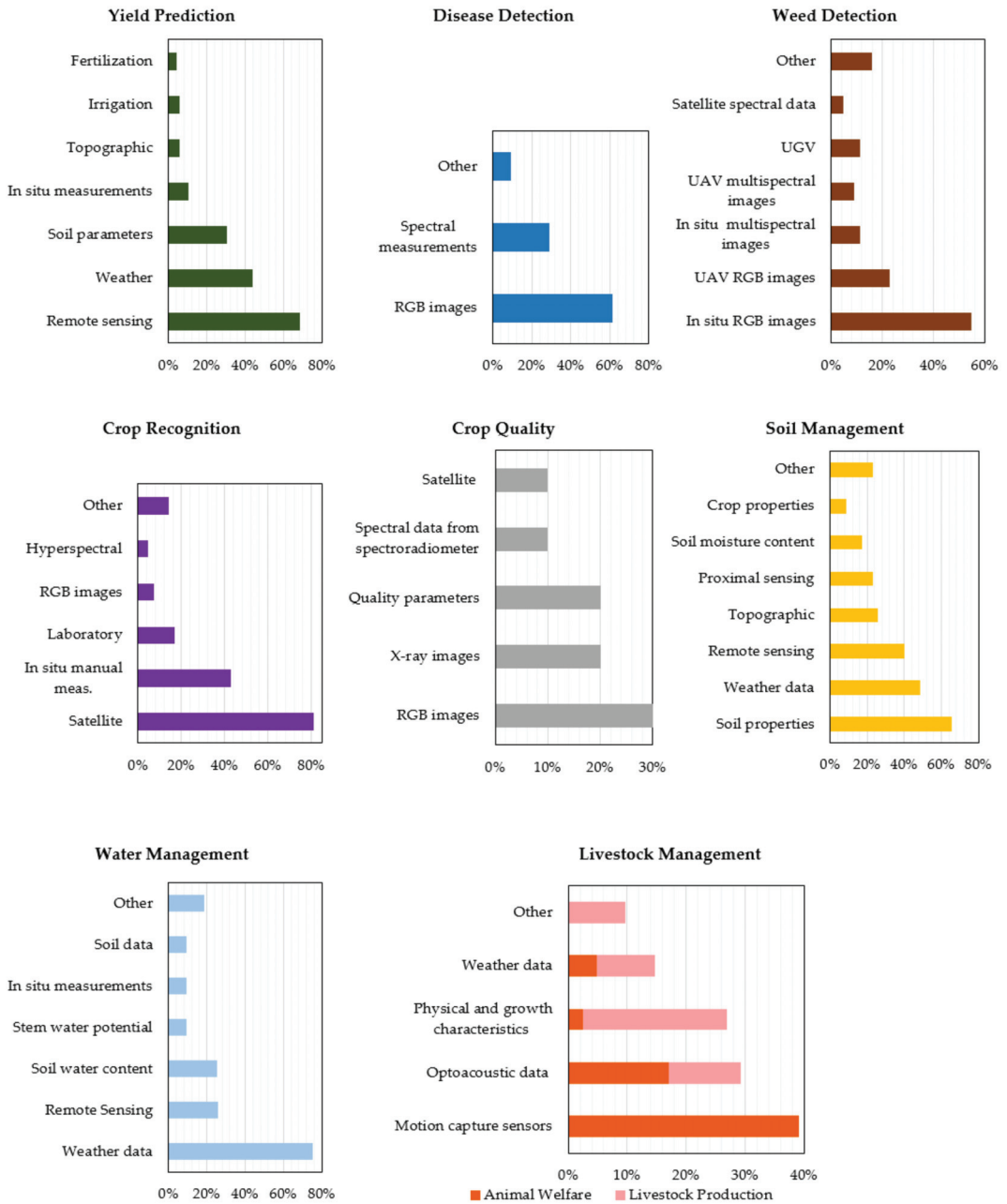


**Figure 10.** Frequency of animal species in studies concerning livestock management by using machine learning models.

#### 4.2.3. Most Studied Features and Technologies

As mentioned in the beginning of this study, modern agriculture has to incorporate large amounts of heterogeneous data, which have originated from a variety of sensors over large areas at various spatial scale and resolution. Subsequently, such data are used as input into ML algorithms for their iterative learning up until modeling of the process in the most effective way possible. Figure 11 shows the features and technologies that were used in the reviewed studies, separately for each category, for the sake of better comprehending the results of the analysis.

Data coming from remote sensing were the most common in the yield prediction sub-category. Remote sensing, in turn, was primarily based on data derived from satellites (40.6% of the total studies published in this sub-category) and, secondarily, from UAVs (23.2% of the total studies published in this sub-category). A remarkable observation is the rapid increase of the usage of UAVs versus satellites from the year 2018 towards 2020, as UAVs seem to be a reliable alternative that can give faster and cheaper results, usually in higher resolution and independent of the weather conditions. Therefore, UAVs allow for discriminating details of localized circumscribed regions that the satellites' lowest resolution may miss, especially under cloudy conditions. This explosion in the use of UAV systems in agriculture is a result of the developing market of drones and sensing solutions attached to them, rendering them economically affordable. In addition, the establishment of formal regulations for UAV operations and the simplification and automatization of the operational and analysis processes had a significant contribution on the increasing popularity of these systems. Data pertaining to the weather conditions of the investigated area were also of great importance as well as soil parameters of the farm at hand. An additional way of getting the data was via in situ manual measurements, involving measurements such as crop height, plant growth, and crop maturity. Finally, data concerning topographic, irrigation, and fertilization aspects were presented with approximately equal frequency.

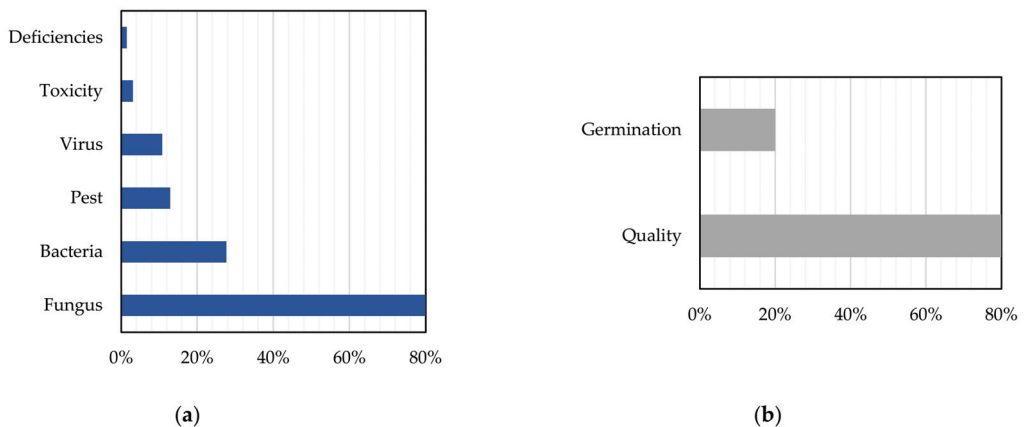


**Figure 11.** Distribution of the most usual features implemented as input data in the machine learning algorithms for each category/sub-category.

As far as disease detection is concerned, Red-Green-Blue (RGB) images appear to be the most usual input data for the ML algorithms (in 62% of the publications). Normally, deep learning methods like CNNs are implemented with the intention of training a classifier to discriminate images depicting healthy leaves, for example, from infected ones. CNNs



use some particular operations to transform the RGB images so that the desired features are enhanced. Subsequently, higher weights are given to the images having the most suitable features. This characteristic constitutes a significant advantage of CNNs as compared to other ML algorithms, when it comes to image classification [79]. The second most common input data came from either multispectral or hyperspectral measurements originated from spectroradiometers, UAVs, and satellites. Concerning the investigated diseases, fungal diseases were the most common ones with diseases from bacteria following, as is illustrated in Figure 12a. This kind of disease can cause major problems in agriculture with detrimental economic consequences [96]. Other examined origins of crop diseases were, in descending order of frequency, pests, viruses, toxicity, and deficiencies.



**Figure 12.** Distribution of the most usual output features of the machine learning algorithms regarding: (a) Disease detection and (b) Crop quality.

Images were also the most used input data for weed detection purposes. These images were RGB images that originated mainly from in situ measurements as well as from UGVs and UAVs and, secondarily, multispectral images from the aforementioned sources. Finally, other parameters that were observed, although with lower frequency, were satellite multispectral images, mainly due to the considerably low resolution they provide, video recordings, and hyperspectral and greyscale images. Concerning crop recognition, the majority of the studies used data coming mostly from satellites and, secondarily, from in situ manual measurements. This is attributed to the fact that most of the studies in this category concern crop classification, a sector where satellite imaging is the most widely used data source owing to its potential for analysis of time series of extremely large surfaces of cultivated land. Laboratory measurements followed, while RGB and greyscale images as well as hyperspectral and multispectral measurements from UAVs were observed with lower incidence.

The input data pertaining to crop quality consisted mainly of RGB images, while X-ray images were also utilized (for seed germination monitoring). Additionally, quality parameters, such as color, mass, and flesh firmness, were used. There were also two studies using spectral data either from satellites or spectroradiometers. In general, the studies belonging in this sub-category dealt with either crop quality (80%) or seed germination potential (20%) (Figure 12b). The latter refers to the seed quality assessment that is essential for the seed production industry. Two studies were found about germination that both combined X-ray images analysis and ML.

Concerning soil management, various soil properties were taken into account in 65.7% of the studies. These properties included salinity, organic matter content, and electrical conductivity of soil and soil organic carbon. Usage of weather data was also



very common (in 48.6% of the studies), while topographic and data pertaining to the soil moisture content (namely the ratio of the water mass over the dry soil) and crop properties were presented with lower frequency. Additionally, remote sensing, including satellite and UAV multispectral and hyperspectral data, as well as proximal sensing, to a lesser extent, were very frequent choices (in 40% of the studies). Finally, properties associated with soil temperature, land type, land cover, root microbial dynamics, and groundwater salinity make up the rest of data, which are labeled as “other” in the corresponding graph of Figure 11.

In water management, weather data stood for the most common input data (appeared in the 75% of the studies), with ET being used in the vast majority of them. In many cases, accurate estimation of ET (the summation of the transpiration via the plant canopy and the evaporation from plant, soil, and open water surface) is among the most central elements of hydrologic cycle for optimal management of water resources [97]. Data from remote sensors and measurements of soil water content were also broadly used in this category. Soil water availability has a central impact on crops’ root growth by affecting soil aeration and nutrient availability [98]. Stem water potential, appearing in three studies, is actually a measure of water tension within the xylem of the plant, therefore functioning as an indicator of the crop’s water status. Furthermore, in situ measurements, soil, and other parameters related to cumulative water infiltration, soil and water quality, field topography, and crop yield were also used, as can be seen in Figure 11.

Finally, in what concerns livestock management, motion capture sensors, including accelerometers, gyroscopes, and pedometers, were the most common devices giving information about the daily activities of animals. This kind of sensors was used solely in the studies investigating animal welfare. Images, audio, and video recordings came next, however, appearing in both animal welfare and livestock production sub-categories. Physical and growth characteristics followed, with slightly less incidence, by appearing mainly in livestock production sub-category. These characteristics included the animal’s weight, gender, age, metabolites, biometric traits, backfat and muscle thickness, and heat stress. The final characteristic may have detrimental consequences in livestock health and product quality [99], while through the measurement of backfat and muscle thickness, estimations of the carcass lean yield can be made [100].

## 5. Discussion and Main Conclusions

The present systematic review study deals with ML in agriculture, an ever-increasing topic worldwide. To that end, a comprehensive analysis of the present status was conducted concerning the four generic categories that had been identified in the previous review by Liakos et al. [12]. These categories pertain to crop, water, soil, and livestock management. Thus, by reviewing the relative literature of the last three years (2018–2020), several aspects were analyzed on the basis of an integrated approach. In summary, the following main conclusions can be drawn:

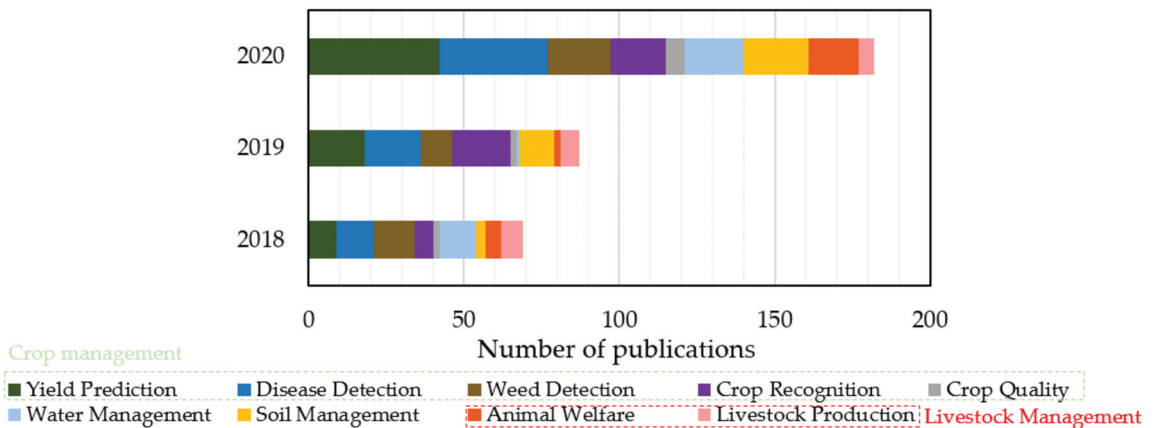
- The majority of the journal papers focused on crop management, whereas the other three generic categories contributed almost with equal percentage. Considering the review paper of [12] as a reference study, it can be deduced that the above picture remains, more or less, the same, with the only difference being the decrease of the percentage of the articles regarding livestock from 19% to 12% in favor of those referring to crop management. Nonetheless, this reveals just one side of the coin. Taking into account the tremendous increase in the number of relative papers published within the last three years (in particular, 40 articles were identified in [12] comparing to the 338 of the present literature survey), approximately 400% more publications were found on livestock management. Another important finding was the increasing research interest on crop recognition.
- Several ML algorithms have been developed for the purpose of handling the heterogeneous data coming from agricultural fields. These algorithms can be classified in families of ML models. Similar to [12], the most efficient ML models proved to be

ANNs. Nevertheless, in contrast to [12], the interest also been shifted towards EL, which can combine the predictions that originated from more than one model. SVM completes the group with the three most accurate ML models in agriculture, due to some advantages, such as its high performance when it works with image data [101].

- As far as the most investigated crops are concerned, mainly maize and, secondarily, wheat, rice, and soybean were widely studied by using ML. In livestock management, cattle along with sheep and goats stood out constituting almost 85% of the studies. Comparing to [12], more species have been included, while wheat and rice as well as cattle, remain important specimens for ML applications.
- A very important result of the present review study was the demonstration of the input data used in the ML algorithms and the corresponding sensors. RGB images constituted the most common choice, thus, justifying the broad usage of CNNs due to their ability to handle this type of data more efficiently. Moreover, a wide range of parameters pertaining to weather as well as soil, water, and crop quality was used. The most common means of acquiring measurements for ML applications was remote sensing, including imaging from satellites, UAVs and UGVs, while in situ and laboratory measurements were also used. As highlighted above, UAVs are constantly gaining ground against satellites mainly because of their flexibility and ability to provide images with high resolution under any weather conditions. Satellites, on the other hand, can supply time-series over large areas [102]. Finally, animal welfare-related studies used mainly devices such as accelerometers for activity recognition, whereas those ones referring to livestock production utilized primary physical and growth characteristics of the animal.

As can be inferred from the geographical distribution (illustrated in Figure 6) in tandem with the broad spectrum of research fields, ML applications for facilitating various aspects of management in the agricultural sector is an important issue on an international scale. As a matter of fact, its versatile nature favors convergence research. Convergence research is a relatively recently introduced approach that is based on shared knowledge between different research fields and can have a positive impact on the society. This can refer to several aspects, including improvement of the environmental footprint and assuring human's health. Towards this direction, ML in agriculture has a considerable potential to create value.

Another noteworthy finding of the present analysis is the capturing of the increasing interest on topics concerning ML analyses in agricultural applications. More specifically, as can be shown in Figure 13, an approximately 26% increase was presented in the total number of the relevant studies, if a comparison is made between 2018 and 2019. The next year (i.e., 2020), the corresponding increase jumped to 109% against 2019 findings; thus, resulting in an overall 164% rise comparing with 2018. The accelerating rate of the research interest on ML in agriculture is a consequence of various factors, following the considerable advancements of ICT systems in agriculture. Moreover, there exists a vital need for increasing the efficiency of agricultural practices while reducing the environmental burden. This calls for both reliable measurements and handling of large volumes of data as a means of providing a wide overview of the processes taking place in agriculture. The currently observed technological outbreak has a great potential to strengthen agriculture in the direction of enhancing food security and responding to the rising consumers' demands.



**Figure 13.** Temporal distribution of the reviewed studies focusing on machine learning in agriculture, which were published within 2018–2020.

In a nutshell, ICT in combination with ML, seem to constitute one of our best hopes to meet the emerging challenges. Taking into account the rate of today’s data accumulation along with the advancement of various technologies, farms will certainly need to advance their management practices by adopting Decision Support Systems (DSSs) tailored to the needs of each cultivation system. These DSSs use algorithms, which have the ability to work on a wider set of cases by considering a vast amount of data and parameters that the farmers would be impossible to handle. However, the majority of ICT necessitates upfront costs to be paid, namely the high infrastructure investment costs that frequently prevent farmers from adopting these technologies. This is going to be a pressing issue, mainly in developing economies, where agriculture is an essential economic factor. Nevertheless, having a tangible impact is a long-haul game. A different mentality is required by all stakeholders so as to learn new skills, be aware of the potential profits of handling big data, and assert sufficient funding. Overall, considering the constantly increasing recognition of the value of artificial intelligence in agriculture, ML will definitely become a behind-the-scenes enabler for the establishment of a sustainable and more productive agriculture. It is anticipated that the present systematic effort is going to constitute a beneficial guide to researchers, manufacturers, engineers, ICT system developers, policymakers, and farmers and, consequently, contribute towards a more systematic research on ML in agriculture.

**Author Contributions:** Conceptualization, D.B.; methodology, L.B., G.D., R.B., D.K. and A.C.T.; investigation, L.B. and G.D.; writing—original draft preparation, L.B. and A.C.T.; writing—review and editing, L.B., G.D., D.K., A.C.T., R.B. and D.B.; visualization, L.B.; supervision, D.B. All authors have read and agreed to the published version of the manuscript.

**Funding:** This work has been partly supported by the Project “BioCircular: Bio-production System for Circular Precision Farming” (project code: T1EDK- 03987) co-financed by the European Union and the Greek national funds through the Operational Programme Competitiveness, Entrepreneurship and Innovation, under the call RESEARCH—CREATE—INNOVATE.

**Conflicts of Interest:** The authors declare no conflict of interest.

## Appendix A

In this section, the reviewed articles are summarized within the corresponding Tables as described in Table 2.

Table A1. Crop Management: Yield Prediction.

Ref	Crop	Input Data	Functionality	Models/Algorithms	Best Output
[103]	Coffee	Weather data, soil fertility	Prediction of Robusta coffee yield by using various soil fertility properties	ELM, RF, MLR	ELM: Model with SOM, K, S: RMSE = 496.35 kg ha <sup>-1</sup> , MAE = 326.40 kg ha <sup>-1</sup>
[104]	Maize	Weather and satellite spectral data	Silage maize yield estimation via Landsat 8 OLI data	BRT, RFR, SVR, GPR	BRT: R = 0.89, RMSE = 4.66
[105]	Maize	Soil properties, topographic, multispectral aerial images	Prediction of corn yield and soil properties (SOM, CEC, Mg, K, pH)	RF, ANN, SVM, GBM, Cubist	(1) Corn yield: RF (R <sup>2</sup> = 0.53); (2) SOM: NN (R <sup>2</sup> = 0.64); (3) CEC: NN (R <sup>2</sup> = 0.67); (4) K: SVM (R <sup>2</sup> = 0.21); (5) Mg: SVM (R <sup>2</sup> = 0.22); (6) pH: GBM (R <sup>2</sup> = 0.15)
[106]	Cotton	Satellite spectral data	Cotton yield estimation	ANN	(1) 2013: Yield vs. CI (R = -0.2–0.60), best ANN (R = 0.68); (2) 2014: Yield vs. CI (R = -0.79–0.84), best ANN (R = 0.86)
[107]	Apple	RGB images	Detection and estimation of the number of apples in canopy images	MLR	Yield relative error = -10–13%, Yield relative error STD = 28% of average tree yield
[108]	Maize	Crop data—CERES model, satellite spectral data	Forecasting spring maize yield from Landsat-8 images	SVM, RF, DT, LDA, KNN	RS: SVM: Acc = 97%, RMSE = 397 kg ha <sup>-1</sup>
[109]	Maize, soybean	Satellite spectral data	Estimation of corn and soybean yield via Landsat and SPOT images	MLR, ANN	R <sup>2</sup> values: (1) Maize: ANN: 0.92, (2) Soybean: ANN: 0.90
[110]	Turmeric	Soil fertility, weather data	Forecasting oil yield produced from turmeric rhizomes	ANN	Multilayer-feed-forward NN with 12 nodes: R <sup>2</sup> = 0.88
[111]	Sunflower	Plant height, SPAD	Prediction of sunflower seed yield	PLSR, ANN	(1) ANN: RMSE = 0.66 tha <sup>-1</sup> , R <sup>2</sup> = 0.86; (2) PLSR: RMSE = 0.93 tha <sup>-1</sup> , R <sup>2</sup> = 0.69
[112]	Pistachio	Irrigation, soil characteristics	Estimation of pistachio yield in orchards	MLR, ANN	Acc values: ANN: 90%, MLR: 28%
[113]	Rice	Weather data, irrigation, planting area, fertilization	Evaluation of feature subsets for prediction of paddy crop yield	ANN, SVR, KNN, RF	Forward Feature Selection: RF: RMSE = 0.085, MAE = 0.055, R = 0.93
[114]	Potato	Satellite spectral data	Prediction of potato yield via Sentinel 2 satellite data	MLR, RQL, LB, SVM, RF, MARS, KNN, ANN	(1) Reduced dataset: LB: MAE = 8.95%, R <sup>2</sup> = 0.89; (2) No feature selection: SVM: MAE = 8.64%, R <sup>2</sup> = 0.93; (3) 1–2 months prior to harvest: RF: MAE = 8.71%, R <sup>2</sup> = 0.89
[115]	Wheat	Satellite spectral data	Prediction of wheat yield	SVM, RF, ANN	R <sup>2</sup> values: (1) SVM: 0.74; (2) RF: 0.68; (3) ANN: 0.68
[116]	Soybean, Maize	Hydrological, weather and satellite spectral data	Prediction of soybean and corn yields	DNN, RF, SVM, MARS, ERT, ANN	DNN (1) Corn: 21–33% more accurate (2) Soybean: 17–22% more accurate
[117]	Wheat, barley	Multispectral images from UAV	Prediction of barley and wheat yields	CNN	(1) Early growth phase (<25%): MAE = 484.3 kg ha <sup>-1</sup> , MAPE = 8.8%; (2) Later growth phase (>25%): MAE = 484.3 kg ha <sup>-1</sup> , MAPE = 8.8%
[118]	Strawberry	Multispectral images from UAV	Detection and counting of strawberry species for yield prediction	CNN	Faster RCNN: (1) Detection: MaP = 0.83 (at 2 m), MaP = 0.72 (at 3 m); (2) Count: Acc = 84.1%, Average occlusion = 13.5%
[119]	Rice	Weather data, irrigation, planting area, fertilization	Prediction of paddy fields yield	ANN, MLR, SVR, KNN, RF	ANN-MLR: R = 0.99, RMSE = 0.051, MAE = 0.041
[120]	Soybean	Weather and satellite spectral data	Prediction of soybean yield in 15 states of USA	CNN, LSTM	2011–2015: End-of-season RMSE = 329.53 kg ha <sup>-1</sup> , R <sup>2</sup> = 0.78
[121]	Maize	Satellite spectral data	Prediction of maize yield	MLR, RF, SVM	RF: (1) yield: R <sup>2</sup> = 0.6; (2) GNDVI: R <sup>2</sup> = 0.48; Best monitoring period: Crop age = 105–135 days
[122]	Mango	Multispectral data from UGV	Estimation of mango maturity level by simulating imaging devices of optical filters	SVM	Estimation of dry matter by using a 4-sensor device with 4 filters: R <sup>2</sup> = 0.69
[123]	Rapeseed, barley, wheat	EC, STI, gamma radiometrics and weather data	Forecasting crop yield	RF	RMSE = 0.36–0.42 t/ha, Lin's CCC = 0.89–0.92
[53]	Maize	Genetic information of hybrids, soil and weather data	Prediction of maize yield	DNN	(1) With predicted weather data: RMSE = 12% of average yield, 50% of STD; (2) Using ideal weather data: RMSE = 11% of average yield, 46% of STD
[124]	Rice	RGB leaf images	Prediction of nutrient deficiencies (P, N, K) in image leaves from paddy fields	ANN	Acc = 77%

Table A1. Cont.

Ref	Crop	Input Data	Functionality	Models/Algorithms	Best Output
[125]	Rice	RGB and multispectral images from UAV	Estimation of rice grain yield	CNN	R <sup>2</sup> values: (1) Only RGB images: 0.424–0.499; (2) RGB and multispectral images: 0.464–0.511
[126]	Maize	Satellite spectral data, crop modeling data	Estimation of end-of-season and early maize yield	RF	(1) Early maize yield: R <sup>2</sup> = 0.53, RMSE = 271 kg ha <sup>-1</sup> , MAE = 202 kg ha <sup>-1</sup> ; (2) End-of-season maize yield: R <sup>2</sup> = 0.59, RMSE = 258 kg ha <sup>-1</sup> , MAE = 201 kg ha <sup>-1</sup>
[127]	Potato	Soil parameters and tillage treatments	Forecasting of organic potato yield	ANN, MLR	(1) MLR: R <sup>2</sup> = 0.894, RMSE = 0.431, MAE = 0.327; (2) ANN: R <sup>2</sup> = 0.95, RMSE = 0.431, MAE = 0.327
[128]	Maize	Simulations data, weather and soil data	Prediction of crop yield based on gridded crop meta-models	RF, XGBoost	(1) XGBoost: (a) growing season climate: R <sup>2</sup> = 0.91, MAE = 0.74, (b) annual climate: R <sup>2</sup> = 0.92, MAE = 0.66; (2) RF: (a) growing season climate: R <sup>2</sup> = 0.94, MAE = 0.71, (b) annual climate: R <sup>2</sup> = 0.95, MAE = 0.58
[129]	Soybean	Satellite spectral data, precipitation and daytime	Forecasting soybean yield	RF, multivariate OLS, LSTM	(1) DOY 16: OLS: MAE = 0.42 Mg ha <sup>-1</sup> ; (2) DOY 32: LSTM: MAE = 0.42 Mg ha <sup>-1</sup> ; (3) DOY 48: LSTM: MAE = 0.25 Mg ha <sup>-1</sup> ; (4) DOY 64: LSTM: MAE = 0.24 Mg ha <sup>-1</sup>
[130]	Potato	Topography, soil EC, soil chemistry and multispectral data from ground based sensors	Potato tuber yield prediction via ground based proximal sensing	LR, KNN, EN, SVR	Best models: (1) SVR: 2017: (a) New Brunswick: RMSE = 5.97 tha <sup>-1</sup> , (b) Prince Edward Island: RMSE = 6.60 tha <sup>-1</sup> ; (2) 2018: (a) New Brunswick: RMSE = 4.62 tha <sup>-1</sup> , (b) Prince Edward Island: RMSE = 6.17 tha <sup>-1</sup>
[131]	Rice, maize, millet, ragi	Weather data	Prediction of various kharif crops yield	MANN, SVR	Overall RMSE = 79.85%
[132]	Wheat	Soil, weather, and satellite spectral data	Winter wheat prediction from four mid-season timings	RF, GPR, SVM, ANN, KNN, DT, BT	(1) RF: R <sup>2</sup> = 0.81, RMSE = 910–920 kg ha <sup>-1</sup> , MAE = 740 kg ha <sup>-1</sup> ; (2) GPR: R <sup>2</sup> = 0.78, RMSE = 920–960 kg ha <sup>-1</sup> , MAE = 735–767 kg ha <sup>-1</sup>
[133]	Maize	Data derived from various cropping systems	Maize grain yield prediction from CA and conventional cropping systems	LDA, MLR, GNB, KNN, CART, SVM	Best results: LDA: Acc = 0.61, Precision = 0.59, Recall = 0.59, F1-score = 0.59
[134]	Soybean	Multispectral, RGB and thermal images from UAV	Estimation of soybean grain yield	DNN, PLSR, RFR, SVR	DNN: (1) Intermediate-level feature fusion: R <sup>2</sup> = 0.720, Relative RMSE = 15.9%; (2) input-level feature fusion: R <sup>2</sup> = 0.691, Relative RMSE = 16.8% CNN-RNN: RMSE values (bushels/acre): (1) Soybean: 2016: 4.15, 2017: 4.32, 2018: 4.91; (2) Maize: 2016: 16.48, 2017: 15.74, 2018: 17.64
[135]	Soybean, Maize	Weather data and soil data	Soybean and corn yield forecasting	CNN-RNN, RF, LASSO, DNN	(1) Only NDVI: RMSE = 1.2 kg/vine, Relative error = 28.7%; (2) Both NDVI ANF VFC: RMSE = 0.9 kg/vine, Relative error = 21.8%
[136]	Grape	Multispectral images from UAV	Estimation of vineyard final yield	MLP	(1) HD NDVI: RF: RMSE = 11.2%, MAE = 9.1%, SVM: RMSE = 8.7%, MAE = 5.6%; (2) HDM NDVI: RF: RMSE = 11.3%, MAE = 9.2%, SVM: RMSE = 8.7%, MAE = 5.6%
[137]	Rice	Satellite spectral data	Prediction of rice crop yield	RF, SVM	Average value for 9 fields in the USA: RMSE = 0.7
[138]	Maize	Fertilization, planting density, soil EC, satellite spectral data	Prediction of corn yield response to nitrogen and seed rate management	CNN	RMSE = 0.31 tha <sup>-1</sup> , MAE = 0.39 tha <sup>-1</sup> , MAPE = 5.18%
[139]	Sugarcane	Monthly precipitation data	Forecasting of sugarcane yield	RNN	SVR: RMSE = 0.55 tha <sup>-1</sup> , R <sup>2</sup> = 0.77
[140]	Wheat	Satellite spectral and weather data	Estimation of wheat yield	SVR, RF, Cubist, XGBoost, MLP, GPR, KNN, MARS	ANN: (1) Corn: RMSE = 4.83–8.41, R = 0.91–0.99; (2) Soybean: RMSE = 5.18–7.77, R = 0.79–0.99
[141]	Maize, Soybean	Satellite spectral data	Forecasting of maize and soybean yield	MLR, ANN	(1) Drought cases: R = 0.954; (2) Heatwave cases: R = 0.887–0.914
[142]	Maize	Satellite spectral and weather data	Prediction of maize yield under severe weather conditions	DNN	R = 0.78–1.00, MSE = 0.040–0.204
[143]	Rice	Weather data	Paddy yield prediction	ANN	WEL: RMSE = 1.138 kg ha <sup>-1</sup>
[144]	Maize	Plant population, soil and weather data	Maize yield forecasting in 3 US states of Corn Belt	XGBoost, RF, LASSO, GBM, WEL	R <sup>2</sup> = 0.76, RMSE = 0.038 tha <sup>-1</sup>
[145]	Maize	Satellite spectral and weather data	Estimation of maize yield	DLS	

Table A1. Cont.

Ref	Crop	Input Data	Functionality	Models/Algorithms	Best Output
[146]	Various crops	Satellite spectral and weather data	Prediction of autumn crops yield	SVR, RF, DNN	RMSE values ( $\times 10^4$ tons) SVR = 501.98; RF = 477.45; DNN = 253.74
[147]	Wheat	Multispectral images from UAV	Growth monitoring and yield prediction of wheat in key growth stages	LR, SMLR, PLSR, ANN, RF	Best results: RF: $R^2 = 0.78$ , RMSE = 0.103
[148]	Cotton	Topographic, weather, soil and satellite spectral data	Within-field yield prediction	RF, GB	Best results: RF: RMSE = 0.20 $\text{tha}^{-1}$ , CCC = 0.50–0.66
[149]	Cotton	Satellite spectral data	Yield prediction	RF, CART	RF: RMSE = 62.77 $\text{Kg ha}^{-1}$ , MAPE = 0.32
[150]	Rice	Multispectral images from UAV	Prediction of rice grain yield	RF	RMSE = 62.77 $\text{Kg ha}^{-1}$ , MAPE = 0.32
[151]	Soybean	Multispectral images from UAV	Yield estimation in soybean	MLP	$R = 0.92$
[152]	Potato	Weather, irrigation, and satellite spectral data	Forecasting of yield in potato fields at municipal level	RF, SVM, GLM	(1) winter cycle: $R^2 = 0.757$ , %RMSE = 18.9; (2) summer cycle: $R^2 = 0.858$ , %RMSE = 14.9
[153]	Sugarcane	Satellite spectral data	Prediction of sugarcane yield	MLR	$R^2 = 0.92$ –0.99
[154]	Cotton	Multispectral images from UAV	Estimation of cotton yield	ANN, SVR, RFR	ANN: $R^2 = 0.9$
[155]	Rice	Weather and soil data	Prediction of rice yields from Blockchain nodes	RF, MLR, GBR, DTR	RF: $R^2 = 0.941$ , %RMSE = 0.62, MAE = 0.72
[156]	Maize	Multispectral images from UAV	Prediction of maize yield at specific phenological stages	GB	Stage V10: $R^2 = 0.90$ ; Stage VT: $R^2 = 0.93$
[157]	Wheat	Satellite spectral and weather data, soil hydraulic properties	Forecasting of wheat yield	RF, MLR	RF: 1 month before harvest: $R = 0.85$ , RMSE = 0.70 $\text{tha}^{-1}$ , ROC = 0.90
[158]	Maize	Soil and weather data	Estimation of maize yield with publicly available data Finding optimal features gathering for forecasting paddy yield	LSTM, LASSO, RF, SVR, AdaBoost	LSTM: MAE = 0.83 ( $\text{buac}^{-1}$ ), MAPE = 0.48%
[159]	Rice	Soil and weather data	Soil and weather data	RF, DT, GBM	RF: MSE = 0.07, $R^2 = 0.67$ ;
[160]	Alfalfa	Hyperspectral data from UAV	In-season alfalfa yield forecast	Combination of RF, SVR, KNN	$R^2 = 0.874$
[161]	Maize	Multispectral images from UAV	Yield prediction of maize	BPNN, SVM, RF, ELM	SVM: RMSE = 1.099, MAE = 0.886
[162]	Mentha	Satellite spectral data, field inventory data (soil, plant height, biomass)	Mentha crop biomass forecasting	MLP	$R^2 = 0.762$ , RMSE = 2.74 $\text{th}^{-1}$
[163]	Wheat	Multispectral images from UAV	Prediction of wheat grain yield	LR, RF, SVM, ANN	LR: RMSE = 972 $\text{kg ha}^{-1}$ , $R^2 = 0.62$
[164]	Maize	Multispectral images from UAV	Prediction of maize yield	RF, RF+R, RF+BAG, SVM, LR, KNN, ANN	RF: $R = 0.78$ , MAE = 853.11 $\text{kg ha}^{-1}$
[165]	Potato	Hyperspectral data from UAV	Yield prediction at two growth stages	RF, PLSR	RF: $R^2 = 0.63$ , MAE = 853.11 $\text{kg ha}^{-1}$
[166]	Carrot	Satellite spectral data	Carrot yield Mapping	RF	$R^2 = 0.82$ , RMSE = 2.64 $\text{Mgha}^{-1}$ ; MAE = 1.74 $\text{Mgha}^{-1}$
[167]	Soybean	Multispectral images from UAV	Predicting yield	DT	RMSE = 196 $\text{kg ha}^{-1}$
[168]	Wheat	Satellite spectral, soil and weather data	Winter wheat yield prediction at a regional level	Combination of LSTM and CNN	$R^2 = 0.75$ , RMSE = 732 $\text{kg ha}^{-1}$ ;
[169]	Potato	Hyperspectral data from UAV	Yield prediction at two growth stages	RF, PLSR	$R^2$ values: RF: 0.63; PLSR: 0.81
[170]	Wheat	Satellite spectral and weather data	Winter yield prediction in the Conterminous United States	OLS, LASSO, SVM, RF, AdaBoost, DNN	AdaBoost: $R^2 = 0.86$ , RMSE = 0.51 $\text{tha}^{-1}$ , MAE = 0.39 $\text{tha}^{-1}$

Acc: Accuracy; CA: Conservation Agriculture; CI: Crop Indices; CEC: Cation Exchange Capacity; CCC: Concordance Correlation Coefficient; DOY: Day Of Year; EC: Electrical Conductivity; HD: Heading Date; HDM: Heading Date to Maturity; K: Potassium; Mg: Magnesium; N: Nitrogen; OLI: Operational Land Imager; P: Phosphorus; RGB: Red-Green-Blue; S: Sulphur; SOM: Soil Organic Matter; SPAD: Soil and Plant Analyzer Development; STI: Soil Texture Information; STD: Standard Deviation; UAV: Unmanned Aerial Vehicle; UGV: Unmanned Ground Vehicle.

Table A2. Crop Management: Disease Detection.

Ref	Crop	Input Data	Functionality	Models/Algorithms	Best Output
[171]	Various crops	RGB images	Detection and diagnosis of plant diseases	CNN	Acc = 99.53%
[172]	Melon	Fluorescence, thermal images	Detection of <i>Dickeya dadantii</i> in melon plants	LR, SVM, ANN	ANN: Whole leaves: Acc = 96%; F1 score = 0.99
[173]	Tomato	RGB images	Recognition of 10 plant diseases and pests in tomato plants	CNN	Recognition rate = 96%



Table A2. Cont.

Ref	Crop	Input Data	Functionality	Models/Algorithms	Best Output
[174]	Avocado	Hyperspectral images	Detection of nitrogen and iron deficiencies and laurel wilt disease in avocado	DT, MLP	MLP: Detection at early stage: Acc = 100%
[175]	Maize	RGB images	Examination of nine factors affecting disease detection in maize fields	CNN	Acc values: (1) Original dataset: 76%; Background removed: 79%; (2) Subdivided (full): 87%; (3) Subdivided (reduced): 81%
[176]	Milk thistle	Spectral measurements from spectroradiometer	Identification of <i>Microbotryum silybum</i> in milk thistle plants	MLP-ARD	Acc = 90.32%
[177]	Tomato	Spectral measurements from spectroradiometer	Detection of leaf diseases (target, bacterial spots and late blight) in tomato	KNN	Acc values: (1) Healthy leaves: 100%, (2) Asymptomatic: 100%, (3) Early stage: 97.8%, (4) Late stage: 100%
[178]	Maize	RGB images	Identification of eight types of leaf diseases in maize	CNN	(1) GoogLeNet: Acc = 98.9%; (2) Cifar10: Acc = 98.8%
[179]	Various crops	RGB images	Identification of six plant leaf diseases	RBFN	(1) Early blight: Acc = 0.8914; (2) Common rusts: Acc = 0.8871
[180]	Citrus	RGB images	Detection and classification of citrus diseases	SVM	Acc values: 1st dataset: 97%; 1st and 2nd dataset: 89%; 3rd dataset: 90.4%
[181]	Grape	Multispectral images from UAV	Identification of infected areas	CNN	(1) Color space YUV: Acc = 95.84%; (2) Color space YUV and ExGR: Acc = 95.92%
[182]	Soybean	RGB images	Detection and classification of three leaf diseases in soybeans	SVM	(1) Healthy: Acc = 82%; (2) Downy mildew: Acc = 79%; (3) Frog eye: Acc = 95.9%; (4) Septoria leaf blight: Acc = 90%
[183]	Millet	RGB images	Identification of fungal disease (mildew) in pearl millet	CNN	Acc = 95.00%, Precision = 90.50%, Recall = 94.50%, F1 score = 91.75%
[184]	Maize	RGB images from UAV	Detection of northern leaf blight in maize	CNN	Acc = 95.1%
[185]	Wheat	RGB images from UAV	Classification of <i>helminthosporium</i> leaf blotch in wheat	CNN	Acc = 91.43%
[186]	Avocado	RGB images, multispectral images	Detection of laurel wilt disease in healthy and stressed avocado plants in early stage	MLP, KNN	Healthy vs. Nitrogen deficiency using 6 bands images: (1) MLP: Acc = 98%; (2) KNN: Acc = 86%
[187]	Basil	RGB images	Identification and classification of five types of leaf diseases in four kinds of basil leaves	DT, RF, SVM, AdaBoost, GLM, ANN, NB, KNN, LDA	RF: Acc = 98.4%
[188]	Various crops	RGB images	Identification of several diseases on leaves	CNN	Acc values: (1) Healthy: 89%; (2) Mildly diseased: 31%; (3) Moderately diseased: 87%; (4) Severely diseased: 94%
[189]	Tea	RGB images from UAV	Identification of tea red Scab, tea leaf blight and tea red leaf spot diseases in tea leaves	SVM, DT, RF, CNN	CNN: Acc values: (1) tea red Scab: 0.7; (2) tea leaf blight: 1.0; (3) tea red leaf spot: 1.0
[190]	Wheat	Hyperspectral images from UAV	Detection of yellow rust in wheat plots	CNN	Acc = 0.85
[191]	Grape	RGB images	Detection of grapevine yellows in red grapes	CNN	Sensitivity = 98.96% Specificity = 99.40%
[192]	Maize	RGB images from UAV	Detection of northern leaf blight in maize	CNN	Acc = 0.9979, F1 score = 0.7153
[193]	Sugar beet	RGB images	Detection and classification of diseased leaf spots in sugar beet	CNN	Acc = 95.48%
[194]	Various crops	RGB images	Identification of various plant leaf diseases	CNN	Acc = 96.46%
[195]	Strawberry	RGB images	Detection of powdery mildew in strawberry leaves	LDA	(1) Artificial lighting conditions: recall = 95.26%, precision = 95.45%, F1 score = 95.37%; (2) Natural lighting conditions: recall = 81.54%, precision = 72%, F1 score = 75.95%
[196]	Various different crops	RGB images	Detection of diseased plants	DL	Acc = 93.67%
[197]	Citrus	Hyperspectral images from UAV	Detection of canker disease on leaves and immature fruits	RBFN, KNN	RBFN: Acc values: (a) asymptomatic: 94%, (b) early stage: 96%, (c) late stage: 100%
[198]	Grape	RGB images	Detection of diseased vine on leaves	SVM	Acc = 95%
[199]	Wheat	RGB images	Identification of three leaf diseases in wheat	CNN	Acc values: (1) Septoria: 100%; (2) Tan Spot: 99.32%; (3) Rust: 99.29%

Table A2. Cont.

Ref	Crop	Input Data	Functionality	Models/Algorithms	Best Output
[200]	Grape	Spectral measurements form spectroradiometer	Classification of Flavescence dorée disease in grapevines	SVM, LDA	SVM: Acc = 96%
[201]	Papaya	RGB images	Recognition of five papaya diseases	SVM	Acc = 90%, Precision = 85.6%
[202]	Rice	RGB images	Recognition and classification of rice infected leaves	KNN, ANN	ANN: Acc = 90%, Recall = 88%
[203]	Tomato	Hyperspectral images from UAV	Detection of bacterial spot and target spot on tomato leaves	MLP, STDA	MLP: Acc values: (a) bacterial spot: 98%, (b) target spot: 97%
[204]	Squash	Hyperspectral images from UAV and laboratory measurements	Classification of powdery mildew in squash	RBFN	Acc values: (1) Laboratory: Asymptomatic: 82%, Late stage: 99%; (2) Field conditions: Early stage: 89%, Late disease stage: 96%
[205]	Tomato	Hyperspectral images from UAV and laboratory measurements	Detection of bacterial spot and target spot on tomato leaves	RBFN, STDA	Field conditions: Acc values: (a) Healthy vs. BS: 98%, (b) Healthy vs. TS: 96%, (c) Healthy vs. TYLC: 100%
[206]	Tomato	RGB images	Identification of various diseases in tomato	CNN	Acc values: (1) PV dataset: 98.4%; (2) 2nd dataset: 98.7%; (3) Field data: 86.27%
[79]	Walnut	RGB images	Identification of anthracnose infected leaves	CNN	Acc values: (1) RGB: 95.97%; (2) Grayscale: 92.47%; (3) Fast Fourier: 92.94%
[207]	Various crops	RGB images	Classification of infected leaves	DBN	Acc = 0.877, Sensitivity = 0.862, Specificity = 0.877
[208]	Grape	Multispectral images from UAV	Detection of Mildew disease in vineyards	CNN	Acc values: (1) Grapevine-level: 92%; (2) Leaf level: 87%
[209]	Rice	RGB images, videos	Video detection of brown spot, stem borer and sheath blight in rice	CNN	(1) Brown spot: Recall = 75.0%, Precision = 90.0%; (2) Stem borer: Recall = 45.5%, Precision = 71.4%; (3) Sheath blight: Recall = 74.1%, Precision = 90.9%
[210]	Cassava	RGB images	Detection and classification of diseased leaves of fine-grain cassava	CNN	Acc = 93%
[211]	Banana	Satellite spectral data, Multispectral images from UAV, RGB images from UAV	Detection of banana diseases in different African landscapes	RF, SVM	RF: Acc = 97%, omissions error = 10%; commission error = 10%; Kappa coefficient = 0.96
[212]	Tomato	RGB images	Detection of early blight, leaf mold and late blight on tomato leaves	CNN	Acc = 98%
[213]	Pepper	Spectral reflectance at 350–2500 nm	Detection of fusarium disease in pepper leaves	ANN, NB, KNN	KNN: Average success rate = 100%
[214]	Tomato	Spectral measurements form spectroradiometer	Detection of fusarium disease on pepper leaves	CNN	Acc = 98.6%
[215]	Citrus	Multispectral images from UAV	Detection of citrus greening in citrus orchards	SVM, KNN, MLR, NB, AdaBoost, ANN	AdaBoost: Acc = 100%
[216]	Soybean	RGB images	Prediction of charcoal rot disease in soybean	GBT	Sensitivity = 96.25%, specificity = 97.33%
[217]	Wheat	RGB images from UAV	Detection of wheat lodging	RF, CNN, SVM	CNN: Acc = 93%
[218]	Tomato	Weather data	Prediction of powdery mildew disease in tomato plants	ELM	Acc = 89.19%, AUC = 88.57%
[219]	Soybean	RGB images	Diagnosis of soybean leaf diseases	CNN	Acc = 98.14%
[220]	Potato	RGB images	Identification of early and late blight disease	NB, KNN, SVM	SVM: Average Acc = 99.67%
[221]	Various crops	RGB images	Quantification of uncertainty in detection of plant diseases	BDL	Mean softmax probability values: (1) Healthy: 0.68; (2) Non-Healthy: 0.72;
[222]	Coffee	Satellite spectral data	Identification of coffee berry necrosis via satellite imagery	MLP, RF, NB	NB: Acc = 0.534
[223]	Tomato	RGB images	Recognition of blight, powdery mildew, leaf mold fungus and tobacco mosaic virus diseases	CNN	Faster RCNN: mAP = 97.01%
[224]	Maize	RGB images	Diagnosis of northern leaf blight, gray leaf spot, and common rust diseases	CNN	Acc = 98.2%; macro average precision = 0.98
[225]	Grape	RGB images	Detection of black measles, black rot, leaf blight and mites on leaves	CNN	mAP = 81.1%
[226]	Grape	Weather data, expert input (disease incidence form visual inspection)	Forecasting downy mildew in vineyards	GLM, LASSO, RF, GB	GB: AUC = 0.85



Table A2. Cont.

Ref	Crop	Input Data	Functionality	Models/Algorithms	Best Output
[227]	Maize	RGB images	Detection of northern leaf blight in maize	CNN	mAP = 91.83%
[228]	Onion	RGB images	Detection of downy mildew symptoms in onions field images	WSL	mAP@0.5 = 74.1–87.2%
[229]	Coffee	RGB images	Detection of coffee leaf rust via remote sensing and wireless sensor networks	CNN	F1 score = 0.775, p-value = 0.231
[230]	Tomato	Weather data, multispectral images captured from UAV	Detection of late blight disease	CNN	Acc values: AlexNet: (1) Transfer learning: 89.69%; (2) Feature extraction: 93.4%, average Acc = 94.64%
[231]	Rice	RGB images	Detection of brown rice planthopper	CNN	Average recall rate = 81.92%, average Acc = 94.64%
[232]	Grape	UAV multispectral images, depth map information	Detection of vine diseases	CNN	VddNet: Accuracy = 93.72%
[233]	Apple	RGB images	Identification of apple leaf diseases (S, FS, CR)	CNN	Improved VGG16: Acc = 99.40%(H), 98.04%(S), 98.33%(FS), 100%(CR)
[234]	Cotton	UAV multispectral images	Disease classification of cotton root rot	KM, SVM	KM: Acc = 88.39%, Kappa = 0.7198

Acc: Accuracy; AUC: Area Under Curve; CR: Cedar Rust; ExGR: Excess Green Minus Excess Red; FS: Frogeye Spot; H: Healthy; mAP: mean Average Precision; RGB: Red-Green-Blue; S: Scab; TYLC: Tomato Yellow Leaf Curl; UAV: Unmanned Aerial Vehicle; VddNet: Vine Disease Detection Network.

Table A3. Crop Management: Weed Detection.

Ref	Input Data	Functionality	Models/Algorithms	Best Output
[235]	RGB images	Classification of thistle (monocots), broa leaf (dicots) weeds	AdaBoost with NB	Acc values: (1) Original dataset: 98.40%; (2) expanded dataset: 94.72%
[236]	RGB images from UAV	Detection of weeds in bean, spinach fields	CNN	Acc values: (1) Bean field: 88.73%; (2) Spinach field: 94.34%
[237]	RGB images	Detection of four weed species in sugar beet fields	SVN, ANN	Overall Acc: SVM: 95.00%; Weed classification: SVM: 93.33%; Sugar beet plants: SVM: 96.67%
[238]	RGB images from UAV, multispectral images	Detection of Gramineae weed in rice fields	ANN	Best system: 80% < M/MGT < 108%, 70% < MP < 85%
[239]	RGB images	Classification of crops (three species) and weeds (nine species)	CNN	Average Acc: 98.21±0.55%
[240]	Multispectral and RGB images from UAV	Weed mapping between and within crop rows, (1) cotton; (2) sunflower	RF	Weed detection Acc: (1) Cotton: 84%; (2) Sunflower: 87.9%
[241]	Hyperspectral images	Recognition of three weed species in maize crops	RF	Mean correct classification rate: (1) Zea mays: 1.0; (2) Convolvulus arvensis: 0.789; Rumex: 0.691; Cirsium arvense 0.752
[242]	RGB images from UAV	Detection of weeds in early season maize fields	RF	Overall Acc = 0.945, Kappa = 0.912
[243]	RGB images from UAV	Weed mapping and prescription map generation in rice field	FCN	Overall Acc = 0.9196, mean intersection over union (mean IU) = 0.8473
[244]	Handheld multispectral data	Weed detection in maize and sugar beet row-crops with: (1) spectral method; (2) spatial; (3) both methods	SVM	Mean detection rate: (1) spectral method: 75%; (2) spatial: 79%; (3) both methods: 89%
[245]	Multispectral images from UAV	Development of Weed/crop segmentation, mapping framework in sugar beet fields	DNN	AUC: (1) background: 0.839; (2) crop: 0.681; (3) weed: 0.576
[246]	RGB images	Classification of potato plant and three weed species	ANN	Acc = 98.1%
[247]	RGB images	Estimation of weed growth stage (18 species)	CNN	Maximum Acc = 78% (Polygonum spp.), minimum Acc = 46% (blackgrass), average Acc = 70% (the number of leaves) and 96% for deviation of two leaves
[248]	Multispectral images	Classification of corn (crop) and silver beet (weed)	SVM	Precision = 98%, Acc = 98%
[249]	RGB images	Classification of Carolina Geranium within strawberry plants	CNN	F1 score values: (1) DetectNet: 0.94, highest; (2) VGGNet: 0.77; (3) GoogLeNet: 0.62
[250]	RGB images	Classification of weeds in organic carrot production	CNN	Plant-based evaluation: Acc = 94.6%, Precision = 93.20%, Recall = 97.5%, F1 Score = 95.32%

Table A3. Cont.

Ref	Input Data	Functionality	Models/Algorithms	Best Output
[251]	Grayscale images from UGV	Recognition of Broad-leaved dock in grasslands	CNN, SVM	VGG-F: Acc = 96.8%
[252]	Multispectral images from UAV	Mapping of Black-grass weed in winter wheat fields	CNN	Baseline model: AUC = 0.78; Weighted kappa = 0.59; Average misclassification rate = 17.8%
[253]	RGB images	Segmentation of rice and weed images at seedling stage in paddy fields	FCN	Semantic segmentation: Average Acc rate = 92.7%
[254]	RGB images from UGV	Creation of multiclass dataset for classification of eight Australian rangelands weed species	CNN	RS-50: Average Acc = 95.7%, average inference time = 53.4 ms per image
[255]	RGB images	Evaluation of weed detection, spraying and mapping system. Two Scenarios: (1) artificial weeds, plants; (2) real weeds, plants	CNN	Scenario: (1) Acc = 91%, Recall = 91%; (2) Acc = 71%, Precision = 78% (for plant detection and spraying Acc)
[256]	RGB images	Detection of goldenrod weed in wild blueberry crops	LC, QC	QC: Acc = 93.80%
[257]	RGB images	Detection of five weed species in turfgrass	CNN	Precision values: Dollar weed: VGGNet (0.97); old world diamond-flower: VGGNet (0.99); Florida pusley: VGGNet (0.98); annual bluegrass: DetectNet (1.00) Precision values: Dandelion: DetectNet (0.99); ground ivy: VGGNet (0.99), spotted spurge: AlexNet (0.87)
[258]	RGB images	Detection of three weed species in perennial ryegrass	CNN	Overall: Mean precision = 91.3%, Mean recall = 96.3%
[259]	RGB images, multispectral images from UGV	Crop-weed classification along with stem detection	FCN	
[260]	RGB images	Identification of crops (cotton, tomato) and weeds (velvetleaf and nightsade)	CNN, SVM, XGBoost, LR	Densenet and SVM: micro F1 score = 99.29%
[261]	Videos recordings	Classification of two weeds species in rice field	ANN, KNN	Acc values: Right channel (76.62%), Left channel (85.59%)
[262]	RGB images	Weed and crop discrimination in paddy fields	MCS, SRF, SVM	Acc values: Right channel (76.62%), Left channel (85.59%)
[263]	Gray-scale and RGB images	Weed and crop discrimination in carrot fields	RF	Acc = 94%
[264]	Multispectral and RGB images	Discrimination of weed and crops with similar morphologies	CNN	Acc = 98.6%
[265]	RGB images	Detection of C. sepium weed and sugar beet plants	CNN	mAP = 0.751–0.829 AP <sub>s</sub> @IoU0.5 = 0.761–0.897
[266]	RGB images	Recognition of eight types of weeds in rangelands	CNN, RNN	DeepWeeds dataset: Acc = 98.1%
[267]	Multispectral images from UAV	Weed estimation on lettuce crops	SVM, CNN	F1 score values: (1) SVM: 88%; (2) CNN-YOLOv3: 94%; (3) Mask R-CNN: 94%
[268]	RGB images	Examination of pre-trained DNN for improvements in weed identification	CNN	(1) Xception: improvement = 0.51%; (2) Inception-Resnet: improvement = 1.89%
[269]	RGB images from UAV	Detection of five weeds in soybean fields	CNN	Faster RCNN: precision = 0.65, recall = 0.68, F1 score = 0.66, IoU = 0.85
[270]	RGB images	Detection of goose grass weed in tomato, strawberry fields	CNN	(1) Strawberry: (a) entire plant: F1 score = 0.75, (b) leaf blade: F1 score = 0.85; (2) Tomato: (a) entire plant: F1 score = 0.56, (b) leaf blade: F1 score = 0.65 Correct classification rate = 98.33%
[271]	Video recordings	Detection of five weed species in Marfona potato fields	ANN	
[272]	In situ measurements, satellite spectral data	Identification of gamba grass in pasture fields	XGBoost	Balanced Acc = 86.9%
[273]	RGB images from UAV, satellite spectral data	Weed maps creation in oat fields	RF	Acc values: (1) Subset A: 89.0%; (2) Subset B: 87.1%
[274]	In situ measurements, RGB images from UAV	Identification of Italian ryegrass in early growth wheat	DNN	Precision = 95.44%, recall = 95.48%, F score = 95.56%
[275]	RGB images from UGV	Weed detection evaluation of a spraying robot in potato fields on: (1) Image-level; (2) application-level; (3) field-level	CNN	YOLOv3: (1) Image-level: recall = 57%, precision = 84%; (2) application-level: plants detected = 83%; (3) field-level: correct spraying = 96%
[276]	RGB images from UGV	Detection of four weed species in maize and bean crops	CNN	Average precision = 0.15–0.73
[277]	RGB images from UAV	Detection of Colchicum autumnale in grassland sites	CNN	U-Net: Precision = 0.692, Recall = 0.886, F2 score = 0.839
[278]	RGB images from UAV	Weed mapping of Rumex obtusifolius in native grasslands	CNN	VGG16: Acc = 92.1%, F1 score = 78.7%

Acc: Accuracy; AUC: Area under Curve; IoU: Intersection over Union; mAP: mean Average Precision; RGB: Red-Green-Blue; UAV: Unmanned Aerial Vehicle; UGV: Unmanned Ground Vehicle.

Table A4. Crop Management: Crop Recognition.

Ref	Crop	Input Data	Functionality	Models/Algorithms	Best Output
[279]	Various crops	Satellite spectral data	Classification of early-season crops	RF	Beginning of growth stage: acc = 97.1%, kappa = 93.5%
[280]	Various crops	Satellite spectral and phenological data	Identification of various crops from remote sensing imagery	SVM, RF, DF	DF: (1) 2015: overall acc = 88%; (2) 2016: overall acc = 85%
[281]	Maize, Rice, Soybean	Satellite spectral data	Three-dimensional classification of various crops	CNN, SVM, KNN	CNN: (1) 2015: overall acc = 0.939, kappa = 0.902; (2) 2016: overall acc = 0.959, kappa = 0.924
[282]	Various crops	Satellite spectral data, in situ data	Identification of crops growing under plastic covered greenhouses	DT	Overall acc = 75.87%, Kappa = 0.63
[283]	Various crops	Satellite data, phenological, in situ data	Classification of various crops	NB, DT, KM	KM: overall acc = 92.04%, Kappa = 0.7998
[284]	Cabbage, Potato	RGB images from UAV, in situ data	Classification of potato and cabbage crops	SVM, RF	SVM: overall acc = 90.85%
[285]	Various crops	Satellite spectral data	Classification of various crops	SVM	Overall acc = 94.32%
[286]	Various crops	Satellite spectral data, in situ data	Classification of various crops in large areas	EBT, DT, WNN	EBT: overall acc = 87%
[287]	Various crops	Satellite spectral data, in situ data	Classification of various crops	SVM	overall acc = 92.64%
[288]	Various crops	Field location, in situ and satellite spectral data	Classification of six crops with small sample sizes	FFNN, ELM, MKL, SVM	MKL: accuracy = 92.1%
[289]	Wolfberry, Maize, Vegetables	Satellite spectral data	Crop classification in cloudy and rainy areas	RNN	Landsat-8: overall acc = 88.3%, Kappa = 0.86
[290]	Maize, Canola, Wheat	Satellite spectral data, in situ data	Crop classification	RF, ANN, SVM	RF: overall acc = 0.93, Kappa = 0.91
[291]	Various crops	Satellite spectral data	Classification of various crop types	Combination of FCN-LSTM	Acc = 86%, IoU = 0.64
[292]	Various crops	Satellite spectral data	Crop classification of various crops	LightGBM	Highest acc: 92.07%
[293]	Maize, Peanut, Soybeans, Rice	Satellite spectral and in situ data	Prediction of different crop types	FCN, SVM, RF	Best crop mapping: FCN: acc = 85%, Kappa = 0.82
[294]	Various crops	Satellite spectral and in situ data	Classification of early growth crops	CNN, RNN, RF	Highest Kappa: 1D CNN: 0.942
[295]	Various crops	Satellite spectral and in situ data	Classification of various crops	CNN, LSTM, RF, XGBoost, SVM	CNN: acc = 85.54%, F1 score = 0.73
[296]	Various crops	Satellite spectral data	Classification of parcel-based crops	LSTM, DCN	DCN: overall acc = 89.41%
[297]	Various crops	Satellite spectral data	Classification of crops in farmland parcel maps	LSTM, RF, SVM	LSTM: overall acc = 83.67%, kappa = 80.91%
[298]	Various crops	Satellite spectral data, in situ data	Crop classification	SVM, RF, CNN-RNN, GBM	Pixel R-CNN: acc = 96.5%
[299]	Zea mays, Canola, radish	Grayscale testbed data	Classification of the crops	SVM	Quadratic SVM: Precision = 91.87%, Recall = 91.85%, F1 score = 91.83%
[300]	Rice	Morphological data	Classification of two rice species (Osmancik-97 and Cammeo)	LR, MLP, SVM, DT, RF, NB, KNN	LR: acc = 93.02%
[301]	Soybean	Hyperspectral data, seed properties	Discrimination of 10 soybean seed varieties	TS-FFNN, SIMCA, PLS-DA, BPNN	TS-FFNN in terms of identification Acc, stability and computational cost
[302]	Cotton	Hyperspectral data, seed properties	Identification of seven cotton seed varieties: (1) Full spectra, (2) Effective wavelengths	PLS-DA, LGR, SVM, CNN	(1) Full spectra: CNN-SoftMax: 88.838%; (2) Effective wavelengths: CNN-SVM: 84.260%
[303]	Various plants	RGB images of leaves	Recognition of 15 plant species of Swedish leaf dataset	CNN	Macro average: (1) Precision = 0.97, (2) Recall = 0.97, (3) F1 score = 0.97
[304]	Various shrubs and trees	RGB images of leaves	Identification of 30 shrub and trees species	RF, SVM, AdaBoost, ANN	SVM: acc = 96.5–98.4%
[305]	Various plants	RGB images of leaves	Identification of seven plant species	BPNN, SOM, KNN, SVM	BPNN: Recognition rate = 92.47%
[306]	Various crops	Satellite spectral data	Crop classification	SVM	SVM (RBF): overall acc values: (1) 2016: 88.3%; (2) 2017: 91%; (3) 2018: 85.00%
[307]	Various crops	Satellite spectral data	Crop classification	FCN	3D FCN: overall acc = 97.56%, Kappa = 95.85%
[308]	Cotton, Rice, Wheat, Gram	Satellite spectral data	Crop classification	RF, KM	RF: acc = 95.06%
[309]	Various crops	Satellite spectral data	Crop classification	SVM, RF, CART	RF: overall acc = 97.85%, Kappa = 0.95
[310]	Various crops	Satellite spectral data, in situ data	Crop classification	RF	overall acc = 75%, Kappa = 72%
[311]	Maize, Soybean	Satellite spectral data	Crop classification	RF, MLP, LSTM	LSTM: confidence interval = 95%
[312]	Various crops	Satellite spectral and in situ data	Crop classification	XGBoost, SVM, RF, MLP, CNN, RNN	CNN: overall acc = 96.65%

Table A4. Cont.

Ref	Crop	Input Data	Functionality	Models/Algorithms	Best Output
[313]	Rice	Satellite spectral data	Crop classification	CNN, SVM, RF, XGboost, MLP	CNN: overall acc = 93.14%, F1 score = 0.8552
[314]	Various crops	Satellite spectral and in situ data	Crop classification	RF	Overall acc = 0.94, Kappa = 0.93
[315]	Various crops	Satellite spectral data	Crop classification	CNN, LSTM, SVM	CNN: overall acc = 95.44%, Kappa = 94.51%
[316]	Various crops	Satellite spectral data	Crop classification prior to harvesting	DT, KNN, RF, SVM	RF: overall acc = 81.5%, Kappa = 0.75
[317]	Various crops	Satellite spectral data	Crop classification	CNN	Overall acc = 98.19%
[318]	Various crops	Satellite spectral data	Crop classification	SVM, DA, DT, NNL	NNL: F1 score = 0.88
[319]	Banana, Rice, Sugarcane, Cotton	Satellite spectral and in situ data	Crop classification	SVM	Overall acc = 89%
[320]	Various crops	Satellite spectral and in situ data	Crop classification	RF	Overall acc = 93.1%

Acc: Accuracy; IoU: Intersection over Union; RGB: Red-Green-Blue; UAV: Unmanned Aerial Vehicle.

Table A5. Crop Management: Crop Quality.

Ref	Crop	Input Data	Functionality	Models/Algorithms	Best Output
[64]	Apples	Quality features, (flesh firmness, soluble solids, fruit mass and skin color)	Classification of apple total quality: very poor, poor, medium, good and excellent	FIS, ANFIS	FIS: acc values: (1) 2005: 83.54%; 2006: 92.73%; 2007: 96.36%
[321]	Pepper	RGB images, quality features (color, mass and density of peppers)	Recognition of pepper seed quality	BLR, MLP	MLP: 15 traits, stability = 99.4%, predicted germination = 79.1%, predicted selection rate = 90.0%
[322]	Soybeans	Satellite spectral and soil data	Estimation of crop gross primary productivity	RF, ANN	ANN: $R^2 = 0.92$ , RMSE = 1.38 $gCdm^{-2}$
[323]	Wheat	RGB images captured by UAV	Estimation of aboveground nitrogen content combining various VI and WFs	PLSR, PSO-SVR	PSO-SVR: $R^2 = 0.9025$ , RMSE = 0.3287
[324]	Millet, rye, maize	RGB images captured in laboratory	Assessment of grain crops seed quality	CNN	Faster R-CNN: (1) Pearl millet: mAP = 94.3%; (2) rye: mAP = 94.2%; (3) Maize: mAP = 97.9%
[325]	Jatropha curcas	X-ray imaging	Prediction of vigor and germination	LDA	Acc values: Fast germination: 82.08%; Slow germination: 76.00%; Non-germinated: 88.24%
[326]	Various legumes	Spectral data form spectroradiometer	Estimation of five warm-season legumes forage quality	PLS, SVM, GP	SVM: All five crops: $Acc = \frac{R_{RF}^2}{R_{RF}^2} = 0.92-0.99$ , IVTD: $Acc = \frac{R_{IVTD}^2}{R_{IVTD}^2} = 0.42-0.98$
[327]	Forage grass	X-ray imaging	Prediction of vigor and seed germination	LDA, PLS-DA, RF, NB, SVM	PLS-DA: Acc values: (1) Vigor: FT-NIR: 0.61, X-ray: 0.68, Combination: 0.58; (2) Germination: FT-NIR: 0.82, X-ray: 0.86, Combination: 0.82
[328]	Tomato	RGB images	Dimensions and mass estimation for quality inspection	(1) DSM, (2) Mass estimation on: (a) MMD (BET, GPR, SVR, ANN, GPR), (b) EDG (BET, GPR, SVR, ANN)	(1) DSM: precision = 99.7%; MAE values: (2) Width (2.38), Length (2.58); (3) Mass estimation: (a) MMD (4.71), (b) EDG (13.04)
[329]	Peach	Hyperspectral images	Estimation of soluble solids content	SAE-RF	$R^2 = 0.9184$ , RMSE = 0.6693

Acc: Accuracy; DSM: Detection and Segmentation Module; EDG: Estimated Dimensions Geometry; IVTD: In Vitro True Digestibility; RGB: Red-Green-Blue; MMD: Manually Measured Dimensions; mAP: mean Average Precision; PSO: Particle Swarm Optimization; RGB: Red-Green-Blue; SAE: Stacked AutoEncoder; VI: Vegetation Indices; WF: Wavelet Features.

Table A6. Water management.

Ref	Property	Input Data	Functionality	Models/Algorithms	Best Output
[330]	Crop water status	Weather data, crop water status, thermal images	Prediction of vineyard's water status. Scenario A: with RT; Scenario B: without RT	REPTree	(1) Scenario A: prediction: $R^2 = 0.58$ , RMSE = 0.204 MPa; (2) Scenario B: prediction: $R^2 = 0.65$ , RMSE = 0.184 MPa.
[331]	Crop water status	Crop water status, hyperspectral data	Discrimination of stressed and non-stressed vines	RF, XGBoost	RF: Acc = 83.3%, Kappa = 0.67
[332]	Groundwater level	Water table depth, weather data	Prediction of water table depth	LSTM, FFNN,	LSTM: $R^2 = 0.789-0.952$
[333]	Irrigation scheduling	Weather, irrigation, soil moisture, yield data	Prediction of weekly irrigation plan in jojoba orchards	DTR, RFR, GBRT, MLR, BTC	(1) Regression: GBRT: Acc = 93%; (2) Classification: GBRT: Acc = 95%

Table A6. Cont.

Ref	Property	Input Data	Functionality	Models/Algorithms	Best Output
[334]	Crop water status	Water status, multispectral UAV data	Estimation of vineyard water status	MLR, ANN	ANN: $R^2 = 0.83$
[335]	ET	Weather data	Estimation of daily $ET_0$	ELM, WANN	ELM: RMSE values: Region case A: 0.1785 mm/day; Region case B: 0.359 mm/day
[336]	ET	Weather data	Estimation of daily $ET_0$	RF, M5Tree, GBDT, XGBoost, SVM, RF	XGBoost: RMSE = 0.185–0.817 $mmday^{-1}$
[337]	Soil water content	Weather data, volumetric soil moisture content	Prediction of one-day-ahead volumetric soil moisture content	FFNN, LSTM	LSTM: $R^2 > 0.94$
[338]	Infiltration	Field data, moisture content, cumulative infiltration of soil	Estimation of cumulative infiltration of soil	SVM, ANN, ANFIS	ANFIS: RMSE = 0.8165 cm, CC = 0.9943
[339]	Soil water content	Weather data, soil moisture difference, ultraviolet radiation	Prediction of soil moisture	SVR	$R = 0.98$ , $R^2 = 0.96$ , MSE = 0.10
[340]	Soil water content	Simulated soil moisture data, weather data	Forecasting of monthly soil moisture for: Scenario A: upper; Scenario B: lower layers	ELM	(1) Scenario A: RRMSE = 19.16%; (2) Scenario B: RRMSE = 18.99%
[341]	ET	Weather and in situ crop data	Estimation of actual ET Scenario A: rainfed maize field under non-mulching; Scenario B: partial plastic film mulching	ANN, SVM	ANN: Scenario A: ET = 399.3 mm, RMSE = 0.469, MAE = 0.376; Scenario B: ET = 361.2 mm, RMSE = 0.421, MAE = 0.322
[342]	Infiltration and infiltration rate	Soil and hydraulic data	Prediction of cumulative infiltration and infiltration rate in arid areas	ANFIS, SVM, RF	SVM: RMSE values: cumulative infiltration: 0.2791 cm, infiltration rate: 0.0633 $cmh^{-1}$
[343]	Water quality	NIR spectroscopy.	Estimation of water pollution level	CNN	RMSE = 25.47 $mgL^{-1}$
[344]	ET	Weather data, simulated ET data	Estimation of $ET_0$ : (1) 2011–2015; (2) 2016–2017	LSTM	(1) Predictions in 3 sites: $R^2 > 0.90$ ; (2) All sites: RMSE = 0.38–0.58 $mmday^{-1}$
[345]	Soil water content	Weather data, potential ET, simulated soil moisture data	Estimation of soil moisture	FFNN, Ross-IES	FFNN: RMSE = 0.15–0.25, NSE = 0.71–0.91
[346]	ET	Weather data, simulated ET data, soil data	Estimation of daily kikuyu grass crop ET	RT, SVR, MLP, KNN, LGR, MLR, BN, RFC	RFC: $R = 0.9936$ , RMSE = 0.183 $mmday^{-1}$ , MRE = 6.52% Most influential parameters: farmer's age, education level, years of experience and number of cultivated land plots
[347]	Drought	Weather data	Evaluation of farmers' drought perception	RF, DT	
[348]	ET	Weather and soil data; simulated ET	Prediction of daily potato ET	ANN, AdaBoost, KNN	KNN: $R^2 = 0.8965$ , RMSE = 0.355 $mm day^{-1}$ , MSE = 0.126 $mm day^{-1}$
[349]	Soil water erosion	In situ data, geological, and weather data	Susceptibility mapping of soil erosion from water	RF, GP, NB	RF: Acc = 0.91, kappa = 0.94, POD = 0.94
[350]	ET, drought	Weather data, simulated ET index	Prediction of drought	SVR	Fuzzy-SVR: $R^2 = 0.903$ , RMSE = 0.137, MAE = 0.105
[351]	ET	Weather data, simulated $ET_0$	Estimation of daily $ET_0$	CNN, ANN, XGBoost, RF	CNN: (1) Regional: $R^2 = 0.91$ , RMSE = 0.47; (2) Local: $R^2 = 0.92$ , RMSE = 0.37
[352]	ET	Weather data	Estimation of daily $ET_0$	ELM, ANN, RF	ELM: $R^2 = 0.920$ , MAE = 0.394 $mmday^{-1}$
[353]	ET	Weather data	Prediction of ET in semi-arid and arid regions	CART, CCNN, SVM	SVM: (1) Station I: $R^2 = 0.92$ ; (1) Station II: $R^2 = 0.97$
[354]	Pan evaporation	Weather data	Prediction of monthly pan evaporation	ELM, ANN, M5Tree	ELM: $R^2 = 0.864$ –0.924, RMSE = 0.3069–0.4212
[355]	ET	Weather data, simulated $ET_0$	Evaluation of ML algorithms in daily reference ET prediction	Cubist, SVM, ANN, MLR	Cubist: $R^2 = 0.99$ , RMSE = 0.10 $mmday^{-1}$ , MAE = 0.07 $mmday^{-1}$
[356]	ET	Weather data, simulated ET	Estimation of $ET_0$	SVM, MLP, CNN, GRNN, GMDH	SVM: $R = 0.96$ –1.00, ME = 95–99%
[357]	Drought	Weather data, simulated Palmer Z-index values	Estimation of Palmer drought severity index	ANN, DT, LR, SVM	ANN: $R = 0.98$ , MSE = 0.40, RMSE = 0.56
[358]	Water quality	In-situ water quality data, hyperspectral, satellite data.	Estimation of inland water quality.	LSTM, PLSR, SVR, DNN	DNN: $R^2 = 0.81$ , MSE = 0.29, RMSE = 0.54
[359]	Groundwater	In-situ water quality data, hyperspectral, satellite spectral data	Estimation of water quality	DT	Acc = 81.49%, ROC = 87.75%
[360]	Groundwater	Weather data, ET, satellite spectral data, land use	Estimation of groundwater withdrawals	RF	$R^2 = 0.93$ , MAE = 4.31 mm, RMSE = 13.50 mm
[361]	Groundwater nitrate concentration	Various geo-environmental data	Comparison of different ML models for estimating nitrate concentration	SVM, Cubist, RF, Bayesian-ANN	RF: $R^2 = 0.89$ , RMSE = 4.24, NSE = 0.87

Acc: Accuracy; CC: Coefficient of Correlation; ET: Evapotranspiration;  $ET_0$ : reference EvapoTranspiration; ROC: Receiver Operating Characteristic; ME: Model Efficiency; NSE: Nash-Sutcliffe model efficiency Coefficient; POD: Probability Of Detection.

Table A7. Soil management.

Ref	Property	Input Data	Functionality	Models/Algorithms	Best Output
[362]	Soil organic matter	Soil properties, spectrometer NIR data	Estimation of soil organic matter	ELM, SVM	TRI-ELM: $R^2 = 0.83$ , RPIQ = 3.49
[363]	Soil microbial dynamics	Microbial dynamics measurements from root samples	Prediction of microbial dynamics: (1) BP; (2) PS and (3) ACCA	ANN, SVR, FIS	SCFIS: (1) BP: RMSE = 1350000, $R^2 = 1.00$ ; (2) PS: RMSE = 45.28, $R^2 = 1.00$ ; (3) ACCA: RMSE = 271, $R^2 = 0.52$
[364]	Soil salinity	Soil salinity, hyperspectral data, satellite data	Prediction of soil salinity	Bootstrap BPNN	BPNN with hyperspectral data: $R^2 = 0.95$ , RMSE = 4.38 g/kg
[365]	Soil properties	Simulated topographic attributes, satellite data	Prediction of SOC, CCE, clay content	Cu, RF, RT, MLR	(1) CCE: Cu: $R^2 = 0.30$ , RMSE = 9.52; (2) SOC: Cu, RF: $R^2 = 0.55$ ; (3) Clay contents: RF: $R^2 = 0.15$ , RMSE = 7.86
[366]	Soil organic matter	Soil properties, weather data, terrain, satellite spectral data	Prediction of soil organic matter	DT, BDT, RF, GBRT	GBRT: ME = 1.26 g/kg, RMSE = 5.41 g/kg, CCC = 0.72
[367]	Soil organic matter	Soil properties, satellite, land cover, topographic, weather data	Prediction of soil organic matter	CNN, RF, XGBoost	XGBoost: ME = 0.3663 g/kg, MSE = 1.0996 g/kg
[368]	Electrical conductivity	Soil properties, simulated electrical conductivity	Prediction of soil electrical conductivity	MLP	MLP: $WI = 0.780$ , $E_{NS} = 0.725$ , $E_{LM} = 0.552$
[369]	Soil moisture content	Hyperspectral images data, UAV, soil moisture content data samples	Estimation of soil moisture content	RF, ELM	RF: $R^2 = 0.907$ , RMSEP = 1.477, RPD = 3.396
[370]	Soil temperature	Weather data	Estimation of soil temperature at various depths	ELM, GRNN, BPNN, RF	ELM: RMSE = 2.26–2.95 °C, MAE = 1.76–2.26 °C, NSE = 0.856–0.930, CC = 0.925–0.965, $R^2 = 0.74–0.84$ , RMSEP = 0.14–0.18%, RPD = 1.98–2.5
[371]	SOC	Soil properties, vis-NIR spectral data	Estimation of SOC	RF	RMSEP = 0.14–0.18%, RPD = 1.98–2.5
[372]	Soil properties	Soil properties, visible-NIR, MIR spectral data	Prediction of total carbon, cation exchange capacity and SOC	PLSR, Cu, CNN	CNN: $R^2 = 0.95–0.98$
[373]	Soil properties	Soil properties, simulated organic, mineral samples, soil spectral data	Estimation of various soil properties	CNN	RMSE values: OC: 28.83 g/kg, CEC: 8.68 cmol <sup>+</sup> /kg, Clay: 7.47%, Sand: 18.03%, pH: 0.5 g/kg, N: 1.52 g/kg
[374]	Soil moisture content, soil ET	Soil properties, water, weather and crop data	Estimation of soil moisture content and soil ET	NN-RBF	Soil MC: RMSE = 0.428, RSE = 0.985, MSE = 0.183, RPD = 8.251
[375]	Soil salinity	Soil salinity, crop field temperature	Estimation of leaching water requirements for saline soils	Naive Bayes classifier	Acc = 85%
[376]	Soil erosion	Weather data, satellite, soil chemical data	Estimation of soil erosion susceptibility	Combination of GWR-ANN	GWR-ANN: AUC = 91.64% (1) Productivity: RMSEC = 0.20 T/ha, RMSECV = 0.54 T/ha, $R^2 = 0.9189$ ; (2) Organic matter: $R^2 = 0.9345$ , RMSECV = 0.54%; (3) Clay: $R^2 = 0.9239$ , RMSECV = 5.28%
[377]	Soil fertility	Spectral, weather data, EC, soil properties	Prediction of soil fertility and productivity	PLS	
[378]	Soil moisture	Multispectral images from UAV, in situ soil moisture, weather data	Retrieval of surface soil moisture	BRT, RF, SVR, RVR	BRT: MAE = 3.8%
[379]	Soil moisture	Soil samples, simulated PWP, field capacity data	Estimation of PWP and field capacity	ANN, KNN, DL	$R^2 = 0.829$ , R = 0.911, MAE = 0.027
[380]	Soil temperature	Weather data	Estimation of soil temperature	GMDH, ELM, ANN, CART, MLR	ELM: R = 0.99
[381]	Soil moisture	Soil samples, on-field thermal, simulated soil moisture data	Estimation of soil moisture content	ANN, SVM, ANFIS	SVM: R = 0.849, RMSE = 0.0131
[382]	Gully erosion	Geological, environmental, geographical data	Evaluation of gully erosion susceptibility mapping	RF, CDTree, BFTree, KLR	RF: AUC = 0.893
[383]	Groundwater salinity	Topographic, groundwater salinity data	Evaluation of groundwater salinity susceptibility maps	StoGB, RotFor, BGLM	BGLM: Kappa = 0.85
[384]	Heavy metals transfer	Soil and crop properties	Identification of factors related to heavy metals transfer	RF, GBM, GLM	RF: $R^2 = 0.17–0.84$
[385]	Land suitability	Soil properties, weather, topography data	Prediction of land suitability maps	SVM, RF	RF: Kappa = 0.77, overall acc = 0.79
[386]	SOC	Soil properties, satellite, simulated environmental data	Prediction of SOC	MLR, SVM, Cu, RF, ANN	RF: $R^2 = 0.68$
[387]	Electrical conductivity, SOC	Soil properties, weather data	Electrical conductivity and SOC prediction	GLM	(1) EC: MSPE = 0.686, MAPE = 0.635; (2) OC: MSPE = 0.413, MAPE = 0.474
[388]	SOC, soil moisture	Proximal spectral data, electrical conductivity, soil samples data	Prediction of SOC and soil moisture 3D maps	Cu, RF	Cu: $R^2 = 0.76$ , CCC = 0.84, RMSE = 0.38%



Table A7. Cont.

Ref	Property	Input Data	Functionality	Models/Algorithms	Best Output
[389]	Soil aggregate stability	Soil samples data	Prediction of soil aggregate stability	GLM, ANN	ANN: $R^2 = 0.82$
[390]	SOC	Soil samples, weather, topographic, satellite data	Prediction of SOC	Cu, RF, SVM, XGBoost, KNN	Best SOC prediction: RF: RMSE = 0.35%, $R^2 = 0.6$
[391]	Soil moisture	In situ soil moisture, satellite data	Estimation of surface soil moisture	SVM, RF, ANN, EN	RF: NSE = 0.73
[392]	SOC	Composite surface soil, satellite, weather data	Prediction of SOC	SVM, ANN, RT, RF, XGBoost, DNN	DNN: MAE = 0.59%, RMSE = 0.75%, $R^2 = 0.65$ , CCC = 0.83
[393]	Gully erosion	Topographic, weather, soil data	Mapping of gully erosion susceptibility	LMT, NBTree, ADTree	LMT: AUC = 0.944
[394]	Gully erosion	Satellite spectral data	Identification of gully erosion	LDA, SVM, RF	Best overall acc: RF: 98.7%
[395]	Gully erosion	Satellite, weather, land type maps data	Gully erosion mapping	LGR	Acc = 68%, Kappa = 0.42

ACCA: Aminocyclopropane-1-carboxylate; AUC: Area Under Curve; BP: Bacterial Population; CC: Coefficient of Correlation; CCC: Concordance Correlation Coefficient; CCE: Calcium Carbonate Equivalent; ET: Evaporotranspiration; MIR: Mid InfraRed; NSE: Nash-Sutcliffe model efficiency Coefficient; NIR: Near-InfraRed; PS: Phosphate Solubilization; PWP: Permanent Wilting Point; RPIQ: Ratio of Performance to Interquartile Range; RPD: Relative Percent Deviation; SOC: Soil Organic Carbon; WI: Willmott's Index.

Table A8. Livestock Management: Animal Welfare.

Ref	Animal	Input Data	Functionality	Models/Algorithms	Best Output
[396]	Swine	3D, 2D video images	Detection of pigs tail posture as a sign of tail biting	LMM	Low vs. not low tails: Acc = 73.9%, Sensitivity = 88.4%, Specificity = 66.8%
[397]	Sheep	Accelerometer and gyroscope attached to the ear and collar of sheep	Classification of Grazing and Rumination Behavior in Sheep	RF, SVM, KNN, Adaboost	RF: Highest overall acc: collar: 92%; ear: 91%
[398]	Sheep	Accelerometer, gyroscope data	Classification of sheep behavior (lying, standing and walking)	RF	Acc = 95%, F1-score = 91–97% for: ear: 32 Hz, 7 s, collar: 32 Hz, 5 s
[399]	Swine	RGB images	Recognition of pigs feeding behavior	CNN	Faster R-CNN: Precision = 99.6%, recall = 86.93% Faster R-CNN: Sow posture: (1) Recumbency: night: 92.9%, daytime: 84.1%; (2) Standing: at night: 0.4%, daytime: 10.5%; (3) Sitting: night: 0.55%, daytime: 3.4%
[400]	Swine	RGB images, depth images	Recognition of lactating sow postures	CNN	(1) Recumbency: night: 92.9%, daytime: 84.1%; (2) Standing: at night: 0.4%, daytime: 10.5%; (3) Sitting: night: 0.55%, daytime: 3.4%
[401]	Cattle, Sheep, sheepdog	Audio field recordings data	Classification of animals' vocalization	SVM	Acc: cattle: 95.78%, sheep: 99.29%, dogs: 99.67%
[402]	Cattle	Accelerometer data	Detection of sheep rumination.	SVM	Acc = 86.1%
[403]	Sheep	Ear-borne accelerometer data, observation recordings	Classification of grazed sheep behavior Scenario A: walking, standing, lying, grazing Scenario B: active/inactive Scenario C: body posture	CART, SVM, LDA, QDA	(1) Scenario A: SVM Acc: 76.9%; (2) Scenario B: CART Acc: 98.1%; (3) Scenario C: Acc: LDA 90.6%
[404]	Goat	On-farm videos, weather data	Classification of goats behavior (1) Anomaly detection (2) Feeding/non-feeding	KNN, SVR, CNN	(1) Most accurate: KNN: Acc = 95.02–96.5%; (2) Faster R-CNN: Eating: 55.91–61.33 %, Non-feeding (Resting): 79.91–81.53 %
[405]	Cattle, sheep	UAV Video data	Counting and classification of cattle, sheep	CNN	Mask R-CNN: Cattle: Acc = 96%; Sheep: Acc = 92%
[406]	Cattle	Accelerometer data	Prediction of dairy cows behavior at pasture	XGBoost, SVM, AdaBoost, RF	Best predictions for most behaviours: XGBoost: sensitivity = 0.78
[407]	Cattle	Pedometers	Detection of early lameness in dairy cattle	RF, KNN	RF: acc = 91%
[408]	Cattle	Environmental heat stressors data	Evaluation of heat stressors influence in dairy cows physiological responses	RF, GBM, ANN, PLR	RF: (1) RR: RMSE = 9.695 respmin <sup>-1</sup> ; (2) ST: RMSE = 0.334 °C
[409]	Cattle	Diets nutrient levels data	Prediction of dairy cows diet energy digestion	ELM, LR, ANN, SVM	Best performance: kernel-ELM: (1) DE: $R^2 = 0.8879$ , MAE = 4.0606; (2) ED: $R^2 = 0.899$ , MAE = 2.3272
[410]	Cattle	Routine herd data	Detection of lameness in dairy herds	GLM, RF, GBM, XGBoost, CART	GBM: AUC = 0.75, Sensitivity = 0.58, Specificity = 0.83

Table A8. Cont.

Ref	Animal	Input Data	Functionality	Models/Algorithms	Best Output
[411]	Poultry	Air quality data	Early prediction of Coccidiosis in poultry farms	KNN	AUC = 0.897–0.967
[412]	Cattle	On-farm questionnaires, clinical and milk records	Prediction of mastitis infection in dairy herds	RF	CONT vs. ENV: Acc = 95%, PPV = 100%, NPV = 95%
[413]	Cattle	Location (transceiver) and accelerometer data	Detection of dairy cows in estrus	KNN, LDA, CART, BPNN, KNN	BPNN: specificity = 85.71%
[414]	Cattle	Mid-NIR spectral data using spectrometer	Prediction of bovine tuberculosis in dairy cows	CNN	Accuracy = 71%, sensitivity = 0.79, specificity = 0.65
[415]	Cattle	Metabolomics data from serum samples	Evaluation of metabolotypes existence in overconditioned dairy cows	RF, NB, SMO, ADT	ADT: acc = 84.2%
[416]	Cattle	Accelerometer data	Classification of cows' behavior	GBDT, SVM, RF, KNN	GBDT: acc = 86.3%, sensitivity = 80.6%
[417]	Sheep	Gyroscope and accelerometer ear sensors	Detection of lame and non-lame sheep in three activities	RF, SVM, MLP, AdaBoost	RF: overall acc = 80%
[418]	Cattle	Activity and rumination data	Prediction of calving day in cattle	RNN, RF, LDA, KNN, SVM	RNN/LSTM: Sensitivity = 0.72, Specificity = 0.98

AUC: Area Under Curve; Cont: Contagious; DE: Digestible Energy; ED: Energy Digestibility; ENV: Environmental; DWT: Discrete Wavelet Transform; MFCCs: Mel-Frequency Cepstral Coefficients; NIR: Near InfraRed; NPV: Negative Predictive Value; PTZ: Pan-Tilt-Zoom; PPV: Positive Predictive Value; RGB: Red-Green-Blue; RR: Respiration Rate; ST: Skin Temperature.

Table A9. Livestock Management: Livestock Production.

Ref	Animal	Input Data	Functionality	Models/Algorithms	Best Output
[419]	Cattle	Depth images in situ BCS evaluation data	Estimation of BCS, Scenario A: HER = 0.25; Scenario B: HER = 0.5	CNN	Scenario A: Acc = 78%; Scenario B: Acc = 94%
[420]	Swine	Weather, physiological data	Prediction of piglets temperature Scenario A: skin-surface; Scenario B: hair-coat; Scenario C: core	DNN, GBR, RF, GLR	Best prediction: Scenario C: DNN: error = 0.36%
[421]	Poultry	Depth, RGB images data	Classification of flock of chickens' behavior Classification of cattle behaviour	CNN	Acc = 99.17%
[422]	Cattle	Accelerometer, observations recordings data	Scenario A: grazing; Scenario B: standing; Scenario C: ruminating	RF	Highest F-scores: RF: Scenario A: 0.914; Scenario B: 0.89; Scenario C: 0.932
[423]	Sheep	Phenotypic, weather data	Prediction of on-farm water and electricity consumption on pasture based Irish dairy farms	BAG, ANN, MT	Scenario 3: MT: R = 0.95, MAE = 0.88 $\mu$ m, RMSE = 1.19
[424]	Cattle	Milk production, environmental data	Prediction of on-farm water and electricity consumption on pasture based Irish dairy farms	CART, RF, ANN, SVM	Electricity consumption prediction: SVM: relative prediction error = 12%
[425]	Goat	RGB data	Detection of dairy goats from surveillance video	CNN	Faster R-CNN: Acc = 92.49 %
[426]	Cattle	Animal feed, machinery, milk yield data	Estimation of energy use targets for buffalo farms	ANN	30.5 % of total energy input can be saved if targeted inputs are followed ANN: Liveweight: R <sup>2</sup> = 0.7, RMSE = 42; CCW: R <sup>2</sup> = 0.88, RMSE = 14; SMY: R <sup>2</sup> = 0.72, RMSE = 14
[427]	Cattle	3D images data	Prediction of liveweight and carcass characteristics	ANN, SLR	MAE = 1.67, RMSE = 2.13, detection speed = 42 ms per image
[428]	Swine	RGB images	Detection and pig counting on farms	CNN	SVM: Neck weight: R <sup>2</sup> = 0.63, RMSE = 0.09 kg; HCW: R <sup>2</sup> = 0.84, RMSE = 0.64
[429]	Sheep	Biometric traits, body condition score data	Prediction of commercial meat cuts and carcass traits	MLR, ANN, SVR, BN	
[430]	Cattle	Data produced by REIMS	Prediction of beef attributes (muscle tenderness, production background, breed type and quality grade)	SVM, RF, KNN, LDA, PDA, XGBoost, LogitBoost, PLS-DA	Best Acc: SVM: 99%
[431]	Sheep	Carcass, live weight and environmental records	Estimation of sheep carcass traits (IMF, HCW, CTLEAN, GRFAT, LW)	DL, GBT, KNN, MT, RF	Highest prediction of all traits: RF: (1) IMF: R = 0.56, MAE = 0.74; (2) HCW: R = 0.88, MAE = 1.19; (3) CTLEAN: R = 0.88, MAE = 0.76
[432]	Swine	ADG, breed, MT, gender and BBFT	Identification of pigs' limb condition	RF, KNN, ANN, SVM, NB, GLM, Boost, LDA	RF: Acc = 0.8846, Kappa = 0.7693
[433]	Cattle	Activity, weather data	Prediction of cows protein and fat content, milk yield and actual concentrate feed intake, Scenario (1) only cows with similar heat tolerance; Scenario (2) all cows	ANN	(1) Scenario A: n = 116, 456; R = 0.87; slope = 0.76; (2) Scenario B: n = 665, 836; R = 0.86; slope = 0.74



Table A9. Cont.

Ref	Animal	Input Data	Functionality	Models/Algorithms	Best Output
[434]	Cattle	Animal behavior, feed intake, estrus events data	Detection of estrus in dairy heifers	GLM, ANN, RF	RF: Acc = 76.3–96.5%
[435]	Cattle	Infrared thermal images	Estimation of deep body temperature	LRM, QRM	Higher correlation: QRM: R <sup>2</sup> = 0.922
[436]	Cattle	Liveweight, biophysical measurements data	Prediction of Carcass traits and marbling score in beef cattle	LR, MLP, MT, RF, SVM	SVM: carcass weight: R = 0.945, MAE = 0.139; EMA: R = 0.676, MAE = 4.793; MS: R = 0.631, MAE = 1.11

ACFW: Adult Clean Fleece Weight; ADG: Average Daily Gain; AFD: Adult Fibre Diameter; AGFW: Adult Greasy Fleece Weight; ASL: Adult Staple Length; ASS: Adult Staple Strength; BBFT: Bacon/BackFat Thickness; BCS: Body Condition Score; CCW: Cold Carcass Weights; CTLEAN: Computed Tomography Lean Meat Yield; DBT: Deep Body Temperature; EMA: Eye Muscle Area; GWAS: Genome-Wide Association Studies; GRFAT: Greville Rule Fat Depth; HER: Human Error Range; IMF: IntraMuscular Fat; HCW: Hot Carcass Weight; LW: Loin Weight; MS: Marbling Score; MT: Muscle Thickness; REIMS: Rapid Evaporative Ionization Mass Spectrometry; RGB: Red-Green-Blue; SMY: Saleable Meat Yield.

Table A10. Abbreviations for machine learning models.

Abbreviation	Model
ANN	Artificial Neural Network
BM	Bayesian Models
DL	Deep Learning
DR	Dimensionality Reduction
DT	Decision Trees
EL	Ensemble Learning
IBM	Instance Based Models
SVM	Support Vector Machine

Table A11. Abbreviations for machine learning algorithms.

Abbreviation	Model	Model
AdaBoost	EL	Adaptive Boosting
ADT	DT	Alternating Decision Trees
ANFIS	ANN	Adaptive-Neuro Fuzzy Inference Systems
ARD	BM	Automatic Relevance Determination
Bayesian-ANN	ANN	Bayesian Artificial Neural Network
BAG	EL	Bagging Algorithm
BDT	DT	Bagging Decision Trees
BDL	BM,ANN	Bayesian Deep Learning
BET	EL	Bagged Ensemble Tree
BGLM	BM, Regression	Bayesian Generalized Linear Model
BLR	Regression	Binary Logistic Regression
BN	BM	Bayesian Network
BPNN	ANN	Back-Propagation Neural Networks
BRT	DT,EL	Boosted Regression Trees
BTC	EL	Boosted Trees Classifiers
CART	DT	Classification And Regression Trees
CCNN	ANN	Cascade Correlation Neural Networks
CDTree	DT	Credal Decision Trees
CNN	ANN	Convolutional Neural Networks
Cu	Regression	Cubist
DBN	ANN	Deep Belief Networks
DF	EL,SVM	Decision Fusion
DLS	Regression	Damped Least Squares
DNN	ANN	Deep Neural Networks
DTR	DT, Regression	Decision Tree Regression
EBT	DT,EL	Ensemble Bagged Trees
ERT	DT	Extremely Randomized Trees
ELM	ANN	Extreme Learning Machines
EN	Regression	Elastic Net
FCN	ANN	Fully Convolutional Networks
FIS	ANN	Fuzzy Inference System
FFNN	ANN	Feed Forward Neural Networks
GBM	EL	Gradient Boosting Model
GBT	DT	Gradient Tree Boosting
GBR	Regression	Gradient Boosted Regression
GBRT	DT, Regression	Gradient Boosted Regression Trees
GBDT	DT,EL	Gradient Boosted Decision Trees

Table A11. Cont.

Abbreviation	Model	Model
GLM	Regression	General Linear Model
GMDH	DR	Group Method of Data Handling
GNB	BM	Gaussian Naive Bayes
GP	BM	Gaussian Processes
GPR	BM	Gaussian Process Regression
GRNN	ANN	Generalized Regression Neural Networks
GWR	Regression	Geographically Weighted Regression
KM	IBM	K-Means
KNN	IBM	K-Nearest Neighbors
LASSO	Regression	Least Absolute Shrinkage and Selection Operator
LDA	DR	Linear Discriminant Analysis
LightGBM	EL	Light Gradient Boosting Machine
LMT	Regression, DT	Logistic Model Trees
LGR	Regression	LoGistic Regression
LMM	Regression	Linear Mixed Model
LR	Regression	Linear Regression
LSTM	ANN	Long-Short Term Memory
LogitBoost	EL	Logistic Boosting
M5Tree	DT	M5 model Trees
MANN	ANN	Modular Artificial Neural Networks
MARS	Regression	Multivariate Adaptive Regression Splines
MCS	EL	Multiple Classifier System
MKL	DR	Multiple Kernel Learning
MLP	ANN	Multi-Layer Perceptron
MLR	Regression	Multiple Linear Regression
MT	DT	Model Trees
NB	BM	Naive Bayes
NBTree	BM, DT	Naive Bayes Trees
NNL	IBM	Nearest Neighbor Learner
OLS	Regression	Ordinary Least Squares
PLSR	Regression	Partial Least Squares Regression
PLS-DA	Regression, DR	Partial Least Squares Discriminant Analysis
QC	Regression	Quadratic Classifier
QDA	DR	Quadratic Discriminant Analysis
QRM	Regression	Quadratic Regression Model
RBFN	ANN	Radial Basis Function Networks
REPtree	DT	Reduced Error Pruning Tree
RFC	EL	Randomizable Filtered Classifier
RFR	EL, Regression	Random Forest Regression
RNN	ANN	Recurrent Neural Network
RQL	Regression	Regression Quantile LASSO
RF	EL	Random Forest
Ross-IES	EL	Ross Iterative Ensemble Smoother
RotFor	EL	Rotation Forest
RVMR	Regression	Relevance Vector Machine Regression
SCFIS	ANN	Subtractive Clustering Fuzzy Inference System
STDA	DR	Stepwise Discriminant Analysis
SMO	SVM	Sequential Minimal Optimization
SMLR	Regression	Stepwise Multiple Linear Regression
SOM	DR	Self-Organising Maps
StoGB	EL	Stochastic Gradient Boosting
SVR	SVM	Support Vector Regression
TS-FNN	ANN	Takagi-Sugeno Fuzzy Neural Networks
XGBoost	EL	Extreme Gradient Boosting
WANN	ANN	Wavelet Artificial Neural Networks
WEL	EL	Weighted Ensemble Learning
WNN	IBM	Weighted Nearest Neighbors
WSL	EL	Weakly Supervised Learning

## References

- Thayer, A.; Vargas, A.; Castellanos, A.; Lafon, C.; McCarl, B.; Roelke, D.; Winemiller, K.; Lacher, T. Integrating Agriculture and Ecosystems to Find Suitable Adaptations to Climate Change. *Climate* **2020**, *8*, 10. [\[CrossRef\]](#)
- Nassani, A.A.; Awan, U.; Zaman, K.; Hyder, S.; Aldakhil, A.M.; Abro, M.M.Q. Management of natural resources and material pricing: Global evidence. *Resour. Policy* **2019**, *64*, 101500. [\[CrossRef\]](#)
- Conrad, Z.; Niles, M.T.; Neher, D.A.; Roy, E.D.; Tichenor, N.E.; Jahns, L. Relationship between food waste, diet quality, and environmental sustainability. *PLoS ONE* **2018**, *13*. [\[CrossRef\]](#)
- Benos, L.; Bechar, A.; Bochtis, D. Safety and ergonomics in human-robot interactive agricultural operations. *Biosyst. Eng.* **2020**, *200*, 55–72. [\[CrossRef\]](#)
- Lampridi, M.; Sørensen, C.; Bochtis, D. Agricultural Sustainability: A Review of Concepts and Methods. *Sustainability* **2019**, *11*, 5120. [\[CrossRef\]](#)
- Zecca, F. The Use of Internet of Things for the Sustainability of the Agricultural Sector: The Case of Climate Smart Agriculture. *Int. J. Civ. Eng. Technol.* **2019**, *10*, 494–501.

7. Sørensen, C.A.G.; Kateris, D.; Bochtis, D. ICT Innovations and Smart Farming. In *Communications in Computer and Information Science*; Springer: Berlin/Heidelberg, Germany, 2019; Volume 953, pp. 1–19.
8. Sonka, S. Big Data: Fueling the Next Evolution of Agricultural Innovation. *J. Innov. Manag.* **2016**, *4*, 114–136. [[CrossRef](#)]
9. Meng, T.; Jing, X.; Yan, Z.; Pedrycz, W. A survey on machine learning for data fusion. *Inf. Fusion* **2020**, *57*, 115–129. [[CrossRef](#)]
10. Evstatiev, B.I.; Gabrovska-Evstatieva, K.G. A review on the methods for big data analysis in agriculture. In Proceedings of the IOP Conference Series: Materials Science and Engineering, Borovets, Bulgaria, 26–29 November 2020; IOP Publishing Ltd.: Bristol, UK, 2020; Volume 1032, p. 012053.
11. Helm, J.M.; Swiergosz, A.M.; Haeberle, H.S.; Karnuta, J.M.; Schaffer, J.L.; Krebs, V.E.; Spitzer, A.I.; Ramkumar, P.N. Machine Learning and Artificial Intelligence: Definitions, Applications, and Future Directions. *Curr. Rev. Musculoskelet. Med.* **2020**, *13*, 69–76. [[CrossRef](#)]
12. Liakos, K.; Busato, P.; Moshou, D.; Pearson, S.; Bochtis, D. Machine Learning in Agriculture: A Review. *Sensors* **2018**, *18*, 2674. [[CrossRef](#)]
13. Abade, A.; Ferreira, P.; Vidal, F. Plant Diseases recognition on images using Convolutional Neural Networks: A Systematic Review. *arXiv* **2020**, arXiv:2009.04365.
14. Yashodha, G.; Shalini, D. An integrated approach for predicting and broadcasting tea leaf disease at early stage using IoT with machine learning—A review. *Mater. Today Proc.* **2020**. [[CrossRef](#)]
15. Yuan, Y.; Chen, L.; Wu, H.; Li, L. Advanced agricultural disease image recognition technologies: A review. *Inf. Process. Agric.* **2021**. [[CrossRef](#)]
16. Mayuri, K. Role of Image Processing and Machine Learning Techniques in Disease Recognition, Diagnosis and Yield Prediction of Crops: A Review. *Int. J. Adv. Res. Comput. Sci.* **2018**, *9*, 788–795.
17. Wang, A.; Zhang, W.; Wei, X. A review on weed detection using ground-based machine vision and image processing techniques. *Comput. Electron. Agric.* **2019**, *158*, 226–240. [[CrossRef](#)]
18. Su, W.-H. Advanced Machine Learning in Point Spectroscopy, RGB- and Hyperspectral-Imaging for Automatic Discriminations of Crops and Weeds: A Review. *Smart Cities* **2020**, *3*, 767–792. [[CrossRef](#)]
19. Chlingaryan, A.; Sukkarieh, S.; Whelan, B. Machine learning approaches for crop yield prediction and nitrogen status estimation in precision agriculture: A review. *Comput. Electron. Agric.* **2018**, *151*, 61–69. [[CrossRef](#)]
20. Van Klompenburg, T.; Kassahun, A.; Catal, C. Crop yield prediction using machine learning: A systematic literature review. *Comput. Electron. Agric.* **2020**, *177*, 105709. [[CrossRef](#)]
21. Pushpanathan, K.; Hanafi, M.; Mashohor, S.; Fazlil Ilahi, W.F. Machine learning in medicinal plants recognition: A review. *Artif. Intell. Rev.* **2021**, *54*, 305–327. [[CrossRef](#)]
22. Wäldchen, J.; Rzanny, M.; Seeland, M.; Mäder, P. Automated plant species identification—Trends and future directions. *PLoS Comput. Biol.* **2018**, *14*, e1005993. [[CrossRef](#)]
23. Virnodkar, S.S.; Pachghare, V.K.; Patil, V.C.; Jha, S.K. Remote sensing and machine learning for crop water stress determination in various crops: A critical review. *Precis. Agric.* **2020**, *21*, 1121–1155. [[CrossRef](#)]
24. Sun, A.Y.; Scanlon, B.R. How can Big Data and machine learning benefit environment and water management: A survey of methods, applications, and future directions. *Environ. Res. Lett.* **2019**, *14*, 73001. [[CrossRef](#)]
25. Li, N.; Ren, Z.; Li, D.; Zeng, L. Review: Automated techniques for monitoring the behaviour and welfare of broilers and laying hens: Towards the goal of precision livestock farming. *Animal* **2020**, *14*, 617–625. [[CrossRef](#)]
26. García, R.; Aguilar, J.; Toro, M.; Pinto, A.; Rodríguez, P. A systematic literature review on the use of machine learning in precision livestock farming. *Comput. Electron. Agric.* **2020**, *179*, 105826. [[CrossRef](#)]
27. Ellis, J.L.; Jacobs, M.; Dijkstra, J.; van Laar, H.; Cant, J.P.; Tulpan, D.; Ferguson, N. Review: Synergy between mechanistic modelling and data-driven models for modern animal production systems in the era of big data. *Animal* **2020**, *14*, s223–s237. [[CrossRef](#)]
28. Lovarelli, D.; Bacenetti, J.; Guarino, M. A review on dairy cattle farming: Is precision livestock farming the compromise for an environmental, economic and social sustainable production? *J. Clean. Prod.* **2020**, *262*, 121409. [[CrossRef](#)]
29. Patrício, D.I.; Rieder, R. Computer vision and artificial intelligence in precision agriculture for grain crops: A systematic review. *Comput. Electron. Agric.* **2018**, *153*, 69–81. [[CrossRef](#)]
30. Cravero, A.; Sepúlveda, S. Use and Adaptations of Machine Learning in Big Data—Applications in Real Cases in Agriculture. *Electronics* **2021**, *10*, 552. [[CrossRef](#)]
31. Ang, K.L.-M.; Seng, J.K.P. Big Data and Machine Learning with Hyperspectral Information in Agriculture. *IEEE Access* **2021**, *9*, 36699–36718. [[CrossRef](#)]
32. Jose, A.; Nandagopalan, S.; Venkata, C.M.; Akana, S. Artificial Intelligence Techniques for Agriculture Revolution: A Survey. *Ann. Rom. Soc. Cell Biol.* **2021**, *25*, 2580–2597.
33. Jung, J.; Maeda, M.; Chang, A.; Bhandari, M.; Ashapure, A.; Landivar-Bowles, J. The potential of remote sensing and artificial intelligence as tools to improve the resilience of agriculture production systems. *Curr. Opin. Biotechnol.* **2021**, *70*, 15–22. [[CrossRef](#)]
34. Vieira, S.; Lopez Pinaya, W.H.; Mechelli, A. *Introduction to Machine Learning*; Mechelli, A., Vieira, S.B.T.-M.L., Eds.; Academic Press: Cambridge, MA, USA, 2020; Chapter 1; pp. 1–20. ISBN 978-0-12-815739-8.
35. Domingos, P. A few useful things to know about machine learning. *Commun. ACM* **2012**, *55*, 78–87. [[CrossRef](#)]
36. Lopez-Arevalo, I.; Aldana-Bobadilla, E.; Molina-Villegas, A.; Galeana-Zapién, H.; Muñoz-Sánchez, V.; Gausin-Valle, S. A Memory-Efficient Encoding Method for Processing Mixed-Type Data on Machine Learning. *Entropy* **2020**, *22*, 1391. [[CrossRef](#)]

37. Anagnostis, A.; Papageorgiou, E.; Bochtis, D. Application of Artificial Neural Networks for Natural Gas Consumption Forecasting. *Sustainability* **2020**, *12*, 6409. [CrossRef]
38. Zheng, A.; Casari, A. *Feature Engineering for Machine Learning: Principles and Techniques for Data Scientists*; O'Reilly Media, Inc.: Sebastopol, CA, USA, 2018.
39. LeCun, Y.; Bengio, Y.; Hinton, G. Deep learning. *Nature* **2015**, *521*, 436–444. [CrossRef]
40. Kokkoti, C.; Moustakidis, S.; Papageorgiou, E.; Giakas, G.; Tsaopoulos, D.E. Machine learning in knee osteoarthritis: A review. *Osteoarthr. Cartil. Open* **2020**, *2*, 100069. [CrossRef]
41. Simeone, O. A Very Brief Introduction to Machine Learning With Applications to Communication Systems. *IEEE Trans. Cogn. Commun. Netw.* **2018**, *4*, 648–664. [CrossRef]
42. Choi, R.Y.; Coyner, A.S.; Kalpathy-Cramer, J.; Chiang, M.F.; Peter Campbell, J. Introduction to machine learning, neural networks, and deep learning. *Transl. Vis. Sci. Technol.* **2020**, *9*, 14. [CrossRef] [PubMed]
43. Cheng, Q.; Zhang, S.; Bo, S.; Chen, D.; Zhang, H. Augmented Reality Dynamic Image Recognition Technology Based on Deep Learning Algorithm. *IEEE Access* **2020**, *8*, 137370–137384. [CrossRef]
44. Anvarjon, T.; Mustaqeem; Kwon, S. Deep-Net: A Lightweight CNN-Based Speech Emotion Recognition System Using Deep Frequency Features. *Sensors* **2020**, *20*, 5212. [CrossRef]
45. Fujiyoshi, H.; Hirakawa, T.; Yamashita, T. Deep learning-based image recognition for autonomous driving. *IATSS Res.* **2019**, *43*, 244–252. [CrossRef]
46. Rai, A.K.; Dwivedi, R.K. Fraud Detection in Credit Card Data using Unsupervised Machine Learning Based Scheme. In Proceedings of the International Conference on Electronics and Sustainable Communication Systems (ICESC), Coimbatore, India, 2–4 July 2020; Institute of Electrical and Electronics Engineers Inc.: Piscataway, NJ, USA, 2020; pp. 421–426.
47. Carta, S.; Ferreira, A.; Podda, A.S.; Reforgiato Recupero, D.; Sanna, A. Multi-DQN: An ensemble of Deep Q-learning agents for stock market forecasting. *Expert Syst. Appl.* **2021**, *164*, 113820. [CrossRef]
48. Sofos, F.; Karakasidis, T.E. Machine Learning Techniques for Fluid Flows at the Nanoscale. *Fluids* **2021**, *6*, 96. [CrossRef]
49. Gangavarapu, T.; Jaidhar, C.D.; Chanduka, B. Applicability of machine learning in spam and phishing email filtering: Review and approaches. *Artif. Intell. Rev.* **2020**, *53*, 5019–5081. [CrossRef]
50. Lučin, I.; Grbić, L.; Čarija, Z.; Kranjčević, L. Machine-Learning Classification of a Number of Contaminant Sources in an Urban Water Network. *Sensors* **2021**, *21*, 245. [CrossRef]
51. Anagnostis, A.; Benos, L.; Tsaopoulos, D.; Tagarakis, A.; Tsolakis, N.; Bochtis, D. Human activity recognition through recurrent neural networks for human-robot interaction in agriculture. *Sensors* **2021**, *11*, 2188. [CrossRef]
52. Yvoz, S.; Petit, S.; Biju-Duval, L.; Cordeau, S. A framework to type crop management strategies within a production situation to improve the comprehension of weed communities. *Eur. J. Agron.* **2020**, *115*, 126009. [CrossRef]
53. Khaki, S.; Wang, L. Crop Yield Prediction Using Deep Neural Networks. *Front. Plant Sci.* **2019**, *10*, 621. [CrossRef]
54. Harvey, C.A.; Rakotobe, Z.L.; Rao, N.S.; Dave, R.; Razafimahatratra, H.; Rabarijohn, R.H.; Rajaofara, H.; MacKinnon, J.L. Extreme vulnerability of smallholder farmers to agricultural risks and climate change in Madagascar. *Philos. Trans. R. Soc. B Biol. Sci.* **2014**, *369*. [CrossRef]
55. Jim Isleib Signs and Symptoms of Plant Disease: Is It Fungal, Viral or Bacterial? Available online: [https://www.canr.msu.edu/news/signs\\_and\\_symptoms\\_of\\_plant\\_disease\\_is\\_it\\_fungal\\_viral\\_or\\_bacterial](https://www.canr.msu.edu/news/signs_and_symptoms_of_plant_disease_is_it_fungal_viral_or_bacterial) (accessed on 19 March 2021).
56. Zhang, J.; Rao, Y.; Man, C.; Jiang, Z.; Li, S. Identification of cucumber leaf diseases using deep learning and small sample size for agricultural Internet of Things. *Int. J. Distrib. Sens. Netw.* **2021**, *17*, 1–13. [CrossRef]
57. Anagnostis, A.; Tagarakis, A.C.; Asiminari, G.; Papageorgiou, E.; Kateris, D.; Moshou, D.; Bochtis, D. A deep learning approach for anthracnose infected trees classification in walnut orchards. *Comput. Electron. Agric.* **2021**, *182*, 105998. [CrossRef]
58. Islam, N.; Rashid, M.M.; Wibowo, S.; Xu, C.-Y.; Morshed, A.; Wasimi, S.A.; Moore, S.; Rahman, S.M. Early Weed Detection Using Image Processing and Machine Learning Techniques in an Australian Chilli Farm. *Agriculture* **2021**, *11*, 387. [CrossRef]
59. Slaughter, D.C.; Giles, D.K.; Downey, D. Autonomous robotic weed control systems: A review. *Comput. Electron. Agric.* **2008**, *61*, 63–78. [CrossRef]
60. Zhang, L.; Li, R.; Li, Z.; Meng, Y.; Liang, J.; Fu, L.; Jin, X.; Li, S. A Quadratic Traversal Algorithm of Shortest Weeding Path Planning for Agricultural Mobile Robots in Cornfield. *J. Robot.* **2021**, *2021*, 6633139. [CrossRef]
61. Bonnet, P.; Joly, A.; Goëau, H.; Champ, J.; Vignau, C.; Molino, J.-F.; Barthélémy, D.; Boujemaa, N. Plant identification: Man vs. machine. *Multimed. Tools Appl.* **2016**, *75*, 1647–1665. [CrossRef]
62. Seeland, M.; Rzanny, M.; Alaqraa, N.; Wäldchen, J.; Mäder, P. Plant species classification using flower images—A comparative study of local feature representations. *PLoS ONE* **2017**, *12*, e0170629. [CrossRef]
63. Zhang, S.; Huang, W.; Huang, Y.; Zhang, C. Plant species recognition methods using leaf image: Overview. *Neurocomputing* **2020**, *408*, 246–272. [CrossRef]
64. Papageorgiou, E.I.; Aggelopoulou, K.; Gemtos, T.A.; Nanos, G.D. Development and Evaluation of a Fuzzy Inference System and a Neuro-Fuzzy Inference System for Grading Apple Quality. *Appl. Artif. Intell.* **2018**, *32*, 253–280. [CrossRef]
65. Neupane, J.; Guo, W. Agronomic Basis and Strategies for Precision Water Management: A Review. *Agronomy* **2019**, *9*, 87. [CrossRef]
66. El Bilali, A.; Taleb, A.; Brouziyne, Y. Groundwater quality forecasting using machine learning algorithms for irrigation purposes. *Agric. Water Manag.* **2021**, *245*, 106625. [CrossRef]

67. Lu, Y.-C.; Sadler, E.J.; Camp, C.R. Economic Feasibility Study of Variable Irrigation of Corn Production in Southeast Coastal Plain. *J. Sustain. Agric.* **2005**, *26*, 69–81. [[CrossRef](#)]
68. Mauget, S.A.; Adhikari, P.; Leiker, G.; Baumhardt, R.L.; Thorp, K.R.; Ale, S. Modeling the effects of management and elevation on West Texas dryland cotton production. *Agric. For. Meteorol.* **2017**, *247*, 385–398. [[CrossRef](#)]
69. Chasek, P.; Safriel, U.; Shikongo, S.; Fuhrman, V.F. Operationalizing Zero Net Land Degradation: The next stage in international efforts to combat desertification? *J. Arid Environ.* **2015**, *112*, 5–13. [[CrossRef](#)]
70. Fournel, S.; Rousseau, A.N.; Laberge, B. Rethinking environment control strategy of confined animal housing systems through precision livestock farming. *Biosyst. Eng.* **2017**, *155*, 96–123. [[CrossRef](#)]
71. Salina, A.B.; Hassan, L.; Saharee, A.A.; Jajere, S.M.; Stevenson, M.A.; Ghazali, K. Assessment of knowledge, attitude, and practice on livestock traceability among cattle farmers and cattle traders in peninsular Malaysia and its impact on disease control. *Trop. Anim. Health Prod.* **2020**, *53*, 15. [[CrossRef](#)]
72. Akhigbe, B.I.; Munir, K.; Akinade, O.; Akanbi, L.; Oyedele, L.O. IoT Technologies for Livestock Management: A Review of Present Status, Opportunities, and Future Trends. *Big Data Cogn. Comput.* **2021**, *5*, 10. [[CrossRef](#)]
73. Wathes, C.M.; Kristensen, H.H.; Aerts, J.-M.; Berckmans, D. Is precision livestock farming an engineer’s daydream or nightmare, an animal’s friend or foe, and a farmer’s panacea or pitfall? *Comput. Electron. Agric.* **2008**, *64*, 2–10. [[CrossRef](#)]
74. Berckmans, D.; Guarino, M. From the Editors: Precision livestock farming for the global livestock sector. *Anim. Front.* **2017**, *7*, 4–5. [[CrossRef](#)]
75. PRISMA. Available online: <http://prisma-statement.org/prismastatement/flowdiagram.aspx> (accessed on 1 February 2021).
76. Labarrière, F.; Thomas, E.; Calistri, L.; Optasanu, V.; Gueugnon, M.; Ornetti, P.; Laroche, D. Machine Learning Approaches for Activity Recognition and/or Activity Prediction in Locomotion Assistive Devices—A Systematic Review. *Sensors* **2020**, *20*, 6345. [[CrossRef](#)]
77. Benos, L.; Stanev, D.; Spyrou, L.; Moustakas, K.; Tsaopoulos, D.E. A Review on Finite Element Modeling and Simulation of the Anterior Cruciate Ligament Reconstruction. *Front. Bioeng. Biotechnol.* **2020**, *8*. [[CrossRef](#)]
78. Mostafa, S.S.; Mendonça, F.; Ravelo-García, A.G.; Morgado-Dias, F. A Systematic Review of Detecting Sleep Apnea Using Deep Learning. *Sensors* **2019**, *19*, 4934. [[CrossRef](#)]
79. Anagnostis, A.; Asiminari, G.; Papageorgiou, E.; Bochtis, D. A Convolutional Neural Networks Based Method for Anthracnose Infected Walnut Tree Leaves Identification. *Appl. Sci.* **2020**, *10*, 469. [[CrossRef](#)]
80. De Myttenaere, A.; Golden, B.; Le Grand, B.; Rossi, F. Mean Absolute Percentage Error for regression models. *Neurocomputing* **2016**, *192*, 38–48. [[CrossRef](#)]
81. Lehmann, E.L.; Casella, N. *Theory of Point Estimation*, 2nd ed.; Springer: New York, NY, USA, 1998; ISBN 978-0-387-98502-2.
82. Hosseini, S.; Ivanov, D.; Dolgui, A. Review of quantitative methods for supply chain resilience analysis. *Transp. Res. Part E Logist. Transp. Rev.* **2019**, *125*, 285–307. [[CrossRef](#)]
83. Benos, L.; Tsaopoulos, D.; Bochtis, D. A review on ergonomics in agriculture. part I: Manual operations. *Appl. Sci.* **2020**, *10*, 1905. [[CrossRef](#)]
84. Benos, L.; Tsaopoulos, D.; Bochtis, D. A Review on Ergonomics in Agriculture. Part II: Mechanized Operations. *Appl. Sci.* **2020**, *10*, 3484. [[CrossRef](#)]
85. Chen, Y.-Y.; Lin, Y.-H.; Kung, C.-C.; Chung, M.-H.; Yen, I.-H. Design and Implementation of Cloud Analytics-Assisted Smart Power Meters Considering Advanced Artificial Intelligence as Edge Analytics in Demand-Side Management for Smart Homes. *Sensors* **2019**, *19*, 2047. [[CrossRef](#)] [[PubMed](#)]
86. Sadiq, R.; Rodriguez, M.J.; Mian, H.R. *Empirical Models to Predict Disinfection By-Products (DBPs) in Drinking Water: An Updated Review*, 2nd ed.; Nriagu, J.B.T.-E., Ed.; Elsevier: Oxford, UK, 2019; pp. 324–338. ISBN 978-0-444-63952-3.
87. De Oliveira, M.A.; Monteiro, A.V.; Vieira Filho, J. A New Structural Health Monitoring Strategy Based on PZT Sensors and Convolutional Neural Network. *Sensors* **2018**, *18*, 2955. [[CrossRef](#)] [[PubMed](#)]
88. Yang, B.; Ma, J.; Yao, X.; Cao, W.; Zhu, Y. Estimation of Leaf Nitrogen Content in Wheat Based on Fusion of Spectral Features and Deep Features from Near Infrared Hyperspectral Imagery. *Sensors* **2021**, *21*, 613. [[CrossRef](#)] [[PubMed](#)]
89. Sagi, O.; Rokach, L. Ensemble learning: A survey. *Wiley Interdiscip. Rev. Data Min. Knowl. Discov.* **2018**, *8*, e1249. [[CrossRef](#)]
90. Pisner, D.A.; Schnyer, D.M. *Support Vector Machine*; Mechelli, A., Vieira, S.B.T.-M.L., Eds.; Academic Press: Cambridge, MA, USA, 2020; Chapter 6; pp. 101–121. ISBN 978-0-12-815739-8.
91. Verhaeghe, H.; Nijssen, S.; Pesant, G.; Quimper, C.-G.; Schaus, P. Learning optimal decision trees using constraint programming. *Constraints* **2020**, *25*, 226–250. [[CrossRef](#)]
92. Khosravi, P.; Vergari, A.; Choi, Y.; Liang, Y.; Van den Broeck, G. Handling Missing Data in Decision Trees: A Probabilistic Approach. *arXiv* **2020**, arXiv:2006.16341.
93. FAO. Bread Wheat—Improvement and Production. Available online: <http://www.fao.org/3/y4011e/y4011e00.htm> (accessed on 24 February 2021).
94. UN. Food and Agriculture Organization Corporate Statistical Database (FAOSTAT) Crops/Regions/World List/Production Quantity (Pick Lists), Rice (Paddy). Available online: <http://www.fao.org/faostat/en/#data/QC> (accessed on 24 February 2021).
95. Badole, S.L.; Patil, K.Y.; Rangari, V.D. *Antihyperglycemic Activity of Bioactive Compounds from Soybeans*; Watson, R.R., Dokken, B.B.B.T.-G.I., Eds.; Academic Press: Boston, MA, USA, 2015; Chapter 18; pp. 225–227. ISBN 978-0-12-800093-9.



96. Moshou, D.; Bravo, C.; Oberti, R.; West, J.S.; Ramon, H.; Vougioukas, S.; Bochtis, D. Intelligent multi-sensor system for the detection and treatment of fungal diseases in arable crops. *Biosyst. Eng.* **2011**, *108*, 311–321. [[CrossRef](#)]
97. Abdullah, S.S.; Malek, M.A.; Abdullah, N.S.; Kisi, O.; Yap, K.S. Extreme Learning Machines: A new approach for prediction of reference evapotranspiration. *J. Hydrol.* **2015**, *527*, 184–195. [[CrossRef](#)]
98. Voroney, P. *Soils for Horse Pasture Management*; Sharpe, P.B.T.-H.P.M., Ed.; Academic Press: Cambridge, MA, USA, 2019; Chapter 4; pp. 65–79. ISBN 978-0-12-812919-7.
99. Gonzalez-Rivas, P.A.; Chauhan, S.S.; Ha, M.; Fegan, N.; Dunshea, F.R.; Warner, R.D. Effects of heat stress on animal physiology, metabolism, and meat quality: A review. *Meat Sci.* **2020**, *162*, 108025. [[CrossRef](#)]
100. Pomar, C.; Marcoux, M.; Gispert, M.; Font i Furnols, M.; Daumas, G. 21—Determining the lean content of pork carcasses. In *Woodhead Publishing Series in Food Science, Technology and Nutrition*; Kerry, J.P., Ledward, D.B.T.-I., Eds.; Woodhead Publishing: Cambridge, UK, 2009; pp. 493–518. ISBN 978-1-84569-343-5.
101. Chandra, M.A.; Bedi, S.S. Survey on SVM and their application in image classification. *Int. J. Inf. Technol.* **2018**. [[CrossRef](#)]
102. Emilien, A.-V.; Thomas, C.; Thomas, H. UAV & satellite synergies for optical remote sensing applications: A literature review. *Sci. Remote Sens.* **2021**, *3*, 100019. [[CrossRef](#)]
103. Kouadio, L.; Deo, R.C.; Byrareddy, V.; Adamowski, J.F.; Mushtaq, S.; Phuong Nguyen, V. Artificial intelligence approach for the prediction of Robusta coffee yield using soil fertility properties. *Comput. Electron. Agric.* **2018**, *155*, 324–338. [[CrossRef](#)]
104. Aghighi, H.; Azadbakht, M.; Ashourloo, D.; Shahrabi, H.S.; Radiom, S. Machine Learning Regression Techniques for the Silage Maize Yield Prediction Using Time-Series Images of Landsat 8 OLI. *IEEE J. Sel. Top. Appl. Earth Obs. Remote Sens.* **2018**, *11*, 4563–4577. [[CrossRef](#)]
105. Khanal, S.; Fulton, J.; Klopfenstein, A.; Douridas, N.; Shearer, S. Integration of high resolution remotely sensed data and machine learning techniques for spatial prediction of soil properties and corn yield. *Comput. Electron. Agric.* **2018**, *153*, 213–225. [[CrossRef](#)]
106. Haghverdi, A.; Washington-Allen, R.A.; Leib, B.G. Prediction of cotton lint yield from phenology of crop indices using artificial neural networks. *Comput. Electron. Agric.* **2018**, *152*, 186–197. [[CrossRef](#)]
107. Linker, R. Machine learning based analysis of night-time images for yield prediction in apple orchard. *Biosyst. Eng.* **2018**, *167*, 114–125. [[CrossRef](#)]
108. Ahmad, I.; Saeed, U.; Fahad, M.; Ullah, A.; Habib ur Rahman, M.; Ahmad, A.; Judge, J. Yield Forecasting of Spring Maize Using Remote Sensing and Crop Modeling in Faisalabad-Punjab Pakistan. *J. Indian Soc. Remote Sens.* **2018**, *46*, 1701–1711. [[CrossRef](#)]
109. Sayago, S.; Bocco, M. Crop yield estimation using satellite images: Comparison of linear and non-linear models. *AgriScientia* **2018**, *35*, 1–9. [[CrossRef](#)]
110. Akbar, A.; Kuanar, A.; Patnaik, J.; Mishra, A.; Nayak, S. Application of Artificial Neural Network modeling for optimization and prediction of essential oil yield in turmeric (*Curcuma longa* L.). *Comput. Electron. Agric.* **2018**, *148*, 160–178. [[CrossRef](#)]
111. Zeng, W.; Xu, C.; Gang, Z.H.A.O.; Wu, J.; Huang, J. Estimation of Sunflower Seed Yield Using Partial Least Squares Regression and Artificial Neural Network Models. *Pedosphere* **2018**, *28*, 764–774. [[CrossRef](#)]
112. Pourmohammadali, B.; Hosseinifard, S.J.; Hassan Salehi, M.; Shirani, H.; Esfandiarpour Boroujeni, I. Effects of soil properties, water quality and management practices on pistachio yield in Rafsanjan region, southeast of Iran. *Agric. Water Manag.* **2019**, *213*, 894–902. [[CrossRef](#)]
113. Maya Gopal, P.S.; Bhargavi, R. Performance Evaluation of Best Feature Subsets for Crop Yield Prediction Using Machine Learning Algorithms. *Appl. Artif. Intell.* **2019**, *33*, 621–642. [[CrossRef](#)]
114. Gómez, D.; Salvador, P.; Sanz, J.; Casanova, J.L. Potato Yield Prediction Using Machine Learning Techniques and Sentinel 2 Data. *Remote Sens.* **2019**, *11*, 1745. [[CrossRef](#)]
115. Cai, Y.; Guan, K.; Lobell, D.; Potgieter, A.B.; Wang, S.; Peng, J.; Xu, T.; Asseng, S.; Zhang, Y.; You, L.; et al. Integrating satellite and climate data to predict wheat yield in Australia using machine learning approaches. *Agric. For. Meteorol.* **2019**, *274*, 144–159. [[CrossRef](#)]
116. Kim, N.; Ha, K.-J.; Park, N.-W.; Cho, J.; Hong, S.; Lee, Y.-W. A Comparison Between Major Artificial Intelligence Models for Crop Yield Prediction: Case Study of the Midwestern United States, 2006–2015. *ISPRS Int. J. Geo-Inf.* **2019**, *8*, 240. [[CrossRef](#)]
117. Nevuuri, P.; Narra, N.; Lipping, T. Crop yield prediction with deep convolutional neural networks. *Comput. Electron. Agric.* **2019**, *163*, 104859. [[CrossRef](#)]
118. Chen, Y.; Lee, W.S.; Gan, H.; Peres, N.; Fraisse, C.; Zhang, Y.; He, Y. Strawberry Yield Prediction Based on a Deep Neural Network Using High-Resolution Aerial Orthoimages. *Remote Sens.* **2019**, *11*, 1584. [[CrossRef](#)]
119. Maya Gopal, P.S.; Bhargavi, R. A novel approach for efficient crop yield prediction. *Comput. Electron. Agric.* **2019**, *165*, 104968. [[CrossRef](#)]
120. Sun, J.; Di, L.; Sun, Z.; Shen, Y.; Lai, Z. County-level soybean yield prediction using deep CNN-LSTM model. *Sensors* **2019**, *19*, 4363. [[CrossRef](#)]
121. Kayad, A.; Sozzi, M.; Gatto, S.; Marinello, F.; Pirotti, F. Monitoring Within-Field Variability of Corn Yield using Sentinel-2 and Machine Learning Techniques. *Remote Sens.* **2019**, *11*, 2873. [[CrossRef](#)]
122. Gutiérrez, S.; Wendel, A.; Underwood, J. Spectral filter design based on in-field hyperspectral imaging and machine learning for mango ripeness estimation. *Comput. Electron. Agric.* **2019**, *164*, 104890. [[CrossRef](#)]

123. Filippi, P.; Jones, E.J.; Wimalathunge, N.S.; Somarathna, P.D.S.N.; Pozza, L.E.; Ugbaje, S.U.; Jephcott, T.G.; Paterson, S.E.; Whelan, B.M.; Bishop, T.F.A. An approach to forecast grain crop yield using multi-layered, multi-farm data sets and machine learning. *Precis. Agric.* **2019**, *20*, 1015–1029. [[CrossRef](#)]
124. Shidnal, S.; Latte, M.V.; Kapoor, A. Crop yield prediction: Two-tiered machine learning model approach. *Int. J. Inf. Technol.* **2019**, *1*–9. [[CrossRef](#)]
125. Yang, Q.; Shi, L.; Han, J.; Zha, Y.; Zhu, P. Deep convolutional neural networks for rice grain yield estimation at the ripening stage using UAV-based remotely sensed images. *Field Crop. Res.* **2019**, *235*, 142–153. [[CrossRef](#)]
126. Leroux, L.; Castets, M.; Baron, C.; Escorihuela, M.J.; Bégué, A.; Lo Seen, D. Maize yield estimation in West Africa from crop process-induced combinations of multi-domain remote sensing indices. *Eur. J. Agron.* **2019**, *108*, 11–26. [[CrossRef](#)]
127. Abrougui, K.; Gabsi, K.; Mercatoris, B.; Khemis, C.; Amami, R.; Chehaibi, S. Prediction of organic potato yield using tillage systems and soil properties by artificial neural network (ANN) and multiple linear regressions (MLR). *Soil Tillage Res.* **2019**, *190*, 202–208. [[CrossRef](#)]
128. Folberth, C.; Baklanov, A.; Balkovič, J.; Skalský, R.; Khabarov, N.; Obersteiner, M. Spatio-temporal downscaling of gridded crop model yield estimates based on machine learning. *Agric. For. Meteorol.* **2019**, *264*, 1–15. [[CrossRef](#)]
129. Schwalbert, R.A.; Amado, T.; Corassa, G.; Pott, L.P.; Prasad, P.V.V.; Ciampitti, I.A. Satellite-based soybean yield forecast: Integrating machine learning and weather data for improving crop yield prediction in southern Brazil. *Agric. For. Meteorol.* **2020**, *284*, 107886. [[CrossRef](#)]
130. Abbas, F.; Afzaal, H.; Farooque, A.A.; Tang, S. Crop yield prediction through proximal sensing and machine learning algorithms. *Agronomy* **2020**, *10*, 1046. [[CrossRef](#)]
131. Khosla, E.; Dharavath, R.; Priya, R. Crop yield prediction using aggregated rainfall-based modular artificial neural networks and support vector regression. *Environ. Dev. Sustain.* **2020**, *22*, 5687–5708. [[CrossRef](#)]
132. Han, J.; Zhang, Z.; Cao, J.; Luo, Y.; Zhang, L.; Li, Z.; Zhang, J. Prediction of Winter Wheat Yield Based on Multi-Source Data and Machine Learning in China. *Remote Sens.* **2020**, *12*, 236. [[CrossRef](#)]
133. Mupangwa, W.; Chipindu, L.; Nyagumbo, I.; Mkuhlani, S.; Sisito, G. Evaluating machine learning algorithms for predicting maize yield under conservation agriculture in Eastern and Southern Africa. *SN Appl. Sci.* **2020**, *2*, 1–14. [[CrossRef](#)]
134. Maimaitijiang, M.; Sagan, V.; Sidike, P.; Hartling, S.; Esposito, F.; Fritschi, F.B. Soybean yield prediction from UAV using multimodal data fusion and deep learning. *Remote Sens. Environ.* **2020**, *237*, 111599. [[CrossRef](#)]
135. Khaki, S.; Wang, L.; Archontoulis, S.V. A CNN-RNN Framework for Crop Yield Prediction. *Front. Plant Sci.* **2020**, *10*, 1750. [[CrossRef](#)]
136. Ballesteros, R.; Intrigliolo, D.S.; Ortega, J.F.; Ramírez-Cuesta, J.M.; Buesa, I.; Moreno, M.A. Vineyard yield estimation by combining remote sensing, computer vision and artificial neural network techniques. *Precis. Agric.* **2020**, *21*, 1242–1262. [[CrossRef](#)]
137. Son, N.T.; Chen, C.F.; Chen, C.R.; Guo, H.Y.; Cheng, Y.S.; Chen, S.L.; Lin, H.S.; Chen, S.H. Machine learning approaches for rice crop yield predictions using time-series satellite data in Taiwan. *Int. J. Remote Sens.* **2020**, *41*, 7868–7888. [[CrossRef](#)]
138. Barbosa, A.; Trevisan, R.; Hovakimyan, N.; Martin, N.F. Modeling yield response to crop management using convolutional neural networks. *Comput. Electron. Agric.* **2020**, *170*, 105197. [[CrossRef](#)]
139. Murali, P.; Revathy, R.; Balamurali, S.; Tayade, A.S. Integration of RNN with GARCH refined by whale optimization algorithm for yield forecasting: A hybrid machine learning approach. *J. Ambient Intell. Hum. Comput.* **2020**, 1–13. [[CrossRef](#)]
140. Kamir, E.; Waldner, F.; Hochman, Z. Estimating wheat yields in Australia using climate records, satellite image time series and machine learning methods. *ISPRS J. Photogramm. Remote Sens.* **2020**, *160*, 124–135. [[CrossRef](#)]
141. Saranya, C.P.; Nagarajan, N. Efficient agricultural yield prediction using metaheuristic optimized artificial neural network using Hadoop framework. *Soft Comput.* **2020**, *24*, 12659–12669. [[CrossRef](#)]
142. Kim, N.; Na, S.-I.; Park, C.-W.; Huh, M.; Oh, J.; Ha, K.-J.; Cho, J.; Lee, Y.-W. An Artificial Intelligence Approach to Prediction of Corn Yields under Extreme Weather Conditions Using Satellite and Meteorological Data. *Appl. Sci.* **2020**, *10*, 3785. [[CrossRef](#)]
143. Amaratunga, V.; Wickramasinghe, L.; Perera, A.; Jayasinghe, J.; Rathnayake, U.; Zhou, J.G. Artificial Neural Network to Estimate the Paddy Yield Prediction Using Climatic Data. *Math. Probl. Eng.* **2020**, *2020*. [[CrossRef](#)]
144. Shahhosseini, M.; Hu, G.; Archontoulis, S.V. Forecasting Corn Yield with Machine Learning Ensembles. *Front. Plant Sci.* **2020**, *11*, 1120. [[CrossRef](#)]
145. Mwaurea, J.L.; Kenduiywo, B.K. County level maize yield estimation using artificial neural network. *Model. Earth Syst. Environ.* **2020**, 1–8. [[CrossRef](#)]
146. Dang, C.; Liu, Y.; Yue, H.; Qian, J.X.; Zhu, R. Autumn Crop Yield Prediction using Data-Driven Approaches:- Support Vector Machines, Random Forest, and Deep Neural Network Methods. *Can. J. Remote Sens.* **2020**. [[CrossRef](#)]
147. Fu, Z.; Jiang, J.; Gao, Y.; Krienke, B.; Wang, M.; Zhong, K.; Cao, Q.; Tian, Y.; Zhu, Y.; Cao, W.; et al. Wheat Growth Monitoring and Yield Estimation based on Multi-Rotor Unmanned Aerial Vehicle. *Remote Sens.* **2020**, *12*, 508. [[CrossRef](#)]
148. Leo, S.; Migliorati, M.D.A.; Grace, P.R. Predicting within-field cotton yields using publicly available datasets and machine learning. *Agron. J.* **2020**, 1150–1163. [[CrossRef](#)]
149. Prasad, N.R.; Patel, N.R.; Danodia, A. Crop yield prediction in cotton for regional level using random forest approach. *Spat. Inf. Res.* **2020**, 1–12. [[CrossRef](#)]
150. Wan, L.; Cen, H.; Zhu, J.; Zhang, J.; Zhu, Y.; Sun, D.; Du, X.; Zhai, L.; Weng, H.; Li, Y.; et al. Grain yield prediction of rice using multi-temporal UAV-based RGB and multispectral images and model transfer—A case study of small farmlands in the South of China. *Agric. For. Meteorol.* **2020**, *291*, 108096. [[CrossRef](#)]

151. Eugenio, F.C.; Grohs, M.; Venancio, L.P.; Schuh, M.; Bottega, E.L.; Ruoso, R.; Schons, C.; Mallmann, C.L.; Badin, T.L.; Fernandes, P. Estimation of soybean yield from machine learning techniques and multispectral RPAS imagery. *Remote Sens. Appl. Soc. Environ.* **2020**, *20*, 100397. [[CrossRef](#)]
152. Salvador, P.; Gómez, D.; Sanz, J.; Casanova, J.L. Estimation of Potato Yield Using Satellite Data at a Municipal Level: A Machine Learning Approach. *ISPRS Int. J. Geo-Inf.* **2020**, *9*, 343. [[CrossRef](#)]
153. Rahman, M.M.; Robson, A. Integrating Landsat-8 and Sentinel-2 Time Series Data for Yield Prediction of Sugarcane Crops at the Block Level. *Remote Sens.* **2020**, *12*, 1313. [[CrossRef](#)]
154. Ashapure, A.; Jung, J.; Chang, A.; Oh, S.; Yeom, J.; Maeda, M.; Maeda, A.; Dube, N.; Landivar, J.; Hague, S.; et al. Developing a machine learning based cotton yield estimation framework; using multi-temporal UAS data. *ISPRS J. Photogramm. Remote Sens.* **2020**, *169*, 180–194. [[CrossRef](#)]
155. Nesarani, A.; Ramar, R.; Pandian, S. An efficient approach for rice prediction from authenticated Block chain node using machine learning technique. *Environ. Technol. Innov.* **2020**, *20*, 101064. [[CrossRef](#)]
156. Barzin, R.; Pathak, R.; Lotfi, H.; Varco, J.; Bora, G.C. Use of UAS Multispectral Imagery at Different Physiological Stages for Yield Prediction and Input Resource Optimization in Corn. *Remote Sens.* **2020**, *12*, 2392. [[CrossRef](#)]
157. Sun, J.; Lai, Z.; Di, L.; Sun, Z.; Tao, J.; Shen, Y. Multilevel Deep Learning Network for County-Level Corn Yield Estimation in the U.S. Corn Belt. *IEEE J. Sel. Top. Appl. Earth Obs. Remote Sens.* **2020**, *13*, 5048–5060. [[CrossRef](#)]
158. Jiang, Z.; Liu, C.; Ganapathysubramanian, B.; Hayes, D.J.; Sarkar, S. Predicting county-scale maize yields with publicly available data. *Sci. Rep.* **2020**, *10*, 1–12. [[CrossRef](#)]
159. Elavarasan, D.; Vincent P M, D.R.; Srinivasan, K.; Chang, C.-Y. A Hybrid CFS Filter and RF-RFE Wrapper-Based Feature Extraction for Enhanced Agricultural Crop Yield Prediction Modeling. *Agriculture* **2020**, *10*, 400. [[CrossRef](#)]
160. Feng, L.; Zhang, Z.; Ma, Y.; Du, Q.; Williams, P.; Drewry, J.; Luck, B. Alfalfa Yield Prediction Using UAV-Based Hyperspectral Imagery and Ensemble Learning. *Remote Sens.* **2020**, *12*, 2828. [[CrossRef](#)]
161. Guo, Y.; Wang, H.; Wu, Z.; Wang, S.; Sun, H.; Senthilnath, J.; Wang, J.; Robin Bryant, C.; Fu, Y. Modified Red Blue Vegetation Index for Chlorophyll Estimation and Yield Prediction of Maize from Visible Images Captured by UAV. *Sensors* **2020**, *20*, 55. [[CrossRef](#)]
162. Khan, M.S.; Semwal, M.; Sharma, A.; Verma, R.K. An artificial neural network model for estimating Mentha crop biomass yield using Landsat 8 OLI. *Precis. Agric.* **2020**, *21*, 18–33. [[CrossRef](#)]
163. Zhou, X.; Kono, Y.; Win, A.; Matsui, T.; Tanaka, T.S.T. Predicting within-field variability in grain yield and protein content of winter wheat using UAV-based multispectral imagery and machine learning approaches. *Plant Prod. Sci.* **2020**, 1–15. [[CrossRef](#)]
164. Marques Ramos, A.P.; Prado Osco, L.; Elis Garcia Furuya, D.; Nunes Gonçalves, W.; Cordeiro Santana, D.; Pereira Ribeiro Teodoro, L.; Antonio da Silva Junior, C.; Fernando Capristo-Silva, G.; Li, J.; Henrique Rojo Baio, F.; et al. A random forest ranking approach to predict yield in maize with uav-based vegetation spectral indices. *Comput. Electron. Agric.* **2020**, *178*, 105791. [[CrossRef](#)]
165. Sun, C.; Feng, L.; Zhang, Z.; Ma, Y.; Crosby, T.; Naber, M.; Wang, Y. Prediction of End-Of-Season Tuber Yield and Tuber Set in Potatoes Using In-Season UAV-Based Hyperspectral Imagery and Machine Learning. *Sensors* **2020**, *20*, 5293. [[CrossRef](#)]
166. Wei, M.C.F.; Maldaner, L.F.; Ottoni, P.M.N.; Molin, J.P. Carrot Yield Mapping: A Precision Agriculture Approach Based on Machine Learning. *AI* **2020**, *1*, 229–241. [[CrossRef](#)]
167. Da Silva, E.E.; Rojo Baio, F.H.; Ribeiro Teodoro, L.P.; da Silva Junior, C.A.; Borges, R.S.; Teodoro, P.E. UAV-multispectral and vegetation indices in soybean grain yield prediction based on in situ observation. *Remote Sens. Appl. Soc. Environ.* **2020**, *18*, 100318. [[CrossRef](#)]
168. Wang, X.; Huang, J.; Feng, Q.; Yin, D. Winter Wheat Yield Prediction at County Level and Uncertainty Analysis in Main Wheat-Producing Regions of China with Deep Learning Approaches. *Remote Sens.* **2020**, *12*, 1744. [[CrossRef](#)]
169. Li, B.; Xu, X.; Zhang, L.; Han, J.; Bian, C.; Li, G.; Liu, J.; Jin, L. Above-ground biomass estimation and yield prediction in potato by using UAV-based RGB and hyperspectral imaging. *ISPRS J. Photogramm. Remote Sens.* **2020**, *162*, 161–172. [[CrossRef](#)]
170. Wang, Y.; Zhang, Z.; Feng, L.; Du, Q.; Runge, T. Combining Multi-Source Data and Machine Learning Approaches to Predict Winter Wheat Yield in the Conterminous United States. *Remote Sens.* **2020**, *12*, 1232. [[CrossRef](#)]
171. Ferentinos, K.P. Deep learning models for plant disease detection and diagnosis. *Comput. Electron. Agric.* **2018**. [[CrossRef](#)]
172. Pineda, M.; Pérez-Bueno, M.L.; Barón, M. Detection of Bacterial Infection in Melon Plants by Classification Methods Based on Imaging Data. *Front. Plant Sci.* **2018**, *9*, 164. [[CrossRef](#)]
173. Fuentes, A.F.; Yoon, S.; Lee, J.; Park, D.S. High-Performance Deep Neural Network-Based Tomato Plant Diseases and Pests Diagnosis System with Refinement Filter Bank. *Front. Plant Sci.* **2018**, *9*, 1162. [[CrossRef](#)]
174. Abdulridha, J.; Ampatzidis, Y.; Ehsani, R.; de Castro, A.I. Evaluating the performance of spectral features and multivariate analysis tools to detect laurel wilt disease and nutritional deficiency in avocado. *Comput. Electron. Agric.* **2018**, *155*, 203–211. [[CrossRef](#)]
175. Barbedo, J.G.A. Factors influencing the use of deep learning for plant disease recognition. *Biosyst. Eng.* **2018**, *172*, 84–91. [[CrossRef](#)]
176. Tamouridou, A.; Pantazi, X.; Alexandridis, T.; Lagopodi, A.; Kontouris, G.; Moshou, D. Spectral Identification of Disease in Weeds Using Multilayer Perceptron with Automatic Relevance Determination. *Sensors* **2018**, *18*, 2770. [[CrossRef](#)]
177. Lu, J.; Ehsani, R.; Shi, Y.; de Castro, A.I.; Wang, S. Detection of multi-tomato leaf diseases (late blight, target and bacterial spots) in different stages by using a spectral-based sensor. *Sci. Rep.* **2018**, *8*, 1–11. [[CrossRef](#)]
178. Zhang, X.; Qiao, Y.; Meng, F.; Fan, C.; Zhang, M. Identification of maize leaf diseases using improved deep convolutional neural networks. *IEEE Access* **2018**, *6*, 30370–30377. [[CrossRef](#)]



179. Chouhan, S.S.; Kaul, A.; Singh, U.P.; Jain, S. Bacterial foraging optimization based radial basis function neural network (BRBFNN) for identification and classification of plant leaf diseases: An automatic approach towards plant pathology. *IEEE Access* **2018**, *6*, 8852–8863. [[CrossRef](#)]
180. Sharif, M.; Khan, M.A.; Iqbal, Z.; Azam, M.F.; Lali, M.I.U.; Javed, M.Y. Detection and classification of citrus diseases in agriculture based on optimized weighted segmentation and feature selection. *Comput. Electron. Agric.* **2018**, *150*, 220–234. [[CrossRef](#)]
181. Kerkech, M.; Hafiane, A.; Canals, R. Deep leaning approach with colorimetric spaces and vegetation indices for vine diseases detection in UAV images. *Comput. Electron. Agric.* **2018**, *155*, 237–243. [[CrossRef](#)]
182. Kaur, S.; Pandey, S.; Goel, S. Semi-automatic leaf disease detection and classification system for soybean culture. *IET Image Process.* **2018**, *12*, 1038–1048. [[CrossRef](#)]
183. Coulibaly, S.; Kamsu-Foguem, B.; Kamissoko, D.; Traore, D. Deep neural networks with transfer learning in millet crop images. *Comput. Ind.* **2019**, *108*, 115–120. [[CrossRef](#)]
184. Wu, H.; Wiesner-Hanks, T.; Stewart, E.L.; DeChant, C.; Kaczmar, N.; Gore, M.A.; Nelson, R.J.; Lipson, H. Autonomous Detection of Plant Disease Symptoms Directly from Aerial Imagery. *Plant Phenome J.* **2019**, *2*, 1–9. [[CrossRef](#)]
185. Huang, H.; Deng, J.; Lan, Y.; Yang, A.; Zhang, L.; Wen, S.; Zhang, H.; Zhang, Y.; Deng, Y. Detection of Helminthosporium Leaf Blotch Disease Based on UAV Imagery. *Appl. Sci.* **2019**, *9*, 558. [[CrossRef](#)]
186. Abdulridha, J.; Ehsani, R.; Abd-Elrahman, A.; Ampatzidis, Y. A remote sensing technique for detecting laurel wilt disease in avocado in presence of other biotic and abiotic stresses. *Comput. Electron. Agric.* **2019**, *156*, 549–557. [[CrossRef](#)]
187. Dhingra, G.; Kumar, V.; Joshi, H.D. A novel computer vision based neutrosophic approach for leaf disease identification and classification. *Meas. J. Int. Meas. Confed.* **2019**, *135*, 782–794. [[CrossRef](#)]
188. Arnal Barbedo, J.G. Plant disease identification from individual lesions and spots using deep learning. *Biosyst. Eng.* **2019**, *180*, 96–107. [[CrossRef](#)]
189. Hu, G.; Wu, H.; Zhang, Y.; Wan, M. A low shot learning method for tea leaf's disease identification. *Comput. Electron. Agric.* **2019**, *163*, 104852. [[CrossRef](#)]
190. Zhang, X.; Han, L.; Dong, Y.; Shi, Y.; Huang, W.; Han, L.; González-Moreno, P.; Ma, H.; Ye, H.; Sobeih, T. A Deep Learning-Based Approach for Automated Yellow Rust Disease Detection from High-Resolution Hyperspectral UAV Images. *Remote Sens.* **2019**, *11*, 1554. [[CrossRef](#)]
191. Cruz, A.; Ampatzidis, Y.; Pierro, R.; Materazzi, A.; Panattoni, A.; De Bellis, L.; Luvisi, A. Detection of grapevine yellows symptoms in *Vitis vinifera* L. with artificial intelligence. *Comput. Electron. Agric.* **2019**, *157*, 63–76. [[CrossRef](#)]
192. Wiesner-Hanks, T.; Wu, H.; Stewart, E.; DeChant, C.; Kaczmar, N.; Lipson, H.; Gore, M.A.; Nelson, R.J. Millimeter-Level Plant Disease Detection from Aerial Photographs via Deep Learning and Crowdsourced Data. *Front. Plant Sci.* **2019**, *10*, 1550. [[CrossRef](#)]
193. Ozguven, M.M.; Adem, K. Automatic detection and classification of leaf spot disease in sugar beet using deep learning algorithms. *Phys. A Stat. Mech. Appl.* **2019**, *535*, 122537. [[CrossRef](#)]
194. Geetharamani, G.; Arun Pandian, J. Identification of plant leaf diseases using a nine-layer deep convolutional neural network. *Comput. Electr. Eng.* **2019**, *76*, 323–338. [[CrossRef](#)]
195. Sultan Mahmud, M.; Zaman, Q.U.; Esau, T.J.; Price, G.W.; Prithiviraj, B. Development of an artificial cloud lighting condition system using machine vision for strawberry powdery mildew disease detection. *Comput. Electron. Agric.* **2019**, *158*, 219–225. [[CrossRef](#)]
196. Arsenovic, M.; Karanovic, M.; Sladojevic, S.; Anderla, A.; Stefanovic, D. Solving Current Limitations of Deep Learning Based Approaches for Plant Disease Detection. *Symmetry* **2019**, *11*, 939. [[CrossRef](#)]
197. Abdulridha, J.; Batuman, O.; Ampatzidis, Y. UAV-based remote sensing technique to detect citrus canker disease utilizing hyperspectral imaging and machine learning. *Remote Sens.* **2019**, *11*, 1373. [[CrossRef](#)]
198. Pantazi, X.E.; Moshou, D.; Tamouridou, A.A. Automated leaf disease detection in different crop species through image features analysis and One Class Classifiers. *Comput. Electron. Agric.* **2019**, *156*, 96–104. [[CrossRef](#)]
199. Picon, A.; Alvarez-Gila, A.; Seitz, M.; Ortiz-Barredo, A.; Echazarra, J.; Johannes, A. Deep convolutional neural networks for mobile capture device-based crop disease classification in the wild. *Comput. Electron. Agric.* **2019**, *161*, 280–290. [[CrossRef](#)]
200. Al-Saddik, H.; Simon, J.C.; Cointault, F. Assessment of the optimal spectral bands for designing a sensor for vineyard disease detection: The case of 'Flavescence dorée'. *Precis. Agric.* **2019**, *20*, 398–422. [[CrossRef](#)]
201. Habib, M.T.; Majumder, A.; Jakaria, A.Z.M.; Akter, M.; Uddin, M.S.; Ahmed, F. Machine vision based papaya disease recognition. *J. King Saud Univ. Comput. Inf. Sci.* **2020**, *32*, 300–309. [[CrossRef](#)]
202. Ramesh, S.; Vydeki, D. Recognition and classification of paddy leaf diseases using Optimized Deep Neural network with Jaya algorithm. *Inf. Process. Agric.* **2020**, *7*, 249–260. [[CrossRef](#)]
203. Abdulridha, J.; Ampatzidis, Y.; Kakarla, S.C.; Roberts, P. Detection of target spot and bacterial spot diseases in tomato using UAV-based and benchtop-based hyperspectral imaging techniques. *Precis. Agric.* **2020**, *21*, 955–978. [[CrossRef](#)]
204. Abdulridha, J.; Ampatzidis, Y.; Roberts, P.; Kakarla, S.C. Detecting powdery mildew disease in squash at different stages using UAV-based hyperspectral imaging and artificial intelligence. *Biosyst. Eng.* **2020**, *197*, 135–148. [[CrossRef](#)]
205. Abdulridha, J.; Ampatzidis, Y.; Qureshi, J.; Roberts, P. Laboratory and UAV-based identification and classification of tomato yellow leaf curl, bacterial spot, and target spot diseases in tomato utilizing hyperspectral imaging and machine learning. *Remote Sens.* **2020**, *12*, 2732. [[CrossRef](#)]
206. Agarwal, M.; Gupta, S.K.; Biswas, K.K. Development of Efficient CNN model for Tomato crop disease identification. *Sustain. Comput. Inform. Syst.* **2020**, *28*, 100407. [[CrossRef](#)]

207. Cristin, R.; Kumar, B.S.; Priya, C.; Karthick, K. Deep neural network based Rider-Cuckoo Search Algorithm for plant disease detection. *Artif. Intell. Rev.* **2020**, *53*, 4993–5018. [[CrossRef](#)]
208. Kerkech, M.; Hafiane, A.; Canals, R. Vine disease detection in UAV multispectral images using optimized image registration and deep learning segmentation approach. *Comput. Electron. Agric.* **2020**, *174*, 105446. [[CrossRef](#)]
209. Li, D.; Wang, R.; Xie, C.; Liu, L.; Zhang, J.; Li, R.; Wang, F.; Zhou, M.; Liu, W. A Recognition Method for Rice Plant Diseases and Pests Video Detection Based on Deep Convolutional Neural Network. *Sensors* **2020**, *20*, 578. [[CrossRef](#)]
210. Sambasivam, G.; Opiyo, G.D. A predictive machine learning application in agriculture: Cassava disease detection and classification with imbalanced dataset using convolutional neural networks. *Egypt. Inform. J.* **2020**. [[CrossRef](#)]
211. Gomez Selvaraj, M.; Vergara, A.; Montenegro, F.; Alonso Ruiz, H.; Safari, N.; Raymaekers, D.; Ocimati, W.; Ntamwira, J.; Tits, L.; Omondi, A.B.; et al. Detection of banana plants and their major diseases through aerial images and machine learning methods: A case study in DR Congo and Republic of Benin. *ISPRS J. Photogramm. Remote Sens.* **2020**, *169*, 110–124. [[CrossRef](#)]
212. Karthik, R.; Hariharan, M.; Anand, S.; Mathikshara, P.; Johnson, A.; Menaka, R. Attention embedded residual CNN for disease detection in tomato leaves. *Appl. Soft Comput. J.* **2020**, *86*, 105933. [[CrossRef](#)]
213. Karadağ, K.; Tenekeci, M.E.; Taşaltın, R.; Bilgili, A. Detection of pepper fusarium disease using machine learning algorithms based on spectral reflectance. *Sustain. Comput. Inform. Syst.* **2020**, *28*, 100299. [[CrossRef](#)]
214. Sharma, P.; Berwal, Y.P.S.; Ghai, W. Performance analysis of deep learning CNN models for disease detection in plants using image segmentation. *Inf. Process. Agric.* **2020**, *7*, 566–574. [[CrossRef](#)]
215. Lan, Y.; Huang, Z.; Deng, X.; Zhu, Z.; Huang, H.; Zheng, Z.; Lian, B.; Zeng, G.; Tong, Z. Comparison of machine learning methods for citrus greening detection on UAV multispectral images. *Comput. Electron. Agric.* **2020**, *171*, 105234. [[CrossRef](#)]
216. Khalili, E.; Kouchaki, S.; Ramazi, S.; Ghanati, F. Machine Learning Techniques for Soybean Charcoal Rot Disease Prediction. *Front. Plant Sci.* **2020**, *11*, 2009. [[CrossRef](#)]
217. Zhang, Z.; Flores, P.; Igathinathane, C.; Naik, D.L.; Kiran, R.; Ransom, J.K. Wheat Lodging Detection from UAS Imagery Using Machine Learning Algorithms. *Remote Sens.* **2020**, *12*, 1838. [[CrossRef](#)]
218. Bhatia, A.; Chug, A.; Prakash Singh, A. Application of extreme learning machine in plant disease prediction for highly imbalanced dataset. *J. Stat. Manag. Syst.* **2020**, *23*, 1059–1068. [[CrossRef](#)]
219. Karlekar, A.; Seal, A. SoyNet: Soybean leaf diseases classification. *Comput. Electron. Agric.* **2020**, *172*, 105342. [[CrossRef](#)]
220. Abdu, A.M.; Mokji, M.M.; Sheikh, U.U. Automatic vegetable disease identification approach using individual lesion features. *Comput. Electron. Agric.* **2020**, *176*, 105660. [[CrossRef](#)]
221. Hernández, S.; López, J.L. Uncertainty quantification for plant disease detection using Bayesian deep learning. *Appl. Soft Comput. J.* **2020**, *96*, 106597. [[CrossRef](#)]
222. Da Rocha Miranda, J.; de Carvalho Alves, M.; Ampelio Pozza, E.; Santos Neto, H. Detection of coffee berry necrosis by digital image processing of landsat 8 oli satellite imagery. *Int. J. Appl. Earth Obs. Geoinf.* **2020**, *85*, 101983. [[CrossRef](#)]
223. Zhang, Y.; Song, C.; Zhang, D. Deep Learning-Based Object Detection Improvement for Tomato Disease. *IEEE Access* **2020**, *8*, 56607–56614. [[CrossRef](#)]
224. Darwish, A.; Ezzat, D.; Hassanien, A.E. An optimized model based on convolutional neural networks and orthogonal learning particle swarm optimization algorithm for plant diseases diagnosis. *Swarm Evol. Comput.* **2020**, *52*, 100616. [[CrossRef](#)]
225. Xie, X.; Ma, Y.; Liu, B.; He, J.; Li, S.; Wang, H. A Deep-Learning-Based Real-Time Detector for Grape Leaf Diseases Using Improved Convolutional Neural Networks. *Front. Plant Sci.* **2020**, *11*, 751. [[CrossRef](#)]
226. Chen, M.; Brun, F.; Raynal, M.; Makowski, D. Forecasting severe grape downy mildew attacks using machine learning. *PLoS ONE* **2020**, *15*, e0230254. [[CrossRef](#)]
227. Sun, J.; Yang, Y.; He, X.; Wu, X. Northern Maize Leaf Blight Detection under Complex Field Environment Based on Deep Learning. *IEEE Access* **2020**, *8*, 33679–33688. [[CrossRef](#)]
228. Kim, W.S.; Lee, D.H.; Kim, Y.J. Machine vision-based automatic disease symptom detection of onion downy mildew. *Comput. Electron. Agric.* **2020**, *168*, 105099. [[CrossRef](#)]
229. Velásquez, D.; Sánchez, A.; Sarmiento, S.; Toro, M.; Maiza, M.; Sierra, B. A Method for Detecting Coffee Leaf Rust through Wireless Sensor Networks, Remote Sensing, and Deep Learning: Case Study of the Caturra Variety in Colombia. *Appl. Sci.* **2020**, *10*, 697. [[CrossRef](#)]
230. Verma, S.; Chug, A.; Singh, A.P. Application of convolutional neural networks for evaluation of disease severity in tomato plant. *J. Discret. Math. Sci. Cryptogr.* **2020**, *23*, 273–282. [[CrossRef](#)]
231. He, Y.; Zhou, Z.; Tian, L.; Liu, Y.; Luo, X. Brown rice planthopper (*Nilaparvata lugens* Stal) detection based on deep learning. *Precis. Agric.* **2020**, *21*, 1385–1402. [[CrossRef](#)]
232. Kerkech, M.; Hafiane, A.; Canals, R. VddNet: Vine Disease Detection Network Based on Multispectral Images and Depth Map. *Remote Sens.* **2020**, *12*, 3305. [[CrossRef](#)]
233. Yan, Q.; Yang, B.; Wang, W.; Wang, B.; Chen, P.; Zhang, J. Apple Leaf Diseases Recognition Based on An Improved Convolutional Neural Network. *Sensors* **2020**, *20*, 3535. [[CrossRef](#)] [[PubMed](#)]
234. Wang, T.; Thomasson, J.A.; Yang, C.; Isakeit, T.; Nichols, R.L. Automatic Classification of Cotton Root Rot Disease Based on UAV Remote Sensing. *Remote Sens.* **2020**, *12*, 1310. [[CrossRef](#)]
235. Ahmad, J.; Muhammad, K.; Ahmad, I.; Ahmad, W.; Smith, M.L.; Smith, L.N.; Jain, D.K.; Wang, H.; Mehmood, I. Visual features based boosted classification of weeds for real-time selective herbicide sprayer systems. *Comput. Ind.* **2018**, *98*, 23–33. [[CrossRef](#)]

236. Bah, M.D.; Hafiane, A.; Canals, R. Deep learning with unsupervised data labeling for weed detection in line crops in UAV images. *Remote Sens.* **2018**, *10*, 1690. [\[CrossRef\]](#)
237. Bakhshipour, A.; Jafari, A. Evaluation of support vector machine and artificial neural networks in weed detection using shape features. *Comput. Electron. Agric.* **2018**, *145*, 153–160. [\[CrossRef\]](#)
238. Barrero, O.; Perdomo, S.A. RGB and multispectral UAV image fusion for Gramineae weed detection in rice fields. *Precis. Agric.* **2018**, *19*, 809–822. [\[CrossRef\]](#)
239. Chavan, T.R.; Nandedkar, A.V. AgroAVNET for crops and weeds classification: A step forward in automatic farming. *Comput. Electron. Agric.* **2018**, *154*, 361–372. [\[CrossRef\]](#)
240. De Castro, A.; Torres-Sánchez, J.; Peña, J.; Jiménez-Brenes, F.; Csilik, O.; López-Granados, F. An Automatic Random Forest-OBIA Algorithm for Early Weed Mapping between and within Crop Rows Using UAV Imagery. *Remote Sens.* **2018**, *10*, 285. [\[CrossRef\]](#)
241. Gao, J.; Nuytens, D.; Lootens, P.; He, Y.; Pieters, J.G. Recognising weeds in a maize crop using a random forest machine-learning algorithm and near-infrared snapshot mosaic hyperspectral imagery. *Biosyst. Eng.* **2018**, *170*, 39–50. [\[CrossRef\]](#)
242. Gao, J.; Liao, W.; Nuytens, D.; Lootens, P.; Vangeyte, J.; Pižurica, A.; He, Y.; Pieters, J.G. Fusion of pixel and object-based features for weed mapping using unmanned aerial vehicle imagery. *Int. J. Appl. Earth Obs. Geoinf.* **2018**, *67*, 43–53. [\[CrossRef\]](#)
243. Huang, H.; Deng, J.; Lan, Y.; Yang, A.; Deng, X.; Wen, S.; Zhang, H.; Zhang, Y. Accurate Weed Mapping and Prescription Map Generation Based on Fully Convolutional Networks Using UAV Imagery. *Sensors* **2018**, *18*, 3299. [\[CrossRef\]](#)
244. Louargant, M.; Jones, G.; Faroux, R.; Paoli, J.-N.; Maillot, T.; Gée, C.; Villette, S. Unsupervised Classification Algorithm for Early Weed Detection in Row-Crops by Combining Spatial and Spectral Information. *Remote Sens.* **2018**, *10*, 761. [\[CrossRef\]](#)
245. Sa, I.; Popović, M.; Khanna, R.; Chen, Z.; Lottes, P.; Liebisch, F.; Nieto, J.; Stachniss, C.; Walter, A.; Siegwart, R. WeedMap: A Large-Scale Semantic Weed Mapping Framework Using Aerial Multispectral Imaging and Deep Neural Network for Precision Farming. *Remote Sens.* **2018**, *10*, 1423. [\[CrossRef\]](#)
246. Sabzi, S.; Abbaspour-Gilandeh, Y. Using video processing to classify potato plant and three types of weed using hybrid of artificial neural network and particle swarm algorithm. *Meas. J. Int. Meas. Confed.* **2018**, *126*, 22–36. [\[CrossRef\]](#)
247. Teimouri, N.; Dyrmann, M.; Nielsen, P.; Mathiassen, S.; Somerville, G.; Jørgensen, R. Weed Growth Stage Estimator Using Deep Convolutional Neural Networks. *Sensors* **2018**, *18*, 1580. [\[CrossRef\]](#)
248. Akbarzadeh, S.; Paap, A.; Ahderom, S.; Apopei, B.; Alameh, K. Plant discrimination by Support Vector Machine classifier based on spectral reflectance. *Comput. Electron. Agric.* **2018**, *148*, 250–258. [\[CrossRef\]](#)
249. Sharpe, S.M.; Schumann, A.W.; Boyd, N.S. Detection of Carolina Geranium (*Geranium carolinianum*) Growing in Competition with Strawberry Using Convolutional Neural Networks. *Weed Sci.* **2019**, *67*, 239–245. [\[CrossRef\]](#)
250. Knoll, F.J.; Czymmek, V.; Harders, L.O.; Hussmann, S. Real-time classification of weeds in organic carrot production using deep learning algorithms. *Comput. Electron. Agric.* **2019**, *167*, 105097. [\[CrossRef\]](#)
251. Kounalakis, T.; Triantafyllidis, G.A.; Nalpantidis, L. Deep learning-based visual recognition of rumex for robotic precision farming. *Comput. Electron. Agric.* **2019**, *165*, 104973. [\[CrossRef\]](#)
252. Lambert, J.P.; Childs, D.Z.; Freckleton, R.P. Testing the ability of unmanned aerial systems and machine learning to map weeds at subfield scales: A test with the weed *Alopecurus myosuroides* (Huds). *Pest Manag. Sci.* **2019**, *75*, 2283–2294. [\[CrossRef\]](#)
253. Ma, X.; Deng, X.; Qi, L.; Jiang, Y.; Li, H.; Wang, Y.; Xing, X. Fully convolutional network for rice seedling and weed image segmentation at the seedling stage in paddy fields. *PLoS ONE* **2019**, *14*, e0215676. [\[CrossRef\]](#)
254. Olsen, A.; Konovalov, D.A.; Philippa, B.; Ridd, P.; Wood, J.C.; Johns, J.; Banks, W.; Girgenti, B.; Kenny, O.; Whinney, J.; et al. DeepWeeds: A multiclass weed species image dataset for deep learning. *Sci. Rep.* **2019**, *9*, 1–12. [\[CrossRef\]](#)
255. Partel, V.; Charan Kakarla, S.; Ampatzidis, Y. Development and evaluation of a low-cost and smart technology for precision weed management utilizing artificial intelligence. *Comput. Electron. Agric.* **2019**, *157*, 339–350. [\[CrossRef\]](#)
256. Rehman, T.U.; Zaman, Q.U.; Chang, Y.K.; Schumann, A.W.; Corscadden, K.W. Development and field evaluation of a machine vision based in-season weed detection system for wild blueberry. *Comput. Electron. Agric.* **2019**, *162*, 1–13. [\[CrossRef\]](#)
257. Yu, J.; Sharpe, S.M.; Schumann, A.W.; Boyd, N.S. Deep learning for image-based weed detection in turfgrass. *Eur. J. Agron.* **2019**, *104*, 78–84. [\[CrossRef\]](#)
258. Yu, J.; Schumann, A.W.; Cao, Z.; Sharpe, S.M.; Boyd, N.S. Weed Detection in Perennial Ryegrass with Deep Learning Convolutional Neural Network. *Front. Plant Sci.* **2019**, *10*, 1422. [\[CrossRef\]](#) [\[PubMed\]](#)
259. Lottes, P.; Behley, J.; Chebrolu, N.; Milioto, A.; Stachniss, C. Robust joint stem detection and crop-weed classification using image sequences for plant-specific treatment in precision farming. *J. Field Robot.* **2020**, *37*, 20–34. [\[CrossRef\]](#)
260. Espejo-García, B.; Mylonas, N.; Athanasakos, L.; Fountas, S.; Vasilakoglou, I. Towards weeds identification assistance through transfer learning. *Comput. Electron. Agric.* **2020**, *171*, 105306. [\[CrossRef\]](#)
261. Dadashzadeh, M.; Abbaspour-Gilandeh, Y.; Mesri-Gundoshmian, T.; Sabzi, S.; Hernández-Hernández, J.L.; Hernández-Hernández, M.; Arribas, J.I. Weed Classification for Site-Specific Weed Management Using an Automated Stereo Computer-Vision Machine-Learning System in Rice Fields. *Plants* **2020**, *9*, 559. [\[CrossRef\]](#)
262. Kamath, R.; Balachandra, M.; Prabhu, S. Paddy Crop and Weed Discrimination: A Multiple Classifier System Approach. *Int. J. Agron.* **2020**, *2020*. [\[CrossRef\]](#)
263. Kamath, R.; Balachandra, M.; Prabhu, S. Crop and weed discrimination using Laws' texture masks. *Int. J. Agric. Biol. Eng.* **2020**, *13*, 191–197. [\[CrossRef\]](#)

264. Le, V.N.T.; Aherom, S.; Alameh, K. Performances of the lbp based algorithm over cnn models for detecting crops and weeds with similar morphologies. *Sensors* **2020**, *20*, 2193. [\[CrossRef\]](#)
265. Gao, J.; French, A.P.; Pound, M.P.; He, Y.; Pridmore, T.P.; Pieters, J.G. Deep convolutional neural networks for image-based *Convolvulus sepium* detection in sugar beet fields. *Plant Methods* **2020**, *16*, 29. [\[CrossRef\]](#)
266. Hu, K.; Coleman, G.; Zeng, S.; Wang, Z.; Walsh, M. Graph weeds net: A graph-based deep learning method for weed recognition. *Comput. Electron. Agric.* **2020**, *174*, 105520. [\[CrossRef\]](#)
267. Osorio, K.; Puerto, A.; Pedraza, C.; Jamaica, D.; Rodríguez, L. A Deep Learning Approach for Weed Detection in Lettuce Crops Using Multispectral Images. *AgriEngineering* **2020**, *2*, 471–488. [\[CrossRef\]](#)
268. Espejo-Garcia, B.; Mylonas, N.; Athanasakos, L.; Fountas, S. Improving weeds identification with a repository of agricultural pre-trained deep neural networks. *Comput. Electron. Agric.* **2020**, *175*, 105593. [\[CrossRef\]](#)
269. Veeranampalayam Sivakumar, A.N.; Li, J.; Scott, S.; Psota, E.; Jhala, A.J.; Luck, J.D.; Shi, Y. Comparison of Object Detection and Patch-Based Classification Deep Learning Models on Mid- to Late-Season Weed Detection in UAV Imagery. *Remote Sens.* **2020**, *12*, 2136. [\[CrossRef\]](#)
270. Sharpe, S.M.; Schumann, A.W.; Boyd, N.S. Goosegrass Detection in Strawberry and Tomato Using a Convolutional Neural Network. *Sci. Rep.* **2020**, *10*, 1–8. [\[CrossRef\]](#)
271. Sabzi, S.; Abbaspour-Gilandeh, Y.; Arribas, J.I. An automatic visible-range video weed detection, segmentation and classification prototype in potato field. *Heliyon* **2020**, *6*, e03685. [\[CrossRef\]](#)
272. Shendryk, Y.; Rossiter-Rachor, N.A.; Setterfield, S.A.; Levick, S.R. Leveraging High-Resolution Satellite Imagery and Gradient Boosting for Invasive Weed Mapping. *IEEE J. Sel. Top. Appl. Earth Obs. Remote Sens.* **2020**, *13*, 4443–4450. [\[CrossRef\]](#)
273. Gašparović, M.; Zrinjski, M.; Barković, Đ.; Radočaj, D. An automatic method for weed mapping in oat fields based on UAV imagery. *Comput. Electron. Agric.* **2020**, *173*, 105385. [\[CrossRef\]](#)
274. Sapkota, B.; Singh, V.; Neely, C.; Rajan, N.; Bagavathiannan, M. Detection of Italian Ryegrass in Wheat and Prediction of Competitive Interactions Using Remote-Sensing and Machine-Learning Techniques. *Remote Sens.* **2020**, *12*, 2977. [\[CrossRef\]](#)
275. Ruijgrok, T.; van Henten, E.; Booi, J.; van Boheemen, K.; Kootstra, G. Application-Specific Evaluation of a Weed-Detection Algorithm for Plant-Specific Spraying. *Sensors* **2020**, *20*, 7262. [\[CrossRef\]](#)
276. Champ, J.; Mora-Fallas, A.; Goëau, H.; Mata-Montero, E.; Bonnet, P.; Joly, A. Instance segmentation for the fine detection of crop and weed plants by precision agricultural robots. *Appl. Plant Sci.* **2020**, *8*. [\[CrossRef\]](#) [\[PubMed\]](#)
277. Petrich, L.; Lohrmann, G.; Neumann, M.; Martin, F.; Frey, A.; Stoll, A.; Schmidt, V. Detection of *Colchicum autumnale* in drone images, using a machine-learning approach. *Precis. Agric.* **2020**, *21*, 1291–1303. [\[CrossRef\]](#)
278. Lam, O.H.Y.; Dogotari, M.; Prüm, M.; Vithlani, H.N.; Roers, C.; Melville, B.; Zimmer, F.; Becker, R. An open source workflow for weed mapping in native grassland using unmanned aerial vehicle: Using *Rumex obtusifolius* as a case study. *Eur. J. Remote Sens.* **2020**, 1–18. [\[CrossRef\]](#)
279. Abad, M.; Abkar, A.; Mojaradi, B. Effect of the Temporal Gradient of Vegetation Indices on Early-Season Wheat Classification Using the Random Forest Classifier. *Appl. Sci.* **2018**, *8*, 1216. [\[CrossRef\]](#)
280. Ghazaryan, G.; Dubovyk, O.; Löw, F.; Lavreniuk, M.; Kolotii, A.; Schellberg, J.; Kussul, N. A rule-based approach for crop identification using multi-temporal and multi-sensor phenological metrics. *Eur. J. Remote Sens.* **2018**, *51*, 511–524. [\[CrossRef\]](#)
281. Ji, S.; Zhang, C.; Xu, A.; Shi, Y.; Duan, Y. 3D Convolutional Neural Networks for Crop Classification with Multi-Temporal Remote Sensing Images. *Remote Sens.* **2018**, *10*, 75. [\[CrossRef\]](#)
282. Nemmaoui, A.; Aguilar, M.A.; Aguilar, F.J.; Novelli, A.; García Lorca, A. Greenhouse Crop Identification from Multi-Temporal Multi-Sensor Satellite Imagery Using Object-Based Approach: A Case Study from Almería (Spain). *Remote Sens.* **2018**, *10*, 1751. [\[CrossRef\]](#)
283. Xu, L.; Zhang, H.; Wang, C.; Zhang, B.; Liu, M. Crop Classification Based on Temporal Information Using Sentinel-1 SAR Time-Series Data. *Remote Sens.* **2018**, *11*, 53. [\[CrossRef\]](#)
284. Kwak, G.-H.; Park, N.-W. Impact of Texture Information on Crop Classification with Machine Learning and UAV Images. *Appl. Sci.* **2019**, *9*, 643. [\[CrossRef\]](#)
285. Paul, S.; Kumar, D.N. Evaluation of Feature Selection and Feature Extraction Techniques on Multi-Temporal Landsat-8 Images for Crop Classification. *Remote Sens. Earth Syst. Sci.* **2019**, *2*, 197–207. [\[CrossRef\]](#)
286. Piedelobo, L.; Hernández-López, D.; Ballesteros, R.; Chakhar, A.; Del Pozo, S.; González-Aguilera, D.; Moreno, M.A. Scalable pixel-based crop classification combining Sentinel-2 and Landsat-8 data time series: Case study of the Duero river basin. *Agric. Syst.* **2019**, *171*, 36–50. [\[CrossRef\]](#)
287. Song, Q.; Xiang, M.; Hovis, C.; Zhou, Q.; Lu, M.; Tang, H.; Wu, W. Object-based feature selection for crop classification using multi-temporal high-resolution imagery. *Int. J. Remote Sens.* **2019**, *40*, 2053–2068. [\[CrossRef\]](#)
288. Sonobe, R. Parcel-Based Crop Classification Using Multi-Temporal TerraSAR-X Dual Polarimetric Data. *Remote Sens.* **2019**, *11*, 1148. [\[CrossRef\]](#)
289. Sun, Y.; Luo, J.; Wu, T.; Zhou, Y.; Liu, H.; Gao, L.; Dong, W.; Liu, W.; Yang, Y.; Hu, X.; et al. Synchronous Response Analysis of Features for Remote Sensing Crop Classification Based on Optical and SAR Time-Series Data. *Sensors* **2019**, *19*, 4227. [\[CrossRef\]](#)
290. Sun, C.; Bian, Y.; Zhou, T.; Pan, J. Using of Multi-Source and Multi-Temporal Remote Sensing Data Improves Crop-Type Mapping in the Subtropical Agriculture Region. *Sensors* **2019**, *19*, 2401. [\[CrossRef\]](#)



291. Teimouri, N.; Dyrmann, M.; Jørgensen, R.N. A Novel Spatio-Temporal FCN-LSTM Network for Recognizing Various Crop Types Using Multi-Temporal Radar Images. *Remote Sens.* **2019**, *11*, 990. [[CrossRef](#)]
292. Ustuner, M.; Balik Sanli, F. Polarimetric Target Decompositions and Light Gradient Boosting Machine for Crop Classification: A Comparative Evaluation. *ISPRS Int. J. Geo Inform.* **2019**, *8*, 97. [[CrossRef](#)]
293. Wei, S.; Zhang, H.; Wang, C.; Wang, Y.; Xu, L. Multi-Temporal SAR Data Large-Scale Crop Mapping Based on U-Net Model. *Remote Sens.* **2019**, *11*, 68. [[CrossRef](#)]
294. Zhao, H.; Chen, Z.; Jiang, H.; Jing, W.; Sun, L.; Feng, M. Evaluation of Three Deep Learning Models for Early Crop Classification Using Sentinel-1A Imagery Time Series—A Case Study in Zhanjiang, China. *Remote Sens.* **2019**, *11*, 2673. [[CrossRef](#)]
295. Zhong, L.; Hu, L.; Zhou, H. Deep learning based multi-temporal crop classification. *Remote Sens. Environ.* **2019**, *221*, 430–443. [[CrossRef](#)]
296. Zhou, Y.; Luo, J.; Feng, L.; Zhou, X. DCN-Based Spatial Features for Improving Parcel-Based Crop Classification Using High-Resolution Optical Images and Multi-Temporal SAR Data. *Remote Sens.* **2019**, *11*, 1619. [[CrossRef](#)]
297. Zhou, Y.; Luo, J.; Feng, L.; Yang, Y.; Chen, Y.; Wu, W. Long-short-term-memory-based crop classification using high-resolution optical images and multi-temporal SAR data. *GIScience Remote Sens.* **2019**, *56*, 1170–1191. [[CrossRef](#)]
298. Mazzia, V.; Khaliq, A.; Chiaberge, M. Improvement in Land Cover and Crop Classification based on Temporal Features Learning from Sentinel-2 Data Using Recurrent-Convolutional Neural Network (R-CNN). *Appl. Sci.* **2019**, *10*, 238. [[CrossRef](#)]
299. Nguyen Thanh Le, V.; Apopei, B.; Alameh, K. Effective plant discrimination based on the combination of local binary pattern operators and multiclass support vector machine methods. *Inf. Process. Agric.* **2019**, *6*, 116–131. [[CrossRef](#)]
300. Cinar, I. Classification of Rice Varieties Using Artificial Intelligence Methods. *Int. J. Intell. Syst. Appl. Eng.* **2019**, *7*, 188–194. [[CrossRef](#)]
301. Tan, K.; Wang, R.; Li, M.; Gong, Z. Discriminating soybean seed varieties using hyperspectral imaging and machine learning. *J. Comput. Methods Sci. Eng.* **2019**, *19*, 1001–1015. [[CrossRef](#)]
302. Zhu, S.; Zhou, L.; Gao, P.; Bao, Y.; He, Y.; Feng, L. Near-Infrared Hyperspectral Imaging Combined with Deep Learning to Identify Cotton Seed Varieties. *Molecules* **2019**, *24*, 3268. [[CrossRef](#)] [[PubMed](#)]
303. Bisen, D. Deep convolutional neural network based plant species recognition through features of leaf. *Multimed. Tools Appl.* **2020**, *80*, 6443–6456. [[CrossRef](#)]
304. Bambil, D.; Pistori, H.; Bao, F.; Weber, V.; Alves, F.M.; Gonçalves, E.G.; de Alencar Figueiredo, L.F.; Abreu, U.G.P.; Arruda, R.; Bortolotto, I.M. Plant species identification using color learning resources, shape, texture, through machine learning and artificial neural networks. *Environ. Syst. Decis.* **2020**, *40*, 480–484. [[CrossRef](#)]
305. Huixian, J. The Analysis of Plants Image Recognition Based on Deep Learning and Artificial Neural Network. *IEEE Access* **2020**, *8*, 68828–68841. [[CrossRef](#)]
306. Shelestov, A.; Lavreniuk, M.; Vasiliev, V.; Shumilo, L.; Kolotii, A.; Yailymov, B.; Kussul, N.; Yailymova, H. Cloud Approach to Automated Crop Classification Using Sentinel-1 Imagery. *IEEE Trans. Big Data* **2020**, *6*, 572–582. [[CrossRef](#)]
307. Ji, S.; Zhang, Z.; Zhang, C.; Wei, S.; Lu, M.; Duan, Y. Learning discriminative spatiotemporal features for precise crop classification from multi-temporal satellite images. *Int. J. Remote Sens.* **2020**, *41*, 3162–3174. [[CrossRef](#)]
308. Bhuyar, N. Crop Classification with Multi-Temporal Satellite Image Data. *Int. J. Eng. Res.* **2020**, *V9*. [[CrossRef](#)]
309. Zhang, H.; Kang, J.; Xu, X.; Zhang, L. Accessing the temporal and spectral features in crop type mapping using multi-temporal Sentinel-2 imagery: A case study of Yi'an County, Heilongjiang province, China. *Comput. Electron. Agric.* **2020**, *176*, 105618. [[CrossRef](#)]
310. Kyere, L.; Astor, T.; Graf, R.; Wachendorf, M. Agricultural crop discrimination in a heterogeneous low-mountain range region based on multi-temporal and multi-sensor satellite data. *Comput. Electron. Agric.* **2020**, *179*, 105864. [[CrossRef](#)]
311. Xu, J.; Zhu, Y.; Zhong, R.; Lin, Z.; Xu, J.; Jiang, H.; Huang, J.; Li, H.; Lin, T. DeepCropMapping: A multi-temporal deep learning approach with improved spatial generalizability for dynamic corn and soybean mapping. *Remote Sens. Environ.* **2020**, *247*, 111946. [[CrossRef](#)]
312. Liao, C.; Wang, J.; Xie, Q.; Al Baz, A.; Huang, X.; Shang, J.; He, Y. Synergistic Use of Multi-Temporal RADARSAT-2 and VEN $\mu$ S Data for Crop Classification Based on 1D Convolutional Neural Network. *Remote Sens.* **2020**, *12*, 832. [[CrossRef](#)]
313. Zhang, W.; Liu, H.; Wu, W.; Zhan, L.; Wei, J. Mapping Rice Paddy Based on Machine Learning with Sentinel-2 Multi-Temporal Data: Model Comparison and Transferability. *Remote Sens.* **2020**, *12*, 1620. [[CrossRef](#)]
314. Yi, Z.; Jia, L.; Chen, Q. Crop Classification Using Multi-Temporal Sentinel-2 Data in the Shiyang River Basin of China. *Remote Sens.* **2020**, *12*, 4052. [[CrossRef](#)]
315. Guo, J.; Li, H.; Ning, J.; Han, W.; Zhang, W.; Zhou, Z.-S. Feature Dimension Reduction Using Stacked Sparse Auto-Encoders for Crop Classification with Multi-Temporal, Quad-Pol SAR Data. *Remote Sens.* **2020**, *12*, 321. [[CrossRef](#)]
316. Maponya, M.G.; van Niekerk, A.; Mashimbye, Z.E. Pre-harvest classification of crop types using a Sentinel-2 time-series and machine learning. *Comput. Electron. Agric.* **2020**, *169*, 105164. [[CrossRef](#)]
317. Minallah, N.; Tariq, M.; Aziz, N.; Khan, W.; Rehman, A.U.; Belhaouari, S.B. On the performance of fusion based planet-scope and Sentinel-2 data for crop classification using inception inspired deep convolutional neural network. *PLoS ONE* **2020**, *15*, e0239746. [[CrossRef](#)]
318. Chakhar, A.; Ortega-Terol, D.; Hernández-López, D.; Ballesteros, R.; Ortega, J.F.; Moreno, M.A. Assessing the Accuracy of Multiple Classification Algorithms for Crop Classification Using Landsat-8 and Sentinel-2 Data. *Remote Sens.* **2020**, *12*, 1735. [[CrossRef](#)]
319. Mandal, D.; Kumar, V.; Rao, Y.S. An assessment of temporal RADARSAT-2 SAR data for crop classification using KPCA based support vector machine. *Geocarto Int.* **2020**. [[CrossRef](#)]

320. Kobayashi, N.; Tani, H.; Wang, X.; Sonobe, R. Crop classification using spectral indices derived from Sentinel-2A imagery. *J. Inf. Telecommun.* **2020**, *4*, 67–90. [\[CrossRef\]](#)
321. Tu, K.-L.; Li, L.-J.; Yang, L.-M.; Wang, J.-H.; Sun, Q. Selection for high quality pepper seeds by machine vision and classifiers. *J. Integr. Agric.* **2018**, *17*, 1999–2006. [\[CrossRef\]](#)
322. Wolanin, A.; Camps-Valls, G.; Gómez-Chova, L.; Mateo-García, G.; van der Tol, C.; Zhang, Y.; Guanter, L. Estimating crop primary productivity with Sentinel-2 and Landsat 8 using machine learning methods trained with radiative transfer simulations. *Remote Sens. Environ.* **2019**, *225*, 441–457. [\[CrossRef\]](#)
323. Yang, B.; Wang, M.; Sha, Z.; Wang, B.; Chen, J.; Yao, X.; Cheng, T.; Cao, W.; Zhu, Y. Evaluation of Aboveground Nitrogen Content of Winter Wheat Using Digital Imagery of Unmanned Aerial Vehicles. *Sensors* **2019**, *19*, 4416. [\[CrossRef\]](#)
324. Genze, N.; Bharti, R.; Grieb, M.; Schultheiss, S.J.; Grimm, D.G. Accurate machine learning-based germination detection, prediction and quality assessment of three grain crops. *Plant Methods* **2020**, *16*, 157. [\[CrossRef\]](#)
325. De Medeiros, A.D.; Pinheiro, D.T.; Xavier, W.A.; da Silva, L.J.; dos Santos Dias, D.C.F. Quality classification of *Jatropha curcas* seeds using radiographic images and machine learning. *Ind. Crop. Prod.* **2020**, *146*, 112162. [\[CrossRef\]](#)
326. Baath, G.S.; Baath, H.K.; Gowda, P.H.; Thomas, J.P.; Northup, B.K.; Rao, S.C.; Singh, H. Predicting Forage Quality of Warm-Season Legumes by Near Infrared Spectroscopy Coupled with Machine Learning Techniques. *Sensors* **2020**, *20*, 867. [\[CrossRef\]](#) [\[PubMed\]](#)
327. Medeiros, A.D.D.; Silva, L.J.D.; Ribeiro, J.P.O.; Ferreira, K.C.; Rosas, J.T.F.; Santos, A.A.; Silva, C.B.D. Machine Learning for Seed Quality Classification: An Advanced Approach Using Merger Data from FT-NIR Spectroscopy and X-ray Imaging. *Sensors* **2020**, *20*, 4319. [\[CrossRef\]](#) [\[PubMed\]](#)
328. Lee, J.; Nazki, H.; Baek, J.; Hong, Y.; Lee, M. Artificial Intelligence Approach for Tomato Detection and Mass Estimation in Precision Agriculture. *Sustainability* **2020**, *12*, 9138. [\[CrossRef\]](#)
329. Yang, B.; Gao, Y.; Yan, Q.; Qi, L.; Zhu, Y.; Wang, B. Estimation Method of Soluble Solid Content in Peach Based on Deep Features of Hyperspectral Imagery. *Sensors* **2020**, *20*, 5021. [\[CrossRef\]](#)
330. Gutiérrez, S.; Diago, M.P.; Fernández-Navales, J.; Tardaguila, J. Vineyard water status assessment using on-the-go thermal imaging and machine learning. *PLoS ONE* **2018**, *13*, e0192037. [\[CrossRef\]](#)
331. Loggenberg, K.; Strever, A.; Greyling, B.; Poona, N. Modelling Water Stress in a Shiraz Vineyard Using Hyperspectral Imaging and Machine Learning. *Remote Sens.* **2018**, *10*, 202. [\[CrossRef\]](#)
332. Zhang, J.; Zhu, Y.; Zhang, X.; Ye, M.; Yang, J. Developing a Long Short-Term Memory (LSTM) based model for predicting water table depth in agricultural areas. *J. Hydrol.* **2018**, *561*, 918–929. [\[CrossRef\]](#)
333. Goldstein, A.; Fink, L.; Meitin, A.; Bohadana, S.; Lutenberg, O.; Ravid, G. Applying machine learning on sensor data for irrigation recommendations: Revealing the agronomist's tacit knowledge. *Precis. Agric.* **2018**, *19*, 421–444. [\[CrossRef\]](#)
334. Romero, M.; Luo, Y.; Su, B.; Fuentes, S. Vineyard water status estimation using multispectral imagery from an UAV platform and machine learning algorithms for irrigation scheduling management. *Comput. Electron. Agric.* **2018**, *147*, 109–117. [\[CrossRef\]](#)
335. Kisi, O.; Alizamir, M. Modelling reference evapotranspiration using a new wavelet conjunction heuristic method: Wavelet extreme learning machine vs wavelet neural networks. *Agric. For. Meteorol.* **2018**, *263*, 41–48. [\[CrossRef\]](#)
336. Fan, J.; Yue, W.; Wu, L.; Zhang, F.; Cai, H.; Wang, X.; Lu, X.; Xiang, Y. Evaluation of SVM, ELM and four tree-based ensemble models for predicting daily reference evapotranspiration using limited meteorological data in different climates of China. *Agric. For. Meteorol.* **2018**, *263*, 225–241. [\[CrossRef\]](#)
337. Adeyemi, O.; Grove, I.; Peets, S.; Domun, Y.; Norton, T. Dynamic Neural Network Modelling of Soil Moisture Content for Predictive Irrigation Scheduling. *Sensors* **2018**, *18*, 3408. [\[CrossRef\]](#)
338. Angelaki, A.; Singh Nain, S.; Singh, V.; Sihag, P. Estimation of models for cumulative infiltration of soil using machine learning methods. *ISH J. Hydraul. Eng.* **2018**. [\[CrossRef\]](#)
339. Goap, A.; Sharma, D.; Shukla, A.K.; Rama Krishna, C. An IoT based smart irrigation management system using Machine learning and open source technologies. *Comput. Electron. Agric.* **2018**, *155*, 41–49. [\[CrossRef\]](#)
340. Prasad, R.; Deo, R.C.; Li, Y.; Maraseni, T. Soil moisture forecasting by a hybrid machine learning technique: ELM integrated with ensemble empirical mode decomposition. *Geoderma* **2018**, *330*, 136–161. [\[CrossRef\]](#)
341. Tang, D.; Feng, Y.; Gong, D.; Hao, W.; Cui, N. Evaluation of artificial intelligence models for actual crop evapotranspiration modeling in mulched and non-mulched maize croplands. *Comput. Electron. Agric.* **2018**, *152*, 375–384. [\[CrossRef\]](#)
342. Sihag, P.; Singh, V.P.; Angelaki, A.; Kumar, V.; Sepahvand, A.; Golia, E. Modelling of infiltration using artificial intelligence techniques in semi-arid Iran. *Hydrol. Sci. J.* **2019**, *64*, 1647–1658. [\[CrossRef\]](#)
343. Chen, H.; Chen, A.; Xu, L.; Xie, H.; Qiao, H.; Lin, Q.; Cai, K. A deep learning CNN architecture applied in smart near-infrared analysis of water pollution for agricultural irrigation resources. *Agric. Water Manag.* **2020**, *240*, 106303. [\[CrossRef\]](#)
344. Afzaal, H.; Farooque, A.A.; Abbas, F.; Acharya, B.; Esau, T. Computation of Evapotranspiration with Artificial Intelligence for Precision Water Resource Management. *Appl. Sci.* **2020**, *10*, 1621. [\[CrossRef\]](#)
345. Li, P.; Zha, Y.; Shi, L.; Tso, C.H.M.; Zhang, Y.; Zeng, W. Comparison of the use of a physical-based model with data assimilation and machine learning methods for simulating soil water dynamics. *J. Hydrol.* **2020**, *584*, 124692. [\[CrossRef\]](#)
346. Fernández-López, A.; Marín-Sánchez, D.; García-Mateos, G.; Ruiz-Canales, A.; Ferrández-Villena-García, M.; Molina-Martínez, J.M. A Machine Learning Method to Estimate Reference Evapotranspiration Using Soil Moisture Sensors. *Appl. Sci.* **2020**, *10*, 1912. [\[CrossRef\]](#)

347. Xavier, L.C.P.; Carvalho, T.M.N.; Pontes Filho, J.D.; Souza Filho, F.D.A.; Silva, S.M.O.D. Use of Machine Learning in Evaluation of Drought Perception in Irrigated Agriculture: The Case of an Irrigated Perimeter in Brazil. *Water* **2020**, *12*, 1546. [\[CrossRef\]](#)
348. Yamaç, S.S.; Todorovic, M. Estimation of daily potato crop evapotranspiration using three different machine learning algorithms and four scenarios of available meteorological data. *Agric. Water Manag.* **2020**, *228*, 105875. [\[CrossRef\]](#)
349. Mosavi, A.; Sajedi-Hosseini, F.; Choubin, B.; Taromideh, F.; Rahi, G.; Dineva, A. Susceptibility Mapping of Soil Water Erosion Using Machine Learning Models. *Water* **2020**, *12*, 1995. [\[CrossRef\]](#)
350. Fung, K.F.; Huang, Y.F.; Koo, C.H.; Mirzaei, M. Improved svr machine learning models for agricultural drought prediction at downstream of langat river basin, Malaysia. *J. Water Clim. Chang.* **2020**, *11*, 1383–1398. [\[CrossRef\]](#)
351. Ferreira, L.B.; da Cunha, F.F. New approach to estimate daily reference evapotranspiration based on hourly temperature and relative humidity using machine learning and deep learning. *Agric. Water Manag.* **2020**, *234*, 106113. [\[CrossRef\]](#)
352. Zhu, B.; Feng, Y.; Gong, D.; Jiang, S.; Zhao, L.; Cui, N. Hybrid particle swarm optimization with extreme learning machine for daily reference evapotranspiration prediction from limited climatic data. *Comput. Electron. Agric.* **2020**, *173*, 105430. [\[CrossRef\]](#)
353. Yaseen, Z.M.; Al-Juboori, A.M.; Beyaztas, U.; Al-Ansari, N.; Chau, K.-W.; Qi, C.; Ali, M.; Salih, S.Q.; Shahid, S. Prediction of evaporation in arid and semi-arid regions: A comparative study using different machine learning models. *Eng. Appl. Comput. Fluid Mech.* **2020**, *14*, 70–89. [\[CrossRef\]](#)
354. Wu, L.; Huang, G.; Fan, J.; Ma, X.; Zhou, H.; Zeng, W. Hybrid extreme learning machine with meta-heuristic algorithms for monthly pan evaporation prediction. *Comput. Electron. Agric.* **2020**, *168*, 105115. [\[CrossRef\]](#)
355. Dos Santos Farias, D.B.; Althoff, D.; Rodrigues, L.N.; Filgueiras, R. Performance evaluation of numerical and machine learning methods in estimating reference evapotranspiration in a Brazilian agricultural frontier. *Theor. Appl. Climatol.* **2020**, *142*, 1481–1492. [\[CrossRef\]](#)
356. Raza, A.; Shoaib, M.; Faiz, M.A.; Baig, F.; Khan, M.M.; Ullah, M.K.; Zubair, M. Comparative Assessment of Reference Evapotranspiration Estimation Using Conventional Method and Machine Learning Algorithms in Four Climatic Regions. *Pure Appl. Geophys.* **2020**, *177*, 4479–4508. [\[CrossRef\]](#)
357. Tufaner, F.; Özbeyaz, A. Estimation and easy calculation of the Palmer Drought Severity Index from the meteorological data by using the advanced machine learning algorithms. *Environ. Monit. Assess.* **2020**, *192*, 576. [\[CrossRef\]](#) [\[PubMed\]](#)
358. Sagan, V.; Peterson, K.T.; Maimaitijiang, M.; Sidike, P.; Sloan, J.; Greeling, B.A.; Maalouf, S.; Adams, C. Monitoring inland water quality using remote sensing: Potential and limitations of spectral indices, bio-optical simulations, machine learning, and cloud computing. *Earth Sci. Rev.* **2020**, *205*, 103187. [\[CrossRef\]](#)
359. Lee, S.; Hyun, Y.; Lee, S.; Lee, M.-J. Groundwater Potential Mapping Using Remote Sensing and GIS-Based Machine Learning Techniques. *Remote Sens.* **2020**, *12*, 1200. [\[CrossRef\]](#)
360. Majumdar, S.; Smith, R.; Butler, J.J.; Lakshmi, V. Groundwater Withdrawal Prediction Using Integrated Multitemporal Remote Sensing Data Sets and Machine Learning. *Water Resour. Res.* **2020**, *56*, e2020WR028059. [\[CrossRef\]](#)
361. Band, S.S.; Janizadeh, S.; Pal, S.C.; Chowdhuri, I.; Siabi, Z.; Norouzi, A.; Melesse, A.M.; Shokri, M.; Mosavi, A. Comparative Analysis of Artificial Intelligence Models for Accurate Estimation of Groundwater Nitrate Concentration. *Sensors* **2020**, *20*, 5763. [\[CrossRef\]](#)
362. Hong, Y.; Chen, S.; Zhang, Y.; Chen, Y.; Yu, L.; Liu, Y.; Liu, Y.; Cheng, H.; Liu, Y. Rapid identification of soil organic matter level via visible and near-infrared spectroscopy: Effects of two-dimensional correlation coefficient and extreme learning machine. *Sci. Total Environ.* **2018**, *644*, 1232–1243. [\[CrossRef\]](#)
363. Jha, S.K.; Ahmad, Z. Soil microbial dynamics prediction using machine learning regression methods. *Comput. Electron. Agric.* **2018**, *147*, 158–165. [\[CrossRef\]](#)
364. Wang, X.; Zhang, F.; Ding, J.; Kung, H.T.; Latif, A.; Johnson, V.C. Estimation of soil salt content (SSC) in the Ebinur Lake Wetland National Nature Reserve (ELWNNR), Northwest China, based on a Bootstrap-BP neural network model and optimal spectral indices. *Sci. Total Environ.* **2018**, *615*, 918–930. [\[CrossRef\]](#)
365. Zeraatpisheh, M.; Ayoubi, S.; Jafari, A.; Tajik, S.; Finke, P. Digital mapping of soil properties using multiple machine learning in a semi-arid region, central Iran. *Geoderma* **2019**, *338*, 445–452. [\[CrossRef\]](#)
366. Chen, D.; Chang, N.; Xiao, N.; Zhou, Q.; Wu, W. Mapping dynamics of soil organic matter in croplands with MODIS data and machine learning algorithms. *Sci. Total Environ.* **2019**, *669*, 844–855. [\[CrossRef\]](#)
367. Wu, T.; Luo, J.; Dong, W.; Sun, Y.; Xia, L.; Zhang, X. Geo-Object-Based Soil Organic Matter Mapping Using Machine Learning Algorithms with Multi-Source Geo-Spatial Data. *IEEE J. Sel. Top. Appl. Earth Obs. Remote Sens.* **2019**, *12*, 1091–1106. [\[CrossRef\]](#)
368. Ghorbani, M.A.; Deo, R.C.; Kashani, M.H.; Shahabi, M.; Ghorbani, S. Artificial intelligence-based fast and efficient hybrid approach for spatial modelling of soil electrical conductivity. *Soil Tillage Res.* **2019**, *186*, 152–164. [\[CrossRef\]](#)
369. Ge, X.; Wang, J.; Ding, J.; Cao, X.; Zhang, Z.; Liu, J.; Li, X. Combining UAV-based hyperspectral imagery and machine learning algorithms for soil moisture content monitoring. *PeerJ* **2019**, *7*, e6926. [\[CrossRef\]](#)
370. Feng, Y.; Cui, N.; Hao, W.; Gao, L.; Gong, D. Estimation of soil temperature from meteorological data using different machine learning models. *Geoderma* **2019**, *338*, 67–77. [\[CrossRef\]](#)
371. Nawar, S.; Mouazen, A.M. On-line vis-NIR spectroscopy prediction of soil organic carbon using machine learning. *Soil Tillage Res.* **2019**, *190*, 120–127. [\[CrossRef\]](#)

372. Ng, W.; Minasny, B.; Montazerolghaem, M.; Padarian, J.; Ferguson, R.; Bailey, S.; McBratney, A.B. Convolutional neural network for simultaneous prediction of several soil properties using visible/near-infrared, mid-infrared, and their combined spectra. *Geoderma* **2019**, *352*, 251–267. [[CrossRef](#)]
373. Padarian, J.; Minasny, B.; McBratney, A.B. Using deep learning to predict soil properties from regional spectral data. *Geoderma Reg.* **2019**, *16*, e00198. [[CrossRef](#)]
374. Mohapatra, A.G.; Lenka, S.K.; Keswani, B. Neural Network and Fuzzy Logic Based Smart DSS Model for Irrigation Notification and Control in Precision Agriculture. *Proc. Natl. Acad. Sci. India Sect. A Phys. Sci.* **2019**, *89*, 67–76. [[CrossRef](#)]
375. Bashir, R.N.; Bajwa, I.S.; Shahid, M.M.A. Internet of Things and Machine-Learning-Based Leaching Requirements Estimation for Saline Soils. *IEEE Internet Things J.* **2020**, *7*, 4464–4472. [[CrossRef](#)]
376. Chakraborty, R.; Pal, S.C.; Sahana, M.; Mondal, A.; Dou, J.; Pham, B.T.; Yunus, A.P. Soil erosion potential hotspot zone identification using machine learning and statistical approaches in eastern India. *Nat. Hazards* **2020**, 1–36. [[CrossRef](#)]
377. Helfer, G.A.; Victória Barbosa, J.L.; dos Santos, R.; da Costa, A. Ben A computational model for soil fertility prediction in ubiquitous agriculture. *Comput. Electron. Agric.* **2020**, *175*, 105602. [[CrossRef](#)]
378. Araya, S.; Fryjoff-Hung, A.; Anderson, A.; Viers, J.; Ghezzehei, T. Advances in Soil Moisture Retrieval from Multispectral Remote Sensing Using Unmanned Aircraft Systems and Machine Learning Techniques. *Hydrol. Earth Syst. Sci. Discuss.* **2020**, 1–33. [[CrossRef](#)]
379. Yamaç, S.S.; Şeker, C.; Neğiş, H. Evaluation of machine learning methods to predict soil moisture constants with different combinations of soil input data for calcareous soils in a semi arid area. *Agric. Water Manag.* **2020**, *234*, 106121. [[CrossRef](#)]
380. Alizamir, M.; Kisi, O.; Ahmed, A.N.; Mert, C.; Fai, C.M.; Kim, S.; Kim, N.W.; El-Shafie, A. Advanced machine learning model for better prediction accuracy of soil temperature at different depths. *PLoS ONE* **2020**, *15*, e0231055. [[CrossRef](#)]
381. Sanuade, O.A.; Hassan, A.M.; Akanji, A.O.; Oloajo, A.A.; Oladunjoye, M.A.; Abdulraheem, A. New empirical equation to estimate the soil moisture content based on thermal properties using machine learning techniques. *Arab. J. Geosci.* **2020**, *13*, 377. [[CrossRef](#)]
382. Lei, X.; Chen, W.; Avand, M.; Janizadeh, S.; Kariminejad, N.; Shahabi, H.; Costache, R.; Shahabi, H.; Shirzadi, A.; Mosavi, A. GIS-Based Machine Learning Algorithms for Gully Erosion Susceptibility Mapping in a Semi-Arid Region of Iran. *Remote Sens.* **2020**, *12*, 2478. [[CrossRef](#)]
383. Mosavi, A.; Hosseini, F.S.; Choubin, B.; Goodarzi, M.; Dineva, A.A. Groundwater Salinity Susceptibility Mapping Using Classifier Ensemble and Bayesian Machine Learning Models. *IEEE Access* **2020**, *8*, 145564–145576. [[CrossRef](#)]
384. Hu, B.; Xue, J.; Zhou, Y.; Shao, S.; Fu, Z.; Li, Y.; Chen, S.; Qi, L.; Shi, Z. Modelling bioaccumulation of heavy metals in soil-crop ecosystems and identifying its controlling factors using machine learning. *Environ. Pollut.* **2020**, *262*, 114308. [[CrossRef](#)]
385. Taghizadeh-Mehrjardi, R.; Nabiollahi, K.; Rasoli, L.; Kerry, R.; Scholten, T. Land Suitability Assessment and Agricultural Production Sustainability Using Machine Learning Models. *Agronomy* **2020**, *10*, 573. [[CrossRef](#)]
386. JOHN, K.; Abraham Isong, I.; Michael Kebonye, N.; Okon Ayito, E.; Chapman Agyeman, P.; Marcus Afu, S. Using Machine Learning Algorithms to Estimate Soil Organic Carbon Variability with Environmental Variables and Soil Nutrient Indicators in an Alluvial Soil. *Land* **2020**, *9*, 487. [[CrossRef](#)]
387. Benke, K.K.; Norng, S.; Robinson, N.J.; Chia, K.; Rees, D.B.; Hopley, J. Development of pedotransfer functions by machine learning for prediction of soil electrical conductivity and organic carbon content. *Geoderma* **2020**, *366*, 114210. [[CrossRef](#)]
388. Rentschler, T.; Werban, U.; Ahner, M.; Behrens, T.; Gries, P.; Scholten, T.; Teuber, S.; Schmidt, K. 3D mapping of soil organic carbon content and soil moisture with multiple geophysical sensors and machine learning. *Vadose Zone J.* **2020**, *19*, e20062. [[CrossRef](#)]
389. Rivera, J.L.; Bonilla, C.A. Predicting soil aggregate stability using readily available soil properties and machine learning techniques. *Catena* **2020**, *187*, 104408. [[CrossRef](#)]
390. Mahmoudzadeh, H.; Matinfar, H.R.; Taghizadeh-Mehrjardi, R.; Kerry, R. Spatial prediction of soil organic carbon using machine learning techniques in western Iran. *Geoderma Reg.* **2020**, *21*, e00260. [[CrossRef](#)]
391. Adab, H.; Morbidelli, R.; Saltalippi, C.; Moradian, M.; Ghalhari, G.A. Machine Learning to Estimate Surface Soil Moisture from Remote Sensing Data. *Water* **2020**, *12*, 3223. [[CrossRef](#)]
392. Emadi, M.; Taghizadeh-Mehrjardi, R.; Cherati, A.; Danesh, M.; Mosavi, A.; Scholten, T. Predicting and Mapping of Soil Organic Carbon Using Machine Learning Algorithms in Northern Iran. *Remote Sens.* **2020**, *12*, 2234. [[CrossRef](#)]
393. Arabameri, A.; Chen, W.; Loche, M.; Zhao, X.; Li, Y.; Lombardo, L.; Cerda, A.; Pradhan, B.; Bui, D.T. Comparison of machine learning models for gully erosion susceptibility mapping. *Geosci. Front.* **2020**, *11*, 1609–1620. [[CrossRef](#)]
394. Phinzi, K.; Abriha, D.; Bertalan, L.; Holb, I.; Szabó, S. Machine Learning for Gully Feature Extraction Based on a Pan-Sharpended Multispectral Image: Multiclass vs. Binary Approach. *ISPRS Int. J. Geo-Inf.* **2020**, *9*, 252. [[CrossRef](#)]
395. Du Plessis, C.; van Zijl, G.; Van Tol, J.; Manyevere, A. Machine learning digital soil mapping to inform gully erosion mitigation measures in the Eastern Cape, South Africa. *Geoderma* **2020**, *368*, 114287. [[CrossRef](#)]
396. D'Eath, R.B.; Jack, M.; Futro, A.; Talbot, D.; Zhu, Q.; Barclay, D.; Baxter, E.M. Automatic early warning of tail biting in pigs: 3D cameras can detect lowered tail posture before an outbreak. *PLoS ONE* **2018**, *13*, e0194524. [[CrossRef](#)]
397. Mansbridge, N.; Mitsch, J.; Bollard, N.; Ellis, K.; Miguel-Pacheco, G.; Dottorini, T.; Kaler, J. Feature Selection and Comparison of Machine Learning Algorithms in Classification of Grazing and Rumination Behaviour in Sheep. *Sensors* **2018**, *18*, 3532. [[CrossRef](#)]
398. Walton, E.; Casey, C.; Mitsch, J.; Vázquez-Diosdado, J.A.; Yan, J.; Dottorini, T.; Ellis, K.A.; Winterlich, A.; Kaler, J. Evaluation of sampling frequency, window size and sensor position for classification of sheep behaviour. *R. Soc. Open Sci.* **2018**, *5*, 171442. [[CrossRef](#)]



399. Yang, Q.; Xiao, D.; Lin, S. Feeding behavior recognition for group-housed pigs with the Faster R-CNN. *Comput. Electron. Agric.* **2018**, *155*, 453–460. [[CrossRef](#)]
400. Zheng, C.; Zhu, X.; Yang, X.; Wang, L.; Tu, S.; Xue, Y. Automatic recognition of lactating sow postures from depth images by deep learning detector. *Comput. Electron. Agric.* **2018**, *147*, 51–63. [[CrossRef](#)]
401. Bishop, J.C.; Falzon, G.; Trotter, M.; Kwan, P.; Meek, P.D. Livestock vocalisation classification in farm soundscapes. *Comput. Electron. Agric.* **2019**, *162*, 531–542. [[CrossRef](#)]
402. Hamilton, A.; Davison, C.; Tachtatzis, C.; Andonovic, I.; Michie, C.; Ferguson, H.; Somerville, L.; Jonsson, N. Identification of the Rumination in Cattle Using Support Vector Machines with Motion-Sensitive Bolus Sensors. *Sensors* **2019**, *19*, 1165. [[CrossRef](#)]
403. Fogarty, E.S.; Swain, D.L.; Cronin, G.M.; Moraes, L.E.; Trotter, M. Behaviour classification of extensively grazed sheep using machine learning. *Comput. Electron. Agric.* **2020**, *169*, 105175. [[CrossRef](#)]
404. Rao, Y.; Jiang, M.; Wang, W.; Zhang, W.; Wang, R. On-farm welfare monitoring system for goats based on Internet of Things and machine learning. *Int. J. Distrib. Sens. Netw.* **2020**, *16*, 155014772094403. [[CrossRef](#)]
405. Xu, B.; Wang, W.; Falzon, G.; Kwan, P.; Guo, L.; Sun, Z.; Li, C. Livestock classification and counting in quadcopter aerial images using Mask R-CNN. *Int. J. Remote Sens.* **2020**, *41*, 8121–8142. [[CrossRef](#)]
406. Riaboff, L.; Poggi, S.; Madouasse, A.; Couvreur, S.; Aubin, S.; Bédère, N.; Goumand, E.; Chauvin, A.; Plantier, G. Development of a methodological framework for a robust prediction of the main behaviours of dairy cows using a combination of machine learning algorithms on accelerometer data. *Comput. Electron. Agric.* **2020**, *169*, 105179. [[CrossRef](#)]
407. Taneja, M.; Byabazaire, J.; Jalodia, N.; Davy, A.; Olariu, C.; Malone, P. Machine learning based fog computing assisted data-driven approach for early lameness detection in dairy cattle. *Comput. Electron. Agric.* **2020**, *171*, 105286. [[CrossRef](#)]
408. Gorczyca, M.T.; Gebremedhin, K.G. Ranking of environmental heat stressors for dairy cows using machine learning algorithms. *Comput. Electron. Agric.* **2020**, *168*, 105124. [[CrossRef](#)]
409. Fu, Q.; Shen, W.; Wei, X.; Zhang, Y.; Xin, H.; Su, Z.; Zhao, C. Prediction of the diet energy digestion using kernel extreme learning machine: A case study with Holstein dry cows. *Comput. Electron. Agric.* **2020**, *169*, 105231. [[CrossRef](#)]
410. Warner, D.; Vasseur, E.; Lefebvre, D.M.; Lacroix, R. A machine learning based decision aid for lameness in dairy herds using farm-based records. *Comput. Electron. Agric.* **2020**, *169*, 105193. [[CrossRef](#)]
411. Borgonovo, F.; Ferrante, V.; Grilli, G.; Pascuzzo, R.; Vantini, S.; Guarino, M. A Data-Driven Prediction Method for an Early Warning of Coccidiosis in Intensive Livestock Systems: A Preliminary Study. *Animals* **2020**, *10*, 747. [[CrossRef](#)]
412. Hyde, R.M.; Down, P.M.; Bradley, A.J.; Breen, J.E.; Hudson, C.; Leach, K.A.; Green, M.J. Automated prediction of mastitis infection patterns in dairy herds using machine learning. *Sci. Rep.* **2020**, *10*, 4289. [[CrossRef](#)]
413. Wang, J.; Bell, M.; Liu, X.; Liu, G. Machine-Learning Techniques Can Enhance Dairy Cow Estrus Detection Using Location and Acceleration Data. *Animals* **2020**, *10*, 1160. [[CrossRef](#)]
414. Denholm, S.J.; Brand, W.; Mitchell, A.P.; Wells, A.T.; Krzyzalewski, T.; Smith, S.L.; Wall, E.; Coffey, M.P. Predicting bovine tuberculosis status of dairy cows from mid-infrared spectral data of milk using deep learning. *J. Dairy Sci.* **2020**, *103*, 9355–9367. [[CrossRef](#)]
415. Ghaffari, M.H.; Jahanbekam, A.; Post, C.; Sadri, H.; Schuh, K.; Koch, C.; Sauerwein, H. Discovery of different metabotypes in overconditioned dairy cows by means of machine learning. *J. Dairy Sci.* **2020**, *103*, 9604–9619. [[CrossRef](#)]
416. Khanh, P.C.P.; Tran, D.T.; Duong, V.T.; Thinh, N.H.; Tran, D.N. The new design of cows' behavior classifier based on acceleration data and proposed feature set. *Math. Biosci. Eng.* **2020**, *17*, 2760–2780. [[CrossRef](#)]
417. Kaler, J.; Mitsch, J.; Vázquez-Diosdado, J.A.; Bollard, N.; Dottorini, T.; Ellis, K.A. Automated detection of lameness in sheep using machine learning approaches: Novel insights into behavioural differences among lame and non-lame sheep. *R. Soc. Open Sci.* **2020**, *7*. [[CrossRef](#)] [[PubMed](#)]
418. Keceli, A.S.; Catal, C.; Kaya, A.; Tekinerdogan, B. Development of a recurrent neural networks-based calving prediction model using activity and behavioral data. *Comput. Electron. Agric.* **2020**, *170*, 105285. [[CrossRef](#)]
419. Rodríguez Alvarez, J.; Arroqui, M.; Mangudo, P.; Toloza, J.; Jatip, D.; Rodríguez, J.M.; Teyseyre, A.; Sanz, C.; Zunino, A.; Machado, C.; et al. Body condition estimation on cows from depth images using Convolutional Neural Networks. *Comput. Electron. Agric.* **2018**, *155*, 12–22. [[CrossRef](#)]
420. Gorczyca, M.T.; Milan, H.F.M.; Maia, A.S.C.; Gebremedhin, K.G. Machine learning algorithms to predict core, skin, and hair-coat temperatures of piglets. *Comput. Electron. Agric.* **2018**, *151*, 286–294. [[CrossRef](#)]
421. Pu, H.; Lian, J.; Fan, M. Automatic Recognition of Flock Behavior of Chickens with Convolutional Neural Network and Kinect Sensor. *Int. J. Pattern Recognit. Artif. Intell.* **2018**, *32*. [[CrossRef](#)]
422. Rahman, A.; Smith, D.V.; Little, B.; Ingham, A.B.; Greenwood, P.L.; Bishop-Hurley, G.J. Cattle behaviour classification from collar, halter, and ear tag sensors. *Inf. Process. Agric.* **2018**, *5*, 124–133. [[CrossRef](#)]
423. Shahinfar, S.; Kahn, L. Machine learning approaches for early prediction of adult wool growth and quality in Australian Merino sheep. *Comput. Electron. Agric.* **2018**, *148*, 72–81. [[CrossRef](#)]
424. Shine, P.; Murphy, M.D.; Upton, J.; Scully, T. Machine-learning algorithms for predicting on-farm direct water and electricity consumption on pasture based dairy farms. *Comput. Electron. Agric.* **2018**, *150*, 74–87. [[CrossRef](#)]
425. Wang, D.; Tang, J.L.; Zhu, W.; Li, H.; Xin, J.; He, D. Dairy goat detection based on Faster R-CNN from surveillance video. *Comput. Electron. Agric.* **2018**, *154*, 443–449. [[CrossRef](#)]

426. Elahi, E.; Weijun, C.; Jha, S.K.; Zhang, H. Estimation of realistic renewable and non-renewable energy use targets for livestock production systems utilising an artificial neural network method: A step towards livestock sustainability. *Energy* **2019**, *183*, 191–204. [[CrossRef](#)]
427. Miller, G.A.; Hyslop, J.J.; Barclay, D.; Edwards, A.; Thomson, W.; Duthie, C.-A. Using 3D Imaging and Machine Learning to Predict Liveweight and Carcass Characteristics of Live Finishing Beef Cattle. *Front. Sustain. Food Syst.* **2019**, *3*, 30. [[CrossRef](#)]
428. Tian, M.; Guo, H.; Chen, H.; Wang, Q.; Long, C.; Ma, Y. Automated pig counting using deep learning. *Comput. Electron. Agric.* **2019**, *163*, 104840. [[CrossRef](#)]
429. Alves, A.A.C.; Pinzon, A.C.; da Costa, R.M.; da Silva, M.S.; Vieira, E.H.M.; de Mendonca, I.B.; Lôbo, R.N.B. Multiple regression and machine learning based methods for carcass traits and saleable meat cuts prediction using non-invasive in vivo measurements in commercial lambs. *Small Rumin. Res.* **2019**, *171*, 49–56. [[CrossRef](#)]
430. Gredell, D.A.; Schroeder, A.R.; Belk, K.E.; Broeckling, C.D.; Heuberger, A.L.; Kim, S.Y.; King, D.A.; Shackelford, S.D.; Sharp, J.L.; Wheeler, T.L.; et al. Comparison of Machine Learning Algorithms for Predictive Modeling of Beef Attributes Using Rapid Evaporative Ionization Mass Spectrometry (REIMS) Data. *Sci. Rep.* **2019**, *9*, 1–9. [[CrossRef](#)]
431. Shahinfar, S.; Kelman, K.; Kahn, L. Prediction of sheep carcass traits from early-life records using machine learning. *Comput. Electron. Agric.* **2019**, *156*, 159–177. [[CrossRef](#)]
432. Bakoev, S.; Getmantseva, L.; Kolosova, M.; Kostyunina, O.; Chartier, D.R.; Tatarinova, T.V. PigLeg: Prediction of swine phenotype using machine learning. *PeerJ* **2020**, *2020*, e8764. [[CrossRef](#)]
433. Fuentes, S.; Gonzalez Viejo, C.; Cullen, B.; Tongson, E.; Chauhan, S.S.; Dunshea, F.R. Artificial Intelligence Applied to a Robotic Dairy Farm to Model Milk Productivity and Quality based on Cow Data and Daily Environmental Parameters. *Sensors* **2020**, *20*, 2975. [[CrossRef](#)]
434. Cairo, F.C.; Pereira, L.G.R.; Campos, M.M.; Tomich, T.R.; Coelho, S.G.; Lage, C.F.A.; Fonseca, A.P.; Borges, A.M.; Alves, B.R.C.; Dorea, J.R.R. Applying machine learning techniques on feeding behavior data for early estrus detection in dairy heifers. *Comput. Electron. Agric.* **2020**, *179*, 105855. [[CrossRef](#)]
435. Ma, S.; Yao, Q.; Masuda, T.; Higaki, S.; Yoshioka, K.; Arai, S.; Takamatsu, S.; Itoh, T. Development of an Anomaly Detection System for Cattle Using Infrared Image and Machine Learning. *Sens. Mater.* **2020**, *32*, 4139–4149. [[CrossRef](#)]
436. Shahinfar, S.; Al-Mamun, H.A.; Park, B.; Kim, S.; Gondro, C. Prediction of marbling score and carcass traits in Korean Hanwoo beef cattle using machine learning methods and synthetic minority oversampling technique. *Meat Sci.* **2020**, *161*, 107997. [[CrossRef](#)]



## Article

# Weed Classification Using Explainable Multi-Resolution Slot Attention

Sadaf Farkhani \*, Søren Kelstrup Skovsen, Mads Dyrmann, Rasmus Nyholm Jørgensen and Henrik Karstoft

Department of Electrical and Computer Engineering, Aarhus University, 8200 Aarhus, Denmark; ssk@ece.au.dk (S.K.S.); madsdyrmann@ece.au.dk (M.D.); rnj@agrointelli.com (R.N.J.); hka@ece.au.dk (H.K.)  
\* Correspondence: farkhanis@ece.au.dk

**Abstract:** In agriculture, explainable deep neural networks (DNNs) can be used to pinpoint the discriminative part of weeds for an imagery classification task, albeit at a low resolution, to control the weed population. This paper proposes the use of a multi-layer attention procedure based on a transformer combined with a fusion rule to present an interpretation of the DNN decision through a high-resolution attention map. The fusion rule is a weighted average method that is used to combine attention maps from different layers based on saliency. Attention maps with an explanation for why a weed is or is not classified as a certain class help agronomists to shape the high-resolution weed identification keys (WIK) that the model perceives. The model is trained and evaluated on two agricultural datasets that contain plants grown under different conditions: the Plant Seedlings Dataset (PSD) and the Open Plant Phenotyping Dataset (OPPD). The model represents attention maps with highlighted requirements and information about misclassification to enable cross-dataset evaluations. State-of-the-art comparisons represent classification developments after applying attention maps. Average accuracies of 95.42% and 96% are gained for the negative and positive explanations of the PSD test sets, respectively. In OPPD evaluations, accuracies of 97.78% and 97.83% are obtained for negative and positive explanations, respectively. The visual comparison between attention maps also shows high-resolution information.

**Keywords:** transformer; slot attention; explainable neural network; fusion rule; weed classification; weed identification key; precision agriculture

**Citation:** Farkhani, S.; Skovsen, S.K.; Dyrmann, M.; Jørgensen, R.N.; Karstoft, H. Weed Classification Using Explainable Multi-Resolution Slot Attention. *Sensors* **2021**, *21*, 6705. <https://doi.org/10.3390/s21206705>

Academic Editors: Asim Biswas, Dionysis Bochtis and Aristotelis C. Tagarakis

Received: 30 June 2021  
Accepted: 1 October 2021  
Published: 9 October 2021

**Publisher's Note:** MDPI stays neutral with regard to jurisdictional claims in published maps and institutional affiliations.



**Copyright:** © 2021 by the authors. Licensee MDPI, Basel, Switzerland. This article is an open access article distributed under the terms and conditions of the Creative Commons Attribution (CC BY) license (<https://creativecommons.org/licenses/by/4.0/>).

## 1. Introduction

Weeds compete with crops to capture sunlight and take up nutrients and water; this competition leads to significant yield losses around the world every year [1]. Furthermore, there are considerable indirect negative externalities that should be taken into consideration when combating weeds [2]. Currently, the use of conventional weed control methods usually results in soil erosion, global warming, and human health problems [3–6]. Weeds are usually not distributed evenly across farmlands. Therefore, weed management could be greatly improved by collecting information about the location, type, and amount of weeds in an area [7].

In general, there are three primary weed management strategies: biological, chemical, and physical [8]. Biological weed management refers to weed control through the use of other organisms, such as insects or bacteria, to maintain weed populations at a lower level [9]. Biological weed control is, however, a prolonged procedure that reduces the growth of a specific species. Selective chemical weed management using an autonomous and unmanned vehicle is one solution for controlling the weed population and requires the use of considerably lower contamination doses [10]. In the physical approach, weeds are controlled without herbicide; this is typically accomplished through the use of mechanical tools. Physical weed control requires extra precision in the detection of weeds, as non-selective and incorrect weed detection can harm the crop.

In physical and chemical methods, weed management is conducted in two steps: capturing images in the field and weed detection/classification [11]. The earlier step can feasibly be carried out through the use of new imaging technologies. In the second step, however, collecting and labeling data is a time-consuming and error-prone procedure, especially in agricultural areas where many different kinds of plants are mixed in [12–14]. In artificial neural network (ANN) modeling, it is possible to determine imprecise temporal and spatial parameters [15,16]. Thus, autonomous weed management methods combined with computer vision approaches could help farmers to detect and classify weeds and consequently improve weed management and decision-making [17,18]. Thus, the application of an accurate weed classification method plays a critical role in precise farming, helping to determine the weed-combating approach used, maximize crop yields, and improve economical returns [19–22].

CNNs have shown promising performance for image classification, including agricultural applications. However, one of the main challenges with deep neural networks (DNNs) is the lack of explanation, known as the *black-box* problem, concerning the human perception of the model's logic within the classification [23]. Therefore, an interpretable map is an efficient means of explaining the model's prediction as well as understanding the data better.

To mitigate the aforementioned challenges, explainable artificial intelligence (XAI) is proposed to present a better explanation of *black-box* DNN models [24]. In classification methods based on XAI, the model identifies the class prediction and highlights the critical data content to draw attention to a given decision. Therefore, the models are also called attention models.

In agriculture, the model's explanation map supports a research area called the weed identification key (WIK), which is mainly adopted to discriminate species with a higher accuracy [25]. WIKs assist agronomists in classifying both common and uncommon features between species with an acceptable level of accuracy. Therefore, the model's transparency helps us to create and understand the WIKs perceived by the model.

Positive and negative explanation maps, which explain why a model does or does not classify an image into a corresponding category, introduce both mutual and distinctive perceptible features from different classes. The negative explanation is especially informative in classification problems with high similarities between classes, such as in agricultural datasets [26].

Conventional WIKs include both positive and negative explanations simultaneously. In computer vision problems, self-attention transformers are utilized to discriminate the locations of objects. According to [27], the slot attention module includes multi-head attention blocks with dynamic weights [28,29]. Slot attention describes the latent features of DNNs by training a set of abstract representations, called slots, for different classes. In a slot attention module, discriminative object regions will be extracted without the need to use humans for supervision. The slot attention, however, will have a low resolution due to the poor resolution of the DNN's latent features [26].

In this paper, two agricultural datasets are employed in the analysis: the Plant Seedlings Dataset (PSD) [30] and the Open Plant Phenotyping Database (OPPD) [31]. Both datasets have a weed species-annotated bounding-box for each plant. To improve the resolution of the slot attention with high-level semantics and fine details, a multi-resolution mechanism is adopted here that is based on the slot attention module. Afterwards, to manipulate different feature layers' impacts on the resulting attention map, a weighted mean approach is used to combine multi-resolution maps regarding their saliency. Three main aspects are used for creating the slot attention in agricultural applications, and the proposed model is evaluated based on them: (1) the resolution of the attention map, (2) the size of the area covering the object, and (3) the features of the weed species that cause the model to not classify the weed as another class (hereafter called negative explanation).

The proposed framework for multi-resolution slot attention and the proposed weighted average method in this paper are described in Section 2. Then, in Section 3, the results are elaborated within two different setups. Lastly, the discussion and conclusion are provided in Sections 4 and 5, respectively.

## 2. Materials and Methods

### 2.1. Utilized Datasets

The model was trained and tested with two different datasets to evaluate how well it could support attention on mutual features. Hence, two plant seedling datasets, PSD and OPPD, were employed in this paper. Differences in the growing medium were used to evaluate the proposed model on agricultural datasets with changing settings.

In Table 1, the European and Mediterranean Plant Protection Organization (EPPO) labels for the species utilized in this paper are shown. Monocot and dicot species are represented by M and D, respectively, in Table 1.

**Table 1.** EPPO code and English name of the species utilized in this paper.

EPPO Code	English Name	Mono/Dicot
ALOMY	Black grass	M
APESV	Loose silky-bent	M
BEAVP	Sugar beet	D
CAPBP	Shepherd's purse	D
CHEAL	Fat hen	D
GALAP	Cleavers	D
GERMO	Small-flowered crane's bill	D
MATIN	Scentless mayweed	D
SINAR	Charlock	D
STEME	Common chickweed	D
TRZAW	Common wheat	D
ZEAMA	Maize	M

The PSD contains images of 960 unique plants across 12 plant species in several growth stages with a ground sampling distance of 10 pixels per mm [30]. The camera (Canon 600D) was placed at a 110–115 cm distance above the soil surface. Plants in the PSD are grown indoors with even illumination conditions. The surface of the soil in the PSD is covered with stones to avoid green indoor moss artifacts and to ease the distinction between plants and the background. There is no specific plant color variation in the PSD. In the PSD, weed species are detected and cropped out.

The original OPPD is comprised of 64,292 unique crop plants. These plants include 47 different species in multiple growth stages with a ground sampling distance of 6.6 pixels per mm [31]. In our work, we only considered growth stages and species that are common in the PSD. Therefore, 21,653 and 5393 plant images are utilized as training and test sets here, respectively. Images were illuminated using a ring flash to ensure consistent light conditions during the image acquisition. The OPPD was able to better capture the naturally occurring variability in the plant morphology of the species in abnormal conditions. To meet this goal, plants were grown with different amounts of water and levels of nutrition stress. As with the PSD, there is only one plant per image for training and testing the model.

Figure 1 shows different samples from species that are common to both the PSD and OPPD, respectively. Images are sorted from the left to right according to the growth stage. Three samples are shown for the OPPD and two for the PSD, since growth stage diversity is higher in the OPPD. There are multiple images for each plant in the growing procedure. The images depicted in Figure 1 were resized to a common resolution. Moreover, the samples in the training and test sets were randomly divided into proportions of 80% and 20%, respectively. The training and test samples were randomly separated for each image.

There are nine mutual species in the PSD and OPPD. Twelve species from the PSD were utilized in experiments when the PSD was employed for both training and testing. Otherwise, only the nine common species of the PSD and OPPD were fed into the network. The two datasets have different illumination conditions. For instance, there is a bright area around the terminal bud in the later growth stages of *CHEAL*, which is a deterministic feature. However, this feature is more apparent in the OPPD than in the PSD due to the illumination. Therefore, the combination of these two datasets could assist us in finding which features were brought out by the model and whether the absent features were essential.

It is necessary to mention that the scale of the images is varied due to the data augmentation technique (explained in Section 2.3) applied to the training set. Therefore, the differences in resolution between the two datasets cause no serious problem. On the other hand, the model's generalizability was examined under changing light, acquisition, and growth conditions. We recommend that the reader review [30,31] if more details about the data acquisition process used in the PSD and OPPD are required.

## 2.2. Neural Network Architecture

The overall framework of the proposed pyramid representation—hereafter called high-resolution attention—was inspired by feature pyramid networks [32,33]. By extracting features from different levels, a high-resolution representation of the attention map was achieved (Figure 2).

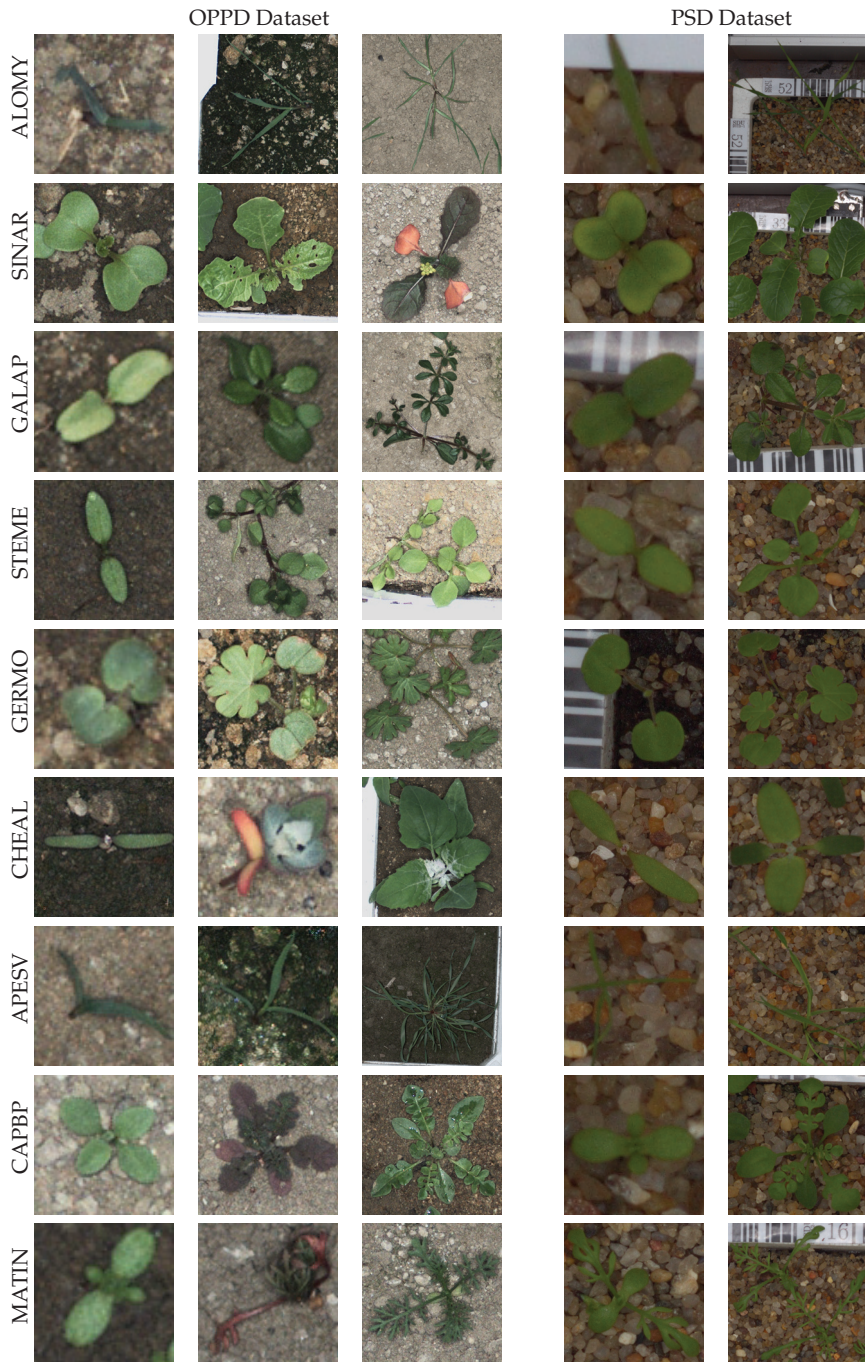
The RGB input image is passed through a DNN to extract features at multiple depths and spatial resolutions (Figure 2a). The extracted features are then passed through the slot attention module (Figure 2b). The slot attention module mainly consists of a transformer. Ultimately, the extracted attention maps gained for other classes from different resolution levels are merged to obtain the high-resolution attention map as the output.

### 2.2.1. Slot Attention

The slot attention is generated based on the feature regions with a great explainability of the class. The impact of different regions is formulated using positional encoding in Figure 2b. In this section, we illustrate not only the attention mechanism utilized [27], but also the method proposed to be used for extracting multi-resolution attention maps.

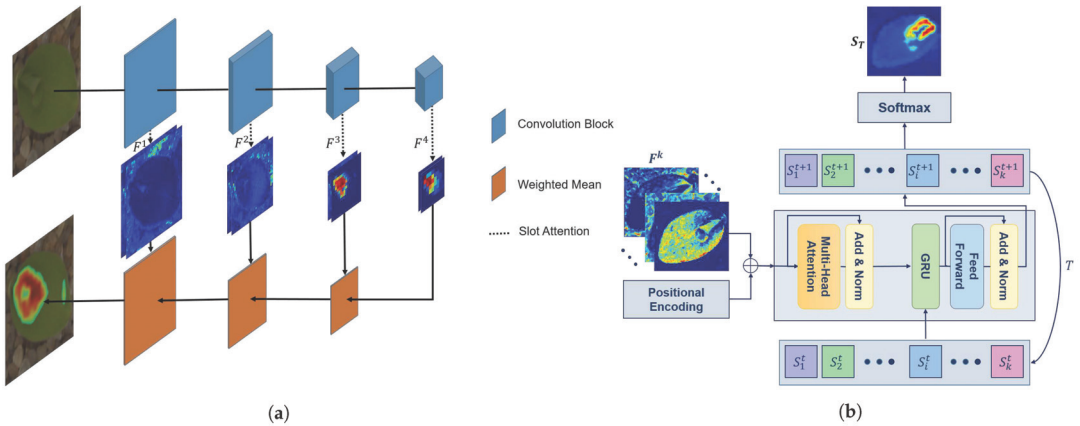
In Figure 2, the features were first extracted from different levels  $F^n$  of the backbone.  $n$  depends on the number of spatial downsampling processes used in the DNN, which was four in the ResNet50 [34] adopted in this study. Then,  $F^n$ s were individually passed through the slot attention module to extract highlighted regions. Slot attention based on a transformer is an iterative module with  $K$  slots, where each slot describes a class in a  $K$ -classification problem. Through extracted features and positional encoding, the slots are trained to present maps with a high ability to explain the object. Slots are shown by  $S_i^t$  and randomly initialized using a Gaussian distribution.





**Figure 1.** Examples of nine common species from the OPPD and PSD samples during different maturity stages, from left to right. OPPD samples were also selected from non-stressed and stressed samples.





**Figure 2.** The proposed architecture for plant classification using the slot attention module. (a) The overall architecture for extracting features using convolutional blocks (in blue), including obtaining the highlighted attention areas from different convolutional blocks and combining multi-resolution slot attention to generate the final attention map (orange blocks). (b) The slot attention module applied to K-class weed classification using the transformer concept. Slots are depicted as  $S_i^t$  for class  $i$  in iteration  $t$ .

In the multi-head attention block shown in Figure 2, there are three main learnable vectors: keys ( $k$ ), queries ( $q$ ), and values ( $v$ ) [35]. The  $q$  are the slots  $S_k$  updated within  $T$  iterations. According to [27], the slots are trained to be sufficiently precise after three iterations. While  $q$  is formed based on the labels used,  $k$  and  $v$  are based on the inputs. The higher the similarity gained between  $q$  and  $k$  is, the better the model has been trained with respect to precision of explanation:

$$U^{t+1} = \langle \text{Softmax}\left(\frac{1}{\sqrt{D}} \langle k(\text{inputs}), q(\text{slots})^T \rangle\right)^T, v(\text{inputs}) \rangle, \quad (1)$$

where Equation (1) is the multi-head attention block shown in Figure 2;  $D$  is the common dimension space between three vectors  $q$ ,  $k$ , and  $v$  utilized as a normalization term; and  $U^{t+1}$  is the updated slots obtained in iteration  $t$ . The inner product  $\langle \cdot, \cdot \rangle$  of the vectors is computed to find the vectors' similarities. Softmax is then applied to normalize the attention maps and suppress the attention gained for the other classes. Then, a gated recurrent unit (GRU) is utilized to update the slots [36]. GRU is a learnable recurrent function that is used for updating slots with the aggregated updates and previous slots. In [27], the investigations show improvements in the model's performance when a multi-layer perceptron (MLP) is adopted after the GRU,

$$S^{t+1} = \text{MLP}(\text{GRU}(S^t, e \cdot U^{t+1})), S^t = [S_1^t, S_2^t, \dots, S_k^t], \quad (2)$$

where  $S^t$  and  $S^{t+1}$  are the previous and updated slots, respectively. Therefore, all the slots are updated in each iteration. To easily switch between positive and negative explanations, the sign parameter  $e$  is determined. A comprehensive description of the negative explanation and Equation (2) is provided in the study of [26].

Instead of interpolating the last layer features to gain an attention map with the same input dimension, we applied the slot attention after four convolutional blocks in ResNet50. Afterwards, slots from different layers with different resolutions were combined using a fusion rule described in the next section.

### 2.2.2. Fusion Rule

In slot attention, deeper layers have a sparse but high accuracy regarding the object explanation, albeit with a lower spatial resolution. On the other hand, shallower layers

have a high spatial resolution with a lower accuracy regarding object localization. When combining different layers of slot attention, the degree of certainty should impact the dedicated weight of the fused attention maps. The higher the average values of the slots are, the higher the model's certainty will be with regard to localization. Therefore, a slot attention map with higher average values should have a higher impact on the fused attention map. The following equation was used for this purpose to combine different layer attention maps:

$$S_F = \sum_{l=1}^n \frac{W_l}{\sum_{j=1}^n W_j} \cdot S^l, \quad (3)$$

where  $W_l$  is the summation of elements in the updated slots for the  $l$ th layer of the backbone. In other words, the attention map with the highest  $W_l$  had the greatest effect on the fused slots  $S_F$ . In Figure 2, the fusion rule is represented by an orange block. Therefore, the final attention map was formed based on the combination of shallow layers with a high precision and deep layers with a high resolution. The proposed weighted mean approach preserves the highlighted areas through the use of upsampling.

### 2.2.3. Loss

Two loss functions were required for this problem: one for the classification and the other for the attention. For the classification, the cross-entropy ( $L_{CE}$ ) of the deepest layer of the backbone was computed, ref. [26] presents SCOUTER loss, defining how large the attention area should be through the formula:

$$L_{SCOUTER} = L_{CE} + \lambda W, \quad (4)$$

where  $W$  is the sum of elements in the slots gained from different backbone layers controlled by the hyperparameter  $\lambda$ .  $\lambda$  is adjusted based on how broad the attention areas are in the specific dataset.

### 2.3. Parameter Setting

Input images in both PSD and OPPD have square dimensions. Input images were first resized to  $360 \times 360$  pixels with bilinear interpolation to balance images with different dimensions at different growth stages. Then, ResNet50 [34] was used as the backbone in order to extract the latent features. There are four convolutional blocks in ResNet50. Thus, four slot attention modules were implemented on intermediate features to merge the attention maps created based on their saliency. The model is implemented by PyTorch v1.7. The model was pretrained using ImageNet [37]. The batch size was 32, the initial learning rate was  $10^{-4}$ , and AdamW [38] was utilized as the optimizer. The attention was shown in positive and negative explanations. In Equation (4),  $\lambda$  was set to 2 in all evaluations based on trial and error. The number of iterations used for the slot attention was set to three. Additionally, the model was trained in 80 epochs. In the training procedure, the model was trained using multiple training processes on four GPUs (48 GB).

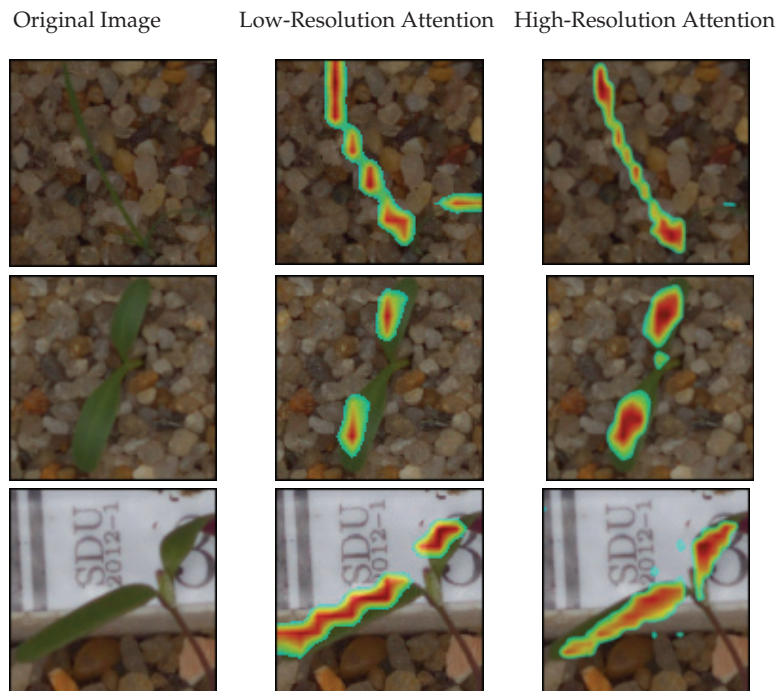
Translation, rotation, scaling, shear, cut-out, image corruption, Gaussian noise, and color space-changing methods were utilized as data augmentation techniques (color augmentation was only employed for generating results in Section 3.3). The translation (along the x and y axes), rotation, scaling, and shear were randomly selected within  $[-0.1, 0.1]$  of the input's dimension,  $[-10^\circ, 10^\circ]$ ,  $[0.8, 1]$ , and  $[-20^\circ, 20^\circ]$ , respectively. Only a few data augmentation methods were randomly applied to the data each time in order to avoid significant variations in the images.

## 3. Results

This section is ordered into an exploration of attention maps from different backbone layers, an evaluation of the PSD, and a cross-evaluation of the OPPD and PSD.

### 3.1. Multi-Resolution Attention

Figure 3 shows the attention maps gained using three examples from different classes (narrow and broad leaves). The attention map was utilized as the alpha channel, with areas with values close to zero neglected by applying a threshold. The original images are shown to give a better view of where weeds are located. Low-resolution attention was obtained by using only the backbone's last layer of slot attention. High-resolution attention was obtained by applying the weighted average to the attention maps gained from different levels.



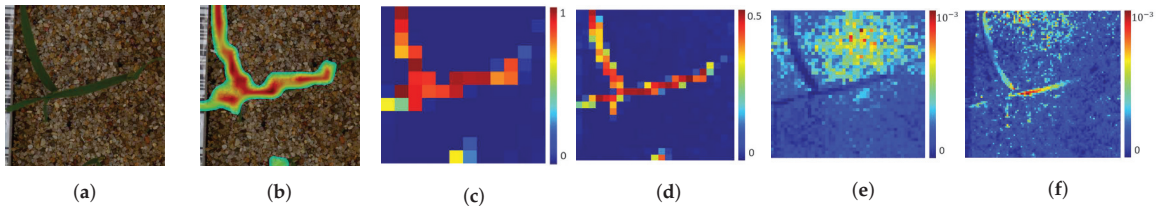
**Figure 3.** Comparison between the low- and high-resolution predicted attention map for three samples from different classes.

The attention map gained from only the last layer of the backbone is highly precise in terms of discriminating the salient features of weeds, as shown in the middle column of Figure 3. In the low-resolution attention map, highlighted areas were roughly distributed along the horizontal and vertical axes due to the interpolation (the middle column in Figure 3). Moreover, attention spots in the low-resolution map were not placed precisely on the weed. Contrarily, the high-resolution attention map was distributed smoothly along the plant (the right column in Figure 3).

It is worth mentioning that the predicted attention was partly placed on the background in some cases of high-resolution attention (such as the last row in Figure 3). This phenomenon was likely due to the impact of shallower layers on the combined attention map. This result could also be related to noisy backgrounds, blurred features, etc. For example, in the last row of Figure 3, the high-resolution attention map also points to stones and the box in the background.

Additionally, attention maps from different layers on a weed-specific sample are shown in Figure 4. All slots from different layers are scaled up in Figure 4. The two last layers (Figure 4e,f) had an excellent resolution compared with the slot attention from the other layers (Figure 4c,d). Normalized heatmaps from various slots are presented here in order to give a better demonstration of each layer's attention. The scale bar for

each slot is presented alongside it. It is necessary to mention that the legends are not directly comparable between figures. The 4th and 3th layers' weights, referred to as  $W_j$  in Equation (3), were considerably more important than the 2nd and 1st layers. In other words, while the attention maps extracted from the deeper layers (Figure 4c,d) had a higher accuracy in identifying plants, the attention maps from shallower layers (Figure 4e,f) had lower attention weights for the whole image.

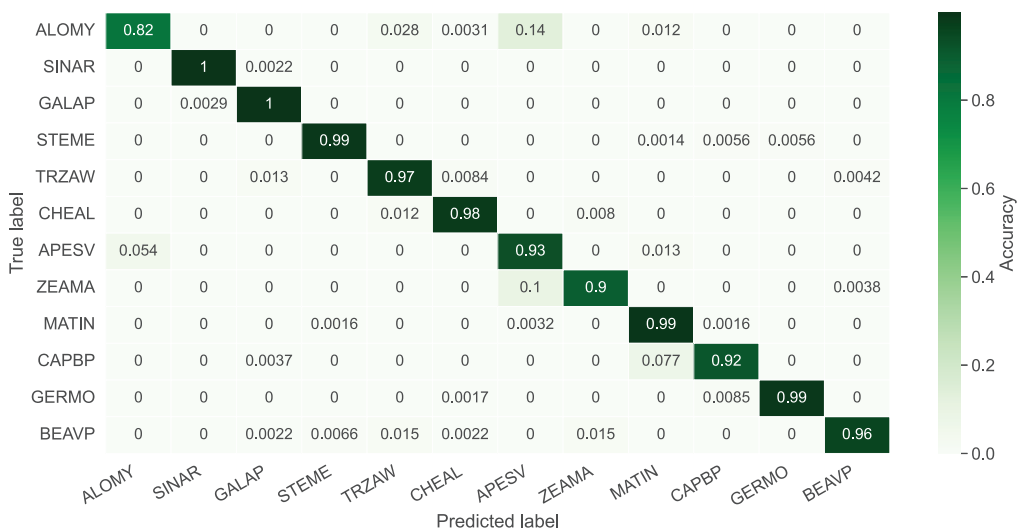


**Figure 4.** The impact of multi-resolution attention maps. (a) The original image and (b) the weighted averaged attention map. (c) 4th layer, (d) 3rd layer, (e) 2nd layer, and (f) 1st layer slot attention gained from the backbone layers. The bluish areas in (b) were filtered to improve the clarity of the visualization.

The weighted average fusion rule provides a balance between accurate, low-resolution attention from the last layer and inaccurate, high-resolution attention from the first layer. In Figure 4b, the attention map has a multi-directional explanation from shallower layers with a high accuracy in detecting weeds from deeper layers simultaneously. Therefore, the distribution of the attention maps was enhanced and developed to provide precise, omnidirectional attention maps. The omnidirectional attention map was created using high-resolution attention maps from shallower layers.

### 3.2. Evaluations on the PSD

In this section, all 12 species in the PSD are employed for training and inference. In Figure 5, the average confusion matrix for the test set is shown for the negative explanation across ten repeats. The negative attention helps us to explicitly understand the data better. The average is then computed, since the model performance slightly changes for the random data augmentation and weight initialization. All samples visualized in attention matrices were selected from correctly classified instances.

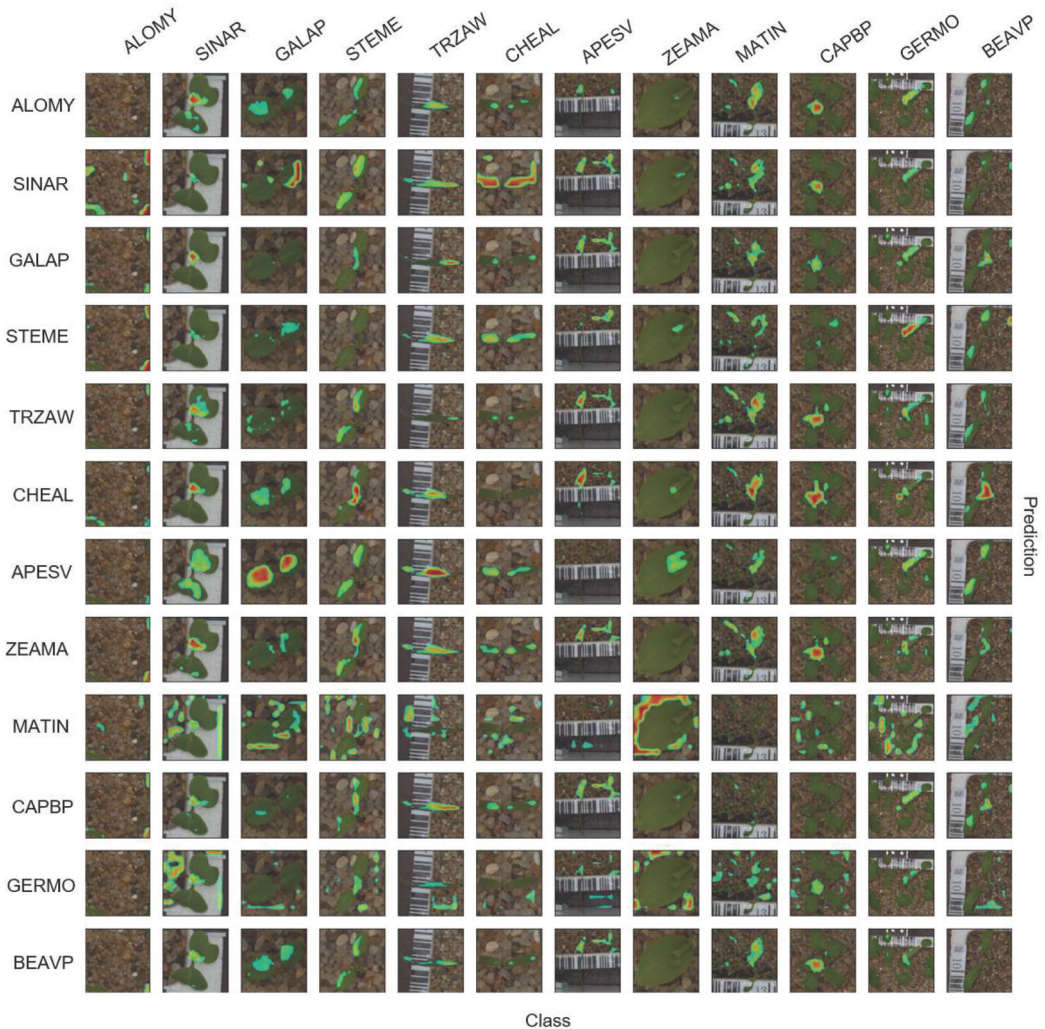


**Figure 5.** The average confusion matrix for the negative explanation of the PSD test set with 12 classes. The overall accuracy gained was 95.42%.



In Figure 5, the average accuracy is 95.42%. The diagonal of the matrix has a more than 90% accuracy for all samples, except *ALOMY*. *ALOMY* and *APESV* are both monocots (narrow leaves), and it is hard to discriminate them using an agronomist. Since *APESV* comprises more samples than *ALOMY*, the model presented a clear bias towards misclassifying monocot samples as *APESV* when the uncertainty is high. Additionally, the model showed a clear tendency to classify *ZEAMA* (also monocot) as *APESV*. However, *ZEAMA* has a particular feature in earlier growth stages, making it easier for the model to identify it than *ALOMY*. Therefore, the model has a higher certainty for *ZEAMA*, particularly in the earlier growth stages.

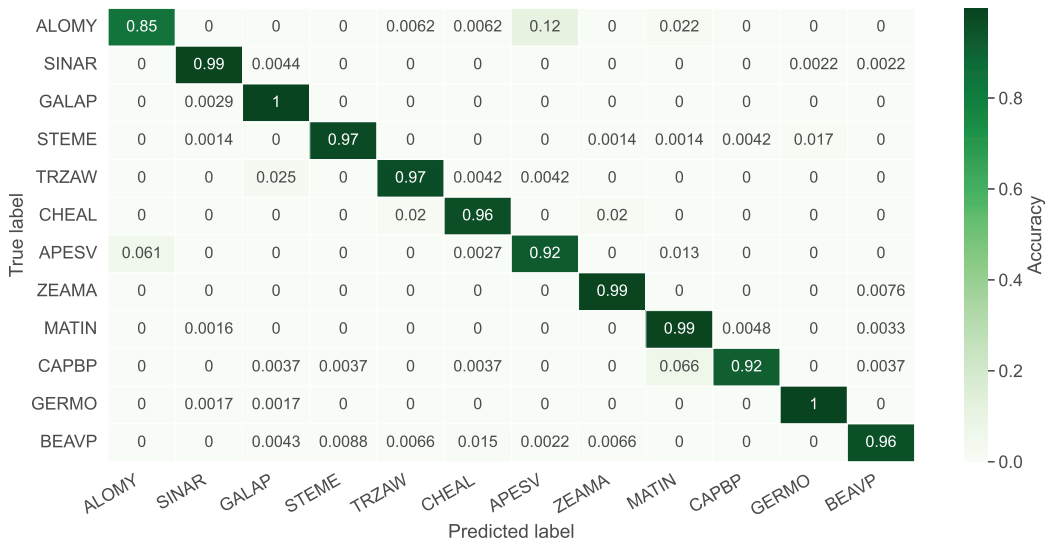
In Figure 6, the attention confusion for the negative explanation is shown. It is expected that the highlighted areas will be absent in the diagonal, while the non-diagonal images will have meaningful distinctive attention areas.



**Figure 6.** Negative attention matrix for PSD dataset with 12 classes. Columns are classes and rows are model predictions. The attention matrix's diagonal has remarkably less attention, since the model classifies using the negative loss value in Equation (2).

The feature is well represented by the highlighted area, which is used for predicting APESV for ZEAMA. In Figure 6, the highlighted spots on the background were supposed to be generated for two reasons: (i) the scale of the stones varied regarding the growth stage (input images were re-scaled to  $360 \times 360$ ) and the background had remarkable impacts in classes with small changes across different growth stages, and (ii) the positive layer's weights were on the background while the negative layer's weights were on the foreground.

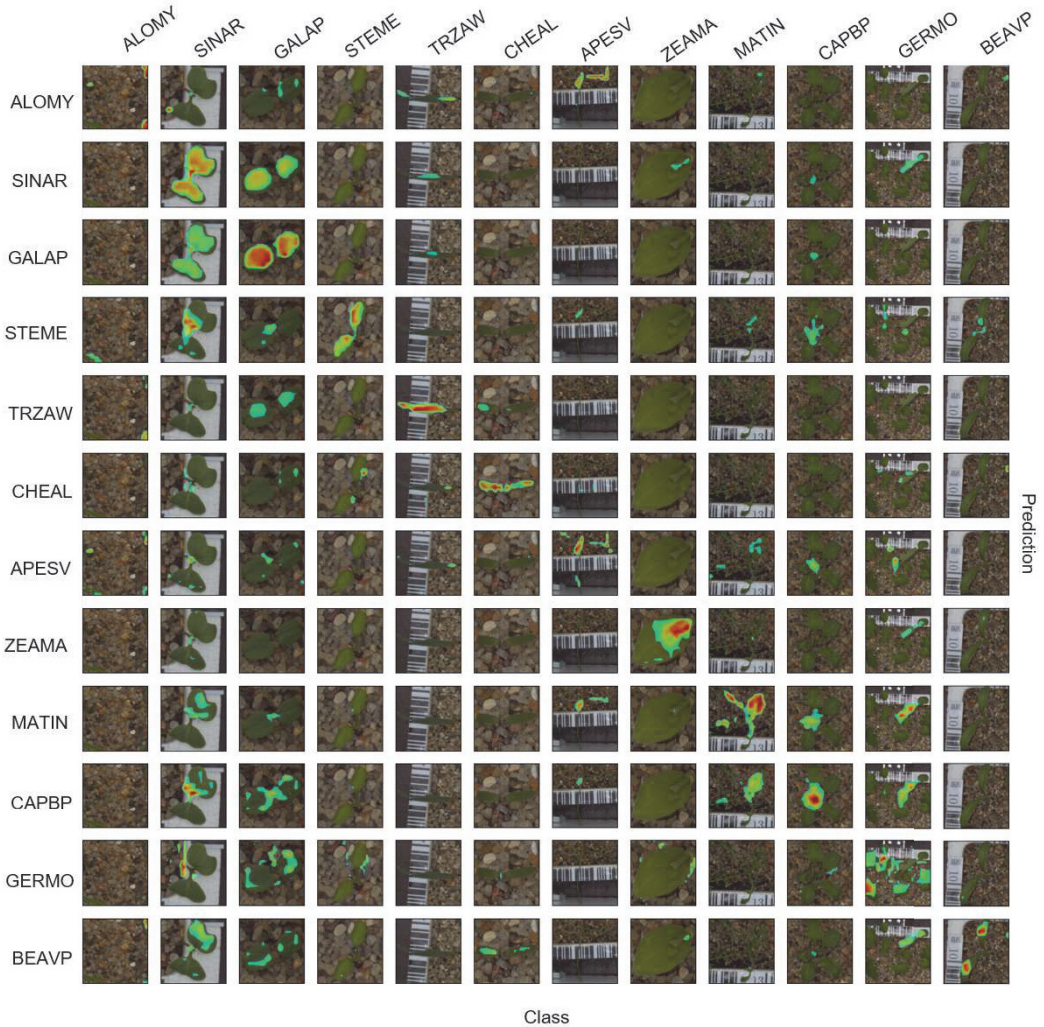
The positive confusion matrix is shown in Figure 7, which led to a similar trend as that for the negative explanation. The non-diagonal predictions for the same class are helpful for understanding which features were missed in the dataset or which species had higher similarities that made the model uncertain. Therefore, a high number of doubtful species were recognized and could be utilized as an alarm in the other field classification.



**Figure 7.** Confusion matrix for the positive explanation of the PSD test set with 12 classes. The average gained accuracy was 96%. The diagonal with a dark heatmap is desirable.

The same samples in the negative explanation are selected for the positive explanation in Figure 8. The diagonal attention areas show which part of the plant has a significant weight in classification during training. In other words, the positive explanation emphasizes species patterns that are necessary for the model. In class ZEAMA, for instance, the highlighted area shows the particular part that is unique in the class and not the whole leaf. Comparing Figure 7 with Figure 5, it can be seen that the accuracy of the class ZEAMA improved by approximately 9% from the negative to the positive explanation. The reason for this was that ZEAMA has similarities to both monocots and dicots (broadleaves). As a result, it was simpler for the network to reveal the unique feature for ZEAMA (in Figure 8) in the negative explanation (in Figure 6). This also reveals the accuracy improvement from the negative to positive explanation.

In Figure 8, the model came with different parts of plants in different classes or growth stages, depending on the similarities between species. For instance, while the model's attention was on the whole leaves for GALAP, as an example of a case that is difficult to classify during early growth stages, the main attention was on the center of the plant for CAPBP, as an example of a case that is easier to classify in the later growth stages.



**Figure 8.** The positive attention matrix for the PSD test set with 12 classes. The diagonal images bold out the particular features that the model uses for the classification.

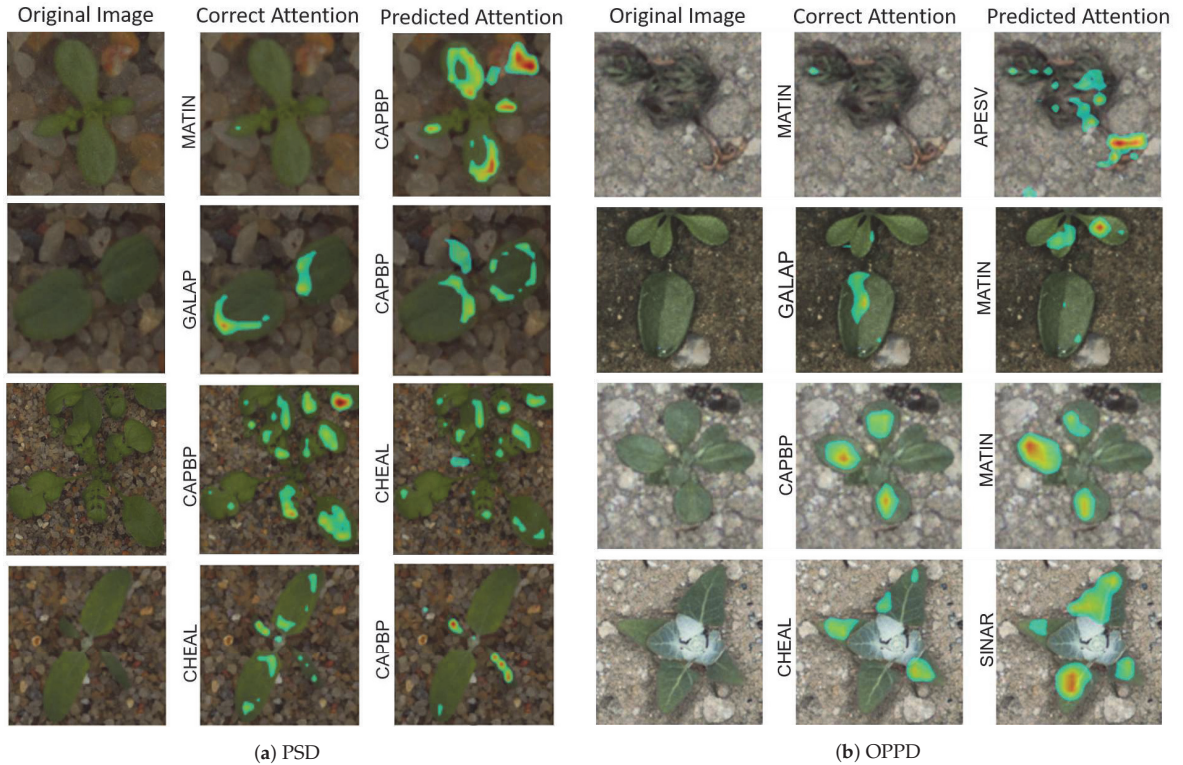
### 3.3. Evaluations on PSD and OPPD

In this section, the model was trained on the PSD and inferred on the OPPD as a cross-dataset evaluation. In Figure 9, eight misclassified samples are shown through cross-dataset evaluation. For each sample, correct and predicted positive attention maps are depicted on the original image. The label for each slot attention is presented on the left side of the image. Four class species are shown for two cross-dataset evaluations: (i) in Figure 9a, the model was trained on the OPPD and evaluated on the PSD, while (ii) in Figure 9b the model was trained on the PSD and tested on the OPPD.

Classes *CAPBP* and *MATIN* look similar in their earlier growth stages, which made prediction harder. Furthermore, samples of stressed species from the OPPD were misclassified in most cases. For instance, a stressed sample from class *MATIN* is shown in Figure 9b from the OPPD which was predicted as class *APESV*.



In Table 2, a comparison between the use of the proposed method and state-of-the-art methods on the PSD and OPPD is shown. The proposed method in this study was evaluated with both a positive explanation, *Ours+*, and a negative explanation, *Ours-*. For the PSD, two other state-of-the-art methods are compared in Table 2.



**Figure 9.** Misclassified samples in cross-dataset evaluation. In (a), the model was trained on the OPPD with positive attention, while the inference was trained on the PSD. Conversely, in (b), the model was trained on the PSD with positive attention, while the inference was trained on the OPPD.

**Table 2.** The comparison between the use of multi-resolution attention on the PSD and OPPD test sets with the state-of-the-art methods.

	Dataset	Accuracy (%)	Parameters (M)
EffNet [39]	OPPD	95.44	7.8
ResNet50 [40]	OPPD	95.23	25
<b>Ours-</b>	OPPD	95.42	23.98
<b>Ours+</b>	OPPD	<b>96.00</b>	23.98
SE-Module [41]	PSD	96.32	1.79
<b>Ours-</b>	PSD	97.78	23.54
<b>Ours+</b>	PSD	<b>97.83</b>	23.54

In Table 2, the proposed method was found to outperform the previous methods in both OPPD and PSD evaluations, ref. [39] conducted the training with a five-fold cross-validation of the PSD using EfficientNet. The number of parameters used was lower in our methods (the negative and positive attention models) in spite of the use of the multiple slot attention module, since the fully connected layer is omitted. However, the number




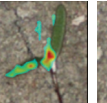
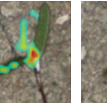








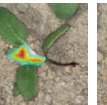

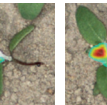

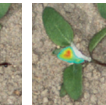



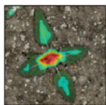

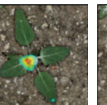
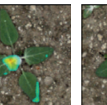
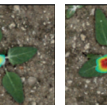
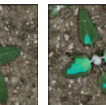
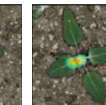
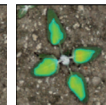



of parameters utilized in [41] is considerably lower than that in the attention method proposed in this paper.

The OPPD was published quite recently and only one applied method is given as a comparison in Table 2. In the OPPD study conducted by [41], the SE-module is implemented for classification. The SE-module is a multi-scale fusion approach that does not utilize attention. The proposed method outperformed the method described in the study by [41] in terms of accuracy.

Instances from different growth stages of the class *CHEAL* are presented in Table 3 to emphasize the importance of contrast and color space in classification. The result in Table 3 was gained by a model that had been both trained and tested on the OPPD. In the first growth stage, attention was also paid to leaves (the last row). However, the attention was attracted to the center in later growth stages (the first and middle rows).

**Table 3.** Positive and negative explanation of the class *CHEAL* by the model trained and tested on the OPPD dataset. Images are sorted in order of increasing growth stage. The model had different highlighted areas and understandings of *CHEAL* in different growth stages.

Original Image	Positive Attention	Negative Attention							
		ALOMY	SINAR	GALAP	STEME	GERMO	APESV	CAPBP	MATIN
									
									
									

The impact of growth stage on *CHEAL* is shown in Table 3. In the OPPD, the class *CHEAL* was a prominent feature in the later growth stages; there are white hairs on the leaves that are more obvious in the center of plants. In the PSD, however, the whitish domain is less visible due to the different brightness and contrast. Therefore, the attention gained from the training and inference with the PSD and the OPPD, respectively, highlighted areas over leaves, not over stems.

The model shows the leaves for monocot species in Table 3—i.e., *ALOMY* and *MATIN*—since the broad leaves are distinctive areas in the later growth stages. For dicot species, the white center area gained the model’s attention.

#### 4. Discussion

The proposed model presented a high-resolution attention map of weed species; the map enabled us to better perceive the model’s decision [42]. In the previous transformer-based methods, the resolution of the attention map was low due to the interpolation applied for resizing the attention map from  $12 \times 12$  to  $360 \times 360$  [43]. This challenge was mitigated in the approach proposed in this paper by providing a multi-layer attention mechanism. In general, the model has a lower certainty regarding attention in the first few layers [44,45], but its precision is higher. Therefore, the proposed algorithm merged multi-layer attention maps from different layers to generate a precise high-resolution representation that included principle features for weed discrimination.

The positive explanation maps help us to differentiate weed species during the early growth stages and are frequently utilized in transformers [42,46]. Moreover, the negative explanation maps support the model's classification, particularly during the mature growth stages, where the dissimilarities between species are substantial [26]. Moreover, the model's uncertainty should help farmers to decide which species should be reconsidered during weed management [47].

In terms of statistical comparison, the proposed model outperformed the state-of-the-art methods using positive attention, as illustrated in Table 2. The performances of the proposed model showed slight improvements compared with those shown in the study by [40]. This is likely due to the attention explanation, better data augmentation, tuning of the hyper-parameters, etc. The attention loss also showed improvements in terms of classification for the positive and negative explanations of the PSD.

The model's challenges in cross-dataset evaluation (Section 3.3) showed that a model applied to one agricultural dataset might not be robust on the other datasets [48]. The proposed model presented interpretable information about the differences between the two datasets, which made the model unable to classify properly. Moreover, only diversity was not sufficient to improve the performance, since the model that was trained with the OPPD and had a wider variety still struggled when applied to the PSD. Nevertheless, the proposed method should help us determine what areas showed significant differences between the two datasets. Therefore, there should be a better explanation as to why the model achieved a lower accuracy during the classification. The cross-dataset evaluation also highlighted the necessity of understanding the data better during the training and test phases in DNNs.

In the cross-dataset evaluation, three characteristics that will be considered in future research were not taken into account:

1. Growth stage;
2. Partial or heavy occlusion;
3. Partial plant appearance.

The model's performance is expected to be improved when a growth stage label is also given to the model due to species variation in different growth stages [13,49]. Furthermore, two critical factors observed from Figure 9 were the impact of occlusion and partial appearance due to the classification. For instance, class *GALAP* showed a partial appearance in Figure 9b (where only half of the plant is visualized), while class *CAPBP* showed partial occlusion due to the neighboring plant in Figure 9a. A great quantity of real in-field annotated images would support our knowledge about the model's performance regarding the existence of occlusion, stress, neighboring plants, etc. In conclusion, the characteristics mentioned above should be investigated in future research.

## 5. Conclusions

In this paper, a high-resolution attention architecture was proposed in order to improve the resolution and location of highlighted weed areas in weed management. The resulting explanation is a foolproof approach for interpreting the similarities and dissimilarities between different weed species through automated weed control. By understanding the black-box model better, we were able to gain more transparency regarding the model's classification of different weed species through maturation. Therefore, self-attention maps from different layers of a ResNet model were extracted to improve the attention precision. The proposed method was able to simultaneously preserve the accuracy from deeper layers and develop the resolution using shallower layers. In addition, this explanation is useful when studying the generalizability of a model for cross-dataset evaluations. The proposed precise and high-resolution attention map was able to explain the datasets better in terms of their visual aspect. Furthermore, the high-resolution attention map highlighted different patterns in a species through various growth stages. The influence of growth stage on attention maps through weed classification is a matter that should be investigated in future studies.

**Author Contributions:** Conceptualization, R.N.J.; methodology, S.F. and S.K.S.; software, S.F.; formal analysis, S.F., S.K.S. and R.N.J.; writing—review and editing, S.F., S.K.S., M.D. and H.K.; visualization, S.F. and S.K.S.; supervision, R.N.J. and H.K.; funding acquisition, R.N.J. All authors have read and agreed to the published version of the manuscript.

**Funding:** This research was funded by the Green Development and Demonstration Program (GUDP) under the Danish Ministry for Food, Agriculture, and Fisheries (project: Square Meter Farming (SqM-Farm), journal number: 34009-17-1303).

**Institutional Review Board Statement:** Not applicable.

**Informed Consent Statement:** Not applicable.

**Data Availability Statement:** Publicly available datasets were analyzed in this study. The data [30,31] can be found from: <https://vision.eng.au.dk/plant-seedlings-dataset/> and <https://gitlab.au.dk/AUENG-Vision/OPPD>, accessed on 17 September 2021, respectively.

**Conflicts of Interest:** The authors declare no conflict of interest.

## Abbreviations

The following abbreviations are used in this paper:

CNN	Convolutional neural network
D	Dicot
DNN	Deep neural network
EPPO	European and Mediterranean Plant Protection Organization
GRU	Gated recurrent unit
M	Monocot
MLP	Multi-layer perceptron
OPPD	Open Plant Phenotyping Dataset
PSD	Plant Seedlings Dataset
ReLU	Rectified linear unit
WIK	Weed identification key
XAI	Explainable artificial intelligence

## References

1. Singh, C.B. Grand Challenges in Weed Management. *Front. Agron.* **2020**, *1*. [CrossRef]
2. Sharma, A.; Shukla, A.; Attri, K.; Kumar, M.; Kumar, P.; Suttee, A.; Singh, G.; Barnwal, R.P.; Singla, N. Global trends in pesticides: A looming threat and viable alternatives. *Ecotoxicol. Environ. Saf.* **2020**, *201*, 110812. [CrossRef]
3. Abbas, T.; Zahir, Z.A.; Naveed, M. Field application of allelopathic bacteria to control invasion of little seed canary grass in wheat. *Environ. Sci. Pollut. Res.* **2021**, *28*, 9120–9132. [CrossRef]
4. Ren, W.; Banger, K.; Tao, B.; Yang, J.; Huang, Y.; Tian, H. Global pattern and change of cropland soil organic carbon during 1901–2010: Roles of climate, atmospheric chemistry, land use and management. *Geogr. Sustain.* **2020**, *1*, 59–69. [CrossRef]
5. Maggipinto, M.; Beghi, A.; McLoone, S.; Susto, G. DeepVM: A Deep Learning-based Approach with Automatic Feature Extraction for 2D Input Data Virtual Metrology. *J. Process. Control* **2019**, *84*, 24–34. [CrossRef]
6. Bručienė, I.; Aleliūnas, D.; Šarauskis, E.; Romaneckas, K. Influence of Mechanical and Intelligent Robotic Weed Control Methods on Energy Efficiency and Environment in Organic Sugar Beet Production. *Agriculture* **2021**, *11*, 449. [CrossRef]
7. Veeranampalayam Sivakumar, A.N.; Li, J.; Scott, S.; Psota, E.; Jhala, A.J.; Luck, J.D.; Shi, Y. Comparison of object detection and patch-based classification deep learning models on mid-to late-season weed detection in UAV imagery. *Remote Sens.* **2020**, *12*, 2136. [CrossRef]
8. Olsen, A. Improving the Accuracy of Weed Species Detection for Robotic Weed Control in Complex Real-Time Environments. Ph.D. Thesis, James Cook University, Queensland, Australia, 2020.
9. Schwarzländer, M.; Hinz, H.L.; Winston, R.; Day, M. Biological control of weeds: An analysis of introductions, rates of establishment and estimates of success, worldwide. *BioControl* **2018**, *63*, 319–331. [CrossRef]
10. Gonzalez-de Santos, P.; Ribeiro, A.; Fernandez-Quintanilla, C.; Lopez-Granados, F.; Brandstötter, M.; Tomic, S.; Pedrazzi, S.; Peruzzi, A.; Pajares, G.; Kaplanis, G.; et al. Fleets of robots for environmentally-safe pest control in agriculture. *Precis. Agric.* **2017**, *18*, 574–614. [CrossRef]
11. Awan, A.F. Multi-Sensor Weed Classification Using Deep Feature Learning. Ph.D. Thesis, Australian Defence Force Academy, Canberra, Australia, 2020.
12. Dyrmann, M.; Mortensen, A.K.; Midtby, H.S.; Jørgensen, R.N. Pixel-wise classification of weeds and crops in images by using a Fully Convolutional neural network. In Proceedings of the International Conference on Agricultural Engineering, Aarhus, Denmark, 26–29 June 2016.

13. Skovsen, S.; Dyrmann, M.; Mortensen, A.K.; Laursen, M.S.; Gislum, R.; Eriksen, J.; Farkhani, S.; Karstoft, H.; Jørgensen, R.N. The GrassClover Image Dataset for Semantic and Hierarchical Species Understanding in Agriculture. In Proceedings of the IEEE/CVF Conference on Computer Vision and Pattern Recognition (CVPR) Workshops, Seattle, WA, USA, 14–19 June 2019.
14. Lu, Y.; Young, S. A survey of public datasets for computer vision tasks in precision agriculture. *Comput. Electron. Agric.* **2020**, *178*, 105760. [[CrossRef](#)]
15. Wang, Y.; Fang, Z.; Wang, M.; Peng, L.; Hong, H. Comparative study of landslide susceptibility mapping with different recurrent neural networks. *Comput. Geosci.* **2020**, *138*, 104445. [[CrossRef](#)]
16. Rai, A.K.; Mandal, N.; Singh, A.; Singh, K.K. Landsat 8 OLI Satellite Image Classification Using Convolutional Neural Network. *Procedia Comput. Sci.* **2020**, *167*, 987–993. [[CrossRef](#)]
17. Castañeda-Miranda, A.; Castaño-Meneses, V.M. Internet of things for smart farming and frost intelligent control in greenhouses. *Comput. Electron. Agric.* **2020**, *176*, 105614. [[CrossRef](#)]
18. Büyüksahin, Ü.Ç.; Ertekin, Ş. Improving forecasting accuracy of time series data using a new ARIMA-ANN hybrid method and empirical mode decomposition. *Neurocomputing* **2019**, *361*, 151–163. [[CrossRef](#)]
19. Farkhani, S.; Skovsen, S.K.; Mortensen, A.K.; Laursen, M.S.; Jørgensen, R.N.; Karstoft, H. Initial evaluation of enriching satellite imagery using sparse proximal sensing in precision farming. In Proceedings of the Remote Sensing for Agriculture, Ecosystems, and Hydrology XXII, London, UK, 20–25 September 2020; SPIE: Bellingham, WA, USA, 2020; Volume 11528, pp. 58–70.
20. Jiang, H.; Zhang, C.; Qiao, Y.; Zhang, Z.; Zhang, W.; Song, C. CNN feature based graph convolutional network for weed and crop recognition in smart farming. *Comput. Electron. Agric.* **2020**, *174*, 105450. [[CrossRef](#)]
21. Sharma, A.; Jain, A.; Gupta, P.; Chowdary, V. Machine learning applications for precision agriculture: A comprehensive review. *IEEE Access* **2020**, *9*, 4843–4873. [[CrossRef](#)]
22. Hasan, A.M.; Sohel, F.; Diepeveen, D.; Laga, H.; Jones, M.G. A survey of deep learning techniques for weed detection from images. *Comput. Electron. Agric.* **2021**, *184*, 106067. [[CrossRef](#)]
23. Chandra, A.L.; Desai, S.V.; Guo, W.; Balasubramanian, V.N. Computer vision with deep learning for plant phenotyping in agriculture: A survey. *arXiv* **2020**, arXiv:2006.11391.
24. Masuda, K.; Suzuki, M.; Baba, K.; Takeshita, K.; Suzuki, T.; Sugiura, M.; Niikawa, T.; Uchida, S.; Akagi, T. Noninvasive Diagnosis of Seedless Fruit Using Deep Learning in Persimmon. *Hortic. J.* **2021**, *90*, 172–180. [[CrossRef](#)]
25. Leggett, R.; Kirchoff, B.K. Image use in field guides and identification keys: Review and recommendations. *AoB Plants* **2011**, *2011*, plr004. [[CrossRef](#)] [[PubMed](#)]
26. Li, L.; Wang, B.; Verma, M.; Nakashima, Y.; Kawasaki, R.; Nagahara, H. SCOUTER: Slot attention-based classifier for explainable image recognition. *arXiv* **2020**, arXiv:2009.06138.
27. Locatello, F.; Weissenborn, D.; Unterthiner, T.; Mahendran, A.; Heigold, G.; Uszkoreit, J.; Dosovitskiy, A.; Kipf, T. Object-centric learning with slot attention. *arXiv* **2020**, arXiv:2006.15055.
28. Vaswani, A.; Shazeer, N.; Parmar, N.; Uszkoreit, J.; Jones, L.; Gomez, A.N.; Kaiser, L.; Polosukhin, I. Attention is all you need. *arXiv* **2017**, arXiv:1706.03762.
29. Han, K.; Wang, Y.; Chen, H.; Chen, X.; Guo, J.; Liu, Z.; Tang, Y.; Xiao, A.; Xu, C.; Xu, Y.; et al. A Survey on Visual Transformer. *arXiv* **2020**, arXiv:2012.12556.
30. Giselsson, T.M.; Dyrmann, M.; Jørgensen, R.N.; Jensen, P.K.; Midtby, H.S. A Public Image Database for Benchmark of Plant Seedling Classification Algorithms. *arXiv* **2017**, arXiv:1711.05458.
31. Madsen, S.L.; Mathiassen, S.K.; Dyrmann, M.; Laursen, M.S.; Paz, L.C.; Jørgensen, R.N. Open Plant Phenotype Database of Common Weeds in Denmark. *Remote Sens.* **2020**, *12*, 1246. [[CrossRef](#)]
32. Lin, T.Y.; Dollár, P.; Girshick, R.; He, K.; Hariharan, B.; Belongie, S. Feature pyramid networks for object detection. In Proceedings of the IEEE Conference on Computer Vision and Pattern Recognition, Honolulu, HI, USA, 21–26 July 2017; pp. 2117–2125.
33. Zhao, Q.; Sheng, T.; Wang, Y.; Tang, Z.; Chen, Y.; Cai, L.; Ling, H. M2det: A single-shot object detector based on multi-level feature pyramid network. In Proceedings of the AAAI Conference on Artificial Intelligence, Honolulu, HI, USA, 27 January–1 February 2019; Volume 33, pp. 9259–9266.
34. He, K.; Zhang, X.; Ren, S.; Sun, J. Deep residual learning for image recognition. In Proceedings of the IEEE Conference on Computer Vision and Pattern Recognition, Las Vegas, NV, USA, 27–30 June 2016; pp. 770–778.
35. Vyas, A.; Katharopoulos, A.; Fleuret, F. Fast transformers with clustered attention. *arXiv* **2020**, arXiv:2007.04825.
36. Yu, Y.; Si, X.; Hu, C.; Zhang, J. A review of recurrent neural networks: LSTM cells and network architectures. *Neural Comput.* **2019**, *31*, 1235–1270. [[CrossRef](#)] [[PubMed](#)]
37. Deng, J.; Dong, W.; Socher, R.; Li, L.J.; Li, K.; Fei-Fei, L. ImageNet: A Large-Scale Hierarchical Image Database. In Proceedings of the 2009 IEEE Conference on Computer Vision and Pattern Recognition, Miami, FL, USA, 20–25 June 2009.
38. Loshchilov, I.; Hutter, F. Decoupled weight decay regularization. *arXiv* **2017**, arXiv:1711.05101.
39. Ofori, M.; El-Gayar, O. An Approach for Weed Detection Using CNNs And Transfer Learning. In Proceedings of the 54th Hawaii International Conference on System Sciences, Hawaii, HI, USA, 5–8 January 2021; p. 888.
40. Gupta, K.; Rani, R.; Bahia, N.K. Plant-Seedling Classification Using Transfer Learning-Based Deep Convolutional Neural Networks. *Int. J. Agric. Environ. Inf. Syst.* **2020**, *11*, 25–40. [[CrossRef](#)]
41. Haoyu, L.; Rui, F. Weed Seeding Recognition Based on Multi-Scale Fusion Convolutional Neural Network. *Comput. Sci. Appl.* **2020**, *10*, 2406.

42. Zhang, P.; Dai, X.; Yang, J.; Xiao, B.; Yuan, L.; Zhang, L.; Gao, J. Multi-scale vision longformer: A new vision transformer for high-resolution image encoding. *arXiv* **2021**, arXiv:2103.15358.
43. Caron, M.; Touvron, H.; Misra, I.; Jégou, H.; Mairal, J.; Bojanowski, P.; Joulin, A. Emerging properties in self-supervised vision transformers. *arXiv* **2021**, arXiv:2104.14294.
44. Tian, C.; Xu, Y.; Li, Z.; Zuo, W.; Fei, L.; Liu, H. Attention-guided CNN for image denoising. *Neural Netw.* **2020**, *124*, 117–129. [[CrossRef](#)]
45. Chen, G.; Li, C.; Wei, W.; Jing, W.; Woźniak, M.; Blažauskas, T.; Damaševičius, R. Fully convolutional neural network with augmented atrous spatial pyramid pool and fully connected fusion path for high resolution remote sensing image segmentation. *Appl. Sci.* **2019**, *9*, 1816. [[CrossRef](#)]
46. Tay, Y.; Dehghani, M.; Aribandi, V.; Gupta, J.; Pham, P.; Qin, Z.; Bahri, D.; Juan, D.C.; Metzler, D. Omninet: Omnidirectional representations from transformers. *arXiv* **2021**, arXiv:2103.01075.
47. Brdar, M.; Brdar-Szabó, R.; Perak, B. Separating (non-) figurative weeds from wheat. In *Figurative Meaning Construction in Thought and Language*; John Benjamins Publishing Company: Amsterdam, The Netherlands, 2020; pp. 46–70. Available online: <https://benjamins.com/catalog/ftl.9.02brd> (accessed on 17 September 2021).
48. Saikawa, T.; Cap, Q.H.; Kagiwada, S.; Uga, H.; Iyatomi, H. AOP: An anti-overfitting pretreatment for practical image-based plant diagnosis. In Proceedings of the 2019 IEEE International Conference on Big Data (Big Data), Los Angeles, CA, USA, 9–12 December 2019; pp. 5177–5182.
49. Takahashi, Y.; Dooliokhuu, M.; Ito, A.; Murata, K. How to Improve the Performance of Agriculture in Mongolia by ICT. Applied Studies in Agribusiness and Commerce. Ph.D. Thesis, University of Debrecen, Debrecen, Hungary, 2019.



# Orchard Mapping with Deep Learning Semantic Segmentation

Athanasios Anagnostis <sup>1,2</sup>, Aristotelis C. Tagarakis <sup>1</sup>, Dimitrios Kateris <sup>1,\*</sup>, Vasileios Moysiadis <sup>1</sup>,  
Claus Grøn Sørensen <sup>3</sup>, Simon Pearson <sup>4</sup> and Dionysis Bochtis <sup>1,5</sup>

<sup>1</sup> Institute for Bio-Economy and Agri-Technology (iBO), Centre for Research and Technology–Hellas (CERTH), GR57001 Thessaloniki, Greece; a.anagnostis@certh.gr (A.A.); a.tagarakis@certh.gr (A.C.T.); v.moisiadis@certh.gr (V.M.); d.bochtis@certh.gr (D.B.)

<sup>2</sup> Department of Computer Science & Telecommunications, University of Thessaly, GR35131 Lamia, Greece

<sup>3</sup> Department of Electrical and Computer Engineering, Aarhus University, DK-8000 Aarhus C, Denmark; claus.soerensen@ece.au.dk

<sup>4</sup> Lincoln Institute for Agri-Food Technology (LIAT), University of Lincoln, Lincoln LN6 7TS, UK; spears@lincoln.ac.uk

<sup>5</sup> farmB Digital Agriculture P.C., Doiranis 17, GR54639 Thessaloniki, Greece

\* Correspondence: d.kateris@certh.gr; Tel.: +30-242-109-6740

**Abstract:** This study aimed to propose an approach for orchard trees segmentation using aerial images based on a deep learning convolutional neural network variant, namely the U-net network. The purpose was the automated detection and localization of the canopy of orchard trees under various conditions (i.e., different seasons, different tree ages, different levels of weed coverage). The implemented dataset was composed of images from three different walnut orchards. The achieved variability of the dataset resulted in obtaining images that fell under seven different use cases. The best-trained model achieved 91%, 90%, and 87% accuracy for training, validation, and testing, respectively. The trained model was also tested on never-before-seen orthomosaic images or orchards based on two methods (oversampling and undersampling) in order to tackle issues with out-of-the-field boundary transparent pixels from the image. Even though the training dataset did not contain orthomosaic images, it achieved performance levels that reached up to 99%, demonstrating the robustness of the proposed approach.

**Keywords:** precision agriculture; orchard mapping; deep learning; computer vision; semantic segmentation; orthomosaic

**Citation:** Anagnostis, A.; Tagarakis, A.C.; Kateris, D.; Moysiadis, V.; Sørensen, C.G.; Pearson, S.; Bochtis, D. Orchard Mapping with Deep Learning Semantic Segmentation. *Sensors* **2021**, *21*, 3813. <https://doi.org/10.3390/s21113813>

Academic Editor: Asim Biswas

Received: 21 April 2021

Accepted: 27 May 2021

Published: 31 May 2021

**Publisher's Note:** MDPI stays neutral with regard to jurisdictional claims in published maps and institutional affiliations.



**Copyright:** © 2021 by the authors. Licensee MDPI, Basel, Switzerland. This article is an open access article distributed under the terms and conditions of the Creative Commons Attribution (CC BY) license (<https://creativecommons.org/licenses/by/4.0/>).

## 1. Introduction

The latest advances in sensing technologies dedicated to agricultural systems have led to the emergence and development of a modern management concept, namely precision agriculture, which focuses on efficient management of the temporal and spatial variability of field and crop properties using information and communication technology (ICT) [1]. A plethora of different sensors and technologies are utilized in relation to this concept to form a detailed view of fields' properties, capturing the spatial and temporal variability and searching for the specific factors responsible for their occurrence, which are to be treated accordingly. Therefore, mapping the field and crop properties is a fundamental aspect in the application of such management systems.

Remote sensing is defined as the non-contact measurement of crop properties based on the radiation reflected from the plants, using ground based or aerial platforms, and it is widely used for mapping tasks in agricultural systems [2]. Recent technological advances have made unmanned aerial systems (UASs), i.e., sensing systems mounted on unmanned aerial vehicles (UAVs), commercially available. These systems provide high spatial resolution images and, in combination with their ease of use, quick acquisition times, and low operational cost, they have become particularly popular for monitoring agricultural fields [3]. Several studies have utilized UASs for crop management purposes,

such as yield prediction and site-specific fertilization [4] by capturing multispectral images, irrigation using thermal imaging [5], or for field scouting using RGB (Red-Green-Blue) orthomosaics [6].

In tandem with the development of remote sensing and image capturing techniques, machine learning (ML) has leaped forward both in terms of performance as well as in terms of its applicability in almost all scientific domains. Agriculture in general, and specifically precision agriculture, has benefited from the rise of machine learning in multiple ways since complex tasks, hard to deal with using traditional programming, can be tackled with the help of a plethora of different ML algorithms [7–9]. Particularly with regard to computer vision, there has been extensive implementation of machine and deep learning in tasks of classification [10], object detection [11], and semantic segmentation [12].

Classification tasks employ self-learning algorithms for the assignment of a class to an image according to its content. Examples of classification in agricultural applications include the identification of diseases on leaves in real-life environment images with the help of convolutional neural networks (CNNs) [13], the identification of trees from UAV images with a combination of k-nearest neighbors (kNNs) and GoogLeNet [14], and tree species assignment from UAV images and multispectral data with random forest algorithms [15]. Object detection algorithms differ because they predict the location of objects and assign the appropriate class to them [16]. Examples of object detection applications include the detection of disease-infected leaves at tree level from UGV images [17], the detection of trees with the use of Faster RCNN (Regions with CNN features) and YOLO (You Only Look Once) [6], and the mapping of operational environments in orchards with classical computer vision techniques or Fast RCNN [18]. Image segmentation, on the other hand, is a pixel-wise operation where a class is appointed to each individual pixel, thus creating detailed outlines of objects and maintaining their exact shape. U-net [19] is one of the most famous algorithms for image segmentation and has been used for tree segmentation from satellite images [20], mapping of forests [21], and pomegranate canopy segmentation in comparison to Mask RCNN [22]. Segmentation algorithms for tree canopy mapping have also been used in tandem with object detection approaches, like Segnet and YOLO [23], or classification approaches, like the multi-resolution segmentation algorithm used with state-of-the-art CNNs and support vector machines (SVMs) [24].

Applications of image segmentation with images acquired by UAS have used several machine learning algorithms: point-cloud data with the use of deep neural networks (DNNs) for tree canopy segmentation [25], support vector machines and image pre-processing filters for citrus trees segmentation [26], random forest (RF) super pixel classification for tree canopy extraction [27], and for the automatic segmentation of canopies with Deeplab v3+, a type of encoder-decoder network, for automatic segmentation of canopies [28].

Several approaches, listed in the bibliography, have attempted to find solutions to the problem of automatic segmentation of trees from aerial images. However, all approaches had as a prerequisite a full, healthy canopy. All aforementioned studies also tackled the problem with methods of unsupervised learning or object detection. These methods present shortcomings, either regarding the identification performance per se or the precise shape of the canopy excluding surroundings. Subsequent tasks, such as canopy size estimation and orchard mapping, rely on the results of these methods; therefore, the respective shortcomings propagate to them as well. According to our knowledge, semantic segmentation has not been implemented in the task of canopy detection of orchards with the use of UAS-derived images. Furthermore, a gap has been identified in the proper identification of tree canopies within orchards, throughout all seasons and in every step of their growth.

This study aimed to propose, develop, and validate an approach for orchard trees segmentation using aerial images based on a custom variant of a deep learning convolutional neural network, namely the U-net network. The purpose was the automated detection and localization of the canopy of orchard trees under various conditions (i.e., different



seasons, different tree ages, different levels of weed coverage). The results of this study contribute to the farming community by providing a robust tool for instant scouting of orchard environments by automatically segmenting the tree canopies from aerial images. This work is a preliminary step in the development of an integrated tool to support farmers in decision making.

## 2. Methodology

The proposed approach is structured around data-driven algorithms and computer vision techniques. An annotated dataset was generated from a large number of UAV captured images by masking the canopies of the trees in order to create a large dataset for supervised learning. This annotated dataset was used to train the model with the selected deep-learning algorithm so that it could properly identify tree canopies and segment them from the background. A mask image is produced as an output, containing the shapes of all predicted tree canopies. Following the segmentation, the weighted average of each mask, i.e., its moment, is used for the calculation of its centroid, so that it can be used as a reasonable approximation of the location of the tree's trunk. Provided that the geodetic coordinates of the photographed location are retained in the orthomosaic images, the tree trunk locations can be computed with high accuracy.

In order to deal with the complexity of orchard environments, in terms of the presence of weeds in the image background, and the high variability in the phenomenology of canopies due to seasonality, a deep learning algorithm, namely U-net, was considered and tweaked to fit the problem's requirements.

### 2.1. U-Net Variant

U-net is an advanced type of convolutional neural network which consists of two modules, an encoder and a decoder. Such networks aim to encode the input into a latent space in order to create the desired output based on the said input. U-net's characteristic feature, which distinguishes it from the case of simple encoder-decoder networks, is that it contains direct "skip" connections between the shallow encoder and decoder layers alongside the sequential structure of the architecture [29]. In this way, certain features from the encoding/input layers are fed directly to the decoding/output layers. For the approach presented here, two modifications were made to the standard U-net architecture; the input layer was tweaked to both 3- and 6-channel images and a dropout layer was added between the convolutional layers per block, to avoid the tendency towards overfitting that would occur in such a small dataset with similar representations. A schematic of the U-net used in this work is shown in Figure 1.

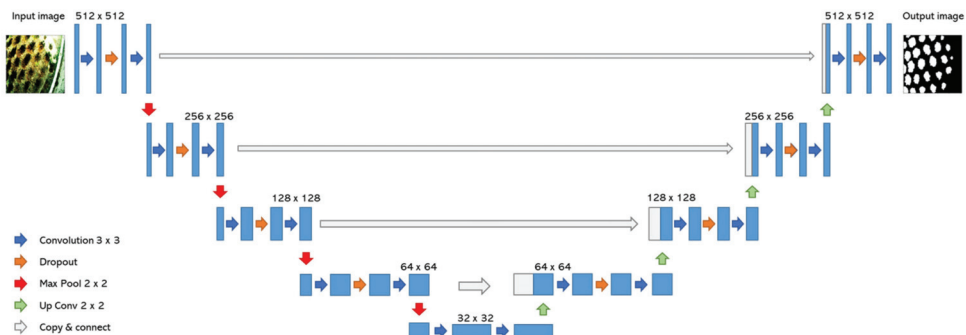


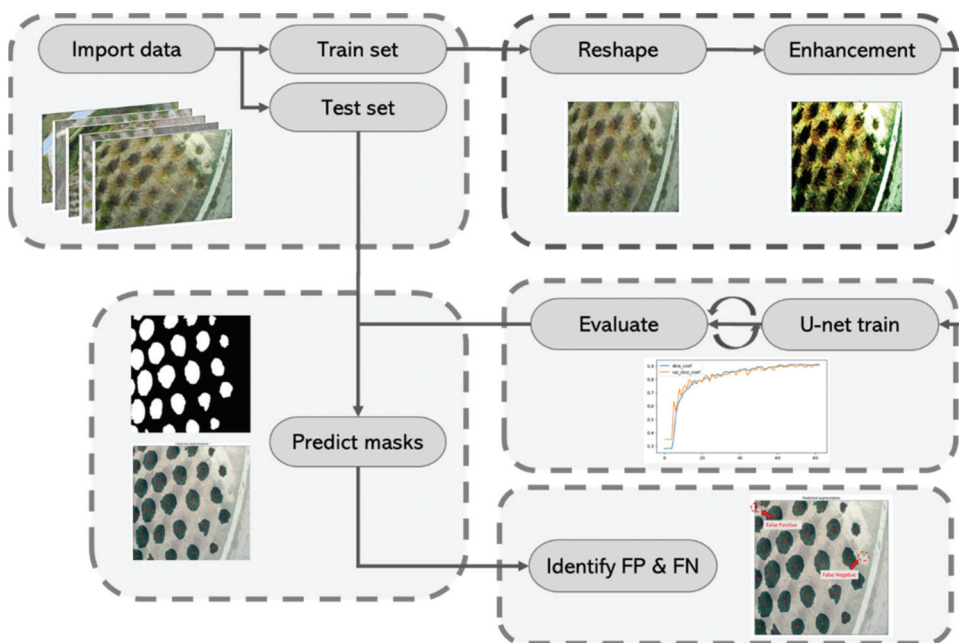
Figure 1. Architecture of the modified U-net network implemented in the approach.

## 2.2. Process Flow

The methodology developed for creating segmentation predictions follows a sequential process which consists of several preprocessing, training, and evaluation steps. The complete process flow can be summarized as follows:

- Data are imported and split into train and test sets. For the implementation of the approach, the test set is required to contain at least one image from each use case;
- Each image is reshaped (into a predefined aspect ratio) and, additionally, color enhancements such as contrast equalization are applied;
- The training data are fed into the U-net and the model learns to create proper segmentations for each image. An evaluation metric is used across a randomly selected validation set comprising 10% of the training set, so that the trained model can learn to create better segmentation masks;
- The trained model produces segmentation masks for the test images and the evaluation metric is applied;
- The segmentation masks are compared with the real masks created during annotation and the presence of false positive or false negative segmentations is manually investigated;
- The overall performance of the model is defined by the accuracy of the trained model on the test dataset, as well as the ratio of false positives and false negatives over the total amount of trees in the image.

A visual representation is shown in Figure 2.



**Figure 2.** Process flow of the proposed methodology for creating segmentation predictions. FN: false negative; FP: false positive.

## 3. Implementation

Three sites of commercial walnut orchards, located in Thessaly, Central Greece, were used in the present study. The orchards covered a range of tree ages and soil surface features. Correspondingly, the images represented different seasons, with the aim of capturing the different tree conditions and stages throughout the growing season, namely: defoliated,

canopy developing, canopy fully developed, and brown canopy before defoliation. Additionally, the orchards varied in terms of background soil conditions, including: soil surface free from weeds, soil surface partly covered by weeds, and untreated soil with complete weeds coverage. A total number of 106 images from the three orchards led to the definition of seven different use cases which were used for the training and testing of the proposed methodology. A detailed list of the characteristics' use cases is presented in Table 1.

**Table 1.** Orchards' characteristics and categorization into separate use cases.

Use Case No.	Yearly Season	Weeds Coverage	Canopy Size	Foliage Color	Ground Color
1	Autumn	Low	-	Brown	Brown
2	Autumn	Low	-	Mixed	Brown
3	Summer	Low	Small	Green	Brown
4	Summer	Low	Medium	Green	Brown
5	Summer	Low	Medium	Green	Mixed
6	Summer	Low	Large	Green	Brown
7	Summer	High	Large	Green	Green

All use cases were adequately represented by several images in the training set and, more importantly, the test set was constructed so that it would always contain at least one image of each use case. This way, the trained models would be tested for all different combinations of characteristics, ensuring the maximum generalization. Sample images for each use case are presented in Appendix A.

### 3.1. Data Acquisition

From 2018 to 2020, a number of test flights were conducted over the aforementioned orchards with two different types of UAV, a quadcopter (Phantom 4, DJI Technology Co., Ltd., Shenzhen, China) and a fixed-wing UAV (eBee, senseFly, Cheseaux-sur-Lausanne, Switzerland), both equipped with high-accuracy GNSS (real-time kinematic (RTK) positioning) and high-resolution cameras, i.e.,  $5472 \times 3648$ , at a 3:2 aspect ratio.

The use of RTK GNSS was a requisite to accurately geotag the acquired images. To achieve further exploration, the automated flights were maintained with the necessary criteria to produce high-accuracy orthomosaics. The parameters of each automated flight were fine-tuned (UAV flight height, speed, number of captured images, side overlap and forward overlap ratio) to produce high-resolution, below-centimeter pixel size, orthomosaics, which are presented in detail in Table 2.

**Table 2.** Information concerning the flights performed in each use case for the acquisition of images and the creation of the orthomosaics used in the study.

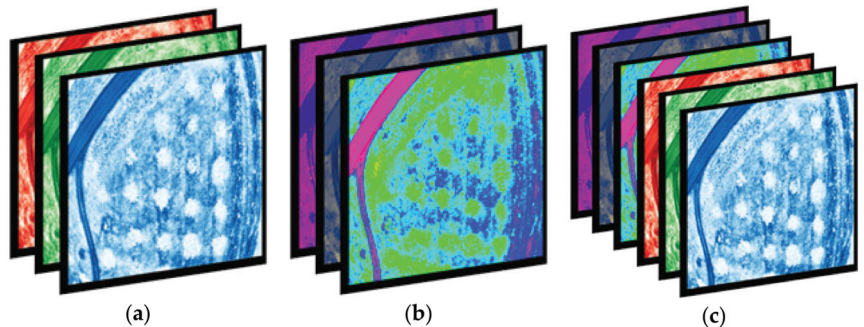
Use Case No.	Acquisition Date	Number of Trees	Number of Images	Overlap	GSD	Air Speed (m/s)	Cloud Coverage (%)
1	1 November 2018	1399	283	75%	1.3	<3	49
2	30 August 2020	569	522	75%	1.3	3	32
3	19 June 2020	358	330	75%	1.3	<3	5
4	3 June 2020	506	244	75%	1.5	<3	35
5	12 August 2020	2118	510	75%	1.5	<3	40
6	7 May 2019	296	193	75%	1.3	<3	12
7	15 May 2020	632	465	75%	1.3	<3	5

### 3.2. Data Pre-Processing

Image pre-processing is a fundamental aspect of computer vision tasks, especially when employing self-learning algorithms. The reason for this is the need to transform the images into proper sizes/shapes, in order for the numerical computations to take place. In the present study, each of the raw images captured from the study sites utilized over 30 MB of storage each and had a  $5472 \times 3648$  pixel rectangular shape. Size reduction was the first step that took place along with the reshaping of all images to dimensions of  $512 \times 512$  pixels.

The effect of image preprocessing in terms of color and colorspaces was another aspect investigated in this study. Histogram equalization (EQ) [30] and contrast-limited adaptive histogram equalization (CLAHE) [31] are two methods usually used for contrast enhancement in RGB images, both of which expand the contrast by adapting the range of the image's pixel values either globally or locally. Besides the RGB spectrum, the HSV colorspace—which represents color with hue, saturation, and value, all assigned to cylindrical coordinates—was also investigated since it amplifies different features of an image, which could lead to increased performance.

A novel approach to increasing contrast and extracting features by combining an RGB contrast-enhanced instance of an image and an HSV instance of an image into a single 6-channel image was attempted. Such images contain “double” information from a regular 3-channel image; however, the addition of more color channels does not necessarily imply that the added value increases as well [32]. A visual representation of how the 3- and 6-channel images are constructed is shown in Figure 3.

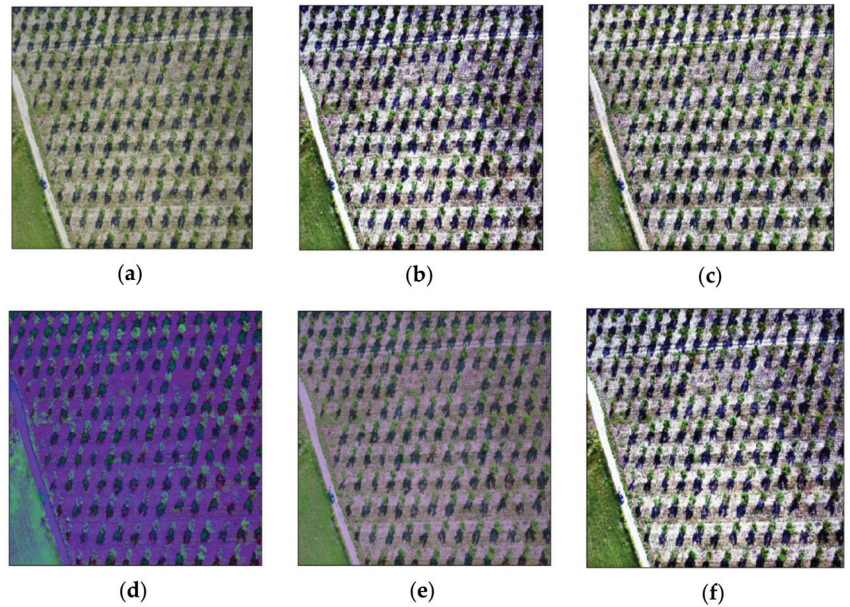


**Figure 3.** Channel deconstructing of (a) RGB, (b) HSV, and (c) fused images.

Two variants of the fused images were tested, namely the RGB image without any contrast enhancement and the CLAHE method for adaptive contrast enhancement, alongside the HSV colorspace image. The visual differences between all methods are presented in Figure 4.

### 3.3. Performance Metric

The Sørensen–Dice coefficient [33] was selected as the performance metric for the segmentation of trees against their background. It was preferred over the intersection over union (IoU), also known as the Jaccard index [34] because the IoU penalizes bad classifications harder [35] and, in the case of tree foliage, the exact details of the foliage shape is not of high importance. As a loss function, the negative value of the dice coefficient was used, as is common in image segmentation tasks [36].

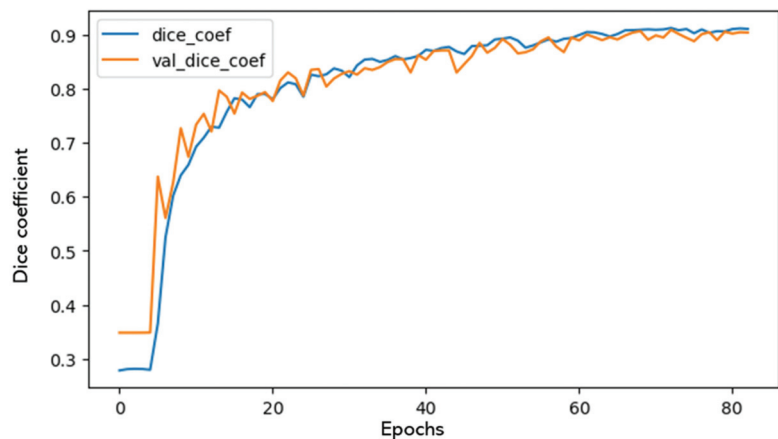


**Figure 4.** Image color transformations used in the study: (a) RGB image, (b) EQ image, (c) CLAHE image, (d) HSV colorspace image, (e) 6-channel RGB and HSV fused image, and (f) 6-channel CLAHE and HSV fused image.

## 4. Results

### 4.1. Validation on Dataset

All models were trained on an NVIDIA Titan 1080 Ti GPU with between 40 and 100 epochs, a visualization of which is seen in Figure 5. Early stopping was used for preventing overfitting of the models. The models were trained and tested on 96 and 10 images respectively, which were randomly selected from the 106 images of the dataset, including all seven use cases (use cases presented in Table 1). In this way, the generalization of the model was ensured. The accuracy achieved by the models under the differently pre-processed datasets is shown in Table 3.



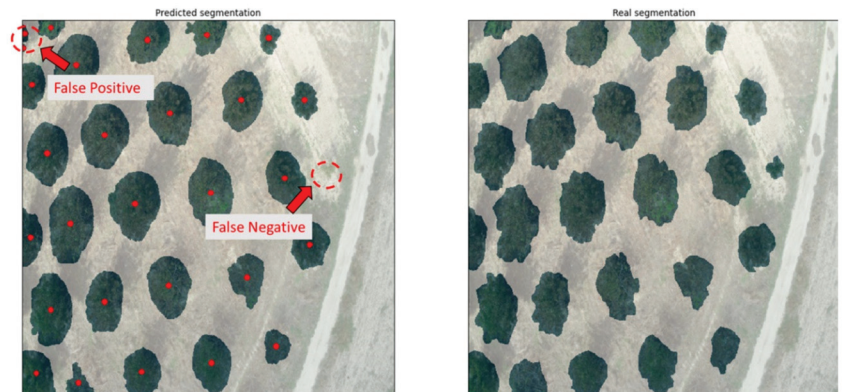
**Figure 5.** Learning plot with training and validation accuracy.



**Table 3.** Accuracy (dice coefficient) for investigated methods of segmentation.

Image Colorspace	RGB	EQ	CLAHE	HSV	RGB + HSV	CLAHE + HSV
Channels	3			6		
Training accuracy	0.91	0.90	0.90	0.92	0.91	0.91
Validation accuracy	0.90	0.88	0.89	0.90	0.89	0.90
Testing accuracy	0.87	0.77	0.86	0.86	0.85	0.86

As mentioned previously, the dice coefficient is used for benchmarking the performance of trained models. However, the ability of a trained model to properly segment trees is measured by visual inspection. The system was validated by applying the trained models to never-before-seen images of entirely different use cases and comparing the results to the identification of a human expert. The false positives (FPs), i.e., incorrectly identifying trees at locations where there were none, and false negatives (FNs), i.e., failing to identify trees, could thus be registered. On top of the tree canopy segmentation, the exact location of a tree's trunk was computed based on the predicted masks. The method for computing this location was based on the centroids of the image moments, i.e., the weighted average of the predicted masks. Therefore, for each mask representing a tree canopy, and with the condition that it was isolated and in no way connected to an adjacent mask, a single point was calculated to signify the position of the tree trunk, considering a fairly symmetrical canopy shape. A visual example of the predicted segmentation (left) and the real annotation (right), both overlaid on the original images, is given in Figure 6.

**Figure 6.** Examples of false positive and false negative segmentation predicted by the developed system (left) as compared to the real segmentation (right).

Since this study aimed to primarily solve the issue of mapping the locations of trees within orchards, the absolute intersection between all pixels was mostly considered for the training phase. The rough shape and size of a properly identified tree canopy was what would lead to a correct computation of the trunk location and the estimation of the tree's age. Therefore, in order to choose the best-trained model for the application, the test set was manually investigated across the predicted segmentations from each approach. In this way, FPs and FNs were identified and, finally, each model received a score based on the ratio of FPs, FNs, and their sum over the total amount of trees in each image, as seen in Table 4.

**Table 4.** Overall performance evaluation, expressed as percentages (%), of the models examined in the test set of the study, in terms of false positives (FPs), false negatives (FNs), and their sum ratios over the total number of trees in the test set.

Image Colorspace	RGB	EQ	CLAHE	HSV	RGB + HSV	CLAHE + HSV
FPs (%)	7.49	9.41	16.17	7.57	7.49	4.99
FNs (%)	5.81	8.73	15.17	6.48	10.66	16.22
Total misidentifications (%)	13.30	18.14	31.34	14.05	18.16	21.21

From the overall evaluation of the models' performance, the RGB model was identified as the simplest and provided the best results. Therefore, it was selected as the primary model to be investigated further. In the next step, the performance of the RGB model was investigated for each use case separately. In this way, the strengths and weaknesses of the selected approach could be identified and therefore tackled in future work. The results of the RGB method were further broken down per test image, covering all use cases that were included in the present study, as shown in Table 5.

**Table 5.** Performance evaluation of the RGB model (best performing) applied to the separate test images for each use case, expressed as percentages (%) of false positives, false negatives, and their sum total.

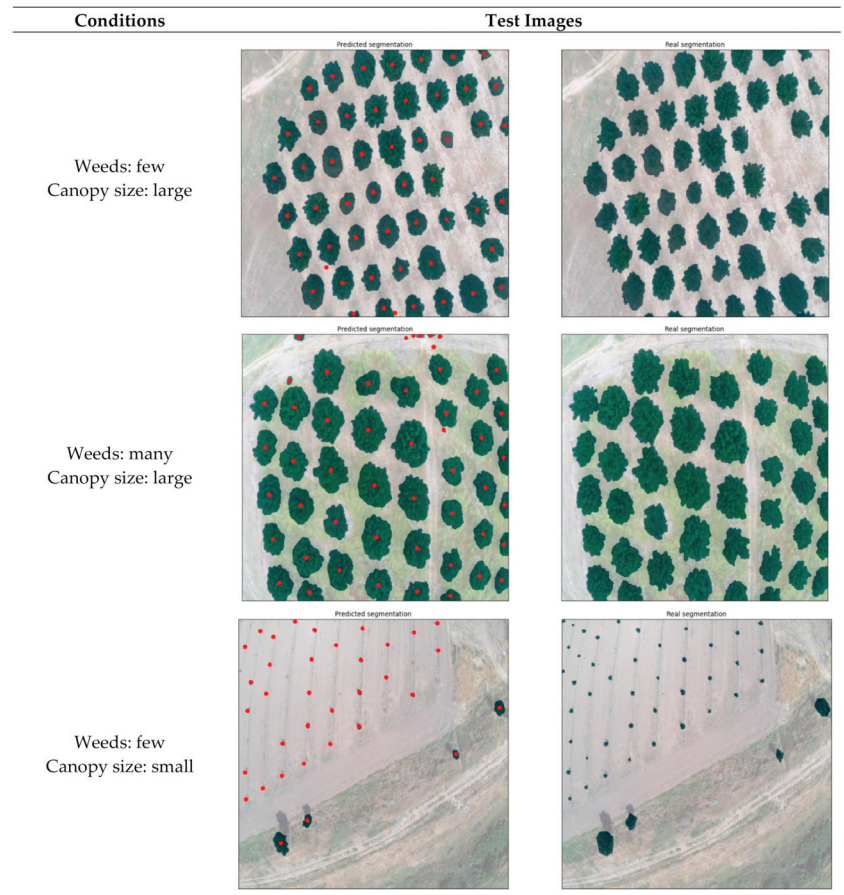
Test Image	1	2	3	4	5	6	7	8	9	10	Mean
Use Case	2	1	5	4	4	6	6	5	7	3	
FPs (%)	7.69	8.33	16.67	9.09	2.08	1.82	2.33	12.64	14.29	0.00	7.49
FNs (%)	0.00	4.17	4.17	18.18	0.00	1.82	0.00	3.45	2.38	23.94	5.81
Total (%)	7.69	12.50	20.83	27.27	2.08	3.64	2.33	16.09	16.67	23.94	13.30

The accuracy achieved for all use cases using the RGB model ranged between 72.7% and 97.9%, which can be considered as a satisfactory result. Comparing images 6 and 7 with 9, the effect of the presence of weeds' on the accuracy of the model is evident, since the first two images, which belong to use case 6 (large trees; few weeds), performed considerably better compared to image 9, which belongs to use case 7 (large trees; many weeds). In the latter, the FPs were the primary reason for limiting the system's performance. This signifies that the developed weeds within the image frame led to increased FP misclassifications (weeds classified as trees). Interestingly, when running test images from use cases 1 and 2 (i.e., images captured during autumn when the canopy was turning brown), accuracy was notably high, albeit with a low level of weeds coverage.

With regard to common characteristics between use cases, three indicative results from the RGB model are presented in Figure 7. These three categories cover the most contrasting situations; (a) ideal conditions with medium/large tree canopies and ground with only a small amount of weeds, (b) intermediate conditions with large tree canopies but weed-infested ground, and (c) unfavorable conditions with small tree canopies and some weeds present. The first image belongs to use case 4, containing clear green canopies and ground covered by only a few weeds. The second image, which represents use case 7, shows large green canopies; however, the ground is almost entirely covered with weeds of a similar shade of green. The third image is from an orchard free of weeds (use case 3); however, the canopies are particularly small in size due to the young age of the trees. Use cases 4 and 6 are the most ideal, considering canopy and background color contrast due to the season and the lack of weeds. A noteworthy outcome is that even though use cases 4 and 5 both had medium-sized canopies, the trained model's accuracy was completely different due to the presence of weeds. Additionally, use cases 1 and 2 demonstrated similar behavior as use cases 3 and 4, since all of them were almost free of weeds, with the only difference being the more brownish color, making it slightly harder to identify



all canopies. In all images, a mask overlay of 50% transparency was applied in order to visualize the segmentations; therefore, the real shades of the images were altered.



**Figure 7.** Results of indicative RGB images covering a range of different conditions.

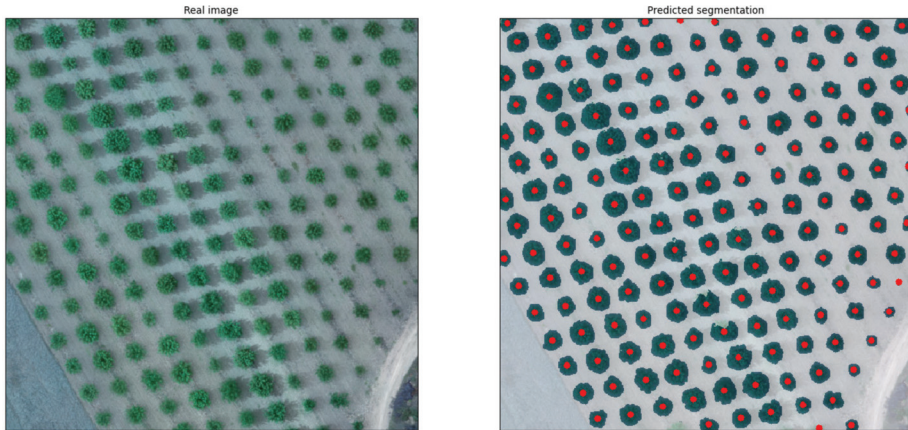
#### 4.2. Validation on Orthomosaics

The system as presented above showed its ability to recognize tree canopies with high accuracy when applied to high resolution images of certain dimensions. However, investigating the performance of the system with orthomosaics covering the entirety or a large part of the orchard area was also considered to be of great interest. Therefore, in a further analysis, the trained models were applied to orthomosaics captured from orchards with pixel resolution considerably lower than the original training dataset. The aim of this test was to examine the extent of the trained models' capabilities considering the pixel resolution range of all canopies. Applying the models directly to the orthomosaics produced errors due to the presence of "transparent" pixels that denote areas outside the bounds of the appointed orchard. Two methods were used to overcome this inconvenience: "oversampling", i.e., filling the transparent pixels with the dominant ground color; or "undersampling", i.e., cropping the largest area possible that did not contain "out-of-borders" areas.

The test included (a) analysis of orthomosaics treated as a whole (i.e., as one image) and (b) analysis of sub-images clipped from the orthomosaic. It is important to note

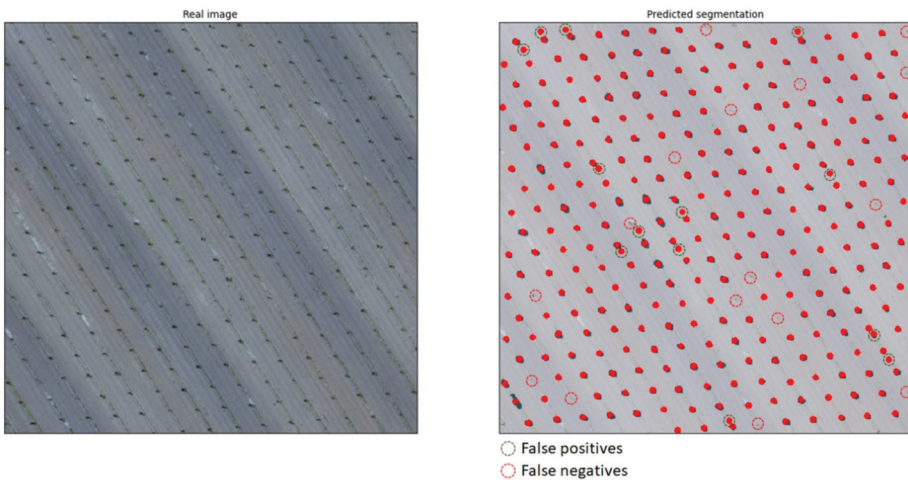
that these were never-before-seen images that had not been a part of the original dataset. Similarly to the training phase, orthomosaics of three different use cases were selected.

Case A. The first case displayed an orchard with large- to medium-sized canopies. As mentioned above, the pixel resolution was smaller than that of the training dataset. The accuracy reached 99%, with only a small FP segmentation on the right section of the middle of the image detected (Figure 8).



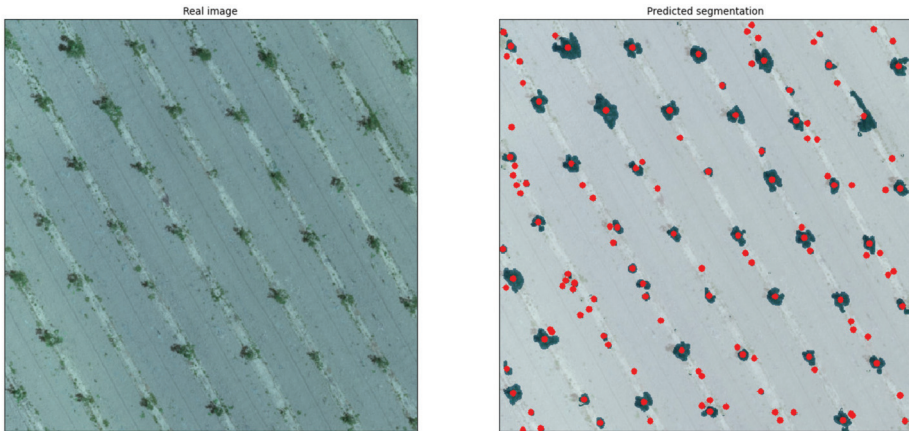
**Figure 8.** Undersampled orthomosaic of an orchard with large- to medium-sized canopies (left) and the segmentation predicted by the model (right).

Case B. The second use case was an undersampled orthomosaic of an orchard with young trees (Figure 9). It was observed that even though the canopies were significantly small, the trained model was able to achieve a high accuracy of 90.5% with only 5.3% FNs and 4.3% FPs.



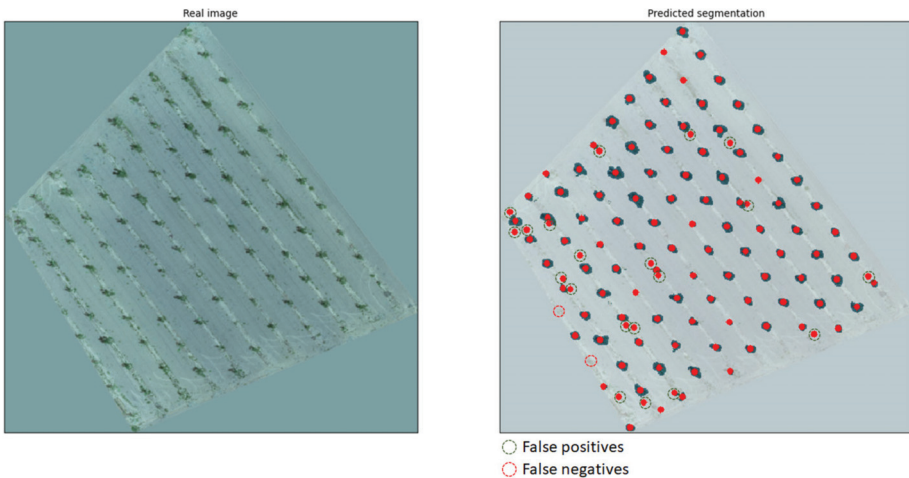
**Figure 9.** Undersampled orthomosaic of an orchard with young trees featuring small-sized canopies (left) and the segmentation predicted by the model (right).

Case C. Finally, an orthomosaic with a higher resolution compared to the previous case of an orchard with small-sized canopies was undersampled and tested. However, the presence of developed weeds dispersed throughout the orchard produced many FPs in the segmentation, as seen in Figure 10.



**Figure 10.** Undersampled orthomosaic of an orchard with small canopies, not treated for weeds (**left**), and the segmentation predicted by the model (**right**).

Even though a rule-based condition could eliminate such small segmentations, this could be counterproductive for cases with young-aged trees with small canopies. However, the original orthomosaic, as seen in Figure 11, produced significantly fewer FPs compared to the undersampled one above.



**Figure 11.** Complete orthomosaic of a study orchard with trees with small-sized canopies, not treated for weeds (**left**), and the segmentation predicted by the model (**right**).

The accuracy achieved for the orthomosaic was notably high, reaching 82%, and the segmentation prediction showed 16.4% FPs and only 1.6% FNs. It is worth mentioning that all the FPs were recognized as trees due to the presence of large surfaces covered by weeds, simulating the size and the shape of the top view of the tree canopy. This indicates that

the model can be expected to demonstrate excellent performance with weed-free orchards. Furthermore, the FNs were located at the edges of the orthomosaic where part of the canopy of the respective trees was missing.

#### 4.3. Ablation Study

The aim of this section is to demonstrate the effectiveness of the additional components (layers) and modifications that were added to the U-net architecture. The scope of evaluation in this paragraph is the effectiveness of the dropout layer that was placed between the two convolutional layers in each step. Even though a dropout layer makes intuitive sense since it improves generalization by mitigating overfitting, its actual effect should be investigated. A baseline (vanilla) U-net with no dropout layer included and a variant with the dropout layer placed before the max-pooling and the up-convolution layers were tested in comparison to the proposed variant. All models were trained with the RGB images dataset, since it was selected as the best method, and the results of the three trained models, including the proposed one, are presented in Table 6.

**Table 6.** Results of the ablation study for the baseline (vanilla) U-net, a variant with a dropout layer placed after the convolutional layers, and the proposed variant.

	Vanilla	Variant No. 1	Proposed Variant
Training accuracy	0.89	0.86	0.91
Validation accuracy	0.78	0.85	0.90
Testing accuracy	0.74	0.81	0.87
FPs (%)	13.56	9.93	7.49
FNs (%)	12.48	8.74	5.81
Total misidentifications (%)	26.04	18.67	13.30

An approach without dropout overfitted the model and this was evident because the training accuracy was high while the validation and testing accuracies were low. This poor performance was also reflected in the number of epochs required for the model to achieve proper training, which was significantly lower (approximately 10–20 epochs) than the other approaches. Adding a dropout layer allows the model to train for a longer time (<40 epochs); however, the position of the dropout layer affects the performance of the model [37]. The variant where the dropout layer preceded the max-pooling layer performed measurably worse since, in a general sense, both dropout and pooling layers reduce learned information. The ideal combination arises when the dropout layer is placed between the two convolutional layers, since the network maintains a balance between learning and forgetting information from the input images.

#### 4.4. Comparison with Baselines and Other Methods

A comparison of the proposed approach with other traditional computer vision techniques, unsupervised machine learning methods, object detection approaches, and other image segmentation deep learning techniques is presented in this section. For all methods, baseline versions were used with minor tuning of parameters. For the traditional computer vision techniques, blob, feature, and color detection were implemented with the assistance of OpenCV Python library [38]. Specifically, for the feature detection, oriented FAST and rotated BRIEF (ORB) was used as a baseline. With regard to the unsupervised machine learning approach, a K-means algorithm [39] was implemented from Python's SciKit-Learn library [40]. For the object detection approach, the single shot detection (SSD) algorithm [41] with a ResNet50 [42] backbone was used, and for the segmentation approach, the Mask R-CNN algorithm with a ResNet101 [42] backbone, both implemented with the Keras library [43] with the Tensorflow backend [44]. Since all methods have different ways to extract information from images, the characterization of FPs and FNs was conducted by a domain expert agronomist. The total percentage of both FP and FN instances was used as a metric of comparison, and all methods were tested on the same test images from the



study. The supervised learning algorithms were trained with the default parameters and with early stopping on the same training dataset. The results for all methods are presented in Table 7.

**Table 7.** Comparison of the proposed approach (in bold) with other computer vision baselines and machine learning methods using total percentage of misidentifications as a metric (sum of false positives and false negatives).

Test Image	1	2	3	4	5	6	7	8	9	10	Mean
Use Case	2	1	5	4	4	6	6	5	7	3	
Blob detection	63.65	56.81	34.35	34.57	31.73	28.00	25.75	28.54	65.39	39.57	40.84
Feature detection (ORB)	65.68	59.56	49.72	46.85	48.38	50.24	47.90	48.81	63.40	43.74	52.43
Color detection	53.88	52.96	35.32	32.27	31.12	29.62	29.03	27.51	55.88	27.45	37.50
Clustering (K-means)	52.25	54.17	40.19	39.12	38.69	36.47	36.16	36.20	53.55	42.97	42.98
Object detection (SSD)	12.34	15.28	21.68	29.16	5.92	7.03	7.05	19.39	21.01	27.10	16.60
Mask R-CNN	8.31	13.01	19.80	27.21	3.45	3.98	2.80	16.59	17.98	23.00	13.61
<b>Proposed U-net</b>	<b>7.69</b>	<b>12.50</b>	<b>20.83</b>	<b>27.27</b>	<b>2.08</b>	<b>3.64</b>	<b>2.33</b>	<b>16.09</b>	<b>16.67</b>	<b>23.94</b>	<b>13.30</b>

Blob detection performed poorly on use cases 1 and 2 due to the canopies being brown or leafless, on 4 and 5 due to the canopies' shadows, and on 7 due to the matching green color on the weed-rich ground. On use case 3, no significant drawbacks were noted. Feature detection resulted in too many FP identifications in all cases because of the leaf-like appearances of most objects present in the aerial orchard photos. Color detection achieved better performance on use cases 3–6 compared to the previous two methods, but with manual tweaking of the color values for each image separately; however, when foliage and ground color bore a resemblance, there were almost no identifications. When K-means was tuned to create two clusters, for trees and backgrounds, it took into account all pixels that belonged to weeds or similar fauna. The algorithm trained with SSD was able to find most trees; however, the locations of the tree trunks, which were computed as the center of the bounding box, had noticeable deviations from the ground truth. Finally, Mask R-CNN is a two-stage approach but, even though it performed similarly to the proposed U-net approach, the generated model was five to ten times larger (the size of the proposed U-net-based model was ~22 Mb), thus rendering the lightweight implementation prerequisite as null. All methods offer benefits and drawbacks; however, it is evident that, to meet all requirements needed to tackle the problem at hand, the proposed U-net approach appears to be the optimal one.

## 5. Discussion

The present study is an initial attempt to address the problem of accurately mapping orchards via UAS. The primary focus was to construct a methodology of tree segmentation and mapping of orchards. During the testing phase of the models, useful insights were produced, along with some outcomes that showed both FP and FN misidentifications. In general, the FPs in the presented system referred to:

- Identification of shrubs and weeds as tree canopies; and
- Segmentation splits of a single instance into multiple high-density instances.

On the other hand, the FNs referred to:

- Circumstantial inadequacy in identifying small canopies; and
- Limitations in identifying trees with leafless canopies.

Considering the preprocessing method that was used, more outcomes can be discussed. For example, the simple EQ, according to the original image brightness and the size of the trees, either produced FPs next to canopies, most of them being weeds, or failed to find the trees entirely, especially if their canopy was small in size. The CLAHE methodology, a valuable tool performing well under different brightness conditions, slimmed down the canopies to a higher degree than desirable, leading to different shapes and sizes compared to the actual canopy. In many cases, this slimming splits canopies in two, which

meant that the size of the tree and the location of its trunk could be incorrectly calculated. When the images were transformed into the HSV colorspace, the trained model performed well in identifying rough shapes, yet missed some obvious canopies which were not missed by other methods, leading to a high number of FNs. The fused approach demonstrated that the shortcomings of each method affected the predicted segmentations, therefore leading to models with worse performance than their best-performing counterparts. Nevertheless, the RGB model achieved the highest training and validation accuracy, the best testing accuracy, and the best performance considering FPs and FNs. This approach demonstrated robustness with all types of orchards and all seasons and for all different sizes, proving that it was the best approach for the problem at hand. Another factor that mostly affected the presence of FNs was the reshaping that images underwent in order to be fed into the training algorithm and consequently to the trained model. Resizing can compress information and in some cases this compression made small canopies “disappear”. However, even though some vital information could have been lost due to resizing, the FN errors remained at a low ratio.

The present study also demonstrated that the majority of FP segmentations were either (a) trees or bushes that were outside of the orchard, (b) developed weeds dispersed throughout the field area, or (c) split canopies resulting in two separate masks. The first category is easy to handle since the coordinates of the orchard are known and therefore any masks outside of it can be disregarded. Since the tree trunks can be calculated based on the shape of the canopy, their distances can be measured and a set of rules applied to the orchard’s structure could identify such misidentifications. The latter could serve as a good solution to address the misidentification problems caused by weeds. The third category can also be addressed by applying methods that identify the lines on which each tree is planted, therefore deducting whether the calculated coordinates of a trunk fall within an acceptable limit. All the above indicate future research directions for the continuation of this work.

The second misidentification factor can also be addressed by changing the resolution of the processed images. According to the results of the model performance evaluation on orthomosaics, in orchards with young trees featuring small canopies and filled with developed weeds, the performance was rather poor. This was attributed to the fact that the top view of the weeds was similarly colored, shaped, and sized as the very small trees within the image. This led to the identification of a large number of FPs. The resolution of the images used in the procedure played an important role in the accuracy. Running the same model on the complete orthomosaic, the results were remarkably improved, reaching 82% accuracy. This was attributed to the fact that the lower pixel resolution resulted in smoothing of the image, merging the pixels that included small weeds with the surroundings, thus making the trees stand out in the image.

Higher accuracy with regard to the overlapping area of pixels may be desired as this is a confident performance metric for model training. However, since the annotation was conducted with high detail on the canopy while the prediction was not required to outline fine details, the metric based on FP and FN predictions was additionally used to identify which method achieved the best results. Regarding the accuracy metric, the best model achieved 91% for training, 90% for validation, and 87% for testing accuracy. Considering the false predictions ratio, 13.3% was achieved for both positive and negative misidentifications of segmented canopies.

In general, image segmentation has been used in many areas; however, this is the first time, based on the authors’ knowledge, that it has been applied to UAV images of orchards. Image segmentation was selected over object detection due to a number of benefits, some of which can be summarized in the following bullet points:

- The trees’ canopy size can be distinguished;
- The trees’ canopy shape can be identified;
- Gaps in the planting scheme due to missing or defoliated and diseased trees can be identified;



- The 2D surface of the imaged canopies can be computed;
- The 3D surface and volume of the trees' canopy can be computed;
- The trees' ages can be approximated;
- The amount of pesticide/water needed for individual trees can be reduced by assigning proportionate amounts;
- The orchard's yield potential can be calculated based on UAV imagery.

There are diverse possibilities for applying image segmentation to orchards and it can cover multiple aspects of operational activities in agriculture. This can be achieved with the use of deep learning, as it has proven its use in multiple occasions [45]. Additionally, semantic segmentation is an active domain with novel approaches being proposed systematically [46], some of which have direct associations with the specific shortcomings of remote sensing [47].

For the present study, U-net was utilized and tweaked to match the addressed problem and the available dataset. U-net might be considered as a relatively basic neural network considering the existence of autoencoders; however, several benefits of its use are apparent from this study:

- It achieved consistent performance >85% with all image datasets even if they had not been enhanced;
- High performance could be obtained even with a small number (~100) of images and even without image augmentation;
- The trained model could produce masks instantaneously.

These outcomes render the selection of U-net as optimal for free field deployment on UAV images. The lightness of the architecture leads to trained models which can run with on-board devices using low-power processors. This ease of application, combined with the high performance for the selected RGB model and the fact that this performance was achieved with a small dataset, leads to the conclusion that the proposed methodology is a promising start in the development of a highly sophisticated system that can identify trees in orchards and extrapolate a multitude of information useful for a variety of related operations.

The current study could be further advanced by investigating the use of other sensing tools with different capabilities and functions. These sensors might include hyperspectral or multispectral cameras, stereo/depth cameras, or thermal cameras. Each of these sensing tools has different pros and cons:

- Hyper/multispectral and thermal cameras. These cameras have multiple applications in agriculture, especially for crop monitoring. The main advantage is the high-value data related to crop and soil status. The disadvantages of this type of camera are the high computational cost that is required to transform the raw data, the high purchase cost, and the operational constraints due to various calibrations that have to take place before each flight and their dependence on weather conditions since cloud coverage greatly affects their measurements.
- Stereo/depth cameras. These are a type of camera commonly used in UGV applications due to their accurate depth perception in tandem with RGB depiction. There are two major disadvantages that constrain the use of these sensors; their low range of operational distance (most cameras have a 20 m range) and increased onboard computational requirements.
- Thermal cameras. These cameras provide high-value data, similar to the hyper- and multispectral cameras. However, they have high computational and operational costs.

However, using one of these sensors, or a combination of them, would increase the complexity of the system, adding computational costs. Since our goal was to develop a widely acceptable rapid system for on-the-go applications, we based the methodology on using RGB camera, thus making it accessible to the majority of UAS users. In this study, an initial approach for developing a simple tree segmentation system that provides instant

and accurate results was proposed. Evaluating the use of the abovementioned sensors is part of our future plans for further development.

The proposed system can serve as a tool for identifying the locations of trees and obstacles within orchards and can be used as part of situation awareness and path planning for agricultural robots and autonomous vehicles. In future work, this model could serve as a UAV-based scouting tool in a UAV-UGV synergetic scheme for autonomous UGV operations within orchards. Additionally, this system can identify gaps within tree rows, thus serving as a subsystem of a farm management information system (FMIS).

## 6. Conclusions

This study addressed the problem of accurately identifying and segmenting tree canopies in a variety of orchards from UAS-captured images. The potential uses of tree segmentation cover a variety of applications, such as, for example, mapping orchard environments in order to identify the coordinates of tree trunks for autonomous ground vehicle navigation. Additionally, the system can serve as a tool to properly calculate the volume of tree canopies within orchards and consequently estimate the trees' ages and yield potential. These operations are crucial for the next age of precision agriculture, in which on-field visual inspection by experts will be less frequent, or extensive and less time-consuming. Agricultural environments are highly complex; therefore, the ability to accurately segment tree canopies, regardless of the growth stage and the season, provides added value to any subsequent operations that take place within orchards.

The proposed approach employed a deep learning architecture, namely U-net, to create a model able to segment tree canopies from UAS-captured images. The implemented dataset was composed of images from three different orchards at different seasons throughout the year, growing trees of different ages and with different canopy sizes. The achieved variability of the dataset resulted in obtaining images that fell under seven different use cases. The best-trained model achieved 91%, 90%, and 87% accuracy for training, validation, and testing, respectively. The results of the test dataset were also hand-examined by experts in order to identify false positive and false negative instances of the produced segmentation. The mean of all false positive instances throughout the whole test dataset was 7.49% and for all false negative instances it was 5.81%. The trained model was also tested on never-before-seen orthomosaic images or orchards based on two methods in order to tackle issues with out-of-the-field boundary transparent pixels in the image. Even though the trained model did not contain orthomosaic images, it achieved performance levels that reached up to 99%, demonstrating the robustness of the proposed approach. Additionally, this study revealed issues that are present in computer vision tasks in highly complex environments, such as in agricultural production. These issues have been documented and will be the focus of upcoming studies. Other future plans include the verification of the present study's results by testing and evaluating the performance of the trained models on different types of trees and orchard structures. Additionally, auxiliary methodologies will be developed to address the problem of densely located or merged false positives.

**Author Contributions:** Conceptualization, A.A. and D.B.; methodology, A.A., S.P., and D.B.; software, A.A., V.M.; validation, D.K., C.G.S., and A.C.T.; formal analysis, C.G.S., D.K., S.P., and A.C.T.; investigation, A.A.; data curation, A.A., A.C.T., and V.M.; writing—original draft preparation, A.A. and A.C.T.; review and editing, D.B., C.G.S., and S.P.; visualization, V.M. and A.A.; supervision, D.B. All authors have read and agreed to the published version of the manuscript.

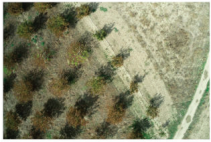


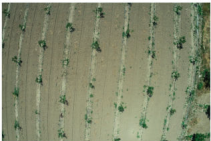



**Funding:** This research received no external funding.

**Acknowledgments:** This research was supported by the project "Human-Robot Synergetic Logistics for High Value Crops" (project acronym: SYNERGIE), funded by the General Secretariat for Research and Innovation (GSRI) under reference no. 2386.

**Conflicts of Interest:** The authors declare no conflict of interest.

## Appendix A

**Table A1.** Sample images of the seven use cases included in the study.

Use Case No.	Conditions	Sample Image
1	Yearly season: Autumn Weeds coverage: Low Canopy size: - Foliage color: Brown Ground color: Brown	
2	Yearly season: Autumn Weeds coverage: Low Canopy size: - Foliage color: Mixed Ground color: Brown	
3	Yearly season: Summer Weeds coverage: Low Canopy size: Small Foliage color: Green Ground color: Brown	
4	Yearly season: Summer Weeds coverage: Low Canopy size: Medium Foliage color: Green Ground color: Brown	
5	Yearly season: Summer Weeds coverage: Low Canopy size: Medium Foliage color: Green Ground color: Mixed	
6	Yearly season: Summer Weeds coverage: Low Canopy size: Large Foliage color: Green Ground color: Brown	
7	Yearly season: Summer Weeds coverage: High Canopy size: Large Foliage color: Green Ground color: Green	

## References

- Gemtos, T.; Fountas, S.; Tagarakis, A.; Liakos, V. Precision Agriculture Application in Fruit Crops: Experience in Handpicked Fruits. *Procedia Technol.* **2013**, *8*, 324–332. [[CrossRef](#)]
- Mulla, D.J. Twenty five years of remote sensing in precision agriculture: Key advances and remaining knowledge gaps. *Biosyst. Eng.* **2013**, *114*, 358–371. [[CrossRef](#)]
- Berni, J.A.J.; Zarco-Tejada, P.J.; Suárez, L.; González-Dugo, V.; Fereres, E. Remote sensing of vegetation from UAV platforms using lightweight multispectral and thermal imaging sensors. *Int. Arch. Photogramm. Remote Sens. Spat. Inform. Sci.* **2009**, *38*, 6.
- Maresma, A.; Chamberlain, L.; Tagarakis, A.; Kharel, T.; Godwin, G.; Czymmek, K.J.; Shields, E.; Ketterings, Q.M. Accuracy of NDVI-derived corn yield predictions is impacted by time of sensing. *Comput. Electron. Agric.* **2020**, *169*. [[CrossRef](#)]

5. Messina, G.; Modica, G. Applications of UAV Thermal Imagery in Precision Agriculture: State of the Art and Future Research Outlook. *Remote. Sens.* **2020**, *12*, 1491. [[CrossRef](#)]
6. Ampatzidis, Y.; Partel, V.; Costa, L. Agroview: Cloud-based application to process, analyze and visualize UAV-collected data for precision agriculture applications utilizing artificial intelligence. *Comput. Electron. Agric.* **2020**, *174*, 105457. [[CrossRef](#)]
7. Anagnostis, A.; Benos, L.; Tsaopoulos, D.; Tagarakis, A.; Tsolakis, N.; Bochtis, D. Human Activity Recognition through Recurrent Neural Networks for Human–Robot Interaction in Agriculture. *Appl. Sci.* **2021**, *11*, 2188. [[CrossRef](#)]
8. Liakos, K.G.; Busato, P.; Moshou, D.; Pearson, S.; Bochtis, D. Machine learning in agriculture: A review. *Sensors* **2018**, *18*, 2674. [[CrossRef](#)]
9. Benos, L.; Tagarakis, A.C.; Dolias, G.; Berruto, R.; Kateris, D. Machine Learning in Agriculture: A Comprehensive Updated Review. *Sensors* **2021**, *21*, 3758. [[CrossRef](#)]
10. Ofori, M.; El-Gayar, O. Towards deep learning for weed detection: Deep convolutional neural network architectures for plant seedling classification. In Proceedings of the 26th Americas Conference on Information Systems, AMCIS 2020, Salt Lake City, UT, USA, 10–14 August 2020.
11. Zheng, Y.-Y.; Kong, J.-L.; Jin, X.-B.; Wang, X.-Y.; Zuo, M. CropDeep: The Crop Vision Dataset for Deep-Learning-Based Classification and Detection in Precision Agriculture. *Sensors* **2019**, *19*, 1058. [[CrossRef](#)]
12. Bosilj, P.; Aptoula, E.; Duckett, T.; Cielniak, G. Transfer learning between crop types for semantic segmentation of crops versus weeds in precision agriculture. *J. Field Robot.* **2019**, *37*, 7–19. [[CrossRef](#)]
13. Anagnostis, A.; Asiminari, G.; Papageorgiou, E.; Bochtis, D. A Convolutional Neural Networks Based Method for Anthracnose Infected Walnut Tree Leaves Identification. *Appl. Sci.* **2020**, *10*, 469. [[CrossRef](#)]
14. Onishi, M.; Ise, T. Automatic classification of trees using a UAV onboard camera and deep learning. *arXiv* **2018**, arXiv:1804.10390.
15. Franklin, S.E.; Ahmed, O.S. Deciduous tree species classification using object-based analysis and machine learning with unmanned aerial vehicle multispectral data. *Int. J. Remote. Sens.* **2018**, *39*, 5236–5245. [[CrossRef](#)]
16. Zhao, Z.-Q.; Zheng, P.; Xu, S.-T.; Wu, X. Object Detection with Deep Learning: A Review. *IEEE Trans. Neural Netw. Learn. Syst.* **2019**, *30*, 3212–3232. [[CrossRef](#)] [[PubMed](#)]
17. Anagnostis, A.; Tagarakis, A.; Asiminari, G.; Papageorgiou, E.; Kateris, D.; Moshou, D.; Bochtis, D. A deep learning approach for anthracnose infected trees classification in walnut orchards. *Comput. Electron. Agric.* **2021**, *182*, 105998. [[CrossRef](#)]
18. Moisiadis, V.; Tsolakis, N.; Katikaridis, D.; Sørensen, C.G.; Pearson, S.; Bochtis, D. Mobile Robotics in Agricultural Operations: A Narrative Review on Planning Aspects. *Appl. Sci.* **2020**, *10*, 3453. [[CrossRef](#)]
19. Ronneberger, O.; Fischer, P.; Brox, T. U-net: Convolutional networks for biomedical image segmentation. In Proceedings of the International Conference on Medical Image Computing and Computer-Assisted Intervention, Cham, Switzerland, 5–9 October 2015; pp. 234–241.
20. Brandt, M.; Tucker, C.J.; Kariryaa, A.; Rasmussen, K.; Abel, C.; Small, J.; Chave, J.; Rasmussen, L.V.; Hiernaux, P.; Diouf, A.A.; et al. An unexpectedly large count of trees in the West African Sahara and Sahel. *Nat. Cell Biol.* **2020**, *587*, 78–82. [[CrossRef](#)] [[PubMed](#)]
21. Schiefer, F.; Kattenborn, T.; Frick, A.; Frey, J.; Schall, P.; Koch, B.; Schmidlein, S. Mapping forest tree species in high resolution UAV-based RGB-imagery by means of convolutional neural networks. *ISPRS J. Photogramm. Remote. Sens.* **2020**, *170*, 205–215. [[CrossRef](#)]
22. Zhao, T.; Yang, Y.; Niu, H.; Chen, Y.; Wang, D. Comparing U-Net convolutional networks with fully convolutional networks in the performances of pomegranate tree canopy segmentation. In Proceedings of the SPIE Asia-Pacific Remote Sensing Conference, Multispectral, Hyperspectral, Ultraspectral Remote Sensing Technology Techniques and Applications VII, Honolulu, HI, USA, 24–26 September 2018; p. 64. [[CrossRef](#)]
23. Ochoa, K.S.; Guo, Z. A framework for the management of agricultural resources with automated aerial imagery detection. *Comput. Electron. Agric.* **2019**, *162*, 53–69. [[CrossRef](#)]
24. Onishi, M.; Ise, T. Explainable identification and mapping of trees using UAV RGB image and deep learning. *Sci. Rep.* **2021**, *11*, 1–15. [[CrossRef](#)]
25. Hu, X.; Li, D. Research on a Single-Tree Point Cloud Segmentation Method Based on UAV Tilt Photography and Deep Learning Algorithm. *IEEE J. Sel. Top. Appl. Earth Obs. Remote. Sens.* **2020**, *13*, 4111–4120. [[CrossRef](#)]
26. Chen, Y.; Hou, C.; Tang, Y.; Zhuang, J.; Lin, J.; He, Y.; Guo, Q.; Zhong, Z.; Lei, H.; Luo, S. Citrus Tree Segmentation from UAV Images Based on Monocular Machine Vision in a Natural Orchard Environment. *Sensors* **2019**, *19*, 5558. [[CrossRef](#)] [[PubMed](#)]
27. Adhikari, A.; Kumar, M.; Agrawal, S.; Raghavendra, S. An Integrated Object and Machine Learning Approach for Tree Canopy Extraction from UAV Datasets. *J. Indian Soc. Remote. Sens.* **2021**, *49*, 471–478. [[CrossRef](#)]
28. Morales, G.; Kemper, G.; Sevillano, G.; Arteaga, D.; Ortega, I.; Telles, J. Automatic Segmentation of *Mauritia flexuosa* in Unmanned Aerial Vehicle (UAV) Imagery Using Deep Learning. *Forests* **2018**, *9*, 736. [[CrossRef](#)]
29. Soni, A.; Koner, R.; Villuri, V.G.K. M-UNet: Modified U-Net Segmentation Framework with Satellite Imagery. In *Advances in Intelligent Systems and Computing*; Springer Science and Business Media LLC: Berlin/Heidelberg, Germany, 2020; pp. 47–59.
30. Chen, S.-D.; Ramli, A. Minimum mean brightness error bi-histogram equalization in contrast enhancement. *IEEE Trans. Consum. Electron.* **2003**, *49*, 1310–1319. [[CrossRef](#)]
31. Reza, A.M. Realization of the Contrast Limited Adaptive Histogram Equalization (CLAHE) for Real-Time Image Enhancement. *J. VLSI Signal Process. Syst. Signal Image Video Technol.* **2004**, *38*, 35–44. [[CrossRef](#)]

32. Papandrianos, N.; Papageorgiou, E.; Anagnostis, A.; Papageorgiou, K. Efficient Bone Metastasis Diagnosis in Bone Scintigraphy Using a Fast Convolutional Neural Network Architecture. *Diagnostics* **2020**, *10*, 532. [CrossRef]
33. Carass, A.; Roy, S.; Gherman, A.; Reinhold, J.C.; Jesson, A.; Arbel, T.; Maier, O.; Handels, H.; Ghafoorian, M.; Platel, B.; et al. Evaluating White Matter Lesion Segmentations with Refined Sørensen-Dice Analysis. *Sci. Rep.* **2020**, *10*, 1–19. [CrossRef]
34. Jaccard, P. The Distribution of the Flora in the Alpine Zone. *New Phytol.* **1912**, *11*, 37–50. [CrossRef]
35. Zhang, Y.; Mehta, S.; Caspi, A. Rethinking Semantic Segmentation Evaluation for Explainability and Model Selection. *arXiv* **2021**, arXiv:2101.08418.
36. Khryashchev, V.; Larionov, R. Wildfire Segmentation on Satellite Images using Deep Learning. In Proceedings of the 2020 Moscow Workshop on Electronic and Networking Technologies (MWENT), Moscow, Russia, 11–13 March 2020; pp. 1–5.
37. Park, S.; Kwak, N. Analysis on the dropout effect in convolutional neural networks. In Proceedings of the Asian Conference on Computer Vision, Taipei, Taiwan, 20–24 November 2016. [CrossRef]
38. Bradski, G. *The OpenCV Library*; Dr. Dobb's J. Software Tools: New York, NY, USA, 2000.
39. Hartigan, A.; Wong, M.A. A K-Means Clustering Algorithm. *J. R. Stat. Soc.* **1979**, *28*.
40. Pedregosa, F.; Varoquaux, G.; Gramfort, A.; Michel, V.; Thirion, B.; Grisel, O.; Blondel, M.; Prettenhofer, P.; Weiss, R.; Dubourg, V.; et al. Scikit-learn: Machine learning in Python. *J. Mach. Learn. Res.* **2011**, *12*, 2825–2830.
41. Liu, W.; Anguelov, D.; Erhan, D.; Szegedy, C.; Reed, S.; Fu, C.Y.; Berg, A.C. SSD: Single shot multibox detector. In Proceedings of the Lecture Notes in Computer Science, Milan, Italy, 14–16 November 2016; Volume 9905, pp. 21–37.
42. He, K.; Zhang, X.; Ren, S.; Sun, J. Deep residual learning for image recognition. In Proceedings of the IEEE Conference on Computer Vision and Pattern Recognition, Las Vegas, NV, USA, 27–30 June 2016; pp. 770–778.
43. Chollet, F. and Others, Keras. 2015. Available online: [https://www.scirp.org/\(S\(351jmbntvnjsjt1aadkposzje\)\)/reference/ReferencesPapers.aspx?ReferenceID=1887532](https://www.scirp.org/(S(351jmbntvnjsjt1aadkposzje))/reference/ReferencesPapers.aspx?ReferenceID=1887532) (accessed on 30 May 2021).
44. Abadi, M.; Agarwal, A.; Barham, P.; Brevdo, E.; Chen, Z.; Citro, C.; Corrado, G.S.; Davis, A.; Dean, J.; Devin, M.; et al. TensorFlow: Large-Scale Machine Learning on Heterogeneous Distributed Systems. *arXiv* **2016**, arXiv:1603.04467.
45. Garcia-Garcia, A.; Orts-Escolano, S.; Oprea, S.O.; Villena-Martinez, V.; Garcia-Rodriguez, J. A review on deep learning techniques applied to semantic segmentation. *arXiv* **2017**, arXiv:1704.06857.
46. Yuan, Y.; Chen, X.; Wang, J. Object-Contextual Representations for Semantic Segmentation. In *Transactions on Petri Nets and Other Models of Concurrency XV*; Springer Science and Business Media LLC: Berlin/Heidelberg, Germany, 2020; pp. 173–190.
47. Li, Y.; Shi, T.; Zhang, Y.; Chen, W.; Wang, Z.; Li, H. Learning deep semantic segmentation network under multiple weakly-supervised constraints for cross-domain remote sensing image semantic segmentation. *ISPRS J. Photogramm. Remote Sens.* **2021**, *175*, 20–33. [CrossRef]

## Article

# Detecting Animal Contacts—A Deep Learning-Based Pig Detection and Tracking Approach for the Quantification of Social Contacts

Martin Wutke <sup>1,2,\*</sup>, Felix Heinrich <sup>1</sup>, Pronaya Prosun Das <sup>3</sup>, Anita Lange <sup>2</sup>, Maria Gentz <sup>2</sup>, Imke Traulsen <sup>2</sup>, Friederike K. Warns <sup>4</sup>, Armin Otto Schmitt <sup>1,5</sup> and Mehmet Gültas <sup>5,6,\*</sup>

- <sup>1</sup> Breeding Informatics Group, Department of Animal Sciences, Georg-August University, Margarethe von Wrangell-Weg 7, 37075 Göttingen, Germany; felix.heinrich@uni-goettingen.de (F.H.); armin.schmitt@uni-goettingen.de (A.O.S.)
  - <sup>2</sup> Livestock Systems, Department of Animal Sciences, Georg-August University, Albrecht-Thaer-Weg 3, 37075 Göttingen, Germany; anita.lange@agr.uni-goettingen.de (A.L.); maria.gentz@thuenen.de (M.G.); imke.traulsen@uni-goettingen.de (I.T.)
  - <sup>3</sup> Bioinformatics Group, Fraunhofer Institute for Toxicology and Experimental Medicine (Fraunhofer ITEM), Nikolai-Fuchs-Str. 1, 30625 Hannover, Germany; pronaya.prosun.das@item.fraunhofer.de
  - <sup>4</sup> Agricultural Test and Education Centre House Düsse, Chamber of Agriculture North Rhine-Westphalia, Haus Düsse 2, 59505 Bad Sassendorf, Germany; Friederike.Warns@LWK.NRW.DE
  - <sup>5</sup> Center for Integrated Breeding Research (CiBreed), Georg-August University, Albrecht-Thaer-Weg 3, 37075 Göttingen, Germany
  - <sup>6</sup> Statistics and Data Science, Faculty of Agriculture, South Westphalia University of Applied Sciences, 59494 Soest, Germany
- \* Correspondence: martin.wutke@uni-goettingen.de (M.W.); gultas.mehmet@fh-swf.de (M.G.)

**Citation:** Wutke, M.; Heinrich, F.; Das, P.P.; Lange, A.; Gentz, M.; Traulsen, I.; Warns, F.K.; Schmitt, A.O.; Gültas, M. Detecting Animal Contacts—A Deep Learning-Based Pig Detection and Tracking Approach for the Quantification of Social Contacts. *Sensors* **2021**, *21*, 7512. <https://doi.org/10.3390/s21227512>

Academic Editors: Dionysis Bochtis and Aristotelis C. Tagarakis

Received: 18 October 2021

Accepted: 10 November 2021

Published: 12 November 2021

**Publisher's Note:** MDPI stays neutral with regard to jurisdictional claims in published maps and institutional affiliations.



**Copyright:** © 2021 by the authors. Licensee MDPI, Basel, Switzerland. This article is an open access article distributed under the terms and conditions of the Creative Commons Attribution (CC BY) license (<https://creativecommons.org/licenses/by/4.0/>).

**Abstract:** The identification of social interactions is of fundamental importance for animal behavioral studies, addressing numerous problems like investigating the influence of social hierarchical structures or the drivers of agonistic behavioral disorders. However, the majority of previous studies often rely on manual determination of the number and types of social encounters by direct observation which requires a large amount of personnel and economical efforts. To overcome this limitation and increase research efficiency and, thus, contribute to animal welfare in the long term, we propose in this study a framework for the automated identification of social contacts. In this framework, we apply a convolutional neural network (CNN) to detect the location and orientation of pigs within a video and track their movement trajectories over a period of time using a Kalman filter (KF) algorithm. Based on the tracking information, we automatically identify social contacts in the form of head–head and head–tail contacts. Moreover, by using the individual animal IDs, we construct a network of social contacts as the final output. We evaluated the performance of our framework based on two distinct test sets for pig detection and tracking. Consequently, we achieved a Sensitivity, Precision, and F1-score of 94.2%, 95.4%, and 95.1%, respectively, and a *MOTA* score of 94.4%. The findings of this study demonstrate the effectiveness of our keypoint-based tracking-by-detection strategy and can be applied to enhance animal monitoring systems.

**Keywords:** pig detection; pig tracking; convolutional neural network; Kalman filter; precision livestock farming

## 1. Introduction

Today, it is well known that domestic pigs are highly social animals, maintaining hierarchical structures and socially organized groups. In commercial farming systems, the established social orders are frequently disrupted due to mixing groups as they are transferred between different housing and production stages [1,2]. Mixing of unacquainted animals leads to the establishment of a new social hierarchy going along with agonistic interactions which may result in reduced animal welfare and health [3–5].



In order to enhance animal welfare and health in future husbandry systems, the analysis of animal interactions as well as their monitoring and prediction is of high importance in research and commercial farming. Reasons for agonistic or aggressive behavior are manifold [2,6–10], contribute to a certain extent to the animal specific behavior, and also include a high variation between animals [2].

Nowadays, video recordings are a standard tool in research for observing pig pens due to their non-invasive nature. Recent technological advances including deep learning techniques, led to the rise of precision livestock farming applications to partially automate the time consuming video evaluation process [11]. Within the area of precision livestock farming, the tasks of multiple object detection and motion tracking have been studied intensively in recent years, in order to remotely monitor several animals and to capture the animals activity [11–15]. While multiple object detection refers to the task of locating several objects belonging to a category of interest within an image [16], multiple object tracking can be described as tracing the movement of objects throughout a consecutive number of video frames and consistently assigning individual object IDs [17].

With the recent advances in the area of deep learning, convolutional neural network (CNN)-based applications achieved state-of-the-art results in various image and video object detection scenarios [18]. Here, the most frequently used detection approaches aim to localize an object of interest by computing a bounding box around the object [19–21]. Although these approaches work successfully for various problem settings, due to the overlapping of the predicted bounding boxes, their applicability is limited for the analysis of videos with high utilization rates and several pigs in a close environment [22,23]. Furthermore, the standard bounding box approach only provides the positional information without taking the orientation of the animal into account which is a key information in order to reliably differentiate distinctive contact types like head–head interactions.

To overcome this limitation, an alternative detection approach was developed by Psota et al. [23]. The authors proposed a keypoint-based CNN for the detection of individual body parts of pigs. After processing the CNN output with a cross-check matching algorithm for assigning the individual body parts, they were able to successfully differentiate multiple animals even in a close proximity environment. Achieving a sensitivity, precision rate and an F1-score of 96%, 100%, and 98%, respectively, their approach proved to be highly successful in identifying the location and orientation of individual animals. As an extension, Psota et al. [11] applied this method to deal with the problem of tracking individual animals by using a second object detection CNN to detect ear tags which serve as a pig-individual identifier. Although this approach shows a lot of practical potential, using individual ear tags requires additional effort for the attachment of the ear-tags. Furthermore, the detectability of the corresponding ear-tags must be ensured, as the visibility of the tags is often prevented by heavy interactions between the animals, bad lighting conditions or a high degree of pollution in the pig compartment. As a possible solution, it seems beneficial to use the detected body parts directly for animal tracking which could increase the applicability of the keypoint-based detection approach, while simultaneously reducing the complexity without the need to train a second CNN for object detection.

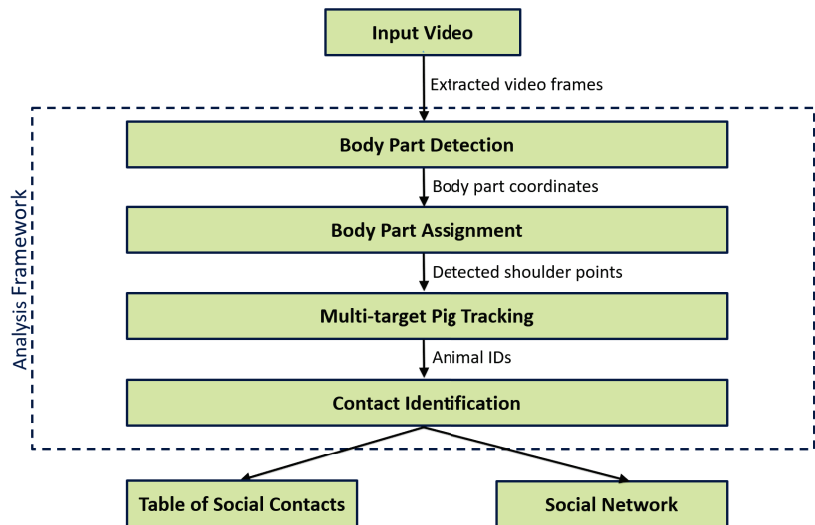
Therefore, by following the idea in [23] we implement a CNN based framework for detecting individual body parts of pigs and use the predicted shoulder–tail information directly as the input for a Kalman filter (KF)-based tracking algorithm. The KF is currently one of the most frequently used approaches for tracking the motion activity of multiple objects within a video [24,25] which allows the assignment of individual animal IDs in this study. Subsequently, by collecting the shoulder–tail information as well as the animal ID in our framework we differentiate between specific head–head and head–tail contacts. As a result of this, our framework is able to determine a table of social contacts and to compute a graphical network of the social relationships. Such type of contacts could provide crucial information about social interactions including tail and ear biting. Consequently, using the proposed framework we aim to automate the process of video data analysis by quantifying the number of social encounters for several pigs within a video sequence. This information

can then be used by researchers to specifically analyze scenes of interest within their respective fields or to directly perform a SNA.

The remainder of this article is structured as follows. Section 2 describes the data used for this analysis and explains the methodical foundation as well as the evaluation rationale applied in this article. Next, the results for the animal detection, animal tracking, and social contact identification are presented and discussed in Section 3. Section 4 concludes this article.

## 2. Materials and Methods

In this section, the data used for the analysis as well as the different stages of the proposed method and the evaluation rationale are described in detail. The underlying multi-stage framework of the proposed method is illustrated in Figure 1.



**Figure 1.** Flowchart of the analysis applied in this study.

The proposed method follows a tracking-by-detection (TBD) approach with the goal of tracking a known number of pigs within the pig compartment. As the input signal, a video sequence represented by a series of consecutive frames  $S = (s_1, s_2, \dots, s_N)$  is used, where  $N$  is the number of frames. In this context, TBD refers to first detecting objects of interest in each video frame using a pre-trained detector and then linking the independent detections at the temporal dimension over a longer period of frames [26,27].

In this study, the location and orientation of each pig within the video is determined frame-wise using a keypoint-based CNN to output the coordinates of important body parts (shoulder, tail, left ear, and right ear). After associating the body parts and assigning a unique ID to each pig, the shoulder coordinates in time  $T$  are used as the input signal for a Kalman filter to predict and track the location of future shoulder positions in  $T + i$  with  $i = (1, 2, \dots, N - T)$ . By tracking the shoulder points, two distinct types of body part contacts are identified as being either a head-head or head-tail contact. If two shoulder points are close to each other, the encounter is marked as a head-head contact. If a shoulder point is close to a tail point, the encounter is marked as a head-tail contact. Finally, by incorporating the frame number information, animal IDs and types of contact, a table of social contacts as well as a graphical representation in form of a social network is constructed as an output.

### 2.1. Data Acquisition and Processing

The video data used for this study was collected by [28,29] between October and December 2018 at the research farm Futterkamp of the Chamber of Agriculture of Schleswig-Holstein in Germany during a research project to investigate the effects of different farrowing and rearing systems on the stress level of piglets. For this purpose, a single static camera of the type AXIS M3024-LVE (Axis Communications AB, Lund, Sweden) was assembled 3 m above the ground which recorded all videos with a frame-per-second (fps) rate of 10 frames and a display resolution of  $1280 \times 800$  pixels. For this study, sequences with a varying number of animals and a fixed camera angle have been selected. Figure 2 shows three example frames of structurally identical pens.



**Figure 2.** Example frames of the pig compartment under investigation with a known number of pigs.

In our analysis, we extracted all video frames and converted them to a grayscale format with a pixel dimension of  $640 \times 400$  pixels, in order to avoid a potential bias of the CNN by differentiating between day and night recordings [30]. The dimensionality reduction was carried out to reduce CNN training time and, thereby, increase the computational efficiency.

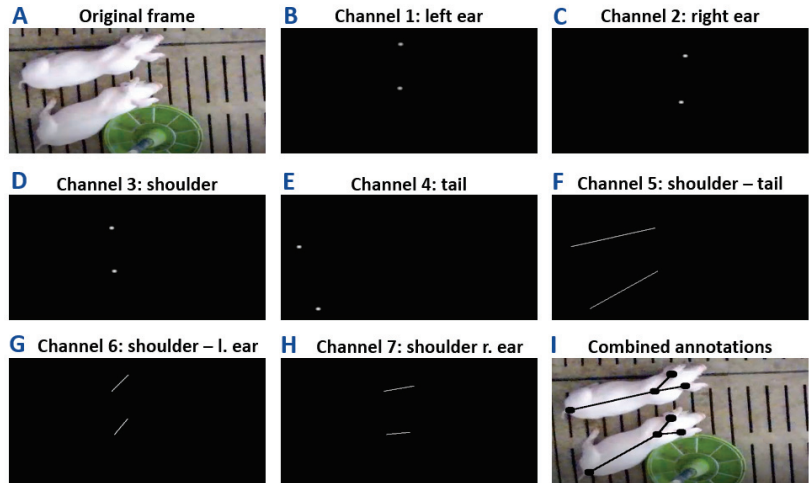
### 2.2. Pig Detection

An essential step in the tracking of individual pigs is their successful detection. For this purpose, Psota et al. [23] established a keypoint-based CNN to detect distinct body parts of pigs and highlighted the advantage of this approach over existing bounding box detections. Using this keypoint approach, we implemented a CNN to receive a video frame and to output the coordinates of four individual body parts for each animal. Similar to the work in [23], we stored the coordinate information of the left ear, right ear, shoulder and tail point directly as a binary image in a separate image channel (Figure 3B–E). Additionally, the information for the connection lines shoulder–tail, shoulder–left ear, and the shoulder–right ear are included (Figure 3F–H). In comparison to conventional top-down detection methods, which output bounding box or ellipsoid coordinates, the detected keypoints directly provide a pose representation which facilitates the contact identification of the animals [23].

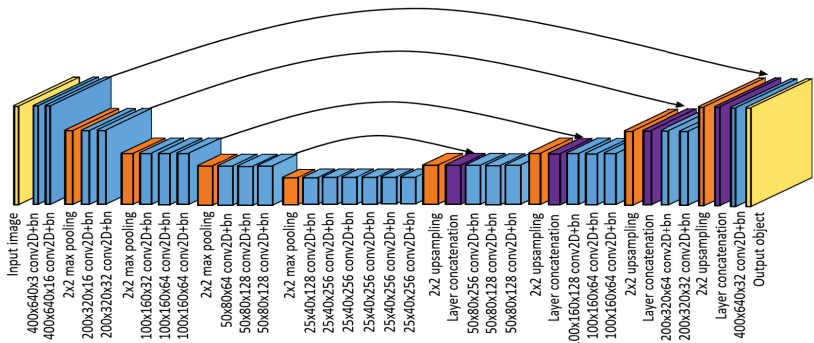
During the training process, a CNN is trained to map the input image to the ground truth annotations by highlighting the important pixels of the corresponding body parts. The architecture of our CNN follows an autoencoder structure which is illustrated in Figure 4.

The CNN consists of 25 convolutional layers combined with  $2 \times 2$  max pooling and upsampling layers. The first ten layers are used to reduce the input dimension from  $640 \times 400$  pixels to a latent representation of  $40 \times 25$  pixels and extract the main features for the body part detection. At the lowest dimension, six stacked convolutional layers forward the latent image representation to a set of upsampling and convolutional layers, which step-wise increase the image dimension back to  $640 \times 400$  pixels and output the approximate body part coordinates. After each upsampling layer, a residual connection with a concatenation layer is used to copy a representation from the encoder layers to the decoder layers to decrease the reconstruction loss and improve the training efficiency [23,31]. All convolutional layers are implemented with a ReLU activation function, zero padding and a stride parameter of 1. Using the Adam optimizer [32] and binary cross-entropy loss, the

network applies a sigmoid activation for the last layer to output pixel intensities between 0 and 1.



**Figure 3.** (A) The original image which serves as the input for the CNN. (B–H) The corresponding ground truth annotations containing the positional body part information which are used for the training process. (I) The original image combined with the ground truth annotations.



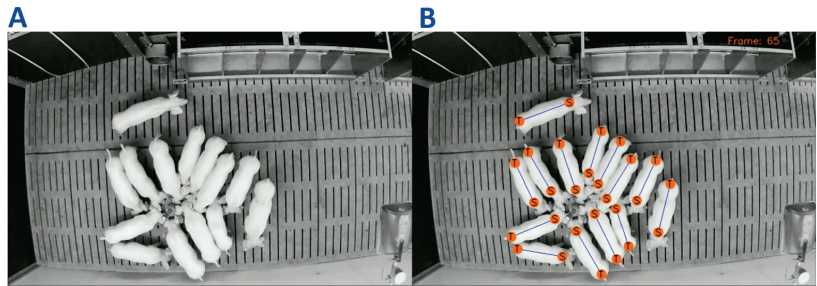
**Figure 4.** The implemented CNN follows an autoencoder structure to create the seven-channel output object given a gray-scaled video frame. For each convolutional layer the dimensional information is given in the format height  $\times$  width  $\times$  number of convolutional filters.

The CNN was implemented in Python (version 3.7.6) [33] using the deep learning framework Keras (version 2.2.4) [34] with TensorFlow (version 2.0) [35] as a backend. The model training was carried out on a workstation equipped with two Intel Xeon Gold 6138 CPUs, 512 GB RAM, and a NVIDIA Quadro P5000 GPU.

Subsequently, to train the CNN, we annotated a training data set consisting of 2457 images. To increase the overall sample size and to enable the model to see more heterogenous animal postures, we augmented the training images as well as the corresponding ground truth annotations using vertical and horizontal shifting, shrinking and image rotation. After augmentation, the total training data set had a size of 12,285 images of which 90% were used for training and 10% for the model validation after each epoch.

After the CNN has learned to predict the positions of the individual body parts in the two-dimensional image space, the location and orientation of each pig are determined based on the CNN output. For this step, we mainly focus on the analysis of Channel 5

(Figure 3F), as it mainly carried the most accurate and robust information. By extracting the start and end coordinates of each shoulder–tail line, a depth-first-search algorithm (DFS) [36] is applied to determine the pigs location. However, Channel 5 does not contain the information of the animal’s orientation. Therefore, we incorporate the information of Channels 1–4 to identify shoulder and tail points of each pig. An example frame after the detection process is given in Figure 5.



**Figure 5.** Example of the CNN pig detection showing the original frame (A) and the detected shoulder and tail points (B). The frame shows a feeding situation in which several pigs are in close proximity to each other. Each pig is marked by highlighting the corresponding shoulder and tail points as well as the connection line.

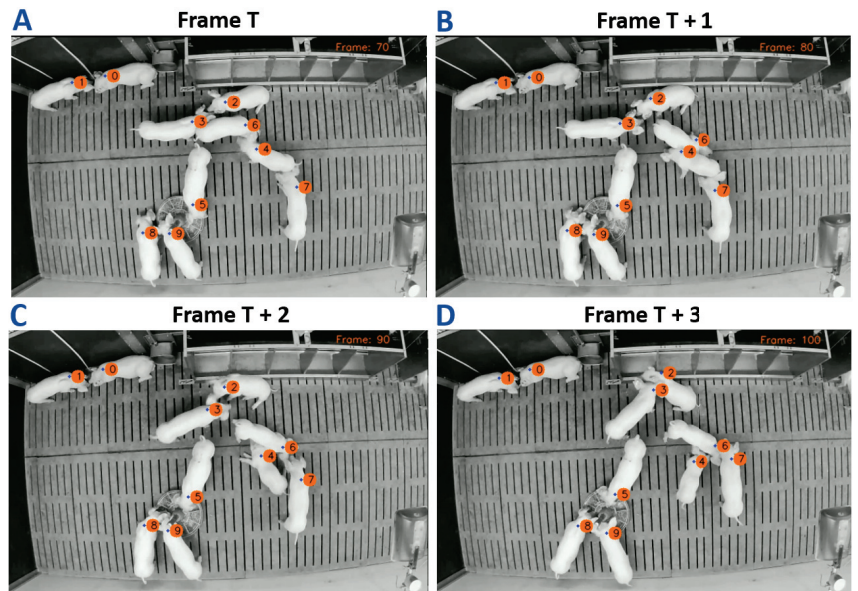
### 2.3. Pig Tracking

After determining the location and orientation of each pig, this step aims to track the pigs’ movement and to link their trajectories over the total sequence of frames. While previous approaches mainly focused on pig tracking using bounding box detections [19,37–39], the suitability of these approaches is limited to identify social contacts in close proximities because they do not incorporate the animals’ orientation and show a high risk of ID switches in situations of overlapping boxes. To reduce this limitation, we apply for the first time a combination of a KF tracking approach [40] with the body part detections as the input signal to track individual animals and to determine distinct contact types. While the CNN output can still contain false detections, we use the KF as an unsupervised, dynamic model to estimate and track the shoulder positions, even in frames in which the true point could not be detected by the CNN.

The KF process is divided into two phases: a prediction and an update phase. In the prediction phase, a prediction of the shoulder position for the current time step  $k$  is computed based on the KF estimate of the shoulder point of the previous time step  $k - 1$ . During the update phase, new CNN detections at  $k$  are used to adjust the current prediction and to compute the KF estimate at time  $k$ , which is used as new input for the prediction phase of the next time step  $k + 1$ . In the case of false positive or false negative CNN detections, the input signal variance is increased, which leads the KF to weight down the importance of the CNN input and to increase the weight of the previous KF prediction [41]. Consequently, the KF yields a more robust estimate of the shoulder point coordinates which overcomes the problem of shoulder–tail swaps and misdetections.

After the KF is initialized, it is applied to the ordered shoulder points produced by the CNN. While all videos have been recorded with a fps rate of 10 frames, even intense motion changes of the animals caused just slight pixel variations in the consecutive frames. Therefore, a KF shoulder point in frame  $k$  is mapped to the corresponding KF shoulder point in frame  $k + 1$  by minimizing the Euclidean distance. Consequently, each KF shoulder estimate is assigned an individual animal ID. An example of the pig tracking and ID assignment is shown in Figure 6.





**Figure 6.** The multi-target pig tracking, shown for an example sequence of four frames, on a one second interval. The frame number is printed on the top, and the fps-rate was set to ten frames. The KF estimate of the shoulder point is highlighted by the blue dot, near the shoulder region of each pig. The corresponding ID is placed right of it.

#### 2.4. Identifying Contact Information

The last stage of our proposed framework aims to identify animal contacts in the form of either head–head or head–tail contacts, which may be related to tail biting or nosing behavior. We use the KF shoulder and tail estimates, as well as the pig orientation to define a region of interest at the head and tail area of each pig. If at least two pigs are nearby to each other so that either both head regions or one head and one tail region are sufficiently close, the head and tail regions are intersecting, which indicates a potential contact. To account for different age and size levels of the animals, the average length of each shoulder–tail line per frame is calculated and used to scale the head and tail regions to a radius  $r$ , defined as:

$$r = \frac{1}{\alpha N} \sum_{i=1}^N \sqrt{(s_i - t_i)^2} \quad (1)$$

where  $s_i$  and  $t_i$  are the shoulder and tail coordinates of the  $i$ -th pig,  $N$  the total number of pigs in the given frame, and  $\alpha$  a scaling factor. In this study, an  $\alpha$  value of 3 was empirically deemed to be optimal for computing an area of interest large enough to cover the essential part of the head and tail region, but being small enough to avoid potential false detections in the form of animals walking by. Figure 7 shows an example of the region computation and contact identification.





**Figure 7.** Based on the KF estimates, a region of interest for each head and tail area is computed. By detecting the intersection of at least two regions, the type of contact and the associated animals can be identified. Exemplarily, a head–tail contact can be detected between pigs 5 and 11 and a head–head contact for pigs 1 and 10.

### 2.5. Pig Detection and Tracking Evaluation Rationale

In order to assess the overall performance of our framework, we evaluated both the CNN detection stage as well as the multi-target pig tracking stage separately. For the CNN detection, we additionally annotated 100 randomly selected images and used these frames as a test set to evaluate the CNN’s ability to predict the location of individual pigs by detecting their shoulder points. To avoid confusion we used the subscript “*D*” and “*T*” to differentiate between the detection evaluation and the tracking evaluation. For the detection stage, we computed the number of *True Positives* ( $TP_D$ ), *False Positives* ( $FP_D$ ), and *False Negatives* ( $FN_D$ ) over all test images and calculated the *Sensitivity*, *Precision* rate, and *F1-score* defined as

$$\text{Sensitivity} = \frac{TP_D}{P_D} \quad (2)$$

$$\text{Precision} = \frac{TP_D}{TP_D + FP_D} \quad (3)$$

$$F1 = \frac{2TP_D}{2TP_D + FP_D + FN_D} \quad (4)$$

In order to determine  $TP_D$ ,  $FP_D$ , and  $FN_D$ , a circular detection region around the true shoulder point was defined by computing the average distance from the true shoulder point to the true left and right ear points over all pigs of the given frame as the radius. If exactly one shoulder point was predicted by the CNN within the detection region, this point has been classified as  $TP_D$ . If more than one point was predicted within the region or outside the detection region, these points have been classified as  $FP_D$ . If no point was detected within the region, the point was classified as  $FN_D$ .

Despite the recent advances of multiple object tracking applications, there is still a lack of large-scale benchmarks and comparable evaluation metrics [42,43]. While the majority of existing object tracking publications applies a bounding box approach using the intersection over union (IoU) as an evaluation criterion between the annotated and predicted box, our proposed framework applies a keypoint-based approach, for which the IoU is not suitable. Therefore, we followed previous studies [21,38,44] and calculated the *Multiple Object Tracking Accuracy* (MOTA) defined as

$$\text{MOTA} = 1 - \frac{FP_T + FN_T + IDSW}{N_{CNN}} \quad (5)$$

by manually determining the number of falsely tracked pigs ( $FP_T$ ), pigs which have not been tracked ( $FN_T$ ), the number of ID switches ( $IDSW$ ), and the number of pigs detected

by the CNN ( $N_{CNN}$ ). While the total tracking error can be further divided into detection errors, association errors, and localization errors [42,45],  $FP_T$  and  $FN_T$  account for the detection errors and  $IDSW$  accounts for the association errors. If a detected pig is not tracked by the KF tracker, it is classified as  $FN_T$ . If the tracker tracks something different than a pig, it is classified as an  $FP_T$ . We further increased the number of  $FP_T$  to account for the localization errors if a pig is tracked, but the corresponding tracking point is too far away from the target point. To determine the  $MOTA$  value we randomly selected 70 videos as test sequences with an average length of 20 seconds. These sequences have been analyzed by the CNN in advance, in order to obtain the coordinates of the detected body parts.

### 3. Results and Discussion

By applying our pig detection and tracking framework, we first analyzed in this study several video frames including different scenarios, in order to assess the detection and tracking performance. After that, three distinct animal contact network visualizations are presented and discussed to demonstrate the applicability and functionality of our framework.

#### 3.1. Pig Detection and Tracking

As the performance of a tracking-by-detection (TBD) algorithm depends strongly on the accuracy of the corresponding detector [46], we evaluated the CNN performance for locating the pig position and determining its orientation using the *Sensitivity*, *Precision*, and *F1-Score* metric, respectively. For this purpose, we analyzed the manually annotated detection test set containing 100 randomly selected frames. Consequently, in total 1054 shoulder points have been annotated and considered for the evaluation analysis (see Table 1). In a following step, we focused on the tracking ability of the implemented KF and used 70 randomly selected video sequences as the tracking evaluation data. The results for the detection as well as for the tracking are provided in Table 1. The data sets used for the detection and tracking evaluation are made publicly available at [https://github.com/MartinWut/Supp\\_DetAnIn](https://github.com/MartinWut/Supp_DetAnIn) (accessed on 9 November 2021).

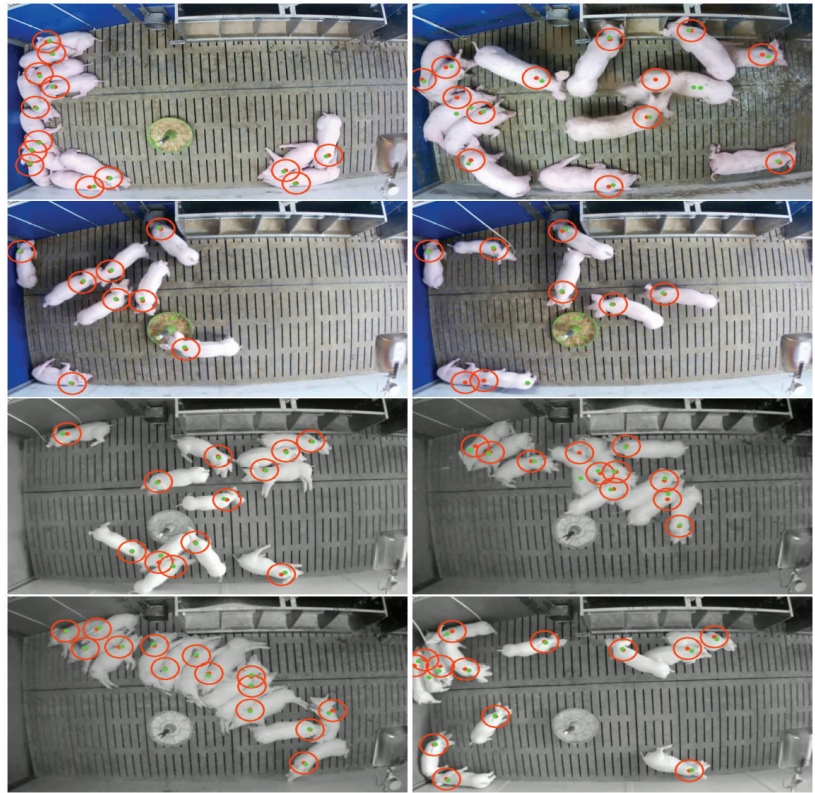
**Table 1.** Evaluation results for the pig detection set and tracking set.

Test Set	TP	FP	FN	IDSW	Sensitivity (%)	Precision (%)	F1 (%)	MOTA (%)
Detection	1019	51	35	-	94.2	95.4	95.1	-
Tracking	640	20	8	10	-	-	-	94.4

Table 1 shows that the majority of shoulder points was successfully detected by the CNN resulting in high performance values, in terms of *Sensitivity*, *Precision*, and *F1-Score*. While in total 1054 shoulder points have been manually annotated, only a relatively small fraction of these points have not been detected. On the other hand, the number of falsely detected pigs ( $FP = 51$ ) indicates that the detection CNN still has limitations in challenging situations like object occlusion. Figure 8 illustrates several example frames from the test set showing cases of successful and failed detections.

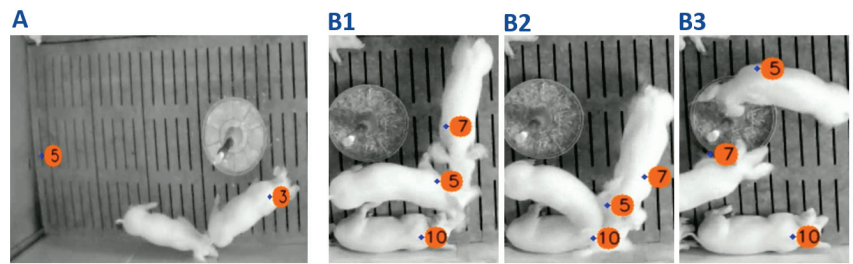
In Figure 8, it can be observed that the CNN successfully detected most of the pigs. Focusing on the failed detections, the large majority of failures was produced in situations in which one pig has been occluded by another pig, which led to a false negative detection. However, the problem of object occlusion and the resulting degradation in performance is not linked to the design of this study. In fact, the issue of object detection under the influence of occlusion is a challenging task which negatively affects the robustness of most detection algorithms [47]. While current approaches aim to tackle this problem by applying a compositional neural network structure in combination with an occluder model [47–50], the majority of approaches focus on the problem of partial occlusion and would, therefore, be of limited suitability for this study. Moreover, during the tracking process, the negative effect of object occlusion can be reduced to some extent, by applying a predictive model like

the KF algorithm, which internally interprets the CNN detections as noisy measurement information. In cases of extreme volatility, like the loss of an object due to occlusion, the KF reduces the influence of the measurement input by increasing the importance of the Kalman prediction [51,52]. To reduce the effect of a missing shoulder or tail point to some extent, we computed the number of detected objects frame-wise and marked the corresponding frames as corrupted in cases of missing detections. Corrupted frames have then been excluded for the KF tracking where we used the previous KF estimates as the new measurement input instead.



**Figure 8.** Example frames from the detection test set for day and night frames showing cases of a completely successful pig detection (**left column**) and cases in which at least one pig was not detected correctly (**right column**). A true shoulder point is highlighted by a red dot in the middle of the detection region (red circle). A green dot represents the predicted shoulder point from the CNN.

To assess the tracking performance, we further analyzed 70 test sequences containing various scenarios like feeding, resting, or interactions. As it can be seen in Table 1, the implemented KF was able to track 640 out of 678 shoulder points correctly resulting in a *MOTA* score of 94.4%. However, in 38 cases the tracking of the detected shoulder points failed: (i) 20 animals have not been tracked, (ii) eight animals have been tracked at the wrong position, and (iii) ten cases occurred in which the assigned ID of two pigs switched. Examples of a *FP*-track, a *FN*-track, and an ID switch are given in Figure 9.



**Figure 9.** Examples of a failed tracking performance. (A) While the shoulder point of the lower pig was not tracked (FN), the corresponding ID was computed at an empty spot in the compartment (FP). (B1–B3) A case of an ID switch due to a close proximity interaction and the occlusion of an animal. Before the interaction takes place, ID 5 and ID 7 have been assigned correctly (B1). After the interaction the IDs switched so that the ID 5 was assigned ID 7 and vice versa (B3).

In line with previous studies [26], we observed that if the detector is able to detect all pigs correctly, the corresponding pig tracking is working without producing corrupted tracks. In contrast, if the detection of the body parts fails, the tracker predicts the shoulder point based on the movement pattern of the previous frames. While the consequences are minor for short periods of detection failures, longer phases of missing detections lead to the effect of misplaced tracking IDs. However, this limitation is not specific to this study. Although the most successful tracking approaches are based on a TBD-strategy, the consequence of missing detections can be a significant reduction in their performance [53]. An example of a misplaced tracking ID is given in Figure 9A.

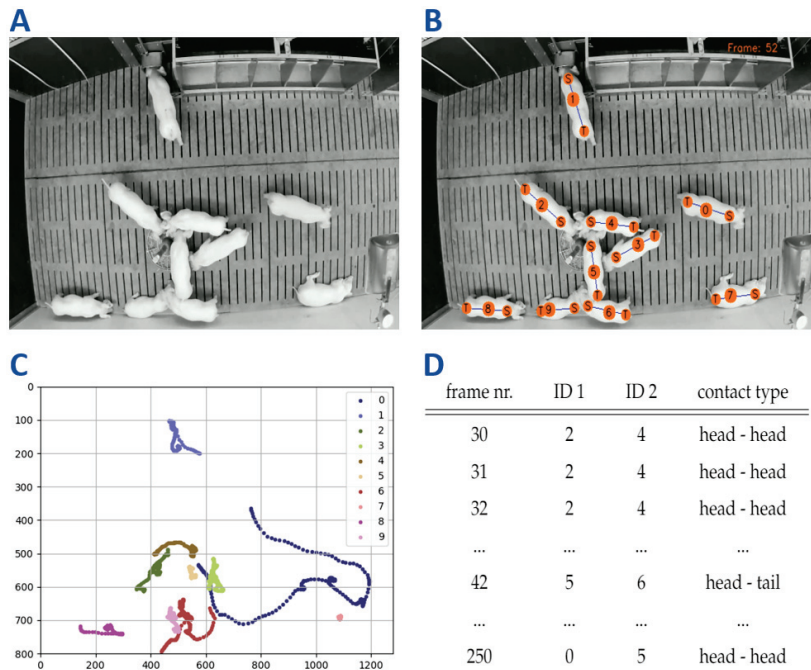
Another fundamental issue in the field of multiple object tracking, is the problem of ID switches, which is shown in Figure 9(B1–B3) [21,39,44,54]. In Figure 9(B1), the pigs with IDs 5, 7, and 10 are successfully detected and tracked. During the sequence, pigs 5 and 7 are occluding the shoulder point of pig 10, which leads to a missed detection of this animal by the detector (Figure 9(B2)). However, after all shoulder points reappear in the video, the KF tracker estimates the position of the shoulder points, but swaps IDs 5 and 7 (Figure 9(B3)).

Unlike previous bounding box-based studies, the problem of ID switches in our study only occurs in cases when the shoulder points of the animals disappear due to different obstacles, thus preventing the detection of these points. While several existing bounding box tracking applications suffer from ID switches arising from highly overlapping boxes [39], the keypoint-based approach applied in this study considers a much smaller tracking area. Therefore, a strong overlap of two or more tracked shoulder points is less likely to occur, which explains the relatively low number of ID switches given in Table 1. Of particular interest, we further studied all cases of ID switches in the test set in order to establish the main reason for the ID switch issue. We found that nine out of ten ID switches have been caused by a missed detection rather than by two detected IDs in a short distance. Only in one case a false detection caused the ID switch.

### 3.2. Animal-to-Animal Contact Identification

The knowledge about social interactions is fundamental to enhance farming conditions and animal welfare. Thus, the final stage of the framework proposed in this study aims to identify such behavior patterns based on pig interactions. In particular, by focusing on close proximity contacts between at least two animals, our framework automatically takes into account head–head as well as head–tail contacts. After that, based on these contact information, we construct a trajectory map to highlight individual movement patterns, which finally provides an information table about the social contacts. An example of the identification process for one test sequence is given in Figure 10.

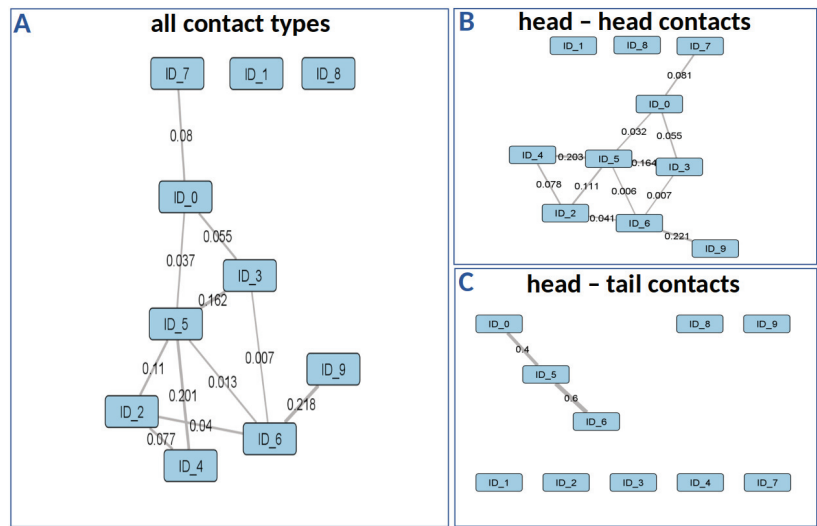




**Figure 10.** The social contact identification starts with a raw video frame (A). After detecting the shoulder and tail position (B), the trajectories are computed and analyzed over time (C). By identifying cases of close distances, a table of social contacts is constructed automatically (D).

The table of social contacts (Figure 10D) contains highly essential information about the contact pattern of animals over all video frames. As Smith et al. [55] pointed out, these data are crucial in the field of behavioral ecology and the automatic contact identification can reduce observer bias as a limiting factor. To address different research questions like the investigation of hierarchical structures, agonistic behavior patterns or pen utilization, the necessary information can be derived from this table as required. Further, this table can be used for extracting a distinct contact period by restricting the frame and ID information. However, the aim of this study is to differentiate between individual contacts. Therefore, the extraction process primarily focuses on the contact type information which is used to visualize the social relationships of the observed animals. Figure 11 shows an example for the visualization depicting both type of contacts (Figure 11A) as well as the specific head–head and head–tail contact types (Figures 11B,C).

Each of the three social networks in Figure 11 is constructed by using the individual animal ID as the node information and the contact frequency as an intensity score for the edge weight. In particular, for a holistic analysis, the consideration of all contact types is crucial to establish the general contact patterns between all animals in a compartment (Figure 11A). On the other hand, with regard to specific research questions [56–58], a more differentiated network design focusing on a distinct type of contact can be advantageous (Figures 11B,C). As a result, the structure of the specific network types differs from the holistic network which arises from the alterations in the edge weights.



**Figure 11.** Examples of three social networks from one test sequence.

In comparison to previous studies which aim to tackle the issue of identifying social interactions by following a bounding box approach [59], our strategy is not restricted to specific behavioral patterns like escaping and chasing motion activities. Even in challenging situations like resting behavior where most of the pigs are lying down in a very small area, our proposed framework is able to identify social contacts to a certain extent.

To further extend the performance of the proposed framework, future work could focus on the implementation of more sophisticated network topologies. In this regard, recent studies [60,61] successfully showed the potential of attention mechanisms, introduced by Bahdanau et al. [62], to leverage the power of deep learning for highlighting important features. Ghaffarian et al. [60] performed a literature review analyzing 176 articles focusing on image classification, object detection, and change detection. As a result, the authors concluded that the majority of deep learning-based research studies reported a performance increase when applying an attention mechanism. This improvement could have the potential to further reduce the number of false positive predicted body parts and could enable additional filtering steps to detect corrupted video frames.

#### 4. Conclusions

Today, the usage of video technology for animal monitoring is well established. However, extracting useful information is often challenging and thus limiting the potential of animal video analysis. In this study, we propose a framework for the automatic detection of social contacts to address the limitations of animal behavioral studies. By applying a keypoint-based body part detection and a subsequent pig tracking algorithm, we are able to determine the time, the animals involved, and the type of a social contact. We further process the information to construct a social network based on the contact type. To the best of our knowledge, this is the first study incorporating both a body part detection CNN as well as a Kalman filter tracking algorithm to identify social contacts. Our findings show the applicability of our approach to monitor a known number of pigs which can be used as part of early warning systems for the detection of behavioral changes. Overall, we suggest that our framework is applicable for different livestock animal monitoring systems.



**Author Contributions:** M.G. (Mehmet Gültas), I.T. and A.O.S. supervised the research. M.W. developed the model together with M.G. (Mehmet Gültas) and participated in the design of the study, prepared the data sets, conducted the analyses, and implemented the framework. F.H., P.P.D. and I.T. were involved in the interpretation of the results, together with M.W. and M.G. (Mehmet Gültas). A.L., F.K.W. and M.G. (Maria Gentz) provided the video data. M.W. and M.G. (Mehmet Gültas) wrote the final version of the manuscript. M.G. (Mehmet Gültas), A.O.S. and I.T. conceived the study. M.G. (Mehmet Gültas) designed the study and managed the project. All authors have read and agreed to the published version of the manuscript.

**Funding:** The project (InnoPig) was supported by funds of the German Government's Special Purpose Fund deposited at the Landwirtschaftliche Rentenbank (project no.: 2817205413; 758914).

**Institutional Review Board Statement:** The authors declare that the experiment was in accordance with current German law. As such, no part of this research was subject to approval of an ethics committee.

**Informed Consent Statement:** Not applicable.

**Data Availability Statement:** The data sets used for the detection and tracking evaluation are made publicly available at [https://github.com/MartinWut/Supp\\_DetAnIn](https://github.com/MartinWut/Supp_DetAnIn) (accessed on 9 November 2021).

**Acknowledgments:** We thank A. Rajavel (Breeding Informatics Group, University of Göttingen) for proofreading and her valuable advice. We thank the Chamber of Agriculture of Schleswig-Holstein for their support in data acquisition. We acknowledge support by the German Research Foundation and the Open Access Publication Funds of the Göttingen University.

**Conflicts of Interest:** The authors declare no conflict of interest.

## Abbreviations

The following abbreviations are used in this manuscript:

CNN	Convolutional neural network
KF	Kalman filter
SNA	Social network analysis
TBD	Tracking-by-detection

## References

- Verdon, M.; Rault, J.L. Aggression in group housed sows and fattening pigs. In *Advances in Pig Welfare*; Woodhead Publishing: Oxford, UK, 2018; pp. 235–260.
- Foister, S.; Doeschl-Wilson, A.; Roehe, R.; Arnott, G.; Boyle, L.; Turner, S. Social network properties predict chronic aggression in commercial pig systems. *PLoS ONE* **2018**, *13*, e0205122. [[CrossRef](#)] [[PubMed](#)]
- Büttner, K.; Scheffler, K.; Czycholl, I.; Krieter, J. Social network analysis-centrality parameters and individual network positions of agonistic behavior in pigs over three different age levels. *Springerplus* **2015**, *4*, 185. [[CrossRef](#)] [[PubMed](#)]
- Rhim, S.J.; Son, S.H.; Hwang, H.S.; Lee, J.K.; Hong, J.K. Effects of mixing on the aggressive behavior of commercially housed pigs. *Asian-Australas. J. Anim. Sci.* **2015**, *28*, 1038. [[CrossRef](#)] [[PubMed](#)]
- Stukenborg, A.; Traulsen, I.; Puppe, B.; Presuhn, U.; Krieter, J. Agonistic behaviour after mixing in pigs under commercial farm conditions. *Appl. Anim. Behav. Sci.* **2011**, *129*, 28–35. [[CrossRef](#)]
- Morrone, B.; Bernardino, T.; Tatemoto, P.; Rodrigues, F.A.M.L.; de Moraes, J.E.; da Cruz, T.D.A.; Zanella, A.J. Indication that the presence of older conspecifics reduces agonistic behaviour in piglets at weaning. *Appl. Anim. Behav. Sci.* **2021**, *234*, 105201. [[CrossRef](#)]
- Camerlink, I.; Proßegger, C.; Kubala, D.; Galunder, K.; Rault, J.L. Keeping littermates together instead of social mixing benefits pig social behaviour and growth post-weaning. *Appl. Anim. Behav. Sci.* **2021**, *235*, 105230. [[CrossRef](#)]
- Marinelli, L.; Mongillo, P.; Carnier, P.; Schiavon, S.; Gallo, L. A Short Period of Darkness after Mixing of Growing Pigs Intended for PDO Hams Production Reduces Skin Lesions. *Animals* **2020**, *10*, 1729. [[CrossRef](#)] [[PubMed](#)]
- Brajon, S.; Ahloy-Dallaire, J.; Devillers, N.; Guay, F. The role of genetic selection on agonistic behavior and welfare of gestating sows housed in large semi-static groups. *Animals* **2020**, *10*, 2299. [[CrossRef](#)]
- Weller, J.E.; Camerlink, I.; Turner, S.P.; Farish, M.; Arnott, G. Socialisation and its effect on play behaviour and aggression in the domestic pig (*Sus scrofa*). *Sci. Rep.* **2019**, *9*, 4180. [[CrossRef](#)]
- Psota, E.; Schmidt, T.; Mote, B.; Pérez, L.C. Long-term tracking of group-housed livestock using keypoint detection and map estimation for individual animal identification. *Sensors* **2020**, *20*, 3670. [[CrossRef](#)] [[PubMed](#)]

12. Li, G.; Huang, Y.; Chen, Z.; Chesser, G.D.; Purswell, J.L.; Linhoss, J.; Zhao, Y. Practices and Applications of Convolutional Neural Network-Based Computer Vision Systems in Animal Farming: A Review. *Sensors* **2021**, *21*, 1492. [[CrossRef](#)]
13. Liu, C.; Zhou, H.; Cao, J.; Guo, X.; Su, J.; Wang, L.; Lu, S.; Li, L. Behavior Trajectory Tracking of Piglets Based on DLC-KPCA. *Agriculture* **2021**, *11*, 843. [[CrossRef](#)]
14. Matthews, S.G.; Miller, A.L.; Clapp, J.; Plötz, T.; Kyriazakis, I. Early detection of health and welfare compromises through automated detection of behavioural changes in pigs. *Vet. J.* **2016**, *217*, 43–51. [[CrossRef](#)] [[PubMed](#)]
15. Brünger, J.; Traulsen, I.; Koch, R. Randomized global optimization for robust pose estimation of multiple targets in image sequences. *Math. Model. Comput. Methods* **2015**, *2*, 45–53.
16. Russakovsky, O.; Deng, J.; Su, H.; Krause, J.; Satheesh, S.; Ma, S.; Huang, Z.; Karpathy, A.; Khosla, A.; Bernstein, M.; et al. Imagenet large scale visual recognition challenge. *Int. J. Comput. Vis.* **2015**, *115*, 211–252. [[CrossRef](#)]
17. Kale, K.; Pawar, S.; Dhulekar, P. Moving object tracking using optical flow and motion vector estimation. In Proceedings of the 2015 4th International Conference on Reliability, Infocom Technologies and Optimization (ICRITO) (Trends and Future Directions), Noida, India, 2–4 September 2015; pp. 1–6.
18. Padilla, R.; Netto, S.L.; da Silva, E.A. A survey on performance metrics for object-detection algorithms. In Proceedings of the 2020 International Conference on Systems, Signals and Image Processing (IWSSIP), Niteroi, Brazil, 1–3 July 2020; pp. 237–242.
19. Van Der Zande, L.; Guzhva, O.; Rodenburg, T.B. Individual detection and tracking of group housed pigs in their home pen using computer vision. *Front. Anim. Sci.* **2021**, *2*, 10. [[CrossRef](#)]
20. Ahn, H.; Son, S.; Kim, H.; Lee, S.; Chung, Y.; Park, D. EnsemblePigDet: Ensemble Deep Learning for Accurate Pig Detection. *Appl. Sci.* **2021**, *11*, 5577. [[CrossRef](#)]
21. Zhang, L.; Gray, H.; Ye, X.; Collins, L.; Allinson, N. Automatic individual pig detection and tracking in pig farms. *Sensors* **2019**, *19*, 1188. [[CrossRef](#)]
22. Steffen Küster, P.; Nolte, C.; Meckbach, B.; Stock, I.; Traulsen, I. Automatic behavior and posture detection of sows in loose farrowing pens based on 2D-video images. *Front. Anim. Sci.* **2021**, *2*, 23.
23. Psota, E.T.; Mittek, M.; Pérez, L.C.; Schmidt, T.; Mote, B. Multi-pig part detection and association with a fully-convolutional network. *Sensors* **2019**, *19*, 852. [[CrossRef](#)]
24. Madhukar, P.S.; Prasad, L. State Estimation using Extended Kalman Filter and Unscented Kalman Filter. In Proceedings of the 2020 International Conference on Emerging Trends in Communication, Control and Computing (ICONC3), Lakshmgarh, India, 21–22 February 2020; pp. 1–4.
25. Corrales, J.A.; Candelas, F.; Torres, F. Hybrid tracking of human operators using IMU/UWB data fusion by a Kalman filter. In Proceedings of the 2008 3rd ACM/IEEE International Conference on Human-Robot Interaction (HRI), Amsterdam, The Netherlands, 12–15 March 2008; pp. 193–200.
26. Sun, Z.; Chen, J.; Chao, L.; Ruan, W.; Mukherjee, M. A survey of multiple pedestrian tracking based on tracking-by-detection framework. *IEEE Trans. Circuits Syst. Video Technol.* **2020**, *31*, 1819–1833. [[CrossRef](#)]
27. Bogun, I.; Ribeiro, E. Robstruck: Improving occlusion handling of structured tracking-by-detection using robust kalman filter. In Proceedings of the 2016 IEEE International Conference on Image Processing (ICIP), Phoenix, AZ, USA, 25–28 September 2016; pp. 3479–3483.
28. Lange, A.; Gentz, M.; Hahne, M.; Lambertz, C.; Gauly, M.; Burfeind, O.; Traulsen, I. Effects of different farrowing and rearing systems on post-weaning stress in piglets. *Agriculture* **2020**, *10*, 230. [[CrossRef](#)]
29. Gentz, M.; Lange, A.; Zeidler, S.; Lambertz, C.; Gauly, M.; Burfeind, O.; Traulsen, I. Tail lesions and losses of docked and undocked pigs in different farrowing and rearing systems. *Agriculture* **2020**, *10*, 130. [[CrossRef](#)]
30. Wutke, M.; Schmitt, A.O.; Traulsen, I.; Gültas, M. Investigation of Pig Activity Based on Video Data and Semi-Supervised Neural Networks. *AgriEngineering* **2020**, *2*, 581–595. [[CrossRef](#)]
31. Deepak, K.; Chandrakala, S.; Mohan, C.K. Residual spatiotemporal autoencoder for unsupervised video anomaly detection. *Signal Image Video Process.* **2021**, *15*, 215–222. [[CrossRef](#)]
32. Kingma, D.P.; Ba, J. Adam: A method for stochastic optimization. *arXiv* **2014**, arXiv:1412.6980.
33. Rossum, G.V. Python Software Foundation. Python Language Reference, Version 3.7. 1995. Available online: <http://www.python.org> (accessed on 9 November 2021).
34. Chollet, F. Keras. 2015. Available online: <https://keras.io> (accessed on 9 November 2021).
35. Abadi, M.; Agarwal, A.; Barham, P.; Brevdo, E.; Chen, Z.; Citro, C.; Corrado, G.S.; Davis, A.; Dean, J.; Devin, M.; et al. TensorFlow: Large-Scale Machine Learning on Heterogeneous Systems. 2015. Available online: <https://www.tensorflow.org/> (accessed on 9 November 2021).
36. Spampinato, D.G.; Sridhar, U.; Low, T.M. Linear algebraic depth-first search. In Proceedings of the 6th ACM SIGPLAN International Workshop on Libraries, Languages and Compilers for Array Programming, Phoenix, AZ, USA, 22 June 2019; pp. 93–104.
37. Sun, L.; Li, Y. Multi-target pig tracking algorithm based on joint probability data association and particle filter. *Int. J. Agric. and Biol. Eng.* **2021**, *14*, 199–207. [[CrossRef](#)]
38. Gan, H.; Ou, M.; Zhao, F.; Xu, C.; Li, S.; Chen, C.; Xue, Y. Automated piglet tracking using a single convolutional neural network. *Biosyst. Eng.* **2021**, *205*, 48–63. [[CrossRef](#)]

39. Bochinski, E.; Senst, T.; Sikora, T. Extending IOU based multi-object tracking by visual information. In Proceedings of the 2018 15th IEEE International Conference on Advanced Video and Signal Based Surveillance (AVSS), Auckland, New Zealand, 27–30 November 2018; pp. 1–6.
40. Kalman, R.E. A new approach to linear filtering and prediction problems. *J. Basic Eng.* **1960**, *82*, 35–45. [\[CrossRef\]](#)
41. Welch, G.; Bishop, G. *An Introduction to the Kalman Filter*; University of North Carolina, Department of Computer Science: Chapel Hill, NC, USA, 1995.
42. Luiten, J.; Osep, A.; Dendorfer, P.; Torr, P.; Geiger, A.; Leal-Taixé, L.; Leibe, B. Hota: A higher order metric for evaluating multi-object tracking. *Int. J. Comput. Vis.* **2021**, *129*, 548–578. [\[CrossRef\]](#)
43. Fan, H.; Bai, H.; Lin, L.; Yang, F.; Chu, P.; Deng, G.; Yu, S.; Huang, M.; Liu, J.; Xu, Y.; et al. Lasot: A high-quality large-scale single object tracking benchmark. *Int. J. Comput. Vis.* **2021**, *129*, 439–461. [\[CrossRef\]](#)
44. Cowton, J.; Kyriazakis, I.; Bacardit, J. Automated individual pig localisation, tracking and behaviour metric extraction using deep learning. *IEEE Access* **2019**, *7*, 108049–108060. [\[CrossRef\]](#)
45. Leichter, I.; Krupka, E. Monotonicity and error type differentiability in performance measures for target detection and tracking in video. *IEEE Trans. Pattern Anal. Mach. Intell.* **2013**, *35*, 2553–2560. [\[CrossRef\]](#) [\[PubMed\]](#)
46. Luo, W.; Xing, J.; Milan, A.; Zhang, X.; Liu, W.; Kim, T.K. Multiple object tracking: A literature review. *Artif. Intell.* **2020**, *293*, 103448. [\[CrossRef\]](#)
47. Wang, A.; Sun, Y.; Kortylewski, A.; Yuille, A.L. Robust object detection under occlusion with context-aware compositionalnets. In Proceedings of the IEEE/CVF Conference on Computer Vision and Pattern Recognition, Seattle, WA, USA, 13–19 June 2020; pp. 12645–12654.
48. Kortylewski, A.; Liu, Q.; Wang, A.; Sun, Y.; Yuille, A. Compositional convolutional neural networks: A robust and interpretable model for object recognition under occlusion. *Int. J. Comput. Vis.* **2021**, *129*, 736–760. [\[CrossRef\]](#)
49. Cosgrove, C.; Kortylewski, A.; Yang, C.; Yuille, A. Robustness Out of the Box: Compositional Representations Naturally Defend Against Black-Box Patch Attacks. *arXiv* **2020**, arXiv:2012.00558.
50. Kortylewski, A.; He, J.; Liu, Q.; Yuille, A.L. Compositional convolutional neural networks: A deep architecture with innate robustness to partial occlusion. In Proceedings of the IEEE/CVF Conference on Computer Vision and Pattern Recognition, Seattle, WA, USA, 13–19 June 2020; pp. 8940–8949.
51. Jeong, J.M.; Yoon, T.S.; Park, J.B. Kalman filter based multiple objects detection-tracking algorithm robust to occlusion. In Proceedings of the 2014 Proceedings of the SICE Annual Conference (SICE), Sapporo, Japan, 9–12 September 2014; pp. 941–946.
52. Li, X.; Wang, K.; Wang, W.; Li, Y. A multiple object tracking method using Kalman filter. In Proceedings of the 2010 IEEE International Conference on Information and Automation, Harbin, China, 20–23 June 2010; pp. 1862–1866.
53. Hou, X.; Wang, Y.; Chau, L.P. Vehicle tracking using deep sort with low confidence track filtering. In Proceedings of the 2019 16th IEEE International Conference on Advanced Video and Signal Based Surveillance (AVSS), Taipei, Taiwan, 18–21 September 2019; pp. 1–6.
54. Frossard, D.; Urtasun, R. End-to-end learning of multi-sensor 3D tracking by detection. In Proceedings of the 2018 IEEE International Conference on Robotics and Automation (ICRA), Brisbane, Australia, 21–25 May 2018; pp. 635–642.
55. Smith, J.E.; Pinter-Wollman, N. Observing the unwatchable: Integrating automated sensing, naturalistic observations and animal social network analysis in the age of big data. *J. Anim. Ecol.* **2021**, *90*, 62–75. [\[CrossRef\]](#)
56. Kakanis, M.; Sossidou, E.; Kritas, S.; Tzika, E. Update on Tail biting in pigs: An undesirable damaging behaviour. *J. Hell. Vet. Med Soc.* **2021**, *72*, 2629–2646. [\[CrossRef\]](#)
57. Larsen, M.L.V.; Pedersen, L.J.; Edwards, S.; Albanie, S.; Dawkins, M.S. Movement change detected by optical flow precedes, but does not predict, tail-biting in pigs. *Livest. Sci.* **2020**, *240*, 104136. [\[CrossRef\]](#)
58. D’Eath, R.B.; Jack, M.; Futro, A.; Talbot, D.; Zhu, Q.; Barclay, D.; Baxter, E.M. Automatic early warning of tail biting in pigs: 3D cameras can detect lowered tail posture before an outbreak. *PLoS ONE* **2018**, *13*, e0194524.
59. Liu, D.; Oczak, M.; Maschat, K.; Baumgartner, J.; Pletzer, B.; He, D.; Norton, T. A computer vision-based method for spatial-temporal action recognition of tail-biting behaviour in group-housed pigs. *Biosyst. Eng.* **2020**, *195*, 27–41. [\[CrossRef\]](#)
60. Ghaffarian, S.; Valente, J.; Van Der Voort, M.; Tekinerdogan, B. Effect of Attention Mechanism in Deep Learning-Based Remote Sensing Image Processing: A Systematic Literature Review. *Remote Sens.* **2021**, *13*, 2965. [\[CrossRef\]](#)
61. Xu, R.; Tao, Y.; Lu, Z.; Zhong, Y. Attention-mechanism-containing neural networks for high-resolution remote sensing image classification. *Remote Sens.* **2018**, *10*, 1602. [\[CrossRef\]](#)
62. Bahdanau, D.; Cho, K.; Bengio, Y. Neural machine translation by jointly learning to align and translate. *arXiv* **2014**, arXiv:1409.0473.



## Article

# Behavioural Classification of Cattle Using Neck-Mounted Accelerometer-Equipped Collars

Dejan Pavlovic <sup>1,\*</sup>, Mikolaj Czerkawski <sup>2</sup>, Christopher Davison <sup>2</sup>, Oskar Marko <sup>1</sup>, Craig Michie <sup>2</sup>, Robert Atkinson <sup>2</sup>, Vladimir Crnojevic <sup>1</sup>, Ivan Andonovic <sup>2</sup>, Vladimir Rajovic <sup>3</sup>, Goran Kvascev <sup>3</sup> and Christos Tachtatzis <sup>2</sup>

<sup>1</sup> BioSense Institute, 21101 Novi Sad, Serbia; oskar.marko@biosense.rs (O.M.); crnojevic@biosense.rs (V.C.)

<sup>2</sup> Department of Electronic and Electrical Engineering, University of Strathclyde, Glasgow G1 1RD, UK; mikolaj.czerkawski@strath.ac.uk (M.C.); christopher.davison@strath.ac.uk (C.D.); c.michie@strath.ac.uk (C.M.); robert.atkinson@strath.ac.uk (R.A.); i.andonovic@strath.ac.uk (I.A.); christos.tachtatzis@strath.ac.uk (C.T.)

<sup>3</sup> School of Electrical Engineering, University of Belgrade, 11000 Belgrade, Serbia; rajo@etf.rs (V.R.); kvascev@etf.bg.ac.rs (G.K.)

\* Correspondence: dejan.pavlovic@biosense.rs

**Abstract:** Monitoring and classification of dairy cattle behaviours is essential for optimising milk yields. Early detection of illness, days before the critical conditions occur, together with automatic detection of the onset of oestrus cycles is crucial for obviating prolonged cattle treatments and improving the pregnancy rates. Accelerometer-based sensor systems are becoming increasingly popular, as they are automatically providing information about key cattle behaviours such as the level of restlessness and the time spent ruminating and eating, proxy measurements that indicate the onset of heat events and overall welfare, at an individual animal level. This paper reports on an approach to the development of algorithms that classify key cattle states based on a systematic dimensionality reduction process through two feature selection techniques. These are based on Mutual Information and Backward Feature Elimination and applied on knowledge-specific and generic time-series extracted from raw accelerometer data. The extracted features are then used to train classification models based on a Hidden Markov Model, Linear Discriminant Analysis and Partial Least Squares Discriminant Analysis. The proposed feature engineering methodology permits model deployment within the computing and memory restrictions imposed by operational settings. The models were based on measurement data from 18 steers, each animal equipped with an accelerometer-based neck-mounted collar and muzzle-mounted halter, the latter providing the truthing data. A total of 42 time-series features were initially extracted and the trade-off between model performance, computational complexity and memory footprint was explored. Results show that the classification model that best balances performance and computation complexity is based on Linear Discriminant Analysis using features selected through Backward Feature Elimination. The final model requires  $1.83 \pm 1.00$  ms to perform feature extraction with  $0.05 \pm 0.01$  ms for inference with an overall balanced accuracy of 0.83.

**Keywords:** precision agriculture; cattle behaviour monitoring; feature selection

**Citation:** Pavlovic, D.; Czerkawski, M.; Davison, C.; Marko, O.; Michie, C.; Atkinson, R.; Crnojevic, V.; Andonovic, I.; Rajovic, V.; Kvascev, G.; et al. Behavioural Classification of Cattle Using Neck-Mounted Accelerometer-Equipped Collars. *Sensors* **2022**, *22*, 2323. <https://doi.org/10.3390/s22062323>

Academic Editors: Dionysis Bochtis and Aristotelis C. Tagarakis

Received: 17 February 2022

Accepted: 14 March 2022

Published: 17 March 2022

**Publisher's Note:** MDPI stays neutral with regard to jurisdictional claims in published maps and institutional affiliations.



**Copyright:** © 2022 by the authors. Licensee MDPI, Basel, Switzerland. This article is an open access article distributed under the terms and conditions of the Creative Commons Attribution (CC BY) license (<https://creativecommons.org/licenses/by/4.0/>).

## 1. Introduction

Autonomous cattle behaviour monitoring systems have grown in importance over the recent past. Sensor-based technologies are now starting to be accepted as an enhancement to traditional visual inspection, the latter being both time-consuming and labour-intensive. In the UK, there has been a steady decline in the number of milk producers, whilst at the same time the average size per herd has risen as small-scale farm holdings have departed the industry sector due to the economic pressure. The average number of cows per herd has also grown from ~75 in 1996 to ~155 in 2020 [1]; and during the same period, milk

production has increased marginally, from ~13 M litres in 2008 to ~15 M litres in 2020 [1]. As a direct consequence, the time available to observe herds has reduced significantly, with farmers now more amenable to relying on technology-based systems for extensive monitoring [2,3].

Systems such as neck-mounted collars, leg and ear tags that monitor dairy and beef cattle are now enjoying increased adoption. Such systems provide early information on health and welfare issues, and identify the onset of oestrus, both of which form the basis for a decision support system that advises farmers on the most appropriate interventions that enhance the efficiency of current practices [4–6].

In this paper, the use of a neck-mounted accelerometer-based collar to identify eating and rumination signatures is reported. A muzzle-mounted halter pressure sensor was used in order to collect the ground truth data. The halter has proved to yield high correlation between identified and visually observed behaviours and has become a widely accepted means of gathering ground truth data throughout the precision livestock community. A study by [7] compared halter-based labels and video annotations and reported an F1 Score of 0.932 for rumination. Additionally, a high Spearman correlation of 0.96 and 0.75 for rumination, and 0.96 and 0.81 for eating, respectively, was reported in [8,9]. Three classification algorithms are considered here and a comparison of their ability to discriminate different cattle states has been performed. Data from 18 steers were acquired during three farm trials in the United Kingdom (Easter Howgate Farm, Edinburgh, UK). A total of 42 features were initially extracted from the data, followed by a systematic reduction in dimensionality to decrease model complexity, easing the transformation of the raw sensor data into actionable information and optimising the trade-off between model performance, computation complexity and memory footprint.

The paper is organised as follows. Section 1 represents a brief introduction and Section 2 provides a summary of related work. Section 3 presents a short description of the data acquisition methodology. Section 4 describes the adopted methodology and details the dimensionality reduction methods, while Section 5 describes the classification algorithms considered. Section 6 evaluates the accuracy of the classifications and the efficiency of implementation of the proposed approaches. Section 7 draws conclusions and summarises key findings. The full range of feature definitions are given in the Appendix A.

## 2. Related Work

A range of solutions for cattle behaviour identification have been reported, many based on classical Machine Learning (ML) algorithms [10–17], but the recent adaption of Deep Learning (DL) techniques has significantly increased the potential to optimise the efficiency of artificial intelligence enabled classification solutions [18–21].

Convolutional Neural Networks (CNNs) have been used for classification of grazing and non-grazing periods [18]; given the output is binary, the development is less demanding compared to multi-state behavioural classification. A highly accurate performance classifier based on a 3-axis accelerometer/gyroscope/magnetometer data and a Recurrent Neural Network with Long Short-Term Memory (RNN-LSTM) able to identify 8 cattle behaviours has been reported in [19]. Although the RNN-LSTM algorithm achieved accurate cattle behaviour classification, its operational deployment on low-cost, low-power processors is prohibitively challenging due to significant model complexity. The approach which overcomes the operational implementation challenges of complex Deep Learning (DL) models was implemented through an iterative structured pruning process in [21]. The results confirm that the CNN architecture can be supported on low-power micro-controllers with an operational lifetime of 5.7 years. The methodology achieved a model compression of 14.30 with minimal loss of performance; however, additional effort to create the approach that overcomes the implementation challenges is required.

In most instances, although classical ML algorithms do not require model reduction, a further decrease in computational complexity and memory footprint requirement will enhance device efficiency and prolong battery lifetime. An approach [12] based on Decision



Tree (DT) and Support Vector Machine (SVM) algorithms, using data from neck-mounted collars sampled at 10 Hz, demonstrated high performance classification for three cattle states viz. ‘eating’, ‘rumination’ and ‘other’. The overall accuracy, validated by human observation, was 0.90 and 0.93 using DT and SVM algorithms, the latter classifying ‘eating’ and ‘rumination’ with a precision of 0.92 and 0.88 and sensitivity of 0.85 and 0.92, respectively. Data were acquired from 10 animals over a period of 5 days giving a total monitoring time of 60 h. A similar study also demonstrated the use of a SVM to identify a larger number of cattle states including ‘eating’, ‘rumination’, ‘standing’, ‘lying’ and ‘walking’ [11] using accelerometer measurement data sampled at 10 Hz from 30 animals. The approach produced results with a precision of  $0.78 \pm 0.01$ , with ‘eating’ and ‘rumination’ classified with a precision of  $0.81 \pm 0.03$  and  $0.86 \pm 0.02$  and sensitivity of  $0.75 \pm 0.04$  and  $0.75 \pm 0.02$ , respectively. The classification accuracy of both states was reported to be  $0.96 \pm 0.01$  and  $0.92 \pm 0.01$ . Ground truth data, obtained through both direct animal observation and video annotation, provided a highly appropriate validation dataset; nevertheless, owing to the significant effort required, a relatively small dataset of 95.5 h in total was acquired.

The present paper advances the state-of-the-art in several areas: It proposes a methodology to systematically reduce the dimensionality using a number of feature selection techniques and, coupled with appropriate ML algorithms, to deliver accurate identification of ‘eating’, ‘rumination’ and ‘other’ cattle behaviours using data from 3-axis accelerometer neck-mounted collars. The development harnesses a comparable dataset size to other reported studies in terms of the number of animals, but the total number of observation hours is significantly higher. The studies conducted in [11,12] proposed the use of 28 and 16 features, respectively, derived from the raw accelerometer data; however, the motivation for selecting the corresponding number of features and the features themselves was not directly specified. The methodology reported here begins with 42 knowledge-specific and generic time-series features and follows a systematic feature reduction process, resulting in 7 features that yield near optimum classification performance while maintaining low model complexity. As most datasets are not publicly available, a comparison of the classification performance of the proposed model with the data used to develop other algorithms was not possible. The data underpinning the current study have been made publicly accessible to stimulate the creation of new algorithms and permit the community to perform direct comparisons.

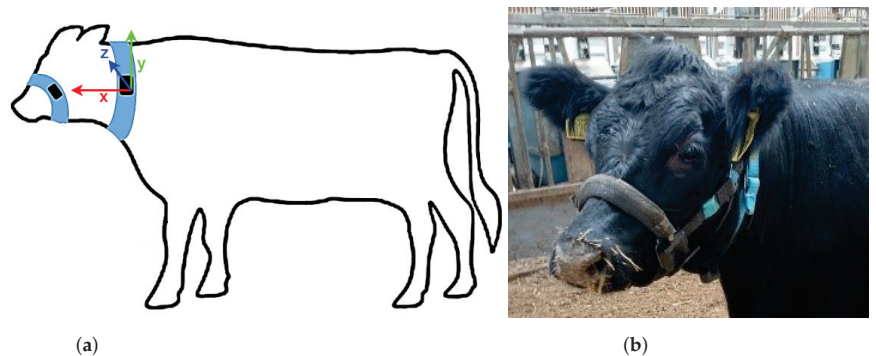
### 3. Data

The cattle were housed indoors in a straw setting and fed a Total Mixed Ration (TMR) ad libitum. Data, collected during three farm trials in the United Kingdom (Easter Howgate Farm, Edinburgh, UK) were acquired from a total of 18 Limousin Cross-Breed steers equipped with Afimilk Silent Herdsman [5] neck-mounted collars and Rumiwatch halters [22] mounted on the muzzle (Figure 1). The collar comprised a 3-axis accelerometer sampled at 10 Hz with range of  $\pm 2$  g and 12-bit resolution, an SD card for storage, and a Real Time Clock (RTC). The halter consisted of a pressure sensor, an SD card and RTC producing behaviour classification at frequency of 10 Hz. The SD cards from both systems were collected and the recordings with total duration of 3460 h were verified for time alignment (the dataset is publicly available at <https://www.doi.org/10.5281/zenodo.4064802>, accessed on 16 February 2022).

The collars provided acceleration values orientated in x-, y- and z-directions, i.e., parallel, vertical and perpendicular to the body of the animal, capturing both head and neck muscle motions. The halter, through pressure changes induced by movements of the jaw, provided the ground truth of the following animal states:

- Eating—the animal is ingesting food.
- Rumination—the animal is regurgitating to further breakdown ingested food and improve nutrient absorption.
- Other—the animal is engaged in an activity which is neither ruminating or eating.





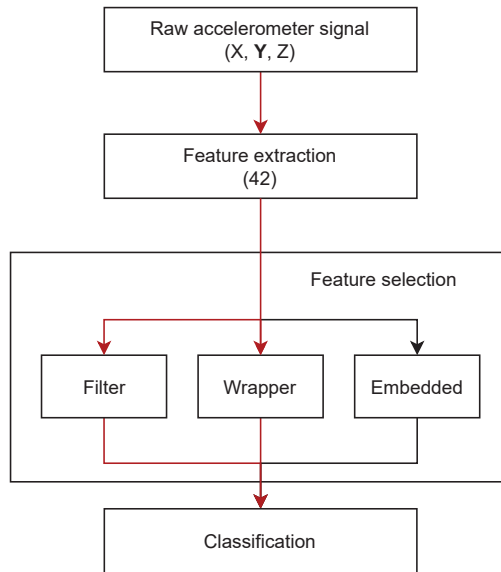
**Figure 1.** Placement of a RumiWatch muzzle-mounted halter and Afimilk Silent Herdsman neck-mounted collar. (a) Axis orientation diagram. (b) Photograph illustrating sensor placement.

#### Data Preparation

At the outset, both the accelerometer and halter time sequences were segmented into 90 s blocks [10,12,19], with each block of the accelerometer signal assigned to only one behaviour state for truthing. The acceleration in y-direction—oriented vertical to the animal body i.e., perpendicular to the ground—is the one that captures both head and neck muscle motions, central to the identification of the target cattle states; for that reason, only y-axis data was used for analysis [15]. Considering that the halter provides measurements at a frequency of 10 Hz and that there are instances of more than one cattle behaviour during the 90 s period, a majority vote was applied within each block to indicate the primary behaviour.

#### 4. Model Design

A total of 42 features, defined in the Appendix A (Table A1), were extracted from raw accelerometer signals for each of the 90 s blocks as the basis for the discrimination between cattle behaviours. All features used within the analysis are derived using the *tsfresh* Python package [23] with the exception of two knowledge-specific features; *FFT amplitude* in the band 2–4 Hz and *Spectral flatness*. Specific features were selected, informed by the knowledge that the dominant frequency of the rumination motion is centered around ~3 Hz and manifests as a significant spectral peak, while the eating frequency content is spread over a wider band, characterised by a relatively flat spectrum. Given the relatively high number of extracted features, the performance of the classification model is compromised due to the curse of dimensionality. A highly dimensional feature space also has ramifications in respect of increased computation complexity and memory footprint hindering the ability to deploy low-cost, low-power on-farm implementations. Therefore, a systematic reduction of features was performed in order to decrease model complexity but not at the expense of a reduction in discrimination performance between three cattle states of ‘eating’, ‘rumination’ and ‘other’. The reduction phase is followed by evaluation of three classification algorithms, namely, Hidden Markov Model (HMM), Linear Discriminant Analysis (LDA) and Partial Least Squares Discriminant Analysis (PLS-DA). A schematic of the end-to-end development pipeline is illustrated in Figure 2, the red arrows representing the applied process flow, while the black arrows illustrate an alternative, relevant methodology not considered here. All components of the adopted methodology presented within the block diagram are further analysed in more detail.



**Figure 2.** A block diagram showing the methodology starting from the raw data to training and evaluation of the classification algorithms. The red arrows indicate the adopted methodology followed in this work.

#### 4.1. Training and Validation

Three steers from the total of 18, each drawn from a distinct farm trial, were randomly selected to form a dataset prior to any pre-processing. The data from the three steers are used at the final stage only in order to evaluate the methodology and are not considered in the dimensionality reduction process nor in the training of the classification model. The remaining 15 steers are used to optimise the combination of features and classification model parameters through a 5-fold cross-validation process; twelve steers are used as the training set, with the remaining three forming the validation set. The cross-validation process is repeated 5 times so that each steer is present in the validation set precisely once. Further, the complete 5-fold cross-validation is repeated 5 times resulting in a total of 25 training/validation iterations. In order to eliminate the bias from individual steers, i.e., so that each steer has an equal contribution during model training, the training set was balanced. More precisely, each steer was represented with the same number of observations as the steer with the shortest observational period across all 12 individual animals. The remaining segments derived from steers with longer observational periods are under-sampled randomly, with the time-order of given observations remaining unchanged. Further, each feature is standardised, so that each feature time-series had zero-mean and unit-variance, to ensure that feature scales are comparable i.e.,:

$$x'_i = \frac{x_i - \mu_i}{\sigma_i}, \forall i \in \{1, \dots, 42\}, \quad (1)$$

where  $x_i$  and  $x'_i$  represent the original and standardised feature vectors, respectively, while  $\mu_i$  and  $\sigma_i$  refer to the mean and standard deviation of the corresponding feature prior to standardisation. Both  $\mu_i$  and  $\sigma_i$  are estimated on the training set and consequently each fold results in different normalisation parameters but those parameters are used for both training and validation sets.

Naturally, each steer spends varying amounts of time in each of the states and as a consequence resulting in an unequal number of observations per class; for that reason, a balanced accuracy is used to evaluate model performance;

$$\text{Balanced accuracy} = \frac{TP}{P} + \frac{TN}{N} \quad (2)$$

Equation (2) relates to binary classification problems. In cases where more than 2 classes are present (as is the case in the study reported here), individual class estimations are required and the average balanced accuracy can be used to evaluate overall performance. True Positives (*TP*) represent the number of accurately detected observations of a certain class, while True Negatives (*TN*), the number of observations accurately detected as not belonging to that particular class. Variables *P* and *N* refer to the actual number of observations belonging to the class of interest and the actual number of observations of all other classes, respectively.

#### 4.2. Feature Reduction

The process of dimensionality reduction i.e., the representation of high-dimensional data in a lower-dimensional feature space, not only mitigates the curse of dimensionality but also reduces the computing resource requirements, model training and inference times [24].

A reduction of data dimensionality can be performed through feature transformation, feature selection, or a combination of both, providing the intrinsic dimensionality (minimum number of parameters needed to account for the observed properties of the data [25]) of the original feature set. Feature transformation methods are a reconstruction process of the original features into a new feature set. However, it should be noted that these techniques do not reduce the number of features that need to be selected from the raw data but rather, re-project the original features onto a new domain. The goal of feature selection is to establish a subset of features, retaining those with a higher discriminatory power. The selection can be executed in a number of ways depending on the goal, available resources, and the target level of optimisation [26]. Feature selection methods are most commonly classified into three categories: filters, wrappers, and embedded methods (Figure 2). Filter methods estimate feature relevance based on a ranking function which observes input or input/output data and drops low-scoring features. Filter methods are computationally inexpensive and independent of classification model, and as such, need only to be executed once to obtain the most appropriate features, which can be subsequently used to create and evaluate classification models [27]; both the wrapper and embedded approaches require the training of the model. In particular, the wrapper method requires multiple training iterations for multiple feature combinations, increasing significantly the computational cost. Embedded methods are based on intrinsic properties of the classifier and performed during model training. Although the two approaches are based on an interaction between the extracted features and classification model, common drawbacks of the wrapper approach are a higher risk of over-fitting as well as consuming greater levels of computing resources compared to filter methods.

Here, two feature selection methods are evaluated, namely, the filter method based on the Mutual Information (MI) score and the wrapper method based on the Backward Feature Elimination (BFE) technique. Embedded approaches are not considered since feature ranking is not implicitly supported by other reported classification algorithms. MI is a statistical measure which estimates the dependence between different sets of data, the value of zero referring to completely independent sets, while higher values represent a higher dependency. In this particular case, the dependence between individual features and labels is analysed. The most applied approach for MI estimation assumes the partitioning of the datasets into bins of finite size. However, here, MI was estimated using the k-nearest neighbour method [28]. A comparison between binning and the nearest neighbour method,

along with the following definition of the MI estimate between discrete and continuous datasets is given in [29];

$$I(X, Y) = \psi(N) - \langle \psi(N_x) \rangle + \psi(k) - \langle \psi(m) \rangle \quad (3)$$

where  $\psi$  is the digamma function, while  $\langle \cdot \rangle$  denotes the average over all samples.  $N_x$  represents the number of points per activity state and  $m$  refers to the number of neighbours from all states that lie within the defined distance determined by parameter  $k$ . Although larger values of  $k$  lead to lower statistical errors, excessively large values of  $k$  should be avoided since the resultant increase in systematic errors could potentially outweigh the decrease in statistical errors. The analysis conducted in [29] indicates that the nearest-neighbor estimator achieves good performance when the parameter  $k$  is set to low integer values ( $1 \leq k \leq 10$ ), whereas the authors in [28] suggested a range between 2 and 4. For that reason, here, the number of nearest neighbours is set as  $k = 3$ .

The second feature selection approach investigated is the wrapper method using BFE, reliant on the use of the classification model to execute feature selection. The approach typically starts by iteratively removing one or more features from the entire feature set  $F = f_1, \dots, f_N$ , governed by the performance of the classification model on the selected subset of features. More precisely, the methodology follows the steps of the algorithm reported in Algorithm 1;

---

**Algorithm 1** Backward Feature Elimination procedure used to reduce features in blocks.

---

```

F = f1, …, fN                                ▷ Total features set
R = F                                          ▷ Remaining features set
P                                              ▷ Declare empty performance array
while |R| > 1 do
  for i ← 1 to R do
    Sf = R − fi                                ▷ Select subset of features Sf ⊂ F
    model.fit(Sf)                               ▷ Train the model with Sf
    P[i] = model.eval(Sf)                       ▷ Compute model performance with Sf features
  end for
  R = R \ ∪j=1k [R \ fargmin(P)] where k ≥ 1    ▷ Update remaining features by excluding low performing features
end while

```

---

## 5. Classification Algorithms

The effectiveness of each feature reduction technique is assessed through three classification algorithms, namely, Hidden Markov Model (HMM), Linear Discriminant Analysis (LDA), and Partial Least Squares Discriminant Analysis (PLS-DA). Note that both the LDA and PLS-DA perform feature transformation in accordance with the classifier operation inherently but do not reduce the number of inputs that must be computed from the raw data.

### 5.1. Hidden Markov Models

A probabilistic time-series model requires the definition of a joint distribution  $p(X_1, \dots, X_T)$  where  $X_t$  represents the features of a 90 s block in a sequence  $t \in 1 \rightarrow T$ . The sequence has many entries with long-range correlations amongst subsequent observations. However, an independent specification of that many entries is impractical; therefore, simplifications are required. The main assumption underpinning Markov chains is that the current  $X_t$  contains sufficient amount of information to predict future states i.e., that the influence of the recent past is more relevant than the influence of a more distant past [30]. A first order Markov chain is defined as follows:

$$p(X_{1:T}) = p(X_1) \prod_{t=2}^T p(X_t | X_{t-1}) \quad (4)$$

where the conditional distribution  $p(X_t|X_{t-1})$  for  $K$  states, can be written as a  $K \times K$  transition matrix when  $X_t \in \{1, \dots, K\}$  and the elements of the matrix represent the transition probabilities between states [31].

HMMs are an extension of Markov chains. Initially, for each observation  $X_t$ , a corresponding hidden variable  $h_t$  is introduced, with  $X_t$  dependent on  $h_t$  through an emission probability  $p(X_t|h_t)$ . A HMM is defined as;

$$p(h_{1:T}, X_{1:T}) = p(X_1|h_1)p(h_1) \prod_{t=2}^T p(X_t|h_t)p(h_t|h_{t-1}) \quad (5)$$

where  $p(h_1)$  is the initial probability. Here, emissions have been constructed through the Gaussian Mixture Model, a linear superposition of  $K$  Gaussian distributions defined as [32]:

$$p(X) = \sum_{k=1}^K \pi_k \mathcal{N}(x|\mu_k, \Sigma_k) \quad (6)$$

where  $\mathcal{N}(x|\mu_k, \Sigma_k)$  denotes the Gaussian component with mean  $\mu_k$  and co-variance  $\Sigma_k$ , and parameter  $\pi_k$ —known as mixing probability—such that  $\pi_k \in [0, 1]$  and  $\sum_{k=1}^K \pi_k = 1$ .

The HMM parameters such as the transition matrix, emission matrix, and initial probability are optimised through an iterative procedure—the Expectation Maximisation (EM), also known as the Baum-Welch algorithm [33]. HMM optimisation requires the implementation of stopping criteria either in terms of the number of iterations or error tolerance. A thorough procedure is followed to estimate the optimal stopping criterion; a tolerance of 0.04 yielded the maximum average performance within an average execution time of 12 s per fold, utilising all 42 features.

HMMs can also consider the temporal behaviour of the signal, taking into account a transition probability between states e.g., from ‘eating’ to ‘rumination’, the main motivation for the evaluation of their potential performance for cattle behavior classification.

### 5.2. Linear Discriminant Analysis

Fitting joint probability density function models to determine a decision boundary can be problematic in data with high dimensions; hence the need to reduce the input data dimensionality [31]. Unlike HMM, LDA is a supervised technique, making use of labels alongside the features in the dataset. LDA searches the dimensions in the underlying space that maximise the distance between the means of different states (inter-class variance) and minimises the variation within each category (intra-class variance) [34]. More formally, LDA creates a linear combination of input features with the goal to maximise the ratio  $\frac{\det|S_b|}{\det|S_w|}$ , where  $S_b$  and  $S_w$  are the intra-class and inter-class scatter matrices respectively as defined in [35]. The disadvantage is that the approach fits a Gaussian density to each class, assuming that all classes share the same co-variance matrix. Furthermore, LDA projects the original space to a lower dimensional space which is limited to  $\leq K - 1$  dimensions (where  $K$  is the number of classes), regardless of the dimensionality of the input.

### 5.3. Partial Least Squares Discriminant Analysis

A Partial Least Squares algorithm is developed initially as a regression technique and extended subsequently for classification tasks and its discriminant form (PLS-DA) [36]. Similar to LDA, a PLS-DA is a supervised technique that combines dimensionality reduction and discriminant analysis. However, unlike LDA, PLS-DA does not assume that the input data fits a single Gaussian distribution. PLS aims to maximise the variance of the response variables (labels) explained by the explanatory ones (features) [37]. The optimisation of the Nonlinear Iterative Partial Least Squares (NIPALS) algorithm involves computing the singular vectors of the cross co-variance matrix. A tolerance of  $10^{-6}$  and 500 iterations are used as stopping criteria for the optimisation, consuming an average execution time of

0.73 s per fold, for all 42 features re-projected into 42 dimensions. The formal definition of PLS-DA used is described in [38].

Given that PLS regression analyses generate a continuum of predicted values, the definition and application of a decision rule is required to translate the predicted values in one of the corresponding classes. The most commonly used reported decision rule is a class assignment based on the maximum positive value [36] of the predicted output variables, henceforth used within this analysis.

## 6. Performance Evaluation

A systematic evaluation of the performance of the classification of cattle states as a function of different combinations of dimensionality reduction and classification techniques is carried out. Dimensionality reduction is implemented using the two feature selection techniques detailed thus far, namely, the filter method based on the MI score and the wrapper method based on the BFE, with three classification algorithms viz. HMM, LDA, and PLS-DA. A grid search to optimise the number of features that optimally discriminate between states is performed for each combination. The number of features decreases gradually starting from the full dataset containing 42 features. The reduction in dimensionality is executed in nine steps as reducing one feature at a time is computationally prohibitive; as a consequence, the number of features is decreased in steps of five until a single feature is reached. Feature transformation methods are not considered as they do not reduce the number of features from the raw data.

The HMM is implemented using *hmmlearn* Python framework (<https://github.com/hmmlearn/hmmlearn>, accessed on 16 February 2022), while LDA and PLS-DA are implemented utilising the *scikit-learn* Python library [39]. The BFE algorithm was implemented in Python as described in Algorithm 1.

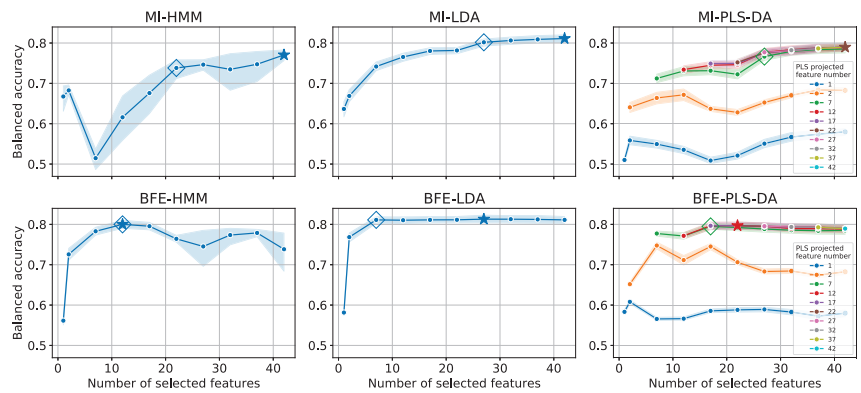
Due to the stochastic nature of the training process, many folds and repetitions may result in elimination of different subsets of features. Thus, a ranking methodology is required to reach consensus on feature importance. For MI, a simple feature ranking process computes the MI feature score for all folds and repetitions in the training set and subsequently utilises the average MI score of each feature as a proxy of importance. The dimensionality of the data is then reduced by eliminating a pre-defined number of the least important features (five in this case). On the other hand, BFE utilises a classification algorithm and thus feature importance can be inferred based on classification performance on the validation set. Here, multiple training/validation stages are performed by excluding one feature at a time for all folds and repetitions; the process yields 25 balanced accuracy results for each feature (five folds with five repetitions). The average balance accuracy is then used to determine the feature importance rank with the lowest average rank features from the pre-defined number eliminated.

The average balanced accuracy and the 95% confidence interval (the Confidence Interval is computed with bootstrapping [40]) on the validation dataset for all combinations, is shown in Figure 3 for varying degrees of reduction. Note that the models with the maximum validation performance are highlighted by a star (\*) and the diamond (◇) represents models that exhibit almost identical performance with the minimum number of features (hence decreasing computational complexity). The '◇' locations are selected manually, taking into consideration the knee point for the line graphs.

The top row plots relate to MI feature selection. Since MI only utilises input and output data for the scoring and not a model, all resultant features at each reduction step are identical for all classification algorithms. As the number of selected features decreases, the balanced accuracy drops as well, indicating that MI is not effective in identifying redundant features for all classification algorithms. Although MI is an efficient statistical measure to estimate the dependence between individual features and output, correlations between features are not considered. As a result, the subset of features that survive the dimensionality reduction have high Mutual Information between input and output but are highly correlated with each other without providing additional discriminatory power.



The performance of the reduction for MI-LDA and MI-PLS-DA is not as steep as MI-HMM, since an inherent re-projection of the input feature space onto a lower dimensional one is performed by eliminating redundant information providing a higher level of robustness against the over-fitting. For PLS-DA the desired size of the lower dimensional space after re-projection is a model hyper-parameter and in order to evaluate the performance, a number of models were trained for a multiple number of re-projected dimensions. In particular, each line in the MI-PLS-DA (and BFE-PLS-DA) corresponds to the dimensionality of the final projected space. For instance, the red line corresponds to balanced accuracy as a function of the number of raw features selected, all re-projected to 12 dimensions; consequently, the line does not extend to below 12 on the horizontal axis.



**Figure 3.** Balanced Accuracy for HMM, LDA and PLS-DA classification algorithms for two feature selection methodologies; MI and BFE for varying number of selected features. For PLS-DA the number of re-projected feature dimensions were varied to explore sensitivity of the hyper-parameter. The  $\star$  denotes models with maximum balanced accuracy performance, while the  $\diamond$  denotes models that were manually selected and balance the trade-off between balanced accuracy and time complexity.

Similarly, the bottom row of the figure, presents the results using BFE. In general, the performance of all models is higher than the corresponding performance with MI, even for a significantly lower number of selected features, attributable to a more structured feature selection methodology. Note that for 42 selected features, the average balanced accuracy obtained through the five folds and five repetitions is lower for BFE-HMM compared to MI-HMM. This is caused by the EM algorithm which is gradient-based and gets stuck in local minima [31] at convergence. In turn creates outlier results with a low balanced accuracy ( $\sim 0.3$ ), also evident by a wider range of the confidence interval. For the band 22–32 of the selected features, the balanced accuracy of BFE-HMM drops owing to the greedy nature of the feature elimination, i.e., decreasing the features in steps of five without reevaluating prior reductions. BFE-LDA and BFE-PLS-DA are more robust to feature reduction, maintaining performance due to their inherent feature transformation. The performance with 7 features is nearly equal to the maximum performance obtained for 27 features for BFE-LDA. For BFE-PLS-DA, the maximum performance is achieved for 22 features which are re-projected to 12; however, the performance is almost identical to 17 features re-projected to 7. The re-projection reduces the computational complexity of the inference, hence, in the manual selection of the ‘ $\diamond$ ’ locations we favoured the re-projections onto lower dimensions.

Table 1 presents the balanced accuracy on the validation set and computation complexity in terms of feature extraction and inference times for all combinations of models and feature selection approaches. In this study, all analyses are conducted on commodity hardware; 64-bit Intel i9 7960x 2.8 GHz 16 cores 128 GB RAM for the purposes of evaluation; however, it is expected that the relative performance differences will translate to low-power

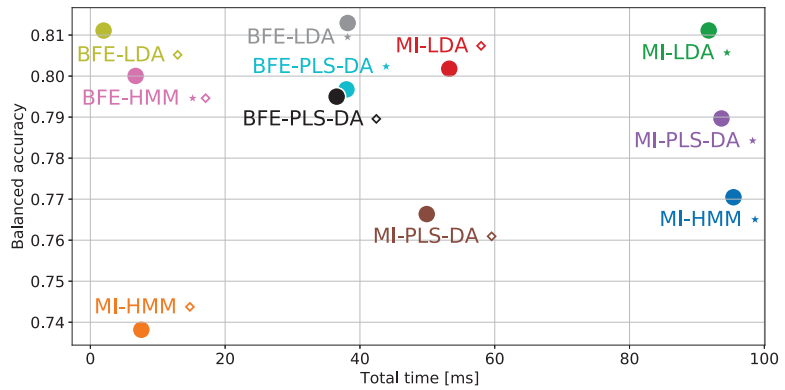
resource constraint processors. Furthermore, Table 1 presents the number of raw features that need to be computed for each methodology. For instance, the LDA classification model with maximum performance ('\*') obtained through BFE technique, requires the extraction of 27 features consuming a computation time of  $38.05 \pm 3.89$  ms and  $0.05 \pm 0.01$  ms for inference, and achieving an average balanced accuracy of 0.81 on the validation dataset. The corresponding BFE-LDA '◇' model requires the computation of 7 raw features which on average, consumes  $1.83 \pm 1.00$  ms for extraction and  $0.05 \pm 0.01$  ms for inference, reducing the total time required ~20 times without loss in balanced accuracy, in contrast to BFE-LDA '\*'.

**Table 1.** Comparison of model performance and time complexity for MI and BFE feature selection approaches for HMM, LDA and PLS-DA classification algorithms. The \* models achieve maximum balanced accuracy performance, while the ◇ models are those that are manually selected and balance the trade-off between balanced accuracy and time complexity.

Feature Selection Technique	Classification Method	# of Input Features	Balanced Accuracy	Time Complexity [ms]			
				Extraction	Inference	Total	
MI	HMM *	42	0.77	$94.68 \pm 9.84$	$0.64 \pm 0.17$	$95.42 \pm 9.91$	
	HMM ◇	22	0.74	$6.99 \pm 0.89$	$0.51 \pm 0.03$	$7.57 \pm 0.91$	
	LDA *	42	0.81	$91.60 \pm 6.65$	$0.05 \pm 0.01$	$91.74 \pm 6.66$	
	LDA ◇	27	0.80	$53.08 \pm 1.21$	$0.05 \pm 0.01$	$53.25 \pm 1.22$	
	PLS-DA *	Projected to 22 features	42	0.79	$93.50 \pm 5.94$	$0.06 \pm 0.01$	$93.64 \pm 5.95$
	PLS-DA ◇		27	0.77	$49.78 \pm 3.06$	$0.04 \pm 0.01$	$49.90 \pm 3.06$
	BFE	HMM ◇*	12	0.80	$6.12 \pm 0.53$	$0.53 \pm 0.03$	$6.71 \pm 0.55$
		LDA *	27	0.81	$38.05 \pm 3.89$	$0.05 \pm 0.01$	$38.18 \pm 3.89$
LDA ◇		7	<b>0.81</b>	<b><math>1.83 \pm 1.00</math></b>	<b><math>0.05 \pm 0.01</math></b>	<b><math>1.96 \pm 1.01</math></b>	
PLS-DA *		Projected to 12 features	22	0.80	$37.86 \pm 4.58$	$0.06 \pm 0.01$	$37.99 \pm 4.58$
PLS-DA ◇			17	0.79	$36.40 \pm 4.24$	$0.05 \pm 0.01$	$36.54 \pm 4.25$

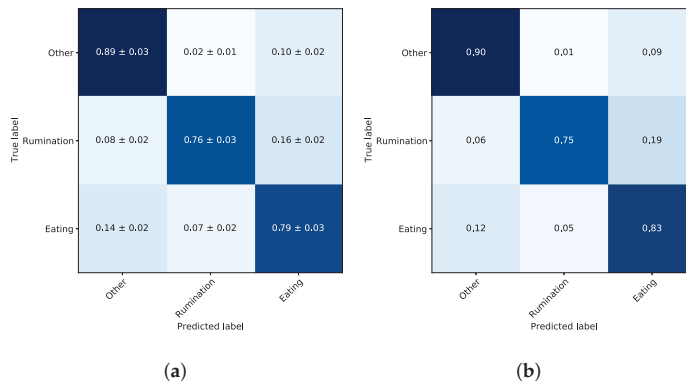
The computational performance difference between a desktop machine and a low-power MCU can be estimated by using the floating point performance as a proxy for the mathematical operations required for feature extraction and inference. An ARM Cortex-M4 [41] requires 9 CPU cycles to complete an FP32 Multiply-and-accumulate (MACC) operation, whereas an Intel i9 can complete 2 MACC per cycle [42]. When the clock speed of each chip is considered, the difference in computational capability between this CPU and an ARM Cortex-M4 such as STM32L476RG [43], is a factor in the region of 1000, with timings scaling appropriately. This factor reduction in computation performance would result in total time complexity increasing; ranging from 1.96s (BFE-LDA '◇') to 95s (MI-HMM '\*'). Hence, the model with the lowest time complexity is still comfortably within a time complexity for deployment to a MCU.

In addition to the information provided within Table 1, Figure 4 presents a graphical comparison between models and illustrates the trade-off between model performance and complexity, through the average validation balanced accuracy and average total processing time, respectively. Although BFE-LDA '\* is highest performing, it is evident that BFE-LDA '◇' achieves almost identical validation performance at significantly lower computational complexity, requiring only  $1.83 \pm 1.00$  ms for feature extraction and  $0.05 \pm 0.01$  ms for inference. Therefore, the BFE-LDA '◇' would be selected for implementation in resource constrained hardware and is the model considered in the remainder of the analysis.



**Figure 4.** Graphical comparison of dimensionality reduction and classification algorithms, in terms of time complexity and performance.

The mean validation performance of BFE-LDA ‘◇’, in terms of the weighted performance metrics of balanced accuracy, precision, and recall are 0.81, 0.85 and 0.82, respectively. The average validation confusion matrix, along with the standard deviations, is shown in Figure 5a. The confusion matrix indicates the normalised individual performance for all states, e.g., the normalised True Positive performance for ‘eating’ is  $0.79 \pm 0.03$ , while ‘rumination’ is mis-classified as ‘eating’  $0.16 \pm 0.02$ ; in all cases, the standard deviation is below 0.03. The BFE-LDA ‘◇’ model with the highest performance on the validation set is selected for evaluation of performance on the test set.

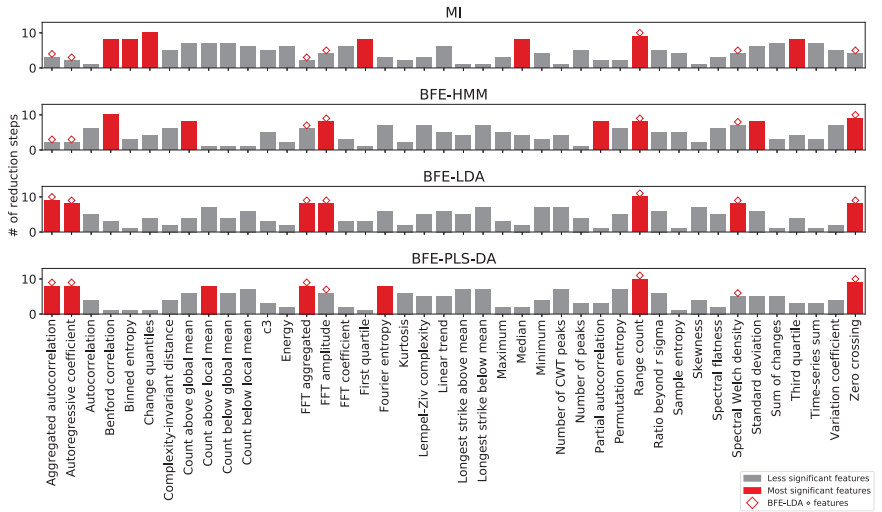


**Figure 5.** Confusion matrices for the selected classification model based on a LDA utilising features selected through BFE that yielded the best trade-off between model performance and complexity—BFE-LDA ‘◇’. (a) Validation dataset. (b) Test dataset.

Further insight arising from the feature selection comparisons can be obtained through the visualisation of the feature importance results for each of the selected combinations of feature reduction method and classification algorithm. Figure 6 shows the feature importance based on the number of reduction steps. Unlike the BFE, MI based feature selection does not depend on the classification algorithm and hence only one graph is shown for all models. Since BFE-LDA ‘◇’ yields the optimum trade-off between performance and time complexity, it is used as a base line for comparison. The seven features selected by BFE-LDA ‘◇’ are annotated in all graphs with a ‘◇’ and the seven most significant features of each approach are annotated in ‘red’. To get consensus between feature selection algorithms, all red bars will be accompanied by a ‘◇’ annotation. It is clear that BFE-PLS-DA and BFE-LDA have the highest agreement in terms of feature significance and

swaps the *FFT amplitude* and *Spectral Welch density* with *Count above global mean* and *Fourier entropy*. Nevertheless, the excluded features have considerable importance. On the other hand, MI and BFE-HMM only agree on ranking feature importance for one and three features respectively. Finally, visualisation of the joint distribution pairs of the seven most important feature combinations selected by BFE-LDA and annotated based on truthing data is presented in Figure 7. Evident is the strength of the knowledge-specific feature *FFT amplitude* which represent the amplitude in the spectral range between 2–4 Hz, aligned with a priori knowledge valuable in guiding the discrimination of the ‘rumination’ class. The *Range count* feature provides a high separation for the ‘other’ class, while for the ‘eating’ class a combination of features are likely to be required. It should be noted that the second knowledge-specific feature *Spectral flatness* only survived 5 reduction steps for BFE-LDA (see Figure 6) inferring that other generic features of higher importance exist.

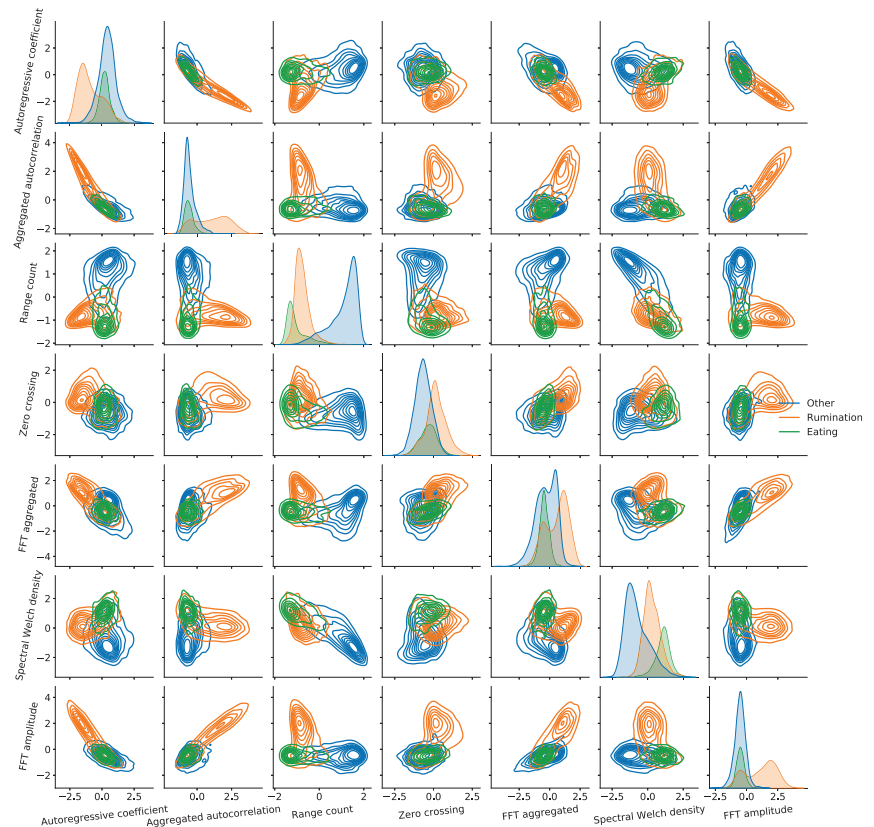
The average weighted metrics for the BFE-LDA ‘o’ in the test set are 0.83, 0.88 and 0.83 for balanced accuracy, precision, and recall, respectively. The metrics were also recorded for individual results per steer on the test set shown in Table 2. Furthermore, the performance of individual classes, ‘eating’ and ‘rumination’, are 0.90 and 0.90 in terms of a precision and 0.86 and 0.90 in terms of recall, respectively.



**Figure 6.** Number of reduction steps the features survived for MI and BFE selection methods. The  $\diamond$  annotations represent the seven features selected by BFE-LDA ‘o’ and red bars the seven features that survived most reductions for each feature selection algorithm.

**Table 2.** Individual classification performance per steer in terms of weighted performance metrics on the test set.

Test Steer	Balanced Accuracy	Precision	Recall
#1	0.82	0.86	0.85
#2	0.86	0.90	0.87
#3	0.80	0.89	0.79
Average	0.83 ± 0.03	0.88 ± 0.02	0.83 ± 0.04



**Figure 7.** Joint distribution of feature pairs selected by BFE-LDA ‘ $\diamond$ ’ with class annotations provided by the truthing data. Note that the diagonal plots are the univariate distributions of each feature.

The normalised confusion matrix on the test set is shown in Figure 5b. Although every attempt is made to mount collars in identical positions around the necks of individual animals, differences in the anatomy and dynamic motion of the animal result in the collars shifting and rotating which results in variations of the accelerometer output, in turn establishing another source of noise that is likely to compromise the accuracy of the classification. It is also clear that the confusion between ‘eating’ and ‘rumination’ is the greatest, as those two states are characterised by similar jaw motions. Given the similarity in these jaw motion patterns, some confusion is to be expected, especially during transition periods. The degree of confusion between other states is lower. In order to place these results in context, assuming the average time spent ruminating is around 400 min per day, an increase in sensitivity of 1% would represent an increase of ~4 min of time spent ruminating.

## 7. Conclusions

Autonomous sensor-based cattle behaviour monitoring systems have grown in importance over the recent past, as an enhancement to traditional visual methods which are both time-consuming and labour-intensive. Systems such as neck-mounted collars monitor dairy and beef cattle continuously, providing a mapping of key behaviours at an individual animal level automatically, the basis for a decision support capability that informs on interventions that enhance the efficiency of current on-farm practices. Here, a novel approach to the development of behaviour classification algorithms, founded on a systematic approach to reducing the dimensionality of the data is reported. Two feature selection techniques based on a MI

score and BFE techniques are applied to both knowledge-specific and generic time-series features extracted from raw accelerometer data. A total of 42 features are extracted from raw accelerometer signals as the starting point, subsequently reduced to 7 with the goal of optimising the degree of discrimination between three key cattle behaviours—‘eating’, ‘rumination’ and ‘other’. The rationale underpinning the selection of the combination of reduction technique and classification algorithm framework is presented and a systematic evaluation of performance provided. The trade-off between model performance, computational complexity and memory footprint is explored. Results show that proposed Backward Feature Elimination to execute on feature selection provides features with higher discriminatory power at the expense of higher computational complexity. Post feature selection, Linear Discriminant Analysis yields a classification model with an overall balanced accuracy of 0.83 and is the most efficient from all of feature reduction/algorithm combinations considered in the paper in terms of implementation in operational settings. In particular, the best combination requires  $1.83 \pm 1.00$  ms to perform feature extraction with  $0.05 \pm 0.01$  ms for inference, thus permitting model deployment within the computation and memory restrictions imposed by operational settings. Evidence is provided that the proposed methodology represents a viable option in the evolution of low-cost neck-mounted accelerometer-equipped collars within precision livestock farming applications.

The dataset generated in this study, including raw data and ground truth annotations from 18 steers, has been made publicly available to stimulate the community to develop new models and facilitate direct comparisons between them (doi:10.5281/zenodo.4064802). Further research should aim to expand in larger trials with more animals and longer observation periods to increase the confidence of behavioural classification and identify novel value-added services.

**Author Contributions:** Conceptualization, C.M., I.A., G.K. and C.T.; Data curation, M.C., C.D., O.M. and C.M.; Formal analysis, D.P.; Investigation, C.D., C.M., I.A. and C.T.; Methodology, D.P. and C.T.; Software, D.P. and C.T.; Supervision, C.T.; Validation, R.A. and V.R.; Visualization, D.P.; Writing—original draft, D.P.; Writing—review and editing, D.P., M.C., C.D., O.M., C.M., R.A., V.C., I.A., V.R., G.K. and C.T. All authors have read and agreed to the published version of the manuscript.

**Funding:** The data were collected under the auspices of BBSRC Project “Precision Beef” [BB/M027333/1]. The analysis was partially supported by the European Union’s Horizon 2020 research and innovation programme “DRAGON—Data Driven Precision Agriculture Services and Skill Acquisition” [810775] and the Ministry of Education, Science and Technological Development of the Republic of Serbia (Grant No. 451-03-68/2022-14/200358).

**Institutional Review Board Statement:** This study was conducted at SRUC’s Beef and Sheep Research Centre situated 6 miles south of Edinburgh UK. The experiment was approved by the Animal Experiment Committee of SRUC and was conducted in accordance with the requirements of the UK Animals (Scientific Procedures) Act 1986.

**Data Availability Statement:** The dataset is publicly available at <https://www.doi.org/10.5281/zenodo.4064802> (accessed on February 2022).

**Acknowledgments:** The authors express their appreciation for providing support to Development and Modeling of Energy-Efficient, Adaptable, Multiprocessor and Multisensor Low-Power Electronic Systems (TR-32043).

**Conflicts of Interest:** The authors declare no conflict of interest.



## Appendix A

**Table A1.** Brief description of generic and knowledge-specific time-series features. All the features used within the analysis are derived using the *tsfresh* Python package [23] with the exception of *FFT amplitude* and *Spectral flatness*.

Features	Definition
Aggregated autocorrelation	Standard deviation of autocorrelation function over a range of different <i>lag</i> values
Autoregressive coefficient	Coefficient of the unconditional maximum likelihood of an autoregressive process
Autocorrelation	$\frac{1}{(n-lag)\sigma^2} \sum_{i=1}^{n-lag} (x_i - \mu)(x_{i+lag} - \mu)$
Benford correlation	Correlation of the time-series first digit distribution with N-B Law distribution
Binned entropy <sup>†</sup>	$-\sum_{i=0}^{\min(nbins,n)} p_i \log p_i * 1_{(p_i>0)}$
Change quantiles	Standard deviation of changes of the time-series within the first and third quartile range
Complexity-invariant distance	$\sqrt{\sum_{i=1}^{n-1} (x_i - x_{i+1})^2}$
Count above global mean	Number of observations higher than the mean value estimated on the training set
Count above local mean	Number of observations higher than the time-series mean
Count below global mean	Number of observations lower than the mean value estimated on the training set
Count below local mean	Number of observations lower than the time-series mean
c3	$\frac{1}{n-2lag} \sum_{i=1}^{n-2lag} (x_{i+2lag} * x_{i+lag} * x_i)$
Energy	$\sum_{i=1}^n x_i^2$
FFT aggregated	Kurtosis of the absolute Fourier transform spectrum
FFT amplitude	Maximum of FFT magnitudes between 2 and 4 Hz
FFT coefficient	Sum of the FFT magnitudes between 2 and 4 Hz
First quartile	The value surpassed by exactly 25% of the time-series data points
Fourier entropy	Binned entropy of the time-series power spectral density
Kurtosis	Difference between the tails of analysed distribution and tails of a normal distribution
Lempel-Ziv complexity	Complexity estimate based on the Lempel-Ziv compression algorithm
Linear trend	Standard error of the estimated linear regression gradient
Longest strike above mean	Length of the longest sequence in time-series higher than its mean value
Longest strike below mean	Length of the longest sequence in time-series lower than its mean value
Maximum	The highest value in time-series
Median	The value surpassed by exactly 50% of the time-series data points
Minimum	The lowest value in time-series.
Number of CWT peaks	Number of peaks within ricker wavelet smoothed time-series
Number of peaks	Number of observations with a value higher than <i>n</i> neighbouring observations
Partial autocorrelation	$\frac{cov(x_t, x_{t-lag}   x_{t-1}, \dots, x_{t-lag+1})}{\sqrt{var(x_t   x_{t-1}, \dots, x_{t-lag+1}) var(x_{t-lag}   x_{t-1}, \dots, x_{t-lag+1})}}$
Permutation entropy	Entropy of ordering permutations occurring in fixed-length time-series window chunks
Range count	Number of observations between the first and the third time-series quartile
Ratio beyond <i>r</i> sigma	Percentage of observations diverging from the mean by more than <i>r</i> standard deviations
Sample entropy	Negative logarithm of the conditional probability that two sequences remain similar
Skewness	Distortion or asymmetry that deviates from the normal distribution
Spectral flatness	Ratio between geometric and arithmetic mean of the power spectrum
Spectral Welch density	Power spectral density estimation using the Welch method at a certain frequency
Standard deviation	$\sqrt{\frac{1}{n} \sum_{i=1}^n (x_i - \mu)^2}$
Sum of changes	$\sum_{i=1}^{n-1}  x_{i+1} - x_i $
Third quartile	The value surpassed by exactly 75% of the time-series data points
Time-series sum	$\sum_{i=1}^n x_i$
Variation coefficient	Relative standard deviation, i.e., ratio of the standard deviation to the mean
Zero crossing	Number of points where time-series signal crosses a zero value

<sup>†</sup> where *p<sub>i</sub>* indicates percentage of samples falling into the given bin.

## References

1. AHDB Dairy. AHDB Dairy Statistics. 2021. Available online: <https://ahdb.org.uk/dairy> (accessed on 17 February 2022).
2. Fricke, P.M.; Carvalho, P.D.; Giordano, J.O.; Valenza, A.; Lopes, G.; Amundson, M.C. Expression and detection of estrus in dairy cows: The role of new technologies. *Animal* **2014**, *8*, 134–143. [CrossRef]

3. Michie, C.; Andonovic, I.; Gilroy, M.; Ross, D.; Duthie, C.A.; Nicol, L. Oestrus Detection in Free Roaming Beef Cattle. In Proceedings of the European Conference on Precision Livestock Farming—EC-PLF 2013, Leuven, Belgium, 10–12 September 2013.
4. Roelofs, J.B.; Van Erp-Van Der Kooij, E. Estrus detection tools and their applicability in cattle: Recent and perspectival situation. *Anim. Reprod.* **2015**, *12*, 498–504. [[CrossRef](#)]
5. Afimilk/NMR. *Silent Herdsman/Better Performing Cows*; NMR: Chippenham, UK, 2012.
6. Stangaferro, M.; Wijma, R.; Caixeta, L.; Al-Abri, M.; Giordano, J. Use of rumination and activity monitoring for the identification of dairy cows with health disorders: Part III. Metritis. *J. Dairy Sci.* **2016**, *99*, 7422–7433. [[CrossRef](#)]
7. Rahman, A.; Smith, D.V.; Little, B.; Ingham, A.B.; Greenwood, P.L.; Bishop-Hurley, G.J. Cattle behaviour classification from collar, halter, and ear tag sensors. *Inf. Process. Agric.* **2018**, *5*, 124–133. [[CrossRef](#)]
8. Zehner, N.; Niederhauser, J.J.; Nydegger, F.; Grothmann, A.; Keller, M.; Hoch, M.; Haeussermann, A.; Schick, M. Validation of a new health monitoring system (RumiWatch) for combined automatic measurement of rumination, feed intake, water intake and locomotion in dairy cows. In Proceedings of the Information Technology, Automation and Precision Farming. International Conference of Agricultural Engineering—CIGR-AgEng 2012: Agriculture and Engineering for a Healthier Life, Valencia, Spain, 8–12 July 2012.
9. Pouloupoulou, I.; Lambertz, C.; Gauly, M. Are automated sensors a reliable tool to estimate behavioural activities in grazing beef cattle? *Appl. Anim. Behav. Sci.* **2019**, *216*, 1–5. [[CrossRef](#)]
10. Hamilton, A.W.; Davison, C.; Tachtatzis, C.; Andonovic, I.; Michie, C.; Ferguson, H.J.; Somerville, L.; Jonsson, N.N. Identification of the rumination in cattle using support vector machines with motion-sensitive bolus sensors. *Sensors* **2019**, *19*, 1165. [[CrossRef](#)]
11. Martiskainen, P.; Järvinen, M.; Skön, J.P.; Tiirikainen, J.; Kolehmainen, M.; Mononen, J. Cow behaviour pattern recognition using a three-dimensional accelerometer and support vector machines. *Appl. Anim. Behav. Sci.* **2009**, *119*, 32–38. [[CrossRef](#)]
12. Benaissa, S.; Tuytens, F.A.; Plets, D.; Cattrysse, H.; Martens, L.; Vandaele, L.; Joseph, W.; Sonck, B. Classification of ingestive-related cow behaviours using RumiWatch halter and neck-mounted accelerometers. *Appl. Anim. Behav. Sci.* **2019**, *211*, 9–16. [[CrossRef](#)]
13. Robert, B.; White, B.J.; Renter, D.G.; Larson, R.L. Evaluation of three-dimensional accelerometers to monitor and classify behavior patterns in cattle. *Comput. Electron. Agric.* **2009**, *67*, 80–84. [[CrossRef](#)]
14. Abell, K.M.; Theurer, M.E.; Larson, R.L.; White, B.J.; Hardin, D.K.; Randle, R.F. Predicting bull behavior events in a multiple-sire pasture with video analysis, accelerometers, and classification algorithms. *Comput. Electron. Agric.* **2017**, *136*, 221–227. [[CrossRef](#)]
15. González, L.A.; Bishop-Hurley, G.J.; Handcock, R.N.; Crossman, C. Behavioral classification of data from collars containing motion sensors in grazing cattle. *Comput. Electron. Agric.* **2015**, *110*, 91–102. [[CrossRef](#)]
16. Riaboff, L.; Aubin, S.; Bedere, N.; Couvreur, S.; Madouasse, A.; Goumand, E.; Chauvin, A.; Plantier, G. Evaluation of pre-processing methods for the prediction of cattle behaviour from accelerometer data. *Comput. Electron. Agric.* **2019**, *165*, 104961. [[CrossRef](#)]
17. Riaboff, L.; Poggi, S.; Madouasse, A.; Couvreur, S.; Aubin, S.; Bédère, N.; Goumand, E.; Chauvin, A.; Plantier, G. Development of a methodological framework for a robust prediction of the main behaviours of dairy cows using a combination of machine learning algorithms on accelerometer data. *Comput. Electron. Agric.* **2020**, *169*, 105179. [[CrossRef](#)]
18. Kasfi, K.T.; Hellicar, A.; Rahman, A. Convolutional Neural Network for Time Series Cattle Behaviour Classification. In Proceedings of the Workshop on Time Series Analytics and Applications—TSA’16, Hobart, TAS, Australia, 6 December 2016; ACM Press: New York, NY, USA, 2016; pp. 8–12. [[CrossRef](#)]
19. Peng, Y.; Kondo, N.; Fujitara, T.; Suzuki, T.; Wulandari; Yoshioka, H.; Itoyama, E. Classification of multiple cattle behavior patterns using a recurrent neural network with long short-term memory and inertial measurement units. *Comput. Electron. Agric.* **2019**, *157*, 247–253. [[CrossRef](#)]
20. Rahman, A.; Smith, D.; Hills, J.; Bishop-Hurley, G.; Henry, D.; Rawnsley, R. A comparison of autoencoder and statistical features for cattle behaviour classification. In Proceedings of the 2016 International Joint Conference on Neural Networks (IJCNN), Vancouver, BC, Canada, 24–29 July 2016; pp. 2954–2960. [[CrossRef](#)]
21. Pavlovic, D.; Davison, C.; Hamilton, A.; Marko, O.; Atkinson, R.; Michie, C.; Crnojević, V.; Andonovic, I.; Bellekens, X.; Tachtatzis, C. Classification of Cattle Behaviours Using Neck-Mounted Accelerometer-Equipped Collars and Convolutional Neural Networks. *Sensors* **2021**, *21*, 4050. [[CrossRef](#)]
22. ITIN+HOCH. RumiWatchSystem: Measurement System for Automatic Health Monitoring in Ruminants. 2014. Available online: <https://www.rumiwatch.com/> (accessed on 17 February 2022).
23. Christ, M.; Braun, N.; Neuffer, J.; Kempa-Liehr, A.W. Time Series Feature Extraction on basis of Scalable Hypothesis tests (tsfresh—A Python package). *Neurocomputing* **2018**, *307*, 72–77. [[CrossRef](#)]
24. Guyon, I.; Elisseeff, A. An introduction to variable and feature selection. *J. Mach. Learn. Res.* **2003**, *3*, 1157–1182.
25. Fukunaga, K. *Introduction to Statistical Pattern Recognition*; Elsevier: Amsterdam, The Netherlands, 2013.
26. Jović, A.; Brkić, K.; Bogunović, N. A review of feature selection methods with applications. In Proceedings of the 2015 38th International Convention on Information and Communication Technology, Electronics and Microelectronics (MIPRO), Opatija, Croatia, 25–29 May 2015; pp. 1200–1205.
27. Saeys, Y.; Inza, I.; Larranaga, P. A review of feature selection techniques in bioinformatics. *Bioinformatics* **2007**, *23*, 2507–2517. [[CrossRef](#)]
28. Kraskov, A.; Stögbauer, H.; Grassberger, P. Estimating mutual information. *Phys. Rev. E* **2004**, *69*, 066138. [[CrossRef](#)]

29. Ross, B.C. Mutual information between discrete and continuous data sets. *PLoS ONE* **2014**, *9*, e87357. [[CrossRef](#)] [[PubMed](#)]
30. Barber, D. *Bayesian Reasoning and Machine Learning*; Cambridge University Press: Cambridge, UK, 2012.
31. Murphy, K.P. *Machine Learning: A probabilistic Perspective*; MIT Press: Cambridge, MA, USA, 2012.
32. Bishop, C.M. *Pattern Recognition and Machine Learning*; Springer: Berlin/Heidelberg, Germany, 2006.
33. Bilmès, J.A. A gentle tutorial of the EM algorithm and its application to parameter estimation for Gaussian mixture and hidden Markov models. *Int. Comput. Sci. Inst.* **1998**, *4*, 126.
34. Tharwat, A.; Gaber, T.; Ibrahim, A.; Hassaniien, A.E. Linear discriminant analysis: A detailed tutorial. *AI Commun.* **2017**, *30*, 169–190. [[CrossRef](#)]
35. Martínez, A.M.; Kak, A.C. PCA versus LDA. *IEEE Trans. Pattern Anal. Mach. Intell.* **2001**, *23*, 228–233. [[CrossRef](#)]
36. Lee, L.C.; Liong, C.Y.; Jemain, A.A. Partial least squares-discriminant analysis (PLS-DA) for classification of high-dimensional (HD) data: A review of contemporary practice strategies and knowledge gaps. *Analyst* **2018**, *143*, 3526–3539. [[CrossRef](#)] [[PubMed](#)]
37. Haenlein, M.; Kaplan, A.M. A beginner’s guide to partial least squares analysis. *Underst. Stat.* **2004**, *3*, 283–297. [[CrossRef](#)]
38. Brereton, R.G.; Lloyd, G.R. Partial least squares discriminant analysis: Taking the magic away. *J. Chemom.* **2014**, *28*, 213–225. [[CrossRef](#)]
39. Pedregosa, F.; Varoquaux, G.; Gramfort, A.; Michel, V.; Thirion, B.; Grisel, O.; Blondel, M.; Prettenhofer, P.; Weiss, R.; Dubourg, V.; et al. Scikit-learn: Machine Learning in Python. *J. Mach. Learn. Res.* **2011**, *12*, 2825–2830.
40. Waskom, M.L. Seaborn: statistical data visualization. *J. Open Source Softw.* **2021**, *6*, 3021. [[CrossRef](#)]
41. ST Microelectronics. UM2526: Introduction Getting Started with X-CUBE-AI Expansion Package for Artificial Intelligence (AI) UM2526 User Manual; 2020. Available online: [https://www.st.com/resource/en/user\\_manual/dm00570145-getting-started-with-xcubeai-expansion-package-for-artificial-intelligence-ai-stmicroelectronics.pdf](https://www.st.com/resource/en/user_manual/dm00570145-getting-started-with-xcubeai-expansion-package-for-artificial-intelligence-ai-stmicroelectronics.pdf) (accessed on 10 March 2022).
42. Intel®. Intel® Intrinsic Guide, 2021. Available online: <https://www.intel.com/content/www/us/en/docs/intrinsics-guide> (accessed on 10 March 2022).
43. ST Microelectronics. Datasheet—STM32L476xx—Ultra-Low-Power Arm®Cortex®-M4. 2019. Available online: <https://www.st.com/resource/en/datasheet/stm32l476je.pdf> (accessed on 10 March 2022).

Review

# Soft Grippers for Automatic Crop Harvesting: A Review

Eduardo Navas \*, Roemi Fernández \*, Delia Sepúlveda, Manuel Armada and Pablo Gonzalez-de-Santos

Centre for Automation and Robotics, UPM-CSIC, Carretera CAMPO-REAL Km 0.2, Arganda del Rey, 28500 Madrid, Spain; delia.sepulveda@csic.es (D.S.); manuel.armada@csic.es (M.A.); pablo.gonzalez@car.upm-csic.es (P.G.-d.-S.)

\* Correspondence: eduardo.navas@csic.es (E.N.); roemi.fernandez@car.upm-csic.es (R.F.)

**Abstract:** Agriculture 4.0 is transforming farming livelihoods thanks to the development and adoption of technologies such as artificial intelligence, the Internet of Things and robotics, traditionally used in other productive sectors. Soft robotics and soft grippers in particular are promising approaches to lead to new solutions in this field due to the need to meet hygiene and manipulation requirements in unstructured environments and in operation with delicate products. This review aims to provide an in-depth look at soft end-effectors for agricultural applications, with a special emphasis on robotic harvesting. To that end, the current state of automatic picking tasks for several crops is analysed, identifying which of them lack automatic solutions, and which methods are commonly used based on the botanical characteristics of the fruits. The latest advances in the design and implementation of soft grippers are also presented and discussed, studying the properties of their materials, their manufacturing processes, the gripping technologies and the proposed control methods. Finally, the challenges that have to be overcome to boost its definitive implementation in the real world are highlighted. Therefore, this review intends to serve as a guide for those researchers working in the field of soft robotics for Agriculture 4.0, and more specifically, in the design of soft grippers for fruit harvesting robots.

**Keywords:** soft robotics; agriculture 4.0; soft grippers; end-effectors; review; harvesting process

**Citation:** Navas, E.; Fernández, R.; Sepúlveda, D.; Armada, M.; Gonzalez-de-Santos, P. Soft Grippers for Automatic Crop Harvesting: A Review. *Sensors* **2021**, *21*, 2689. <https://doi.org/10.3390/s21082689>

Academic Editor: Dionysis Bochtis

Received: 10 March 2021

Accepted: 9 April 2021

Published: 11 April 2021

**Publisher's Note:** MDPI stays neutral with regard to jurisdictional claims in published maps and institutional affiliations.



**Copyright:** © 2021 by the authors. Licensee MDPI, Basel, Switzerland. This article is an open access article distributed under the terms and conditions of the Creative Commons Attribution (CC BY) license (<https://creativecommons.org/licenses/by/4.0/>).

## 1. Introduction

In the last decade, the agricultural sector has undergone a deep transformation to cope with the growing demand for food [1–3]. Among the main tasks in agricultural processes, those that involve the manipulation of fruits and vegetables continue to be one of the most time consuming and labour intensive, resulting in low efficiency and limited competitiveness. This situation is exacerbated by the labour shortages of seasonal workers unable to travel between regions, leading to the accumulation of fresh products and impressive food losses. For these reasons, a great research effort is underway to automate these manual operations, as in the case of selective harvesting, combining multidisciplinary fields such as biological science, control engineering, robotics and artificial intelligence. Special emphasis is being placed on topics such as the modification of plant peduncles [4], which could simplify the harvesting process [5]; machine vision and detection systems [6–10]; decision-making architectures [11–13]; autonomous navigation [14–16]; and dexterous manipulation [17,18]. Another critical topic, often underestimated, is that related to the design of the systems attached to the tip of robotic manipulators and that are in direct contact with the fruit, known as grippers or end-effectors.

In manual harvesting, humans use their hands to move different elements of plants, grasp the fruits and detach them, either directly or with the help of a tool. The kinematics of human hands, the deformability of the skin and muscle, and their sense of touch give us efficient grasping abilities. Attempts to emulate human skills during harvesting have resulted in numerous mechanical end-effectors that can be classified according to their numbers of fingers into two major groups: multi-fingered and parallel grippers [19].

Multi-fingered grippers, such as those proposed in [20–23], include multiple degrees of freedom (DoFs), giving them grasping characteristics similar to the human hand, although they are expensive and difficult to control due to the large number of actuators. On the other hand, parallel grippers exhibit a simpler mechanical structure, making them easier to control, as they have fewer actuators. However, this simplification translates into less adaptability during grasping.

With the emergence of soft robotics, grippers based on soft and deformable materials have recently begun to be proposed for industrial and medical applications [24–31]. These soft grippers, which are able to continuously vary their shape without requiring complex multi-joint mechanisms, have the potential to provide greater adaptability while presenting lower costs and simpler structures and control algorithms than hard end-effectors [32,33].

With all this in mind, this review aims to present and discuss the latest developments in the design and implementation of novel soft grippers and end-effectors. To that end, the suitability of each of the proposed grippers to the movements required during the harvesting processes is studied, as well as their manufacturing processes and low-level control methods. In addition, the picking patterns (i.e., movements required to harvest the fruit) reported in the literature are analysed, and classification is presented in which the correct picking patterns for a considerable number of fruits are identified. Moreover, a list of the remaining challenges for the implementation of soft grippers in robotic crop harvesting is presented.

Therefore, the beneficiaries of this review can be all companies, designers or researchers who want to see a complete picture of the current progress of soft robotics and its suitability for implementation in the agricultural sector. The rest of the review is organized as follows. In Section 2, an overview of the current state of robotic harvesting automation is introduced, delving into the most critical aspects for gripper design, such as the characteristics of the picking patterns and the nature of the different fruits. Section 3 describes the soft technologies applied to existing grippers that could be used for Agriculture 4.0 applications, as well as the main control solutions implemented for soft grippers. Section 4 lists the main challenges of soft grippers for robotic crop harvesting. Finally, Section 5 summarizes the major conclusions.

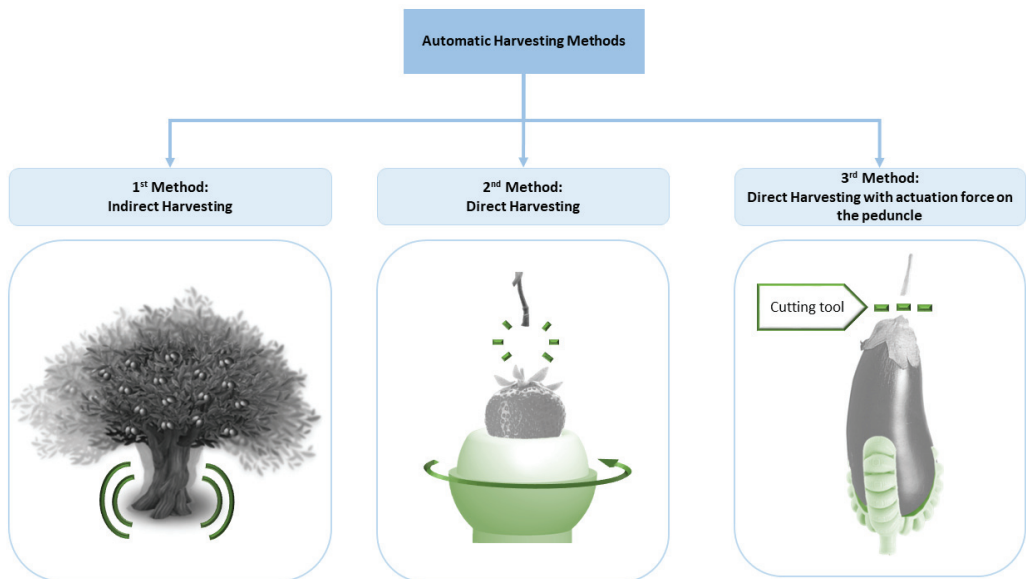
## 2. Harvesting Process

### 2.1. Harvesting Process Classification

Since gripper designs for robotic harvesting are highly dependent on the picking process, the main techniques currently in use are summarized below with the aim of finding the gaps where soft robotics can make the greatest contributions. The general classification presented in [34] divides the detachment of fruits into two methods: (i) mechanical detachment, which involves the removal of pieces of fruit from the tree branch by means of a machine or a mechanical mechanism, and (ii) manual detachment, which consists of the extraction of pieces of fruit from the tree branch by the human hand. In [35], mechanical fruit harvesting processes are classified as follows: (i) those that remove the fruits by shaking the entire plant through air blasting, canopy shaking, limb shaking or trunk shaking; sometimes these methods are assisted with a chemical agent, which makes ripe fruits easier to harvest; and (ii) those that use automatic robotic picking machines that require minimal or no human intervention in their operation.

With the introduction of a wide variety of robotic solutions for fruit harvesting and the design of new grippers and end-effectors in recent years, it is convenient to update the classification of automatic harvesting methods to include these latest technologies. The classification proposed in this review is an extension of that carried out in [36], which classified the removal of the fruits into two groups: (i) those in which the application of direct force to the harvested portion is necessary and (ii) those that deliver the removal energy indirectly as an inertial force response that causes detachment by accelerating the attachment support away from the harvest object. Consequently, harvesting methods are divided into three main groups, which are shown schematically in Figure 1:

1. Indirect harvesting: a technique that involves indirect mechanical movement towards the fruit through a force applied to the plant itself, such as that carried out when harvesting olives [37], almonds [38] or pistachio nuts [39]. To make the fruits fall without any contact points, methods such as air blasting, limb shaking, trunk shaking and canopy shaking are often used [34,35].
2. Direct harvesting: a method used in those crops that, due to the structural characteristics of the plant, cannot be shaken but require the direct application of a mechanical force on the fruit or its peduncle; these picking techniques, which are discussed in more detail in Section 2.2, are also known as picking patterns (e.g., twisting, pulling or bending) and cause fruits to detach from the stem [40]. Examples from this group are the methods used in the harvesting of strawberries [40,41], apples [42–45] and several varieties of tomatoes [46–49].
3. Direct harvesting with an actuation force on the peduncle: a technique that is applied to those fruits that require a direct mechanical movement, or another type of cutting method, applied directly to the stalk since due to their morphology they are connected to the plant by a hard peduncle that must be cut, as in the harvest of aubergines [50,51], melons [52], oranges [53], cucumbers [54] and peppers [55–57].



**Figure 1.** Classification of automatic harvesting methods.

In the classification of the harvesting processes presented above, it is important to highlight that the fruits included in the first group can also be harvested using the methods described in the second group due to the physical characteristics of the peduncle. The most suitable harvesting method to use must be studied on an individual basis depending on the crop. Several factors may influence the choice of the most suitable harvesting method, such as (i) the size and shape of the tree [36], (ii) the structural fragility of the plant [35,36], (iii) the maturity stage of the fruits [34,58], (iv) the lack of preharvesting chemical fruit looseners, which affect the ease of harvesting [34], (v) the requirements of avoiding damage to the fruit or the plant [36,58] and (vi) the financial profitability [34]. Some authors [34,59] discourage the use of products such as chemical fruit looseners before harvest due to their effect on the defoliation of the trees and the subsequent lack of bloom in the following year. This complicates harvesting through indirect contact of the various fruits within the first



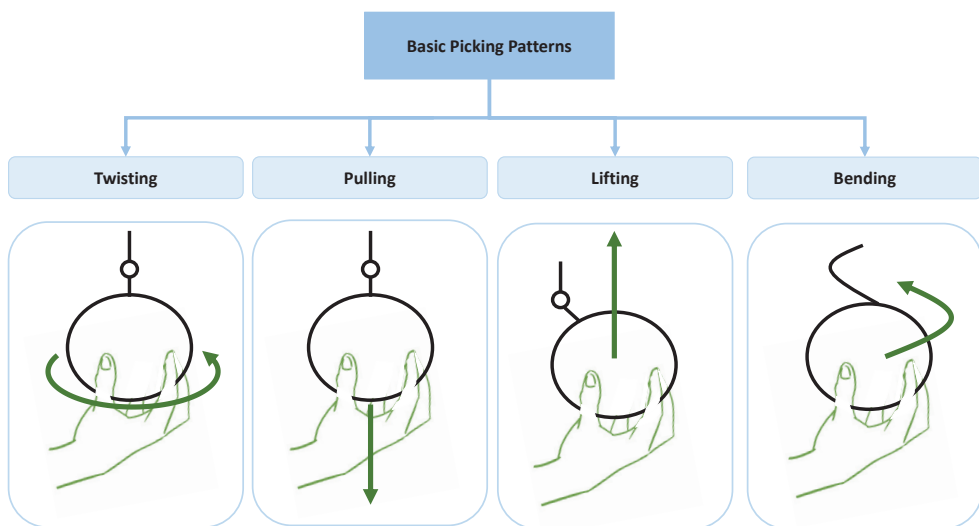
group, which in some cases are collected by air blasting, limb shaking, trunk shaking or canopy shaking [34].

There are also several differences between the requirements of the group 2 and group 3 techniques. For instance, the harvesting methods included in group 3 need a more sophisticated perception system than those in group 2, since in addition to the fruits, they have to detect peduncles; they also require a robotic system with greater precision to locate the peduncle between the blades of the tool and proceed to cut it without damaging the crop [47], while with the group 2 techniques, fruits can be harvested with part of the peduncle with just one picking action.

In the literature, authors of [60] resume the main capabilities of an ideal picking robot as the following: (i) the 3D location of the fruits in the plant, (ii) trajectory planning, (iii) the application of detachment method and adequate storage, and (iv) the application of reliable driving system. These operations must be carried out under the constraints of (i) increasing the harvest ratio between robotic picking and manual picking, (ii) increasing the quality of the harvested fruit, and (iii) being economically justified. Furthermore, ref. [61] highlights two main challenges in fruit harvesting: (i) an adequate manipulation of fruits to avoid the loss of quality and consequently, the loss of value in the market, which implies the development of grippers and end-effectors that meet this requirement, and (ii) the study of the detachment method for removing the fruit from the tree, which varies according to the type of fruit.

## 2.2. Picking Patterns

As stated above, the fruits harvested by means of the methods classified in group 2 pose a challenge in the field of robotic manipulation. One of the research paths in this field is based on the idea of studying and decomposing the human movements performed during the harvesting of fruits and replicating them using robotic grippers. These movements are grouped under the concept of picking patterns, which include, among others, the movements of bending, lifting, twisting, and pulling or a combination of them. In Figure 2, the basic picking patterns are shown conceptually.

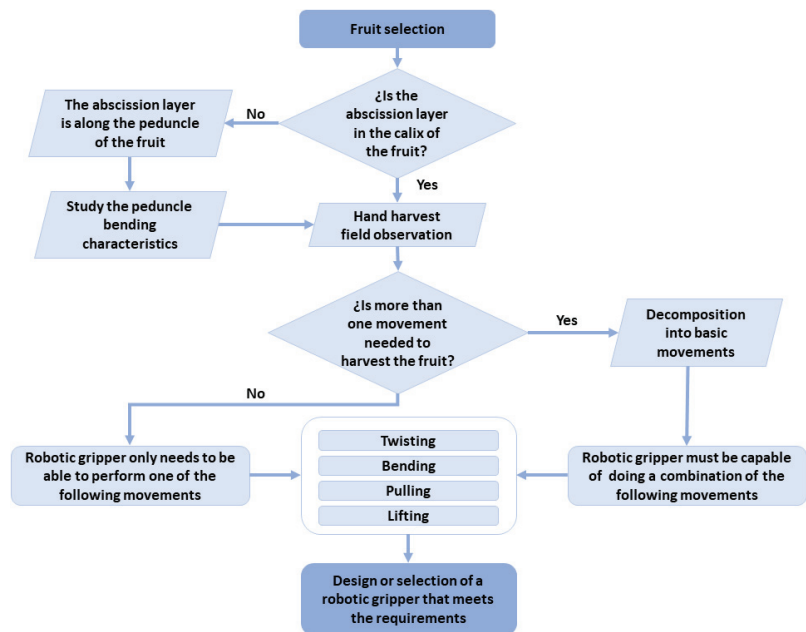


**Figure 2.** Simplified scheme of basic picking techniques.

An important factor that has been studied within the field of biological science for group 2 methods, and particularly for the application of the picking patterns, is the abscis-

sion layer, which is a barrier of thin-walled parenchyma cells that develops between the fruit and the fruit stalk or the fruit stalk and the branch. This development process occurs when the moment of the fall of a fruit from a plant approaches to facilitate detachment [62]. In most cases, fruit harvested before development of the abscission zone will not have well-developed sugar, volatile, or flavour attributes [63]. Some investigations are trying to modify or eliminate this layer by modifying the plant so that the next point of separation of the plant from the fruit is located right in the calyx and the fruit is easier to harvest [5,62]. Therefore, the identification of the abscission layer is important to determine where the fruit separates from the plant at the time of harvest, as well as the picking patterns to apply.

In the literature, there are studies available on picking patterns for (i) tomatoes [46,47,64], (ii) kiwis [65], (iii) apples [61] and (iv) strawberries [66,67]. It is also worth mentioning the study presented in [68], in which the movements of the hand and the human body in the harvesting process are analysed to provide a guide for the design of new grippers and end-effectors of anthropomorphic inspiration. The scheme shown in Figure 3 summarizes the proposed steps to follow for the design or selection of grippers and end-effectors required to harvest fruits by means of direct contact methods.



**Figure 3.** Steps to design or select a gripper or end-effector based on the study of a picking pattern.

Since the picking patterns described in this section involve direct contact with the fruit, the introduction of soft grippers may represent a significant advance in the automation of the harvesting methods classified in group 2, allowing a delicate manipulation that guarantees the integrity of fruits.

### 2.3. Direct Harvesting with an Actuation Force on the Peduncle

Regarding group 3, a comprehensive classification of the types of mechanisms used in grippers coupled to manipulators for the harvesting techniques of group 3 can be found in [2,24]. Research studies on this third group [69–75] have focused on the shear characteristics of the plants, such as the shear ultimate stress, the maximum force and the shear energy. These characteristics could be helpful in the study of the peduncles of fruits, with the aim of developing more energy-efficient cutting tools. For cutting peduncles, there are several techniques that can be classified into two groups: (i) techniques based

on the bending characteristics of the stalk, such as the bending force, bending stress and Young's modulus, and (ii) techniques based on the shear characteristics, such as the shear force, shear strength and shear energy. Table 1 presents the classification of several cutting techniques. According to this table, the tools that do not use the bending force have in common the need to consider the cutting characteristics, in particular, the cutting force and the cutting energy required to separate the fruit from the plant. Since laser cutting is not based on the peduncle characteristics, it has not been included in this table [76].

**Table 1.** Classification of existing grippers.

Type	Bending Characteristics	Shearing Characteristics
Peduncle rotation [61]	X	-
Pushing some object into peduncle [53]	X	-
Knife, one sided blade [53,77]	-	X
Scissors [78]	-	X
Saw [49,53]	-	X
Hot wire [54,79]	-	X

Therefore, harvesting techniques of group 3 are also candidates for the introduction of soft gripper technology, provided they are complemented by a suitable cutting tool.

#### 2.4. Literature Overview of Crop Harvesting Automation

Tables 2 and 3 present a collection of articles that propose technological solutions for automatic harvesting, botanically classified according to the target fruit [80]. This botanical-based classification divides fruits into simple fleshy, aggregate and multiple. Simple fleshy fruits (such as berries, drupes, or pomes) are those derived from a single ovary of and individual flower [81]. Aggregate fruits (such as raspberries) consist of many individual small fruits derived from separate ovaries within a single flower, borne together on a common receptacle [82]. Lastly, multiple fruits (such as figs, mulberries, or pineapples) are those derived from the ovaries of several flowers that coalesce into a single structure [82].

In addition, in each table, the harvesting method used is identified, following the classification of harvesting techniques proposed above and taking as a reference both the information presented in [36,83] and the visualization of the harvesting processes. Although the proposed solutions may be valid for several crops, they have been assigned only to those crops where an experimental study has been reported. Additionally, it is taken into account that the crops classified in groups 2 and 3 are the most suitable for the adoption of soft gripper technology.

**Table 2.** Simple fleshy fruit classification.

Type of Fruit	Name	Actual Harvesting Method	Automatic Harvesting Method
Drupes	Apricot	2	1 [84,85]
	Blackberry	2	1 [86]
	Cafe	2	1 [87,88]
	Cherry	2	1 [89–95], 2 [96], * [97]
	Coconut	3	3 [98,99]
	Loquats	2	-
	Lychee	3	* [100–103]
	Mango	2,3	1 [104], 2 [105], 3 [106–108], * [109]
	Nectarine	2	* [110]
	Olive	1	1 [111–115]
	Peach	2	1 [116], * [117,118]
	Plum	2	2 [119]
	Raspberry	2	1 [120,121]

Table 2. Cont.

Type of Fruit	Name	Actual Harvesting Method	Automatic Harvesting Method
Berries	Avocado	3	* [122]
	Blueberry	2	1 [123]
	Eggplant	3	3 [50,51], * [124]
	Grape	1,3	1 [125–128], 2 [129], * [130]
	Guava	3	* [131]
	Kiwi	2	2 [132–134]
	Papaya	2	3 [105], * [135]
	Passion fruit	2	* [136]
	Pepper	3	3 [55–57,137–139], * [140,141]
	Persimmon	2	2 [142], * [143]
	Pitaya	3	* [144]
	Pomegranate	3	* [145]
	Tomatoes	2,3	2 [46–49], 3 [146,147], * [148–150]
Wolfberry	2	1 [151], 2 [152], * [153]	
Pomes	Apple	1,2	1 [154], 2 [42–45,155,156], 3 [157], * [158,159]
	Pear	2	3 [157], * [160]
	Quince	2	-
Hesperidium and Pepo	Banana	3	* [161]
	Cucumber	3,2	3 [54], * [162,163]
	Grapefruit	3	1 [164]
	Lemon	3	* [165]
	Lime	3	-
	Melon	3	3 [52]
	Orange	3	1 [34,164,166,167], 3[53], * [168,169]
	Pumpkin	3	2 [170], * [171]
Watermelon	3	3 [172]	

(\*) Artificial vision research.

Table 3. Aggregate and multiple fruit classification.

Type of Fruit	Name	Actual Harvesting Method	Automatic Harvesting Method
Aggregate fruit	Custard Apple	2	-
	Strawberry	2	2 [40,41,66,67,173,174], * [175,176]
Multiple fruit	Fig	2	-
	Pineapple	2	2 [177], 3 [178], * [179–181]

(\*) Artificial vision research.

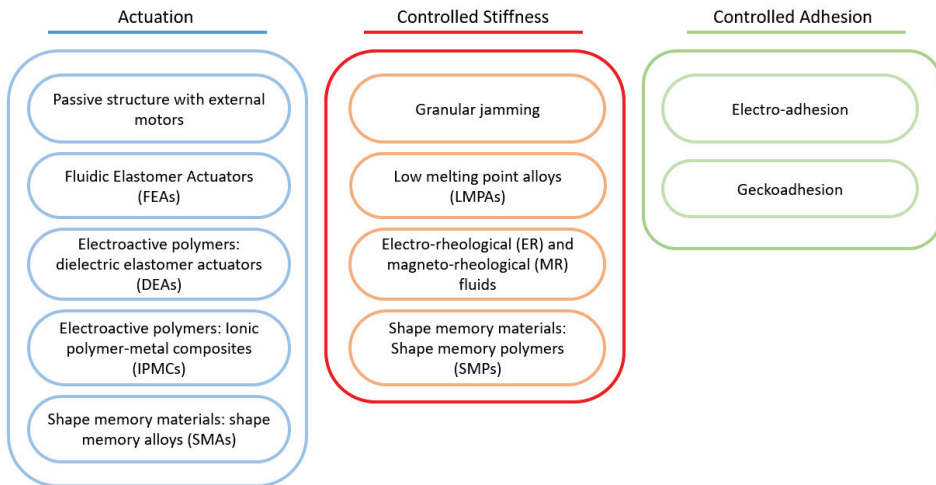
### 3. Soft Grippers

Soft grippers are those end-effectors that use materials and actuation methods that are soft, flexible and compliant and that enable the holding of an object to be manipulated. The softness characteristic provides the adaptability and robustness seen in natural organisms, allowing grasping and manipulation to be achieved with ease. These systems have the potential to interact more safely within an unstructured human environment and deal with dynamic and uncertain tasks [182].

Since fruits must be handled properly to avoid the loss of quality and reach their maximum value in the market, soft grippers are presented as one of the best solutions for harvesting crops, given their adaptability and the delicacy with which they can grasp and manipulate the target products.

In this context, soft technologies can be defined as the set of theories, techniques and procedures that enable key functions of soft robotic grippers, such as actuation, gripping and shape control methods. Although different authors have proposed a great variety of soft technologies [183–187], the main objective of all of them is to guarantee the safe interaction of the device with humans and the environment by using materials with a module similar, in terms of rigidity, to that of soft biological materials [187]. Several

reviews of soft grippers can be found in the literature [19,33,182–184,187–189], presenting various approaches to classify existing technologies. One of the most widely used approaches is the one that classifies the soft gripping technologies according to three different categories [190,191]: (i) actuation, (ii) control stiffness and (iii) controlled adhesion. However, it is currently possible to find devices whose designs simultaneously combine characteristics from several of these categories. Figure 4 shows the complete classification of the current soft gripping technologies based on the mentioned categories.



**Figure 4.** Classification of soft gripping technologies proposed by [190].

From an agricultural point of view, some of these technologies may be more relevant than others. Based on the reviews carried out in [189,190], evaluation criteria adapted to Agriculture 4.0 can be established to perform a quantitative and qualitative analysis of the existing soft grippers. These criteria are listed below.

- **Object size:** This is one of the most critical aspects to evaluate soft technology since its use in certain crops depends on it. Passive structures with external motors, fluidic elastomer actuators (FEAs) and controlled adhesion are the technologies with the best capacity to grasp large objects.
- **Gripper size:** Another criterion is the size of the device, which can be critical to access certain crops.
- **Lifting ratio or operation range:** This variable can be interpreted as the ratio between the mass of the object and the mass of the gripper or as the force that the soft actuator can exert. If interpreted as a ratio, it should always be related to the maximum size of the object that can be grasped. For example, shape memory alloy (SMA) actuators have a higher lift ratio than FEAs but a less manipulable object size, which reduces their suitability for fruit picking.
- **Power consumption:** Each soft technology requires a different type of support device. The technologies that require electric motors or pumps to operate demand the highest energy consumption.
- **Scalability:** This feature takes into account not only the ease of manufacture but also the modularity of the technology used. This is especially important for the adaptation of soft grippers to various types of crops, and it is desirable that they be as universal as possible to increase their viability.
- **Controllability:** Depending on the soft technology used, several proposals for low-level control systems can be found. Normally, the most widely used control method is

open-loop. With respect to fluidic actuators, liquid-based devices can exhibit more linearity than pneumatic devices.

- Response time: This variable can affect the efficiency of the agricultural task. It may be difficult for soft actuators that rely on a fluid to achieve high actuation frequencies due to the fluidic impedance of the channel and the flow actuation level.
- Surface conditions: Soft gripper technologies that require a clean surface, such as controlled adhesion, are less suitable than those that do not have any surface-related requirements.
- Degree of skill to working in unstructured environments: Although soft technology is one of the most suitable for working in unstructured environments, not all soft grippers that can be found in the literature are suitable for agriculture scenarios. This is the case for devices that require complex support devices that are sensitive to large holes or that can suffer tears from sharp objects [192].
- Mechanical compliance: Each soft technology has an advantage in terms of compliance. For instance, FEAs, shape memory polymer (SMP) actuators and dielectric electroactive polymer (DEAP) actuators are inherently compliant due to the materials used. With other technologies, such as SMA actuators, this parameter depends on the shape of their structures.
- Lifetime: The parameter is the number of cycles that a soft actuator can remain in operation before failing or exhibiting altered motion patterns. Lifetime is an important characteristic in FEA technology, which is subjected to constant fill and empty cycles that tend to wear away the material.
- Technology readiness level (TRL) [189]: Another criterion to compare the feasibility of each technology could be the TRL. Those that have experimentally demonstrated their efficiency in real operating environments, as well as those that are also easier to put into production due to the type of support devices they use and the materials and manufacturing process they require, have a higher TRL.

According to this classification, controlled adhesion technology may be difficult to adapt to agricultural tasks, as it requires a special surface to be able to grip an object, although the weight lifted/weight gripper ratio (39 [193]–286.7 [194]) and the size of the object could be suitable ( $0.16 \times 10^{-2}$  m [195] to  $100 \times 10^{-2}$  m [196]). Regarding the grippers grouped around control stiffness, granular jamming ones stand out, since they have a good weight lifted/weight gripper ratio, as well as a good response time and the ability to lift small to medium-size fruits. The other components in this group are discarded for harvest purposes since their performance is not ideal for these tasks. Finally, in the actuation technology group, passive structures with external motors and FEA actuators could be ideal ones for fruit harvesting grippers because (i) they have a large lifted size/gripper weight ratio; (ii) the size of the object can be between 0.01 and  $100 \times 10^{-2}$  m, which includes the sizes of most fruits; (iii) they have a good response time; and (iv) they have the ability to grasp any object. A disadvantage may be their energy consumption since they are hampered by the need for an electric motor or pump. Nevertheless, these technologies present the highest TRL level, which would facilitate their production.

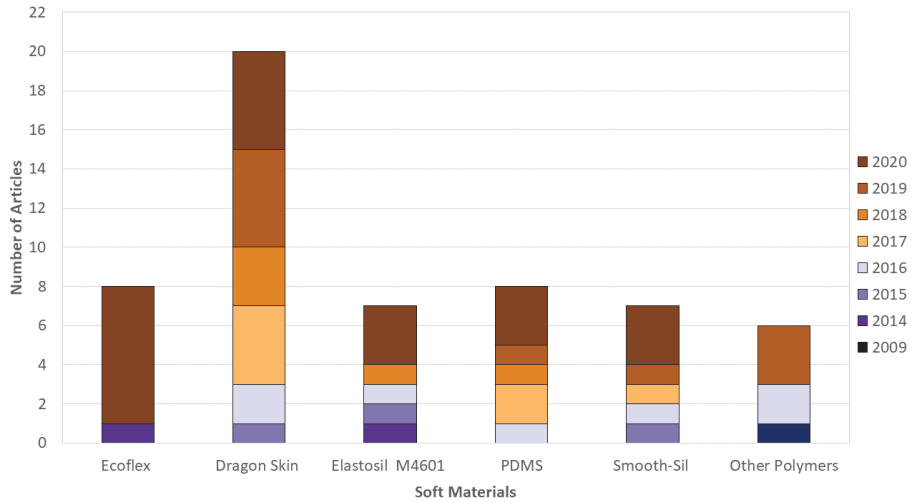
### 3.1. Materials and Manufacturing Methods

#### 3.1.1. Materials

As mentioned above, a wide variety of soft grippers have been proposed. Soft components typically used in the actuators of these grippers include urethanes, hydrogels, braided fabrics, hydraulic fluidics and polymers, such as silicone elastomers [197]. However, actuators based on silicone elastomers have attracted strong interest due to their low cost and ease of manufacture; they do not require the use of complex machinery or skilled labour. In addition, these compliant materials are also advantageous when considering the safety of interaction with biological products, making them appropriate candidates for agricultural applications. Figure 5 presents a bar graph showing the commercially available materials (silicone elastomers and other polymers) that are most frequently reported in the



soft robotics literature and that consequently can be used for soft grippers implementation.



**Figure 5.** Silicone elastomers and other polymers used in soft robotics literature, as well as the corresponding number of citations. For this graph, 45 articles were examined: Ecoflex [198–205], Dragon Skin 10/20/30/FX-Pro [206–225], Elastosil M4601 [199,202,218,226–229], PDMS [198,208,230–232,232–234], Smooth-Sil [200,207,209,218,222,223,227] and Other Polymers [235–241].

Several of these soft materials, particularly silicone elastomers, can be modelled as rubber elastomeric membranes that are hyperelastic and nearly incompressible. Various approaches based on developing free energy density functions can be found to describe the phenomenological constitutive models of rubber-like materials, such as the Neo-Hookean, Mooney–Rivlin (Mooney, 1940; Rivlin, 1948), Ogden (Ogden et al., 2004) and Gent models (Gent, 1996).

As shown in Figure 5, the five most commonly used materials are Dragon Skin, Ecoflex, polydimethylsiloxane (PDMS), Elastosil M4601 and Smooth-Sil, which are all silicone elastomers. Other polymers are Agilus30/VeroClear, ultra-high molecular weight polyethylene, electrostatic discharge (ESD) plastic sheet, thermoplastic elastomers (TPEs) and thermoplastic polyurethane (TPU).

Although there are no specific studies that categorically confirm the suitability of the above materials for the agricultural sector, all materials are declared in their safety data sheet as non-hazardous substances. However, it would be convenient to carry out studies that analyse the life cycle of soft actuators made with these materials, to determine if their degradation may leave particles on the products manipulated.

Dragon Skin, Ecoflex and Smooth-Sil are commonly used for manufacturing objects outside the scientific field, so determining their exact chemical composition is difficult. However, they are versatile, easy to use and handle, and low cost compared to other silicones, and their hardness is between 10 and 50 Shore A. Elastosil M4601 is highly resistant to bending and elongation; it has low viscosity in its uncured form, which makes it easy to mould; and its hardness is approximately 28 Shore A. PDMS has high elasticity [242], it is a thermoset [230], and its behaviour can be mathematically modelled with great precision by means of finite element method (FEM) analysis due to its well-known chemical composition. Furthermore, the variation in its hardness through several mixing ratios has been extensively studied in the literature [243,244]. The main advantage of other soft materials, such as TPU and TPE, is that they can be 3D printed. Additionally, another advantage of TPU-95 is its durability (85A Shore hardness), making it suitable for agricultural environments, where harmful collisions with objects are frequent [236].

A common advantage of all of these silicones is their ability to cure at room temperature, without the need for an oven, although an oven can be used to shorten the cure time.

### 3.1.2. Manufacturing Methods

The main soft actuator manufacturing methods, comprehensively reviewed in [182], are (i) the moulding process, where fused deposition modelling (FDM) printers are commonly used for mould making; (ii) shape deposition manufacturing (SDM), which facilitates the construction of 3D soft actuators composed of multiple materials with different properties; (iii) soft lithography, which facilitates the development of multichannel soft actuators; (iv) lost-wax cast fabrication [245]; and (v) soft 3-D printing. The latter can be considered a promising technology due to the elimination of several moulding stages, which facilitates the manufacturing process and the design of more complex inner chambers or pneumatic networks.

### 3.2. Soft Grippers for Food

In the field of soft robotics, particularly in soft grippers, there is a lack of soft actuators designed for picking fruits and vegetables. This absence is most noticeable for harvesting tasks. Although this is discussed in more detail in the following sections, note that the handling of this type of product requires precise control of the gripper to successfully carry out the movements of the picking patterns that are listed above without damaging the fruit. Furthermore, the current state-of-the-art soft actuators tend to be researched in the field of manipulation, which in many cases is very generalist and is not particular to the diverse characteristics of individual objects.

However, in the field of industrial food handling, there are more research studies that could be considered the basis for soft grippers in Agriculture 4.0 applications. These studies are listed below, classified according to the type of soft actuator they use, indicating the advantages of each technology. Only studies that specifically refer to food handling have been taken into account.

- FEA [206,220,224,225,230,236,246–251]: This type of actuator technology is emerging as a potential winner for fruit handling. This is due to the use of affordable materials, the simplicity of their manufacture and control, and the grip strength obtained. Special mention should be made of the solution proposed in [223], which can be defined as a hybrid gripper, combining vacuum pressure and an origami-inspired compliant structure. This design has a high gripping force of approximately 50 N, and the authors provide a detailed study of its grasping.
- Tendon-driven [252,253]: This type of technology offers other advantages over the previously mentioned technology, such as greater precision in position control. Specifically, this type of technology can be associated with a structure made up of rigid or soft materials that are passively acted upon by tendons that offer soft-type manipulation.
- FEA-tendon-driven [254]: This approach combines both of the above technologies. Tendon drive technology is used for grasping motions, and actuation is achieved by linear soft vacuum actuators. This type of synergy improves the diversity of objects that can be manipulated, as well as the combination of the advantages of each technology. In one particular case [254], the gripper was able to lift a total of 2.7 kg, which represents a maximum payload-to-weight ratio of 7.06.
- Topology-optimized soft grippers [255]: This type of soft gripper, which operates via elastic deformation, can be adapted to the sizes and shapes of objects without mechanical joints or sensors. In one particular case, the gripper could lift maximum loads of 1.4 kg.

Table 4 gathers the main soft grippers that have been proposed for delicate food handling and robotic harvesting applications. All of them are results of ongoing researches in the field of soft robotics.

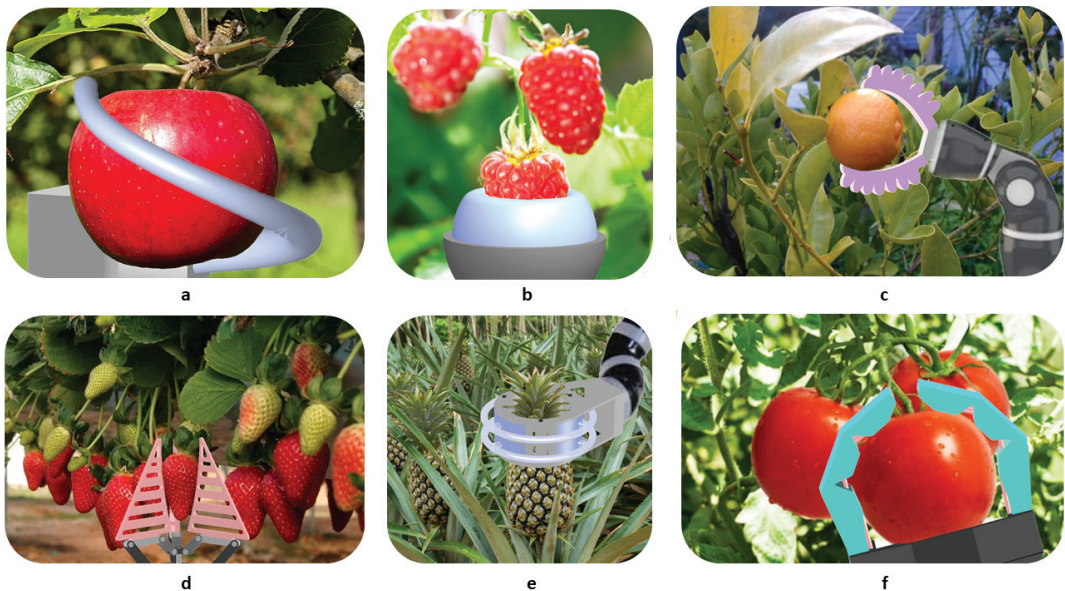
Table 4. Literature review of food soft grippers.

Soft Technology	Reference	Grasped Object	Object Size or Weight	Gripper Type	Gripper Size	Lifting Ratio	Scalability/Controllability	Response Time	Surface Condition	Mechanical Compliance	Lifetime
	[251] *	Lettuce	250 × 250 mm	Two pneumatic actuators and a blade	8000 g, 450 × 450 × 300 mm	-	Close-loop with force sensor feedback	31.7 s	-	✓	-
	[236] *	Apple	-	Three soft finger design	Two fingers length: 95,25 mm One finger length: 152,4 mm	-	Open-loop	7.3 s	-	✓	-
	[230]	Mushroom	-	Three soft chambers in circular shell	Chamber height: 20 mm Chamber arc angle: 60°	30	-	-	Any surface	-	-
	[246]	Apple, Tomato, Carrot, Strawberry	69 mm, 5–150 g	Magnetorheological gripper	-	-	PID	0.46 s	Any surface	✓	-
	[248]	Cupcake liners filled with peanuts	34–64 g	Three soft finger design	Finger size: 82 × 16 × 15 mm	-	FE analysis	-	-	✓	-
	[250]	Cupcake liners filled with red beans, hijiki, ohtashi	75.2 g	Soft fingers	Finger length: 97 mm	1805 %	Open-loop	10 s pick and place (total procedure 3 s for inflation)	-	-	1100
	[224]	Defrosted broccoli	33.54 × 23.94 mm, 3.8–7.0 g	Two soft fingers	Actuator size: 50 × 20 mm	-	-	-	Any surface	-	-
	[225]	Granular kernel corn, Chopped green onion, Boiled hijiki	0.77–26.6 g	Four soft fingers	Finger size: 43 × 61,5 mm	-	Open-loop	-	Any surface	-	-
	[206]	Orange	1000 g	Soft fingers	Finger size: 95 × 20 × 18 mm	-	Open-loop	-	Any surface	-	-
	[220]	Tomato, Kiwifruit, Strawberry	45 to 76 mm	Four soft chambers in circular shell	Internal diameter: 46 mm Height: 30 mm	-	Open-loop	2–5 s	Any surface	✓	-
	[253]	Tomato	500 g	Three soft finger design	-	-	Preprogrammed rotation of motors	-	-	✓	1000
	[252]	Tomato, Cucumber (slices) Avocado (Strips) Cherry Tomato, Olives, Pineapples cubes, Broccoli	-	Quad-Spatula design	-	-	-	-	Flat surfaces	-	-
FEA-Tendon-driven	[254]	Banana, Apple, Grapes	2700 g	Three soft finger design with a suction cup	389.69 g	7.06	Teleoperation Control	0.094 s (Rise time)	Any surface (irregular shapes and sharp corners)	✓	26–20 cycles
Topology optimized soft actuators	[255]	Apple, Grapefruit, Guava, Orange, Kiwifruit	1400 g	Two compliant fingers	-	-	Open-loop (Arduino)	-	-	✓	-

\* Soft Gripper for harvesting purposes. - Data not provided.

As can be seen in Table 4, the cited studies do not list the characteristics of the proposed soft grippers in a homogeneous way, which makes their comparative evaluation difficult. Thus, for example, with regard to the size of the object to be manipulated, each study proposes a different target, which in many cases is carefully selected to ensure an adequate grip. Hence the importance of having standard methods to quantitatively determine and compare the characteristics of soft actuators. It should also be noted that most of the proposed solutions are focused exclusively on the mechanical design, leaving the implementation of the control system for future work. Other crucial aspects such as the adaptation of the grippers to conventional robotic systems, the energy consumption and the power sources required for their operation are not addressed either. More detailed research on the life cycle of actuators is also lacking, which can affect their optimal performance due to the loss of properties that soft materials experience over time.

Figure 6 displays several soft grippers from the literature that could be adapted for precision harvesting of crops.



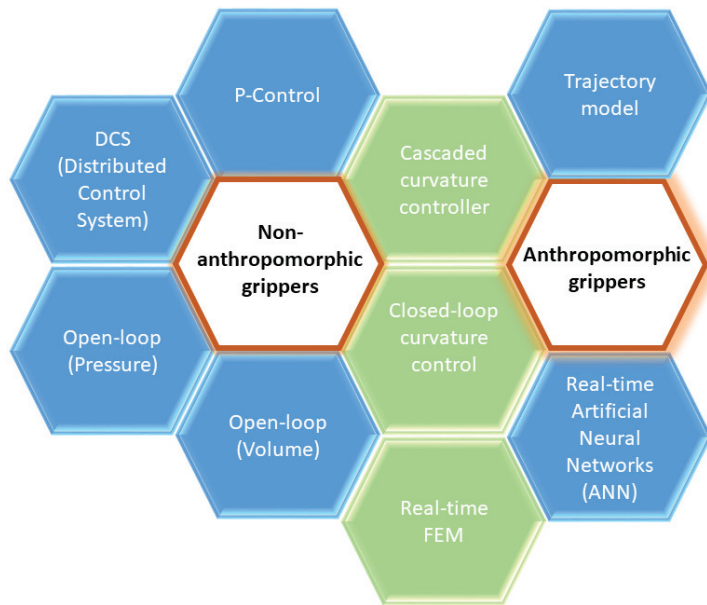
**Figure 6.** Hypothetical harvest scenarios with several soft grippers. (a) Soft continuum gripper based on [256], (b) end-effector based on [257], (c) bellow-type soft gripper based on [224], (d) multi-choice gripper based on [258], (e) circular soft gripper based on [220,230], and (f) tendon-driven soft gripper based on [254].

### 3.3. Control

Deformability and compliance are some of the main characteristics of soft actuators [259], which translate into a large intrinsic number of DoFs. This obviously affects the control system in terms of complexity. Low-level control for soft actuators, which is highly dependent on the soft materials used, can be decentralized to simplify the complexity [260]. For this reason, it is essential, as a design step, to study the passive mechanical dynamics of soft actuators to achieve the desired deformation behaviour [261].

As seen above, there are several soft technologies that have their own implications due to the type of actuator they use. Thus, for example, controlling a servo, actuating a cable in tendon-driven technology, controlling compressors and pressure regulators in FEAs, and controlling the amount of electric charge, electro-adhesion, or a thermal stimulus in SMA actuators are different challenges. The geometry of the actuator also has implications for the control system, as it affects the number of axes and movements that soft actuators can

execute. The widest variety of control philosophies can be found for FEA soft actuators, as summarized in Figure 7.



**Figure 7.** Several control philosophies proposed for FEA-type soft actuators. The control philosophies that have been proposed for a particular type of soft gripper (anthropomorphic or non-anthropomorphic) are presented in blue, while those proposed for both types are shown in green.

Although diverse control strategies have been proposed for FEA-type actuator technology, open-loop control is one of the most frequently used. Several authors [32] report difficulties in controlling certain types of FEA soft actuators due to their deflection around the object. This is especially intricate in anthropomorphic grippers in terms of achieving speed, flexibility and dexterity [191]; not only in FEA actuators but also in passive structures actuated by external motors or tendon motors. This disadvantage can be partially solved by sensing the actuator or by real-time control using FEM [187,262]. On the other hand, tendon-driven soft technology has more mature actuators than pneumatic actuators, and therefore, the control is more straightforward than that of FEAs [237].

#### 4. Challenges of Soft Grippers for Robotic Crop Harvesting

Although a number of different soft actuator technologies have been proposed for various applications, soft grippers for robotic crop harvesting are not yet being sufficiently addressed. This is mainly due to the complexity of the unstructured agricultural environment, the intrinsic challenge posed by soft materials and the need to demonstrate the economic viability of robotic harvesting in the sector. Some of the main barriers that soft robotics, and more particularly soft grippers, face against their possible application in agricultural scenarios are listed below.

- **Design process:** One of the main challenges of soft technology is the design process. A wide diversity of generalist soft grippers can be found in the current state of the art. However, these designs are more focused on achieving new improvements in the field of soft robotics than on developing a specific gripper that solves the issues of the particular field of applications. In terms of robotic crop harvesting, characteristics such as modularity, ease of repair, and the ability to handle food and multiple crops are desired. Apart from this, another gap that needs to be studied is the mathematical model that represents the behaviour of the material in FEM software.

This is directly related to the nature of the various materials used, described in the Materials Subsection.

- **Repeatability:** Another of the main challenges of soft robotics, particular soft grippers, is the need to standardize manufacturing processes. This is the first point to be addressed because it would ensure that the designed soft actuators are suitable for production, facilitating their incorporation into the robotic market. Repeatability studies should research how to mitigate the common effects that appear in soft actuators, such as delamination or interstitial bubbles, that can be the result of faulty manufacturing. To solve these problems, several solutions have been proposed, such as the use of vacuum chambers [227,263–265]. Although positive results from this process have been reported, it is impossible to find a method where, for example, variables such as pressure or time are controlled as a function of volume to ensure the repeatability of the process. Obviously, the method would depend on the material used. On the other hand, in most cases, the manufacturing processes are very hand-made, and therefore, repeatability can be compromised. However, processes based on 3D printing of soft materials, as well as lost wax manufacturing, may become interesting options in the future, given their greater options for achieving repeatability during the manufacturing process.
- **Standard method for determination of soft actuator characteristics:** One of the main gaps that has not yet been addressed in soft actuators is the definition of a method to determine their characteristics. However, it is clear that there is a need for a reliable method that can quantify the soft actuator features to facilitate its evaluation and comparison. Properties such as the contact pressure, contact force, contact area and slip force are crucial for benchmarking and determining room for improvement in this field. Thus, this would not only be useful for selecting the optimal option for each process but also for providing a true picture of the progress of this technology. In the current state of the art, several approaches can be found for the characterization of soft actuators, in which the experimental measurement is always performed with non-standardized objects. However, the proposed methodologies of the studies differ, presenting various approaches, among which the following stand out.
  - The measurement process proposed in [210] consists of grabbing a spherical object connected by an inextensible cable to a force sensor mounted on a motorized platform to measure the slip properties. A similar approach can be seen in [211] but with a six-axis force transducer.
  - Others, such as [218], use a pressure-mapping sensor to obtain the contact force and the pressure. This method offers a reliable measurement for grasping a static object. Grip strength is measured in a similar way to that in the studies mentioned above.
  - In [230], a payload test is presented to obtain the grip strength. Furthermore, the contact pressure is determined by means of FEM software. This last method can give inaccurate solutions due to its dependence on the mathematical model of the material used.
  - Finally, in [266], a deep and detailed analysis is proposed for the measurement of parameters such as grabbing height, pressure and motion acceleration for a soft actuator. In this case, the tests are carried out not only in static but also in dynamic conditions, differentiating between vertical and horizontal positions. Variables such as size, weight and constituent material are also taken into account, as well as the actuation pressure and the grabbing height. Finally, one of the main contributions of this study is the introduction of the handling ratio, which offers a measurable performance comparison.
- **Design of control systems:** Most of the soft grippers that have been proposed use open loop control. All of these grippers also have a low-cost goal associated with them. However, this results in impractical soft grippers that are difficult to implement in the agricultural environment. Their lack of real control of the deformation and



compliance can affect the handling of fruits in different stages of maturity without damaging them. Thus, the study of new control algorithms that take into account the stiffness of the object to be manipulated is essential for the implementation of soft technology in robotic crop harvesting.

- Improvement of energy source systems: Depending on the type of soft actuator used, the energy support required for the gripper can be an electrical source, a pump or air compressor, or a chemical source. In any of these cases, more efficient equipment must be developed to support these technologies. In the literature, descriptions of energy solutions that drive soft-design systems are scarce. Typically, the proposed solutions are suitable for a laboratory or industrial environment, which is far from the unstructured environments of the agricultural sector. Therefore, the development of new energy solutions must be a compromise between functionality and energy consumption. In addition, the optimisation of the system is necessary not only to increase the autonomy of the overall robotic harvester, but also to simplify it, with the aim of enabling its implementation in current agricultural robotics.
- Economic analysis: Economic studies are often the necessary driving force to incentivise research and development in a given area. In the field of Agriculture 4.0, these economic studies can provide information on the most viable way to harvest different crops. However, at present, there is a need for economic research in this field. A study published in 2019 [267] highlights that only 18 investigations in the literature are dedicated to estimating the profitability of crop automation. This affects not only soft robotics but also other automation technologies, hindering its growth in this sector. However, although the lack of research in this direction is noteworthy, it is clear that in certain crops, such as tomatoes and peppers, the labour cost at harvest time represents 30% of the total cost [268,269]. Thus, mechanical harvesting by using soft grippers may be an economically beneficial alternative to manual harvesting [270].

Another challenge, such as the relatively slower actuation speed, is currently addressed in part with the use of pneumatic channels, also known as pneumatic networks [199] or low-pressure actuators [271]. Furthermore, hybrid gripper technology [272], which combines some advantages of soft and hard robotics, may be another potential solution, providing a soft grip and a structural strength capable of withstanding external agents or objects existing in unstructured environments.

## 5. Conclusions

Agriculture mechanization is still in a growth phase. Tasks such as sowing, weeding and harvesting are the spearhead of the development of Agriculture 4.0. Soft robotics is presented as a suitable technology for the manipulation of fruits and vegetables, which are often delicate and easy to mark or bruise and sometimes slippery. This field of robotics can pave the way for the automation of maintenance, harvesting and post-processing tasks in the agro-food industry.

In this article, a detailed review of the latest advancements in the design of novel soft grippers and end-effectors that could be used for robotic harvesting applications is presented. To that end, the current state of automatic picking tasks for several crops is analysed, identifying the main techniques that are commonly used based on the botanical characteristics of the fruits. Since direct harvesting methods based on twisting, bending, pulling, lifting or a combination of them involve the direct contact with the fruits, the introduction of soft grippers for automation of these techniques may represent a significant advantage, allowing a delicate manipulation that guarantees the integrity of fruits. Direct harvesting techniques with an actuation force on the peduncle are also candidates for the introduction of soft gripper technology, provided they are complemented by a suitable cutting tool.

Regarding the material used for the manufacturing of soft grippers, silicone elastomers are attracting strong interest due to their low cost and because they do not require the use of complex machinery or skilled labour. In addition, these compliant materials are also

advantageous when considering the safety of interaction with biological products, making them appropriate candidates for agricultural applications.

It should also be noted that most of the proposed solutions are focused exclusively on the mechanical design, leaving the implementation of the control system for future work. Although diverse control strategies have been proposed for soft actuators, open-loop control is one of the most frequently used. The results of this study also underline that FEA grippers are one of the most promising technologies for robotic harvesting due to their ease of manufacture, compliance and output force. Nevertheless, it is important to note that the implementation of the different soft grippers in agriculture must be associated with the development and improvement in other components of the robotic system, such as artificial vision and navigation.

Furthermore, some of the main challenges that soft grippers still have to overcome to boost is definitive implementation are the design of control systems that consider the stiffness of the fruit to be harvested, the implementation of standardised manufacturing process that guarantee repeatability, the implementation of standard methodologies for the determination of the soft actuators characteristics, and the improvement of the energy sources.

On the other hand, it is important to take into account that the final quality required for fresh market fruits and fruits for the processing industry differs significantly. Soft grippers are presented as the most suitable solution for the harvesting of high value crops, so that mechanical damage is minimised and the products can reach their maximum value in the market. For fruits and vegetables intended for other industrial processing, such as the production of juices, jams and sauces, the economic feasibility of solutions based on soft grippers should be further evaluated. Therefore, future research should be directed to conducting economic studies that provide information on the most viable way to harvest different crops [267], and on the measures that should be taken to minimize losses [273]. Moreover, the study of methods to accurately assess the extent of surface and internal fruit damage caused by excessive external forces should also be addressed [274]. Finally, it would be convenient to carry out studies that analyse the life cycle of soft actuators made with silicone elastomers, to determine if their degradation may leave particles on the products manipulated.

**Author Contributions:** Conceptualization, E.N. and R.F.; methodology, E.N. and P.G.-d.-S.; validation, D.S. and M.A.; formal analysis E.N.; investigation, E.N.; writing—original draft preparation, E.N.; writing—review and editing R.F.; visualization, E.N. and D.S.; supervision R.F.; funding acquisition R.F. and P.G.-d.-S. All authors have read and agreed to the published version of the manuscript.

**Funding:** The research leading to these results has received funding from (i) FEDER/Ministerio de Ciencia, Innovación y Universidades—Agencia Estatal de Investigación/Proyecto ROBOCROP (DPI2017-84253-C2-1-R), (ii) RoboCity2030-DIH-CM, Madrid Robotics Digital Innovation Hub, S2018/NMT-4331, funded by “Programas de Actividades I+D en la Comunidad de Madrid” and cofunded by Structural Funds of the EU, and (iii) CSIC under Grant 202050E099, Proyecto Intramural IAMC-ROBI (Inteligencia Artificial y Mecatrónica Cognitiva para la Manipulación Robótica Bimanual).

**Institutional Review Board Statement:** Not applicable.

**Informed Consent Statement:** Not applicable.

**Conflicts of Interest:** The authors declare no conflict of interest.

## References

1. UN DESA. *United Nations Department of Economic and Social Affairs, Population Division. World Population Prospects: The 2015 Revision, Key Findings and Advance Tables*; Technical Report; Working Paper No. ESA/P/WP. 241; UN DESA: New York, NY, USA, 2015.
2. Vu, Q.; Kuzov, M.; Ronzhin, A. Hierarchical classification of robotic grippers applied for agricultural object manipulations. In *Proceedings of the MATEC Web of Conferences, Samara, Russia, 26–27 November 2018*; Volume 161, p. 03015.

3. Gonzalez-de Santos, P.; Fernández, R.; Sepúlveda, D.; Navas, E.; Emmi, L.; Armada, M. Field Robots for Intelligent Farms—Inhering Features from Industry. *Agronomy* **2020**, *10*, 1638. [[CrossRef](#)]
4. Ito, Y.; Nakano, T. Development and regulation of pedicel abscission in tomato. *Front. Plant Sci.* **2015**, *6*, 442. [[CrossRef](#)] [[PubMed](#)]
5. Zahara, M.; Scheuerman, R. Hand-harvesting jointless vs. jointed-stem tomatoes. *Calif. Agric.* **1988**, *42*, 14.
6. Font, D.; Pallejà, T.; Tresanchez, M.; Runcan, D.; Moreno, J.; Martínez, D.; Teixidó, M.; Palacín, J. A proposal for automatic fruit harvesting by combining a low cost stereovision camera and a robotic arm. *Sensors* **2014**, *14*, 11557–11579. [[CrossRef](#)] [[PubMed](#)]
7. Mehta, S.; Burks, T. Vision-based control of robotic manipulator for citrus harvesting. *Comput. Electron. Agric.* **2014**, *102*, 146–158. [[CrossRef](#)]
8. Cubero, S.; Diago, M.P.; Blasco, J.; Tardáguila, J.; Millán, B.; Aleixos, N. A new method for pedicel/peduncle detection and size assessment of grapevine berries and other fruits by image analysis. *Biosyst. Eng.* **2014**, *117*, 62–72. [[CrossRef](#)]
9. Salinas, C.; Fernández, R.; Montes, H.; Armada, M. A New Approach for Combining Time-of-Flight and RGB Cameras Based on Depth-Dependent Planar Projective Transformations. *Sensors* **2015**, *15*, 24615–24643. [[CrossRef](#)]
10. Sepúlveda, D.; Fernández, R.; Navas, E.; González-de Santos, P.; Armada, M. ROS Framework for Perception and Dual-Arm Manipulation in Unstructured Environments. In Proceedings of the Iberian Robotics Conference, Porto, Portugal, 20–22 November 2019; pp. 137–147.
11. Tabile, R.A.; Godoy, E.P.; Pereira, R.R.; Tangerino, G.T.; Porto, A.J.; Inamasu, R.Y. Design and development of the architecture of an agricultural mobile robot. *Eng. Agric.* **2011**, *31*, 130–142. [[CrossRef](#)]
12. Agostini, A.; Alenya, G.; Fischbach, A.; Scharr, H.; Woergoetter, F.; Torras, C. A cognitive architecture for automatic gardening. *Comput. Electron. Agric.* **2017**, *138*, 69–79. [[CrossRef](#)]
13. Zion, B.; Mann, M.; Levin, D.; Shilo, A.; Rubinstein, D.; Shmulevich, I. Harvest-order planning for a multiarm robotic harvester. *Comput. Electron. Agric.* **2014**, *103*, 75–81. [[CrossRef](#)]
14. Fernández, R.; Montes, H.; Salinas, C. VIS-NIR, SWIR and LWIR Imagery for Estimation of Ground Bearing Capacity. *Sensors* **2015**, *15*, 13994–14015. [[CrossRef](#)]
15. Masuzawa, H.; Miura, J.; Oishi, S. Development of a mobile robot for harvest support in greenhouse horticulture—Person following and mapping. In Proceedings of the 2017 IEEE/SICE International Symposium on System Integration (SII), Taipei, Taiwan, 11–14 December 2017; pp. 541–546. [[CrossRef](#)]
16. Xiong, Y.; Ge, Y.; Grimstad, L.; From, P.J. An autonomous strawberry-harvesting robot: Design, development, integration, and field evaluation. *J. Field Robot.* **2019**, *37*, 202–224. [[CrossRef](#)]
17. Hua, Y.; Zhang, N.; Yuan, X.; Quan, L.; Yang, J.; Nagasaka, K.; Zhou, X.G. Recent Advances in Intelligent Automated Fruit Harvesting Robots. *Open Agric. J.* **2019**, *13*, 101–106. [[CrossRef](#)]
18. Navas, E.; Fernández, R.; Sepúlveda, D.; Armada, M.; Gonzalez-de Santos, P. Modular dual-arm robot for precision harvesting. In Proceedings of the Iberian Robotics Conference, Porto, Portugal, 20–22 November 2019; pp. 148–158.
19. Zhang, B.; Xie, Y.; Zhou, J.; Wang, K.; Zhang, Z. State-of-the-art robotic grippers, grasping and control strategies, as well as their applications in agricultural robots: A review. *Comput. Electron. Agric.* **2020**, *177*, 105694. [[CrossRef](#)]
20. Ozawa, R.; Tahara, K. Grasp and dexterous manipulation of multi-fingered robotic hands: a review from a control view point. *Adv. Robot.* **2017**, *31*, 1030–1050. [[CrossRef](#)]
21. King, J.P.; Bauer, D.; Schlagenhauf, C.; Chang, K.H.; Moro, D.; Pollard, N.; Coros, S. Design, fabrication, and evaluation of tendon-driven multi-fingered foam hands. In Proceedings of the 2018 IEEE-RAS 18th International Conference on Humanoid Robots (Humanoids), Beijing, China, 6–9 November 2018; pp. 1–9.
22. Mizushima, K.; Oku, T.; Suzuki, Y.; Tsuji, T.; Watanabe, T. Multi-fingered robotic hand based on hybrid mechanism of tendon-driven and jamming transition. In Proceedings of the 2018 IEEE International Conference on Soft Robotics (RoboSoft), Livorno, Italy, 24–28 April 2018; pp. 376–381.
23. Vulliez, P.; Gazeau, J.P.; Laguillaumie, P.; Mnyusiwalla, H.; Seguin, P. Focus on the mechatronics design of a new dexterous robotic hand for inside hand manipulation. *Robotica* **2018**, *36*, 1206–1224. [[CrossRef](#)]
24. Blanes, C.; Mellado, M.; Ortiz, C.; Valera, A. Technologies for robot grippers in pick and place operations for fresh fruits and vegetables. *Span. J. Agric. Res.* **2011**, *9*, 1130–1141. [[CrossRef](#)]
25. Morales, R.; Badesa, F.; Garcia-Aracil, N.; Sabater, J.; Zollo, L. Soft robotic manipulation of onions and artichokes in the food industry. *Adv. Mech. Eng.* **2014**, *6*, 345291. [[CrossRef](#)]
26. Chu, C.Y.; Patterson, R.M. Soft robotic devices for hand rehabilitation and assistance: a narrative review. *J. Neuroeng. Rehabil.* **2018**, *15*, 9. [[CrossRef](#)]
27. Cianchetti, M.; Laschi, C.; Menciassi, A.; Dario, P. Biomedical applications of soft robotics. *Nat. Rev. Mater.* **2018**, *3*, 143–153. [[CrossRef](#)]
28. Awad, L.N.; Bae, J.; O’donnell, K.; De Rossi, S.M.; Hendron, K.; Sloop, L.H.; Kudzia, P.; Allen, S.; Holt, K.G.; Ellis, T.D. A soft robotic exosuit improves walking in patients after stroke. *Sci. Transl. Med.* **2017**, *9*, eaai9084. [[CrossRef](#)] [[PubMed](#)]
29. Roche, E.T.; Horvath, M.A.; Wamala, I.; Alazmani, A.; Song, S.E.; Whyte, W.; Machaidze, Z.; Payne, C.J.; Weaver, J.C.; Fishbein, G. Soft robotic sleeve supports heart function. *Sci. Transl. Med.* **2017**, *9*, eaaf3925. [[CrossRef](#)] [[PubMed](#)]
30. Polygerinos, P.; Wang, Z.; Galloway, K.C.; Wood, R.J.; Walsh, C.J. Soft robotic glove for combined assistance and at-home rehabilitation. *Robot. Auton. Syst.* **2015**, *73*, 135–143. [[CrossRef](#)]

31. Díaz, C.E.; Fernández, R.; Armada, M.; Gutiérrez, F.d.J.G. State of the art in robots used in minimally invasive surgeries. Natural orifice transluminal surgery (NOTES) as a particular case. *Ind. Robot. Int. J.* **2015**, *42*, 508–532. [\[CrossRef\]](#)
32. Polygerinos, P.; Correll, N.; Morin, S.A.; Mosadegh, B.; Onal, C.D.; Petersen, K.; Cianchetti, M.; Tolley, M.T.; Shepherd, R.F. Soft robotics: Review of fluid-driven intrinsically soft devices; manufacturing, sensing, control, and applications in human-robot interaction. *Adv. Eng. Mater.* **2017**, *19*, 1700016. [\[CrossRef\]](#)
33. Lee, C.; Kim, M.; Kim, Y.J.; Hong, N.; Ryu, S.; Kim, H.J.; Kim, S. Soft robot review. *Int. J. Control. Autom. Syst.* **2017**, *15*, 3–15. [\[CrossRef\]](#)
34. Sanders, K. Orange harvesting systems review. *Biosyst. Eng.* **2005**, *90*, 115–125. [\[CrossRef\]](#)
35. Li, P.; Lee, S.h.; Hsu, H.Y. Review on fruit harvesting method for potential use of automatic fruit harvesting systems. *Procedia Eng.* **2011**, *23*, 351–366. [\[CrossRef\]](#)
36. Srivastava, A.K.; Goering, C.E.; Rohrbach, R.P.; Buckmaster, D.R. *Engineering Principles of Agricultural Machines*; ASABE: St. Joseph, MI, USA, 1993.
37. Nasini, L.; Proietti, P. Olive harvesting. In *The Extra-Virgin Olive Oil Handbook*; John Wiley & Sons: Hoboken, NJ, USA, 2014; pp. 87–105.
38. Polat, R.; Guner, M.; Dursun, E.; Erdogan, D.; Gezer, I.; Bilim, H.C. Mechanical harvesting of almond with an inertia type limb shaker. *Asian J. Plant Sci.* **2007**, *6*, 528–532. [\[CrossRef\]](#)
39. Polat, R.; Gezer, I.; Guner, M.; Dursun, E.; Erdogan, D.; Bilim, H.C. Mechanical harvesting of pistachio nuts. *J. Food Eng.* **2007**, *79*, 1131–1135. [\[CrossRef\]](#)
40. Dimeas, F.; Sako, D.V.; Moulaniotis, V.C.; Aspragathos, N.A. Design and fuzzy control of a robotic gripper for efficient strawberry harvesting. *Robotica* **2015**, *33*, 1085–1098. [\[CrossRef\]](#)
41. Hayashi, S.; Shigematsu, K.; Yamamoto, S.; Kobayashi, K.; Kohno, Y.; Kamata, J.; Kurita, M. Evaluation of a strawberry-harvesting robot in a field test. *Biosyst. Eng.* **2010**, *105*, 160–171. [\[CrossRef\]](#)
42. De-An, Z.; Jidong, L.; Wei, J.; Ying, Z.; Yu, C. Design and control of an apple harvesting robot. *Biosyst. Eng.* **2011**, *110*, 112–122. [\[CrossRef\]](#)
43. Baeten, J.; Donné, K.; Boedrij, S.; Beckers, W.; Claesen, E. Autonomous fruit picking machine: A robotic apple harvester. In *Field and Service Robotics*; Springer: Berlin/Heidelberg, Germany, 2008; pp. 531–539.
44. Li, J.; Karkee, M.; Zhang, Q.; Xiao, K.; Feng, T. Characterizing apple picking patterns for robotic harvesting. *Comput. Electron. Agric.* **2016**, *127*, 633–640. [\[CrossRef\]](#)
45. Davidson, J.R.; Silwal, A.; Hohimer, C.J.; Karkee, M.; Mo, C.; Zhang, Q. Proof-of-concept of a robotic apple harvester. In Proceedings of the 2016 IEEE/RSJ International Conference on Intelligent Robots and Systems (IROS), Daejeon, Korea, 9–14 October 2016; pp. 634–639.
46. Monta, M.; Kondo, N.; Ting, K.C. End-effectors for tomato harvesting robot. In *Artificial Intelligence for Biology and Agriculture*; Springer: Berlin/Heidelberg, Germany, 1998; pp. 1–25.
47. Yaguchi, H.; Nagahama, K.; Hasegawa, T.; Inaba, M. Development of an autonomous tomato harvesting robot with rotational plucking gripper. In Proceedings of the 2016 IEEE/RSJ International Conference on Intelligent Robots and Systems (IROS), Daejeon, Korea, 9–14 October 2016; pp. 652–657.
48. Li, Z.; Li, P.; Yang, H.; Wang, Y. Stability tests of two-finger tomato grasping for harvesting robots. *Biosyst. Eng.* **2013**, *116*, 163–170. [\[CrossRef\]](#)
49. Zhao, Y.; Gong, L.; Liu, C.; Huang, Y. Dual-arm robot design and testing for harvesting tomato in greenhouse. *IFAC PapersOnLine* **2016**, *49*, 161–165. [\[CrossRef\]](#)
50. Hayashi, S.; Ganno, K.; Ishii, Y.; Tanaka, I. Robotic harvesting system for eggplants. *Jpn. Agric. Res. Q.* **2002**, *36*, 163–168. [\[CrossRef\]](#)
51. Sepúlveda, D.; Fernández, R.; Navas, E.; Armada, M.; González-De-Santos, P. Robotic aubergine harvesting using dual-arm manipulation. *IEEE Access* **2020**, *8*, 121889–121904. [\[CrossRef\]](#)
52. Edan, Y.; Rogozin, D.; Flash, T.; Miles, G.E. Robotic melon harvesting. *IEEE Trans. Robot. Autom.* **2000**, *16*, 831–835. [\[CrossRef\]](#)
53. Muscato, G.; Prestifilippo, M.; Abbate, N.; Rizzuto, I. A prototype of an orange picking robot: past history, the new robot and experimental results. *Ind. Robot. Int. J.* **2005**, *32*, 128–138. [\[CrossRef\]](#)
54. Van Henten, E.J.; Hemming, J.; Van Tuijl, B.; Kornet, J.; Meuleman, J.; Bontsema, J.; Van Os, E. An autonomous robot for harvesting cucumbers in greenhouses. *Auton. Robot.* **2002**, *13*, 241–258. [\[CrossRef\]](#)
55. Hemming, J.; Bac, C.; Van Tuijl, B.; Barth, R.; Bontsema, J.; Pekkeriet, E.; Van Henten, E. A robot for harvesting sweet-pepper in greenhouses. In Proceedings of the International Conference of Agricultural Engineering, Zurich, Switzerland, 6–10 July 2014.
56. Bac, C.W.; Hemming, J.; Van Tuijl, B.; Barth, R.; Wais, E.; Van Henten, E.J. Performance evaluation of a harvesting robot for sweet pepper. *J. Field Robot.* **2017**, *34*, 1123–1139. [\[CrossRef\]](#)
57. Lehnert, C.; English, A.; McCool, C.; Tow, A.W.; Perez, T. Autonomous sweet pepper harvesting for protected cropping systems. *IEEE Robot. Autom. Lett.* **2017**, *2*, 872–879. [\[CrossRef\]](#)
58. Tong, J.; Zhang, Q.; Karkee, M.; Jiang, H.; Zhou, J. Understanding the dynamics of hand picking patterns of fresh market apples. In Proceedings of the 2014 Montreal, Quebec, QC, Canada, 13–16 July 2014; p. 1.
59. Moreno, R.; Torregrosa, A.; Molto, E.; Chueca, P. Effect of harvesting with a trunk shaker and an abscission chemical on fruit detachment and defoliation of citrus grown under Mediterranean conditions. *Span. J. Agric. Res.* **2015**, *13*, 1–12. [\[CrossRef\]](#)

60. Sarig, Y. Robotics of fruit harvesting: A state-of-the-art review. *J. Agric. Eng. Res.* **1993**, *54*, 265–280. [CrossRef]
61. Bulanon, D.M.; Kataoka, T. Fruit detection system and an end effector for robotic harvesting of Fuji apples. *Agric. Eng. Int. CIGR J.* **2010**, *12*, 203–210.
62. Mao, L.; Begum, D.; Chuang, H.w.; Budiman, M.A.; Szymkowiak, E.J.; Irish, E.E.; Wing, R.A. JOINTLESS is a MADS-box gene controlling tomato flower abscissionzone development. *Nature* **2000**, *406*, 910–913. [CrossRef]
63. Erkan, M.; Dogan, A. Harvesting of horticultural commodities. In *Postharvest Technology of Perishable Horticultural Commodities*; Elsevier: Amsterdam, The Netherlands, 2019; pp. 129–159.
64. Chen, X.; Chaudhary, K.; Tanaka, Y.; Nagahama, K.; Yaguchi, H.; Okada, K.; Inaba, M. Reasoning-based vision recognition for agricultural humanoid robot toward tomato harvesting. In Proceedings of the 2015 IEEE/RSJ International Conference on Intelligent Robots and Systems (IROS), Hamburg, Germany, 28 September–2 October 2015; pp. 6487–6494.
65. Mu, L.; Cui, G.; Liu, Y.; Cui, Y.; Fu, L.; Gejima, Y. Design and simulation of an integrated end-effector for picking kiwifruit by robot. *Inf. Process. Agric.* **2020**, *7*, 58–71. [CrossRef]
66. De Preter, A.; Anthonis, J.; De Baerdemaeker, J. Development of a robot for harvesting strawberries. *IFAC PapersOnLine* **2018**, *51*, 14–19. [CrossRef]
67. Huang, Z.; Sklar, E.; Parsons, S. Design of Automatic Strawberry Harvest Robot Suitable in Complex Environments. In Proceedings of the 2020 ACM/IEEE International Conference on Human-Robot Interaction, Cambridge, UK, 23–26 March 2020; pp. 567–569.
68. Li, Z.; Miao, F.; Yang, Z.; Wang, H. An anthropometric study for the anthropomorphic design of tomato-harvesting robots. *Comput. Electron. Agric.* **2019**, *163*, 104881. [CrossRef]
69. Prasad, J.; Gupta, C. Mechanical properties of maize stalk as related to harvesting. *J. Agric. Eng. Res.* **1975**, *20*, 79–87. [CrossRef]
70. Kronbergs, E. Mechanical strength testing of stalk materials and compacting energy evaluation. *Ind. Crop. Prod.* **2000**, *11*, 211–216. [CrossRef]
71. Yu, M.; Womac, A.; Igathinathane, C.; Ayers, P.; Buschermohle, M. Switchgrass ultimate stresses at typical biomass conditions available for processing. *Biomass Bioenergy* **2006**, *30*, 214–219. [CrossRef]
72. Tavakoli, H.; Mohtasebi, S.; Jafari, A. Comparison of mechanical properties of wheat and barley straw. *Agric. Eng. Int. CIGR J.* **2008**, *10*, 1–9.
73. Mou, X.; Liu, Q.; Ou, Y.; Wang, M.; Song, J. Mechanical properties of the leaf sheath of sugarcane. *Trans. ASABE* **2013**, *56*, 801–812.
74. Yu, M.; Cannayen, I.; Hendrickson, J.; Sanderson, M.; Liebig, M. Mechanical shear and tensile properties of selected biomass stems. *Trans. ASABE* **2014**, *57*, 1231–1242.
75. Navas, E.; Fernandez, R.; Sepúlveda, D.; Armada, M.; Gonzalez-de Santos, P. A Design Criterion Based on Shear Energy Consumption for Robotic Harvesting Tools. *Agronomy* **2020**, *10*, 734. [CrossRef]
76. Liu, J.; Li, Z.; Li, P.; Mao, H. Design of a laser stem-cutting device for harvesting robot. In Proceedings of the 2008 IEEE International Conference on Automation and Logistics, Qingdao, China, 1–3 September 2008; pp. 2370–2374.
77. Jia, B.; Zhu, A.; Yang, S.X.; Mittal, G.S. Integrated gripper and cutter in a mobile robotic system for harvesting greenhouse products. In Proceedings of the 2009 IEEE International Conference on Robotics and Biomimetics (ROBIO), Guilin, China, 19–23 December 2009; pp. 1778–1783.
78. Ceccarelli, M.; Figliolini, G.; Ottaviano, E.; Mata, A.S.; Criado, E.J. Designing a robotic gripper for harvesting horticulture products. *Robotica* **2000**, *18*, 105–111. [CrossRef]
79. Bachche, S.; Oka, K. Performance testing of thermal cutting systems for sweet pepper harvesting robot in greenhouse horticulture. *J. Syst. Des. Dyn.* **2013**, *7*, 36–51. [CrossRef]
80. Chunchu G., Chunchu C., Aguirre, Z.H. *Anatomía y Morfología Vegetal*; University of Nebraska de Loja: Loja, Ecuador, 2019.
81. Encyclopædia Britannica, 1993. Available online: <https://www.britannica.com/> (accessed on 10 April 2021).
82. Morris, W. *American Heritage Dictionary of the English Language*; American Heritage Pub. Co.: Rockville, MD, USA, 1969.
83. FAO. *Prevenición de Pérdidas de Alimentos Poscosecha: Frutas, Hortalizas, Raíces y Tubérculos. Manual de Capacitación*; FAO: Rome, Italy, 1993; Volume 2.
84. Erdoğan, D.; Güner, M.; Dursun, E.; Gezer, I. Mechanical harvesting of apricots. *Biosyst. Eng.* **2003**, *85*, 19–28. [CrossRef]
85. Mira, A.T.; Chaparro, O.; Górriz, B.M.; Ortiz, C.; Bernad, J.; Ortí, E.; Gil, J.; Pérez, M. Design, construction and testing of an apricot tractor-trailed harvester. *Span. J. Agric. Res.* **2008**, *3*, 333–340.
86. Crandall, P.C. *Bramble Production: The Management and Marketing of Raspberries and Blackberries*; CRC Press: Boca Raton, FL, USA, 1995.
87. Santinato, F.; SILVA, R.P.D.; Silva, V.D.A.; SILVA, C.D.D.; Tavares, T.D.O. Mechanical harvesting of coffee in high slope. *Rev. Caatinga* **2016**, *29*, 685–691. [CrossRef]
88. Aristizábal, I.; Oliveros, C.; Alvarez, F. Mechanical harvest of coffee applying circular and multidirectional vibrations. In Proceedings of the 2000 ASAE Annual International Meeting, Milwaukee, WI, USA, 9–12 July 2000; pp. 1–14.
89. Halderson, J.L. Fundamental factors in mechanical cherry harvesting. *Trans. ASAE* **1966**, *9*, 681–684. [CrossRef]
90. Norton, R.; Claypool, L.; Leonard, S.; Adrian, P.; Fridley, R.; Charles, F. Mechanical harvesting of sweet cherries: 1961 tests show promise and problems. *Calif. Agric.* **1962**, *16*, 8–10.
91. Peterson, D.; Wolford, S. Mechanical harvester for fresh market quality stemless sweet cherries. *Trans. ASAE* **2001**, *44*, 481. [CrossRef]



92. Zhou, J.; He, L.; Du, X.; Chen, D.; Zhang, Q.; Karkee, M. Dynamic response of sweet cherry tree to the vibration of a limb shaker. In Proceedings of the American Society of Agricultural and Biological Engineers, Dallas, TX, USA, 29 July–1 August 2012; p. 1.
93. Chen, D.; Du, X.; Zhang, Q.; Whiting, M.; Scharf, P.; Wang, S. Performance evaluation of mechanical cherry harvesters for fresh market grade fruits. *Appl. Eng. Agric.* **2012**, *28*, 483–489. [[CrossRef](#)]
94. Zhou, J.; He, L.; Zhang, Q.; Du, X.; Chen, D.; Karkee, M. Evaluation of the influence of shaking frequency and duration in mechanical harvesting of sweet cherry. *Appl. Eng. Agric.* **2013**, *29*, 607–612.
95. He, L.; Zhou, J.; Du, X.; Chen, D.; Zhang, Q.; Karkee, M. Energy efficacy analysis of a mechanical shaker in sweet cherry harvesting. *Biosyst. Eng.* **2013**, *116*, 309–315. [[CrossRef](#)]
96. Tanigaki, K.; Fujiura, T.; Akase, A.; Imagawa, J. Cherry-harvesting robot. *Comput. Electron. Agric.* **2008**, *63*, 65–72. [[CrossRef](#)]
97. Amatya, S.; Karkee, M.; Zhang, Q.; Whiting, M.D. Automated detection of branch shaking locations for robotic cherry harvesting using machine vision. *Robotics* **2017**, *6*, 31. [[CrossRef](#)]
98. Dubey, A.P.; Pattnaik, S.M.; Banerjee, A.; Sarkar, R.; Kumar, S. Autonomous control and implementation of coconut tree climbing and harvesting robot. *Procedia Comput. Sci.* **2016**, *85*, 755–766. [[CrossRef](#)]
99. CCS, M.S.G.; Srinath, P.; Karthikeyan, P. Automatic Coconut Harvesting System. *J. Adv. Res. Embed. Syst.* **2018**, *5*, 1–7.
100. He, Z.L.; Xiong, J.T.; Lin, R.; Zou, X.; Tang, L.Y.; Yang, Z.G.; Liu, Z.; Song, G. A method of green litchi recognition in natural environment based on improved LDA classifier. *Comput. Electron. Agric.* **2017**, *140*, 159–167. [[CrossRef](#)]
101. Xiong, J.; Lin, R.; Liu, Z.; He, Z.; Tang, L.; Yang, Z.; Zou, X. The recognition of litchi clusters and the calculation of picking point in a nocturnal natural environment. *Biosyst. Eng.* **2018**, *166*, 44–57. [[CrossRef](#)]
102. Guo, Q.; Chen, Y.; Tang, Y.; Zhuang, J.; He, Y.; Hou, C.; Chu, X.; Zhong, Z.; Luo, S. Lychee fruit detection based on monocular machine vision in orchard environment. *Sensors* **2019**, *19*, 4091. [[CrossRef](#)] [[PubMed](#)]
103. Li, J.; Tang, Y.; Zou, X.; Lin, G.; Wang, H. Detection of Fruit-bearing Branches and Localization of Litchi Clusters for Vision-based Harvesting Robots. *IEEE Access* **2020**, *8*, 117746–117758. [[CrossRef](#)]
104. Parameswarakumar, M.; Gupta, C.P. Design parameters for vibratory mango harvesting system. *Trans. ASAE* **1991**, *34*, 14–20. [[CrossRef](#)]
105. Hao, H.; Yan, Z.; Dong, L. Design of Mango Picking Machine. *J. Anhui Agric. Sci.* **2012**, *40*, 590–591.
106. Jiuxin, L.; Yan, Z.; Yulan, L.; Dong, L. Research Control System of Mango Picking Machine Based on the PLC. *J. Agric. Mech. Res.* **2012**, *34*, 187–189.
107. Lian, X.W.; Liang, D.; Zhang, Y. *The Design Based on the Hydraulic Control of the Mango Picking Machine*; Advanced Materials Research; Trans Tech Publications: Bäch, Switzerland, 2012; Volume 479, pp. 1468–1475.
108. Konam, S. Agricultural aid for mango cutting (AAM). In Proceedings of the 2014 International Conference on Advances in Computing, Communications and Informatics (ICACCI), Delhi, India, 24–27 September 2014; pp. 1520–1524.
109. Stein, M.; Bargoti, S.; Underwood, J. Image based mango fruit detection, localisation and yield estimation using multiple view geometry. *Sensors* **2016**, *16*, 1915. [[CrossRef](#)]
110. Font, D.; Tresanchez, M.; Pallejà, T.; Teixidó, M.; Martínez, D.; Moreno, J.; Palacín, J. An image processing method for in-line nectarine variety verification based on the comparison of skin feature histogram vectors. *Comput. Electron. Agric.* **2014**, *102*, 112–119. [[CrossRef](#)]
111. Antognozzi, E.; Cartechini, A.; Tombesi, A.; Proietti, P. Effect of cultivar and vibration characteristics on mechanical harvesting of olives. *Int. Symp. Olive Grow.* **1989**, *286*, 417–420. [[CrossRef](#)]
112. Antognozzi, E.; Cartechini, A.; Tombesi, A.; Palliotti, A. Transmission and efficiency of vibrations on ‘Moraiolo’ olive harvesting. *Int. Symp. Olive Grow.* **1989**, *286*, 413–416.
113. Martin, G.C. Mechanical olive harvest: use of fruit loosening agents. *II Int. Symp. Olive Grow.* **1993**, *356*, 284–291. [[CrossRef](#)]
114. Bentaher, H.; Rouina, B.B. Mechanical harvesting of “Chemlali de Sfax” olive-trees. *IV Int. Symp. Olive Grow.* **2000**, *586*, 365–368.
115. Sessiz, A.; Özcan, M. Olive removal with pneumatic branch shaker and abscission chemical. *J. Food Eng.* **2006**, *76*, 148–153. [[CrossRef](#)]
116. Torregrosa, A.; Martín, B.; Brunton, J.G.; Bernad, J. Mechanical harvesting of processed peaches. *Appl. Eng. Agric.* **2008**, *24*, 723–729. [[CrossRef](#)]
117. Liu, Y.; Chen, B.; Qiao, J. Development of a machine vision algorithm for recognition of peach fruit in a natural scene. *Trans. ASABE* **2011**, *54*, 695–702. [[CrossRef](#)]
118. Alosaimi, W.; Alyami, H.; Uddin, M.I. PeachNet: Peach Diseases Detection for Automatic Harvesting. *Comput. Mater. Contin.* **2021**, *67*, 1665–1677. [[CrossRef](#)]
119. Brown, J.; Sukkariéh, S. Design and evaluation of a modular robotic plum harvesting system utilizing soft components. *J. Field Robot.* **2021**, *38*, 289–306. [[CrossRef](#)]
120. Patzlaff, A.W. Beater Assembly for Raspberry Harvester. U.S. Patent 3,611,689, 12 October 1971.
121. Patzlaff, A.W. Raspberry Harvester. U.S. Patent 3,703,072, 21 November 1972.
122. Vasconez, J.P.; Guevara, L.; Cheein, F.A. Social robot navigation based on HRI non-verbal communication: a case study on avocado harvesting. In Proceedings of the 34th ACM/SIGAPP Symposium on Applied Computing, Limassol, Cyprus, 8–12 April 2019; pp. 957–960.
123. Richard, P. *Development of a Mechanical Harvester for Lowbush Blueberries*; ESRI: Redlands, CA, USA, 1982.



124. Saito, Y.; Hatanaka, T.; Uosaki, K.; Shigeto, K. Eggplant classification using artificial neural network. In Proceedings of the International Joint Conference on Neural Networks, Portland, OR, USA, 20–24 July 2003; Volume 2, pp. 1013–1018.
125. Shaulis, N.; Shepardson, E.S.; Jordan, T.D. *Geneva Double Curtain for Concord Grapes*; New York State Agricultural Experiment Station: Geneva, NY, USA, 1966.
126. Shepardson, E.; Shaulis, N.; Moyer, J. Mechanical harvesting of grape varieties grown in New York State. In *Fruit and Vegetable Harvest Mechanization: Technological Implications*; Cargill, B.F., Rossmiller, G.E., Eds.; Rural Manpower Center, Michigan State University: East Lansing, MI, USA, 1969; pp. 571–577.
127. Studer, H.; Olmo, H. Mechanical harvesting of grapes in California: cultural practices and machines. In *Fruit and Vegetable Harvest Mechanization: Technological Implications*; Cargill, B.T., Rossmiller, G.E., Eds.; Michigan State University: East Lansing, MI, USA, 1969; pp. 611–621.
128. Pezzi, F.; Caprara, C. Mechanical grape harvesting: Investigation of the transmission of vibrations. *Biosyst. Eng.* **2009**, *103*, 281–286. [[CrossRef](#)]
129. Monta, M.; Kondo, N.; Shibano, Y. Agricultural robot in grape production system. In Proceedings of 1995 IEEE International Conference on Robotics and Automation, Nagoya, Japan, 21–27 May 1995; Volume 3, pp. 2504–2509.
130. Luo, L.; Tang, Y.; Zou, X.; Wang, C.; Zhang, P.; Feng, W. Robust grape cluster detection in a vineyard by combining the AdaBoost framework and multiple color components. *Sensors* **2016**, *16*, 2098. [[CrossRef](#)] [[PubMed](#)]
131. Lin, G.; Tang, Y.; Zou, X.; Xiong, J.; Li, J. Guava detection and pose estimation using a low-cost RGB-D sensor in the field. *Sensors* **2019**, *19*, 428. [[CrossRef](#)] [[PubMed](#)]
132. Chen, J.; Wang, H.; Jiang, H.; Gao, H.; Lei, W.; Dang, G. Design of end-effector for kiwifruit harvesting robot. *Trans. Chin. Soc. Agric. Mach.* **2012**, *43*, 151–199.
133. Mu, L.; Liu, Y.; Cui, Y.; Liu, H.; Chen, L.; Fu, L.; Gejima, Y. Design of end-effector for kiwifruit harvesting robot experiment. In Proceedings of the 2017 ASABE Annual International Meeting, American Society of Agricultural and Biological Engineers, Spokane, WA, USA, 16–19 July 2017; p. 1.
134. Williams, H.A.; Jones, M.H.; Nejadi, M.; Seabright, M.J.; Bell, J.; Penhall, N.D.; Barnett, J.J.; Duke, M.D.; Scarfe, A.J.; Ahn, H.S.; et al. Robotic kiwifruit harvesting using machine vision, convolutional neural networks, and robotic arms. *Biosyst. Eng.* **2019**, *181*, 140–156. [[CrossRef](#)]
135. BAI, Z.y.; ZHANG, Y. Research on Picking Machine of Papaya. *Hubei Agric. Sci.* **2015**, *2015*, 59.
136. Tu, S.; Xue, Y.; Zheng, C.; Qi, Y.; Wan, H.; Mao, L. Detection of passion fruits and maturity classification using Red-Green-Blue Depth images. *Biosyst. Eng.* **2018**, *175*, 156–167. [[CrossRef](#)]
137. Kitamura, S.; Oka, K. Recognition and cutting system of sweet pepper for picking robot in greenhouse horticulture. In Proceedings of the IEEE International Conference Mechatronics and Automation, Niagara Falls, ON, Canada, 29 July–1 August 2005; Volume 4, pp. 1807–1812.
138. Bac, C.W. *Improving Obstacle Awareness for Robotic Harvesting of Sweet-Pepper*; Wageningen University: Wageningen, The Netherlands, 2015.
139. Arad, B.; Balendonck, J.; Barth, R.; Ben-Shahar, O.; Edan, Y.; Hellström, T.; Hemming, J.; Kurtser, P.; Ringdahl, O.; Tielen, T.; et al. Development of a sweet pepper harvesting robot. *J. Field Robot.* **2020**, *37*, 1027–1039. [[CrossRef](#)]
140. Vitzrabin, E.; Edan, Y. Adaptive thresholding with fusion using a RGBD sensor for red sweet-pepper detection. *Biosyst. Eng.* **2016**, *146*, 45–56. [[CrossRef](#)]
141. Sa, L.; Lehnert, C.; English, A.; McCool, C.; Dayoub, F.; Upcroft, B.; Perez, T. Peduncle detection of sweet pepper for autonomous crop harvesting—Combined color and 3-D information. *IEEE Robot. Autom. Lett.* **2017**, *2*, 765–772. [[CrossRef](#)]
142. Kim, S.; Park, S.; Kim, C.; Kim, C.; Lee, C.; Jy, R. Development of a Persimmon Harvesting System. In Proceedings of the Korean Society for Agricultural Machinery Conference. Korean Society for Agricultural Machinery, Seoul, Korea, 19–22 October 2000; pp. 472–479.
143. Mohammadi, V.; Kheiralipour, K.; Ghasemi-Varnamkhasi, M. Detecting maturity of persimmon fruit based on image processing technique. *Sci. Hortic.* **2015**, *184*, 123–128. [[CrossRef](#)]
144. Li, X.; Qin, Y.; Wang, F.; Guo, F.; Yeow, J.T. Pitaya detection in orchards using the MobileNet-YOLO model. In Proceedings of the 2020 39th Chinese Control Conference (CCC), Shenyang, China, 27–29 July 2020; pp. 6274–6278.
145. Jafari, A.; Bakhshipour, A. A novel algorithm to recognize and locate pomegranate on the tree for a harvesting robot using a stereo vision system. In *Proceedings of the Precision Agriculture*; ResearchGate: Berlin, Germany, 2011.
146. Yeshmukhametov, A.; Koganezawa, K.; Buribayev, Z.; Amirgaliyev, Y.; Yamamoto, Y. Development of Continuum Robot Arm and Gripper for Harvesting Cherry Tomatoes. *Preprints* **2019**. [[CrossRef](#)]
147. Kondo, N.; Yata, K.; Iida, M.; Shiigi, T.; Monta, M.; Kurita, M.; Omori, H. Development of an end-effector for a tomato cluster harvesting robot. *Eng. Agric. Environ. Food* **2010**, *3*, 20–24. [[CrossRef](#)]
148. Arefi, A.; Motlagh, A.M.; Mollazade, K.; Teimourlou, R.F. Recognition and localization of ripen tomato based on machine vision. *Aust. J. Crop. Sci.* **2011**, *5*, 1144–1149.
149. Villaseñor-Aguilar, M.J.; Botello-Álvarez, J.E.; Pérez-Pinal, F.J.; Cano-Lara, M.; León-Galván, M.F.; Bravo-Sánchez, M.G.; Barranco-Gutiérrez, A.I. Fuzzy classification of the maturity of the tomato using a vision system. *J. Sens.* **2019**, *2019*, 3175848. [[CrossRef](#)]
150. Yuan, T.; Lv, L.; Zhang, F.; Fu, J.; Gao, J.; Zhang, J.; Li, W.; Zhang, C.; Zhang, W. Robust cherry tomatoes detection algorithm in greenhouse scene based on SSD. *Agriculture* **2020**, *10*, 160. [[CrossRef](#)]

151. Qiang, L.; Liqin, Y.; Wei, A. The suitable working of wolfberry harvest machine. *J. Agric. Mech. Res.* **2009**, *6*, 126–128.
152. Bing, Z.; Jing, H. Design of simulate hand wolfberry picking machine. *Trans. Chin. Soc. Agric. Eng.* **2011**, *26*, 13–17.
153. Lvcheng, W.; Junmei, T.; Xiaopeng, W.; Tao, L. Wolfberry classification method based on machine vision. *Comput. Eng. Appl.* **2013**, *2013*, 24.
154. Pellerin, R.; Millier, W.; Lakso, A.; Rehkugler, G.; Throop, J. Apple harvesting with an inertial vs. impulse trunk shaker on open-center and central-leader trees—Part II. *Trans. ASAE* **1979**, *22*, 983–988. [[CrossRef](#)]
155. Davidson, J.R.; Hohimer, C.J.; Mo, C.; Karkee, M. Dual robot coordination for apple harvesting. In Proceedings of the 2017 ASABE Annual International Meeting, American Society of Agricultural and Biological Engineers, Spokane, WA, USA, 16–19 July 2017; p. 1.
156. Silwal, A.; Davidson, J.R.; Karkee, M.; Mo, C.; Zhang, Q.; Lewis, K. Design, integration, and field evaluation of a robotic apple harvester. *J. Field Robot.* **2017**, *34*, 1140–1159. [[CrossRef](#)]
157. Guoli, L.; Changying, J.; Baoxing, G.; Weiyue, X.; Mang, D. Kinematics analysis and experiment of apple harvesting robot manipulator with multiple end-effectors. *Trans. Chin. Soc. Agric. Mach* **2016**, *47*, 14–29.
158. Ji, W.; Zhao, D.; Cheng, F.; Xu, B.; Zhang, Y.; Wang, J. Automatic recognition vision system guided for apple harvesting robot. *Comput. Electr. Eng.* **2012**, *38*, 1186–1195. [[CrossRef](#)]
159. Kang, H.; Chen, C. Fast implementation of real-time fruit detection in apple orchards using deep learning. *Comput. Electron. Agric.* **2020**, *168*, 105108. [[CrossRef](#)]
160. Ying, Y.; Jing, H.; Tao, Y.; Zhang, N. Detecting stem and shape of pears using Fourier transformation and an artificial neural network. *Trans. ASAE* **2003**, *46*, 157–162. [[CrossRef](#)]
161. Fu, L.; Duan, J.; Zou, X.; Lin, G.; Song, S.; Ji, B.; Yang, Z. Banana detection based on color and texture features in the natural environment. *Comput. Electron. Agric.* **2019**, *167*, 105057. [[CrossRef](#)]
162. Zhang, L.; Yang, Q.; Xun, Y.; Chen, X.; Ren, Y.; Yuan, T.; Tan, Y.; Li, W. Recognition of greenhouse cucumber fruit using computer vision. *N. Z. J. Agric. Res.* **2007**, *50*, 1293–1298. [[CrossRef](#)]
163. Fernandez, R.; Montes, H.; Surdilovic, J.; Surdilovic, D.; Gonzalez-De-Santos, P.; Armada, M. Automatic detection of field-grown cucumbers for robotic harvesting. *IEEE Access* **2018**, *6*, 35512–35527. [[CrossRef](#)]
164. Gaffney, J.; Miller, W.; Coppock, G.E. Citrus Fruit Injury as Related to Mechanical Harvesting With Limb Shaker-Catch Frame Systems. *Proc. Fla. State Hort. Soc.* **1976**, *89*, 179–182.
165. Li, G.; Huang, X.; Ai, J.; Yi, Z.; Xie, W. Lemon-YOLO: An efficient object detection method for lemons in the natural environment. In *IET Image Processing*; Wiley: Hoboken, NJ, USA, 2021.
166. Peterson, D. Mechanical harvester for process oranges. *Appl. Eng. Agric.* **1998**, *14*, 455–458. [[CrossRef](#)]
167. Whitney, J. Field test results with mechanical harvesting equipment in Florida oranges. *Appl. Eng. Agric.* **1999**, *15*, 205. [[CrossRef](#)]
168. Ganesh, P.; Volle, K.; Burks, T.; Mehta, S. Deep orange: Mask R-CNN based orange detection and segmentation. *IFAC PapersOnLine* **2019**, *52*, 70–75. [[CrossRef](#)]
169. Hannan, M.; Burks, T.; Bulanon, D.M. A machine vision algorithm combining adaptive segmentation and shape analysis for orange fruit detection. *Agric. Eng. Int. CIGR J.* **2010**, *XI*, 1–17.
170. Roshanianfard, A.; Noguchi, N. Pumpkin harvesting robotic end-effector. *Comput. Electron. Agric.* **2020**, *174*, 105503. [[CrossRef](#)]
171. Wittstruck, L.; Kühling, I.; Trautz, D.; Kohlbrecher, M.; Jarmer, T. UAV-Based RGB Imagery for Hokkaido Pumpkin (*Cucurbita max.*) Detection and Yield Estimation. *Sensors* **2021**, *21*, 118. [[CrossRef](#)]
172. Hwang, H.; Kim, S.C. Development of multi-functional tele-operative modular robotic system for greenhouse watermelon. In Proceedings of the 2003 IEEE/ASME International Conference on Advanced Intelligent Mechatronics (AIM 2003), Kobe, Japan, 20–24 July 2003; Volume 2, pp. 1344–1349.
173. Rajendra, P.; Kondo, N.; Ninomiya, K.; Kamata, J.; Kurita, M.; Shiigi, T.; Hayashi, S.; Yoshida, H.; Kohno, Y. Machine vision algorithm for robots to harvest strawberries in tabletop culture greenhouses. *Eng. Agric. Environ. Food* **2009**, *2*, 24–30. [[CrossRef](#)]
174. Klaoudatos, D.S.; Moulianitis, V.C.; Aspragathos, N.A. Development of an Experimental Strawberry Harvesting Robotic System. In Proceedings of the 16th International Conference on Informatics in Control, Automation and Robotics, Prague, Czech Republic, 26–29 July 2019; pp. 437–445.
175. Yu, Y.; Zhang, K.; Yang, L.; Zhang, D. Fruit detection for strawberry harvesting robot in non-structural environment based on Mask-RCNN. *Comput. Electron. Agric.* **2019**, *163*, 104846. [[CrossRef](#)]
176. Lamb, N.; Chuah, M.C. A strawberry detection system using convolutional neural networks. In Proceedings of the 2018 IEEE International Conference on Big Data (Big Data), Seattle, WA, USA, 10–13 December 2018; pp. 2515–2520.
177. Wang, H.; Li, B.; Liu, G.; Xu, L. Design and test of pineapple harvesting manipulator. *Trans. Chin. Soc. Agric. Eng.* **2012**, *28*, 42–46.
178. Anh, N.P.T.; Hoang, S.; Van Tai, D.; Quoc, B.L.C. Developing Robotic System for Harvesting Pineapples. In Proceedings of the 2020 International Conference on Advanced Mechatronic Systems (ICAMEchS), Hanoi, Vietnam, 10–13 December 2020; pp. 39–44.
179. Li, B.; Wang, M.; Wang, N. Development of a real-time fruit recognition system for pineapple harvesting robots. In Proceedings of the American Society of Agricultural and Biological Engineers, Pittsburgh, PA, USA, 20–23 June 2010; p. 1.
180. Li, B.; Ning, W.; Wang, M.; Li, L. In-field pineapple recognition based on monocular vision. *Trans. Chin. Soc. Agric. Eng.* **2010**, *26*, 345–349.
181. Li, B.; Wang, M. In-field recognition and navigation path extraction for pineapple harvesting robots. *Intell. Autom. Soft Comput.* **2013**, *19*, 99–107. [[CrossRef](#)]

182. Hughes, J.; Culha, U.; Giardina, F.; Guenther, F.; Rosendo, A.; Iida, F. Soft manipulators and grippers: a review. *Front. Robot. AI* **2016**, *3*, 69. [[CrossRef](#)]
183. Trivedi, D.; Rahn, C.D.; Kier, W.M.; Walker, I.D. Soft robotics: Biological inspiration, state of the art, and future research. *Appl. Bionics Biomech.* **2008**, *5*, 99–117. [[CrossRef](#)]
184. Kim, S.; Laschi, C.; Trimmer, B. Soft robotics: a bioinspired evolution in robotics. *Trends Biotechnol.* **2013**, *31*, 287–294. [[CrossRef](#)]
185. Majidi, C. Soft robotics: a perspective—current trends and prospects for the future. *Soft Robot.* **2014**, *1*, 5–11. [[CrossRef](#)]
186. Laschi, C.; Cianchetti, M. Soft robotics: new perspectives for robot bodyware and control. *Front. Bioeng. Biotechnol.* **2014**, *2*, 3. [[CrossRef](#)]
187. Rus, D.; Tolley, M.T. Design, fabrication and control of soft robots. *Nature* **2015**, *521*, 467–475. [[CrossRef](#)] [[PubMed](#)]
188. Laschi, C.; Mazzolai, B.; Cianchetti, M. Soft robotics: Technologies and systems pushing the boundaries of robot abilities. *Sci. Robot.* **2016**, *1*, eaah3690. [[CrossRef](#)]
189. Boyraz, P.; Runge, G.; Raatz, A. An overview of novel actuators for soft robotics. *Actuators* **2018**, *7*, 48. [[CrossRef](#)]
190. Shintake, J.; Cacucciolo, V.; Floreano, D.; Shea, H. Soft robotic grippers. *Adv. Mater.* **2018**, *30*, 1707035. [[CrossRef](#)]
191. D’Avella, S.; Tripicchio, P.; Avizzano, C.A. A study on picking objects in cluttered environments: Exploiting depth features for a custom low-cost universal jamming gripper. *Robot.-Comput.-Integr. Manuf.* **2020**, *63*, 101888. [[CrossRef](#)]
192. Tolley, M.T.; Shepherd, R.F.; Mosadegh, B.; Galloway, K.C.; Wehner, M.; Karpelson, M.; Wood, R.J.; Whitesides, G.M. A resilient, untethered soft robot. *Soft Robot.* **2014**, *1*, 213–223. [[CrossRef](#)]
193. Mengüç, Y.; Yang, S.Y.; Kim, S.; Rogers, J.A.; Sitti, M. Gecko-inspired controllable adhesive structures applied to micromanipulation. *Adv. Funct. Mater.* **2012**, *22*, 1246–1254. [[CrossRef](#)]
194. Hawkes, E.W.; Christensen, D.L.; Han, A.K.; Jiang, H.; Cutkosky, M.R. Grasping without squeezing: Shear adhesion gripper with fibrillar thin film. In Proceedings of the 2015 IEEE International Conference on Robotics and Automation (ICRA), Seattle, WA, USA, 26–30 May 2015; pp. 2305–2312.
195. Song, S.; Sitti, M. Soft grippers using micro-fibrillar adhesives for transfer printing. *Adv. Mater.* **2014**, *26*, 4901–4906. [[CrossRef](#)] [[PubMed](#)]
196. Schaler, E.W.; Ruffatto, D.; Glick, P.; White, V.; Parness, A. An electrostatic gripper for flexible objects. In Proceedings of the 2017 IEEE/RSJ International Conference on Intelligent Robots and Systems (IROS), Vancouver, BC, Canada, 24–28 September 2017; pp. 1172–1179.
197. Coyle, S.; Majidi, C.; LeDuc, P.; Hsia, K.J. Bio-inspired soft robotics: Material selection, actuation, and design. *Extrem. Mech. Lett.* **2018**, *22*, 51–59. [[CrossRef](#)]
198. Hsiao, L.Y.; Jing, L.; Li, K.; Yang, H.; Li, Y.; Chen, P.Y. Carbon nanotube-integrated conductive hydrogels as multifunctional robotic skin. *Carbon* **2020**, *161*, 784–793. [[CrossRef](#)]
199. Mosadegh, B.; Polygerinos, P.; Keplinger, C.; Wennstedt, S.; Shepherd, R.F.; Gupta, U.; Shim, J.; Bertoldi, K.; Walsh, C.J.; Whitesides, G.M. Pneumatic networks for soft robotics that actuate rapidly. *Adv. Funct. Mater.* **2014**, *24*, 2163–2170. [[CrossRef](#)]
200. Ellis, D.R.; Venter, M.P.; Venter, G. Soft Pneumatic Actuator with Bimodal Bending Response Using a Single Pressure Source. *Soft Robot.* **2020**. [[CrossRef](#)]
201. Niu, H.; Feng, R.; Xie, Y.; Jiang, B.; Sheng, Y.; Yu, Y.; Baoyin, H.; Zeng, X. MagWorm: A Biomimetic Magnet Embedded Worm-Like Soft Robot. *Soft Robot.* **2020**. [[CrossRef](#)]
202. Gu, G.; Wang, D.; Ge, L.; Zhu, X. Analytical Modeling and Design of Generalized Pneu-Net Soft Actuators with Three-Dimensional Deformations. *Soft Robot.* **2020**. [[CrossRef](#)]
203. Jolaei, M.; Hooshiar, A.; Dargahi, J.; Packirisamy, M. Toward task autonomy in robotic cardiac ablation: Learning-based kinematic control of soft tendon-driven catheters. *Soft Robot.* **2020**. [[CrossRef](#)]
204. Dang, Y.; Liu, Y.; Hashem, R.; Bhattacharya, D.; Allen, J.; Stommel, M.; Cheng, L.K.; Xu, W. SoGut: A Soft Robotic Gastric Simulator. *Soft Robot.* **2020**. [[CrossRef](#)] [[PubMed](#)]
205. Kim, Y.; Cha, Y. Soft Pneumatic Gripper With a Tendon-Driven Soft Origami Pump. *Front. Bioeng. Biotechnol.* **2020**, *8*, 461. [[CrossRef](#)] [[PubMed](#)]
206. Wang, Z.; Or, K.; Hirai, S. A dual-mode soft gripper for food packaging. *Robot. Auton. Syst.* **2020**, *125*, 103427. [[CrossRef](#)]
207. De Barrie, D.; Margetts, R.; Goher, K. SIMPA: Soft-Grasp Infant Myoelectric Prosthetic Arm. *IEEE Robot. Autom. Lett.* **2020**, *5*, 698–703. [[CrossRef](#)]
208. Shih, B.; Drotman, D.; Christianson, C.; Huo, Z.; White, R.; Christensen, H.I.; Tolley, M.T. Custom soft robotic gripper sensor skins for haptic object visualization. In Proceedings of the 2017 IEEE/RSJ international conference on intelligent robots and systems (IROS), Vancouver, BC, Canada, 24–28 September 2017; pp. 494–501.
209. Connolly, F.; Walsh, C.J.; Bertoldi, K. Automatic design of fiber-reinforced soft actuators for trajectory matching. *Proc. Natl. Acad. Sci. USA* **2017**, *114*, 51–56. [[CrossRef](#)]
210. Zhou, J.; Chen, S.; Wang, Z. A soft-robotic gripper with enhanced object adaptation and grasping reliability. *IEEE Robot. Autom. Lett.* **2017**, *2*, 2287–2293. [[CrossRef](#)]
211. Hao, Y.; Gong, Z.; Xie, Z.; Guan, S.; Yang, X.; Ren, Z.; Wang, T.; Wen, L. Universal soft pneumatic robotic gripper with variable effective length. In Proceedings of the 2016 35th Chinese control conference (CCC), Chengdu, China, 27–29 July 2016; pp. 6109–6114.

212. Yirmibesoglu, O.D.; Morrow, J.; Walker, S.; Gosrich, W.; Cañizares, R.; Kim, H.; Daalkhajav, U.; Fleming, C.; Branyan, C.; Menguc, Y. Direct 3D printing of silicone elastomer soft robots and their performance comparison with molded counterparts. In Proceedings of the 2018 IEEE International Conference on Soft Robotics (RoboSoft), Livorno, Italy, 24–28 April 2018; pp. 295–302.
213. Zhong, G.; Hou, Y.; Dou, W. A soft pneumatic dexterous gripper with convertible grasping modes. *Int. J. Mech. Sci.* **2019**, *153*, 445–456. [\[CrossRef\]](#)
214. Yang, H.; Chen, Y.; Sun, Y.; Hao, L. A novel pneumatic soft sensor for measuring contact force and curvature of a soft gripper. *Sens. Actuators A Phys.* **2017**, *266*, 318–327. [\[CrossRef\]](#)
215. Chen, Y.; Guo, S.; Li, C.; Yang, H.; Hao, L. Size recognition and adaptive grasping using an integration of actuating and sensing soft pneumatic gripper. *Robot. Auton. Syst.* **2018**, *104*, 14–24. [\[CrossRef\]](#)
216. Azami, O.; Morisaki, D.; Miyazaki, T.; Kanno, T.; Kawashima, K. Development of the extension type pneumatic soft actuator with built-in displacement sensor. *Sens. Actuators A Phys.* **2019**, *300*, 111623. [\[CrossRef\]](#)
217. Batsuren, K.; Yun, D. Soft robotic gripper with chambered fingers for performing in-hand manipulation. *Appl. Sci.* **2019**, *9*, 2967. [\[CrossRef\]](#)
218. Galloway, K.C.; Becker, K.P.; Phillips, B.; Kirby, J.; Licht, S.; Tchernov, D.; Wood, R.J.; Gruber, D.F. Soft robotic grippers for biological sampling on deep reefs. *Soft Robot.* **2016**, *3*, 23–33. [\[CrossRef\]](#) [\[PubMed\]](#)
219. Lee, H.J.; Prachaseree, P.; Loh, K.J. Rapid Soft Material Actuation Through Droplet Evaporation. *Soft Robot.* **2020**. [\[CrossRef\]](#)
220. Wang, Z.; Kanegae, R.; Hirai, S. Circular Shell Gripper for Handling Food Products. *Soft Robot.* **2020**. [\[CrossRef\]](#) [\[PubMed\]](#)
221. Hashemi, S.; Bentivegna, D.; Durfee, W. Bone-Inspired Bending Soft Robot. *Soft Robot.* **2020**. [\[CrossRef\]](#)
222. Manti, M.; Hassan, T.; Passetti, G.; D’Elia, N.; Laschi, C.; Cianchetti, M. A bioinspired soft robotic gripper for adaptable and effective grasping. *Soft Robot.* **2015**, *2*, 107–116. [\[CrossRef\]](#)
223. Li, S.; Stampfli, J.J.; Xu, H.J.; Malkin, E.; Diaz, E.V.; Rus, D.; Wood, R.J. A vacuum-driven origami “magic-ball” soft gripper. In Proceedings of the 2019 International Conference on Robotics and Automation (ICRA), Montreal, QC, Canada, 20–24 May 2019; pp. 7401–7408.
224. Wang, Z.; Hirai, S. Chamber dimension optimization of a bellow-type soft actuator for food material handling. In Proceedings of the 2018 IEEE International Conference on Soft Robotics (RoboSoft), Livorno, Italy, 24–28 April 2018; pp. 382–387.
225. Kuriyama, Y.; Okino, Y.; Wang, Z.; Hirai, S. A wrapping gripper for packaging chopped and granular food materials. In Proceedings of the 2019 2nd IEEE International Conference on Soft Robotics (RoboSoft), Seoul, Korea, 14–18 April 2019; pp. 114–119.
226. Seibel, A.; Yildiz, M.; Zorlubas, B. A Gecko-Inspired Soft Passive Gripper. *Biomimetics* **2020**, *5*, 12. [\[CrossRef\]](#)
227. Teeple, C.B.; Koutros, T.N.; Graule, M.A.; Wood, R.J. Multi-segment soft robotic fingers enable robust precision grasping. *Int. J. Robot. Res.* **2020**, *39*, 1647–1667. [\[CrossRef\]](#)
228. Polygerinos, P.; Wang, Z.; Overvelde, J.T.; Galloway, K.C.; Wood, R.J.; Bertoldi, K.; Walsh, C.J. Modeling of soft fiber-reinforced bending actuators. *IEEE Trans. Robot.* **2015**, *31*, 778–789. [\[CrossRef\]](#)
229. Hu, W.; Mutlu, R.; Li, W.; Alici, G. A structural optimisation method for a soft pneumatic actuator. *Robotics* **2018**, *7*, 24. [\[CrossRef\]](#)
230. Galley, A.; Knopf, G.K.; Kashkoush, M. Pneumatic Hyperelastic Actuators for Grasping Curved Organic Objects. *Actuators* **2019**, *8*, 76. [\[CrossRef\]](#)
231. Wang, W.; Rodrigue, H.; Kim, H.I.; Han, M.W.; Ahn, S.H. Soft composite hinge actuator and application to compliant robotic gripper. *Compos. Part B Eng.* **2016**, *98*, 397–405. [\[CrossRef\]](#)
232. Breitman, P.; Matia, Y.; Gat, A.D. Fluid mechanics of pneumatic soft robots. *Soft Robot.* **2020**. [\[CrossRef\]](#) [\[PubMed\]](#)
233. Rodrigue, H.; Wang, W.; Kim, D.R.; Ahn, S.H. Curved shape memory alloy-based soft actuators and application to soft gripper. *Compos. Struct.* **2017**, *176*, 398–406. [\[CrossRef\]](#)
234. Zhu, M.; Xie, M.; Lu, X.; Okada, S.; Kawamura, S. A soft robotic finger with self-powered triboelectric curvature sensor based on multi-material 3D printing. *Nano Energy* **2020**, *73*, 104772. [\[CrossRef\]](#)
235. Ltd., F.C. BionicTripod with FinGripper. 2009. Available online: [https://www.festo.com/rep/en\\_corp/assets/pdf/Tripod\\_en.pdf](https://www.festo.com/rep/en_corp/assets/pdf/Tripod_en.pdf) (accessed on 10 April 2021).
236. Hohimer, C.J.; Wang, H.; Bhusal, S.; Miller, J.; Mo, C.; Karkee, M. Design and field evaluation of a robotic apple harvesting system with a 3D-printed soft-robotic end-effector. *Trans. ASABE* **2019**, *62*, 405–414. [\[CrossRef\]](#)
237. Tan, N.; Gu, X.; Ren, H. Design, characterization and applications of a novel soft actuator driven by flexible shafts. *Mech. Mach. Theory* **2018**, *122*, 197–218. [\[CrossRef\]](#)
238. Akbari, S.; Sakhaei, A.H.; Panjwani, S.; Kowsari, K.; Serjouei, A.; Ge, Q. Multimaterial 3D printed soft actuators powered by shape memory alloy wires. *Sens. Actuators A Phys.* **2019**, *290*, 177–189. [\[CrossRef\]](#)
239. Yap, H.K.; Lim, J.H.; Goh, J.C.H.; Yeow, C.H. Design of a soft robotic glove for hand rehabilitation of stroke patients with clenched fist deformity using inflatable plastic actuators. *J. Med. Dev.* **2016**, *10*, 044504. [\[CrossRef\]](#)
240. Alvarez-Palacio, J.M.; Monteiro, E.; Riwan, A.; Mechbal, N. A Novel Inflatable Actuator Based on Simultaneous Eversion Retraction. *Soft Robot.* **2020**. [\[CrossRef\]](#)
241. Yap, H.K.; Ng, H.Y.; Yeow, C.H. High-force soft printable pneumatics for soft robotic applications. *Soft Robot.* **2016**, *3*, 144–158. [\[CrossRef\]](#)
242. Johnston, I.; McCluskey, D.; Tan, C.; Tracey, M. Mechanical characterization of bulk Sylgard 184 for microfluidics and microengineering. *J. Micromech. Microeng.* **2014**, *24*, 035017. [\[CrossRef\]](#)



243. Kim, M.; Moon, B.U.; Hidrovo, C.H. Enhancement of the thermo-mechanical properties of PDMS molds for the hot embossing of PMMA microfluidic devices. *J. Micromech. Microeng.* **2013**, *23*, 095024. [[CrossRef](#)]
244. Kim, T.K.; Kim, J.K.; Jeong, O.C. Measurement of nonlinear mechanical properties of PDMS elastomer. *Microelectron. Eng.* **2011**, *88*, 1982–1985. [[CrossRef](#)]
245. Katzschmann, R.K.; DelPreto, J.; MacCurdy, R.; Rus, D. Exploration of underwater life with an acoustically controlled soft robotic fish. *Sci. Robot.* **2018**, *3*, eaar3449. [[CrossRef](#)]
246. Pettersson, A.; Davis, S.; Gray, J.O.; Dodd, T.J.; Ohlsson, T. Design of a magnetorheological robot gripper for handling of delicate food products with varying shapes. *J. Food Eng.* **2010**, *98*, 332–338. [[CrossRef](#)]
247. Blanes, C.; Mellado, M.; Beltran, P. Novel additive manufacturing pneumatic actuators and mechanisms for food handling grippers. *Actuators* **2014**, *3*, 205–225. [[CrossRef](#)]
248. Wang, Z.; Chathuranga, D.S.; Hirai, S. 3D printed soft gripper for automatic lunch box packing. In Proceedings of the 2016 IEEE International Conference on Robotics and Biomimetics (ROBIO), Qingdao, China, 3–7 December 2016; pp. 503–508.
249. Blanes, C.; Mellado, M.; Beltrán, P. Tactile sensing with accelerometers in prehensile grippers for robots. *Mechatronics* **2016**, *33*, 1–12. [[CrossRef](#)]
250. Wang, Z.; Torigoe, Y.; Hirai, S. A prestressed soft gripper: design, modeling, fabrication, and tests for food handling. *IEEE Robot. Autom. Lett.* **2017**, *2*, 1909–1916. [[CrossRef](#)]
251. Birrell, S.; Hughes, J.; Cai, J.Y.; Iida, F. A field-tested robotic harvesting system for iceberg lettuce. *J. Field Robot.* **2020**, *37*, 225–245. [[CrossRef](#)]
252. Gafer, A.; Heymans, D.; Prattichizzo, D.; Salvietti, G. The Quad-Spatula Gripper: A Novel Soft-Rigid Gripper for Food Handling. In Proceedings of the 2020 3rd IEEE International Conference on Soft Robotics (RoboSoft), New Haven, CT, USA, 15 May–15 July 2020; pp. 39–45.
253. Chen, S.; Pang, Y.; Yuan, H.; Tan, X.; Cao, C. Smart Soft Actuators and Grippers Enabled by Self-Powered Tribo-Skins. *Adv. Mater. Technol.* **2020**, *5*, 1901075. [[CrossRef](#)]
254. Tawk, C.; Gillett, A.; In het Panhuis, M.; Spinks, G.M.; Alici, G. A 3D-printed omni-purpose soft gripper. *IEEE Trans. Robot.* **2019**, *35*, 1268–1275. [[CrossRef](#)]
255. Liu, C.H.; Chiu, C.H.; Chen, T.L.; Pai, T.Y.; Chen, Y.; Hsu, M.C. A soft robotic gripper module with 3D printed compliant fingers for grasping fruits. In Proceedings of the 2018 IEEE/ASME International Conference on Advanced Intelligent Mechatronics (AIM), Auckland, New Zealand, 9–12 July 2018; pp. 736–741.
256. Calisti, M.; Arienti, A.; Giannaccini, M.E.; Follador, M.; Giorelli, M.; Cianchetti, M.; Mazzolai, B.; Laschi, C.; Dario, P. Study and fabrication of bioinspired octopus arm mockups tested on a multipurpose platform. In Proceedings of the 2010 3rd IEEE RAS & EMBS International Conference on Biomedical Robotics and Biomechatronics, Tokyo, Japan, 26–29 September 2010; pp. 461–466.
257. Brown, E.; Rodenberg, N.; Amend, J.; Mozeika, A.; Steltz, E.; Zakin, M.R.; Lipson, H.; Jaeger, H.M. Universal robotic gripper based on the jamming of granular material. *Proc. Natl. Acad. Sci. USA* **2010**, *107*, 18809–18814. [[CrossRef](#)]
258. Festo Corporate. MultiChoiceGripper | Festo Corporate. Available online: <https://www.festo.com/group/en/cms/10221.htm> (accessed on 10 April 2021).
259. Manti, M.; Cacucciolo, V.; Cianchetti, M. Stiffening in soft robotics: A review of the state of the art. *IEEE Robot. Autom. Mag.* **2016**, *23*, 93–106. [[CrossRef](#)]
260. Yang, D.; Verma, M.S.; So, J.H.; Mosadegh, B.; Keplinger, C.; Lee, B.; Khashai, F.; Lossner, E.; Suo, Z.; Whitesides, G.M. Buckling pneumatic linear actuators inspired by muscle. *Adv. Mater. Technol.* **2016**, *1*, 1600055. [[CrossRef](#)]
261. Iida, F.; Laschi, C. Soft robotics: Challenges and perspectives. *Procedia Comput. Sci.* **2011**, *7*, 99–102. [[CrossRef](#)]
262. Largilliere, F.; Verona, V.; Coevoet, E.; Sanz-Lopez, M.; Dequidt, J.; Duriez, C. Real-time control of soft-robots using asynchronous finite element modeling. In Proceedings of the 2015 IEEE International Conference on Robotics and Automation (ICRA), Seattle, WA, USA, 26–30 May 2015; pp. 2550–2555.
263. Friend, J.; Yeo, L. Fabrication of microfluidic devices using polydimethylsiloxane. *Biomicrofluidics* **2010**, *4*, 026502. [[CrossRef](#)] [[PubMed](#)]
264. Rateni, G.; Cianchetti, M.; Ciuti, G.; Menciassi, A.; Laschi, C. Design and development of a soft robotic gripper for manipulation in minimally invasive surgery: a proof of concept. *Meccanica* **2015**, *50*, 2855–2863. [[CrossRef](#)]
265. Linghu, C.; Zhang, S.; Wang, C.; Yu, K.; Li, C.; Zeng, Y.; Zhu, H.; Jin, X.; You, Z.; Song, J. Universal SMP gripper with massive and selective capabilities for multiscaled, arbitrarily shaped objects. *Sci. Adv.* **2020**, *6*, eaay5120. [[CrossRef](#)]
266. Carabin, G.; Palomba, I.; Matt, D.; Vidoni, R. Experimental evaluation and comparison of low-cost adaptive mechatronic grippers. In Proceedings of the International Conference on Robotics in Alpe-Adria Danube Region, Torino, Italy, 21–23 June 2017; pp. 630–637.
267. Lowenberg-DeBoer, J.; Huang, I.Y.; Grigoriadis, V.; Blackmore, S. Economics of robots and automation in field crop production. *Precis. Agric.* **2019**, *21*, 278–299. [[CrossRef](#)]
268. Vermeulen, P. *Kwantitatieve Informatie voor de Glastuinbouw [Quantitative Information on Greenhouse horticulture] 2012–2013*; Wageningen UR Glastuinbouw: Wageningen, The Netherlands, 2012; p. 107.
269. Navarrete, M.; Jeannequin, B. Effect of frequency of axillary bud pruning on vegetative growth and fruit yield in greenhouse tomato crops. *Sci. Hortic.* **2000**, *86*, 197–210. [[CrossRef](#)]

270. Brotons-Martínez, J.; Martín-Gorrioz, B.; Torregrosa, A.; Porras, I. Economic evaluation of mechanical harvesting of lemons. *Outlook Agric.* **2018**, *47*, 44–50. [[CrossRef](#)]
271. Shepherd, R.F.; Ilievski, F.; Choi, W.; Morin, S.A.; Stokes, A.A.; Mazzeo, A.D.; Chen, X.; Wang, M.; Whitesides, G.M. Multigait soft robot. *Proc. Natl. Acad. Sci. USA* **2011**, *108*, 20400–20403. [[CrossRef](#)] [[PubMed](#)]
272. Su, Y.; Fang, Z.; Zhu, W.; Sun, X.; Zhu, Y.; Wang, H.; Tang, K.; Huang, H.; Liu, S.; Wang, Z. A High-Payload Proprioceptive Hybrid Robotic Gripper With Soft Origamic Actuators. *IEEE Robot. Autom. Lett.* **2020**, *5*, 3003–3010. [[CrossRef](#)]
273. Ludwig-Ohm, S.; Dirksmeyer, W.; Klockgether, K. Approaches to Reduce Food Losses in German Fruit and Vegetable Production. *Sustainability* **2019**, *11*, 6576. [[CrossRef](#)]
274. Li, Z.; Thomas, C. Quantitative evaluation of mechanical damage to fresh fruits. *Trends Food Sci. Technol.* **2014**, *35*, 138–150. [[CrossRef](#)]





Article

# Agrobot Lala—An Autonomous Robotic System for Real-Time, In-Field Soil Sampling, and Analysis of Nitrates

Goran Kitić \*, Damir Krklješ, Marko Panić, Csaba Petes, Slobodan Birgermajer and Vladimir Crnojević

BioSense Institute—Research Institute for Information Technologies in Biosystems, University of Novi Sad, Dr. Zorana Đinđića 1a, 21000 Novi Sad, Serbia; dkrkljes@biosense.rs (D.K.); panic@biosense.rs (M.P.); chaba@biosense.rs (C.P.); b.sloba@biosense.rs (S.B.); crnojevic@biosense.rs (V.C.)

\* Correspondence: gkitic@biosense.rs or office@biosense.rs

**Abstract:** This paper presents an autonomous robotic system, an unmanned ground vehicle (UGV), for in-field soil sampling and analysis of nitrates. Compared to standard methods of soil analysis it has several advantages: each sample is individually analyzed compared to average sample analysis in standard methods; each sample is georeferenced, providing a map for precision base fertilizing; the process is fully autonomous; samples are analyzed in real-time, approximately 30 min per sample; and lightweight for less soil compaction. The robotic system has several modules: commercial robotic platform, anchoring module, sampling module, sample preparation module, sample analysis module, and communication module. The system is augmented with an in-house developed cloud-based platform. This platform uses satellite images, and an artificial intelligence (AI) proprietary algorithm to divide the target field into representative zones for sampling, thus, reducing and optimizing the number and locations of the samples. Based on this, a task is created for the robot to automatically sample at those locations. The user is provided with an in-house developed smartphone app enabling overview and monitoring of the task, changing the positions, removing and adding of the sampling points. The results of the measurements are uploaded to the cloud for further analysis and the creation of prescription maps for variable rate base fertilization.

**Keywords:** UGV; precision agriculture; artificial intelligence; soil nutrient analysis; soil sampling

**Citation:** Kitić, G.; Krklješ, D.; Panić, M.; Petes, C.; Birgermajer, S.; Crnojević, V. Agrobot Lala—An Autonomous Robotic System for Real-Time, In-Field Soil Sampling, and Analysis of Nitrates. *Sensors* **2022**, *22*, 4207. <https://doi.org/10.3390/s22114207>

Academic Editor: Sigfredo Fuentes

Received: 20 April 2022

Accepted: 24 May 2022

Published: 31 May 2022

**Publisher's Note:** MDPI stays neutral with regard to jurisdictional claims in published maps and institutional affiliations.



**Copyright:** © 2022 by the authors. Licensee MDPI, Basel, Switzerland. This article is an open access article distributed under the terms and conditions of the Creative Commons Attribution (CC BY) license (<https://creativecommons.org/licenses/by/4.0/>).

## 1. Introduction

With the continuous growth of the world population, the demand for food and cultivated land increases continuously. The prediction of the Food and Agriculture Organization of United Nations (FAO) indicates the presence of constant growth of the population with the rate of 79 million people per year, increasing food demand [1]. Since the cultivated land resources are limited, and acquiring new ones is correlated with degradation of ecosystems, reduction of forests, climate changes, and risks of new pandemic breakouts, as well as degradation of soil properties due to inappropriate cultivation and treatment, there is an urgent need to improve soil treatment, to increase yield in a sustainable manner. The best approach that will enable farming to become more efficient in a sustainable way and reduce the production costs at the same time, is to provide an efficient supply of nutrients and water [2]. Standard and classical methods of soil analysis usually involve taking 1–20 samples per 5 hectares from around 30 cm depth. They are usually mixed and analyzed for an average value of nutrients [3]. A laboratory analysis then takes 10–15 days to obtain the results. The most common soil sampling methods used are hand sampling, hydraulic probes, electric probes, and auger probes [4]. Hand sampling is easy to use and economic, but it is time-consuming, labor-intensive, and could be inconsistent with the sampling depths. Hydraulic probes are fast and have a consistent depth, but are composed of numerous components (engine, hydraulics tank, pump, and lines), vendor locked, and pricy in the range from USD 4000 to 8000 on average. Electric probes demand low maintenance, with no fuel costs, and are more suited for dusty conditions. They do have a slower

cycle time and they are not as powerful as hydraulic ones. Auger probes are the most durable and easy to set up and use. Their main drawback is the cross-contamination due to poor probe cleanout capabilities and they have difficulties with verifying core depth as well with their usage in sandy soils. All the stated sampling methods end up with time-consuming laboratory analysis, which does not provide on-time information to the farmers. Furthermore, due to sample averaging, precise information about nutrients at the exact location is lost. Considering nitrogen, with its large spatial and temporal variations, under and over-fertilization is inevitable. This can lead to a decrease in yield on one hand, and significant pollution of the ecosystems on the other [5].

Sowing and fertilization as phases in the agricultural production process should be completed after soil analysis based on appropriate methods providing information on nutrient availability for the growth and development of the particular plant. Until recently, farmers applied uniform fertilization per plot, which is not optimal from an economic perspective, and unsustainable from an ecologic, environmental, and ecosystem point of view. Plants acquire nutrients in amounts that are needed for normal growth, while any additional artificially applied nutrients by fertilization largely evaporate, creating greenhouse gases, or end up in surface and underground waters, which boosts algae growth in rivers and lakes [6]. Subsequently, lack of oxygen leads to large-scale fish death and other water animals and organisms in their natural habitats, which finally affects humans. All the stated facts impose a need for new systems and methods for real-time georeferenced sampling of soil for nutrients, providing input for precise fertilization.

Precision agriculture, smart farming, and automated agricultural technology have emerged as promising methodologies for increasing crop productivity without sacrificing produced quality. The emergence of various robotics technologies has facilitated the application of these techniques in agricultural processes [7]. In the stated article, the authors provide an overview of the current state of the art in agricultural robots. Classification of the five major operations in open arable farming is presented in the study by [8], where one of them is soil analysis. An implication of soil agrochemical analysis and its accuracy in precision agriculture is given in [9]. The authors suggest that rapid, less labor-intensive, economical, and at least equally accurate methods have to be developed for precision agriculture. They emphasize high soil analysis costs with traditional methods. A suggestion for scales of 10 m or less in precise agriculture is suggested in [8], due to the high spatial variability of the nutrients in the soil. Early work in the automation of soil sampling is presented in [10]. The system collects, packs, and marks samples with georeferencing. Rogo Robotic Soil Sampling [11] represents the state-of-the-art automatic soil sampler, however, it is not on-the-go, as it just collects and packs samples. The paper by Oledo et al. presented a UGV with a custom-built robotic manipulator with a surface scoop-type soil sampler [12]. Cao et al. presented a soil sampling system on a mobile robot with practical implementation in a soil survey in an assault zone [13]. The sampling system is an automatic penetrometer.

Vaeljaots et al. presented soil sampling UGV which can measure some of the soil properties online such as temperature, moisture, and penetration force [14]. It can collect, pack, and label the samples for later laboratory analysis. However, this paper does not present more technical insight, e.g., what are the exact parameters that are measured online, what is the depth of a sample, etc.

The robotic solutions mentioned above are only limited to the soil sampling part of the process and do not offer an insight into the nutrient analysis. In this paper, we propose a novel system for soil sampling and in-field analysis for nitrate-nitrogen that is based on the autonomous robotic platform agrobot Lala. The proposed solution is supported by an AI algorithm for defining optimal sampling locations as well as for fertilization prescription. In this way, a complete solution is offered to the farmers based on what they know on time, what is the spatial need for nitrogen in their fields, and how exactly to apply fertilizer. We believe that the proposed solution will help farmers be more efficient in a sustainable way.

## 2. Materials and Methods

The purpose of an autonomous robotic system, agrobot Lala (Figure 1) is an automation of the in-field, real-time, soil sampling and analysis of nutrient content of the soil. Currently, it supports the measurement of the content of nitrate nitrogen; however, with different probes it could measure other nutrients and soil properties as well (electric conductivity (EC), pH, NPK, and similar). Agrobot Lala is fully autonomous, and it is based on the commercially available UGV platform Husky (Clearpath robotics Inc., Kitchener, ON, Canada) [15]. This platform is equipped with a custom-made system for soil sampling and analysis.



**Figure 1.** An autonomous robotic system—agrobot Lala.

The system can be divided into three major parts:

- Cloud-based application for task management and generation of sample points on the plot based on a proprietary AI algorithm.
- Smartphone application for monitoring and customization of the task.
- Robotic system for acquiring and analysis of soil samples.

### 2.1. Cloud-Based Application

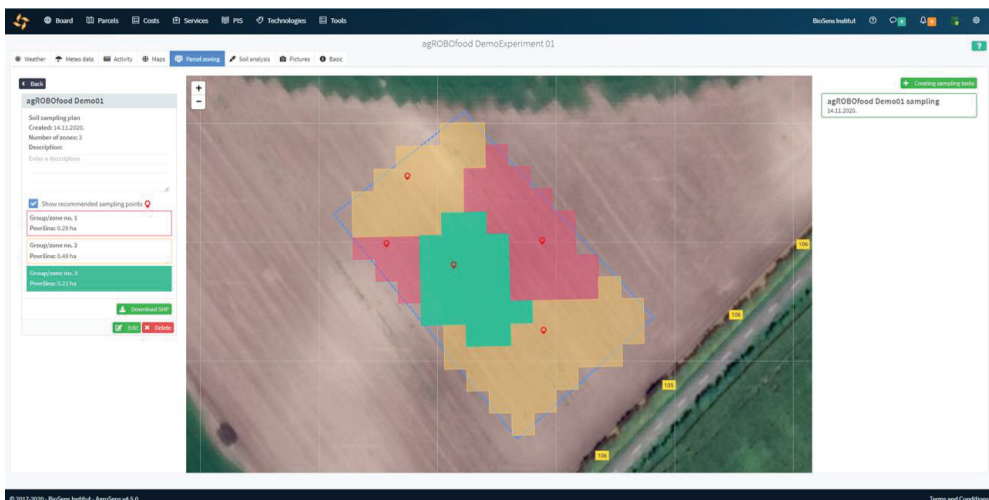
The cloud-based application is a custom-made proprietary solution based on the existing AgroSense digital platform [16]. Through this platform, users can register and associate any of its plots. Various services are then available to support more efficient agricultural production. The platform offers the possibility for the user to perceive, per management zones, specific locations for soil sampling and analysis proposed by the AI algorithm based on satellite or high-resolution drone images. The specified locations are generated according to the assessed variability within the plot and, as such, their number can be lower compared to the number of sampling points obtained from the cell sampling scheme with checkerboard representation [17,18].

In precision agriculture, a management zone defines a sub-region within the same piece of land (plot), which has spatially invariant factors influencing the yield according to which crop management practice is carried out [19,20]. Different types of data have been used for the assessment of spatial variability within the plot such as data about the yield through the years, various soil properties, remotely sensed data, topographic factors, and soil apparent electrical conductivity (ECa) [20–23]. Among the methods proposed to measure within-plot spatial variability for delineating management zones, a statistical cluster analysis, which integrates various data sources, is the most frequently used as a baseline [24]. The developed AI algorithm focus only on remote sensing data, particularly on multispectral Sentinel-2 satellite images [25–28].

Management zone estimation within the defined user plot by the AI algorithm is undertaken in two steps: first, by performing the K-means cluster analysis [29–31] and then by conducting the spatial filtration with the mode filter on the image created from obtained

cluster labels. The K-means takes as input a user-specified parameter K and feature vectors created per minimum area covered by pixels of multispectral images, which is defined by the maximum spatial resolution (10 m × 10 m) achieved by the Sentinel 2 Multispectral Imager (MSI) sensor. The feature vectors can contain various statistics extracted from provided data, such as the vegetation indices [31] calculated from the remote sensing images acquired by satellites or UAVs. For the results presented in this paper, the feature vector contains values of Normalized Difference Vegetation Index (NDVI) calculated using one or more Sentinel-2 images.

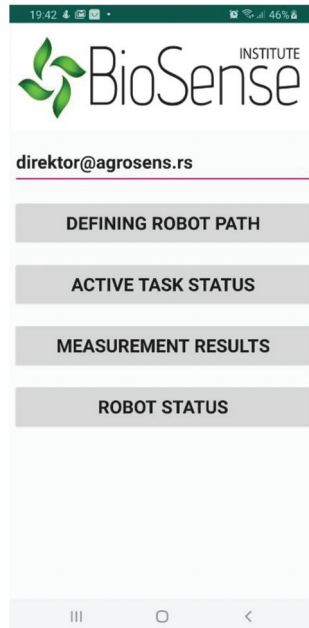
After generating an image with cluster labels obtained from K-means as pixel values, the second step of the AI algorithm consisting of spatial filtration by taking into account spatial statistics of labels is conducted. This step is necessary to obtain a smooth and more regular shape of boundaries of the management zone and to create connected components within the zones, by correcting the pixel labeling with the inclusion of the spatial context, Figure 2. The final step of the AI algorithm generates sampling points one for each of the connected components within the management zone (e.g., two sampling points for the red management zone since it has two connected components (see Figure 2)). Since the selection of sampling point locations is constrained by the maximal spatial resolution provided by input data, then only the GPS location of the pixel center can be selected as a coordinate for the sampling point. A GPS location of the pixel representing the center of the mass of the associated connected component is selected as the coordinate of the sampling point. The spatial filtration step of the AI algorithm can be repeated several times if the shape of the connected component is such that the center of the mass does not fall within the area of the connected component, Figure 2. The algorithm is implemented in the AgroSense platform as a real-time solution for defining the optimal sampling points of the selected field. The algorithm specifies one sampling point per connected component, but it can generate multiple points per management zone. At this moment, it was decided to optimize the system to cover a larger field area and save the battery for this purpose, and not spend it on additional sampling. The user has the option to manually move, add, and remove suggested sampling points. Once the user finishes the rearrangement of the sampling locations, the soil sampling and analysis task can be saved and downloaded using a smartphone application.



**Figure 2.** The results of the executed algorithm for proposing optimal sampling points within the AgroSense platform. Each color represents different management zones, while pin markers represent the optimal sampling points per zone.

## 2.2. Smartphone Application

The smartphone application was made for the robot Operator, the well-trained person that monitors the complete soil sampling and analysis procedure performed by a robotic system in the field. The application called RoboSense is designed to be simple to use and to allow the Operator effortless preparation of a new soil sampling task, have an insight into the current state of the active soil sampling task, edit the currently active soil sampling task, if necessary, as well as the possibility of insight into the state of the robotic system, which will be implemented in future work. Figure 3 shows the main menu of the RoboSense smartphone application.



**Figure 3.** The main menu of the RoboSense smartphone application.

The main menu presents the key functionalities of the application, which are the following:

- A field for entering the email address of the user that defined the soil sampling and analysis task is needed for downloading the task.
- A button “DEFINING ROBOT PATH” is used to define a new robot path.
- A button “ACTIVE TASK STATUS” is used to display the status of the active robot task.
- A button “MEASUREMENT RESULTS” is used to quickly display currently measured nitrate values.
- A button “ROBOT STATUS” is used to display robot status (battery level, water level, and system errors).

## 2.3. Robotic System

The robotic system is a combination of the commercially available UGV platform Husky and a custom-made solution for the task of soil sampling and analysis—minilab. The minilab is mounted on the robotic platform and consists of several main modules:

- Anchoring module.
- Sampling module.
- Sample preparation module.
- Module for soil analysis.



Electronic- and software-wise, a robotic platform is divided into two parts:

- UGV Husky platform, with software based on ROS (Robot Operating System) running on Linux.
- Custom electronics based on ATmega MEGA 2560, with firmware based on C++.

The complete model of the robot Lala, with an exploded view of the modules, is shown in Figure 4.



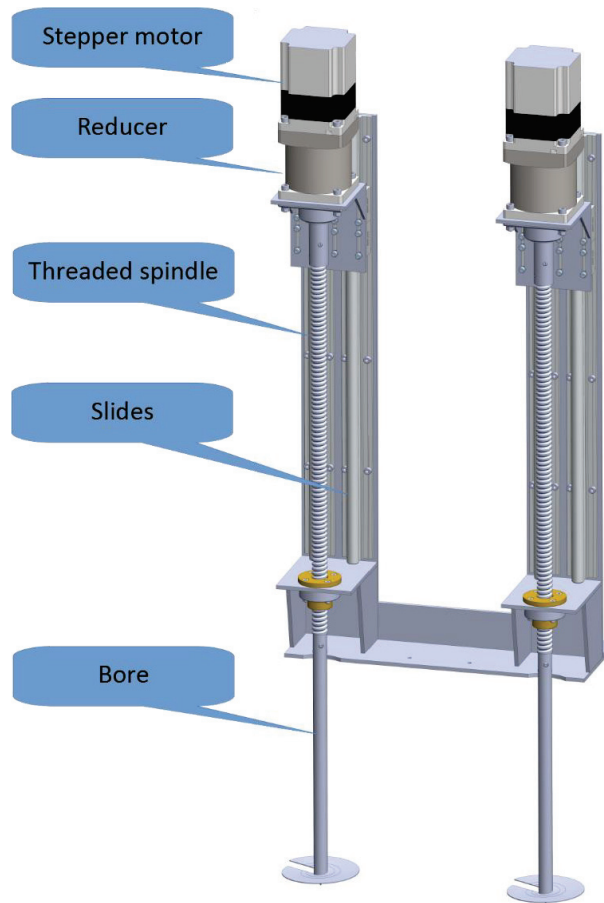
**Figure 4.** The 3D model of the exploded view of the agrobot Lala model.

The UGV platform's external dimensions are  $990 \times 670 \times 390$  mm. It weighs 50 kg and has a maximum payload of 75 kg. The maximum speed is 1.0 m/s and can achieve typically 3 h of autonomy.

The custom-made solution for soil sampling and analysis fits the UGVs width, and expands 40 cm in front of the UGV, with a total height from the ground of 200 cm. It can take samples from a 30 cm depth and can anchor to 15 cm. It can provide penetration force of up to 720 N. The speed of penetration and extraction, where the most reaction forces are exhibited, is 1 mm/s, while the sampler maximum speed is 3 mm/s. The anchoring speed is 2 mm/s for individual anchors, while the total speed is 1 mm/s concerning their reciprocating motion. While not anchoring, the speed is up to 10 mm/s.

### 2.3.1. Anchoring Module

During platform development, it was observed that the penetration forces, especially at higher depths, can be large. They can cause an uplift of the whole platform, which leads to an inadequate sample. This means that the volume of the sample is smaller, but the more severe effect is that the sample does not include a part from the required depth. Furthermore, this uplift can cause damage to the equipment, especially the probe, which can be bent or even broken. To prevent this from happening, the platform is equipped with a custom-made anchoring module, which is shown in Figure 5.



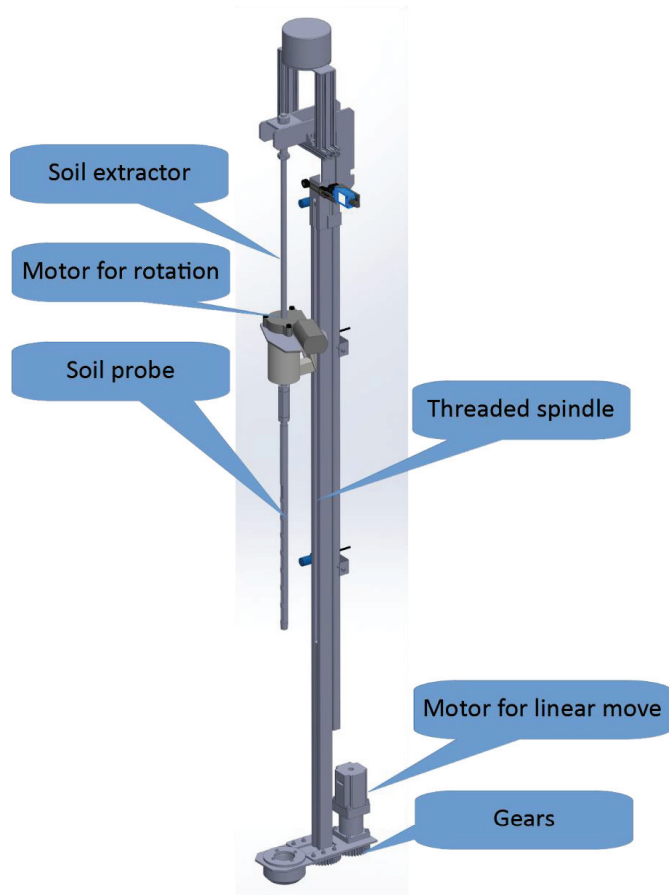
**Figure 5.** Model of the anchoring module.

The anchoring module consists of two linear stages, driven by the stepper motors (NEMA 34, 6.0 A, 8.7 Nm) over the 6:1 reducer. A threaded spindle with a 20 mm step is connected to the output of the reducer. This large step enables firm anchoring while saving instantaneous power needed for drilling. The threaded spindle moves together with motors on slides. The actuating end of the threaded spindle is extended with the bore, which has a single turn of the thread of approximately 80 mm in diameter, and a step equal to the step of the threaded spindle. This constellation enables smooth and efficient anchoring, without the milling effect on the soil. Again, the bore diameter is optimized between firm anchoring and the instantaneous power needed for the drilling. The estimation of the power needed for anchoring and optimization of the parameters was completed in a manual manner, where a manual thread typically used for round hole excavation is used along with a gauge to measure required forces. Due to the battery power, care is taken to minimize peak and overall power consumption.

The module is equipped with three inductive sensors per drive at dedicated positions. These positions indicate the top position, where the anchors are initialized and transported, a position where drilling starts at ground level, and a position at 15 cm anchoring depth. Besides inductive sensors, the anchoring module is also equipped with two mechanical hardwired end switches per drive for safety reasons at the topmost and bottommost positions.

### 2.3.2. Sampling Module

The sampling module serves to take a soil sample (Figure 6). It is based on the electric probe soil sampling method. Similar to the anchoring module, the sampling module is also a linear stage; however, a threaded spindle and a driving motor are at a fixed location, while the moving part is the soil sampling probe and the probe attachment.



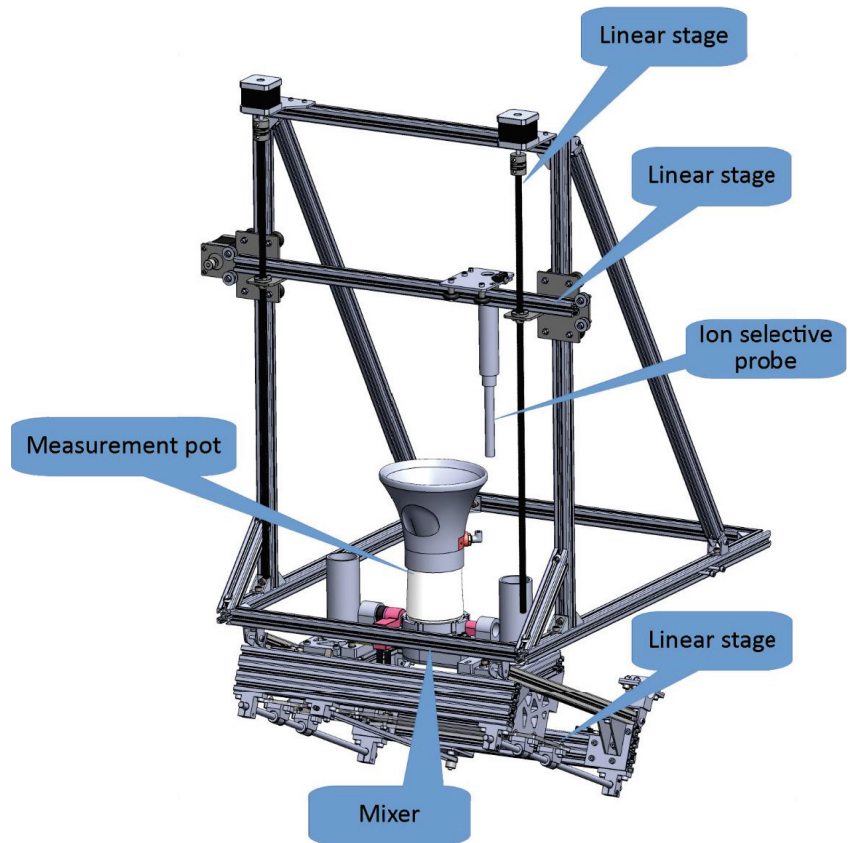
**Figure 6.** Model of the sampling module.

Besides linear movement, the probe also exhibits a rotational movement actuated by the motor placed at the top part of the soil probe. This rotational motion is executed before the probe is pulled from the soil at its lowest point. Namely, this move greatly reduces the initial force needed for a sample removal. Moreover, this rotation is implemented during the sample extraction process, where an extractor end is bore designed, therefore, the rotation creates boring, and the soil starts to fall out from the probe openings before it is extracted at the tip of the probe. This significantly reduces the peak force and power needed for the extraction and minimizes the stress on the material of the probe and the extractor. The threaded spindle has a 3 mm step and is driven by a stepper motor NEMA 23, 3 A, 1.8 Nm over a reducer of gear ratio 6:1. The gearbox and the threaded spindle are colinear and connected using two equal gears at the bottom of the module. The module is equipped with four inductive sensors at dedicated positions. These positions indicate the top position, where the extraction is accomplished, a position where the extraction starts,

a position where the probe tip is at ground level, and a position at 30 cm sample depth. For safety reasons, the sampling module is equipped with two mechanical hardwired end switches for safety reasons at the topmost and bottommost positions.

### 2.3.3. Sample Preparation Module

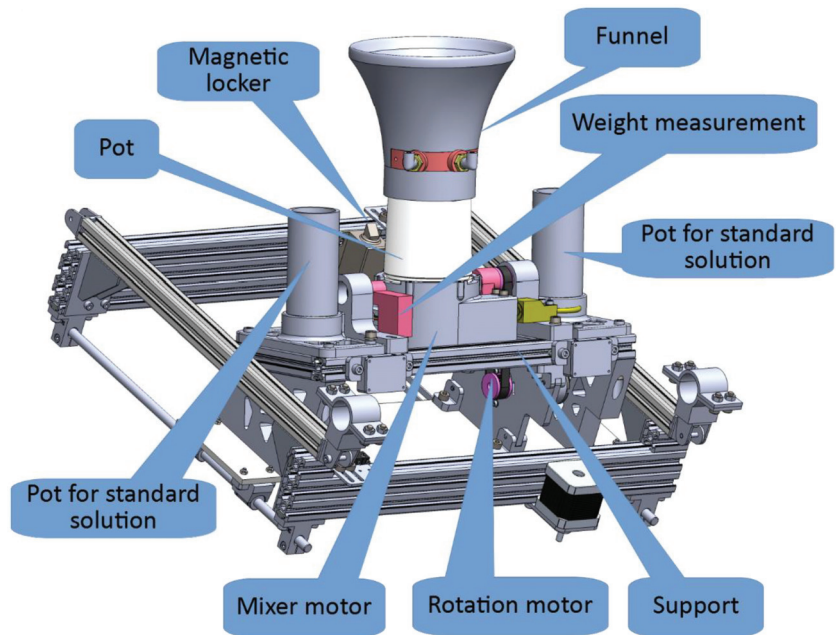
The main purpose of the sample preparation module is to prepare the solution of the soil sample suitable for measurement. It consists of 3-axes linear stages, a measurement pot with one rotational degree of freedom for cleaning purposes, and a mixer. The module is shown in Figure 7.



**Figure 7.** The 3D model of the sample preparation module.

The ion-selective probe used for soil sample measurement can be maneuvered alongside horizontal and vertical linear stages. Namely, horizontal movement enables the probe to position over the referent solutions or the prepared sample, while during vertical movement the probe can be immersed into referent solutions or the prepared sample. The third linear stage is slightly inclined and is used for platform movement. The moving platform is designed to carry the sample preparation pot and supporting parts. Alongside this stage, the measurement pot can be moved under the probe to collect the extracted soil sample or moved to an initial position where measurements with an ion-selective probe are conducted. During the cleaning process, the pot is moved to the dedicated position, where it can be rotated to pour out the sample solution and be cleaned.

The measurement pot consists of the pot, a funnel, support, a weight measurement unit, a motor for rotation, a mixer motor, and a magnetic locker (Figure 8).



**Figure 8.** The 3D model of the measurement pot with parts.

The funnel is used to collect falling parts of the soil sample. It also has integrated water channels and nozzles for two purposes. The first one is for the addition of an exact amount of deionized water (DI water), and the other is for cleaning purposes. Those systems are separated and are driven by different pumps. The pump for the precise addition of DI water is less powerful, therefore more easily controllable, while the pump for cleaning is a more powerful pump that can create a shower effect with many nozzles integrated into the funnel. The weight measurement is used to determine the collected soil sample mass and the mass of added DI water, hence their ratio. The amount of added water is predefined to 4:1; however, it can be less if the sample is heavier, and more if the sample is lighter. The magnetic locker secures the platform in the topmost position, enabling the stepper motors to be de-energized to save power.

Electrically wise, the sample preparation module incorporates:

- Three NEMA 17 stepper motors and associated end switches for linear movement.
- One geared DC motor for the rotation of the pot.
- One brushless motor to mix the sample.
- Two aluminum load cells to measure the soil sample weight, and the weight of added water.
- A magnetic locker.
- Two water pumps with a DI water reservoir.

#### 2.3.4. Module for Soil Analysis

The module for soil analysis is based on an ion-selective electrode (ISE) Vernier NO3-BTA. Besides the electrochemical ISE technique for soil nitrate determination, techniques such as spectrophotometric/spectrometric and biological are available as well. Due to the variable optical signatures of soil, these techniques require considerable site-specific calibration. The biological approach, although promising, should be improved concerning sensor robustness and lifetime. We decided to base our soil analysis module on the ISE probe since it offers the greatest potential for near-term accurate field analysis of nitrates [32].

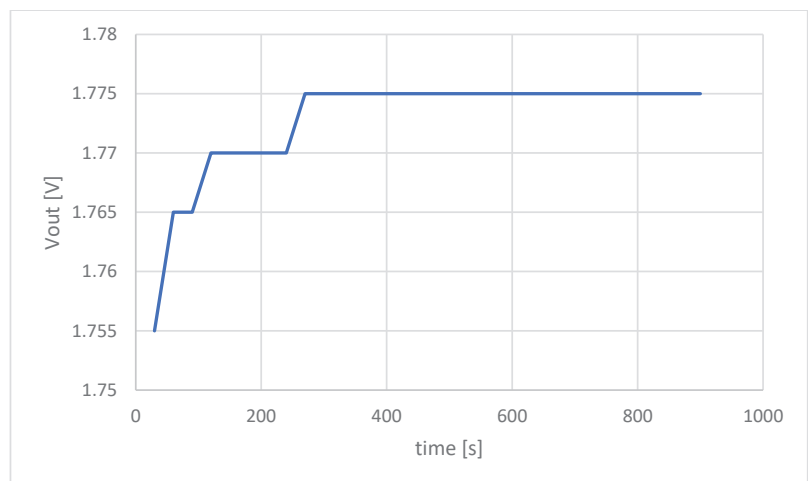
The operating principle of ISE is based on potentiometry, or more precisely, the measurement of the electric potential difference between referent and indicator electrodes which are immersed in a liquid solution with ions that are measured. The most important part of ion-selective electrodes is an ion-selective membrane that enables the passing of particular ions, in this case,  $\text{NO}_3^-$  ions, while preventing the passage of other ones.

The main advantage of ISE nitrates detection is that it does not demand filtration of the sample which significantly simplifies its use in the field.

The module for soil analysis overlaps, to some extent, with the sample preparation module, in the sense that it also uses two linear stages of the sample preparation module to maneuver the probe and the mixer. However, the main part of this module is the ion-selective probe for soil nitrates measurement Vernier  $\text{NO}_3\text{-BTA}$  [33]. Before field operation and any reliable and accurate measurement, the probe must be calibrated. For this purpose, a dedicated plane positioning system was developed consisting of the above-mentioned two linear stages, as well as two pots for standard solutions installed in the module. The calibration procedure is completed automatically on the robotic platform by using 50 and 200 mg/L calibration standards before each soil sampling and analysis task. Based on measurements of standard solutions, a calibration curve of exponential nature is derived. Subsequent measurements of the nitrates are then derived by inserting measured ADC values in this equation. The exact concentration of nitrates is also determined by the proportion of the soil sample mass and the mass of the added water, used to make an appropriate solution of the sample. This ratio is 4:1 in favor of water. Currently, a measurement of soil moisture is not implemented, and this can cause a small error in the measurement.

During the measurement, the sample solution is constantly mixed with a lower mixing speed to achieve a homogeneous solution. The measurement process takes 3.5 min, which is the time needed for the probe to stabilize the response.

Before integrating the module for soil analysis with the robotic platform, a series of benchtop laboratory tests were performed to optimize measurements and to test the accuracy of the proposed method against the referent one. To optimize the measurement time, the ISE probe was immersed in a 200 mg/L nitrate solution to determine dynamic output. As can be seen in Figure 9, the output voltage stabilized after 210 s; therefore, this measurement time was used in the continuation of the measurement.

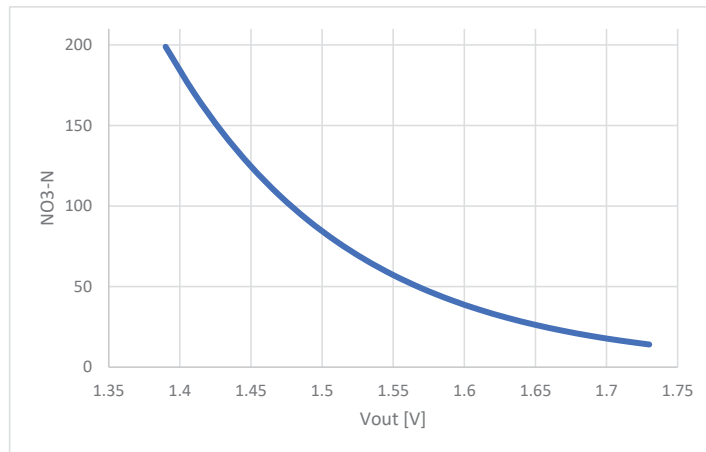


**Figure 9.** Dynamic response of the ISE probe for the nitrate standard concentration of 200 mg/L.

Afterward, a series of nitrate standards were prepared to calibrate the ISE probe. The nitrate concentrations were chosen to cover expected nitrate values in the field and were the



following: 0, 6.25, 12.5, 25, 50, 100, 150, and 200 mg/L. The measurements were performed with each standard and the calibration curve was constructed (Figure 10).



**Figure 10.** Calibration curve that relates ISE probe voltage output with nitrate-nitrogen concentration.

The relation between nitrate concentration and ISE probe voltage output is exponential:

$$C_N = a \times e^{bV_S}, \quad (1)$$

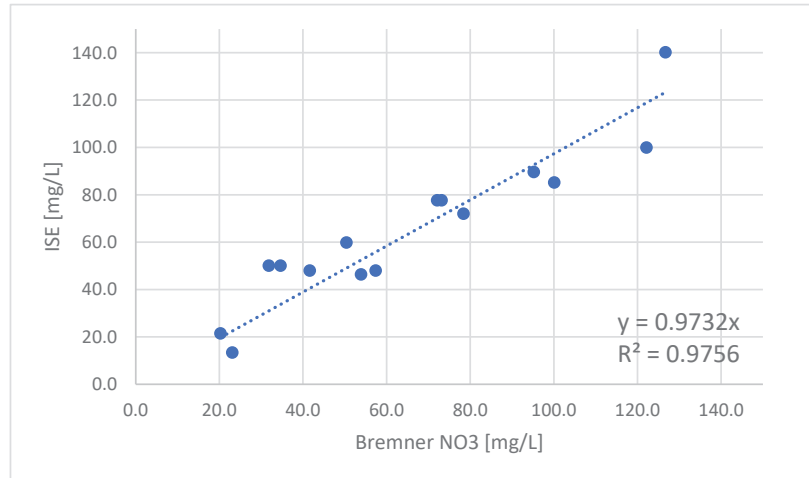
where  $C_N$  is nitrate concentration [mg/L],  $V_S$  is the voltage output of ISE probe [V], while  $a$  and  $b$  are coefficients determined by calibration. From the nature of this relation, it is clear that only two nitrate standards are sufficient to determine the calibration curve. This is also beneficial for the in-field system since there is no need to have all the calibration standards on the platform for the on-site calibration. By analyzing the errors between the calibration curve constructed with all the stated standards and the ones constructed with the help of all the possible standard pairs, it was concluded that the combination of 50 and 200 mg/L gives the lowest relative error with the respect to the full range which was 2.95%.

To test the calibration curve, 15 agricultural soil samples were used, and the results of nitrates measurements were cross compared to the results obtained according to the Bremner method for determination of inorganic nitrogen [34]. The comparison of results is presented in Table 1.

**Table 1.** Comparison between ISE probe nitrate-nitrogen measurement results and results obtained according to the Bremner method.

Sample	Bremner NO3-N [mg/L]	ISE NO3-N [mg/L]
1	20.3	21.4
2	23.1	13.3
3	31.9	50
4	34.7	50
5	41.7	47.9
6	50.4	59.8
7	53.9	46.3
8	57.4	47.9
9	72.1	77.6
10	73.2	77.6
11	78.4	71.9
12	95.2	89.5
13	100.1	85.1
14	122.2	99.9
15	126.7	140.1

The results are compared in graphical form, where the regression line that describes the actual relationship between the two methods is presented (Figure 11). It can be seen that the regression slope is 0.97, while the  $R^2$  factor is 0.97 based on which we can confirm that this method of calibration is validated.



**Figure 11.** Comparison between the referent Bremner method and ISE method for nitrate-nitrogen detection.

### 2.3.5. ROS Implementation

The main control of the platform is implemented through Robotic Operating System (ROS) running under the Linux platform. It comes with preinstalled drivers for all sensors provided by the vendor: LIDAR, Inertial Measurement Unit (IMU), motor drivers with sensors, and RTK GPS module. A ROS navigation package from the manufacturer is preinstalled and used for platform navigation in the field. A module that controls the whole system is developed in-house. This module receives and executes the task from the cloud server. It constantly updates the status of the task and each individual sample point within the task. This status can be monitored by a user (robot Operator) over a dedicated application on a smartphone.

Four ROS nodes are created to communicate with the custom-made electronics for the minilab. The first one publishes control messages for the minilab. The second one receives the responses to the issued commands published by the minilab. The third one receives the measurement results of the nitrate concentration. The last one is used to publish debugging information for the user to monitor the task execution.

There is a substantial list of ROS packages that are installed and used in the robotic platform; therefore, we just want to mention the most important ones in the following list sorted in alphabetical order:

- `actionlib`—provides a standardized interface for interfacing with preemptable tasks.
- `amcl`—a probabilistic localization system for a robot moving in 2D.
- `costmap 2D`—provides an implementation of a 2D costmap that takes in sensor data from the world, builds a 2D or 3D occupancy grid of the data.
- `imu_tools`—contains IMU-related filters and visualizers.
- `navigation`—a 2D navigation stack that takes in information from odometry, sensor streams, and a goal pose and outputs safe velocity commands that are sent to a mobile base.
- `move_base`—provides an implementation of an action that, given a goal in the world, will attempt to reach it with a mobile base.
- `nmea_comms` and `nmea_msgs`—for interfacing GPS.

- rosserial—for wrapping standard ROS serialized messages and multiplexing multiple topics and services over a character device such as a serial port or network socket.
- tf2—lets the user keep track of multiple coordinate frames over time.

### 2.3.6. Electronics

Hardware-wise, the electronics is based on Arduino ATmega MEGA 2560, and a firmware based on C++. The firmware controls all modules of the minilab, including their actuators and sensors. It has two serial interfaces to the external world. The first one is with the ROS platform. This is the main interface during the operation. The second interface serves for debugging and manual control purposes. It can be directly wire-interfaced, or more suitably over a Bluetooth (BT) wireless module, where the status and debug messages can be monitored during the whole process on a smartphone application. This interface, besides high-level commands for the whole processes, also allows low-level commands. The low-level commands are used for testing the individual features, but also for the manual control of the minilab in case of errors during normal operation.

### 2.3.7. An Overview of the System

An overview of the system is presented in Figure 12, based on which the basic procedure can be summarized in the following steps:

1. A farmer defines soil sampling and analysis tasks with the help of the AgroSense platform.
2. The Operator downloads the specific task from the AgroSense platform with the help of the RoboSense smartphone application and defines the optimal route.
3. The task prepared by the Operator is uploaded to the robotic system via the RoboSense server.
4. The robotic system performs the soil sampling and analysis task and during the process, the status of robotic system operations is being refreshed.
5. Once the task is finished, the Operator uploads the measurement results to the AgroSense platform.
6. A farmer selects the task to visualize the results for nitrogen content measurements.
7. A farmer creates a fertilization prescription map for the desired type of fertilizer.

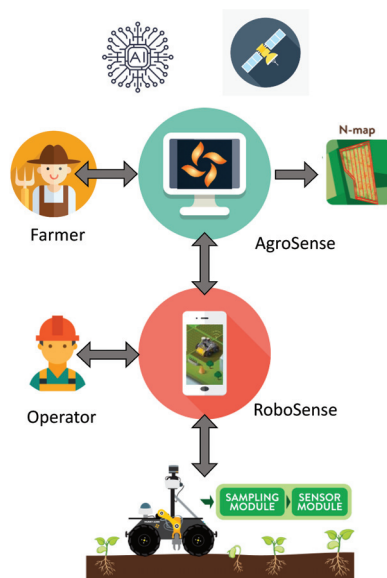


Figure 12. An overview of the system for soil sampling and analysis.

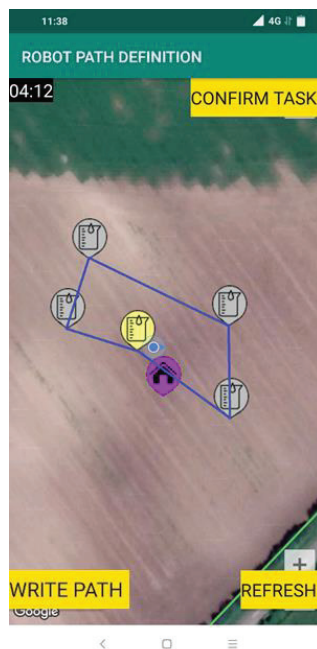
The cost of the entire robotic system is around EUR 50,000. The major expense is a commercial UGV platform, which costs about EUR 40,000. The rest goes to custom-made equipment. With this high cost, a targeted business model for this platform is to be provided as a service, especially having in mind the integration with the AgroSense platform which also provides agricultural services.

### 3. Results

The complete system was tested on the plot within the field of the commercial farm in the locality Krivaja, Serbia. The size of the plot was 1 ha. Plowing and tilling the plot were completed before performing the test of the robotic system.

The process started by defining the soil sampling and analysis task with the help of the cloud-based platform AgroSense. After defining the experimental plot and choosing the relevant satellite image, the algorithm for proposing the locations for soil sampling was initiated. As a result, in total, five points determining sampling locations were estimated within three different management zones (Figure 2). In this way, the soil sampling and analysis task was created, as can be seen in the upper right corner of Figure 2.

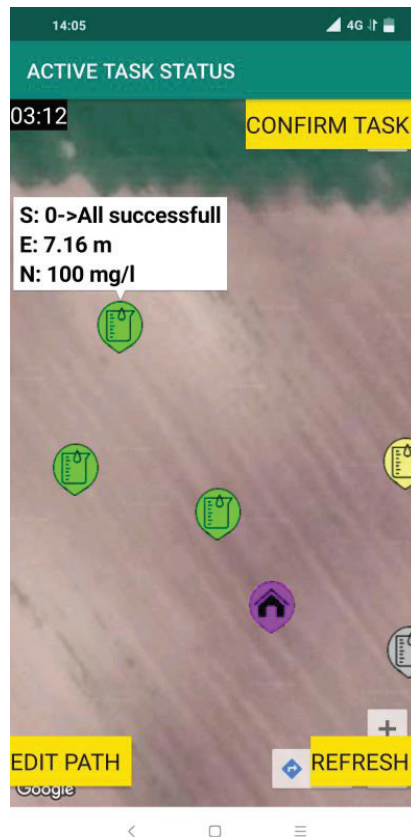
The task created in this way was downloaded using the smartphone application to initiate the soil sampling and analysis process. When the soil sampling task was opened, a Google map was displayed showing the defined sampling points in the form of markers. Next, the optimal route for the robotic system was created as shown by blue connecting lines in Figure 13.



**Figure 13.** Google map with sampling points and optimal route.

It is important to note that if there is a need, the route and sampling points can be edited by the Operator, which was not done in this example case. In this case, the route was confirmed and uploaded to the cloud-based platform by pressing the “WRITE PATH” button. Next, the robotic system was initiated by the Operator, meaning that the system entered the procedure for soil sampling and analysis. First, the robotic system completed the initialization of each module, afterward, the soil sampling and analysis task was downloaded from the AgroSense server. Next, the robotic system visited the

first point in the downloaded list. Before the sampling was completed the robotic system performed the calibration of the ion-selective electrode for measuring nitrate content. After the calibration process, the robotic system undertook routines of anchoring, soil sampling, sample preparation, analysis of the sample, cleaning, un-anchoring, and moving to the next location. The movement of the robotic system was stable, and it successfully overcame all the bumps in the field. If the plot was only plowed, furrow would cause stability issues. The robotic system regularly updated the status of each step of the soil sampling and analysis procedure by sending messages to the AgroSense server, which could be seen by choosing the “ACTIVE TASK STATUS” option from the main menu. Depending on the status, the sampling points were displayed with markers of different colors (Figure 14). The sampling points that have the initial status are shown in gray, meaning the robot has not yet visited the point. The yellow color represents the sampling point at which the robot was currently engaged. The sampling points at which all sampling tasks were performed successfully were shown in green. By clicking on the sampling point marker for a given point additional information such as the current status of the sampling point (status code and brief status description), robot positioning error in meters (distance between specified and achieved robot coordinates), and measured nitrate value if available was displayed.



**Figure 14.** Active task status.

When the robot successfully visited all sampling points by clicking on the “CONFIRM TASK” button the Operator confirms that the active task on the parcel has been completed and the measurement results become available on the AgroSense platform.

The measurement results of this example case are presented in Table 2.

**Table 2.** The measurement results from the test performed on the plot within the field of the commercial farm in the locality Krivaja, Serbia.

Sample	Mass [g]	NO3 [mg/L]	NO3-N [kg N ha <sup>-1</sup> ]
1	37.06	196.38	177.00
2	23.27	175.01	157.74
3	36.05	85.07	76.68
4	45.52	91.70	82.65
5	33.35	98.64	88.91

Based on the measurement results, a fertilization prescription map was generated (Figure 15). Fertilization prescription was completed based on the optimal value of nitrogen in the field which was taken to be 30 ppm. This was just above the critical value of nitrate-nitrogen needed for the maize [35]. Based on the in-field measurement results and nitrogen target value, the amount of missing nitrogen was determined and prescribed to be applied. Green pins represent the locations of the actual sampling points which are different from the proposed ones due to the positioning error.



**Figure 15.** Fertilization prescription map generated based on the measurement results. Red pins represent proposed sampling locations by AI algorithm, while green pins represent actual sampling locations.

#### 4. Discussion

We presented a complete system for soil sampling and analysis intended to help farmers to optimize fertilization in their fields and, in this way, be more efficient in a sustainable way. An overview of the system is presented in Figure 12. The presentation of the system and its functionalities can be seen in a promotional video [36]. The system consists of a user-oriented platform called AgroSense which the farmer uses to define the soil sampling and analysis task with the help of high-resolution satellite images and an AI algorithm. The same platform is used for the visualization of the measurement results and



obtaining the fertilization prescription. The next component of the system is the RoboSense application which is used by the Operator in the field to monitor the soil sampling and analysis task that is performed by the robotic system.

The system was tested in an operational environment in the 1 ha experimental field, during which all the stated functionalities of the system were successfully demonstrated. The complete task took 165 min to be completed, during which five samples were taken. The measurement results showed slightly higher values of nitrate-nitrogen than usual [37] which can be explained by the fact that two days before the tests, the base fertilization was performed.

It should be noted that the fertilization prescription algorithm was tested previously, on another 5 ha experimental field. In this case, soil samples were taken from the field and tested for nitrate concentration with the same ISE probe. Based on the results, a fertilization prescription was completed. The average yield of the experimental field was 1.76% higher in comparison to the entire plot, which is a promising result but should be repeated in future seasons. It should be noted that at the same time more than 7.5% of KAN fertilizer was saved.

At this level, all the functionalities of the system were successfully demonstrated in an operational environment, but it still needs to be further tested to include different real-life scenarios and environmental conditions before it could become commercially available. Furthermore, it should be noted that soil sampling analysis was not corrected for the soil moisture content but mixing the soil sample with water by a ratio of 1:4 reduces the soil moisture influence. In the future, a soil moisture sensor could be integrated into the platform to have more accurate measurements. In addition, since the main challenge of taking the sample from the soil is resolved, a different sensor such as multi-ion probes could be used on the same sample to measure the rest of the important soil nutrients by detecting ions such as  $\text{Ca}^{2+}$ ,  $\text{K}^+$ ,  $\text{Mg}^{2+}$ ,  $\text{NH}_4^+$ ,  $\text{NO}_3^-$ ,  $\text{P}[\text{HPO}_4^{2-}]$ ,  $\text{Cl}^-$ , and  $\text{Na}^+$  [38], together with parameters such as pH and electrical conductivity.

Since the robotic system is equipped with RTK GPS, it could be used for ground-based topographic mapping to generate high-resolution elevation data at the landscape level. The generated maps are highly useful in the understanding of soil water and nutrient movement and would represent an additional valuable level of information for farmers.

In the future, the autonomy of the robotic system could be improved by optimizing soil sampling and analysis procedures as well as by using an advanced battery solution that is based on  $\text{LiFePo}_4$  technology which can offer up to 10 times more capacity.

## 5. Conclusions

This paper represents Agrobot Lala—an autonomous robotic system for real-time, in-field soil sampling and analysis of nitrates. The presented solution helps with fertilization optimization which leads to more efficient production in a sustainable way. The system comprises a cloud-based application for task management and generation of sample points on the plot based on proprietary algorithms of artificial intelligence (AI), a smartphone application for monitoring and customization of the tasks, and a robotic system for fieldwork of acquiring and analysis of soil samples.

With the help of the system, a farmer defines soil sampling and analysis tasks with the help of a cloud-based platform and AI algorithm. The task is performed by the robotic system providing the measurement results in real-time. As the result of the analysis, a fertilization prescription is generated which reached more than 7.5% of KAN fertilizer savings and showed a 1.76% yield improvement during the initial test. All the stated functionalities of the system were verified on the 1 ha experimental field by taking and analyzing 5 soil samples.

The presented system can be significantly improved by introducing a multi-ion probe for detecting additional important nutrients in the soil besides nitrates, as well as additional sensors for pH and electrical conductivity measurements.

**Author Contributions:** Conceptualization G.K., D.K., C.P., S.B. and V.C.; methodology, G.K., D.K., C.P., S.B., M.P. and V.C.; software D.K., C.P. and M.P.; validation G.K., D.K., C.P. and S.B.; investigation M.P.; writing—original draft preparation G.K. and D.K.; writing—review and editing G.K., D.K., M.P. and V.C.; visualization G.K., D.K. and M.P.; project administration G.K. All authors have read and agreed to the published version of the manuscript.

**Funding:** This research was funded by HORIZON 2020 agROBOfood project, Grant agreement ID: 825395 and HORIZON 2020: ANTARES project, Grant agreement ID: 739570. The APC was funded by The Ministry of Education, Science and Technological Development of the Republic of Serbia.

**Institutional Review Board Statement:** Not applicable.

**Informed Consent Statement:** Not applicable.

**Data Availability Statement:** Data is contained within the article.

**Conflicts of Interest:** The authors declare no conflict of interest.

## References

- Bruinsma, J. (Ed.) Chapter 1 Introduction and overview. In *World Agriculture: Towards 2015/2030, An FAO Perspective*, 1st ed.; Earthscan Publications Ltd.: London, UK, 2003; pp. 1–28.
- Houlès, V.; Guérif, M.; Mary, B. Elaboration of a Nitrogen Nutrition Indicator for Winter Wheat Based on Leaf Area Index and Chlorophyll Content for Making Nitrogen Recommendations. *Eur. J. Agron.* **2007**, *27*, 1–11. [[CrossRef](#)]
- Pennock, D.; Yates, T.; Braidek, J. Chapter 1 Soil Sampling design. In *Soil Sampling and Methods of Analysis*, 2nd ed.; Carter, M.R., Gregorich, E.G., Eds.; CRC Press, Taylor & Francis Group: Boca Raton, FL, USA, 2006; pp. 25–38.
- Four Soil Collection Methods That Actually Work. Available online: <https://growers.ag/blog/4-soil-collection-methods-that-actually-work/> (accessed on 13 April 2022).
- Martínez-Dalmau, J.; Berbel, J.; Ordóñez-Fernández, R. Nitrogen Fertilization. A Review of the Risks Associated with the Inefficiency of Its Use and Policy Responses. *Sustainability* **2021**, *13*, 5625. [[CrossRef](#)]
- Sikora, J.; Niemiec, M.; Szlag-Sikora, A.; Gródek-Szostak, Z.; Kuboń, M.; Komorowska, M. The Impact of a Controlled-Release Fertilizer on Greenhouse Gas Emissions and the Efficiency of the Production of Chinese Cabbage. *Energies* **2020**, *13*, 2063. [[CrossRef](#)]
- Aravind, K.R.; Raja, P.; Pérez-Ruiz, M. Task-based agricultural mobile robots in arable farming: A review. *Span J. Agric. Res.* **2007**, *15*, e02R01. [[CrossRef](#)]
- Blackmore, B.S.; Fountas, S.; Gemtos, T.A.; Griepentrog, H.W. A Specification for an Autonomous Crop Production Mechanization System. *Acta Hort.* **2009**, *824*, 201–216. [[CrossRef](#)]
- Rossel, R.A.V.; McBratney, A.B. Soil Chemical Analytical Accuracy and Costs: Implications from Precision Agriculture. *Aust. J. Exp. Agric.* **1998**, *38*, 765. [[CrossRef](#)]
- McGrath, D.; Skotnikov, A. Possibility of Different Soil Sampling Techniques with Automated Soil Sampler. *Commun. Soil Sci. Plant Anal.* **1996**, *27*, 1779–1794. [[CrossRef](#)]
- Rogo Ag. Available online: <https://rogoag.com/> (accessed on 13 April 2022).
- Olmedo, N.A.; Barczyk, M.; Zhang, H.; Wilson, W.; Lipsett, M.G. A UGV-Based Modular Robotic Manipulator for Soil Sampling and Terramechanics Investigations. *J. Unmanned Veh. Syst.* **2020**, *8*, 364–381. [[CrossRef](#)]
- Cao, P.M.; Hall, E.L.; Zhang, E. Soil Sampling Sensor System on a Mobile Robot. *SPIE Proc.* **2003**. [[CrossRef](#)]
- Vaeljaots, E.; Lehiste, H.; Kiik, M.; Leemet, T. Soil Sampling Automation Case-Study Using Unmanned Ground Vehicle. *Eng. Rural. Dev.* **2018**, *17*, 982–987. [[CrossRef](#)]
- HUSKY Unmanned Ground Vehicle. Available online: <https://clearpathrobotics.com/husky-unmanned-ground-vehicle-robot/#~:text=Husky%20is%20a%20medium%20sized,UGV%20by%20our%20integration%20experts> (accessed on 30 March 2022).
- AgroSense Digital Platform. Available online: <https://agrosens.rs/#/app-h/about> (accessed on 13 April 2022).
- Sabbe, W.E.; Marx, D.B. Soil sampling: Spatial and temporal variability. In *Soil Testing: Sampling, Correlation, Calibration, and Interpretation*; SSSA: Washington, DC, USA, 1987; Volume 21, 14p.
- Wollenhaupt, N.C.; Wolkowski, R.P. Grid soil sampling. *Better Crops* **1994**, *78*, 6–9.
- Khosla, R.; Fleming, K.; Delgado, J.A.; Shaver, T.M.; Westfall, D.G. Use of site specific management zones to improve nitrogen management for precision agriculture. *J. Soil Water Conserv.* **2002**, *57*, 513–518.
- Ali, A.; Rondelli, V.; Martelli, R.; Falsone, G.; Lupia, F.; Barbanti, L. Management Zones Delineation through Clustering Techniques Based on Soils Traits, NDVI Data, and Multiple Year Crop Yields. *Agriculture* **2022**, *12*, 231. [[CrossRef](#)]
- Jaynes, D.B.; Kaspar, T.C.; Colvin, T.S.; James, D.E. Cluster Analysis of Spatiotemporal Corn Yield Patterns in an Iowa Field. *Agron. J.* **2003**, *95*, 574–586. [[CrossRef](#)]
- Corwin, D.L.; Lesch, S.M.; Shouse, P.J.; Soppe, R.; Ayars, J.E. Identifying Soil Properties That Influence Cotton Yield Using Soil Sampling Directed by Apparent Soil Electrical Conductivity. *Agron. J.* **2003**, *95*, 352–364. [[CrossRef](#)]

23. Hansen, P.M.; Schjoerring, J.K. Reflectance Measurement of Canopy Biomass and Nitrogen Status in Wheat Crops Using Normalized Difference Vegetation Indices and Partial Least Squares Regression. *Remote Sens. Environ.* **2003**, *86*, 542–553. [[CrossRef](#)]
24. Guastaferro, F.; Castrignano, A.; De Benedetto, D.; Sollitto, D.; Troccoli, A.; Cafarelli, B. A Comparison of Different Algorithms for the Delineation of Management Zones. *Precis. Agric.* **2010**, *11*, 600–620. [[CrossRef](#)]
25. Ormsby, J.P.; Choudhury, B.J.; Owe, M. Vegetation spatial variability and its effect on vegetation indices. *Int. J. Remote Sens.* **1987**, *8*, 1301–1306. [[CrossRef](#)]
26. Townshend, J.R.G.; Justice, C.O. Spatial variability of images and the monitoring of changes in the normalized difference vegetation index. *Int. J. Remote Sens.* **1995**, *16*, 2187–2195. [[CrossRef](#)]
27. Ali, A.; Martelli, R.; Lupia, F.; Barbanti, L. Assessing multiple years' spatial variability of crop yields using satellite vegetation indices. *Remote Sens.* **2019**, *11*, 2384. [[CrossRef](#)]
28. Glenn, E.P.; Huete, A.R.; Nagler, P.L.; Nelson, S.G. Relationship between remotely-sensed vegetation indices, canopy attributes and plant physiological processes: What vegetation indices can and cannot tell us about the landscape. *Sensors* **2008**, *8*, 2136–2160. [[CrossRef](#)] [[PubMed](#)]
29. Marino, S.; Alvino, A. Vegetation Indices Data Clustering for Dynamic Monitoring and Classification of Wheat Yield Crop Traits. *Remote Sens.* **2021**, *13*, 541. [[CrossRef](#)]
30. Praetyo, S.Y.J.; Hartomo, K.D.; Simanjuntak, B.H.; Candra, D.W. Mitigation & identification for local aridity, based of vegetation indices combined with spatial statistics & clustering k means. IOP Publishing. *J. Phys. Conf. Ser.* **2019**, *1235*, 012028. [[CrossRef](#)]
31. Netto, A.F.A.; Martins, R.N.; de Souza, G.S.A.; de Moura Araujo, G.; de Almeida, S.L.H.; Capelini, V.A. Segmentation of RGB images using different vegetation indices and thresholding methods. *Nativa* **2018**, *6*, 389–394. [[CrossRef](#)]
32. Sinfield, J.V.; Fagerman, D.; Colic, O. Evaluation of Sensing Technologies for On-the-Go Detection of Macro-Nutrients in Cultivated Soils. *Comput. Electron. Agric.* **2010**, *70*, 1–18. [[CrossRef](#)]
33. Vernier NO3-BTA. Available online: <https://www.vernier.com/manuals/no3-bta/> (accessed on 13 April 2022).
34. Bremner, J.M. Total Nitrogen. In *Agronomy Monographs*; American Society of Agronomy: Washington, DC, USA, 2016; pp. 1149–1178. [[CrossRef](#)]
35. Olness, A.; Lopez, D.; Archer, D.; Cordes, J.; Sweeney, C.; Mattson, N.; Rinke, J.; Voorhees, W.B. Factors Affecting Microbial Formation of Nitrate-Nitrogen in Soil and Their Effects on Fertilizer Nitrogen Use Efficiency. *Sci. World J.* **2001**, *1*, 122–129. [[CrossRef](#)] [[PubMed](#)]
36. Agrobot Lala. Available online: <https://www.youtube.com/watch?v=seU82D8w9RA> (accessed on 14 April 2022).
37. Cui, Z.; Zhang, F.; Miao, Y.; Sun, Q.; Li, F.; Chen, X.; Li, J.; Ye, Y.; Yang, Z.; Zhang, Q.; et al. Soil Nitrate-N Levels Required for High Yield Maize Production in the North China Plain. *Nutr. Cycl. Agroecosyst.* **2008**, *82*, 187–196. [[CrossRef](#)]
38. CleanGrow Multi-Ion Nutrient Analyzer Kit. Available online: <https://www.ionselectiveelectrode.com/products/cleangrow-multi-ion-nutrient-analyzer-kit> (accessed on 13 April 2022).

## Article

# Proposing UGV and UAV Systems for 3D Mapping of Orchard Environments

Aristotelis C. Tagarakis <sup>1,\*</sup>, Evangelia Filippou <sup>1</sup>, Damianos Kalaitzidis <sup>1</sup>, Lefteris Benos <sup>1</sup>, Patrizia Busato <sup>2</sup> and Dionysis Bochtis <sup>1,3,\*</sup>

<sup>1</sup> Institute for Bio-Economy and Agri-Technology (IBO), Centre for Research and Technology-Hellas (CERTH), 6th km Charilaou-Thermi Rd, GR 57001 Thessaloniki, Greece; e.filippou@certh.gr (E.F.); d.kalaitzidis@certh.gr (D.K.); e.benos@certh.gr (L.B.)

<sup>2</sup> Department of Agriculture, Forestry and Food Science (DISAFA), University of Turin, Largo Braccini 2, 10095 Grugliasco, Italy; patrizia.busato@unito.it

<sup>3</sup> FarmB Digital Agriculture P.C., Doiranis 17, GR 54639 Thessaloniki, Greece

\* Correspondence: a.tagarakis@certh.gr (A.C.T.); d.bochtis@certh.gr (D.B.)

**Abstract:** During the last decades, consumer-grade RGB-D (red green blue-depth) cameras have gained popularity for several applications in agricultural environments. Interestingly, these cameras are used for spatial mapping that can serve for robot localization and navigation. Mapping the environment for targeted robotic applications in agricultural fields is a particularly challenging task, owing to the high spatial and temporal variability, the possible unfavorable light conditions, and the unpredictable nature of these environments. The aim of the present study was to investigate the use of RGB-D cameras and unmanned ground vehicle (UGV) for autonomously mapping the environment of commercial orchards as well as providing information about the tree height and canopy volume. The results from the ground-based mapping system were compared with the three-dimensional (3D) orthomosaics acquired by an unmanned aerial vehicle (UAV). Overall, both sensing methods led to similar height measurements, while the tree volume was more accurately calculated by RGB-D cameras, as the 3D point cloud captured by the ground system was far more detailed. Finally, fusion of the two datasets provided the most precise representation of the trees.

**Keywords:** smart agriculture; depth cameras; 3D mapping; 3D point clouds; situation awareness

**Citation:** Tagarakis, A.C.; Filippou, E.; Kalaitzidis, D.; Benos, L.; Busato, P.; Bochtis, D. Proposing UGV and UAV Systems for 3D Mapping of Orchard Environments. *Sensors* **2022**, *22*, 1571. <https://doi.org/10.3390/s22041571>

Academic Editor: Arturo de la Escalera Hueso

Received: 26 December 2021

Accepted: 14 February 2022

Published: 17 February 2022

**Publisher's Note:** MDPI stays neutral with regard to jurisdictional claims in published maps and institutional affiliations.



**Copyright:** © 2022 by the authors. Licensee MDPI, Basel, Switzerland. This article is an open access article distributed under the terms and conditions of the Creative Commons Attribution (CC BY) license (<https://creativecommons.org/licenses/by/4.0/>).

## 1. Introduction

### 1.1. General Context of RGB-Depth Cameras

Many tasks such as mapping, localization, navigation, 3D reconstruction of object, or scenery, among others, involve computer vision. Computer vision could be described as the technology that combines image processing through computational algorithms to obtain certain information from images [1–3] or vision systems utilizing laser scanners [4]. Focusing on the former case, a lot of studies have used RGB cameras so as to locate and distinguish the targets (e.g., fruits) from other objects by exploiting, for example, the shape, the color and the texture, usually combining their images with machine learning [3,5,6]. However, RGB cameras can only get two-dimensional (2D) information of the scene, while they are susceptible to variable light conditions and occlusions [7]. These challenges have been overcome through acquiring depth measurements of higher resolution, which have the potential to provide more detailed information about the scene. In particular, in the last decade, consumer-grade depth cameras have gained advantage over other sensors, given their low cost, portability, ease of use and measurement accuracy [8]. In brief, an RGB-D camera comprises two parts coupled together to give a dense matrix of pixel values; (a) an RGB camera for providing color information and (b) a depth camera for providing depth information [9]. Consequently, every pixel constructing the image is composed of color and distance values between a view-point and a certain point in the image (RGB-D values).

### 1.2. Use of RGB-D Cameras and Related Research in Agriculture

This type of camera has been applied in a number of areas of interest, such as indoor [10–12] and outdoor mapping [13], 3D reconstruction [14,15], motion and gesture recognition [16–18], and object detection [19]. Moreover, there has been an extensive use in robotics field and more specifically in navigation [19] and localization [2].

In recent years, stereoscopic vision depth cameras have been widely used in 3D reconstruction of objects and 3D mapping related to indoor environments [12,20]. Indicatively, the ZED stereo camera (Stereolabs Inc., San Francisco, CA, USA) has been employed in various indoor scenarios, namely volume designation of simple cubic and cylindrical objects through image segmentation process [21], crack detection and analysis on concrete surfaces using 3D data [22], terrestrial photogrammetry through an aerial mapping system [23], as well as the creation of indoor 3D mapping targeting to be used in studies for “smart” cities [24].

A plethora of researchers have studied the use of depth cameras in agricultural applications and identified their advantages and disadvantages in outdoor sceneries. An evaluation of five different depth cameras of three dissimilar technologies in agricultural applications was made by Condotta et al. [25]. According to their results, all cameras provided effective depth data indoors. Nonetheless, in outdoor environments the cameras using structured light and time-of-flight technology proved to be problematic, due to distortions by the intense lighting conditions. In particular, the aforementioned lighting may cause low contrast in the infrared image and lead to gaps in the corresponding depth image [25]. In outdoors applications, the most reliable data were provided by cameras using stereoscopy. Moreover, depth cameras were applied in agricultural applications for weed detection and above ground biomass volume estimation through 3D point clouds reconstruction [26]. In addition, efficient results in extraction of geometric structural parameters of vegetation with depth measurements were determined [27,28]. An effective approach of measuring the canopy structure on small plant populations in field conditions was presented in [29]. Furthermore, Jiang et al. [30] developed an approach to automatically quantify cotton canopy size in field conditions and showed the potential of using multidimensional traits as yield predictors. Additionally, an experiment using four different depth sensors in agricultural tasks was conducted by Vit and Shani [31], who estimated the quality of depth measurements for geometrical size estimation of agricultural objects with deep learning techniques. In tree crops, size estimation of mango fruits on trees in outdoor environment was made by Wang et al. [32].

Some of the RGB-D cameras are joined or can be combined with other sensors that allow for position and orientation of the camera to be recorded. Such sensors are, for example, inertial measurement units (IMUs) or global positioning system (GPS) sensors that provide positioning, velocity, and time information. As a result, depth cameras can be used to collect geometrical information about the environment and provide them as an input for robot localization and navigation. These added features in depth cameras are very useful for autonomous applications in agriculture or for capturing information about plants’ phenotype and growth. Studies have also been performed on the use of RGB-D cameras along with robotic systems to capture not only color information, but also spatial information about the environment. In addition, in [33] a solution was presented for autonomous obstacle avoidance performance of a UAV by using a deep learning-based object detection method and image processing with a depth camera. Another research, using depth camera mounted on an operational vehicle in an agricultural field, was presented in [34] for the reconstruction of the grapevines’ canopy to measure its volume as well as detect and count the grapevine bunches. Finally, Sa et al. [35] presented an accurate 3D detection method for sweet peppers peduncles in a farm field by using a depth camera on a robotic arm and a supervised machine learning approach.

### 1.3. 3D Mapping Procedures

With 3D mapping, the integration of appearance and shape information from depth sensors can be accomplished [36]. Some of the most commonly used tools for 3D mapping are the Octomap (University of Freiburg, Freiburg im Breisgau, Germany) [37] and real-time appearance-based mapping (RTABMap; Sherbrooke, QC, Canada). In particular, these tools are libraries related to the robot operating system (ROS).

The ROS software [38] for 3D mapping is widely used in robotic applications. More specifically, these tools can simultaneously capture and extract in a 3D map the environment area that a sensor is scanning, with the ability of representing it on a visualization tool. Octomap could be described as a probabilistic tool for 3D mapping, which is based on Octrees. An Octree is an information storing technique in a tree structure, in which there are nodes that each of them has eight “children”. The connection of all these nodes merges all the scanned data and generates continuous 3D maps. Apart from that, Octomap 3D mapping tool is a process which can efficiently recognize changes in the environment dynamically [39]. More specifically, the produced virtual environment with Octomap is composed of less noise from objects and robot position failures. Octomap meets four basic requirements. Firstly, free and occupied space, as it creates full 3D modeling and, secondly, it is updatable. Consequently, it is flexible, as the map can be expanded dynamically, while it is compact, as the produced map can be stored in memory and disk. It is worth mentioning that as compared with other 3D mapping tools, Octomap presents low computational load and memory usage. However, Octomap produces maps with only the depth data, which means that the points have only position information ( $x, y, z$ ) and not color information (RGB).

Opposing Octomap, RTABMap creates 3D maps of the scanned environment with both color and depth data (RGB-D). A notable advantage of this 3D mapping tool is the fact that it provides a complete representation of the environment using the simultaneous localization and mapping (SLAM) algorithm. However, a main disadvantage of RTABMap is that it may lead to noisy maps, as it is unable to recognize dynamic objects [39]. In conclusion, these 3D maps can be stored for further processing and visualized in the ROS visualization tool (Rviz).

### 1.4. 3D Mapping Using Aerial-Based Systems

With the recent technological developments in the agricultural sector and the rise of digital agriculture and artificial intelligence, the use of unmanned aerial systems (UAS) is gaining popularity. This is mainly due to the fact that dedicated systems for commercial use have been made available to public [40]. Moreover, in contrast with satellite imagery, images acquired by UAS tend to demonstrate higher resolutions in both temporal (e.g., daily collections) and spatial (e.g., centimeters) level, while being insusceptible to cloud cover, thus, rendering them suitable for precision agriculture applications [41]. Furthermore, there is a high level of automatization in the analysis of the acquired images providing a range of products, such as orthomosaics with high spatial accuracy and 3D point clouds from the surveyed areas. An indicative recent study of using UAVs for agricultural applications is that of Christiansen et al. [42], where data collected from a LiDAR sensor mounted on a UAV were fused with global navigation satellite system (GNSS) and IMU data to carry out winter wheat field mapping for point clouds. Additionally, Anagnostis et al. [40] used UAS-derived images and deep learning to identify and segment tree canopies of orchards under diverse conditions. In addition, Gašparović et al. [43] combined classification algorithms with UAV images to map weeds in oat fields. Remarkably, RGB images from UAVs in conjunction with convolutional neural networks (CNNs) are constantly gaining ground [44–46], as highlighted in the recent literature review of Benos et al. [3].

### 1.5. Aim of the Present Study

All the above methods presented have certain drawbacks or do not consider RGB-D cameras. The aim of the present study was to investigate the use of RGB-D camera and UGV



platform to autonomously map the environment of commercial orchards, map the location of trees and provide assessments of the tree size in terms of height and canopy volume by exporting and analyzing 3D point clouds. The results from the ground-based mapping system were compared with 3D orthomosaics acquired via an UAS. Finally, the fusion of the two datasets was performed as a means of reaching to a more accurate representation.

## 2. Materials and Methods

A ZED 2 depth camera, consisting of a stereo 2K camera with two color sensors (RGB) was used for the 3D reconstruction of orchard trees. The specific sensor has a horizontal field of view of  $110^\circ$  and can stream at a rate from 15 to 100 FPS, depending on the resolution. The camera's connectivity is compatible to Universal Serial Bus (USB) 2.0. The baseline of 12 cm (distance between the left and right RGB sensor) manages a range of depth perception between 0.2 and 20 m. The most important characteristics of the ZED camera are summarized in Table 1.

**Table 1.** Main characteristics of ZED camera used in the study.

Sensor	RGB		
Lens	<i>f</i> /1.8 aperture		
Depth range	0.2–20 m		
Field of view (horizontal, vertical, diagonal)	110° (H), 70° (V), 120° (D)		
		Resolution (pixels)	Frame rate (Frames per second)
Single image and depth resolution (pixels)	HD2K	2208 × 1242	15 FPS
	HD1080	1920 × 1080	30/15 FPS
	HD720	1280 × 720	60/30/15 FPS
	VGA	672 × 376	100/60/30/15 FPS
Complementary sensors	Accelerometer, Gyroscope, Barometer, Magnetometer, Temperature sensor		

The ZED 2 camera was connected to a NVIDIA Jetson TX2 development kit (NVIDIA Corporation, CA, U.S.A.), with Ubuntu GNU/Linux 18.04 (Canonical Ltd., London, UK) operating system. In this system, the ROS melodic distro was installed to access ROS tools, supporting the ZED 2 camera features. The Jetson TX2 processor was consisted of 8 GB of RAM, 32 GB Flash Storage, 2 Denver 64-bit CPUs, and Quad-Core A57 Complex. For the maximum speed and robustness of the system ensuring the best possible results, all GPU cores were set in full performance. The 3D reconstruction of trees was performed using the spatial mapping module of Stereolabs Software Development Kit (SDK) tool and RTABMap package of ROS. The SDK tool provides drivers for the camera, and several sample functions in Python programming language that were used for the measurements.

Due to the camera's technology basic advantage of providing efficient results also in sunlight environments, this sensor is considered as an ideal solution for a robotic system operating outdoors. Moreover, the small size and compact structure of the camera makes it quite helpful to be used along with a robotic platform for applications such as mapping, object detection, etc. The sensing system was mounted on a Thorvald (SAGA Robotics SA, Oslo, Norway), which is an autonomous all terrain UGV (Figure 1) [47].

The Thorvald robotic vehicle was also equipped with a high accuracy GPS (RTK) as a means of providing the position of the robot and sequentially the position of the camera providing the ability to georeference the point cloud produced by scanning the orchard. Moreover, the scanning system was powered by the Thorvald's battery. The setup was navigated in the field, capturing RGB-D images, collecting the necessary data to construct the 3D point cloud of the orchard.



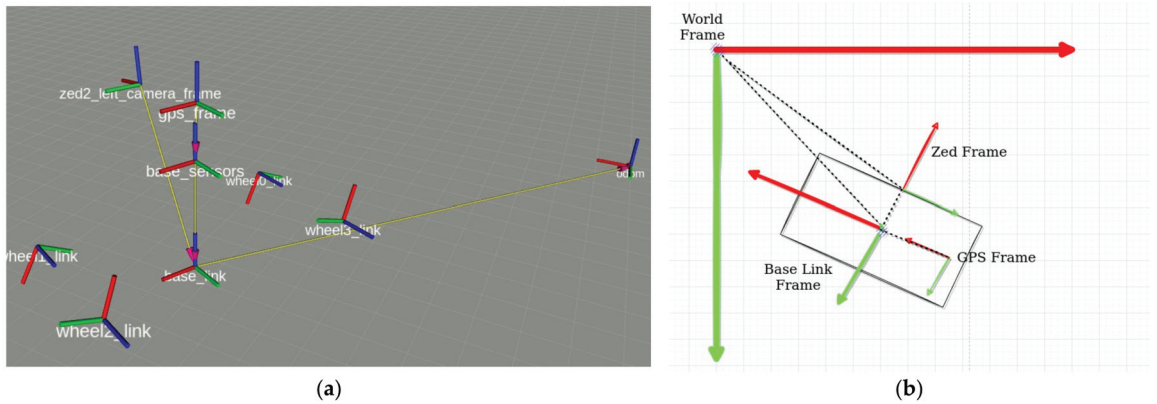
**Figure 1.** Setup of the ground-based scanning system mounted on Thorvald unmanned ground vehicle.

The camera was located on a tripod attached on the Thorvald vehicle at about 1.5 m above the ground level facing sideways towards the trees canopy in horizontal position. In addition, the ZED camera was oriented towards the direction of the tree of interest, and it was manually adjusted as for the viewing angle and the height according to each tree. This adjustment was necessary due to variations in geometry characteristics of the canopy, volume and height of every individual tree.

The RGB-D-based scanning system setup was used in real field conditions to scan and construct the 3D representation of a commercial walnut orchard, located in Thessaly region, in Greece. The field measurements were conducted on sample trees of different height, volume and shape, on a sunny day during September 2020. The robot-camera system was used for in-field navigation, capturing RGB and depth data by steering a circle around each tree, at a distance of 2 m from the canopy, for about one minute. According to the acquisition rate, this procedure produced 3500 frames per sample tree. The camera readings were acquired at a high frame rate, namely 50–60 frames per second, providing sufficient overlapping among the frames for better 3D reconstruction of the model, as the SDK tool (Stereolabs) used for the 3D point cloud generation, merges the additional points of the scene and creates a more complete point cloud. The overlapped areas allow for 3D model construction by estimating the relative position of the camera for each frame. Several parameters of the sensor were adjusted through the SDK tool, such as brightness, saturation and contrast. Furthermore, according to the camera’s application programming interface (API) documentation, several parameters were set to fit in the field conditions. Specifically, the resolution of the camera was set to  $1280 \times 720$  pixels (720p), and the point cloud mapping resolution was set to 2 cm. Additionally, the depth data range was set between 0.4- and 5-m distance from the camera position to create point cloud with high dense geometry and high resolution. Every point cloud of each tree was stored for further processing and saved in an object (OBJ) or polygon (PLY) file format, which is compatible with various point cloud and image processing software, such as Meshlab [48] and CloudCompare [49].

The ROS framework was utilized by the robotic platform to navigate in the field, while supporting data acquisition through the integrated “roscap” tool. The system was recording simultaneously the RGB-D data from the ZED camera and the accurate position of the robotic vehicle utilizing the RTK-GNSS. The ZED camera uses its internal IMU to set the location and direction of the camera in relative coordinates. Therefore, it provides the RGB-D information in relative geodetic system. Combining the two datasets, the relative

coordinates are referenced to the global coordinate system (GPS) “translated” into UTM coordinates (Figure 2). The “ros tf” library was utilized for this task.



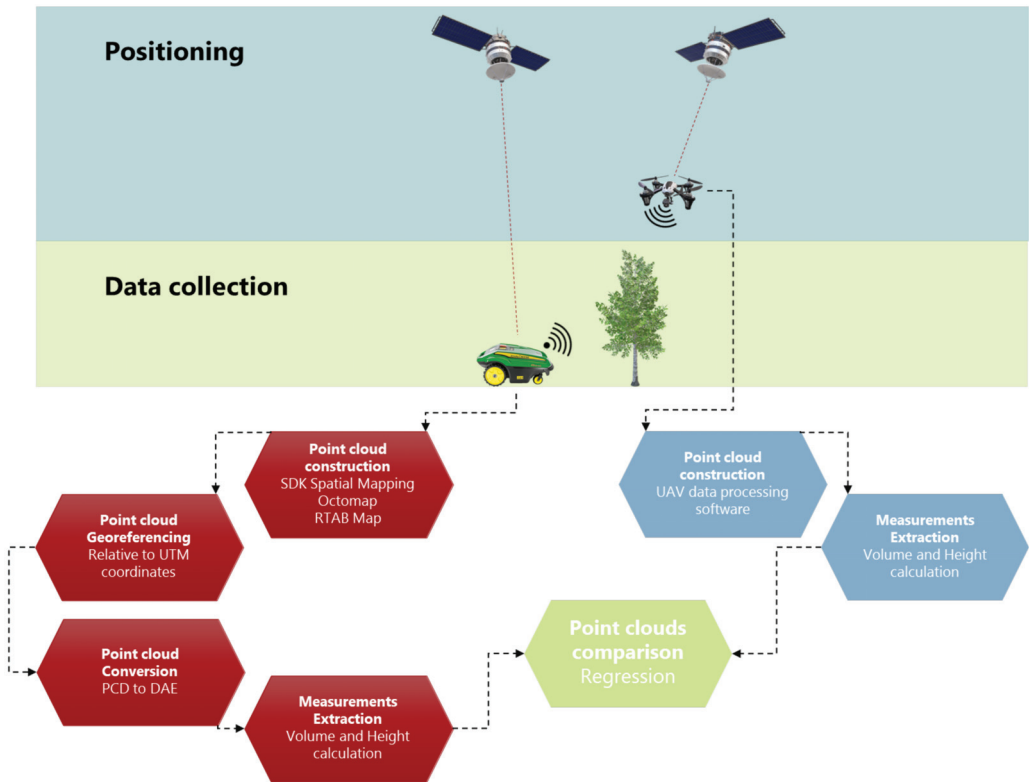
**Figure 2.** Location and orientation of the RGB-D camera in the relative coordinate system using the IMU (a) and georeferencing of the vehicle and the RGB-D to UTM coordinate system (b).

The fusion of the two coordinate systems provided the ability to accurately georeference the spatial data captured by the camera which, after processing, produced the georeferenced 3D point cloud of the orchard corresponding to reality.

After the point cloud extraction, the height and volume of each tree was computed using CloudCompare and its internal tools. During this process, the point cloud is generalized to a surface elevation model and consequently the volume is calculated on the basis of the difference between a fixed ground elevation and the surface model. For the given case, the ground level was set as the lowest point for each tree point cloud. In other words, this technique is similar to draping fabric over the tree and computing the volume under the fabric. The resolution for the volume measurement was set equal to 2 cm. Furthermore, the density of points was calculated. The workflow of the data analysis followed in the study is briefly presented in Figure 3.

In addition to the ground-based scanning system, the orchard’s structure was also mapped from above using a UAV. The flight occurred during the same period with the ground-based measurements to ensure the comparability between the two-point cloud producing methods. The UAV was a quadcopter (Phantom 4, DJI Technology Co., Ltd., Shenzhen, China) equipped with high accuracy GNSS (real-time kinematic—RTK) and high-resolution RGB camera (5472 × 3648 resolution, at a 3:2 aspect ratio). The use of RTK GNSS was necessary in order to accurately geotag the acquired aerial images, while the flight plans were parametrized accordingly (UAV flight height, speed, number of captured images, side overlap, and forward overlap ratio) to produce high accuracy, below centimeter pixel size, orthomosaics. The produced orthomosaic can accurately provide the top view of the tree canopies in 2 dimensions and, thus, it was utilized as the ground truth for measuring the canopies’ surface. The 2D point cloud acquired by the ZED camera was compared with the orthomosaic.

For the purpose of comparing the measurements derived from the ground-based systems against those of aerial-based systems, simple linear regression analysis was utilized taking also into account the 95% confidence interval.



**Figure 3.** Flow chart of the procedure for the 3D point cloud construction using data from ZED 2 camera and its comparison with the UAV derived point cloud.

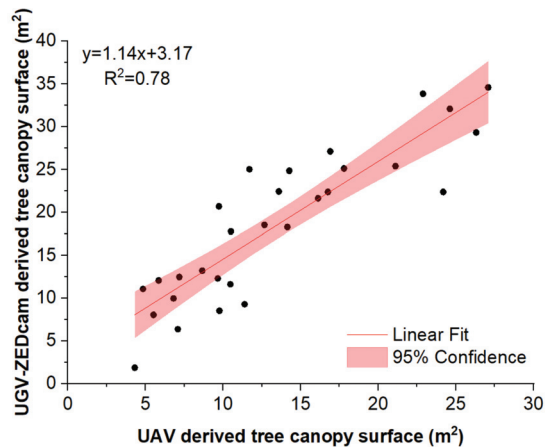
### 3. Results and Discussion

In order to estimate the true position of an object (a tree within the orchard in this case), the first step was to create a 3D model of the object in relative coordinates with the position of the camera as the axis origin and then set it in real-world coordinates by aligning this model to a known point (based on the camera position). This georeferenced point cloud aimed to be compared with a 3D point cloud produced from a UAV. Moreover, the georeferenced point cloud was imported in quantum geographic information system (Q GIS) to check the converted point cloud with a 2D georeferenced raster image of the same area. Reprojecting the point cloud in a real-world coordinate system provided the possibility to be used in various future simulation agricultural applications and robot tasks, such as object detection, spraying, or harvesting [50].

The representation of the orchard in two dimensions provided a general idea of the top view of the trees within the orchard, hence, providing the ability to estimate the canopy surface. This information can be valuable for estimating the age and the yield potential of each tree. In our study, the 2D representation also served as the first stage for the comparison of the two data acquisition methods. In Figure 4, the top view of the georeferenced point cloud acquired by the ground-based measuring system is projected overlaid on the detailed georeferenced orthomosaic constructed from the UAV-derived aerial images. The orchard, at the time of measuring, consisted of trees of different canopy size, color, and stage (fully developed, partly defoliated, or defoliated). Despite of the heterogeneity of the trees within the orchard, the results from the two methods were similar. This was also confirmed by the results of the regression between the two (Figure 5).



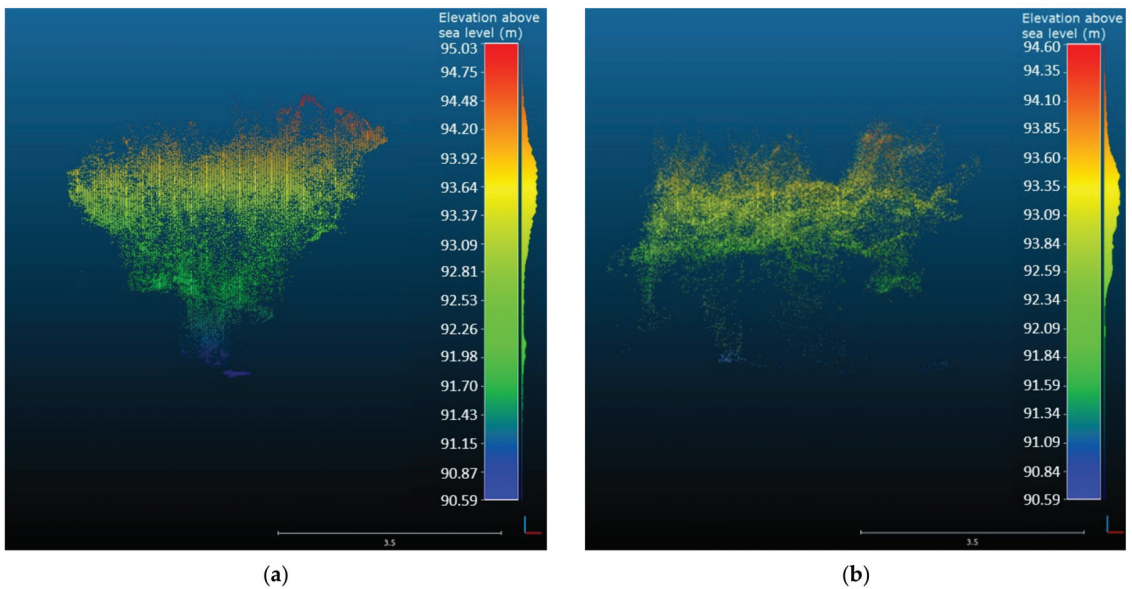
**Figure 4.** The projection of the point cloud (top view) of the orchard in 2D, mapped with the two methods used in the study; the ground-based system using depth camera mounted on Thorvald UGV and the orthomosaic exported from aerial images acquired using UAV.



**Figure 5.** Comparison between the canopy size estimated by the ground-based and the aerial-based systems used in the study; the colored area shows the lower and upper confidence (95%) limits.

For the representation of the collected data in the three-dimensional world, the 3D point clouds were produced and converted to digital asset exchange (DAE) format, as to estimate the tree dimensional parameters, namely the height and canopy volume. Given that the datasets were georeferenced using high accuracy GNSS, the height of the captured trees could be accurately calculated (Figure 6). Furthermore, the robot-camera setup presented accurate results of the volume measurements of the trees confirming that the RGB-D cameras can serve as useful tools for agricultural applications, such as fertilizing and spraying, being part of decision support tools for variable rate applications according to the characteristics of each tree.





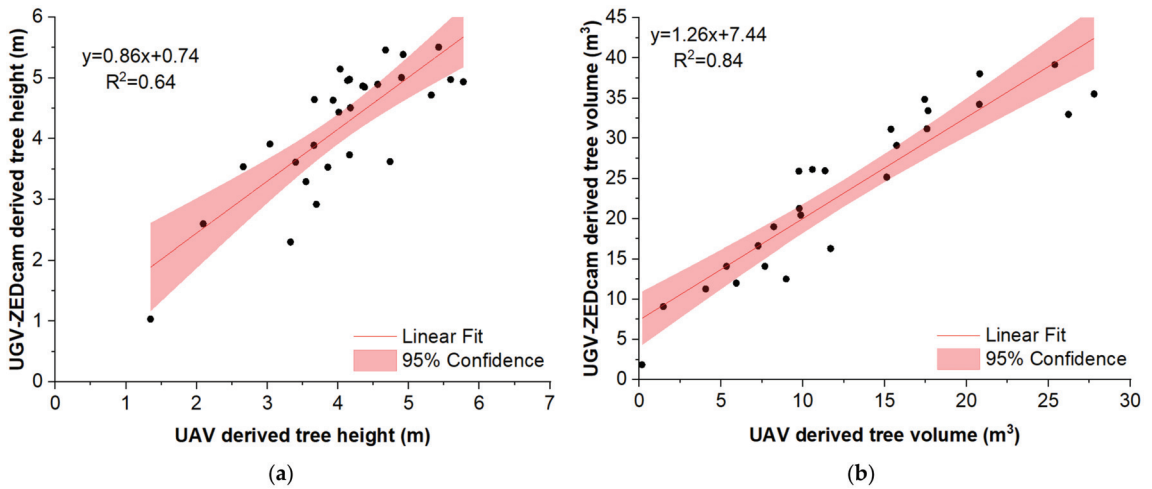
**Figure 6.** The side view of the georeferenced 3D point cloud of a sample tree captured by the ground-based system using the ZED camera (a) and by the UAV aerial-based system (b), used to estimate the tree height.

It is worth mentioning that the ZED camera, with the setup and adjustments used in the study, could not accurately detect the end details of the trees, such as thin branches, individual leaves, or nuts, as it could not provide extremely dense point clouds that are required for such tasks. Increasing the acquisition rate and the camera resolution and scanning more than one circles around each tree would enrich the point clouds producing very detailed point clouds. However, this would not be practical in agricultural applications, since it would be time consuming and hardware requirements for proper data acquisition and processing would significantly increase. In our system setup, despite the limitations, the constructed point cloud provided a model of the trees within the orchard very close to reality. This result is in agreement with the conclusions presented in [51], where the use of low-cost 3D sensors provided reliable results for plant phenotyping and can be applied in automated procedures for agricultural applications.

Comparing the two capturing systems, the ZED camera provided a good representation of the trees, capturing details of the trunk, the lower, and mid canopy. Moreover, the center of the top canopy had some gaps due to the position and the viewing angle of the camera (Figure 6a). Conversely, the point cloud derived from the orthomosaic produced by the UAV aerial images provided a good representation of the top of the canopy, but had poor performance in the representation of the middle and lower canopy and the tree's trunk (Figure 6b). This was expected, since by definition the UAVs can capture the top view of the objects, being unable to penetrate inside and under the canopy. However, some points of the lower canopy, the trunk, and the ground were captured making feasible the accurate estimation of the tree height, calculated by subtracting the ground surface elevation from the top of the canopy elevation. This fact led to similar height measurements from both measuring methods (Figure 7a).

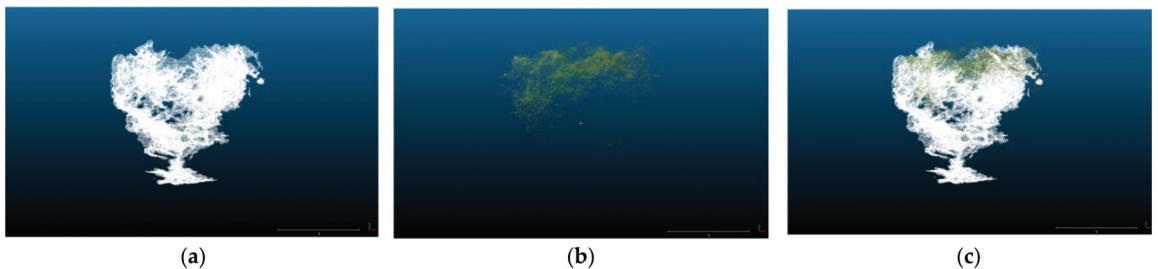
From a practical point of view, a significant drawback of using the ZED camera ground-based system was the time needed to navigate within the orchard and capture the given number of trees. On the other hand, the aerial images derived from the UAV platform could be acquired within a short flight.





**Figure 7.** Comparison between the trees dimension measurements; trees height (a) and trees volume (b), derived by using the two sensing methods; the UAV aerial-based system and the UGV-ZED depth camera ground-based system; the colored areas show the lower and upper confidence (95%) limits.

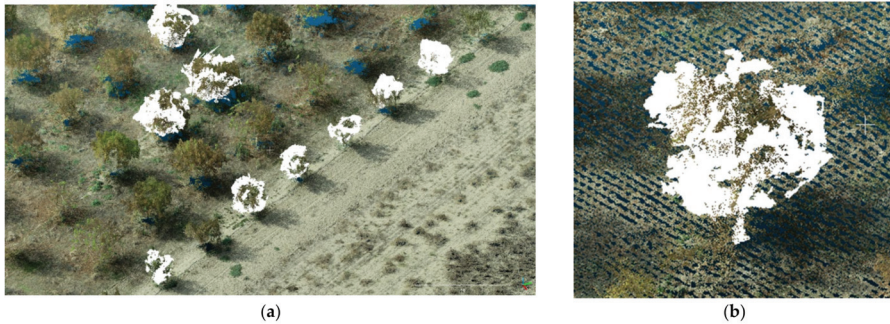
In terms of tree volume measurements, the results from both methods showed similar trend; however, the UAV-derived tree volume was constantly lower by about  $7.4 \text{ m}^3$  while the slope of the relationship was 1.26 (Figure 7b). This is attributed to the fact that the UAVs can capture the upper part of the canopy, thus missing a significant part of the tree volume in the mid and lower canopy as seen in Figure 8b. However, these parts were captured in detail by the ZED camera. The latter managed to capture in detail almost the whole canopy, missing only a part of the middle top. As a consequence, the fusion of the two point clouds into a unified one constructed a more complete 3D model (Figures 8c and 9).



**Figure 8.** Point clouds of a sample tree derived by the UGV-ZED depth camera ground-based system (a), the UAV based aerial system (b), and the fusion of the two point clouds (c).

The constructed point clouds can provide a useful input, by consequently converting them to meshes and importing in Gazebo simulation environment. The resulted virtual orchard environment may be used for testing of the robot navigation and localization. This testing will be carried out for estimation of the robot performance, in tasks such as autonomous navigation and obstacle avoidance before being evaluated in real field conditions. The visualization model in the Gazebo simulation environment can provide an adequate representation of the real orchard field and the possibility to make quality tests in a virtual world. In robotic applications, basic stage of the whole implementation is the algorithm testing part, which is performed in a virtual world before established in the real world. The use of simulation environments in various tasks and different environments, as

to evaluate the robots' performance, could be a quite costly and time effective procedure during the stage of testing and development of an application. As a result, using simulation environments in robotic applications, could optimize the robot behavior before the actual tests in the field [52].



**Figure 9.** The 3D projection of the point clouds exported with the two methods used in the study; the ground-based system using depth camera mounted on Thorvald UGV ((a), white dots) and the orthomosaic exported from aerial images acquired using UAV ((b), colored dots).

#### 4. Conclusions

In this study, the use of RGB-D camera to map the environment of commercial orchards was assessed and compared with 3D orthomosaics acquired using an UAS. The study verified that depth cameras, using stereoscopic vision to calculate the depth values, can provide accurate results in outdoor environments. The system, indeed, showed promising results, as it was capable to work under direct sunlight conditions capturing a high number of points with efficient resolution.

The produced point clouds provided efficient results for the structural parameters of the trees, as their shape and volume were adequately described. In some sample trees, lack of information of the inside and top of the tree canopy was observed. This limitation of the system was due to the initial settings of the camera's parameters and/or due to the finite number of frames captured from each tree, set to the maximum of the hardware's capabilities. Changes in these parameters or increasing of the image frames could possibly improve the 3D model reconstruction, though increasing significantly the processing time, hardware requirements, and, consequently, storage. Furthermore, scanning each tree more than once would significantly increase the point clouds' density and accuracy, but this would affect the time required for the in-field scanning.

Overall, the UAV point cloud provided an accurate representation of the top view of the tree canopies. The orthomosaic, acquired by the RTK GNSS enabled UAS, was utilized as the ground truth for the 2D representation of the surface of the top view of the tree canopies. The 2D point cloud acquired by the ZED camera was successfully compared with the orthomosaic proving that the latter sensor can be an alternative providing accurate results. On the other hand, the point cloud from the ZED camera captured in much detail the structural characteristics of the trees all around, but had lack of information of the top canopy structure. Fusion of the two datasets led to construction of a more complete 3D model with increased accuracy providing a better representation of the tree structure. Focusing on the cost, aerial imaging is affordable, easier to operate and can cover larger areas as compared to on-ground systems. The RGB-D system on the other hand, may be facilitated with conventional agricultural machinery, capturing data while performing in-field operations, thus, minimizing the operational costs. Nevertheless, this study seeks to pave the ground to future applications following the trends of smart-autonomous farming leading towards Agriculture 4.0.

Finally, the 3D point clouds can be imported in Gazebo simulation environment to provide the virtual environment of the orchard to be used for efficient programming evaluation and demonstration of the robotic platform's behavior and interaction in the orchard. Future developments include the automatization of the analysis procedure to provide the results in real time as the system navigates in the orchard. This will enhance situation awareness for safe and undisturbed navigation of the robotic platform in complex environments for the sake of avoiding possible injuries or damages [53]. In a broader perspective, further research is required towards improving the speed and accuracy of the existing cameras and image processing systems as well as decreasing the overall complexity [7,54–56]. Furthermore, fusion of data acquired by a group of unmanned vehicles could allow for better accuracy in a timely manner.

**Author Contributions:** Conceptualization, A.C.T. and D.B.; methodology, E.F., D.K. and P.B.; software, E.F. and D.K.; validation, A.C.T., L.B. and P.B.; writing-original draft preparation, E.F., L.B. and A.C.T.; writing-review and editing, L.B., A.C.T., P.B. and D.B.; visualization, E.F., A.C.T. and L.B.; supervision, A.C.T. and D.B.; project administration, D.B. All authors have read and agreed to the published version of the manuscript.

**Funding:** This research received no external funding.

**Conflicts of Interest:** The authors declare no conflict of interest.

## References

- Han, J.; Shao, L.; Xu, D.; Shotton, J. Enhanced Computer Vision with Microsoft Kinect Sensor: A Review. *IEEE Trans. Cybern.* **2013**, *43*, 1318–1334. [[CrossRef](#)] [[PubMed](#)]
- Ganganath, N.; Leung, H. Mobile robot localization using odometry and kinect sensor. In Proceedings of the 2012 IEEE International Conference on Emerging Signal Processing Applications, Las Vegas, NV, USA, 12–14 January 2012; pp. 91–94.
- Benos, L.; Tagarakis, A.C.; Dolias, G.; Berruto, R.; Kateris, D.; Bochtis, D. Machine Learning in Agriculture: A Comprehensive Updated Review. *Sensors* **2021**, *21*, 3758. [[CrossRef](#)] [[PubMed](#)]
- Lindner, L.; Sergiyenko, O.; Rivas-López, M.; Ivanov, M.; Rodríguez-Quiróñez, J.C.; Hernández-Balbuena, D.; Flores-Fuentes, W.; Tyrsa, V.; Muerrietta-Rico, F.N.; Mercorelli, P. Machine vision system errors for unmanned aerial vehicle navigation. In Proceedings of the 2017 IEEE 26th International Symposium on Industrial Electronics (ISIE), Edinburgh, UK, 19–21 June 2017; pp. 1615–1620.
- Zhao, Y.; Gong, L.; Huang, Y.; Liu, C. A review of key techniques of vision-based control for harvesting robot. *Comput. Electron. Agric.* **2016**, *127*, 311–323. [[CrossRef](#)]
- Fu, L.; Tola, E.; Al-Mallahi, A.; Li, R.; Cui, Y. A novel image processing algorithm to separate linearly clustered kiwifruits. *Biosyst. Eng.* **2019**, *183*, 184–195. [[CrossRef](#)]
- Fu, L.; Gao, F.; Wu, J.; Li, R.; Karkee, M.; Zhang, Q. Application of consumer RGB-D cameras for fruit detection and localization in field: A critical review. *Comput. Electron. Agric.* **2020**, *177*, 105687. [[CrossRef](#)]
- Khoshelham, K.; Elberink, S.O. Accuracy and Resolution of Kinect Depth Data for Indoor Mapping Applications. *Sensors* **2012**, *12*, 1437–1454. [[CrossRef](#)] [[PubMed](#)]
- Liu, H.; Qu, D.; Xu, F.; Zou, F.; Song, J.; Jia, K. Approach for accurate calibration of RGB-D cameras using spheres. *Opt. Express* **2020**, *28*, 19058–19073. [[CrossRef](#)]
- Menna, F.; Remondino, F.; Battisti, R.; Nocerino, E. Geometric investigation of a gaming active device. In *Proceedings of the Videometrics, Range Imaging, and Applications XI*; Remondino, F., Shortis, M.R., Eds.; SPIE: Bellingham, WA, USA, 2011; Volume 8085, pp. 173–187.
- Henry, P.; Krainin, M.; Herbst, E.; Ren, X.; Fox, D. RGB-D Mapping: Using Depth Cameras for Dense 3D Modeling of Indoor Environments BT—Experimental Robotics. In *Proceedings of the 12th International Symposium on Experimental Robotics, New Delhi and Agra, India, 18–21 December 2010*; Khatib, O., Kumar, V., Sukhatme, G., Eds.; Springer: Berlin/Heidelberg, Germany, 2014; pp. 477–491.
- Endres, F.; Hess, J.; Sturm, J.; Cremers, D.; Burgard, W. 3-D Mapping with an RGB-D camera. *IEEE Trans. Robot.* **2014**, *30*, 177–187. [[CrossRef](#)]
- Butkiewicz, T. Low-cost coastal mapping using Kinect v2 time-of-flight cameras. In Proceedings of the 2014 Oceans—St. John's, St. John's, NL, Canada, 14–19 September 2014; pp. 1–9.
- Pan, H.; Guan, T.; Luo, Y.; Duan, L.; Tian, Y.; Yi, L.; Zhao, Y.; Yu, J. Dense 3D reconstruction combining depth and RGB information. *Neurocomputing* **2016**, *175*, 644–651. [[CrossRef](#)]
- Herbst, E.; Henry, P.; Ren, X.; Fox, D. Toward object discovery and modeling via 3-D scene comparison. In Proceedings of the 2011 IEEE International Conference on Robotics and Automation, Shanghai, China, 9–13 May 2011; pp. 2623–2629.
- Wang, K.; Zhang, G.; Bao, H. Robust 3D Reconstruction with an RGB-D Camera. *IEEE Trans. Image Process.* **2014**, *23*, 4893–4906. [[CrossRef](#)]

17. Benos, L.; Bechar, A.; Bochtis, D. Safety and ergonomics in human-robot interactive agricultural operations. *Biosyst. Eng.* **2020**, *200*, 55–72. [CrossRef]
18. Benos, L.; Tsaopoulos, D.; Bochtis, D. A Review on Ergonomics in Agriculture. Part II: Mechanized Operations. *Appl. Sci.* **2020**, *10*, 3484. [CrossRef]
19. Hernández-López, J.-J.; Quintanilla-Olvera, A.-L.; López-Ramírez, J.-L.; Rangel-Butanda, F.-J.; Ibarra-Manzano, M.-A.; Almanza-Ojeda, D.-L. Detecting objects using color and depth segmentation with Kinect sensor. *Procedia Technol.* **2012**, *3*, 196–204. [CrossRef]
20. Marin, G.; Agresti, G.; Minto, L.; Zanuttigh, P. A multi-camera dataset for depth estimation in an indoor scenario. *Data Br.* **2019**, *27*, 104619. [CrossRef]
21. Tran, T.M.; Ta, K.D.; Hoang, M.; Nguyen, T.V.; Nguyen, N.D.; Pham, G.N. A study on determination of simple objects volume using ZED stereo camera based on 3D-points and segmentation images. *Int. J. Emerg. Trends Eng. Res.* **2020**, *8*, 1990–1995. [CrossRef]
22. Sarker, M.M.; Ali, T.A.; Abdelfatah, A.; Yehia, S.; Elaksher, A. A cost-effective method for crack detection and measurement on concrete surface. *ISPRS-Int. Arch. Photogramm. Remote Sens. Spat. Inf. Sci.* **2017**, *42*, 237–241. [CrossRef]
23. Burdziakowski, P. Low cost real time UAV stereo photogrammetry modelling technique-accuracy considerations. In Proceedings of the E3S Web of Conferences; EDP Sciences: Les Ulis, France, 2018; Volume 63, p. 00020.
24. Gupta, T.; Li, H. Indoor mapping for Smart Cities—An affordable approach: Using kinect sensor and ZED stereo camera. In Proceedings of the 2017 International Conference on Indoor Positioning and Indoor Navigation, IPIN 2017, Sapporo, Japan, 18–21 September 2017; Institute of Electrical and Electronics Engineers Inc.: New York, NY, USA, 2017; Volume 2017, pp. 1–8.
25. Condotta, I.C.F.S.; Brown-Brandl, T.M.; Pitla, S.K.; Stinn, J.P.; Silva-Miranda, K.O. Evaluation of low-cost depth cameras for agricultural applications. *Comput. Electron. Agric.* **2020**, *173*, 105394. [CrossRef]
26. Andújar, D.; Dorado, J.; Fernández-Quintanilla, C.; Ribeiro, A. An Approach to the Use of Depth Cameras for Weed Volume Estimation. *Sensors* **2016**, *16*, 972. [CrossRef]
27. Azzari, G.; Goulden, M.L.; Rusu, R.B. Rapid Characterization of Vegetation Structure with a Microsoft Kinect Sensor. *Sensors* **2013**, *13*, 2384–2398. [CrossRef]
28. Andújar, D.; Ribeiro, A.; Fernández-Quintanilla, C.; Dorado, J. Using depth cameras to extract structural parameters to assess the growth state and yield of cauliflower crops. *Comput. Electron. Agric.* **2016**, *122*, 67–73. [CrossRef]
29. Hui, F.; Zhu, J.; Hu, P.; Meng, L.; Zhu, B.; Guo, Y.; Li, B.; Ma, Y. Image-based dynamic quantification and high-accuracy 3D evaluation of canopy structure of plant populations. *Ann. Bot.* **2018**, *121*, 1079–1088. [CrossRef] [PubMed]
30. Jiang, Y.; Li, C.; Paterson, A.H.; Sun, S.; Xu, R.; Robertson, J. Quantitative Analysis of Cotton Canopy Size in Field Conditions Using a Consumer-Grade RGB-D Camera. *Front. Plant. Sci.* **2018**, *8*, 2233. [CrossRef] [PubMed]
31. Vit, A.; Shani, G. Comparing RGB-D Sensors for Close Range Outdoor Agricultural Phenotyping. *Sensors* **2018**, *18*, 4413. [CrossRef] [PubMed]
32. Wang, Z.; Walsh, K.B.; Verma, B. On-Tree Mango Fruit Size Estimation Using RGB-D Images. *Sensors* **2017**, *17*, 2738. [CrossRef]
33. Wang, D.; Li, W.; Liu, X.; Li, N.; Zhang, C. UAV environmental perception and autonomous obstacle avoidance: A deep learning and depth camera combined solution. *Comput. Electron. Agric.* **2020**, *175*, 105523. [CrossRef]
34. Milella, A.; Marani, R.; Petitti, A.; Reina, G. In-field high throughput grapevine phenotyping with a consumer-grade depth camera. *Comput. Electron. Agric.* **2019**, *156*, 293–306. [CrossRef]
35. Sa, I.; Lehnert, C.; English, A.; McCool, C.; Dayoub, F.; Upcroft, B.; Perez, T. Peduncle Detection of Sweet Pepper for Autonomous Crop Harvesting—Combined Color and 3-D Information. *IEEE Robot. Autom. Lett.* **2017**, *2*, 765–772. [CrossRef]
36. Konolige, K. Projected texture stereo. In Proceedings of the 2010 IEEE International Conference on Robotics and Automation, Anchorage, AK, USA, 3–7 May 2010; pp. 148–155.
37. Hornung, A.; Wurm, K.M.; Bennewitz, M.; Stachniss, C.; Burgard, W. OctoMap: An efficient probabilistic 3D mapping framework based on octrees. *Auton. Robot.* **2013**, *34*, 189–206. [CrossRef]
38. ROS—Robot Operating System. Available online: <https://www.ros.org/> (accessed on 13 December 2021).
39. De Silva, K.T.D.S.; Cooray, B.P.A.; Chinthaka, J.I.; Kumara, P.P.; Sooriyaarachchi, S.J. *Comparative Analysis of Octomap and RTABMap for Multi-Robot Disaster Site Mapping*; Institute of Electrical and Electronics Engineers (IEEE): New York, NY, USA, 2019; pp. 433–438.
40. Anagnostis, A.; Tagarakis, A.C.; Kateris, D.; Moysiadis, V.; Sørensen, C.G.; Pearson, S.; Bochtis, D. Orchard Mapping with Deep Learning Semantic Segmentation. *Sensors* **2021**, *21*, 3813. [CrossRef]
41. Zhang, C.; Kovacs, J.M. The application of small unmanned aerial systems for precision agriculture: A review. *Precis. Agric.* **2012**, *13*, 693–712. [CrossRef]
42. Christiansen, M.; Laursen, M.; Jørgensen, R.; Skovsen, S.; Gislum, R. Designing and Testing a UAV Mapping System for Agricultural Field Surveying. *Sensors* **2017**, *17*, 2703. [CrossRef] [PubMed]
43. Gašparović, M.; Zrinjski, M.; Barković, Đ.; Radočaj, D. An automatic method for weed mapping in oat fields based on UAV imagery. *Comput. Electron. Agric.* **2020**, *173*, 105385. [CrossRef]
44. Veeranampalayam Sivakumar, A.N.; Li, J.; Scott, S.; Psota, E.; Jhala, A.; Luck, J.D.; Shi, Y. Comparison of Object Detection and Patch-Based Classification Deep Learning Models on Mid- to Late-Season Weed Detection in UAV Imagery. *Remote Sens.* **2020**, *12*, 2136. [CrossRef]

45. Kerkech, M.; Hafiane, A.; Canals, R. Vine disease detection in UAV multispectral images using optimized image registration and deep learning segmentation approach. *Comput. Electron. Agric.* **2020**, *174*, 105446. [[CrossRef](#)]
46. Barrero, O.; Perdomo, S.A. RGB and multispectral UAV image fusion for Gramineae weed detection in rice fields. *Precis. Agric.* **2018**, *19*, 809–822. [[CrossRef](#)]
47. Grimstad, L.; From, P.J. The Thorvald II Agricultural Robotic System. *Robotics* **2017**, *6*, 24. [[CrossRef](#)]
48. MeshLab. Available online: <https://www.meshlab.net/> (accessed on 17 November 2020).
49. CloudCompare. Available online: <http://www.cloudcompare.org/> (accessed on 17 November 2020).
50. Moysiadis, V.; Tsolakis, N.; Katikaridis, D.; Sørensen, C.G.; Pearson, S.; Bochtis, D. Mobile Robotics in Agricultural Operations: A Narrative Review on Planning Aspects. *Appl. Sci.* **2020**, *10*, 3453. [[CrossRef](#)]
51. Paulus, S.; Behmann, J.; Mahlein, A.-K.; Plümer, L.; Kuhlmann, H. Low-Cost 3D Systems: Suitable Tools for Plant Phenotyping. *Sensors* **2014**, *14*, 3001–3018. [[CrossRef](#)]
52. Guzman, R.; Navarro, R.; Beneto, M.; Carbonell, D. Robotnik—Professional service robotics applications with ROS. *Stud. Comput. Intell.* **2016**, *625*, 253–288. [[CrossRef](#)]
53. Benos, L.; Kokkotis, C.; Tsatalas, T.; Karampina, E.; Tsaopoulos, D.; Bochtis, D. Biomechanical Effects on Lower Extremities in Human-Robot Collaborative Agricultural Tasks. *Appl. Sci.* **2021**, *11*, 11742. [[CrossRef](#)]
54. Rodríguez-Quiñonez, J.C.; Sergiyenko, O.; Flores-Fuentes, W.; Rivas-lopez, M.; Hernandez-Balbuena, D.; Rascón, R.; Mercorelli, P. Improve a 3D distance measurement accuracy in stereo vision systems using optimization methods' approach. *Opto-Electron. Rev.* **2017**, *25*, 24–32. [[CrossRef](#)]
55. Lindner, L.; Sergiyenko, O.; Rodríguez-Quiñonez, J.C.; Tyrsa, V.; Mercorelli, P.; Fuentes, W.F.; Murrieta-Rico, F.N.; Nieto-Hipolito, J.I. Continuous 3D scanning mode using servomotors instead of stepping motors in dynamic laser triangulation. In Proceedings of the 2015 IEEE 24th International Symposium on Industrial Electronics (ISIE), Buzios, Brazil, 3–5 June 2015; pp. 944–949.
56. Rueda-Ayala, V.P.; Peña, J.M.; Höglind, M.; Bengochea-Guevara, J.M.; Andújar, D. Comparing UAV-Based Technologies and RGB-D Reconstruction Methods for Plant Height and Biomass Monitoring on Grass Ley. *Sensors* **2019**, *19*, 535. [[CrossRef](#)] [[PubMed](#)]





Review

# Human–Robot Interaction in Agriculture: A Systematic Review

Lefteris Benos <sup>1</sup>, Vasileios Moysiadis <sup>1,2,3</sup>, Dimitrios Kateris <sup>1</sup>, Aristotelis C. Tagarakis <sup>1</sup>, Patrizia Busato <sup>4</sup>, Simon Pearson <sup>5</sup> and Dionysis Bochtis <sup>1,\*</sup>

<sup>1</sup> Institute for Bio-Economy and Agri-Technology (IBO), Centre of Research and Technology-Hellas (CERTH), Charilaou-Thermi Rd, 57001 Thessaloniki, Greece; e.benos@certh.gr (L.B.); v.moysiadis@farm-b.com (V.M.); d.kateris@certh.gr (D.K.); a.tagarakis@certh.gr (A.C.T.)

<sup>2</sup> Department of Computer Science and Telecommunications, University of Thessaly, 35131 Lamia, Greece

<sup>3</sup> FarmB Digital Agriculture S.A., 17th November 79, 55534 Thessaloniki, Greece

<sup>4</sup> Interuniversity Department of Regional and Urban Studies and Planning (DIST), Polytechnic of Turin, Viale Mattioli 39, 10125 Torino, Italy; patrizia.busato@unito.it

<sup>5</sup> Lincoln Institute for Agri-Food Technology (LIAT), University of Lincoln, Lincoln LN6 7TS, UK; spears@lincoln.ac.uk

\* Correspondence: d.bochtis@certh.gr

**Abstract:** In the pursuit of optimizing the efficiency, flexibility, and adaptability of agricultural practices, human–robot interaction (HRI) has emerged in agriculture. Enabled by the ongoing advancement in information and communication technologies, this approach aspires to overcome the challenges originating from the inherent complex agricultural environments. This paper systematically reviews the scholarly literature to capture the current progress and trends in this promising field as well as identify future research directions. It can be inferred that there is a growing interest in this field, which relies on combining perspectives from several disciplines to obtain a holistic understanding. The subject of the selected papers is mainly synergistic target detection, while simulation was the main methodology. Furthermore, melons, grapes, and strawberries were the crops with the highest interest for HRI applications. Finally, collaboration and cooperation were the most preferred interaction modes, with various levels of automation being examined. On all occasions, the synergy of humans and robots demonstrated the best results in terms of system performance, physical workload of workers, and time needed to execute the performed tasks. However, despite the associated progress, there is still a long way to go towards establishing viable, functional, and safe human–robot interactive systems.

**Keywords:** human–robot synergy; collaborative robotics; communication frameworks; human-centered automation; agriculture 4.0

**Citation:** Benos, L.; Moysiadis, V.; Kateris, D.; Tagarakis, A.C.; Busato, P.; Pearson, S.; Bochtis, D. Human–Robot Interaction in Agriculture: A Systematic Review. *Sensors* **2023**, *23*, 6776. <https://doi.org/10.3390/s23156776>

Academic Editor: David Scaradozzi

Received: 22 June 2023

Revised: 19 July 2023

Accepted: 27 July 2023

Published: 28 July 2023



**Copyright:** © 2023 by the authors. Licensee MDPI, Basel, Switzerland. This article is an open access article distributed under the terms and conditions of the Creative Commons Attribution (CC BY) license (<https://creativecommons.org/licenses/by/4.0/>).

## 1. Introduction

### 1.1. Background

Robots and autonomous systems exploit their capability to sense, scrutinize, analyze, and interact with the physical environment without or with minimal human intervention [1]. Focusing on the agricultural sector, the advent of robotic systems is envisioned to contribute to ending hunger and malnutrition in a sustainable manner by conserving and restoring ecosystems and natural resources [2–4]. Robots are considered as an integral element of Agriculture 4.0, which comes as an evolution of precision agriculture, enabling farmers to utilize the minimum required quantities for specific areas. Agri-robots belong to a broad family of Information and Communications Technologies (ICT), also including, indicatively, wireless sensor networks, farm management information systems, cloud computing, big data, and artificial intelligence, that are prerequisites for the fourth agricultural revolution [5,6].

Taking advantage of the advancement of ICT, along with the reduction in the corresponding costs, because of mass production, robots are being more and more implemented



in agriculture [7]. Robotic systems can increase agricultural productivity, as they optimize the efficiency of the implemented agricultural practices. In addition, robots have the potential to take humans out of hazardous locations and address labor shortages of seasonal workers [8]. Remarkably, the recent coronavirus pandemic has resulted in a spike in investment in agri-robotics as a means of filling labor shortages [9,10]. Indicative examples of agri-robot tasks are also sowing and planting, spraying, weeding, land preparation, insect and disease detection, plant monitoring, and phenotyping [11–13]. Moreover, multi-purposed robots have been developed, thus adding intricacy to both software and hardware and leading to increased costs [14].

In general, robots are able to carry out repetitive and predetermined assignments in stable environments and are closely related to tasks belonging in the so-called “three D’s”, namely dull, dirty, and dangerous tasks [15]. Unlike industrial settings, which contain a stable environment with well-structured objects, agriculture is characterized by uncertainty, heterogeneity, and unpredictable situations. Therefore, advanced technologies must cope with highly complicated environments, variable physical conditions, and live produce, which necessitates gentle and precise manipulations. More specifically, illumination, terrain, and other atmospheric conditions are ill defined, while there is a high variability in crop color, shape, and position that cannot be determined a priori [16]. These features render the replacement of humans by autonomous robots in agriculture very challenging [17].

## 1.2. *The General Context of Human–Robot Interaction in Agriculture*

### 1.2.1. Human–Robot Interaction Definition

With the intention of addressing the challenges provoked by complex agricultural environments, the synergy of humans and robots has been proposed. Human–robot interaction (HRI) constitutes a multidisciplinary research field dealing with investigating, designing, and evaluating these collaborative systems. It combines artificial intelligence, robotics, ergonomics, engineering, computer science, and social science to endow robots and humans with all the required competencies for proper interaction. In particular, HRI refers to the process whereby humans act as a team with robots to achieve a goal and comes from the confluence of information exchange, autonomy, and optimal task shaping [18]. HRI integrates the distinctive cognitive human skills of dexterity, perception, judging, and decision making with those assets of robots concerning repeatable accuracy and strength. The developed robot cognitive capabilities are a result of the integration of several sensors such as laser scanners, radio-frequency identification (RFID), cameras, and actuators. This innovative combination enables versatile use, robustness, flexibility, and adaptability under a constantly evolving workflow [19]. HRI can be accomplished via proximal or remote interaction. The ultimate objective of HRI is to free humans from dangerous and routine tasks. For instance, in the case of pesticide spraying, there can be an operator directing or supervising the task from a safe distance and away from harmful chemicals with the use of a properly designed user interface. These semi-autonomous systems have demonstrated remarkable results, outperforming fully autonomous robots [20]. In short, human–robot synergy can provide many advantages, including flexibility when it comes to system reconfiguration, reduction in the required working area, increasing productivity, improvement of the quality of services, rapid capital depreciation, and the creation of highly skilled jobs [21].

### 1.2.2. Main Design Concepts

One of the most challenging issues in HRI is the design of these synergistic systems, owing to the wide range of different working conditions and levels of interaction that may be faced. Human operators can be easily accused of being responsible for “human error” when they fail to notice an off-nominal instance. Nevertheless, insufficient design of the system and the associated interactions can lead to less-than-optimal compensatory reaction of the humans [22]. Every betterment of HRI is based predominantly on two principles: the autonomy level of the robot and the closeness of human and robot during their interaction.

The level of autonomy that these interactive systems can achieve relies on strategies that enable HRI in such an adaptable way that humans can intercede when it is required. In broad terms, the design should not limit the visual perspectives and mobility of humans or include inconvenient software. Also, robots should be programmed with cognitive skills to interact in an accurate and fluid manner, thus guaranteeing the dynamic autonomy of the system. In addition, different situations should be investigated in relation to proximity, such as following, passing, avoiding, and touching. The design of human–robot interactive systems should also consider the human-to-robot ratio along with the specific roles of the former (programmer, bystander, operator, supervisor, and information consumer). Design concepts also pay attention to adaption, task shaping, and the working time during which humans and robots coexist in the same workspace, while every objective has to match with the next one [23].

### 1.2.3. Communication Frameworks

Interaction, by definition, calls for the development of communication frameworks, which aspire to simplify the knowledge sharing between robots, or machines in general, and humans. In essence, more natural ways of communicating need to be investigated, such as body language and vocal communication. The former term encompasses facial expressions, body postures, and hand gestures, whereas the latter is limited by the noisiness of agricultural environments and the dissimilar ways that someone may pronounce a command. Out of these communication channels, hand gesture recognition, either through acquisition of data from vision sensors or specially designed gloves, has attracted the interest of the scientific literature [24,25]. Furthermore, surface electromyography sensors have been used for recording the electric potential of muscles [26], while hybrid methodologies have also been examined [27]. In brief, the main shortcomings of the above approaches are as follows: (a) vision sensors run into problems whenever changes take place with many people, complex backgrounds, and illumination changes [28]; (b) gloves usually limit natural movements [29]; and (c) electromyography sensors generate massive and noisy datasets [30]. Although the literature on the development of non-verbal communication tools in agriculture is still scarce, some efforts have been presented with encouraging results [24,31]. Finally, face recognition has not yet been widely used in agricultural environments due to the above-mentioned problems associated with vision sensors as well as restrictions imposed by privacy policies [32].

### 1.2.4. Safety and Human Factors

The primary concern concerning these fenceless synergistic systems is to ensure safety and health of humans and disclose all the risk factors that may harm them [33]. Occupational health is centered upon improving the shared workspace to help workers avoiding risky postures that can potentially cause injuries (physical ergonomics). In addition aspects, like mental workload and work stress are taken into consideration (cognitive ergonomics) [34]. On the other hand, occupational safety includes accident control measures. Overall, occupational health and safety can impact the efficiency of the system, response time, quality of work, and collaborative performance. Accordingly, an optimal synergistic human–robot system should be designed from the perspective of mental welfare, psychological comfort, and occupational health and safety. These aspects are related to perceived safety. The key elements that determine perceived safety are considered to be predictability, sense of control, experience, familiarity, transparency, comfort, and trust [35,36]. As a final note, only authorized and qualified workers must work together with a robot, while attention is paid to the establishment and evaluation of safety protocols and risks. The latter must be thoroughly investigated in the design phase, as unweighted factors, including uncertainty in interpreting and possible failures of human or robots, may take place during HRI.

### 1.2.5. Human–Robot Interaction Evaluation and Metrics

The design of synergistic systems necessitates the consideration of the implications of automation on the performance of both robot and human as a means of optimizing the overall benefits for the system. As a result, a significant feature of the design of collaborative tasks is the appraisal of their performance, fluency, effectiveness, and adaptability through adequate metrics allowing for reproducible evaluations. Several studies are concerned with metrics for HRI [37–40]. Indicatively, Vásconez et al. [23] summarized the main metrics that have been studied for evaluating the synergistic systems [41,42] and grouped them into six categories in relation to their usage, namely (a) mission effectiveness (e.g., performance of the mission); (b) human behavior efficiency (e.g., decision making and problem recognition); (c) human cognitive indicators (e.g., situation awareness, trust in robotic systems, and situation awareness); (d) human physiological indicators (comfort and fatigue); (e) robot behavior efficiency (e.g., autonomy level, human awareness, and learnability); and (f) collaborative metrics (e.g., collaborative problem recognition and action implementation efficiency, team situation awareness, and social patterns and roles). As stated in [40], the metrics do not entirely measure the impact of the autonomy level on interaction, since they normally focus on the observation of either humans or robots and not on their capabilities, therefore introducing error in analysis. As a general remark, it is very difficult to evaluate such kinds of systems in a broad and objective assessment. Moreover, the lack of efficient human-in-the-loop assessment has made it problematic to conclude whether such adaptation could bring about satisfying HRI [43]. Finally, the majority of relevant studies are limited to how the robotic system affects the human factors without, however, focusing on the opposite; how human factors impact the system [22].

### 1.2.6. Aim and Structure of the Paper

This paper provides a systematic review investigating the state of the art in HRI and the main challenges that must be addressed, focusing solely on the field of agriculture. The research is conducted through the lenses of different aspects by screening the relevant scholarly literature based on the PRISMA guidelines [44]. The remainder of the present paper is structured as follows. Section 2 describes the implemented methodology for the bibliographic survey, how the methodological quality of the selected studies and level of automation were evaluated, and the classification framework that was used. The results are analyzed in Section 3, also including the list of the selected papers and related statistics. Finally, Section 4 contains the main conclusions of the present review study, along with a discussion from a broader perspective to identify future research directions.

## 2. Materials and Methods

### 2.1. Critical Steps in Performing the Systematic Review

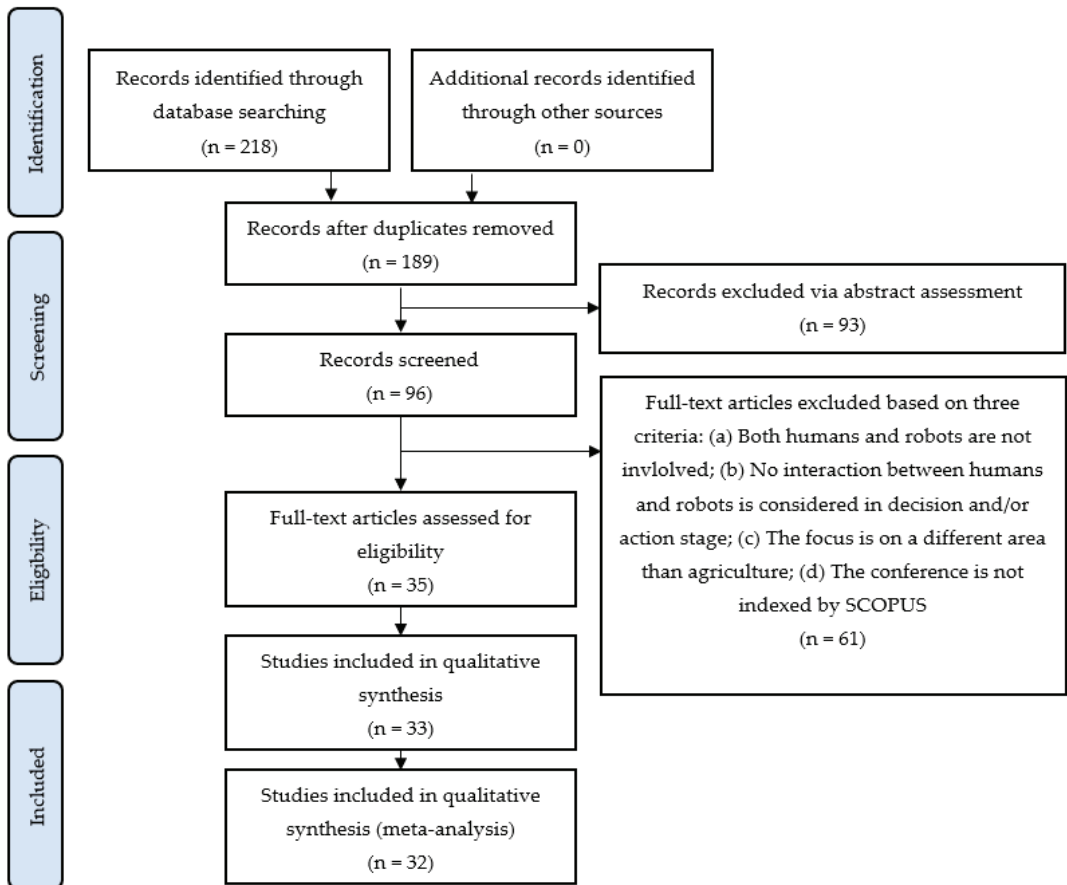
A systematic review is considered a rigorous approach to literature review that involves identifying, synthesizing, and evaluating all the available scientific evidence, both qualitative and quantitative. They are used to produce a robust, empirically derived response to a research question related to a specific topic. By adhering to systematic review principles, they offer distinct advantages over traditional literature reviews. These advantages include enhanced review quality through increased transparency, improved objectivity, and mitigation of researcher bias. Additionally, systematic reviews encourage researchers to critically assess the quality of evidence, thus strengthening the overall review process. While systematic reviews provide comprehensive and unbiased insights, their validity can be influenced by factors such as variations in evidence availability and quality, potential study selection biases, resource limitations, and challenges in addressing complex research inquiries. Nevertheless, systematic reviews remain invaluable tools for evidence synthesis, enabling informed decision making, statistical robustness, and identification of significant patterns and trends. It is important, however, to interpret their findings cautiously within the appropriate contextual framework.

In the present systematic review, seven steps were used in a manner similar to the relevant literature [45,46]:

- (1) Formulation of a primary research question: “What is the state of the art and what are future perspectives in HRI in agriculture?”
- (2) Development of a research protocol: The methodology followed for screening the relevant literature and data extraction and analysis was included in a written document. This was accepted by all the authors of this study, prior to the start of the literature search, to minimize bias.
- (3) Literature search: The methodology for selecting the relevant studies is described in Section 2.2 along with the implemented electronic databases, inclusive criteria, and review stages based on the PRISMA guidelines [44].
- (4) Data extraction: Specific items, regarding references (including journal, title, and authors), objective, method, crop type, interaction modes, automation levels, and key outcomes, were gathered in an online shared spreadsheet.
- (5) Quality appraisal of the selected studies: Although quality remains a challenging concept to define, the present study used the tool developed by Hoy et al. [47] (described in Section 2.3), which comprises specific internal and external validity criteria.
- (6) Data analysis and results: The first step in this procedure included a simple descriptive assessment of each study, presented in tabular form, followed by a statistical analysis.
- (7) Interpretation of results: Conclusions were drawn based on the available scientific evidence, while areas were identified to focus on for future research.

## 2.2. Literature Search

The search engines of Google Scholar, ScienceDirect, Scopus, IEEE Xplore, and MDPI were used for the purpose of seeking publications associated with HRI in agriculture. To that end, Boolean keyword combinations of “human-robot interaction/collaboration/synergy” and “agriculture” were used. Subsequently, the references of each article were scanned with the intention of finding studies that had not been noticed during the initial search. This process was reproduced until there were no more relevant publications. The ultimate search was performed on 15 December 2022. The titles and the abstracts of the resulting papers were then reviewed. As a next step, the full text of the relevant studies was carefully read to ascertain their appropriateness. For the selection of the final scientific literature to be considered, the following criteria should be met: (a) both humans and robots are involved; (b) HRI is considered in the decision and/or action stage; (c) I application domain is agriculture; (d) conference papers are also included, provided that the conference is indexed by SCOPUS. Non-English studies, Master theses, and doctoral dissertations were not included in the research. A final consensus meeting of the co-authors was held to discuss the content and adequacy of the selected papers based on the above criteria and resolve any difference of opinion. A flowchart summarizing the implemented methodology of the present systematic review is depicted in Figure 1, based on the PRISMA guidelines [44] for transparently reporting how the relevant literature was selected. The bibliographic survey on HRI in agriculture resulted in 32 relevant studies that fulfill the imposed inclusion criteria, of which 21 are journal papers and 11 are conference papers.



**Figure 1.** Flow diagram regarding the present systematic review process for selecting the relevant studies.

### 2.3. Methodological Quality Assessment

Assessing the risk of bias of the methodology applied in the selected investigations is very crucial for interpreting literature reviews so as not to underestimate or overestimate their results. In this review study, the risk of bias tool developed by Hoy et al. [47] was considered. This tool is made of 4 and 6 items with reference to external and internal validity criteria, respectively, accompanied by a summary item corresponding to the overall assessment of the quality of the methodology. The first ten items are yes/no questions oriented toward detecting potential bias in measurement methods. If no insufficient information exists, the corresponding answer is “No” [47]. For studies that do not involve participants, such as those developing mathematical models, using simulations, or dealing with design principles, some items may be filled in with “C”. This letter stands for “Can’t say”, similar to [48,49]. These items were not taken into consideration in the final summary item. All the authors of this paper independently took part in the reviewing process by answering all the questions to assess the risk of bias of the methodology for each study. A consensus meeting was held to compare the results and find a commonly accepted final answer. Additional criteria were applied pertaining to “C” cases, such as reliable measurement method and appropriate methodology validation.

As far as the eleventh summary item is concerned, which represents the overall methodological quality, it was rated as follows:

- High (++), indicating low risk of bias;
- Acceptable (+), indicating moderate risk of bias;
- Low (−), indicating high risk of bias.

In practice, depending on the number of “Yes” answers in the first 10 items of the tool of Hoy et al. [47], each paper was scored in the range 0–100% (each “Yes” answer has a 10% contribution to the final score). Similar to [49], 75% was considered as the lower limit, beyond which high (++) overall quality of the methodology was established. Moreover, scores between 50% and the above limit were rated as acceptable, while those below 50% represent studies with relatively low methodological quality.

#### 2.4. Classification of Modes of Human and Robot Working Together

In the present analysis, the classification followed by [12,21,50] is incorporated, where five different modes of robots and humans working together may come about:

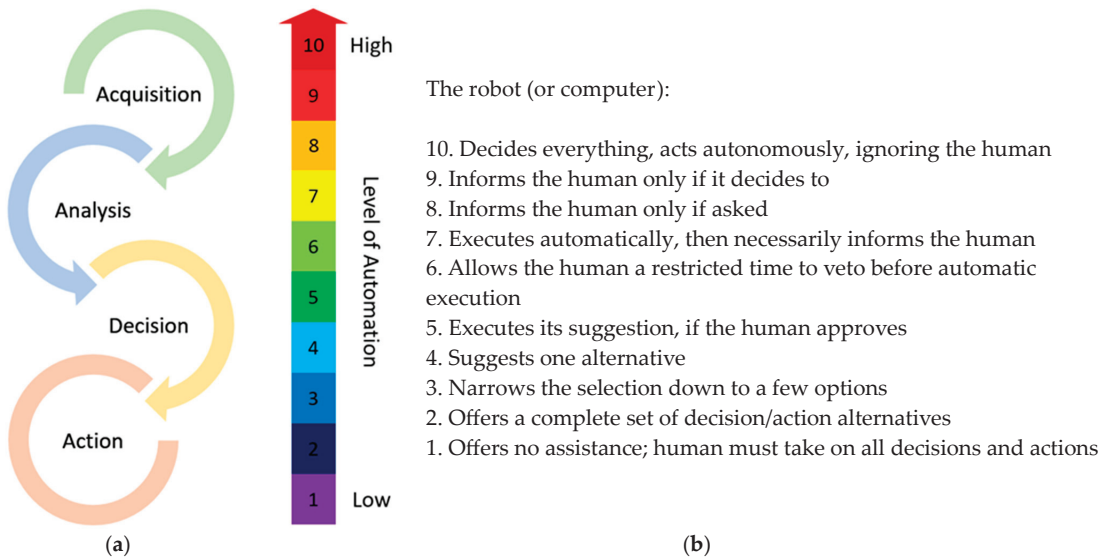
- Isolation mode, where HRI is never permitted, while normally, barriers are used;
- Coexistence mode, which is similar to the above mode, yet without barriers;
- Synchronization mode, where robot and human focus on different tasks in a synchronized manner and work in different working areas;
- Cooperation mode, where robot and human focus, again, on different tasks, however, working in the same working area;
- Collaboration mode, where robot and human focus on the same task and work in the same working area.

Obviously, the isolation mode refers to conventional robots, commonly used in industry, and together with coexistence mode does not consider any interaction between the human and the robot. In contrast, the other three modes correspond to the gradual increase in the level of human–robot synergy. As stressed in [21], it can be problematic to discriminate the existing mode, as this categorization comes from industry. Furthermore, contemporary user interfaces allow for synergy via virtual shared workspaces. In these cases, the criterion was whether robot and human are working on the same task.

#### 2.5. Assessment of the Level of Automation during Decision and Action Stage

In general, automation can take place in four stages [51], namely (a) information acquisition (acquisition stage); (b) information analysis (analysis stage); (c) decision selection (decision stage); and (d) action implementation (action stage). Within each of these stages, automation can be realized at a wide range of levels. Following the analysis of Parasuraman et al. [51] for the decision and action stages, a 10-point scale is used in the present study. In this scale, the higher levels characterize increased autonomy of computer (or robot in the present analysis) over human action. Therefore, if a function can be fully carried out exclusively by a human, the lowest level (i.e., “1”) is given, while the higher level (i.e., “10”) denotes that robot decides and acts autonomously. The intermediate levels of automation represent partial automation and different modes of HRI. Indicatively, at level 4, robot proposes an alternative decision, but the human continuously has the authority to either choose another decision/action or prefer the suggested alternative. In contrast, at level 6, the robot gives a limited time for a veto to the human before automatically executing its own decision. The utilized 10-point scale regarding the levels of autonomy, along with the four classes of functions, are shown in Figure 2. In this regard, it should be emphasized that, usually, a range of automation levels are used instead of a unique level, since there may be different alternative situations during HRI [52,53].





**Figure 2.** (a) A simplified 4-stage model of agricultural applications consisting of information acquisition (acquisition), information analysis (analysis), decision selection (decision), and action implementation (action), and (b) The levels of automation for the decision and action stage according to [51].

### 3. Results

#### 3.1. Preliminary Data Visualization Analysis

Data visualization analysis is regarded as an advantageous practical tool to analyze and illustrate massive data amounts, conduct data-driven judgments, interpret the current trends in the research field of interest, and identify research gaps.

##### 3.1.1. Time Distribution

A preliminary data visualization analysis is presented in this subsection starting from the time distribution of the reviewed studies in Figure 3. As can be deduced from this bar chart, investigation of HRI in agriculture is a recent research field that has concerned scholarly literature for almost the last twenty years, due to the sector-specific extension of “Industry 4.0”. As elaborated in the Introduction, robotics has found fertile ground in agriculture, enlarging their preceding role of performing only non-cognitive and routine missions. However, in contrast with other HRI applications, like those found in industrial settings, rehabilitation and medicine, and education, the peculiar agricultural environment introduces further challenges to the design of synergetic systems. Therefore, only 32 studies were found, most of which were published in recent years. This increase justifies, to some extent, the growing interest in complementary combination of robot and human capabilities in agricultural applications, while also taking advantage of the tremendous progress of ICT.

##### 3.1.2. Distribution of the Contributing International Journals, Conferences, and Disciplines

Subsequently, the sources where the articles were published were reviewed to determine the research approaches, which drew on knowledge from different disciplines. As can be seen in Figure 4a, “Computers and Electronics in Agriculture” was the main international journal of the current survey. This journal is associated with the application of computer hardware and software to meet the challenges emerging in the framework of smart agriculture, in which robotics is of central importance. Other journals with the same objective, but with less contribution, were “Industrial Robot”, “Journal of Field Robotics”,

and “Robotica”, which are not purely interested in the agricultural domain. An interdisciplinary journal with significant contribution was also “Applied Sciences”, which deals with different aspects of applied natural sciences as well as “Biosystems Engineering”. The latter publishes research in engineering for biological systems, including agriculture. “Engineering Proceedings” and “Computers & Industrial Engineering” focus mainly on industrial engineering and the use of computers and electronic communication, which constitute an integral part of it.

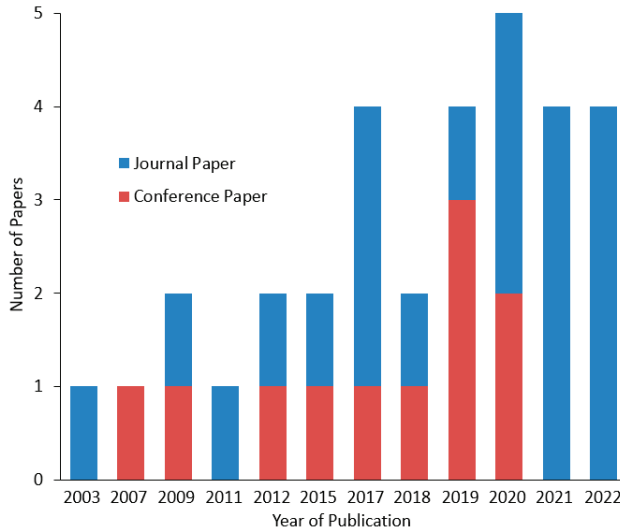


Figure 3. Time distribution of the papers reviewed in the present study.

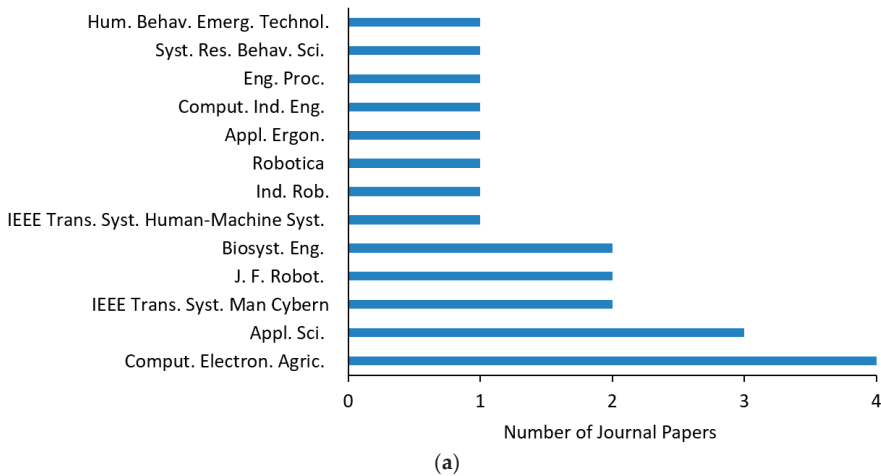
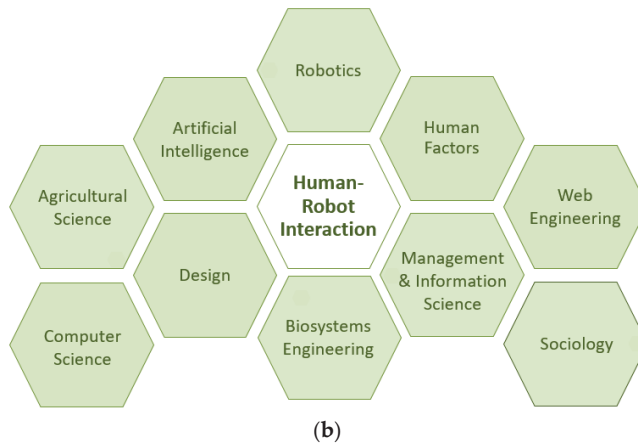


Figure 4. Cont.



**Figure 4.** (a) Distribution of all contributing international journals and (b) different core disciplines engaged in human–robot interaction in agriculture.

In addition, “IEEE Transactions on Systems, Man, and Cybernetics: Systems” and “Systems Research and Behavioral Science” cover the field of systems engineering with a range of engineering methods, including modeling, simulation, and optimization, and examination of issues from an economic and social perspective. Moreover, a journal aimed at investigating the human factors in the design and management of technical systems at work, namely “Applied Ergonomics”, contributed one article. Finally, “Transactions On Human Machine Systems” and “Human Behavior and Emerging Technologies” include human systems and organizational interactions, system testing and assessment, and cognitive ergonomics in systems and organizations. As far as the selected conference papers are concerned, the biggest contribution was from “IFAC-PapersOnLine” (formerly “IFAC Proceedings Volumes”) and IEEE International Conferences emphasizing robotic systems, including human–robot synergetic systems. In conclusion, several disciplines are engaged in finding innovative HRI solutions in agriculture by redefining problems outside the usual boundaries. Based on the scope and scholarly audience of the above journals and conferences, ten disciplines were identified, which are summarized in Figure 4b, whose theories and methodologies are combined so that unique insights are gained to face the challenges of agricultural environments.

### 3.2. Methodological Quality of the Reviewed Studies

The 32 reviewed papers are summarized in the first column of Table 1 in chronological order: from the first study of Bechar and Edan [52], published in 2003, up to the most recent one of Vázquez and Cheein [54], which was published in November 2022. As mentioned in Section 2.2, the tool developed by Hoy et al. [47] is used in the present study for assessing the methodological quality of the reviewed papers. According to the imposed criteria, all studies proved to be of a high methodological quality (with “++” assigned in the eleventh column), which corresponds to low risk of bias. The items that appeared as more questionable were those related to the quality of the sampling. In some studies, the sampling frame was not a close representation of the target population, since, usually, the authors themselves or a few university students may take part in experimental sessions, sometimes selected in a non-random way. Nevertheless, the implemented methodology was of relatively high quality, counterbalancing this disadvantage.

**Table 1.** Assessment of the methodological quality of the reviewed papers. Note that items 1–4 correspond to external while 5–10 correspond to internal validity [47].

Reference	External Validity					Internal Validity					Overall Quality
	1	2	3	4	5	6	7	8	9	10	
[52]	Y	N	Y	Y	Y	Y	Y	Y	Y	Y	++
[55]	C	C	C	C	C	Y	Y	Y	Y	Y	++
[56]	C	C	C	C	C	Y	Y	Y	Y	Y	++
[57]	C	C	C	C	C	Y	Y	Y	Y	Y	++
[58]	C	C	C	C	C	Y	Y	Y	Y	Y	++
[53]	C	C	C	C	C	Y	Y	Y	Y	Y	++
[59]	C	C	C	C	C	Y	Y	Y	Y	Y	++
[60]	C	C	C	C	C	Y	Y	C	Y	Y	++
[61]	C	C	C	C	C	Y	Y	Y	Y	Y	++
[20]	Y	Y	Y	Y	Y	Y	Y	Y	Y	Y	++
[62]	Y	Y	Y	Y	Y	Y	Y	Y	Y	Y	++
[63]	Y	N	Y	Y	Y	Y	Y	Y	Y	Y	++
[64]	C	C	C	C	C	Y	Y	Y	Y	Y	++
[65]	C	C	C	C	C	Y	Y	Y	Y	Y	++
[66]	Y	Y	Y	Y	Y	Y	Y	Y	Y	Y	++
[67]	C	C	C	C	C	Y	Y	Y	Y	Y	++
[68]	C	Y	C	Y	Y	Y	Y	Y	Y	Y	++
[69]	C	C	C	C	C	Y	Y	Y	Y	Y	++
[70]	C	C	C	C	C	Y	Y	Y	Y	Y	++
[71]	C	C	C	C	C	Y	Y	Y	Y	Y	++
[72]	C	Y	Y	Y	Y	Y	Y	Y	Y	Y	++
[21]	C	C	C	C	C	Y	Y	C	C	Y	++
[73]	C	N	C	Y	Y	Y	Y	Y	Y	Y	++
[74]	N	N	Y	Y	Y	Y	Y	Y	Y	Y	++
[75]	Y	N	Y	Y	Y	Y	Y	Y	Y	Y	++
[76]	C	C	C	C	C	Y	Y	Y	Y	Y	++
[77]	Y	Y	Y	Y	Y	Y	Y	Y	Y	Y	++
[78]	Y	N	C	Y	Y	Y	Y	Y	Y	Y	++
[24]	C	N	C	Y	Y	Y	Y	Y	Y	Y	++
[79]	C	C	C	C	C	Y	Y	Y	Y	Y	++
[80]	C	Y	N	C	Y	Y	Y	Y	Y	Y	++
[54]	C	C	C	C	C	Y	Y	Y	Y	Y	++

“C”: cannot say; “N”: no; “Y”: yes; “++”: high quality (low risk of bias); “+”: acceptable (moderate risk of bias); “-”: low quality (high risk of bias). “1”: Was the study’s target population a close representation of the national population in relation to relevant variables, e.g., age, sex, occupation? “2”: Was the sampling frame a true or close representation of the target population? “3”: Was some form of random selection used to select the sample, or, was a census undertaken? “4”: Was the likelihood of non-response bias minimal? “5”: Were data collected directly from the subjects (as opposed to a proxy)? “6”: Was an acceptable case definition used in the study? “7”: Was the study instrument that measured the parameter of interest shown to have reliability and validity (if necessary)? “8”: Was the same mode of data collection used for all subjects? “9”: Was the length of the shortest prevalence period for the parameter of interest appropriate? “10”: Were the numerator(s) and denominator(s) for the parameter of interest appropriate? “11”: Summary item on the overall risk of bias [47].

### 3.3. Brief Review of the Relevant Literature

The selected studies are also included in Table 2, whose columns epitomize some important aspects of them, namely the citation of the paper at hand, its subject, the implemented methodology, the examined crop, the interaction mode (based on the taxonomy described in Section 2.4), the automation level (as described in Section 2.5), and the main results. A summary of the aforementioned aspects, which were investigated by the relevant studies, is provided in Figure 5a–d, while a discussion follows immediately after.

**Table 2.** List of the selected papers along with their citation, subject, implemented methodology, examined crop, interaction mode, automation level, and main results.

Ref <sup>1</sup>	Subject	Method	Crop	Interaction Mode	Automation Level <sup>2</sup>	Main Results
[52]	Target detection	Lab exp <sup>3</sup>	Melon	Isolation; Collaboration	1; 3–4; 5–7; 10	Synergy increased the performance by 4% and by 14% compared with the solely manual or autonomous detection, respectively
[55]	Target detection	Simulation	Melon	Isolation; Collaboration	1; 3–4; 5–7; 10	An objective function was developed for evaluating system performance, while the optimal collaboration level may change depending on human and robot sensitivities
[56]	Target detection	Simulation	Melon	Isolation; Collaboration	1; 3–4; 5–7; 10	The best system performance and collaboration level depend on the environment, the task, and the system characteristics
[57]	Target detection	Simulation	Melon	Isolation; Collaboration	1; 3–4; 5–7; 10	Real-time switching of the synergistic levels was accomplished by developed algorithms for increasing system performance
[58]	Target detection	Simulation	Melon	Isolation; Collaboration	1; 3–4; 5–7; 10	Real-time switching of the synergistic levels was achieved, resulting in improved system performance by more than 90%
[53]	Target detection	Simulation	Melon	Isolation; Collaboration	1; 3–4; 5–7; 10	Operational costs were studied, showing that human decision time strongly affects the performance
[59]	Target detection/ Precision spraying	Lab exp/Simulation	Grape	Isolation; Collaboration	1; 3–4; 5–7; 10	Four levels of HRI <sup>7</sup> were developed and tested, as well as a spraying coverage optimization function
[60]	Robot navigation	Design Principles	N/A	N/A	N/A	A taxonomy was presented and evaluated in terms of an existing user interface for robot teleoperation
[61]	Movements identification	Design Principles	Olive	N/A	N/A	Guidelines are described for addressing problems in sharing human–robot environments
[20]	Robot navigation/ Target detection/ Precision spraying	Field and lab exp	Grape	Synchronization	1–2	Multiple views, head-mounted display, PC <sup>4</sup> keyboard contributed to higher perceived usability

Table 2. Cont.

Ref <sup>1</sup>	Subject	Method	Crop	Interaction Mode	Automation Level <sup>2</sup>	Main Results
[62]	Robot navigation/Target detection/Precision spraying	Field and lab exp	Grape	Synchronization	1–2	Similar results to [20], while camera placement on the top-back of the robot and on the end-effector improved the surroundings and activity awareness
[63]	Target detection/Precision spraying	Field exp	Grape	Isolation; Collaboration	1; 3–4; 5–7; 10	The collaborative spraying system reduces the sprayed material by half
[64]	Social navigation	Simulation	N/A	Coexistence	N/A	A controller modifies the length of personal space and velocity in order to keep a social distance
[65]	Stress management	Simulation	N/A	Isolation; Cooperation	1–3; 10	Collaboration allows for saving time
[66]	Load lift and carrying	Field exp	Strawberry	Cooperation	N/A	The pilot study showed that the experienced workers positively viewed the cooperation and considered it safe
[67]	Stress management	Simulation	N/A	Cooperation; Collaboration	3–5	The developed protocol provides the highest efficiency as compared to a system without synergy
[68]	Fleet of robots (tele-)operation	Field exp	N/A	Collaboration	3–7	The AR <sup>5</sup> system improves the situational awareness of a human for managing a fleet of robots
[69]	Harvesting	Simulation	Orange	N/A	N/A	The developed risk-averse solution minimizes economic costs
[70]	Stress management	Simulation	N/A	Cooperation; Collaboration	3–5	H-R <sup>6</sup> synergy can respond to emergency stresses situations fast and effectively
[71]	Harvesting	Simulation	Strawberries and grapes	Cooperation	N/A	Development of model and simulator to predict efficiencies of coupled operations pertaining to manual harvesting and robot transport
[72]	Harvesting	Field exp/Simulation	Strawberry	Cooperation	N/A	Simulations robustness of [71] was evaluated; 5 robots serving as tray-transport from 25 pickers improved efficiency by 10.2%



Table 2. Cont.

Ref <sup>1</sup>	Subject	Method	Crop	Interaction Mode	Automation Level <sup>2</sup>	Main Results
[21]	Ergonomics and safety	Design Principles	N/A	N/A	N/A	A combined approach is proposed that redefines practical limits, reprioritizes safety measures, and determines the riskiest postures
[73]	Target detection	Lab exp	Strawberry	Collaboration	2–5	Both experienced and non-experienced groups opt for robots producing more false positive results
[74]	Harvesting	Field exp	Tea	Cooperation	N/A	The robot kept on a side-by-side route with two workers
[75]	Human activity recognition	Field exp	N/A	Cooperation	N/A	The prediction of the defined sub-activities demonstrated an 85.6% average accuracy, while fusion of all sensors' data can yield the maximum accuracy
[76]	Harvesting	Simulation	Citrus varieties	N/A	N/A	H-R collaboration can optimize economic viability of robotic harvesters, especially when it occurs in the early stages of harvesting
[77]	Ergonomics	Lab exp	N/A	Cooperation	N/A	A deposit height of robot equal to 90 cm was suggested by avoiding large lumbar flexion
[78]	Human activity recognition	Field exp	N/A	Cooperation	N/A	Six continuous activities with wearable sensors were performed for a HRI scenario under several variants for obtaining a dataset for ergonomics research
[24]	Human activity recognition	Field exp	Pistacia	Cooperation	5	A real-time skeleton-based recognition framework was developed using 5 hand gestures and successfully tested in field experiments

Table 2. Cont.

Ref <sup>1</sup>	Subject	Method	Crop	Interaction Mode	Automation Level <sup>2</sup>	Main Results
[79]	Transitioning toward H-R synergy	Design Principles	N/A	N/A	N/A	The interplay among the socio-economic factors and underlying mental models driving the shift from pure automation to HRI are presented via a systems thinking approach Both groups (computer experts and farmers) made effective use of user interfaces with the tangible one receiving more positive evaluations H-R synergy increases the production but necessitates slightly more energy during harvesting
[80]	Robot navigation/Precision spraying	Field exp/Simulation	Grape	Collaboration	1–3	
[54]	Load lift and carrying	Simulation	Avocado	Cooperation	5	

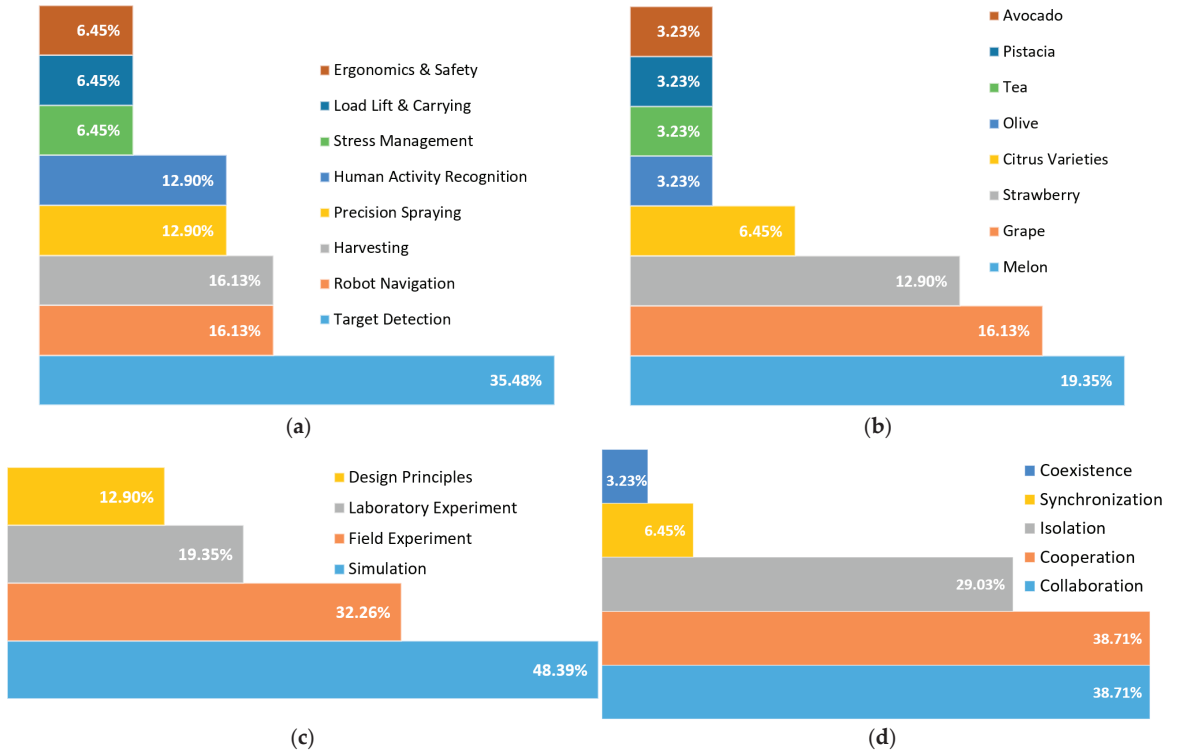
<sup>1</sup> Ref: Reference; <sup>2</sup> automation levels according to Sheridan scale [81]; <sup>3</sup> Exp: Experiments; <sup>4</sup> PC: Personal Computer; <sup>5</sup> AR: Augmented Reality; <sup>6</sup> H-R: Human–Robot; <sup>7</sup> HRI: Human–Robot Interaction.

Starting from the subject of the reviewed papers (Figure 5a), most of them dealt with a very demanding agricultural task, namely target detection. The key problems come from the peculiar agricultural environment. In essence, occlusion and changing illuminations properties, as well as variability in fruit color, size, shape, texture, orientation, and position, are limiting factors. Apart from the problems related to the location of targets, the uneven and continuously changed terrain and atmospheric conditions make target detection more complicated. Several performance measures have been used for target recognition, including detection time, probability of target detection, and non-target detection (false alarm). Automatic target detection in such environments is characterized by poor performance. Consequently, interaction with humans can be advantageous, considering their superior perception and action capabilities allowing them to adapt to unforeseen agricultural events.

The majority of the studies associated with implementing HRI for optimizing target detection [52,53,55–59,63] followed a certain methodology for comparing the performance of four different human–robot types of synergy:

- Humans alone detect and mark the targets, while HRI is never permitted. This is compatible with both level 1 in Sheridan’s scale and isolation mode;
- Robots recommend the targets and humans approve and mark them. In particular, the targets are automatically identified with the use of a detection algorithm. Then, humans recognize the algorithm’s true detections by ignoring the false ones and mark the possible missing targets. This interaction corresponds to levels 3–4 in Sheridan’s scale, as mentioned in these studies. In addition, following the analysis described in Section 2.4, this interaction is classified as collaboration, since both robots and humans focus on the same task;
- The targets are automatically detected by the corresponding machine learning algorithm, with the human role being to cancel the false findings, while, like at the above level, the humans marks the missing items. This type of synergy is equivalent to levels 5–7 in the Sheridan scale and, again, is classified as collaboration;

- Purely autonomous marking of targets takes place, in which human intervention is never permitted. Obviously, similar to the first type of synergy that was mentioned above, no HRI exists, demonstrating the highest level of automation in the Sheridan scale, namely 10.



**Figure 5.** Distribution of the most common aspects investigated in the reviewed studies; (a) subject, (b) examined crop, (c) implemented methodology, and (d) interaction mode.

Most of these studies used melons as a target, while grapes were also investigated corresponding in aggregate to approximately 35.5% of all studies (Figure 5b). On all occasions, the collaboration of humans and robots was found to increase detection performance and the corresponding time needed for detection. Both of these outcomes were observed to strongly depend on human decision time. Interestingly, when a field experiment was conducted to evaluate in practice the impact of the synergy on a site-specific spraying application, the proposed collaborative spraying system demonstrated a 50% reduction in the utilized sprayed pesticide [63]. Preliminary laboratory experiments in [82] investigated the opinion of experienced and non-experienced groups on errors produced by machine learning algorithms in a synergistic task.

Moreover, five studies [20,60,62,64,68] investigated robot navigation, which is also a demanding task, because of the particular nature of the rural environment. Adamides et al. [20,62] examined the usability of two types of output devices, two types of input devices, and single or multiple views toward optimizing a teleoperated robotic sprayer, while in [60], a taxonomy was proposed pertaining to usability guidelines. Similarly, Mallas et al. [80] investigated the efficiency of two user interfaces by using two groups in field and simulation experiments, namely computer experts and farmers. Additionally, in [68], the importance of augmented reality was investigated as a means of supervising two autonomous tractors in a test field. Finally, three computational studies [65,67,70]

concentrated on greenhouse stress management and how human–robot synergy can both provide higher efficiency and save time.

Focusing on HRI for harvesting applications, Rysz et al. [69,76] developed a risk-averse optimization solution and validated it by using a simulated grove setting, including information for different citrus varieties. A vehicle was successfully implemented in [74] for following the worker during tea plucking, as proved by the experimental field results. Furthermore, Seyyedhasani et al. [71,72] investigated the use of harvest-aid robots for carrying trays to decrease the non-productive walking times of pickers by utilizing data collected from two strawberry fields. In the same vein, to increase situation awareness, in [75,78], wearable sensors were used for gathering data during a human–robot synergistic task involving six sub-activities, which were carried out under different variants. Furthermore, in order to provide more natural means of communication between robot and human, Moysiadis et al. [24] developed a skeleton-based recognition system for hand gestures, which enabled a real-time HRI framework tested in field experiments. In [66], the same robotic system (Thorvald, SAGA Robotics SA, Oslo, Norway) with [24] was used for transporting the picked strawberries, and the opinion of workers on their interaction with it was assessed. For that purpose, a brief questionnaire with a five-point scale was employed.

Aiming at occupational health, which has been recognized as an integral element of collaborative robotic systems, kinetic and kinematic data as well as muscle activation levels were collected in [77] from experienced workers in laboratory experiments to investigate the optimal deposit height of an unmanned ground vehicle. For a similar purpose, Vasconez and Cheein [54] evaluated, in simulated scenarios, the expected production and also the physical workload of workers. Benos et al. [21] examined both ergonomics and safety during HRI operations from an agriculture-oriented perspective, while guidelines for addressing problems in shared environments were described in [61]. Finally, the socio-economic factors driving the shift from pure automation to HRI were analyzed through the prism of a systems thinking approach by Aivazidou and Tsolakis [79].

In general, simulated environments were used in the majority of the reviewed studies, while experiments, either in the field or in the laboratory, were also utilized, as well as studies dealing with design principles (Figure 5c). Simulations can be a valuable tool for investigating HRI in agriculture compared to real-world experiments. Benefits associated with simulations are (a) cost-effectiveness, as physical experiments include expensive equipment and land; (b) flexibility to study various scenarios; (c) scalability, enabling researchers to examine large-scale agricultural systems; and (d) risk-free experimentation without the fear of damaging crops or putting human operators at risk. It is worth stressing that simulations cannot fully replicate the intricacies of real-world environments. Therefore, it is essential to validate simulation outcomes by conducting physical experiments. This validation process ensures the dependability and precision of the findings before applying them in real agricultural settings.

Finally, as can be gleaned from Table 2, several automation levels, according to the Sheridan scale, were tested either in field/laboratory experiments or in simulated environments to test the potential of using different interaction levels in agricultural applications. In total, collaboration and cooperation modes, according to the analysis presented in 2.4, were the most usual modes (Figure 5d).

#### 4. Discussion and Conclusions

The present systematic review aimed to shed light on an ever-increasing topic that concerns several sectors worldwide, namely HRI. This emerging research field was methodically analyzed from the perspective of agriculture, which includes complex and dynamic ecosystems as well as live produce highly sensitive to physical and environmental conditions. A comprehensive examination of the present status was carried out by systematically reviewing the relevant literature. In total, 32 scientific papers were found. These studies are a result of the synergistic efforts of multiple disciplines including agricultural sciences,

human factors, sociology, and ICT. After an assessment of their methodological approach, the content of the reviewed articles was discussed in terms of their subject, implemented methodology, examined crop, interaction mode, automation level, and main results.

In summary, most studies dealt with target detection, while studies focusing on detection in combination with precision spraying and/or robot navigation were also observed. Furthermore, simulation was the most preferred methodology, as multiple parameters can be examined. However, field experiments have also been conducted showing encouraging results regarding the benefits of HRI in agriculture. The most studied crops, in descending order of frequency, were melons, grapes, and strawberries, with collaboration and cooperation being the most common interaction modes. These crops have high demands for careful handling, accurate harvesting methods, and precise evaluation of ripeness. Due to the time-consuming and labor-intensive nature of these tasks, the implementation of robotics and automation in these crops can greatly enhance productivity and efficiency. Overall, a range of factors such as the unique attributes of these crops, economic considerations, labor factors, technological feasibility, and research focus collectively contribute to the increased interest in HRI applications, specifically for these high-value crops. These applications can serve as valuable sources of technical knowledge and practices to be disseminated and encouraged among other crop producers. This will aid in the effective adoption of these technologies by considering the requirements, benefits, and potential challenges associated with them. Creating platforms for collaboration and the exchange of knowledge among agricultural growers can bring significant advantages for establishing a supportive ecosystem.

As can be deduced from the existing literature on HRI in agriculture, the brittleness of autonomous robotic systems in uncontrolled and dynamic conditions in tandem with variability in environments and live produce can result in ineffective operations and production losses. To that end, human workers can complement autonomous systems by overcoming their shortcomings. Nevertheless, the path to fully reap the associated benefits of the capabilities of human–robot synergistic systems is still long. A broad range of research areas is open for further development to meet the needs of reliability and feasibility, thus reaching the stage of being commercially available. As human–robot interactive systems consist of several sub-systems, which should be integrated and coordinated to successfully transfer information and execute tasks as a single unit, several factors should be considered, while various issues must be addressed.

First, considering the tremendous progress in ICT and AI, future research should enable the efficient real-time fusion of a variety of complementary sensors to allow sufficient localization, safe robot navigation, and sensing capabilities. The improvement of coordination issues between humans and robots, through providing robots with a better understanding of human intentions and actions, constitutes a promising research area. Moreover, usability issues pertaining to user interfaces should be tackled. The user interface is the point of interaction between humans and robots, allowing the former to control the robotic system to receive feedback from it and achieve effective operation. Consequently, intensive research efforts are required in the direction of developing user-friendly graphical interfaces (GUI). These interfaces should be able to decrease the mental workload, through methods such as avoiding both the inclusion of software that is not convenient to use and restrictions on the mobility of the operator. Advancement in user interfaces will also enable synergy between humans and teams of light-weight unmanned ground or/and aerial vehicles. This constitutes the next demanding step in HRI for addressing the current challenges and optimizing agricultural practices. Toward that direction, human–robot natural communication frameworks should be improved. With the advancement of big data and the enhanced capabilities of computer hardware, deep learning technology exhibits superior reasoning capabilities compared to traditional machine learning algorithms [83]. Hence, it has gained extensive adoption in industrial domains in recent years, where it has been implemented to solve problems related to communication frameworks, such as hand gesture [84,85] and facial expression recognition under various conditions [32,86].

Likewise, advancement in accuracy of machine learning recognition algorithms can further improve the credibility of wearable-sensor-based multi-posture recognition [87].

Future research in the field of HRI in agriculture should give due consideration to the social aspects involved. This entails examining the effects of automation on rural communities, including the exploration of possible changes in skill requirements and socio-economic disparities that may arise [88]. It is imperative to employ user-centered design principles and participatory approaches, actively involving farmers and rural communities during the development process. This approach will ensure that designs are both socially and culturally appropriate, leading to enhanced user acceptance. A deep understanding of social acceptance and trust will be gained by exploring stakeholders' perceptions and attitudes. Factors contributing to trust building, such as transparency, liability, and accountability, should be taken into account [12,89]. Moreover, ethical considerations, encompassing aspects such as privacy and data security, need to be thoroughly examined. By prioritizing these social aspects in future research, a responsible adoption of robotic systems can be accomplished that aligns with the values and needs of society.

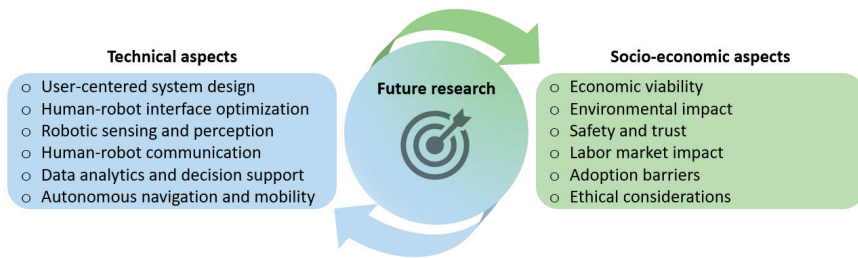
Future research should also put effort into safety aspects in terms of safeguarding workers, crops, and surrounding settings. Also, attention should be paid to the optimal design of HRI systems, including the structure of the team, their specific role, human factors, and complex mechanisms of robotic systems [90,91]. In addition, economic aspects should be investigated in depth regarding the practical use of collaborative robots in agriculture, as farmers will only invest in them on the condition that their investment is going to be profitable after a reasonable time. Future research should also involve the assessment of the environmental implications of using robots, such as their potential to minimize chemical usage and soil erosion and contribute to the advancement of sustainable farming practices.

The introduction of collaborative robotics is, however, not a trivial issue. It requires open dialogue between stakeholders, clear objectives, proper incentives, and information from policy makers. An effective approach would be the organization of frequent symposiums and workshops that involve farmers in the co-design process. These initiatives can provide a space where farmers, robotics experts, policymakers, and researchers can actively participate in meaningful discussions. By facilitating the exchange of knowledge and experiences, these forums can enable the identification of specific limitations, opportunities, and collaborative solutions. Flexible education and training programs need to be developed to equip agricultural workers with the necessary skills to interact with robotic systems effectively. This can involve tailored training modules on robot usage, maintenance, safety protocols, and troubleshooting. Agricultural extension services, technology providers, and vocational training centers can collaborate to provide tailored hands-on training programs that meet farmers' specific needs. To study skill competencies compared to emerging robot demands, interdisciplinary research initiatives should also be undertaken focusing on recognizing areas where skills are lacking, assessing how robotics affect job responsibilities, and investigating the social and economic consequences of their implementation. These endeavors may involve cooperation among agricultural scientists, robotics engineers, and behavioral researchers, with the aim to comprehend the human aspects of productive interaction between humans and robots in agricultural environments.

The above considerations for future research directions, which were discussed in this section, are summarized in Figure 6.

In conclusion, this review paper presents an extensive evaluation of the present state of HRI in agriculture, emphasizing the progress made, capabilities, technological limitations, and potential applications of this technology within the agricultural domain. Through a comprehensive analysis of the existing literature, this review is expected to serve as a valuable reference for researchers, practitioners, and policymakers who aim to gain insights into the dynamic landscape of agricultural robotics. Finally, by identifying areas necessitating further research and development, this paper seeks to stimulate future innovations and collaborations, thereby fostering the seamless integration of robotics to enhance productivity, sustainability, efficiency, and safety in the agricultural sector.





**Figure 6.** Indicative future research areas that are considered to improve human–robot interaction in agriculture.

**Author Contributions:** Conceptualization, L.B., V.M. and D.B.; methodology, L.B., D.K., A.C.T. and P.B.; investigation, P.B., L.B. and V.M.; writing—original draft preparation, L.B., V.M., A.C.T., D.K. and P.B.; writing—review and editing, S.P. and D.B.; visualization, L.B. and V.M.; supervision, S.P. and D.B. All authors have read and agreed to the published version of the manuscript.

**Funding:** This research received no external funding.

**Institutional Review Board Statement:** Not applicable.

**Informed Consent Statement:** Not applicable.

**Data Availability Statement:** No new data were created or analyzed in this study.

**Conflicts of Interest:** The authors declare no conflict of interest.

## References

- Guenat, S.; Purnell, P.; Davies, Z.G.; Nawrath, M.; Stringer, L.C.; Babu, G.R.; Balasubramanian, M.; Ballantyne, E.E.F.; Bylappa, B.K.; Chen, B.; et al. Meeting sustainable development goals via robotics and autonomous systems. *Nat. Commun.* **2022**, *13*, 3559. [CrossRef] [PubMed]
- IFR Press Room Robots Help Reaching UN Goals of Sustainable Development, International Federation of Robotics Reports. Available online: <https://ifr.org/ifr-press-releases/news/robots-help-reaching-un-sdgs> (accessed on 1 June 2023).
- Pearson, S.; Camacho-Villa, T.C.; Valluru, R.; Gaju, O.; Rai, M.C.; Gould, I.; Brewer, S.; Sklar, E. Robotics and Autonomous Systems for Net Zero Agriculture. *Curr. Robot. Rep.* **2022**, *3*, 57–64. [CrossRef]
- Lampridi, M.; Sørensen, C.; Bochtis, D. Agricultural Sustainability: A Review of Concepts and Methods. *Sustainability* **2019**, *11*, 5120. [CrossRef]
- Benos, L.; Makaritis, N.; Kolorizos, V. *From Precision Agriculture to Agriculture 4.0: Integrating ICT in Farming—Information and Communication Technologies for Agriculture—Theme III: Decision*; Bochtis, D.D., Sørensen, C.G., Fountas, S., Moysiadis, V., Pardalos, P.M., Eds.; Springer International Publishing: Cham, Switzerland, 2022; pp. 79–93. ISBN 978-3-030-84152-2.
- Toriyama, K. Development of precision agriculture and ICT application thereof to manage spatial variability of crop growth. *Soil Sci. Plant Nutr.* **2020**, *66*, 811–819. [CrossRef]
- Lampridi, M.G.; Kateris, D.; Vasileiadis, G.; Marinoudi, V.; Pearson, S.; Sørensen, C.G.; Balafoutis, A.; Bochtis, D. A Case-Based Economic Assessment of Robotics Employment in Precision Arable Farming. *Agronomy* **2019**, *9*, 175. [CrossRef]
- Marinoudi, V.; Sørensen, C.G.; Pearson, S.; Bochtis, D. Robotics and labour in agriculture. A context consideration. *Biosyst. Eng.* **2019**, *184*, 111–121. [CrossRef]
- Terazono, E. Farm Robots Given COVID-19 Boost. Available online: <https://www.ft.com/content/0b394693-137b-40a4-992b-0b742202e4e1> (accessed on 22 September 2022).
- Bochtis, D.; Benos, L.; Lampridi, M.; Marinoudi, V.; Pearson, S.; Sørensen, C.G. Agricultural workforce crisis in light of the COVID-19 pandemic. *Sustainability* **2020**, *12*, 8212. [CrossRef]
- Moysiadis, V.; Tsolakis, N.; Katikaridis, D.; Sørensen, C.G.; Pearson, S.; Bochtis, D. Mobile Robotics in Agricultural Operations: A Narrative Review on Planning Aspects. *Appl. Sci.* **2020**, *10*, 3453. [CrossRef]
- Benos, L.; Sørensen, C.G.; Bochtis, D. Field Deployment of Robotic Systems for Agriculture in Light of Key Safety, Labor, Ethics and Legislation Issues. *Curr. Robot. Rep.* **2022**, *3*, 49–56. [CrossRef]
- Oliveira, L.F.P.; Moreira, A.P.; Silva, M.F. Advances in Agriculture Robotics: A State-of-the-Art Review and Challenges Ahead. *Robotics* **2021**, *10*, 52. [CrossRef]
- Droukas, L.; Doulgeri, Z.; Tsakiridis, N.L.; Triantafyllou, D.; Kleitsiotis, I.; Mariolis, I.; Giakoumis, D.; Tzovaras, D.; Kateris, D.; Bochtis, D. A Survey of Robotic Harvesting Systems and Enabling Technologies. *arXiv* **2022**, arXiv:2207.10457. [CrossRef] [PubMed]

15. Van Wynsberghe, A.; Ley, M.; Roeser, S. *Ethical Aspects of Human–Robot Collaboration in Industrial Work Settings BT—The 21st Century Industrial Robot: When Tools Become Collaborators*; Aldinhas Ferreira, M.I., Fletcher, S.R., Eds.; Springer International Publishing: Cham, Switzerland, 2022; pp. 255–266. ISBN 978-3-030-78513-0.
16. Bechar, A.; Vigneault, C. Agricultural robots for field operations: Concepts and components. *Biosyst. Eng.* **2016**, *149*, 94–111. [[CrossRef](#)]
17. Marinoudi, V.; Lampridi, M.; Kateris, D.; Pearson, S.; Sørensen, C.G.; Bochtis, D. The Future of Agricultural Jobs in View of Robotization. *Sustainability* **2021**, *13*, 12109. [[CrossRef](#)]
18. Kruse, T.; Pandey, A.K.; Alami, R.; Kirsch, A. Human-aware robot navigation: A survey. *Rob. Auton. Syst.* **2013**, *61*, 1726–1743. [[CrossRef](#)]
19. Tsarouchi, P.; Makris, S.; Chryssolouris, G. Human–robot interaction review and challenges on task planning and programming. *Int. J. Comput. Integr. Manuf.* **2016**, *29*, 916–931. [[CrossRef](#)]
20. Adamides, G.; Katsanos, C.; Parnet, Y.; Christou, G.; Xenos, M.; Hadzilacos, T.; Edan, Y. HRI usability evaluation of interaction modes for a teleoperated agricultural robotic sprayer. *Appl. Ergon.* **2017**, *62*, 237–246. [[CrossRef](#)] [[PubMed](#)]
21. Benos, L.; Bechar, A.; Bochtis, D. Safety and ergonomics in human-robot interactive agricultural operations. *Biosyst. Eng.* **2020**, *200*, 55–72. [[CrossRef](#)]
22. Hopko, S.; Wang, J.; Mehta, R. Human Factors Considerations and Metrics in Shared Space Human-Robot Collaboration: A Systematic Review. *Front. Robot. AI* **2022**, *9*, 799522. [[CrossRef](#)]
23. Vasconez, J.P.; Kantor, G.A.; Auat Cheein, F.A. Human–robot interaction in agriculture: A survey and current challenges. *Biosyst. Eng.* **2019**, *179*, 35–48. [[CrossRef](#)]
24. Moysiadis, V.; Katikaridis, D.; Benos, L.; Busato, P.; Anagnostis, A.; Kateris, D.; Pearson, S.; Bochtis, D. An Integrated Real-Time Hand Gesture Recognition Framework for Human–Robot Interaction in Agriculture. *Appl. Sci.* **2022**, *12*, 8160. [[CrossRef](#)]
25. Lu, D.; Yu, Y.; Liu, H. Gesture recognition using data glove: An extreme learning machine method. In Proceedings of the 2016 IEEE International Conference on Robotics and Biomimetics (ROBIO), Qingdao, China, 3–7 December 2016; pp. 1349–1354.
26. Jaramillo-Yáñez, A.; Benalcázar, M.E.; Mena-Maldonado, E. Real-Time Hand Gesture Recognition Using Surface Electromyography and Machine Learning: A Systematic Literature Review. *Sensors* **2020**, *20*, 2467. [[CrossRef](#)]
27. Ceolini, E.; Frenkel, C.; Shrestha, S.B.; Taverni, G.; Khacef, L.; Payvand, M.; Donati, E. Hand-Gesture Recognition Based on EMG and Event-Based Camera Sensor Fusion: A Benchmark in Neuromorphic Computing. *Front. Neurosci.* **2020**, *14*, 637. [[CrossRef](#)] [[PubMed](#)]
28. Tran, D.-S.; Ho, N.-H.; Yang, H.-J.; Baek, E.-T.; Kim, S.-H.; Lee, G. Real-Time Hand Gesture Spotting and Recognition Using RGB-D Camera and 3D Convolutional Neural Network. *Appl. Sci.* **2020**, *10*, 722. [[CrossRef](#)]
29. Oudah, M.; Al-Naji, A.; Chah, J. Hand Gesture Recognition Based on Computer Vision: A Review of Techniques. *J. Imaging* **2020**, *6*, 73. [[CrossRef](#)]
30. Su, H.; Ovrur, S.E.; Zhou, X.; Qi, W.; Ferrigno, G.; De Momi, E. Depth vision guided hand gesture recognition using electromyographic signals. *Adv. Robot.* **2020**, *34*, 985–997. [[CrossRef](#)]
31. Vasconez, J.P.; Guevara, L.; Cheein, F.A. Social robot navigation based on HRI non-verbal communication: A case study on avocado harvesting. In Proceedings of the ACM Symposium on Applied Computing, Limassol, Cyprus, 8–2 April 2019; Association for Computing Machinery: New York, NY, USA, 2019; Volume Part F147772, pp. 957–960.
32. Jin, B.; Cruz, L.; Gonçalves, N. Face Depth Prediction by the Scene Depth. In Proceedings of the 2021 IEEE/ACIS 19th International Conference on Computer and Information Science (ICIS), Shanghai, China, 23–5 June 2021; pp. 42–48.
33. Benos, L.; Bochtis, D.D. *An Analysis of Safety and Health Issues in Agriculture Towards Work Automation BT—Information and Communication Technologies for Agriculture—Theme IV: Actions*; Bochtis, D.D., Pearson, S., Lampridi, M., Marinoudi, V., Pardalos, P.M., Eds.; Springer International Publishing: Cham, Switzerland, 2021; pp. 95–117. ISBN 978-3-030-84156-0.
34. Benos, L.; Tsaopoulos, D.; Bochtis, D. A Review on Ergonomics in Agriculture. Part I: Manual Operations. *Appl. Sci.* **2020**, *10*, 1905. [[CrossRef](#)]
35. Akalin, N.; Kristoffersson, A.; Loutfi, A. Do you feel safe with your robot? Factors influencing perceived safety in human-robot interaction based on subjective and objective measures. *Int. J. Hum. Comput. Stud.* **2022**, *158*, 102744. [[CrossRef](#)]
36. Rubagotti, M.; Tusseyeva, I.; Baltabayeva, S.; Summers, D.; Sandygulova, A. Perceived safety in physical human–robot interaction—A survey. *Rob. Auton. Syst.* **2022**, *151*, 104047. [[CrossRef](#)]
37. Hoffman, G. Evaluating Fluency in Human–Robot Collaboration. *IEEE Trans. Hum. Mach. Syst.* **2019**, *49*, 209–218. [[CrossRef](#)]
38. Castro, A.; Silva, F.; Santos, V. Trends of Human-Robot Collaboration in Industry Contexts: Handover, Learning, and Metrics. *Sensors* **2021**, *21*, 4113. [[CrossRef](#)]
39. Mizanoor Rahman, S.M. Performance Metrics for Human-Robot Collaboration: An Automotive Manufacturing Case. In Proceedings of the 2021 IEEE International Workshop on Metrology for Automotive (MetroAutomotive), Bologna, Italy, 1–2 July 2021; pp. 260–265.
40. Murphy, R.R.; Schreckenghost, D. Survey of metrics for human-robot interaction. In Proceedings of the 2013 8th ACM/IEEE International Conference on Human-Robot Interaction (HRI), Tokyo, Japan, 3–6 March 2013; pp. 197–198.
41. Steinfeld, A.; Fong, T.; Kaber, D.; Lewis, M.; Scholtz, J.; Schultz, A.; Goodrich, M. Common Metrics for Human-Robot Interaction. In Proceedings of the 1st ACM SIGCHI/SIGART Conference on Human-Robot Interaction; Association for Computing Machinery, New York, NY, USA, 2–3 March 2006; pp. 33–40.

42. Pina, P.; Cummings, M.; Crandall, J.; Della Penna, M. Identifying generalizable metric classes to evaluate human-robot teams. In Proceedings of the 3rd Annual Conference on Human-Robot Interaction, Amsterdam, The Netherlands, 12–15 March 2008; pp. 13–20.
43. Lasota, P.A.; Shah, J.A. Analyzing the Effects of Human-Aware Motion Planning on Close-Proximity Human–Robot Collaboration. *Hum. Factors* **2015**, *57*, 21–33. [\[CrossRef\]](#)
44. Page, M.J.; McKenzie, J.E.; Bossuyt, P.M.; Boutron, I.; Hoffmann, T.C.; Mulrow, C.D.; Shamseer, L.; Tetzlaff, J.M.; Akl, E.A.; Brennan, S.E.; et al. The PRISMA 2020 statement: An updated guideline for reporting systematic reviews. *BMJ* **2021**, *372*, n71. [\[CrossRef\]](#)
45. Wright, R.W.; Brand, R.A.; Dunn, W.; Spindler, K.P. How to Write a Systematic Review. *Clin. Orthop. Relat. Res.* **2007**, *455*, 23–29. [\[CrossRef\]](#)
46. Lee, C.-L.; Strong, R.; Dooley, K.E. Analyzing Precision Agriculture Adoption across the Globe: A Systematic Review of Scholarship from 1999–2020. *Sustainability* **2021**, *13*, 10295. [\[CrossRef\]](#)
47. Hoy, D.; Brooks, P.; Woolf, A.; Blyth, F.; March, L.; Bain, C.; Baker, P.; Smith, E.; Buchbinder, R. Assessing risk of bias in prevalence studies: Modification of an existing tool and evidence of interrater agreement. *J. Clin. Epidemiol.* **2012**, *65*, 934–939. [\[CrossRef\]](#)
48. Xie, Y.; Szeto, G.; Dai, J. Prevalence and risk factors associated with musculoskeletal complaints among users of mobile handheld devices: A systematic review. *Appl. Ergon.* **2017**, *59*, 132–142. [\[CrossRef\]](#)
49. Benos, L.; Tsaopoulos, D.; Bochtis, D. A Review on Ergonomics in Agriculture. Part II: Mechanized Operations. *Appl. Sci.* **2020**, *10*, 3484. [\[CrossRef\]](#)
50. Matheson, E.; Minto, R.; Zampieri, E.G.G.; Faccio, M.; Rosati, G. Human–Robot Collaboration in Manufacturing Applications: A Review. *Robotics* **2019**, *8*, 100. [\[CrossRef\]](#)
51. Parasuraman, R.; Sheridan, T.B.; Wickens, C.D. A model for types and levels of human interaction with automation. *IEEE Trans. Syst. Man Cybern. Part A Syst. Hum.* **2000**, *30*, 286–297. [\[CrossRef\]](#) [\[PubMed\]](#)
52. Bechar, A.; Edan, Y. Human-robot collaboration for improved target recognition of agricultural robots. *Ind. Rob.* **2003**, *30*, 432–436. [\[CrossRef\]](#)
53. Oren, Y.; Bechar, A.; Edan, Y. Performance analysis of a human-Robot collaborative target recognition system. *Robotica* **2012**, *30*, 813–826. [\[CrossRef\]](#)
54. Vázquez, J.P.; Auat Cheein, F.A. Workload and production assessment in the avocado harvesting process using human-robot collaborative strategies. *Biosyst. Eng.* **2022**, *223*, 56–77. [\[CrossRef\]](#)
55. Bechar, A.; Meyer, J.; Edan, Y. An objective function to evaluate performance of human-robot systems for target recognition tasks. In Proceedings of the 2007 IEEE International Conference on Systems, Man and Cybernetics, Montreal, QC, Canada, 7–10 October 2007; pp. 967–972.
56. Bechar, A.; Meyer, J.; Edan, Y. An objective function to evaluate performance of human-robot collaboration in target recognition tasks. *IEEE Trans. Syst. Man Cybern. Part C Appl. Rev.* **2009**, *39*, 611–620. [\[CrossRef\]](#)
57. Tkach, I.; Edan, Y.; Bechar, A. Algorithms for dynamic switching of collaborative human-robot system in target recognition tasks. *IFAC Proc. Vol.* **2009**, *42*, 2179–2184. [\[CrossRef\]](#)
58. Tkach, I.; Bechar, A.; Edan, Y. Switching between collaboration levels in a human-robot target recognition system. *IEEE Trans. Syst. Man Cybern. Part C Appl. Rev.* **2011**, *41*, 955–967. [\[CrossRef\]](#)
59. Berenstein, R.; Edan, Y. Human-robot cooperative precision spraying: Collaboration levels and optimization function. In *IFAC Proceedings Volumes (IFAC-PapersOnline)*; IFAC Secretariat: Dubrovnik, Croatia, 2012; Volume 45, pp. 799–804.
60. Adamides, G.; Christou, G.; Katsanos, C.; Xenos, M.; Hadzilacos, T. Usability guidelines for the design of robot teleoperation: A taxonomy. *IEEE Trans. Hum. Mach. Syst.* **2015**, *45*, 256–262. [\[CrossRef\]](#)
61. Cheein, F.A.; Herrera, D.; Gimenez, J.; Carelli, R.; Torres-Torriti, M.; Rosell-Polo, J.R.; Escola, A.; Arno, J. Human-robot interaction in precision agriculture: Sharing the workspace with service units. In Proceedings of the IEEE International Conference on Industrial Technology, Seville, Spain, 17–19 March 2015; Volume 2015, pp. 289–295.
62. Adamides, G.; Katsanos, C.; Constantinou, I.; Christou, G.; Xenos, M.; Hadzilacos, T.; Edan, Y. Design and development of a semi-autonomous agricultural vineyard sprayer: Human-robot interaction aspects. *J. Field Robot.* **2017**, *34*, 1407–1426. [\[CrossRef\]](#)
63. Berenstein, R.; Edan, Y. Human-robot collaborative site-specific sprayer. *J. Field Robot.* **2017**, *34*, 1519–1530. [\[CrossRef\]](#)
64. Montesdeoca, J.C.; Toibero, M.; Carelli, R. Person-following based on social navigation into the sensorized environments. In Proceedings of the 2017 IEEE International Conference on Robotics and Biomimetics (ROBIO), Macao, China, 5–8 December 2017; pp. 799–803.
65. Guo, P.; Dusadeerungsikul, P.O.; Nof, S.Y. Agricultural cyber physical system collaboration for greenhouse stress management. *Comput. Electron. Agric.* **2018**, *150*, 439–454. [\[CrossRef\]](#)
66. Baxter, P.; Cielniak, G.; Hanheide, M.; From, P.J. Safe Human-Robot Interaction in Agriculture. In Proceedings of the ACM/IEEE International Conference, New York, NY, USA, 5–8 March 2018.
67. Dusadeerungsikul, P.O.; Nof, S.Y. A collaborative control protocol for agricultural robot routing with online adaptation. *Comput. Ind. Eng.* **2019**, *135*, 456–466. [\[CrossRef\]](#)
68. Huuskonen, J.; Oksanen, T. Augmented Reality for Supervising Multirobot System in Agricultural Field Operation. *IFAC-PapersOnLine* **2019**, *52*, 367–372. [\[CrossRef\]](#)

69. Rysz, M.; Ganesh, P.; Burks, T.F.; Mehta, S.S. Risk-averse Optimization for Improving Harvesting Efficiency of Autonomous Systems through Human Collaboration. *IFAC-PapersOnLine* **2019**, *52*, 207–212. [[CrossRef](#)]
70. Dusadeerungsikul, P.O.; Nof, S.; Bechar, A.; Tao, Y. Collaborative Control Protocol for Agricultural Cyber-Physical System. In Proceedings of the 25th International Conference on Production Research Manufacturing Innovation: Cyber Physical Manufacturing, Chicago, IL, USA, 9–14 August 2019.
71. Seyyedhasani, H.; Peng, C.; Jang, W.; Vougioukas, S.G. Collaboration of human pickers and crop-transporting robots during harvesting—Part I: Model and simulator development. *Comput. Electron. Agric.* **2020**, *172*, 105324. [[CrossRef](#)]
72. Seyyedhasani, H.; Peng, C.; Jang, W.; Vougioukas, S.G. Collaboration of human pickers and crop-transporting robots during harvesting—Part II: Simulator evaluation and robot-scheduling case-study. *Comput. Electron. Agric.* **2020**, *172*, 105323. [[CrossRef](#)]
73. Huang, Z.; Miyachi, G.; Gomez, S.A.; Bird, R.; Amar, S.K.; Jansen, C.; Liu, Z.; Parsons, S.; Sklar, E. Toward robot co-labourers for intelligent farming. In Proceedings of the Companion of the 2020 ACM/IEEE International Conference on Human-Robot Interaction, Cambridge, UK, 23–26 March 2020.
74. Lai, Y.-L.; Chen, P.-L.; Yen, P.-L. A Human-Robot Cooperative Vehicle for Tea Plucking. In Proceedings of the 2020 7th International Conference on Control, Decision and Information Technologies (CoDIT), Prague, Czech Republic, 29 June 2020–2 July 2020; Volume 1, pp. 217–222.
75. Anagnostis, A.; Benos, L.; Tsaopoulos, D.; Tagarakis, A.; Tsolakis, N.; Bochtis, D. Human activity recognition through recurrent neural networks for human-robot interaction in agriculture. *Appl. Sci.* **2021**, *11*, 2188. [[CrossRef](#)]
76. Rysz, M.W.; Mehta, S.S. A risk-averse optimization approach to human-robot collaboration in robotic fruit harvesting. *Comput. Electron. Agric.* **2021**, *182*, 106018. [[CrossRef](#)]
77. Benos, L.; Kokkoti, C.; Tsalas, T.; Karampina, E.; Tsaopoulos, D.; Bochtis, D. Biomechanical Effects on Lower Extremities in Human-Robot Collaborative Agricultural Tasks. *Appl. Sci.* **2021**, *11*, 11742. [[CrossRef](#)]
78. Tagarakis, A.C.; Benos, L.; Aivazidou, E.; Anagnostis, A.; Kateris, D.; Bochtis, D. Wearable Sensors for Identifying Activity Signatures in Human-Robot Collaborative Agricultural Environments. *Eng. Proc.* **2021**, *9*, 5. [[CrossRef](#)]
79. Aivazidou, E.; Tsolakis, N. Transitioning towards human-robot synergy in agriculture: A systems thinking perspective. *Syst. Res. Behav. Sci.* **2023**, *40*, 536–551. [[CrossRef](#)]
80. Mallas, A.; Rigou, M.; Xenos, M. Comparing the Performance and Evaluation of Computer Experts and Farmers when Operating Agricultural Robots: A Case of Tangible vs Mouse-Based UIs. *Hum. Behav. Emerg. Technol.* **2022**, *2022*, 6070285. [[CrossRef](#)]
81. Sheridan, T.; Verplank, W. *Human and Computer Control of Undersea Teleoperators*; Technical Reports; MIT Man-Machine Systems Laboratory: Cambridge, MA, USA, 1978.
82. Huang, Z.; Gomez, A.S.; Bird, R.; Kalsi, A.S.; Jansen, C.; Liu, Z.; Miyachi, G.; Parsons, S.; Sklar, E.I. Understanding human responses to errors in a collaborative human-robot selective harvesting task. In Proceedings of the UKRAS20 Conference: “Robots into the Real World”, Lincoln, UK, 17 April 2020.
83. Benos, L.; Tagarakis, A.C.; Dolias, G.; Berruto, R.; Kateris, D.; Bochtis, D. Machine Learning in Agriculture: A Comprehensive Updated Review. *Sensors* **2021**, *21*, 3758. [[CrossRef](#)] [[PubMed](#)]
84. Sun, J.-H.; Ji, T.-T.; Zhang, S.-B.; Yang, J.-K.; Ji, G.-R. Research on the Hand Gesture Recognition Based on Deep Learning. In Proceedings of the 2018 12th International Symposium on Antennas, Propagation and EM Theory (ISAPE), Hangzhou, China, 3–6 December 2018; pp. 1–4.
85. Hussain, S.; Saxena, R.; Han, X.; Khan, J.A.; Shin, H. Hand gesture recognition using deep learning. In Proceedings of the 2017 International SoC Design Conference (ISOCC), Seoul, Republic of Korea, 5–8 November 2017; pp. 48–49.
86. Jin, B.; Cruz, L.; Gonçalves, N. Pseudo RGB-D Face Recognition. *IEEE Sens. J.* **2022**, *22*, 21780–21794. [[CrossRef](#)]
87. Hong, Z.; Hong, M.; Wang, N.; Ma, Y.; Zhou, X.; Wang, W. A wearable-based posture recognition system with AI-assisted approach for healthcare IoT. *Futur. Gener. Comput. Syst.* **2022**, *127*, 286–296. [[CrossRef](#)]
88. Sørensen, L.B.; Germundsson, L.B.; Hansen, S.R.; Rojas, C.; Kristensen, N.H. What Skills Do Agricultural Professionals Need in the Transition towards a Sustainable Agriculture? A Qualitative Literature Review. *Sustainability* **2021**, *13*, 13556. [[CrossRef](#)]
89. European Parliament Ethical Aspects of Cyber-Physical Systems. Available online: [https://www.europarl.europa.eu/thinktank/en/document/EPRS\\_STU\(2016\)563501](https://www.europarl.europa.eu/thinktank/en/document/EPRS_STU(2016)563501) (accessed on 8 December 2021).
90. Ferland, F.; Reveleau, A.; Leconte, F.; Létourneau, D.; Michaud, F. Coordination mechanism for integrated design of Human-Robot Interaction scenarios. *Paladyn J. Behav. Robot.* **2017**, *8*, 100–111. [[CrossRef](#)]
91. Cammarata, A.; Sinatra, R.; Maddio, P.D. *A Two-Step Algorithm for the Dynamic Reduction of Flexible Mechanisms BT—Mechanism Design for Robotics*; Gasparetto, A., Ceccarelli, M., Eds.; Springer International Publishing: Cham, Switzerland, 2019; pp. 25–32.

**Disclaimer/Publisher’s Note:** The statements, opinions and data contained in all publications are solely those of the individual author(s) and contributor(s) and not of MDPI and/or the editor(s). MDPI and/or the editor(s) disclaim responsibility for any injury to people or property resulting from any ideas, methods, instructions or products referred to in the content.



Review

# Toward the Next Generation of Digitalization in Agriculture Based on Digital Twin Paradigm

Abozar Nasirahmadi \* and Oliver Hensel

Department of Agricultural and Biosystems Engineering, University of Kassel, 37213 Witzenhausen, Germany; agrartechnik@uni-kassel.de

\* Correspondence: aboazar.nasirahmadi@uni-kassel.de

**Abstract:** Digitalization has impacted agricultural and food production systems, and makes application of technologies and advanced data processing techniques in agricultural field possible. Digital farming aims to use available information from agricultural assets to solve several existing challenges for addressing food security, climate protection, and resource management. However, the agricultural sector is complex, dynamic, and requires sophisticated management systems. The digital approaches are expected to provide more optimization and further decision-making supports. Digital twin in agriculture is a virtual representation of a farm with great potential for enhancing productivity and efficiency while declining energy usage and losses. This review describes the state-of-the-art of digital twin concepts along with different digital technologies and techniques in agricultural contexts. It presents a general framework of digital twins in soil, irrigation, robotics, farm machineries, and food post-harvest processing in agricultural field. Data recording, modeling including artificial intelligence, big data, simulation, analysis, prediction, and communication aspects (e.g., Internet of Things, wireless technologies) of digital twin in agriculture are discussed. Digital twin systems can support farmers as a next generation of digitalization paradigm by continuous and real-time monitoring of physical world (farm) and updating the state of virtual world.

**Keywords:** digital twin; digitalization; digital farming; farm management; smart farming

**Citation:** Nasirahmadi, A.; Hensel, O. Toward the Next Generation of Digitalization in Agriculture Based on Digital Twin Paradigm. *Sensors* **2022**, *22*, 498. <https://doi.org/10.3390/s22020498>

Academic Editors: Dionysis Bochtis and Aristotelis C. Tagarakis

Received: 6 December 2021

Accepted: 7 January 2022

Published: 10 January 2022

**Publisher's Note:** MDPI stays neutral with regard to jurisdictional claims in published maps and institutional affiliations.



**Copyright:** © 2022 by the authors. Licensee MDPI, Basel, Switzerland. This article is an open access article distributed under the terms and conditions of the Creative Commons Attribution (CC BY) license (<https://creativecommons.org/licenses/by/4.0/>).

## 1. Introduction

One of the main global challenges is how to ensure food security for the world's growing population whilst ensuring long-term sustainable development. According to the Food and Agriculture Organization, agricultural and food productions will need to grow to feed the world population, which will reach around 10 billion by 2050 [1]. Due to the increase in world population and market demand for higher product quantity and quality standards, the issue of food security, sustainability, productivity, and profitability becomes more important. Furthermore, the economic pressure on the agricultural sector, labor, environmental, and climate change issues are increasing [2,3]. Therefore, the enhancement of efficiency through effective integrated smart technologies and techniques has been widely considered in recent years.

In this context, digital agriculture (also known as smart farming or smart agriculture) tools can support the deeper understanding of interrelations within the agricultural production system and the consequent effects on the performance of farm production while balancing human health and well-being, social and environmental aspects, and sustainability associated with agricultural system [4–6]. Due to advances in data generation, data processing and human-computer interactions, digital farming has progressed in recent years [7]. One of the main features of digitalization in agriculture is the introduction of innovative Information and Communication Technology (ICT), Internet of Things (IoT), big data analytics and interpretation techniques, machine learning and Artificial Intelligence (AI).

Data acquisition and analysis in digital farming by means of smart technologies are supporting complex decision-making approaches [8,9]. They enhance final productivity,



reduce costs, and optimize the decision-making process. Furthermore, ICT tools present advantages for on-farm management, efficiency, quality control, and the food supply chain as well as decision support tools [10]. The AI and big data support better and precise farm monitoring, data acquisition and analytics, improve information extraction from sensors as well as farm management [11]. For instance, crop health and productivity can be monitored and controlled using advanced AI and deep learning techniques [12]. Data-driven approaches augment on-farm decision-making capabilities, improve crop yield, reduce losses, and therefore, benefit farmers. The IoT and wireless technologies enable real-time data transferring and monitoring in digital farming [13,14]. The IoT, along with cloud computing systems, can facilitate communication between software platforms and sensors, pieces of machinery, crops, and animals in digital farming. However, by increasing the number of sensors and generating large amounts of data in digital farming could cause high load on the cloud server and reduce the response speed [15]. In this context, it may be impractical to always store and process data in the cloud systems [16]. An alternative technology which has been recently introduced to the smart farming is edge-computing that enables computation at the edge of the network [17]. It helps to reduce network load and supports real-time data processing in agricultural fields. Furthermore, cyber-physical systems have been introduced through smart farming systems to develop hardware and software, improve adaptability, and safety and security of computer-based algorithms and systems [18]. It enables adaptability, practicality, security, and safety of collected information in agricultural field e.g., climate, irrigation, soil, nutrition, and yield for better management.

According to ref. [19], digital farming approaches can provide farmers with useful information about (I) the use of fertilizers, chemicals, seeds, and irrigation management strategies, (II) the environment protection, (III) pest, climate, and crop monitoring management solutions, (IV) market demands and business conditions. However, agricultural production systems are complex, dynamic, and require sophisticated management [20]. Digitalization approaches are expected to provide more monitoring, data analysis and optimization capabilities, and further decision-making supports.

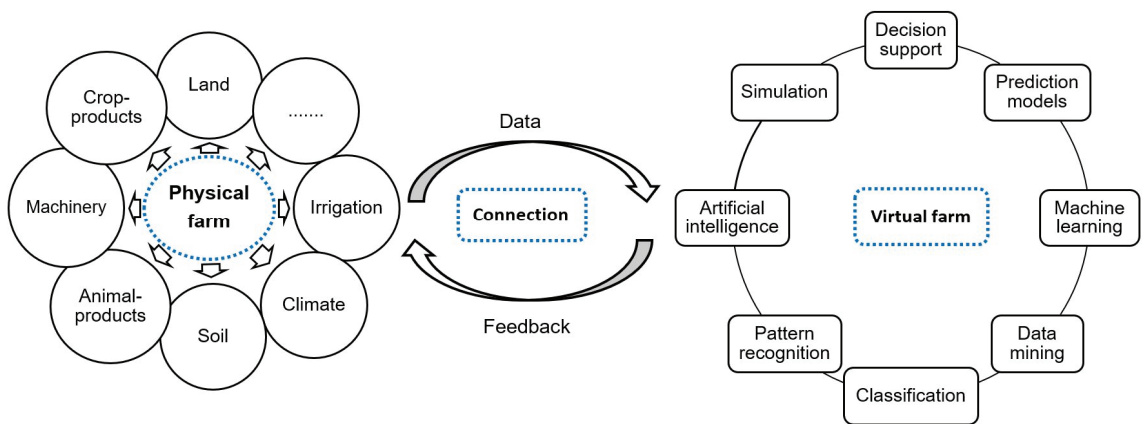
To enhance the efficiency of these systems, an emerging paradigm has been proposed and implemented in digital agriculture, that is, digital twin. The digital twin was firstly presented by NASA for monitoring of spacecraft behavior and can be defined as a virtual or digital representation of physical systems to simulate the behavior of the physical system [21,22]. There are different definitions for digital twin available in the literature which have been reviewed by [23–25]. Based on the reported definitions, the component of digital twin can be characterized by physical and virtual objects, as well as a set of connections between physical and digital assets [26].

The physical system or physical world in agriculture is a complex and dynamic environment and includes basic information and features of the object or device such as shape, position, cooler, material, and live objects [27]. The physical system is one of the key components, and a digital twin without a physical world is a model [28], and system boundaries of a digital twin are identified based on the real physical world [29]. The physical system can be a single component of an object or the whole object with sub-components located in a physical environment [28]. The physical world in agriculture can be an animal itself or located in a farm including building, feeding strategies, number of animals [30], or a crop with different soil, climate, and irrigation conditions [22], robots and agricultural pieces of machinery, e.g., tractors, harvesters and fertilizers, as well as operators. The physical world can include a whole object (e.g., whole machine) or sub-part of the object, or a single asset of the object connected with other objects. In an agricultural context, the physical system may be some aspects of the crop, soil, and irrigation systems, or animal body. The physical world requires measurement technologies and sensors to collect and receive data from the physical object. Examples of digital twins in smart agriculture include optical sensors for plant canopy and disease [31,32], soil and weather sensors for crop [33], barn sensors such as temperature, humidity, ammonia for animals [34],

Global Positioning System (GPS) and Real-Time Kinematic-Global Navigation Satellite for tracking of agricultural robots [35], and food supply chain.

The connection between physical and virtual worlds depends on the developed digital twin. This component enables data transmission between virtual and physical systems. It interprets the collected data from the physical system and updates the state of the virtual system, and transfers feedbacks from the virtual system to the physical world [25]. The connection components can be varied depending on the source, type and volume of data, data transfer rate and speed, as well as the minimum delay between data acquisition and feedbacks. Wireless and IoT techniques have been used in digital twins of agricultural concepts to connect between physical and virtual worlds (such as [34,36,37]).

The models and data of the physical world are represented in a virtual system. The virtual world may also include different processing and simulation concepts, software, machine learning, data mining, and AI models. In this context, data processing and analytics by means of AI techniques to support decision-making and feedback to the physical system were suggested by some researchers [38,39]. The virtual twin may simulate and control the physical system, optimize a process, and predict unseen issues in the physical system. For example, an application layer of a digital twin reported by [22] provides real-time monitoring of weeds, crop growth, and expected yield via cloud dashboards for farmers. A schematic of the digital twin concept in agriculture is shown in Figure 1.



**Figure 1.** Schematic of digital twin concept for agriculture.

Although digital twin concepts in smart farming are in their infancy and early demonstration stages [22,30], there are ongoing interests in implementing this technique in the agricultural context. There are some reviews available in the literature describing digital twin concepts in the agriculture context (listed in Table 1), however, to the best of our knowledge, these works have focused on a specific part of the digital twin, and no comprehensive studies have yet been done to address the application of digital twins in soil, irrigation, agricultural farm pieces of machinery, robots, and post-harvest food processing. Therefore, this review summarizes digital twin concepts as a next-generation paradigm for digitalization in agriculture. This paper is structured in 6 sections. Section 2 illustrates the digital twin of soil and irrigation systems in smart agriculture. Section 3 covers the use of digital twin concepts for crop technologies. Section 4 illustrates digital twin concepts during post-harvest processing. Challenges and future research needs for digital twin are presented in Section 5. Finally, conclusions are discussed in Section 6.

**Table 1.** Previous review studies on digital twin in agriculture.

Concept	Sources
Agriculture-farm management	[40]
Smart farming—Hydroponics	[41]
Food processing	[42]
Food losses—supply chain of fresh products	[43]
Agri-food—societal and ethical aspects	[44]
Food processing—fresh horticulture supply chain	[45]
Agri-food supply chain	[46]
Smart farming—definition and concept	[22]
Agriculture—general application and adoption	[47]

## 2. Digital Twin in Soil and Irrigation

Monitoring and evaluation of soil quality to sustain plant productivity is the basis of land-use strategies in agricultural farms [48]. Crop health and productivity depends on the quality and properties of the soil. More detailed information about the agricultural soil may reduce the potential use of chemical fertilizer and pesticide dosages, therefore improving the underground water, protecting the environment and human health. It also supports defining plant density in a more efficient way. Digital technologies are supporting scientists to better understand and study soil in agriculture. Soil monitoring sensors such as moisture, temperature, organic matter, and soil pollutant sensors are playing critical roles in digital agriculture [49]. For instance, soil moisture information can be used to assess irrigation efficiency in agricultural fields [50]. Furthermore, to support the decision-making process of smart farming, digital soil mapping is an essential paradigm that can be defined as spatial soil information based on field and laboratory investigations coupled with soil inference systems [51]. Digital soil assessment approaches have a direct impact on crop yield and performance by identifying zones that may cause low crop yield. Digital alternative methodologies for soil survey and identifying key soil characteristics could have the possibility to quantify the trend of agricultural soil conditions [52].

The advancement of knowledge and technology (e.g., wireless sensors, IoT, AI) in digital agriculture could lead to digital twin paradigms of soil in agriculture. The recent development of digital soil mapping techniques may support digital twins by digital representation of knowledge obtained from the soil in virtual entrainment [53]. For instance, digital soil mapping could be used to describe soil variation in digital twins using information from complex soil variation at a specific depth, time, and special locations [52].

Additionally, the decision about crop management depends directly on the crop water requirements, soil properties, and availability of water. In order to manage soil and crop requirements in smart farming, digital technologies have been used to meet the requirement of smart or precise water management strategies. Wireless system networks, IoT, edge-computing, local weather-based controllers, and soil sensors are some of the digital tools based on smart irrigation systems. The mentioned tools can be used in the digital twin of soil and irrigation systems. For example, ref. [37] developed a digital twin concept for smart water management in the agricultural domain. Information of air and ground temperature, and humidity sensors, soil moisture, and ambient light as well as geospatial position sensors were collected. An IoT system was used to connect the cloud and the physical system. A virtual environment including decision-making tools and models was designed to inform the data collected by connection device (the IoT system) and to send feedback to the physical system. They also presented a digital twin system architecture including monitoring devices (i.e., soil probe, weather information, irrigation system, machines, and other equipment) in a physical system (farm) with could serve as a connection between the physical and virtual systems to visualize satellite and drone images.

In another study, to evaluate and forecast plants' irrigation requirements, and support irrigation and water distribution planning, a digital twin for a smart water management system was developed by [54]. Data of the physical world (agriculture field) such as

weather, fertilizer, and soil type as well as information from developed models that simulate the behavior of soil and crops were considered as input data for the digital twin. The digital twin concept also consisted of a Soil Agent (includes hydrological models and soil data), Crop Agent (includes crop models and evaporation data), and a Field Avatar, which is a digital representation of the field such as geological models and weather data [54]. In their developed digital twin concept, the information from Soil Avatar and Crop Avatar feed into the Field Avatar, and an IoT system was used for data transformation and connection between the physical and virtual worlds.

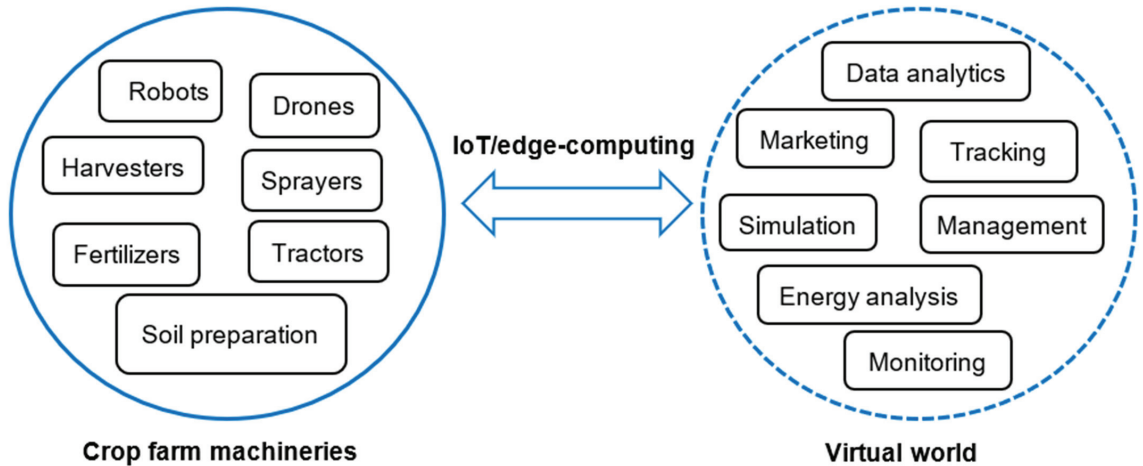
Due to increase in world population, water and energy management, storage, and proper distribution of water become more essential for water users in agricultural sectors, which can be managed through a collective irrigation system [55]. A digital twin of water systems coupled with big data can reduce risk and uncertainty of water management, explore consumption patterns, and optimize operation planning [56]. Furthermore, in a collective irrigation system, improvement of water efficiency could help to reduce water losses. In this context, a digital twin concept was created using field and laboratory tests of a collective irrigation system network to evaluate energy, pumping facilities, water losses and water use efficiencies [57]. The developed digital twin methodology was based on information from the physical system, i.e., infrastructure data, acquired information through telemetry, data analytics from laboratory tests and field measurements, IoT data transferring as connection, energy balance, water balance, and hydraulic model in the virtual system. It was found that the digital twin of the irrigation management system made it possible to understand system processes, maintenance, and management strategies [57].

A digital twin of soil and irrigation systems in smart farming enables digital representation of information from agricultural soil, and provides prediction and fundamental understanding of water requirement and soil components for crop farming. Exchanging information from the soil as a physical system to a virtual system using IoT, cloud, fog, and edge-computing technologies in digital twin may allow evaluating the state of soil and irrigation systems. In particular, the edge-computing technique that saves and performs the data processing near the soil monitoring and irrigation devices can improve the performance and overcome issues of cloud-based system in digital twin concepts. Furthermore, it could offer different irrigation recommendations based on crop requirements which are not solved yet by the researchers.

### 3. Digital Twin in Crop Production

The use of digital and ICT tools in crop production technologies, in particular agricultural machineries, e.g., tractors, combine harvesters, fertilizers, and sprayers, plays an important role in the improvement of overall efficiency by reducing the cost of fuel, fertilizers, human labor, and parameters which affect production efficiency and sustainability [58]. Digitalization has modernized agricultural machinery application and management policies using collected information and advanced data analytics approaches. It allows to optimize the performance and enhance the use of advanced tools in manufacturing. For instance, based on the European Agricultural Machinery Association, a digital farm machine should be able to assist and support drivers by sending and receiving data via sensors and ICT tools, enable the best and optimal use of machinery, and the technology should facilitate the automated operation of the devices [59]. The application of AI, big data analytics, and wireless and IoT technologies have led to significant changes in farm technology roles towards the development of autonomous systems. The role of agricultural machinery in the implementation of digital agriculture was stated by [58] as data collected from sensors mounted on typical and autonomous agricultural machinery and transferred via an IoT platform. Then, the information was analyzed by data analytics such as AI, fuzzy logic, and big data analysis to support farmers, consumers, and markets [58]. In this context, combining digital tools with autonomous machines and robots could help farmers to do more effective practices and improve the quality of products [60]. Nowadays, with advancements in digital technology, the real-time visualization of smart farm equipment

conditions is possible through digital twin approaches [40]. It allows contact to the system (e.g., machinery and robots), simulates the condition of the system, and monitors the behavior and operation as well as the maintenance situation of the machines (Figure 2).



**Figure 2.** An architecture of the digital twin concept for crop production technology.

Digital twin in design and manufacturing of products (e.g., farm machinery) requires (I) geometric (e.g., size, shape) and physical properties of an object, (II) in the detailed information of the product which can illustrate dynamic processing of the object, (III) integration of geometric, physical, and process information [61]. Digital twin approaches make it possible to model, design, simulate, and develop agricultural machinery that would yield more productive machines in terms of energy and power efficiencies. For instance, it was shown that overall energy consumption of machinery could be modeled in digital twin concepts, and the effect of different factors on energy consumption can also be explored there [62]. In the agricultural context, ref. [40] reported that a commercially available digital twin platform for agricultural machinery is able to track the machines in real-time, monitor the energy consumption, economic efficiency of crop management, and trajectories of tractors by considering the specific conditions of the farm. It has also been reported that using digital twins could potentially impact the training of unskilled harvester operators and lead to high macro-economic benefits [63].

Within the digital farming technologies, robotics, as an important technology in crop production, has played an essential role in digitalization and has been drawing more attention in recent years. To optimize the robotic application process, reduce costs, and increase the quality and efficiency of the product, the digital twin concepts can be used for virtualization of the robot environment by introducing a remote operating system [64]. By providing simulation and remote operation possibilities and modeling various interactions between robot and environment in digital twin concepts, accuracy, performance, and flexibility may enhance, and the final product cost may decline. Ref. [65] analyzed the human-robot interactive behaviors using a digital twin platform. Their developed digital twin helps to improve operational productivity and comfort. In another study, a digital twin approach was proposed to assist the remote programming of a robot [66]. The developed digital twin system consists of a robot (as a physical object), and a gaming platform (as a virtual system) which was able to observe the motion of the robot, ease programming for complex environments as well as introduce a remote operating system for communication across different platforms [66]. In the agricultural context, an approach was recommended by [35] that the development of a digital twin paradigm for agricultural robots may improve predictive emulation of the vehicles, operational scheduling, digital-

ization, economic, environmental, and social sustainability in agriculture. Furthermore, the digital twin paradigm makes it possible to overcome common challenges in the control of robot components in the agriculture field. In this context, a research group demonstrated the possibility of a digital twin concept for a desktop version of an agricultural robot [67] to control the motor and indoor localization capabilities of the robot. Besides, the digital twin concept was used to predict movement and monitor the safety mechanism of the robot [67]. However, their developed digital twin concept needs different kinds of calibrations to be applicable in different environmental conditions.

In another study, to simulate complexity of the crop production process, variability of plant, soil, environment, and technologies in the agricultural field, digital twin concepts were developed [68]. Three field robots for different agricultural applications were used to develop different digital twin concepts and optimize sensor-based autonomous navigation. It is reported that the developed concepts could provide considerable information in preparing field experiments, and better evaluation for the use and positioning of sensor systems towards demonstrating and implementation of the developed robotic technologies [68].

Integration of the digital twin systems with technologies and management strategies in crop production can provide a new phenomenon for digitalization in agricultural field. Management strategies can be improved and optimized by providing reliable forecasts of the key parameters in digital twins [69]. The digital twin systems can not only act as a management system, but it may also be used to revolutionize agricultural farm management strategies [40]. For instance, a digital twin concept was applied in a greenhouse to discover, analyze, and extract behavior of farmers [70]. Sensor data were analyzed using deep learning techniques to establish decision-making models to replicate expert farmers' experience for transferring to young farmers. It was found that the developed digital twin module could improve control and management strategies in crop farming [70]. In this context, the use of distributed architecture in digital twin may increase efficiency and reliability of the module by proper resource handling [71]. A distributed digital twin concept was developed to handle resources over different stakeholders and platforms in agricultural landscape [72]. It consists of different components, i.e., stakeholders, applications in agriculture and farm management, sensor data, analytics and simulation tools, virtual model, IoT, and resource registry which makes interoperable and cross-scale management possible in agricultural landscape [71].

In addition, the use of digital twin system as a decision support system can benefit and be adopted for crop farming applications, and optimization of products and farm system performance. A digital twin model was implemented by [36] in sustainable agriculture for monitoring and control of product qualities, adjustment of environmental conditions, identification of forecasting, and decision support scenarios. In addition, a novel approach based on digital twin paradigms was developed to forecast yield, vegetation quality, and duration of plant development [33]. Consequently, the quality of crop production could be improved due to detailed analysis and control of plant growth, and the efficiency of farms could be improved due to automation of decision support processes through the developed digital twin concept. Digital twin along with forecasting models were able to provide feedback to farmers for a better decision-making scenario in a reported study by [73]. Their proposed digital twin system consists of a monitoring system to collect environmental condition data from an underground farm, as well as data analysis and modeling techniques to identify key parameters, critical trends, and forecast operational scenarios. Furthermore, digital twin was able to optimize productivity of crops in a greenhouse environment through climate control strategies and treatments related to crop management [74].

Information from crop production machineries (e.g., tractors, harvesters, robots) have been used in smart farming to optimize the performance and efficiency, and reduce the fuel and energy consumption. However, the digital twin concepts collect real-time data from the devices and characterize the states of the physical object continuously. This capability makes it possible to predict and prescribe solutions using the collected information from



the farm machineries. Hence, big data analytics coupled with AI models are able to detect failures in the machines before or in the early stage of when breakdowns happen. In this context, the use of state-of-the-art edge-computing systems may reduce latency by the limited amount of transmitted data and provide information from the crop production machineries such as autonomous robot, harvesters, and tractors to the digital twin concepts. The digital twin paradigm in crop farming can change production productivity, farm management, and sustainability at farm level. Advanced statistical models, machine learning and data analytic approaches can provide farmers with more precise information to make better decisions that were not possible previously. Based on the past (historical) and current continuous knowledge from crop (sensors deployed at farm) and environment data, the digital twin systems provide information about future states of the farm, and offer solutions for turning the collected information into useful and actionable on-farm knowledge.

#### 4. Digital Twin in Post-Harvest Process

Post-harvest process is a stage of agricultural products after harvesting until consuming the products, which may include transportation, drying, cooling, storage, and marketing. Through digital farming approaches, the post-harvest processes could benefit from loss reduction, improvement of monitoring and optimization of food processing, storage conditions, marketing, and transportation. Digital solutions allow monitoring real-time agri-food supply chain to increase robustness and resilience of the chain [75], and lower food waste and losses. The IoT platform supports the reduction of food losses in post-harvest processing [76], and tracking of the product through the food supply chain. To achieve food security AI and big data analytics enable data processing, optimization, and management in food and crop post-harvest stages [77], also reducing waste and improving overall profitability [78]. The ICT offers solutions to monitor and control quality criteria of food and agricultural products during post-harvest processing [43]. However, different environmental conditions, processing factors, and dynamic features of agricultural product (e.g., shape, size), environmental parameters (e.g., temperature, humidity), handling, transportation, and storage of the products influence the quality of post-harvest process [79].

To overcome these issues and increase the efficiency of the system, digital twin approaches have been used in post-harvest processing to continuously monitor the products and update the processing stages [80]. Digital twins, as an expanding family of digital farming could strengthen agri-food systems, affect knowledge and skills of farm management [44]. Digital twin in post-harvest processes can be defined as a digital representation of harvested agricultural products based on the information collected from the products. In this context, ref. [42] reported the digital twin concept of food processing may include: (I) data collected from a physical system (food process operation) by means of sensors that measure properties and variables of products and environmental parameters, (II) an IoT platform to provide sensor communication, data storage and big data analytics, high-performance computing, and link to the digital twin assets, (III) a simulation platform that uses input data from physical system for optimization, testing and validation of models, and provides decision supports in the virtual world. In order to benefit food processing by developing digital twin models, it is important to include accurate information representing production processes of the product, e.g., equipment, labor, and to create realistic models with all existing boundaries and barriers [81]. In a study reported by [82], a digital twin of mango fruit was developed to simulate and qualify thermal and associated bio-chemical behavior of the fruit through a post-harvest supply chain. In order to develop the digital twin concept, environmental air temperature as input was considered, and the actual supply chain conditions were mimicked within mechanistic finite element models [82]. Moreover, the impact of higher air speed on storage life, cold chain length, and delivery air temperature on the fruit quality were considered in the digital twin. It was reported that the digital twin allows to monitor and predict temperature-dependent fruit quality losses, improve refrigeration and logistic processes, consequently, it can reduce food losses [82]. Furthermore, it is reported that the digital twin can help horticultural

products along with the post-harvest life, and can be used to forecast the shelf-life of agricultural products through the cold chain [45]. It can support food consumers as well as food business owners for tracking of the products, logistics, and marketing decisions; however, the existing digital twin concept needs to be enhanced by considering more biochemical and physical features [45]. Ref. [83] proposed a digital twin concept food supply chain analysis. Their developed digital twin includes: (I) a network based on knowledge from, e.g., customers, suppliers, and factories, (II) some parameters, e.g., in production, transportation, warehouses, sourcing, shipment costs, and policies, (III) various operational parameters, e.g., demand, quality, target inventory, and vehicle capacity. It was found that the developed digital twin can be used for optimization, simulation, and analysis of operation and performance changes in the food supply chain [83].

According to [43], digital twin in post-harvest can be considered as mechanistic, statistical, and intelligent models; however, it was found that the physics-based mechanistic digital twin concepts can evaluate the quality of fresh agricultural products better than the others. Physics-based digital twins were developed on 331 cold chain shipments of four fruits (i.e., cucumber, eggplant, strawberry, raspberry) by [84]. Based on digital twin concepts, it was found that the quality of fruits may be affected (around 43–85%) before being delivered to stores.

The post-harvest processing has improved through the application of digital solutions over the last several years. However, the use of the digital twin paradigm is receiving more attention in post-harvest food processing due to the future product quality prediction and cost reduction. The digital twin of post-harvest processes may be developed to model, optimize, represent, and characterize the design and operational parameters such as quality, safety, ingredients, shelf-life, and product status, which need to be considered by researchers in future studies.

## 5. Challenges and Future Needs

Summary of the digital twin concepts developed in the literature for different purposes in agricultural fields, including soil, irrigation, crop monitoring, robotics, farm machinery, and post-harvest processing, is presented in Tables 2–4. These tables show that the digital twin paradigm is in the early stage of research and development in the agricultural context, and future studies in terms of knowledge, technological, system development, and application aspects of digital twin concepts in different fields of agriculture should be considered.

**Table 2.** Summary of soil and irrigation digital twin concepts.

Concept	Key Components and Benefits	Source
Soil–water	Supporting precision irrigation in agriculture, better irrigation planning and water distribution, reduce crop yield losses	[54]
Soil–water	IoT-based water management platform, monitoring water pattern in soil	[37]
Water	Analyze and optimization of aquaponic systems, minimize water waste	[85]
Irrigation	Urban-integrated hydroponic system, integration of forecasting models for better decision-making assistance	[73]
Irrigation	System management and irrigation decision-making integration, water use, global energy and pumping facilities efficiency evaluation, understanding of irrigation system process	[57]
Water	Development of decision support system, enhancement of cyber-physical implementation in aquaponics	[86]

**Table 3.** Summary of the digital twin in crop production.

Concept	Key Components and Benefits	Source
Vertical farming	Environmental conditions assessment, identification of forecasting and decision support models, monitoring and optimization of agri-food lifecycle	[36]
Plant/tree	Plant condition monitoring including structure, health, stress, and quality of fruit	[31]
Robot	Analysis and performance evaluation, robot selection, and navigation	[35]
Robot	Simulation of field environment, autonomous robot navigation	[68]
Agricultural machinery	Development and advantages of business models for potato harvesting	[59]
Agricultural landscape	Resource distribution management over different stakeholders in agriculture	[72]
Crop	Forecasting yield and duration of plant development	[33]
Agricultural machinery	Development of three-dimensional geometric models, drawings of devices, mechanisms, and the attributive data	[87]
Plant	Detection of plant diseases and nutrient efficiency	[32]
Crop/hydroponic farm	Identification of crop growth parameters such as lighting, external temperature, and ventilation systems	[73]
Crop	Optimize productivity, climate control strategies, and crop treatment management in controlled environment agriculture	[74]
Robot	Co-simulation of robot environment, prediction of robot movement, and safety monitoring	[67]

**Table 4.** Summary of digital twin for post-harvest process.

Concept	Key Components and Benefits	Source
Food supply chain	Thermophysical behavior of fruit during supply chain, storage at different airflow rate, understanding, recording, and predicting losses of temperature-based fruit quality	[82]
Beverage	Predicting possible anomalies and preventing safety issues for employees	[88]
Food	Machine learning-based models for real-time response and quality predictions, maintenance, and data collection	[80]
Food supply chain	Development of practical implementation strategies, enhancing resilience food retail, and capacity management	[83]
Food	Challenges, methodologies, and opportunities for implementation of digital twin in food processing, importance of realistic and accurate models in food processing	[81]
Food	Modeling of equipment, humans, and space for fast-food producing, management of production chain, and performance evaluation	[89]
Post-harvest	Monitoring of retail stores and detection of fruit quality lost	[84]

With rapid technological and sensor development, digital twin of the agricultural soil by considering the soil quality and properties may accommodate plant productivity, health, and yield, save water, and reduce chemical usage. Many elements of the soil, irrigation, and environmental parameters in agricultural land can be continuously monitored, analyzed, and their management strategies optimized using big data analytics, machine learning models, and decision support systems embedded in the digital twin concepts. The combination of soil and irrigation digital twin approaches to record, monitor, and analyze agricultural land changes may lead to improved performance of crop farming. For instance, simulation of soil structure along with data-driven updating models could connect farmers to the farm using the IoT technology and present, in detail, pictures of parameters that impact the soil, irrigation, and crop yield. However, few studies focus on the development of digital twin concepts of agriculture soil with higher degree of flexibility as well as considering a wider range of operation than existing simulation models. Soil sensors could constantly measure and record the dynamic condition of arable soil, e.g.,

water holding capacity, moisture, temperature [53]. These data, along with information from soil structure and simulation techniques, can be transferred to digital twin concepts, and constant feedback from the digital world may advise real-time responses for soil and water management as well as control systems. In recent years, there has been rapid growth in the digital farming scenarios, use of remote sensing, digital soil mapping, and development of software platforms. However, researches needed to fuse the developed techniques along with the IoT, edge-computing, AI, data analytics, and simulation techniques that could lead to development of a digital twin paradigm is in an early stage and needs to be addressed in future studies. Furthermore, researchers need to consider the practical challenges of digital twin-based systems in soil and irrigation as digital twins are multi- and interdisciplinary techniques and require systems engineering perspectives [90].

Digital twin offers real-time simulation of farm machinery and robots that can benefit optimal design of the products, interaction with the environment, energy usage, and maintenance strategies. Digital twin concepts have the possibility to predict failures in farm machinery and support decision-making scenarios in plant production. Farm owners can be able to connect to the machines through virtual world for monitoring and tracking of the devices in agricultural farms. Digital twin systems are accompanied by recording a large amount of data and exchanging information between different assets; hence compiling and analyzing these data is a challenge facing farms, particularly in some rural areas with poor internet and technological infrastructures [91]. Other alternatives, e.g., Long Range technology based on wireless sensor networks communication and edge-computing could be used to mitigate internet access problems in rural areas for the connection part of the digital twin concepts [32,92]. Future opportunities for the implementation of digital twin systems in crop farm technologies could lie in the development of standards as well as data transferring and communication strategies in this context.

The digital twin of crop production using big data collected from crop and farm machinery as well as robots, analytical and AI models, IoT, and satellite and drone information could allow simulating crop, environmental, and farm conditions in the digital world to determine unknown and unseen issues before happening in the physical world. Agricultural objects (crops in particular) need frequent updates in data to support information analysis and decision-making processes [93] which in turn can promote sustainable farming practices and save energy usage in crop productions. In this context, greater effort should be focused in the future on characterization and development of frameworks for more effective practical digital twin paradigms. In crop farming, all information may not be recorded and tracked using digital sensors; however, combining data from different sources could improve the virtual representation of the farm operation and environment [73]. Continuous monitoring of crops in digital twin systems by simulating the dynamic farm conditions and considering the effect of management, climate, and environmental conditions on the plant growth and use of data-driven models along with sensor fusion techniques could help to identify deviations from the normal conditions of the plant, and forecast growth stages to reduce risk of environmental and management effects. In future, different digital twin concepts might be applied to copy the complex physical system of crop farming in the digital world and incorporate variable sensors, data collecting strategies, modeling, forecasting, and simulation approaches in crop farming.

In addition, digital twin concepts can support monitoring, tracking, and analysis of food through the entire supply chain. Development of a digital copy of an agricultural product to monitor post-harvest processing could be used to optimize the process, reduce energy use, labor, and food losses based on information from different sensors and simulation models. Future studies need to be carried out to consider more environmental and post-harvest product features for the development of robust digital twins [45]. Another major challenge in the development of digital twin for post-harvest processing to minimize quality losses and improve the shelf-life of the product is considering the value chain of agricultural products from farm to fork [43], which has not been addressed yet. In post-harvest processing to reduce uncertainty in digital twins and enable the consumer to trust

the output of digital twin concepts, detailed experimental and data collection approaches along with numerical modeling and validation techniques need be considered.

## 6. Conclusions

Employing digital technology has helped agricultural farm managers to improve efficiency, yield, and reduce losses. There are different types of digital farming paradigms in the literature that could be used in digital twin concepts as the next generation of digitalization in the agricultural field. The results of this review show that the digital twin concepts in agriculture and food processing have, so far, been little exploited in research. There are several research challenges and opportunities in different stages of digital farming. Digital twin paradigms can be meaningfully utilized for soil and irrigation, crop, robots and farm machinery, and post-harvest food processing in the agricultural field. In this context, most of the studies have focused on the development of digital twins by considering some limited parameters in agricultural sectors. Deploying of state-of-the-art technologies, e.g., AI, advanced statistical and optimization models, big data analytics, and three-dimensional simulation, offer further possibilities for improvement in farm management. With real-time and continuous information about agricultural assets, virtual models can predict and address unseen issues in the fields. It may support farmers to decline the economic pressure on the agricultural sector and labor issues, and help policy makers responsible for food security and environmental protection, towards strengthening the agriculture sector. In addition, it facilitates the work of researchers exploring methods to track and monitor crop farm machinery, agricultural and post-harvest products or reduce water, chemicals, and energy usage in digital farming. Although many digital twin systems in engineering, manufacturing, and health contexts have been developed, further attempts need to be considered in the agricultural context towards the development of digital twin systems that can monitor, record, and analyze data, to predict and prescribe the best decision for digital farming management.

**Author Contributions:** Conceptualization, A.N. and O.H.; investigation, A.N.; writing—original draft preparation, A.N.; writing—review and editing, A.N. and O.H.; visualization, A.N. All authors have read and agreed to the published version of the manuscript.

**Funding:** This research received no external funding.

**Institutional Review Board Statement:** Not applicable.

**Informed Consent Statement:** Not applicable.

**Data Availability Statement:** Not applicable.

**Conflicts of Interest:** The authors declare no conflict of interest.

## References

1. Food and Agriculture Organization of the United Nations (FAO). *Transforming Food and Agriculture to Achieve the SDGs*; FAO: Rome, Italy, 2018.
2. Prause, L. Digital Agriculture and Labor: A Few Challenges for Social Sustainability. *Sustainability* **2021**, *13*, 5980. [[CrossRef](#)]
3. de Gennaro, B.C.; Forleo, M.B. Sustainability perspectives in agricultural economics research and policy agenda. *Agric. Food Econ.* **2019**, *7*, 17. [[CrossRef](#)]
4. Jakku, E.; Taylor, B.; Fleming, A.; Mason, C.; Fielke, S.; Sounness, C.; Thorburn, P. If they don't tell us what they do with it, why would we trust them? Trust, transparency and benefit-sharing in Smart Farming. *NJAS Wagening. J. Life Sci.* **2019**, *90–91*, 100285. [[CrossRef](#)]
5. Basso, B.; Antle, J. Digital agriculture to design sustainable agricultural systems. *Nat. Sustain.* **2020**, *3*, 254–256. [[CrossRef](#)]
6. Goel, R.K.; Yadav, C.S.; Vishnoi, S.; Rastogi, R. Smart agriculture—Urgent need of the day in developing countries. *Sustain. Comput. Inform. Syst.* **2021**, *30*, 100512. [[CrossRef](#)]
7. Mehrabi, Z.; McDowell, M.J.; Ricciardi, V.; Levers, C.; Martinez, J.D.; Mehrabi, N.; Wittman, H.; Ramankutty, N.; Jarvis, A. The global divide in data-driven farming. *Nat. Sustain.* **2021**, *4*, 154–160. [[CrossRef](#)]
8. Wolfert, S.; Ge, L.; Verdouw, C.; Bogaardt, M.J. Big Data in Smart Farming—A review. *Agric. Syst.* **2017**, *153*, 69–80. [[CrossRef](#)]
9. Ingram, J.; Maye, D. What are the implications of digitalisation for agricultural knowledge? *Front. Sustain. Food Syst.* **2020**, *4*, 66. [[CrossRef](#)]

10. Jakku, E.; Taylor, B.; Fleming, A.; Mason, C.; Thorburn, P. *Big Data, Trust and Collaboration: Exploring the Socio-Technical Enabling Conditions for Big Data in the Grains Industry*; CSIRO: Brisbane, Australia, 2016; p. 34.
11. Smith, M.J. Getting value from artificial intelligence in agriculture. *Anim. Prod. Sci.* **2018**, *60*, 46–54. [[CrossRef](#)]
12. Nasirahmadi, A.; Wilczek, U.; Hensel, O. Sugar Beet Damage Detection during Harvesting Using Different Convolutional Neural Network Models. *Agriculture* **2021**, *11*, 1111. [[CrossRef](#)]
13. Farooq, M.S.; Riaz, S.; Abid, A.; Abid, K.; Naeem, M.A. A Survey on the Role of IoT in Agriculture for the Implementation of Smart Farming. *IEEE Access* **2019**, *7*, 156237–156271. [[CrossRef](#)]
14. Paraforos, D.S.; Griepentrog, H.W. Digital Farming and Field Robotics: Internet of Things, Cloud Computing, and Big Data. In *Fundamentals of Agricultural and Field Robotics. Agriculture Automation and Control*; Karkee, M., Zhang, Q., Eds.; Springer: Cham, Switzerland, 2021.
15. Zhang, X.; Cao, Z.; Dong, W. Overview of Edge Computing in the Agricultural Internet of Things: Key Technologies, Applications, Challenges. *IEEE Access* **2020**, *8*, 141748–141761. [[CrossRef](#)]
16. Sarker, V.K.; Queralta, J.P.; Gia, T.N.; Tenhunen, H.; Westerlund, T. A Survey on LoRa for IoT: Integrating Edge Computing. In Proceedings of the 2019 Fourth International Conference on Fog and Mobile Edge Computing (FMEC), Rome, Italy, 10–13 June 2019; pp. 295–300.
17. Ning, H.; Li, Y.; Shi, F.; Yang, L.T. Heterogeneous edge computing open platforms and tools for internet of things. *Future Gener. Comput. Syst.* **2020**, *106*, 67–76. [[CrossRef](#)]
18. An, W.; Wu, D.; Ci, S.; Luo, H.; Adamchuk, V.; Xu, Z. Agriculture Cyber-Physical Systems. In *Cyber-Physical Systems*; Academic Press: Cambridge, MA, USA, 2017; pp. 399–417.
19. Chergui, N.; Kechadi, M.T.; McDonnell, M. The Impact of Data Analytics in Digital Agriculture: A Review. In Proceedings of the 2020 International Multi-Conference on: Organization of Knowledge and Advanced Technologies (OCTA), Tunis, Tunisia, 6–8 February 2020; pp. 1–13.
20. Walters, J.P.; Archer, D.W.; Sassenrath, G.F.; Hendrickson, J.R.; Hanson, J.D.; Halloran, J.M.; Vadas, P.; Alarcon, V.J. Exploring agricultural production systems and their fundamental components with system dynamics modelling. *Ecol. Model.* **2016**, *333*, 51–65. [[CrossRef](#)]
21. Grieves, M.; Vickers, J. Digital twin: Mitigating Unpredictable, Undesirable Emergent Behavior in Complex Systems. In *Transdisciplinary Perspectives on Complex Systems*; Springer: Cham, Switzerland, 2017; pp. 85–113.
22. Verdouw, C.; Tekinerdogan, B.; Beulens, A.; Wolfert, S. Digital twins in smart farming. *Agric. Syst.* **2021**, *189*, 103046. [[CrossRef](#)]
23. Negri, E.; Fumagalli, L.; Macchi, M. A Review of the Roles of Digital Twin in CPS-based Production Systems. *Procedia Manuf.* **2017**, *11*, 939–948. [[CrossRef](#)]
24. Semeraro, C.; Lezoche, M.; Panetto, H.; Dassisti, M. Digital twin paradigm: A systematic literature review. *Comput. Ind.* **2021**, *130*, 103469. [[CrossRef](#)]
25. VanDerHorn, E.; Mahadevan, S. Digital Twin: Generalization, characterization and implementation. *Decis. Support Syst.* **2021**, *145*, 113524. [[CrossRef](#)]
26. Liu, Y.; Zhang, L.; Yang, Y.; Zhou, L.; Ren, L.; Wang, F.; Liu, R.; Pang, Z.; Deen, M.J. A Novel Cloud-Based Framework for the Elderly Healthcare Services Using Digital Twin. *IEEE Access* **2019**, *7*, 49088–49101. [[CrossRef](#)]
27. Juarez, M.G.; Botti, V.J.; Giret, A.S. Digital Twins: Review and Challenges. *J. Comput. Inf. Sci. Eng.* **2021**, *21*, 030802. [[CrossRef](#)]
28. Wright, L.; Davidson, S. How to tell the difference between a model and a digital twin. *Adv. Modeling Simul. Eng. Sci.* **2020**, *7*, 13. [[CrossRef](#)]
29. Lu, J.; Zheng, X.; Schweiger, L.; Kiritsis, D. A Cognitive Approach to Manage the Complexity of Digital Twin Systems. In *Smart Services Summit*; West, S., Meierhofer, J., Ganz, C., Eds.; Progress in IS; Springer: Cham, Switzerland, 2021.
30. Neethirajan, S.; Kemp, B. Digital Twins in Livestock Farming. *Animals* **2021**, *11*, 1008. [[CrossRef](#)]
31. Moghadam, P.; Lowe, T.; Edwards, E.J. Digital Twin for the Future of Orchard Production Systems. *Multidiscip. Digit. Publ. Inst. Proc.* **2020**, *36*, 92. [[CrossRef](#)]
32. Angin, P.; Anisi, M.H.; Göksel, F.; Gürsoy, C.; Büyükgülcü, A. AgriLoRa: A Digital Twin Framework for Smart Agriculture. *J. Wirel. Mob. Netw. Ubiquitous Comput. Dependable Appl.* **2020**, *11*, 77–96.
33. Skobelev, P.O.; Mayorov, I.V.; Simonova, E.V.; Goryanin, O.I.; Zhilyaev, A.A.; Tabachinskiy, A.S.; Yalovenko, V.V. Development of models and methods for creating a digital twin of plant within the cyber-physical system for precision farming management. *J. Phys. Conf. Ser.* **2020**, *1703*, 012022. [[CrossRef](#)]
34. Jo, S.K.; Park, D.H.; Park, H.; Kim, S.H. Smart livestock farms using digital twin: Feasibility study. In Proceedings of the 2018 International Conference on Information and Communication Technology Convergence (ICTC), Jeju Island, Korea, 17–19 October 2018; pp. 1461–1463.
35. Tsolakis, N.; Bechtsis, D.; Bochtis, D. AgROSos: A Robot Operating System Based Emulation Tool for Agricultural Robotics. *Agronomy* **2019**, *9*, 403. [[CrossRef](#)]
36. Monteiro, J.; Barata, J.; Veloso, M.; Veloso, L.; Nunes, J. Towards sustainable digital twins for vertical farming. In Proceedings of the 2018 Thirteenth International Conference on Digital Information Management (ICDIM), Berlin, Germany, 24–26 September 2018; pp. 234–239.



37. Alves, R.G.; Souza, G.; Maia, R.F.; Tran, A.L.H.; Kamienski, C.; Soininen, J.P.; Aquino, P.T.; Lima, F. A digital twin for smart farming. In Proceedings of the 2019 IEEE Global Humanitarian Technology Conference (GHTC), Santa Clara, CA, USA, 8–11 September 2022; pp. 1–4.
38. Laamarti, F.; Badawi, H.F.; Ding, Y.; Arafsha, F.; Hafidh, B.; El Saddik, A. An ISO/IEEE 11073 Standardized Digital Twin Framework for Health and Well-Being in Smart Cities. *IEEE Access* **2020**, *8*, 105950–105961. [[CrossRef](#)]
39. Gámez Díaz, R.; Yu, Q.; Ding, Y.; Laamarti, F.; El Saddik, A. Digital Twin Coaching for Physical Activities: A Survey. *Sensors* **2020**, *20*, 5936. [[CrossRef](#)]
40. Verdouw, C.N.; Kruize, J.W. Digital twins in farm management: Illustrations from the FIWARE accelerators SmartAgriFood and Fractals. In Proceedings of the 7th Asian-Australasian Conference on Precision Agriculture, Hamilton, New Zealand, 16–18 October 2017; pp. 16–18.
41. Sreedevi, T.R.; Kumar, M.S. Digital Twin in Smart Farming: A Categorical Literature Review and Exploring Possibilities in Hydroponics. In Proceedings of the 2020 Advanced Computing and Communication Technologies for High Performance Applications (ACCTHPA), Cochin, India, 2–4 July 2020; pp. 120–124.
42. Verboven, P.; Defraeye, T.; Datta, A.K.; Nicolai, B. Digital twins of food process operations: The next step for food process models? *Curr. Opin. Food Sci.* **2020**, *35*, 79–87. [[CrossRef](#)]
43. Onwude, D.I.; Chen, G.; Eke-Emezie, N.; Kabutey, A.; Khaled, A.Y.; Sturm, B. Recent Advances in Reducing Food Losses in the Supply Chain of Fresh Agricultural Produce. *Processes* **2020**, *8*, 1431. [[CrossRef](#)]
44. van der Burg, S.; Kloppenburg, S.; Kok, E.J.; van der Voort, M. Digital twins in agri-food: Societal and ethical themes and questions for further research. *NJAS Impact Agric. Life Sci.* **2021**, *93*, 98–125. [[CrossRef](#)]
45. Defraeye, T.; Shrivastava, C.; Berry, T.; Verboven, P.; Onwude, D.; Schudel, S.; Bühlmann, A.; Cronje, P.; Rossi, R.M. Digital twins are coming: Will we need them in supply chains of fresh horticultural produce? *Trends Food Sci. Technol.* **2021**, *109*, 245–258. [[CrossRef](#)]
46. Tebaldi, L.; Vignali, G.; Bottani, E. Digital Twin in the Agri-Food Supply Chain: A Literature Review. In *APMS 2021: Advances in Production Management Systems. Artificial Intelligence for Sustainable and Resilient Production System*; Dolgui, A., Bernard, A., Lemoine, D., von Cieminski, G., Romero, D., Eds.; IFIP Advances in Information and Communication Technology; Springer: Cham, Switzerland, 2021; Volume 633.
47. Pylianidis, C.; Osinga, S.; Athanasiadis, I.N. Introducing digital twins to agriculture. *Comput. Electron. Agric.* **2021**, *184*, 105942. [[CrossRef](#)]
48. Vilček, J.; Štefan, K. Integrated index of agricultural soil quality in Slovakia. *J. Maps* **2018**, *14*, 68–76. [[CrossRef](#)]
49. Yin, H.; Cao, Y.; Marelli, B.; Zeng, X.; Mason, A.J.; Cao, C. Soil Sensors and Plant Wearables for Smart and Precision Agriculture. *Adv. Mater.* **2021**, *33*, 2007764. [[CrossRef](#)] [[PubMed](#)]
50. Basterrechea, D.A.; Rocher, J.; Parra, M.; Parra, L.; Marin, J.F.; Mauri, P.V.; Lloret, J. Design and Calibration of Moisture Sensor Based on Electromagnetic Field Measurement for Irrigation Monitoring. *Chemosensors* **2021**, *9*, 251. [[CrossRef](#)]
51. Söderström, M.; Sohlenius, G.; Rodhe, L.; Piikki, K. Adaptation of regional digital soil mapping for precision agriculture. *Precis. Agric.* **2016**, *17*, 588–607. [[CrossRef](#)]
52. Searle, R.; McBratney, A.; Grundy, M.; Kidd, D.; Malone, B.; Arrouays, D.; Stockman, U.; Zund, P.; Wilson, P.; Wilford, J.; et al. Digital soil mapping and assessment for Australia and beyond: A propitious future. *Geoderma Reg.* **2021**, *24*, e00359. [[CrossRef](#)]
53. Wadoux, A.M.C.; McBratney, A.B. Digital soil science and beyond. *Soil Sci. Soc. Am. J.* **2021**, *85*, 1313–1331. [[CrossRef](#)]
54. Villani, G.; Castaldi, P.; Toscano, A.; Stanghellini, C.; Cinotti, T.S.; Maia, R.F.; Tomei, F.; Taumberger, M.; Zanetti, P.; Panizzi, S. Soil Water Balance Model CRITERIA-ID in SWAMP Project: Proof of Concept. In Proceedings of the 2018 23rd Conference of Open Innovations Association (FRUCT), Bologna, Italy, 13–16 November 2018; pp. 398–404.
55. Cunha, H.; Loureiro, D.; Sousa, G.; Covas, D.; Alegre, H. A comprehensive water balance methodology for collective irrigation systems. *Agric. Water Manag.* **2019**, *223*, 105660. [[CrossRef](#)]
56. Pesantez, J.E.; Alghamdi, F.; Sabu, S.; Mahinthakumar, G.; Berglund, E.Z. Using a Digital Twin to Explore Water Infrastructure Impacts During the COVID-19 Pandemic. *Sustain. Cities Soc.* **2021**, 103520. [[CrossRef](#)]
57. Moreira, M.; Mourato, S.; Rodrigues, C.; Silva, S.; Guimarães, R.; Chibeles, C. Building a Digital Twin for the Management of Pressurised Collective Irrigation Systems. In *ICoWEFS 2021: Proceedings of the 1st International Conference on Water Energy Food and Sustainability (ICoWEFS 2021), Proceedings of the International Conference on Water Energy Food and Sustainability, Leiria, Portugal, 10–12 May 2021*; da Costa Sanches Galvão, J.R., de Brito, P.S.D., dos Santos Neves, F., da Silva Craveiro, F.G., de Amorim Almeida, H., Vasco, J.O.C., Neves, L.M.P., de Jesus Gomes, R., de Jesus Martins Mourato, S., Ribeiro, V.S.S., Eds.; Springer: Cham, Switzerland, 2021.
58. Reis, Á.V.D.; Medeiros, F.A.; Ferreira, M.F.; Machado, R.L.T.; Romano, L.N.; Marini, V.K.; Francetto, T.R.; Machado, A.L.T. Technological trends in digital agriculture and their impact on agricultural machinery development practices. *Revi. Ciência Agronômica* **2021**, *51*, e20207740. [[CrossRef](#)]
59. CEMA. Digital Farming: What Does It Really Mean? 2017. Available online: [https://www.cema-agri.org/images/publications/position-papers/CEMA\\_Digital\\_Farming\\_-\\_Agriculture\\_4.0\\_\\_13\\_02\\_2017\\_0.pdf](https://www.cema-agri.org/images/publications/position-papers/CEMA_Digital_Farming_-_Agriculture_4.0__13_02_2017_0.pdf) (accessed on 4 January 2022).
60. Rotz, S.; Gravely, E.; Mosby, I.; Duncan, E.; Finnis, E.; Horgan, M.; LeBlanc, J.; Martin, R.; Neufeld, H.T.; Nixon, A.; et al. Automated pastures and the digital divide: How agricultural technologies are shaping labour and rural communities. *J. Rural Stud.* **2019**, *68*, 112–122. [[CrossRef](#)]

61. Liu, Q.; Leng, J.; Yan, D.; Zhang, D.; Wei, L.; Yu, A.; Zhao, R.; Zhang, H.; Chen, X. Digital twin-based designing of the configuration, motion, control, and optimization model of a flow-type smart manufacturing system. *J. Manuf. Syst.* **2021**, *58*, 52–64. [[CrossRef](#)]
62. Alamin, K.; Vinco, S.; Poncino, M.; Dall’Ora, N.; Fraccaroli, E.; Quaglia, D. February. Digital Twin Extension with Extra-Functional Properties. In Proceedings of the 2021 Design, Automation & Test in Europe Conference & Exhibition (DATE), Virtual, 1–5 February 2021; pp. 434–439.
63. Kampker, A.; Stich, V.; Jussen, P.; Moser, B.; Kuntz, J. Business Models for Industrial Smart Services—The Example of a Digital Twin for a Product-Service-System for Potato Harvesting. *Procedia CIRP* **2019**, *83*, 534–540. [[CrossRef](#)]
64. Vlădăreanu, L.; Gal, A.I.; Melinte, O.D.; Vlădăreanu, V.; Iliescu, M.; Bruja, A.; Feng, Y.; Ciocîrlan, A. Robot Digital Twin towards Industry 4.0. *IFAC-PapersOnLine* **2020**, *53*, 10867–10872. [[CrossRef](#)]
65. Wang, Q.; Jiao, W.; Wang, P.; Zhang, Y. Digital Twin for Human-Robot Interactive Welding and Welder Behavior Analysis. *IEEE/CAA J. Autom. Sin.* **2020**, *8*, 334–343. [[CrossRef](#)]
66. Garg, G.; Kuts, V.; Anbarjafari, G. Digital Twin for FANUC Robots: Industrial Robot Programming and Simulation Using Virtual Reality. *Sustainability* **2021**, *13*, 10336. [[CrossRef](#)]
67. Lumer-Klabbers, G.; Hausted, J.O.; Kvistgaard, J.L.; Macedo, H.D.; Frasheri, M.; Larsen, P.G. Towards a Digital Twin Framework for Autonomous Robots. In Proceedings of the 2021 IEEE 45th Annual Computers, Software, and Applications Conference (COMPSAC), Madrid, Spain, 12–16 July 2021; pp. 1254–1259.
68. Linz, A.; Hertzberg, J.; Roters, J.; Ruckelshausen, A. “Digitale Zwillinge” als Werkzeug für die Entwicklung von Feldrobotern in landwirtschaftlichen Prozessen. In 39. GIL-Jahrestagung, Digitalisierung für landwirtschaftliche Betriebe in kleinstrukturierten Regionen—ein Widerspruch in sich? Gesellschaft für Informatik: Bonn, Germany, 2019; pp. 125–130. Available online: <https://dl.gi.de/handle/20.500.12116/23075> (accessed on 4 January 2022). (In German)
69. Ford, D.N.; Wolf, C.M. Smart Cities with Digital Twin Systems for Disaster Management. *J. Manag. Eng.* **2020**, *36*, 04020027. [[CrossRef](#)]
70. Tsay, J.R.; Lu, C.T.; Tu, T.C. Application of Common Information Platform to Foster Data-Driven Agriculture in Taiwan. Food Agricultural Policy Platform Article. 2019. Available online: <https://ap.ftcc.org.tw/article/1632> (accessed on 4 January 2022).
71. Villalonga, A.; Negri, E.; Fumagalli, L.; Macchi, M.; Castaño, F.; Haber, R. Local Decision Making based on Distributed Digital Twin Framework. *IFAC-PapersOnLine* **2020**, *53*, 10568–10573. [[CrossRef](#)]
72. Moshrefzadeh, M.; Machl, T.; Gackstetter, D.; Donaubaauer, A.; Kolbe, T.H. Towards a Distributed Digital Twin of the Agricultural Landscape. *J. Digit. Landsc. Archit.* **2020**, *5*, 173–186.
73. Jans-Singh, M.; Leeming, K.; Choudhary, R.; Girolami, M. Digital twin of an urban-integrated hydroponic farm. *Data-Cent. Eng.* **2020**, *1*, e20. [[CrossRef](#)]
74. Chaux, J.D.; Sanchez-Londono, D.; Barbieri, G. A Digital Twin Architecture to Optimize Productivity within Controlled Environment Agriculture. *Appl. Sci.* **2021**, *11*, 8875. [[CrossRef](#)]
75. Lezoche, M.; Hernandez, J.E.; Del Mar Alemany Díaz, M.; Panetto, H.; Kacprzyk, J. Agri-food 4.0: A survey of the supply chains and technologies for the future agriculture. *Comput. Ind.* **2020**, *117*, 103187. [[CrossRef](#)]
76. Purandare, H.; Ketkar, N.; Pansare, S.; Padhye, P.; Ghotkar, A. Analysis of post-harvest losses: An Internet of Things and machine learning approach. In Proceedings of the 2016 International conference on automatic control and dynamic optimization techniques (ICACDOT), Pune, India, 9–10 September 2016; pp. 222–226.
77. Mishra, C.K.; Chakshu. Post-harvest crop management system using IoT and AI. *Int. J. Adv. Res. Dev.* **2019**, *4*, 42–44.
78. Mor, S.; Madan, S.; Prasad, K.D. Artificial intelligence and carbon footprints: Roadmap for Indian agriculture. *Strateg. Chang.* **2021**, *30*, 269–280. [[CrossRef](#)]
79. Bekele, B. Review on Factors Affecting Postharvest Quality of Fruits. *J. Plant Sci. Res.* **2018**, *5*, 180.
80. Eppinger, T.; Longwell, G.; Mas, P.; Goodheart, K.; Badiali, U.; Aglave, R. Increase Food Production Efficiency Using the Executable Digital Twin (xDT). *Chem. Eng. Trans.* **2021**, *87*, 37–42.
81. Koulouris, A.; Misailidis, N.; Petrides, D. Applications of process and digital twin models for production simulation and scheduling in the manufacturing of food ingredients and products. *Food Bioprod. Process.* **2021**, *126*, 317–333. [[CrossRef](#)]
82. Defraeye, T.; Tagliavini, G.; Wu, W.; Prawiranto, K.; Schudel, S.; Kerisima, M.A.; Verboven, P.; Bühlmann, A. Digital twins probe into food cooling and biochemical quality changes for reducing losses in refrigerated supply chains. *Resour. Conserv. Recycl.* **2019**, *149*, 778–794. [[CrossRef](#)]
83. Burgos, D.; Ivanov, D. Food retail supply chain resilience and the COVID-19 pandemic: A digital twin-based impact analysis and improvement directions. *Transp. Res. E Logist. Transp. Rev.* **2021**, *152*, 102412. [[CrossRef](#)] [[PubMed](#)]
84. Shoji, K.; Schudel, S.; Onwude, D.; Shrivastava, C.; Defraeye, T. Mapping the postharvest life of imported fruits from packhouse to retail stores using physics-based digital twins. *Resour. Conserv. Recycl.* **2022**, *176*, 105914. [[CrossRef](#)]
85. Ahmed, A.; Zulfiqar, S.; Ghandar, A.; Chen, Y.; Hanai, M.; Theodoropoulos, G. Digital twin technology for aquaponics: Towards optimizing food production with dynamic data driven application systems. In *AsiaSim 2019: Methods and Applications for Modeling and Simulation of Complex Systems, Proceedings of the Asian Simulation Conference, Singapore, 30 October–1 November 2019*; Springer: Singapore; pp. 3–14.
86. Ghandar, A.; Ahmed, A.; Zulfiqar, S.; Hua, Z.; Hanai, M.; Theodoropoulos, G. A Decision Support System for Urban Agriculture Using Digital Twin: A Case Study With Aquaponics. *IEEE Access* **2021**, *9*, 35691–35708. [[CrossRef](#)]

87. Nemtinov, K.; Eruslanova, M.; Zazulya, A.; Nemtinova, Y.; Haider, S.S. Creating a digital twin of an agricultural machine. In Proceedings of the MATEC Web of Conferences, EDP Sciences, Sevastopol, Russia, 7–11 September 2020; Volume 329, p. 05002.
88. Bottani, E.; Vignali, G.; Tancredi, G.P.C. A digital twin model of a pasteurization system for food beverages: Tools and architecture. In Proceedings of the 2020 IEEE International Conference on Engineering, Technology and Innovation (ICE/ITMC), Cardiff, UK, 15–17 June 2020; pp. 1–8.
89. Chiscop, F.; Necula, B.; Cazacu, C.C.; Stoica, C.E. Using Digital Twinning in Fast-food Production Chain Simulation. In Proceedings of the MATEC Web of Conferences, EDP Sciences, Sibiu, Romania, 2–4 June 2021; Volume 343, p. 03005.
90. Tekinerdogan, B.; Verdouw, C. Systems architecture design pattern catalog for developing digital twins. *Sensors* **2020**, *20*, 5103. [[CrossRef](#)] [[PubMed](#)]
91. Ciruela-Lorenzo, A.M.; Del-Aguila-Obra, A.R.; Padilla-Meléndez, A.; Plaza-Angulo, J.J. Digitalization of Agri-Cooperatives in the Smart Agriculture Context. Proposal of a Digital Diagnosis Tool. *Sustainability* **2020**, *12*, 1325. [[CrossRef](#)]
92. O’Grady, M.J.; Langton, D.; O’Hare, G.M.P. Edge computing: A tractable model for smart agriculture? *Artif. Intell. Agric.* **2019**, *3*, 42–51. [[CrossRef](#)]
93. Komasilovs, V.; Zacepins, A.; Kviešis, A.; Nasirahmadi, A.; Sturm, B. Solution for remote real-time visual expertise of agricultural objects. *Agron. Res.* **2018**, *16*, 464–473.

MDPI  
St. Alban-Anlage 66  
4052 Basel  
Switzerland  
[www.mdpi.com](http://www.mdpi.com)

*Sensors* Editorial Office  
E-mail: [sensors@mdpi.com](mailto:sensors@mdpi.com)  
[www.mdpi.com/journal/sensors](http://www.mdpi.com/journal/sensors)



Disclaimer/Publisher's Note: The statements, opinions and data contained in all publications are solely those of the individual author(s) and contributor(s) and not of MDPI and/or the editor(s). MDPI and/or the editor(s) disclaim responsibility for any injury to people or property resulting from any ideas, methods, instructions or products referred to in the content.





Academic Open  
Access Publishing

[mdpi.com](https://www.mdpi.com)

ISBN 978-3-0365-8809-4